

VOLUME 75

APRIL 29, 1971

NUMBER 9

JPCHAx

THE JOURNAL OF
PHYSICAL
CHEMISTRY

PUBLISHED BIWEEKLY BY THE AMERICAN CHEMICAL SOCIETY

American Chemical Society

"Primary Publications on Microfilm"

Your Key to—

■ Dramatic savings in archival space and dollars . . . over **1,000,000** pages of chemical literature contained in a carousel measuring only 17" x 17" x 39".

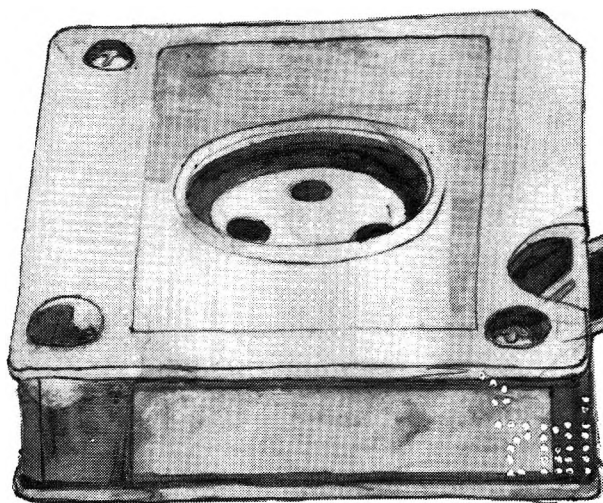
■ Faster access to needed data. Slash costly search and retrieval time required of your scientists and librarians.

■ Unlimited distribution of copyrighted scientific data. "ACS Primary Publications on Microfilm" are available under a unique licensing agreement permitting you to make as many enlarged photocopies per page as desired . . . for distribution throughout your company.

American Chemical Society Primary Publications included in this microfilm program:

JOURNAL OF THE AMERICAN CHEMICAL SOCIETY
INDUSTRIAL & ENGINEERING CHEMISTRY
CHEMICAL TECHNOLOGY
CHEMICAL & ENGINEERING NEWS
CHEMICAL & ENGINEERING NEWS ANNUAL INDEXES
ANALYTICAL CHEMISTRY
JOURNAL OF PHYSICAL CHEMISTRY
JOURNAL OF AGRICULTURAL AND FOOD CHEMISTRY
JOURNAL OF ORGANIC CHEMISTRY
JOURNAL OF CHEMICAL AND ENGINEERING DATA
CHEMICAL REVIEWS
JOURNAL OF CHEMICAL DOCUMENTATION
I&EC FUNDAMENTALS
I&EC PROCESS DESIGN AND DEVELOPMENT
I&EC PRODUCT RESEARCH AND DEVELOPMENT
BIOCHEMISTRY
INORGANIC CHEMISTRY
JOURNAL OF MEDICINAL CHEMISTRY
CHEMISTRY
ENVIRONMENTAL SCIENCE & TECHNOLOGY
ACCOUNTS OF CHEMICAL RESEARCH
MACROMOLECULES

For information on "ACS Primary Publications on Microfilm", write or call:
Mr. George Virvan
Special Issues Sales
American Chemical Society
1155 16th Street, N.W.
Washington, D.C. 20036
(202-737-3337)



THE JOURNAL OF PHYSICAL CHEMISTRY

BRYCE CRAWFORD, Jr., *Editor*

STEPHEN PRAGER, *Associate Editor*

ROBERT W. CARR, Jr., FREDERIC A. VAN CATLEDGE, *Assistant Editors*

EDITORIAL BOARD: A. O. ALLEN (1970-1974), R. BERSOHN (1967-1971), J. R. BOLTON (1971-1975), S. BRUNAUER (1967-1971), M. FIXMAN (1970-1974), H. S. FRANK (1970-1974), J. R. HUIZENGA (1969-1973), M. KASHA (1967-1971), W. J. KAUFMANN (1969-1973), W. R. KRIGBAUM (1969-1973), R. A. MARCUS (1968-1972), W. J. MOORE (1969-1973), J. A. POPLE (1971-1975), B. S. RABINOVITCH (1971-1975), H. REISS (1970-1974), S. A. RICE (1969-1975), R. E. RICHARDS (1967-1971), F. S. ROWLAND (1968-1972), R. L. SCOTT (1968-1972), R. SEIFERT (1968-1972)

CHARLES R. BERTSCH, *Manager, Editorial Production*

AMERICAN CHEMICAL SOCIETY, 1155 Sixteenth St., N.W., Washington, D. C. 20036

FREDERICK T. WALL, *Executive Director*

Books and Journals Division

JOHN K. CRUM, *Director (Acting)*

JOSEPH H. KUNEY, *Head, Business Operations Department*

RUTH REYNARD, *Assistant to the Director*

©Copyright, 1971, by the American Chemical Society. Published biweekly by the American Chemical Society at 20th and Northampton Sts., Easton, Pa. 18042. Second-class postage paid at Easton, Pa.

All manuscripts should be sent to *The Journal of Physical Chemistry*, Department of Chemistry, University of Minnesota, Minneapolis, Minn. 55455.

Additions and Corrections are published once yearly in the final issue. See Volume 74, Number 26 for the proper form.

Extensive or unusual alterations in an article after it has been set in type are made at the author's expense, and it is understood that by requesting such alterations the author agrees to defray the cost thereof.

The American Chemical Society and the Editor of *The Journal of Physical Chemistry* assume no responsibility for the statements and opinions advanced by contributors.

Correspondence regarding accepted copy, proofs, and reprints should be directed to Editorial Production Office, American Chemical Society, 20th and Northampton Sts., Easton, Pa. 18042. Manager: CHARLES R. BERTSCH. Assistant Editor: EDWARD A. BORGER. Editorial Assistant: EVELYN J. UHLER.

Advertising Office: Century Communications Corporation, 142 East Avenue, Norwalk, Conn. 06851.

Business and Subscription Information

Remittances and orders for subscriptions and for single copies,

notices of changes of address and new professional connections, and claims for missing numbers should be sent to the Subscription Service Department, American Chemical Society, 1155 Sixteenth St., N.W., Washington, D. C. 20036. Allow 4 weeks for changes of address. Please include an old address label with the notification.

Claims for missing numbers will not be allowed (1) if received more than sixty days from date of issue, (2) if loss was due to failure of notice of change of address to be received before the date specified in the preceding paragraph, or (3) if the reason for the claim is "missing from files."

Subscription rates (1971): members of the American Chemical Society, \$20.00 for 1 year; to nonmembers, \$40.00 for 1 year. Those interested in becoming members should write to the Admissions Department, American Chemical Society, 1155 Sixteenth St., N.W., Washington, D. C. 20036. Postage to Canada and countries in the Pan-American Union, \$4.00; all other countries, \$5.00. Single copies for current year: \$2.00. Rates for back issues from Volume 56 to date are available from the Special Issues Sales Department, 1155 Sixteenth St., N.W., Washington, D. C. 20036.

This publication and the other ACS periodical publications are now available on microfilm. For information write to: MICROFILM, Special Issues Sales Department, 1155 Sixteenth St., N.W., Washington, D. C. 20036.

CHEMICAL REACTIONS IN ELECTRICAL DISCHARGES

ADVANCES IN CHEMISTRY SERIES NO. 80

Thirty-seven papers from a symposium sponsored by the Division of Fuel Chemistry and the Division of Physical Chemistry of the American Chemical Society, chaired by Bernard D. Blaustein.

A wide range of topics are covered in these papers by chemists, physicists, and engineers including treatments of decomposition and dissociation reactions, ion-molecule reactions, chemical syntheses, and chemical engineering aspects and physics of reactions in electrical discharges.

514 pages with index Clothbound (1969) \$15.00

Set of L.C. cards free with library orders upon request

Other books in ADVANCES IN CHEMISTRY SERIES on topics of industrial interest include:

No. 85 Stabilization of Polymers and Stabilizer Processes. Twenty-two papers survey progress and report recent work on a variety of stabilization problems—thermal stabilization, antioxidants and antiozonants for polyolefins, rubbers, and rubbers containing polymers. Other topics include microbial stabilization, ultraviolet light absorbers, and fire retardants. 332 pages
Cloth (1968) \$12.00

No. 78 Literature of Chemical Technology. Forty articles discuss the literature of many aspects of chemical technology, including chlor-alkali and electrochemistry, ceramics, rocket propulsion, photography, medicinal chemistry, leather and glue, waxes, textile, paper, soap, plastics, coatings, explosives, petroleum, dyes, aerosols, pesticides, and foods. Special attention is given to rubber with eight articles and one on carbon black. Included for each article is discussion of special literature sources and services, books, periodicals, patent classes, and bibliographies. 732 pages
Cloth (1968) \$17.50

No. 76 Oxidation of Organic Compounds—II. Thirty-one papers on gas phase oxidations, homogeneous catalysis, applied oxidation, and synthetic processes. 438 pages
Cloth (1968) \$13.50

No. 70 Homogeneous Catalysis. Industrial Applications and Implications. Concentrates on reactions in solution. Reviews the kinds of substances that can be used as homogeneous catalysts and how they function, contrasts homogeneous with heterogeneous catalysis, reviews industrial applications of homogeneous catalysis, and treats in detail many special topics. 283 pages
Cloth (1968) \$10.50

No. 69 Fuel Gasification. Waning natural gas supplies and the threat of nuclear fuels are renewing interest in converting solid fuels to high B.t.u. gas. Sixteen studies survey current research in the U.S. and elsewhere from which commercial processes seem imminent. 276 pages
Cloth (1967) \$10.50

No. 64 Regenerative EMF Cells. Seventeen papers survey current progress and research on regenerative systems for converting and storing electrical energy. Principal emphasis is on thermally regenerative systems, but chemical and photochemical systems are considered. 309 pages
Cloth (1967) \$11.00

No. 51 Selective Oxidation Processes. Surveys methods for selectively oxidizing petroleum fractions by vapor phase and liquid phase processes, such as hydroxylation of aromatics and olefins; covers use of SO₂, NO₂, and O₃ and surveys carbon anion oxidation. 177 pages
Cloth (1965) \$8.00

No. 48 Plasticization and Plasticizer Processes. Seventeen papers survey recent studies on plasticizer action, properties, and production. Includes chapters on glass transition, plasticizer mobility, processes for phthalates and other plasticizers, and antiplasticizers. 200 pages
Cloth (1965) \$8.00

No. 46 Patents for Chemical Inventions. What to do about your patentable idea before you call the attorney. 117 pages
Cloth (1964) \$5.50

No. 38 Saline Water Conversion—II. Fourteen papers from two symposia; includes recovery of minerals from sea water, minimizing scale formation, wiped thin-film distillation, diffusion still, solar flash evaporation, osmosis, electrodialysis (3 papers), research in Israel, hydrate process. 199 pages
Paper (1963) \$8.00

No. 34 Polymerization and Polycondensation Processes. An I&EC Division symposium with emphasis on unit processes. Twenty-one papers on addition polymerization, polycondensation reactions, commercial polymerization processes, and equipment design. 260 pages
Paper (1962) \$10.00

No. 27 Saline Water Conversion. A Water and Waste Chemistry Division symposium; includes thermodynamics of desalting, solvent extraction, freezing, centrifugal phase barrier recompression distillation, multistage flash evaporation, ion exchange, osmosis, and electrochemical demineralization. 246 pages
Paper (1960) \$9.00

No. 21 Ozone Chemistry and Technology. Sixty papers from the International Ozone Conference; includes ozone chemistry, high concentration ozone, ozone analysis and technology, formation in electrical discharge, toxicity, sterilization, and water purification. 465 pages
Cloth (1959) \$10.00

No. 19 Handling and Uses of Alkali Metals. Nineteen articles on the chemistry, manufacture, and use of the alkali metals; five are devoted solely or partly to lithium, two to potassium, the remainder to sodium. 177 pages
Paper (1957) \$7.00

No. 5 Progress in Petroleum Technology. Survey of 25 years of progress at the ACS Diamond Jubilee. Thirty-two papers on all aspects of petroleum processing and products. 392 pages
Cloth (1951) \$8.00

All books postpaid in U.S. and Canada; plus 20 cents foreign and PUAS.

Order from SPECIAL ISSUES SALES
AMERICAN CHEMICAL SOCIETY
1155 SIXTEENTH ST., N.W.
WASHINGTON, D.C. 20036

THE JOURNAL OF PHYSICAL CHEMISTRY

Volume 75, Number 9 April 29, 1971

The Kinetics of the Decomposition of Freeze-Dried Iron(II) Sulfate	D. W. Johnson and P. K. Gallagher	1179
Electron Spin Resonance Studies of Transient Radicals in Aqueous Solutions	K. Eiben and Richard W. Fessenden	1186
Electron Paramagnetic Resonance Studies in Frozen Aqueous Solutions. Elimination of Freezing Artifacts	John S. Leigh, Jr., and George H. Reed	1202
Electron Spin Resonance Studies of Biradicals of Nitro Aromatic Radical Anions and Alkali Ions	C. A. McDowell and F. Nakano	1205
Anisotropic Solvent Shifts Determined by Factor Analysis	Paul H. Weiner and Edmund R. Malinowski	1207
Nuclear Magnetic Resonance Study of Ion-Exchange Resins. Macroreticular Resins, Carboxylic Acid Resins, and Line-Width Effects	Lawrence S. Frankel	1211
Infrared Study of the Surface of Titanium Dioxides. I. Hydroxyl Groups	Michel Primet, Pierre Pichat, and Michel-Vital Mathieu	1216
Infrared Study of the Surface of Titanium Dioxides. II. Acidic and Basic Properties	Michel Primet, Pierre Pichat, and Michel-Vital Mathieu	1221
The Aggregation of Arylazonaphthols. II. Steric Effects on Dimer Structure in Water	Alan R. Monahan, Nicholas J. Germano, and Daniel F. Blossley	1227
Photophysical Processes of <i>m</i> -Difluorobenzene	Terry L. Brewer	1233
Relaxation Processes of Cholesteryl Methyl Ether	P. F. Mountain and S. Walker	1237
Dielectric Properties of Some Diols	Eiji Ikada	1240
Perchlorodiphenylmethyl Stable Free Radical. X-Ray Analysis of a Disordered Mixed Crystal	J. Silverman, L. J. Soltzberg, N. F. Yannoni, and A. P. Krukoni	1246
Cohesive Energies of the Alkali Hydrides and Deuterides	R. C. Bowman, Jr.	1251
The Thermodynamic Properties of Liquids, Including Solutions. IV. The Entropy of Mixing	Maurice L. Huggins	1255
The Electrical Conductance of Gaseous Mixtures of Aluminum Trichloride and Sodium Tetrachloroaluminate	E. W. Dewing	1260
The Thermochemistry, Thermodynamic Functions, and Molecular Structures of Some Cyclic Hydrocarbons	Richard H. Boyd, Shiv N. Sanwal, Shahrokh Shary-Tehrany, and Donal McNally	1264
The Self-Diffusion of Water in Uranyl Nitrate Hexahydrate	M. L. Franklin and Ted B. Flanagan	1272
Transient Phenomena Caused by Temperature Change on Capacitance of Rutile Film	Masaki Yamazaki and Hiroshi Nozaki	1279
Isotope Effects in the Substitution Reaction of 2.8-eV Tritium Atoms with Methane	C. C. Chou and F. S. Rowland	1283
A Study of the Roles of Chemical Factors in Controlling the Yields of Substitution Reactions by Energetic Tritium Atoms. Electronegativity, Electron Density, and Bond Energy	Yi-Noo Tang, Edward K. C. Lee, Enzo Tachikawa, and F. S. Rowland	1290
Complete Retention of Configuration during the Replacement of Hydrogen by Energetic Tritium in <i>dl</i> - and <i>meso</i> -(CHFCl) ₂	G. F. Palino and F. S. Rowland	1299
The Prediction of Osmotic and Activity Coefficients in Mixed Electrolyte Solutions	P. J. Reilly, R. H. Wood, and R. A. Robinson	1305

NOTES

Isotope Effects in the Diffusion of ^{14}C -Substituted Molecules in the Liquid Phase. II. The Relative Diffusion Rates of Benzene- I - ^{14}C and Benzene- $I,2$ - ^{14}C	Lee B. Eppstein and John G. Albright 1315
On the Photolysis of Ethylene at 1216 \AA	Y. Inel, A. Siddiqi, and G. G. Meisels 1317
An Improved Numerical Method for Evaluating Second-Order Rate Constants	G. R. Howe 1319
Mass Spectrometric Study of the Reaction of Oxygen Atoms with Nitrosyl Chloride	M. R. Dunn, C. G. Freeman, M. J. McEwan, and L. F. Phillips 1320

COMMUNICATIONS TO THE EDITOR

Dielectric Measurements with Time Domain Reflectometry When Large Conductivities Are Involved	M. J. C. van Gemert 1323
Bond Energy Effects in Substitution Reactions of Fluorine-18 Atoms with Methyl Halides	Thomas Smail, R. Subramonia Iyer, and F. S. Rowland 1324
Hexafluoroacetone Imine Filter for 185 nm.	Sidney Toby and Glyn O. Pritchard 1326
Kinetics of Isopropyl Alcohol Radicals by Electron Spin Resonance-Flow Techniques	R. E. James and F. Sicilio 1326
Trifluoroacetic Acid. The Nature of Association in Dilute Solutions in Inert and Slightly Basic Solvents	M. Kirszenbaum, J. Corset, and M. L. Josien 1327
Perfluorinated Aliphatic Carboxylic Acids. Nature of Association in Dilute Solutions in Nonpolar Solvents	T. S. S. R. Murty 1330

AUTHOR INDEX

Albright, J. G., 1315	Frankel, L. S., 1211	Krukonis, A. P., 1246	Nozaki, H., 1279	Siddiqi, A., 1317
Blossey, D. F., 1227	Franklin, M. L., 1272	Lee, E. K. C., 1290	Palino, G. F., 1299	Silverman, J., 1246
Bowman, R. C., Jr., 1251	Freeman, C. G., 1320	Leigh, J. S., Jr., 1202	Phillips, L. F., 1320	Smail, T., 1324
Boyd, R. H., 1264	Gallagher, P. K., 1179	Malinowski, E. R., 1207	Pichat, P., 1216, 1221	Soltzberg, L. J., 1246
Brewer, T. L., 1233	Germano, N. J., 1227	Mathieu, M.-V., 1216, 1221	Primet, M., 1216, 1221	Tachikawa, E., 1290
Chou, C. C., 1283	Howe, G. R., 1319	McDowell, C. A., 1205	Pritchard, G. O., 1326	Tang, Y.-N., 1290
Corset, J., 1327	Huggins, M. L., 1255	McEwan, M. J., 1320	Reed, G. H., 1202	Toby, S., 1326
Dewing, E. W., 1260	Ikada, E., 1240	McNally, D., 1264	Reilly, P. J., 1305	van Gemert, M. J. C., 1323
Dunn, M. R., 1320	Inel, Y., 1317	Meisels, G. G., 1317	Robinson, R. A., 1305	Walker, S., 1237
Eiben, K., 1186	Iyer, R. S., 1324	Monahan, A. R., 1227	Rowland, F. S., 1283, 1290, 1299, 1324	Weiner, P. H., 1207
Eppstein, L. B., 1315	James, R. E., 1326	Mountain, P. F., 1237	Sanwal, S. N., 1264	Wood, R. H., 1305
Fessenden, R. W., 1186	Johnson, D. W., 1179	Murty, T. S. S. R., 1330	Shary-Tehrany, S., 1264	Yamazaki, M., 1279
Flanagan, T. B., 1272	Josien, M. L., 1327	Nakano, F., 1205	Sicilio, F., 1326	Yannoni, N. F., 1246
	Kirszenbaum, M., 1327			

ANNOUNCEMENT

On the last two pages of this issue you will find reproduced the table of contents of the April 1971 issue of the *Journal of Chemical and Engineering Data*.

THE JOURNAL OF PHYSICAL CHEMISTRY

Registered in U. S. Patent Office © Copyright, 1971, by the American Chemical Society

VOLUME 75, NUMBER 9 APRIL 29, 1971

The Kinetics of the Decomposition of Freeze-Dried Iron(II) Sulfate¹

by D. W. Johnson* and P. K. Gallagher

Bell Telephone Laboratories, Inc., Murray Hill, New Jersey (Received December 16, 1970)

Publication costs assisted by the Bell Telephone Laboratories, Inc.

The isothermal decomposition kinetics of iron(II) sulfate has been studied for both the freeze-dried and the reagent sulfate in wet and dry oxygen and nitrogen atmospheres. The decomposition in oxygen atmosphere was studied as a single-step decomposition of a $\text{Fe}_2\text{O}(\text{SO}_4)_2$ phase. In nitrogen it was studied as a resolvable two-step decomposition from FeSO_4 to $\text{Fe}_2\text{O}_2\text{SO}_4$ and then to Fe_2O_3 . The data were fitted quantitatively by computer to several equations. Reasonable fitting was obtained using the Erofeev model, $[-\ln(1-\alpha)]^{1/n} = kt$, usually the best fit was to the contracting geometry models, $1 - (1-\alpha)^{1/n} = kt$, with $0.10 < \alpha < 0.90$ where α is the fraction reacted. Best fits often occurred with nonintegral values of n , but no consistent nonintegral value was found. Activation energies in the range of 45–61 kcal/mol were determined for the various iron(II) sulfate materials prepared and decomposed under the different conditions. The relative rates of decomposition and the kinetic models to which the data fit are discussed in terms of the morphology of the starting materials.

Introduction

While the kinetics of the sulfate decomposition of hydrated FeSO_4 have been studied previously^{2,3} no similar study has been made of the decomposition kinetics of FeSO_4 prepared by the freeze-drying process.⁴ The kinetics of decomposition of freeze-dried inorganic salts is of interest for several reasons. Firstly, it would be expected that the high surface areas observed in these materials would be reflected in the decomposition rate. Secondly, it was hoped that the decomposition rate law would reflect the interesting chained aggregate structure observed in freeze-dried materials.⁵ Finally, in the case of iron(II) sulfate, the kinetic experiments offered the possibility of lending further support to the decomposition scheme proposed by Gallagher, *et al.*⁶

A further impetus for the study of the decomposition kinetics of the FeSO_4 system stems from some disagreement in the published literature. Kubo, *et al.*,³ fit their data to the Prout-Tompkins model

$$\ln\left(\frac{\alpha}{1-\alpha}\right) = kt$$

and get an activation energy for the decomposition of 32.4 kcal/mol. Lumme, *et al.*,^{2b} found that nonisothermal TG data taken for the decomposition in nitrogen gave an activation energy of 58.3 ± 3 kcal/mol. Pechkovskii, *et al.*,^{2a} studied the isothermal decomposition of iron(II) sulfate in air over a temperature range of 676–729°. These data were fitted to the contracting volume model

$$1 - (1 - \alpha)^{1/s} = kt$$

giving an activation energy of 60.4 kcal/mol.

The kinetic study reported here follows the results

- (1) This paper was presented in part at the 160th National Meeting of the American Chemical Society, Chicago, Ill., Sept 1970.
- (2) (a) V. V. Pechkovskii, A. G. Zvezdin, and S. V. Ostrovskii, *J. Appl. Chem. USSR*, **36**, 1403 (1963); (b) P. Lumme and K. Junkkarinen, *Suom. Kemistilehti B*, **41**, 220 (1968).
- (3) T. Kubo, M. Tamguchi, and S. Shirasaki, *Kogyo Kagaku Zasshi*, **64**, 256 (1961); *Chem. Abstr.* **57**, 3076f (1962).
- (4) F. J. Schnettler, F. R. Monforte, and W. W. Rhodes, *Sci. Ceram.*, **4**, 79 (1968).
- (5) D. W. Johnson and F. J. Schnettler, *J. Amer. Ceram. Soc.*, **53**, 440 (1970).
- (6) P. K. Gallagher, D. W. Johnson, and F. Schrey, *ibid.*, **53**, 666 (1970).

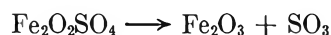
of the decomposition scheme recorded by Gallagher, *et al.*,⁶ for FeSO_4 . This study showed that in an oxygen atmosphere FeSO_4 oxidized by two routes to $\text{Fe}_2\text{O}(\text{SO}_4)_2$. It is the decomposition of this species to Fe_2O_3 in a single step that will be discussed for an oxygen atmosphere. The equation for the reaction is



The study also showed that FeSO_4 decomposed in two resolvable steps in nitrogen atmospheres, which are



and



Experimental Section

Freeze-dried samples were prepared as described by Schnetler, *et al.*,⁴ from 0.5 M solutions of Fisher Certified $\text{FeSO}_4 \cdot 7\text{H}_2\text{O}$. Studies done on the reagent $\text{FeSO}_4 \cdot 7\text{H}_2\text{O}$ were carried out on a -200, +250 mesh seive fraction of the above Fisher $\text{FeSO}_4 \cdot 7\text{H}_2\text{O}$.

Samples (2-3 mg) of the freeze-dried material or 10-13 mg of the reagent iron(II) sulfate were loaded onto the platinum pan of a Cahn Model RG thermobalance. A Perkin-Elmer furnace for which the temperature calibration has been described by Gallagher and Schrey⁷ was used. Each sample was heated to 300° and held to constant weight and then heated to the isothermal decomposition temperature at a rate of 320°/min. Atmospheres of flowing nitrogen or oxygen at the rate of 15-20 cc/min were used. The gases were dried over silica gel or were saturated with H_2O vapor at room temperature. The nitrogen was also passed over hot copper for removal of residual oxygen.

The output from the thermobalance was recorded digitally on paper tape as described by Gallagher and Schrey.⁸ Because the decompositions took place isothermally, only the weight change was recorded. Weight data were recorded at equally spaced time intervals of 10-100 sec depending on the rate of the reaction.

Computer programs were prepared to accept the weight *vs.* time digital data using a GE 635 computer and a special Xerox graphical terminal unit for hard copy plotting of computed data. Several programs were used to process each isothermal run. First, a simple weight *vs.* time plot was generated. Then upon selecting appropriate values for the beginning and final weights, the data were plotted as a preselected function of α *vs.* time where α is the fraction reacted. The 18 equations used in the program are enumerated in Table I.

Visual observation for the straight-line fit of these plots allowed selection of equations with sufficiently good fit for subsequent least-squares fitting of the data by another program. The output from this program gave the least-squares straight-line parameters (of

Table I: Kinetic Models

Name	Equation
1. Power law	$\alpha^n = kt, n = 1, 2, 1/2, 1/3, 1/4$
2. Contracting geometry	$1 - (1 - \alpha)^{1/n} = kt, n = 2, 3$
3. Erofeev	$[-\ln(1 - \alpha)]^{1/n} = kt, n = 1, 3/2, 2, 3, 4$
4. 2D diffusion controlled	$(1 - \alpha) \ln(1 - \alpha) + \alpha = kt$
5. 3D diffusion controlled	$[1 - (2/3)\alpha] - (1 - \alpha)^{2/3} = kt$
6. Jander	$[1 - (1 - \alpha)^{1/3}]^2 = kt$
7. Prout-Tompkins	$\ln \frac{\alpha}{1 - \alpha} = kt$
8. Second order	$\frac{1}{1 - \alpha} - 1 = kt$
9. Exponential	$\ln \alpha = kt$

which the slope is k), and the standard deviation was calculated in terms of the appropriate α function and also the deviation of each point from the lines was converted back into a deviation in α . These deviations were also presented as a standard deviation. This parameter is useful in quantitatively comparing the fit of data to several models and allows the selection of the best model.

Finally, the rate constants computed in the above program were used in another to make an Arrhenius type plot, $\log k$ *vs.* $1/T$, and to least-squares fit a straight line using the reciprocal of the standard deviation as a weight factor for each point. This program calculated the slope as kcalories per mole and the intercept as the preexponential term.

One final program was prepared to least-squares fit the data to either the contracting geometry model or the Erofeev model with a variable value of n . The results were plotted as a standard deviation in α *vs.* n in order to pick the nonintegral value of n which provided the best fit.

Results

Data were collected for the decomposition of freeze-dried FeSO_4 in both wet and dry oxygen and nitrogen. The decomposition of the reagent $\text{FeSO}_4 \cdot 7\text{H}_2\text{O}$ was carried out in dry oxygen and nitrogen. An example of the plots generated as weight *vs.* time are shown in Figure 1 for a freeze-dried FeSO_4 sample decomposed at 500° in both dry nitrogen and oxygen gas. These examples serve to illustrate the type of plot generated by about 800 individual data points. The nitrogen case also serves to illustrate the characteristic break in the vicinity of 2.15 mg for decomposition in nitrogen. The break (accentuated by the dashed lines on Figure 1) corresponds to the expected weight of the $\text{Fe}_2\text{O}_2\text{SO}_4$ compound.

(7) P. K. Gallagher and F. Schrey, *Thermochimica Acta*, **1**, 465 (1970).

(8) P. K. Gallagher and F. Schrey, "Thermal Analysis," Vol. 2, R. F. Schwenker and P. D. Garn, Ed., Academic Press, New York, N. Y., 1969, p. 929.

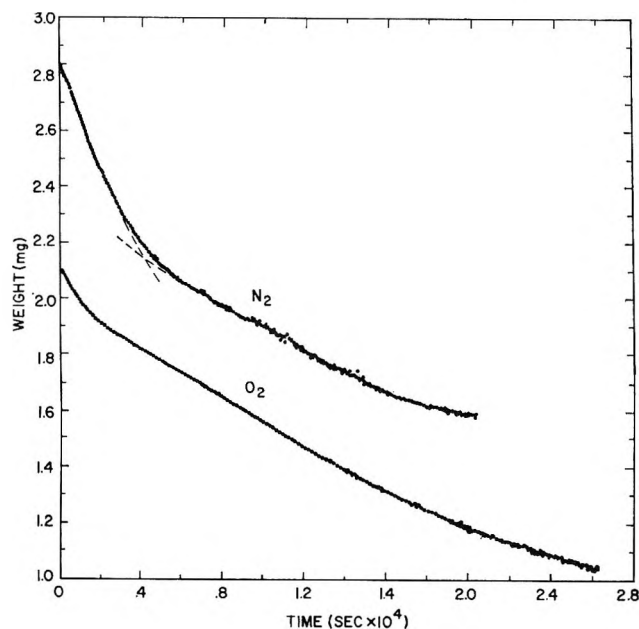


Figure 1. Weight vs. time for freeze-dried iron(II) sulfate in dry O_2 and N_2 .

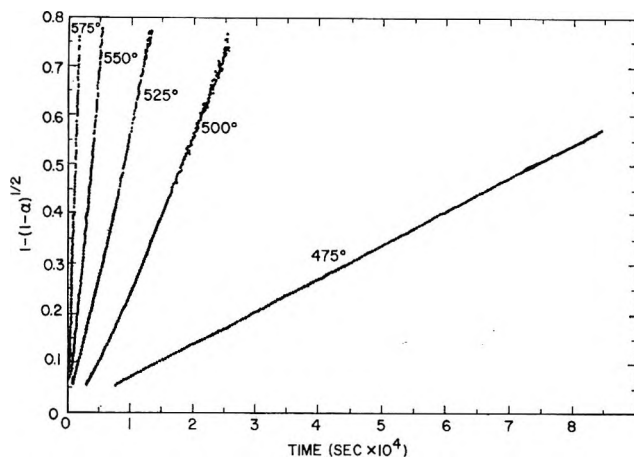


Figure 2. Decomposition of freeze-dried iron(II) sulfate in dry O_2 plotted with the contracting area formula.

Examples of the data plotted as the appropriate functions of α are shown in Figures 2-4 for $0.10 < \alpha < 0.90$. These examples were chosen to illustrate decompositions in oxygen and nitrogen and at the same time illustrate a case for the reagent material and that for a freeze-dried material in a wet and dry atmosphere.

The rate constants obtained by least-squares fitting of the data are most compactly described in Table II showing the activation energies and preexponential terms derived by least-squares fitting of the rate constant data according to the Arrhenius equation. The three best fitting models as determined by the standard deviation are presented for each case. The standard deviations shown in Table II are an average over each temperature of the standard deviation in α of the points from the straight line. As such, they are to be

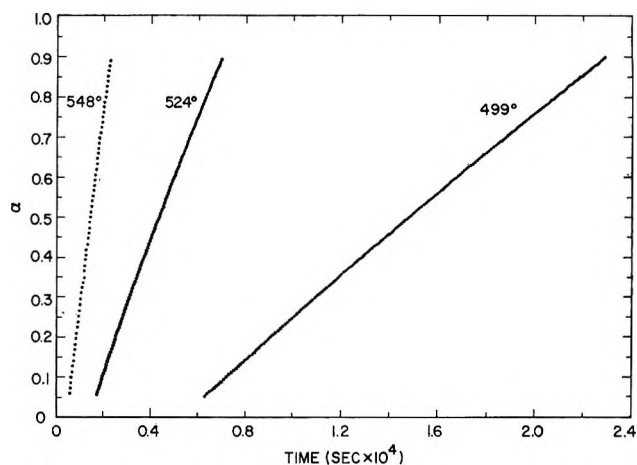


Figure 3. The first step in the decomposition of freeze-dried iron(II) sulfate in wet N_2 plotted with the linear formula.

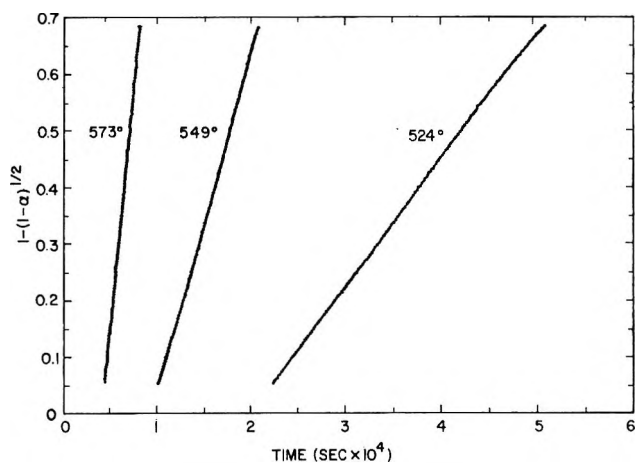


Figure 4. The second step in the decomposition of reagent iron(II) sulfate by dry N_2 plotted with the contracting area formula.

used primarily to compare the fit of one equation with another for the same data.

Examples of the Arrhenius plots for the decomposition in oxygen and for the two decompositions in nitrogen are shown in Figure 5 for the reagent sulfate and freeze-dried sulfate in both wet and dry atmospheres. The kinetic models used to obtain the rate data are not necessarily the ones which give the best fit in each case as shown in Table II, but were selected as a common equation such that the freeze-dried and reagent samples could be compared on the same plot.

Experiments were carried out to optimize the fit of the data to the second and third kinetic equations in Table I by varying n over nonintegral values. An example of the computer results for the freeze-dried $FeSO_4$ in dry oxygen at 500° is shown in Figure 6 for the contracting geometry model. This plot of the standard deviation in α vs. n would suggest the optimum value of n at about 1.7 for this reaction. However, the calculations did not indicate the same opti-

Table II. Numerical Data from Kinetic Model Fitting and Arrhenius Plots

	$\text{FeO}(\text{SO}_4)_2 \rightarrow \text{Fe}_2\text{O}_3 + 2\text{SO}_3$ in O_2 atmosphere $\alpha = 0.10-0.95$	$2\text{FeSO}_4 \rightarrow \text{Fe}_2\text{O}_3\text{SO}_4 + \text{SO}_2$ in N_2 atmosphere $\alpha = 0.05-0.90$	$\text{Fe}_2\text{O}_3\text{SO}_4 \rightarrow \text{Fe}_2\text{O}_3 + \text{SO}_3$ in N_2 atmosphere $\alpha = 0.10-0.90$
Temperatures used, °C	475, 500, 525, 550, 575	425, 450, 475, 500, 525, 550, 575	475, 500, 525, 550, 575
Equation	$1 - \frac{(1-\alpha)^{1/2}}{\alpha} = kt$	$1 - \frac{(1-\alpha)}{\alpha} = kt$	$1 - \frac{(1-\alpha)}{\alpha} = kt$
Activation energy ^a	45.0	45.2	48.5
Preexponential term ^b	1.12×10^8	1.59×10^8	1.03×10^8
Average std deviation	0.020	0.026	0.010
Equation	$1 - \frac{(1-\alpha)}{\alpha} = kt$	$1 - \frac{(1-\alpha)}{\alpha} = kt$	$1 - \frac{(1-\alpha)}{\alpha} = kt$
Activation energy ^a	46.2	46.2	46.2
Preexponential term ^b	2.57×10^8	1.25×10^8	1.82×10^8
Average std deviation	0.013	0.016	0.013
Equation	$1 - \frac{(1-\alpha)}{\alpha} = kt$	$1 - \frac{(1-\alpha)}{\alpha} = kt$	$1 - \frac{(1-\alpha)}{\alpha} = kt$
Activation energy ^a	46.0	46.2	46.0
Preexponential term ^b	2.57×10^8	1.25×10^8	1.82×10^8
Average std deviation	0.013	0.016	0.013
Equation	$1 - \frac{(1-\alpha)}{\alpha} = kt$	$1 - \frac{(1-\alpha)}{\alpha} = kt$	$1 - \frac{(1-\alpha)}{\alpha} = kt$
Activation energy ^a	45.8	45.2	45.8
Preexponential term ^b	6.32×10^7	3.67×10^7	6.32×10^7
Average std deviation	0.012	0.016	0.012
Equation	$1 - \frac{(1-\alpha)}{\alpha} = kt$	$1 - \frac{(1-\alpha)}{\alpha} = kt$	$1 - \frac{(1-\alpha)}{\alpha} = kt$
Activation energy ^a	45.8	45.2	45.8
Preexponential term ^b	6.32×10^7	3.67×10^7	6.32×10^7
Average std deviation	0.012	0.016	0.012

^a In kcal/mol. ^b Sec⁻¹.

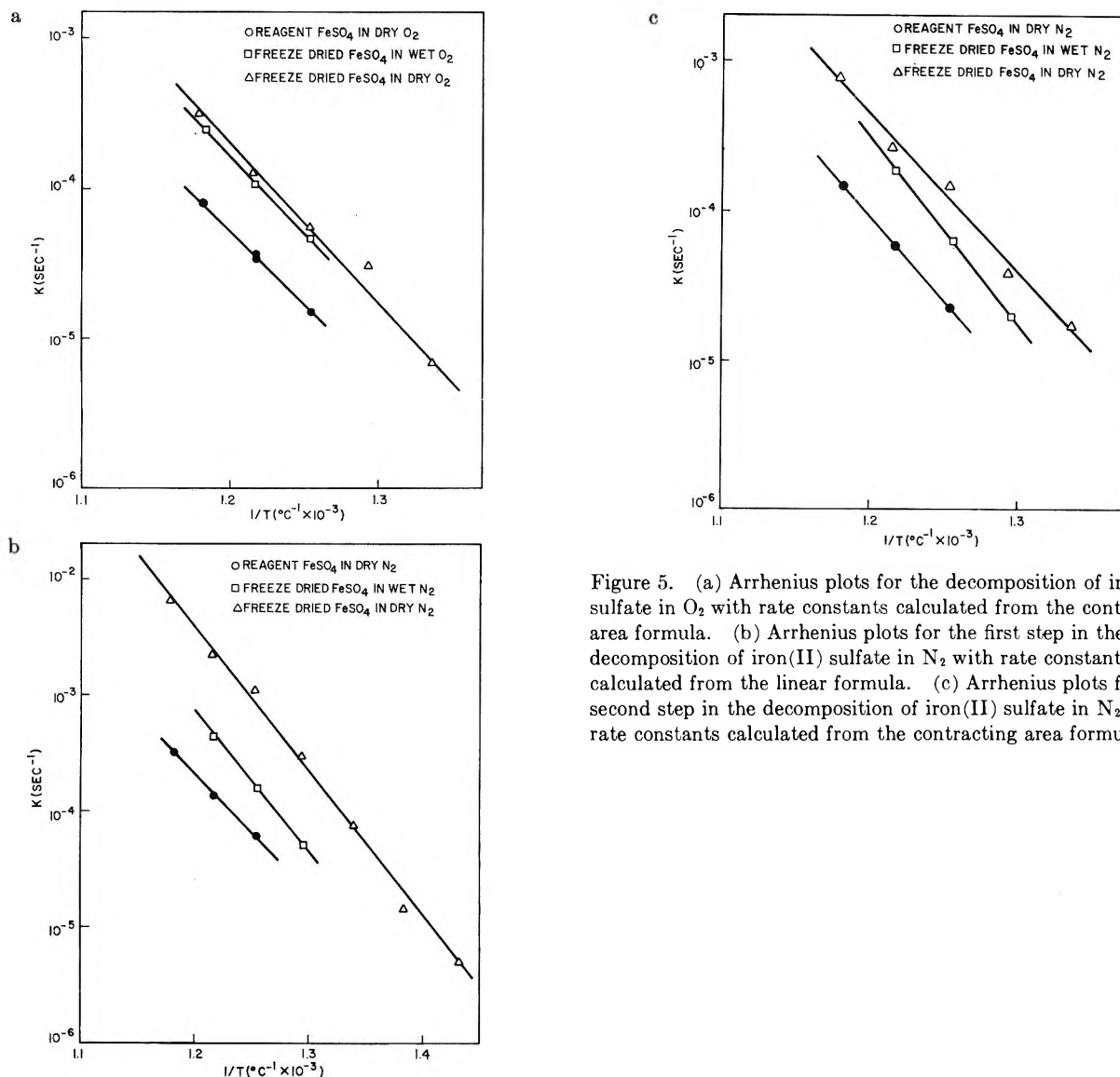


Figure 5. (a) Arrhenius plots for the decomposition of iron(II) sulfate in O_2 with rate constants calculated from the contracting area formula. (b) Arrhenius plots for the first step in the decomposition of iron(II) sulfate in N_2 with rate constants calculated from the linear formula. (c) Arrhenius plots for the second step in the decomposition of iron(II) sulfate in N_2 with rate constants calculated from the contracting area formula.

imum value of n for different temperatures as shown in Figure 7 where the calculated optimum value of n is plotted as a function of temperature for the reaction in dry oxygen.

Discussion of Results

The technique of breaking the decomposition reaction in nitrogen into two parts was used for two reasons. First, the mechanism of the reaction as determined by Gallagher, *et al.*,⁶ indicates that the reaction occurs in two steps; second, the kinetic data show breaks such as that illustrated in Figure 1 which allowed the data to be broken into two portions. This break, however, is most clearly demonstrated for the case of the freeze-dried $FeSO_4$ in dry nitrogen. The same technique has been used by Bond and Jacobs⁹ in analyzing the two-step thermal decomposition of sodium nitrate.

It was recognized that the second decomposition step to some degree takes place simultaneously with the first. However, attempts to synthesize hybrid

equations to cover the entire decomposition range did not improve the fit over the range of α where the two reactions overlap significantly.

Comparison of the actual rates of reaction can be seen in Figures 5a, b, and c. The consistent trend is that the reaction occurs faster in dry atmospheres than in wet and faster for freeze-dried material than for the $-200, +250$ mesh reagent material. The relative rates for the freeze-dried and reagent sulfates were expected since the freeze-dried material has a higher surface area than the reagent. However, from the preliminary TG data it was reported⁶ that the reaction was faster in wet atmospheres than in dry. This conclusion was reached partly on evidence that the Fe_2O_3 crystallites attained greater dimensions in equivalent heat treatments for the freeze-dried sulfate if the atmospheres were wet. The isothermal kinetic data show, however, that the dry atmospheres allow a more rapid

(9) B. D. Bond and P. W. M. Jacobs, *J. Chem. Soc. A*, 1265 (1966).

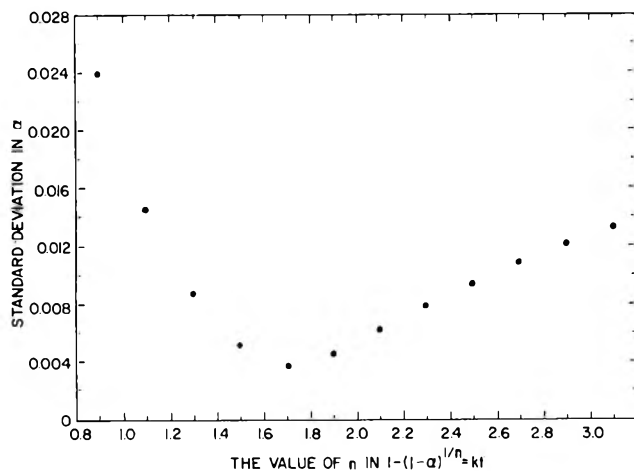


Figure 6. Variation of fitting parameter with n in $1 - (1 - \alpha)^{1/n} = kt$ for freeze-dried iron(II) sulfate decomposed at 500° in dry O_2 .

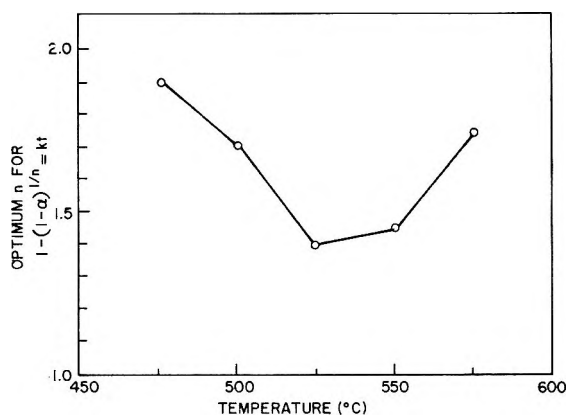


Figure 7. Variation of optimum n in $1 - (1 - \alpha)^{1/n} = kt$ with temperature for freeze-dried iron(II) sulfate decomposed in dry O_2 .

reaction, and it is now clear that the increased crystallite size of the Fe_2O_3 formed in wet atmospheres is due to an increased grain growth phenomenon rather than an increased decomposition rate.

Several interesting observations can be made from the kinetic data in Table II. One is that in some cases one kinetic model fits far better than others. An example is the first decomposition of reagent $FeSO_4 \cdot 7H_2O$ in dry nitrogen. Here the linear model fits considerably better than the others. However, in other cases such as the decomposition of freeze-dried $FeSO_4$ in wet oxygen none of the three best equations stands out as fitting significantly better than the others. Also to be noticed in Table II is the general insensitivity of the activation energy to the model used to calculate the rate constants.

Some trends emerge from the activation energy data presented in Table II. The activation energies for the nitrogen decomposition are consistently higher than those for the decomposition in oxygen. With the exception of the low activation energies for the second

decomposition of freeze-dried $FeSO_4$ in dry nitrogen the overall trend is for the reaction in oxygen to have low activation energies, the first nitrogen reaction to be intermediate, and the second nitrogen reaction to be highest. While the activation energies of the freeze-dried and reagent sulfate are similar for the decomposition in oxygen, the trend of the activation energies is seen for the nitrogen reactions again with the exception of the second decomposition of freeze-dried sulfate in dry nitrogen. This trend shows the activation energies for freeze-dried sulfate in dry nitrogen to be greatest, for the same material in wet nitrogen to be intermediate, and that for the reagent material to be the lowest.

Table II also shows that in almost all cases the data were fit either to the contracting geometry model or the Erofeev model. These models are different from those used by other workers. Kubo, *et al.*,³ found the Prout-Tomkins model to hold. Use of this model in this work showed the fit to be generally satisfactory but was usually surpassed by the other models as shown in Table II. Pechkovskii, *et al.*,^{2a} fit their data to the contracting volume model and specifically state that the Erofeev model was tested also. Again, while in this work the contracting volume model gave a satisfactory fit, it was in no case one of the three best fit equations in Table II.

Another serious deviation from the work of Pechkovskii, *et al.*,^{2a} occurred. They report decomposing the $FeSO_4$ isothermally at temperatures between 676 and 729° while in this work these temperatures proved to be much too high for successful experimentation. The discrepancy is borne out in the rate constants. Pechkovskii, *et al.*,^{2a} report a rate constant of $9.9 \times 10^{-5}/\text{sec}$ at 700° . While in this work, a rate constant of this value is found at a temperature of about 585° for the reagent material in oxygen, a difference of 115° .

The contracting geometry model implies the rapid formation of many nuclei on the surface of the particles. A moving decomposition interface then occurs in one, two, or three dimensions with $n = 1, 2, \text{ or } 3$, respectively. The Erofeev model has been used with $n = 2, 3, \text{ and } 4$, where $n = 2$ and 3 implies the growth of a constant number of nuclei in two or three dimensions, while $n = 4$ implies an increasing number of nuclei growing spherically.

Since the data do in general best fit the contracting geometry model ($n = 1$ and 2), it is interesting to consider the geometrical significance of this model in terms of the morphology of $FeSO_4$. Figure 8 shows scanning electron micrographs of a fractured sphere of freeze-dried $FeSO_4$ after decomposition at 800° in oxygen. The radial texture is common to freeze-dried powders⁵ and occurs during the freezing process as a segregation of sulfate and ice. The interconnecting columns of oxide can account for the fit of the contracting geometry equation. If the material were made of cylindrical columns and if the movement of the de-

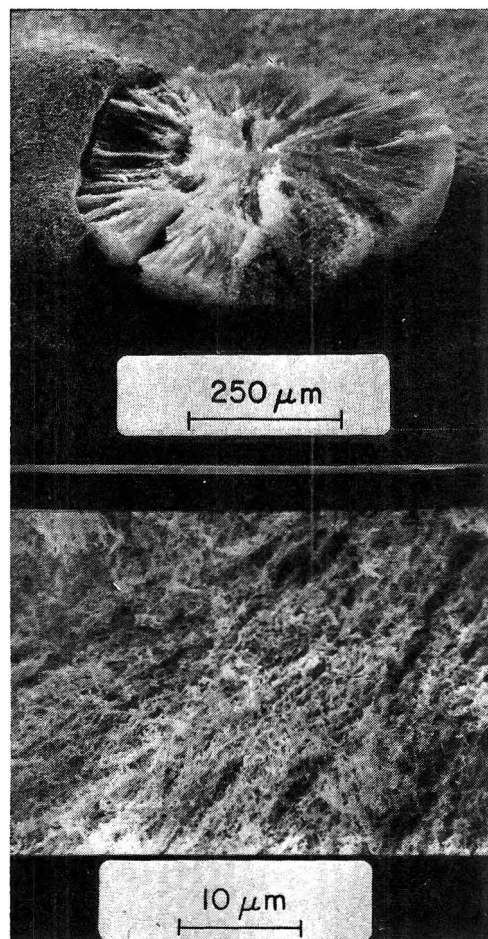


Figure 8. Scanning electron micrographs of a fractured sphere of freeze-dried iron(II) sulfate after decomposition for 2 hr at 800° in O₂.

composition interface were to take place primarily down the length of the column, then a linear model would be expected. On the other hand, if the decomposition interface moved from the cylindrical surface of the column toward the center, then the observed contracting area model would be expected. A similar argument can be made for the reagent material since after

dehydration the scanning electron microscope shows the structure to be similar to that of the freeze-dried material but much more densely packed.

This idealized picture does not hold completely since the actual mechanism could be a combination of both. In fact, this suspicion is backed up by data such as those in Figure 7 where the optimum value of n is often not exactly one or two but something intermediate.

Summary

The following generalities can be made concerning the kinetics of freeze-dried and reagent FeSO₄.

1. The successful application of the two-step decomposition of FeSO₄ in nitrogen atmosphere lends support to the hypothesis of the transient Fe₂O₂SO₄ phase.
2. The relative rates of the decomposition are such that in all cases studied, the freeze-dried sulfate in dry atmospheres decomposes the most rapidly, the same material in wet atmospheres intermediately, and the reagent sulfate in dry atmospheres the most slowly.
3. In almost all cases the isothermal data best fitted the contracting geometry models. This fit is consistent with structures observed in the sulfate and derived oxide by scanning electron microscopy.
4. The optimum value of n in the contracting geometry model

$$1 - (1 - \alpha)^{1/n} = kt$$

is generally in the range of 1 or 2 but is not usually an integral value.

5. In most cases the activation energy for the reaction is nearly independent of the kinetic model used.

6. Activation energies for the reaction fall in the range of 45–61 kcal/mol in all cases. The decompositions occur with a lower activation energy in oxygen than in nitrogen.

Acknowledgments. The authors wish to thank Miss B. Cetlin for her aid in computer programming.

Electron Spin Resonance Studies of Transient Radicals in Aqueous Solutions¹

by K. Eiben

Institut für Strahlenchemie, Kernforschungszentrum, Karlsruhe, West Germany

and Richard W. Fessenden²

Radiation Research Laboratories and Department of Chemistry, Mellon Institute of Science, Carnegie-Mellon University, Pittsburgh, Pennsylvania 15213 (Received October 16, 1970)

Publication costs assisted by Carnegie-Mellon University and the U. S. Atomic Energy Commission

Esr spectroscopy has been used to examine aqueous solutions of various solutes during steady irradiation with a 2.8-MeV electron beam. Radiolysis was carried out directly in the esr cavity; the sample was contained in a silica cell of the usual flat design for aqueous samples. Of the three primary radicals from water (H, OH, and e_{aq}^-) only H could be detected by its esr spectrum, a 503.2-G doublet (but with the low-field line in emission). Reactions of all three primary radicals have been studied. As is usual, use was made of selective scavengers (*e.g.*, N_2O for e_{aq}^- , *t*-butyl alcohol for OH) to help in identifying the source of the various solute radicals. Emphasis has been put upon the ability of esr spectroscopy to provide positive identification of radicals. The technique has been tested upon some well-understood systems and then applied to several more specific problems some of which have been studied by pulse radiolysis. Some of the reactions which were studied are abstraction (by OH) from methyl and isopropyl alcohols and acetate, chloroacetate, malonate, and glycolate ions, addition (of H and OH) to benzene and benzoate ion, attachment of e_{aq}^- to acetone and chloroacetate, and electron transfer from $(CH_3)_2\dot{C}OH$ to several nitrobenzene derivatives. It is noteworthy that in only one case (abstraction from $CH_2(COOH)_2$ to form $\dot{C}H(COOH)_2$) were qualitatively different results found for OH reactions than observed for the active species in the $Ti^{3+}-H_2O_2$ system.

Introduction

Work in these laboratories has shown that esr spectroscopy can be used to detect radicals in liquid hydrocarbons during steady, *in situ* radiolysis with a high-energy electron beam.³ This experimental arrangement, however, is limited to relatively nonpolar materials by the requirement of a large sample volume. The desirability of an extension to other systems, including aqueous solutions, is obvious. An early attempt⁴ to study radicals in aqueous solutions was successful but was confined by sensitivity considerations to radicals with lifetimes longer than those determined by diffusion-controlled reaction. Publications by Smaller, *et al.*,^{5,6} have shown that lossy samples can be studied with small sample volumes if the absorbed dose rate is increased. One of these papers⁶ describes results obtained upon an aqueous solution.

Previously we had determined that the absorbed dose rate could not be greatly increased by using higher electron beam currents because of excessive sample heating and voltage instability problems with the Van de Graaff accelerator. Decreasing the beam diameter and consequently increasing the current density over the beam cross section seemed the only improvement possible. This approach has been implemented by using a hole in the side of the cavity and by moving the beam exit window of the Van de Graaff accelerator closer to the esr cell. A great improvement in signal intensity has resulted, and it is now possible to detect in aqueous

solutions radicals with recombination rate constants as large as 10^9 to $10^{10} M^{-1} sec^{-1}$.

The results presented here are intended to demonstrate some of the potential applications of esr spectroscopy to the study of the radiolysis of aqueous solutions. We have not attempted to investigate the various points in depth but have chosen applications which illustrate the unique properties of esr spectroscopy. (Two papers based on work subsequent to that reported here and describing in more detail the reactions of two classes of compounds have been published.^{7,8})

One major advantage of esr spectroscopy is that radicals can often be identified with only a minimum of other information and that chemically and structurally similar radicals can be distinguished. Esr spectra are clearly better for this purpose than optical spectra as used in conventional pulse radiolysis. We have in several instances investigated reactions which have already been studied by pulse radiolysis to check that the radicals have been properly identified. The esr

(1) Supported in part by the U. S. Atomic Energy Commission.

(2) To whom correspondence should be sent.

(3) R. W. Fessenden and R. H. Schuler, *J. Chem. Phys.*, **39**, 2147 (1963).

(4) K. Eiben and R. W. Fessenden, *J. Phys. Chem.*, **72**, 3387 (1968).

(5) B. Smaller, J. R. Remko, and E. C. Avery, *J. Chem. Phys.*, **48**, 5174 (1968).

(6) E. C. Avery, J. R. Remko, and B. Smaller, *ibid.*, **49**, 951 (1968).

(7) P. Neta and R. W. Fessenden, *J. Phys. Chem.*, **74**, 2263 (1970).

(8) P. Neta and R. W. Fessenden, *ibid.*, **74**, 3362 (1970).

method, of course, has limitations (see below), so that it must also draw on the results of other more conventional studies. It is to be hoped that mutual benefit will arise from any comparison of the results of esr and pulse radiolysis studies of similar systems.

All of the experiments to be described were done with a steady electron beam and not a pulsed one. Although the steady-state method does not allow kinetic information to be obtained directly, it has several other advantages. First, the standard 100-kHz field modulation spectrometer can be used, and the resolution provided by that type of spectrometer is available for the study of complex spectra. (We have not yet taken the steps to provide faster response times as have Smaller, *et al.*⁵) In general before one wishes to study kinetics one must identify the radicals and the reactions they are involved in. The steady-state method allows this. Second, the main difference between pulsed and steady-state experiments is that the latter sees much less of the initial nonequilibrium populations of spin levels with which the radical is formed. This problem, discussed in more detail below, is best avoided for many purposes. Finally, several problems shared by both approaches should be mentioned. If the esr line widths are large, peak heights are reduced and radicals may be undetectable even though present at otherwise adequate concentrations. Also both steady-state and pulsed methods use such high absorbed dose rates that they suffer from the possibility of secondary reactions even with flowing samples. (The pulse repetition period in most pulsed experiments is shorter than the residence time of the sample in the irradiation zone.) In many cases the products of radiolysis can be significantly more reactive toward the primary radicals from the water than the initial solute.

The detailed relationship between the sensitivity of pulsed and steady-state modes has been discussed by Fessenden and Schuler.⁹ This treatment shows that for radicals which disappear bimolecularly the pulsed mode can be made nearly as sensitive as the steady-state one if signal enhancement by time sampling is employed and the average beam current is made equal to that in the steady-state experiment. The technique reported by Smaller, *et al.*,⁵ seems to meet these requirements. Although the two methods have comparable sensitivity, the steady-state one has sacrificed the possibility of studying the time dependence of the esr signals. With the present spectrometer system it is possible to study radical disappearance by using a pulsed electron beam with long pulse duration (~ 1 msec) and a time-average computer but only at considerable loss of signal-to-noise ratio.^{4,10} With such an arrangement radical lifetimes are just long enough (> 1 msec) to be unaffected by the minimum time constant of the 100-kHz unit.

The phenomenon of nonequilibrium initial population of spin states upon radical formation was first observed

by Fessenden and Schuler³ for the hydrogen atom produced in liquid methane. They observed that the esr spectra of both H and D atoms exhibited an inverted low-field line, implying an inverted population difference for the appropriate pairs of spin states. Smaller, *et al.*,⁵ have found this phenomenon to be common to other radicals if observations are made before spin relaxation can occur, and they have published a spectrum of cyclopentyl radical with the low-field half-inverted. It is now clear that this effect is not limited to radicals produced by high-energy radiation but may be common to most, if not all, methods of generating radicals.¹¹ The effect was first observed for radicals other than hydrogen atom by Smaller, *et al.*,⁵ because their experiment was the first in which the spectrum could be examined in a time after radical formation which was comparable to the spin relaxation time, T_1 . Usually only small trends in intensity are observed in spectra taken in the steady-state mode as a result of almost complete spin relaxation over the chemical lifetime of the radicals. Only where the chemical lifetime is relatively short or the relaxation time relatively long is the effect very pronounced. We have found the greatest effect (except for the hydrogen atom) for the hydroxycyclohexadienyl radical and suppose that this radical has a long T_1 through the lowering of the hyperfine anisotropy by the reduced spin densities in this conjugated radical. Some effect is seen for the radical $(\text{CH}_3)_2\dot{\text{C}}\text{OH}$ from isopropyl alcohol.

It is not clear at this time what factors determine the initial population of spin states. It is likely, however, that many of the considerations are similar to those invoked to explain superficially similar multiplet effect in the nmr spectra of samples undergoing radical reactions. Several discussions of the latter effects have been given,¹²⁻¹⁴ and Kaptein and Oosterhoff¹⁵ and also Fischer¹⁶ have specifically considered the esr problem. Their explanation involves the mixing of single and triplet states of a radical pair by the combined action of hyperfine and electron exchange interactions during separation of the radical pair. Although this type of mechanism qualitatively fits many observations (*e.g.*, the effect is larger for larger hyperfine constants), the details are not yet clear enough to be of use in under-

(9) R. W. Fessenden and R. H. Schuler in "Advances in Radiation Chemistry," Vol. 2, M. Burton and J. L. Magee, Ed., Interscience, New York, N. Y., 1970, p 56 ff.

(10) R. W. Fessenden, *J. Phys. Chem.*, **68**, 1508 (1964).

(11) The high-field lines appear stronger in spectra from photolysis, see, *e.g.*, R. Livingston and H. Zeldes, *J. Amer. Chem. Soc.*, **88**, 4333 (1966), or P. J. Krusic and J. K. Kochi, *ibid.*, **90**, 7155 (1968), and also in those from $\text{Ti}^{3+} + \text{H}_2\text{O}_2$ reaction, see, *e.g.*, H. Fischer, *Z. Naturforsch. A*, **19**, 866 (1964).

(12) H. Fischer and J. Bargon, *Accounts Chem. Res.*, **2**, 110 (1969).

(13) R. Kaptein, *Chem. Phys. Lett.*, **2**, 261 (1968).

(14) G. L. Closs, *J. Amer. Chem. Soc.*, **91**, 4552 (1969).

(15) R. Kaptein and J. L. Oosterhoff, *Chem. Phys. Lett.*, **3**, 195 (1969).

(16) H. Fischer, *ibid.*, **4**, 611 (1970).

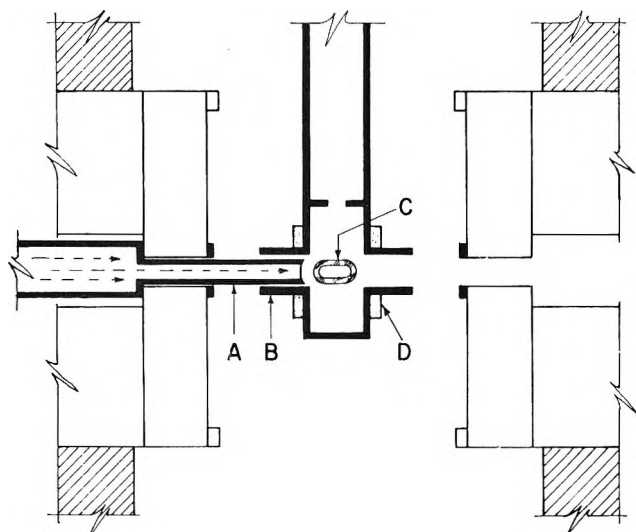


Figure 1. Diagram of irradiation arrangement showing magnet poles and cavity. The extension (A) of the Van de Graaff vacuum system is brought into a chimney (B) on the broad face of the cavity and is terminated by a window (0.025 mm brass) approximately in the plane of the cavity wall. The silica aqueous cell (C, inside cross section 0.5×10 mm) is irradiated edgewise as shown. The two broad faces of the cavity are of 0.45-mm Type 304 stainless steel which has been plated with copper and then silver. The modulation coils are external to these faces (D).

standing the radical formation mechanism. For this paper, therefore, the effect will be ignored as much as possible.

Experimental Section

It was mentioned above that a most important quantity is the production rate of radicals (*i.e.*, current density over the beam cross section) for a given total electron beam current. In the work on nitromethane⁴ the window to the vacuum system of the accelerator was inside the pole piece as in Figure 1 of ref 3, and the beam diameter at the cavity wall was ~ 10 mm. To achieve a significant improvement it was necessary to bring this window very close to the cavity and to make a hole in the face of the cavity. These details are shown in Figure 1. At some point in the reduction of the beam diameter any further decrease will be offset by the spreading of the beam in the dense material of the sample and cell. With the present arrangement the approximate average width of the beam in the sample and cell as measured by the coloring produced in a Pyrex cell is 5–6 mm. Calculations of absorbed dose rate based on this beam cross section agree approximately with that determined chemically (see below).

The increased beam currents used in this work produce considerable ionization of the gas within the cavity, and this conductivity affects both cavity Q and resonant frequency. Because the electron beam is not steady dc but has a considerable ac noise component, a considerable increase in noise output of the spectrometer results. Because the main component of this

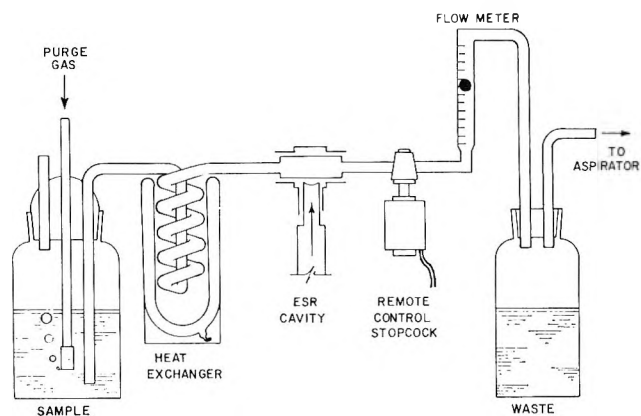


Figure 2. Schematic representation of flow system. ESR cavity, cell, and the electron beam have been rotated for clarity. The electron beam is in a horizontal plane. The sample (in a 4-l. bottle) is bubbled with the desired gas (N_2 or N_2O usually) and forced through the cell by partially evacuating the waste container. A heat exchanger (bath of ethylene glycol-water cooled from an external thermostat bath) is provided to cool the sample. A remote control stopcock is also provided.

conductivity is a result of free electrons, a shortening of electron lifetime reduces the effect on the spectrometer. We have found that a slow flow of pure O_2 through the cavity is sufficient to reduce the interaction of the electron beam with the spectrometer to an insignificant level.

The system for flowing the sample is shown in Figure 2. The sample is degassed in a 4-l. container and is made to flow through the sample cell by partially evacuating the waste container with an aspirator. The cooling coil is to lower the solution temperature to compensate for the temperature rise produced by the radiolysis. The temperature rise is about 5° for a beam current of $10 \mu A$. Because of some overcompensation all results pertain to a solution temperature of about 15° . A motor driven stopcock is used to turn the flow on and off remotely. Both the stopcock and a tungsten current collection electrode are downstream from the irradiation zone. We have used a flat silica cell fabricated from Suprasil II¹⁷ with a 0.5-mm internal spacing. Although this material produces a large esr signal, only ~ 7 G of the spectrum are blanked out when the spectrum is taken as a second derivative with modulation amplitudes appropriate to fairly narrow lines (0.1–0.2-G width).

The esr spectrometer is a Varian V4200 with a 100-kHz modulation unit as described previously.³ A Philco L-4164 detector diode is currently being used (with no amplifier modifications) to give some improvement in signal-to-noise ratio over that for a 1N23G. The field-tracking nmr unit³ has been modified by the use of a transistorized marginal oscillator. Measurements of the g factors are relative to the main peak in

(17) Amersil, Inc., Hillside, N. J.

the signal from the cell which occurs at $g = 2.00044$. These measurements are accurate to about ± 0.00003 .

The electron beam current is collected and monitored at two points: from the cavity itself and from an electrode in the esr cell. The current measured from the cell was $\sim 15\%$ that from the cavity. The current from the cavity plus cell represents substantially the total beam current entering the magnet gap. Typically the current from the cavity was 8–10 μA . Because this represents ~ 25 W of heat for 2.8-MeV energy, it was necessary to water-cool the cavity. The flow of sample solution (~ 1 cm³ sec⁻¹) provides cooling for the cell.

The absorbed dose rate was measured by irradiating an oxygen-saturated ferrous solution. For a 2.5- μA total beam current and a 1-cm³ sec⁻¹ flow rate the production rate of Fe³⁺ corresponded to an absorbed dose of 3×10^{18} eV g⁻¹. A proportional decrease in yield of Fe³⁺ was observed when a higher flow rate was used showing that no depletion of C₂ had occurred. This absorbed dose can be compared with that calculated from a beam diameter of 5 mm and a linear energy loss of 1.8 MeV g⁻¹ cm². The value obtained from this calculation is also 3×10^{18} . The close agreement must be regarded as partially fortuitous because the estimate of the beam average diameter is rather approximate. It is clear, however, that the irradiation conditions are known at least semiquantitatively. This knowledge is important in considering possible solute depletion or secondary reaction.

At 1-cm³ sec⁻¹ flow rate the sample volume of $0.8 \times 0.5 \times 0.05 = 0.020$ cm³ is replenished 50 times per second so that the absorbed dose rate is 1.5×10^{20} eV g⁻¹ sec⁻¹. For a radiation chemical yield of unity this is a radical production rate of 2.5×10^{-3} M sec⁻¹. This production rate combined with a radical recombination rate constant of 10^9 M⁻¹ sec⁻¹ leads to a steady-state radical concentration of 1.6×10^{-6} M. Such a radical concentration is readily detectable if the esr spectrum has relatively narrow lines.

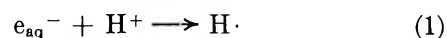
The chemicals in this study were used as received, and no special problems were encountered. Reagent grades were used when available. The water was doubly distilled as previously described.⁴ In the early work pH was adjusted using only KOH or HClO₄. Subsequently it became evident that for near-neutral pH values buffering was necessary. This was accomplished with the appropriate sodium phosphate.

Results and Discussion

As is well known, an important tool in the study of reactions in aqueous solutions during radiolysis is the use of selective scavengers to control the reactions of H, OH, and e_{aq}⁻ with solutes. (The primary yields of these radicals are about 0.6, 2.8, and 2.8, respectively.¹⁸) Such an approach was important for this esr work because without the use of scavengers it would often have been difficult to determine which of the primary

radicals led to the formation of a particular radical. There are two types of scavengers: those that interconvert the primary radicals (*e.g.*, H⁺ and N₂O) and those which yield some other radical. The latter must be chosen so that the spectrum of the radical produced does not interfere with other spectra. The presence of the spectrum derived from the scavenger is useful evidence that the solute is not competing to a great extent with the intended scavenger.

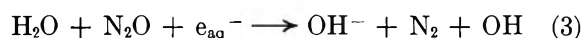
In acid solutions reaction 1 occurs, and a relatively



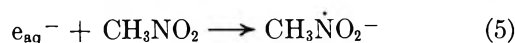
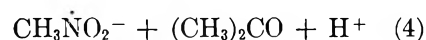
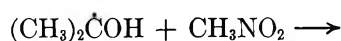
large yield of H is produced. Under these conditions it is possible to study the radicals produced from the solute by reaction of H \cdot . There can also be reactions of OH. Depending on the rate of the OH reaction it may be possible to remove OH by reaction with *t*-butyl alcohol (which is relatively unreactive toward H) and



to study only the reactions of H. In basic solution the main solute reactions are with e_{aq}⁻ and OH because the direct yield of H is only 0.6.¹⁸ Use of the electron scavenger, N₂O, converts e_{aq}⁻ into OH so that its reac-



tions can be studied alone. The study of reactions of e_{aq}⁻ is more difficult because OH reactions are also present. A number of scavengers for OH exist, such as alcohols and formate, but these must be used with caution because the resultant radicals may act as electron transfer or reducing agents and yield⁴ the same radical as does e_{aq}⁻ (*cf.* reactions 4 and 5). Where a



reaction analogous to (4) occurs, use of such OH scavengers is advantageous in studies of spectra because a larger yield of the desired radical is obtained. Where no electron transfer reaction (4) occurs, the existence of a reaction analogous to eq 5 can be demonstrated by the addition of N₂O to the solution. With N₂O present the radical produced from e_{aq}⁻ should disappear (provided the rate constants and concentrations are such that N₂O can compete successfully for e_{aq}⁻). If *t*-butyl alcohol is used as the OH scavenger (eq 2), no complications are expected because $\dot{\text{C}}\text{H}_2(\text{CH}_3)_2\text{COH}$ does not seem to be capable of electron transfer.¹⁹

The discussion immediately above suggests that the radicals observed be discussed as reaction products of

(18) See, *e.g.*, the review by M. Anbar in "Fundamental Processes in Radiation Chemistry," P. Ausloos, Ed., Interscience, New York, N. Y., 1968, p 651.

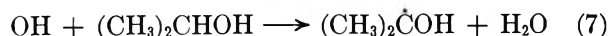
(19) G. E. Adams, B. D. Michael, and R. L. Willson, *Advan. Chem. Ser.*, **81**, 289 (1968).

the three primary radicals or of electron transfer from reducing agents such as alcohol radicals or $\dot{\text{C}}\text{O}_2^-$. This approach will be followed as much as is practical.

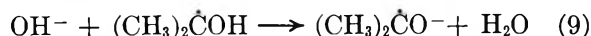
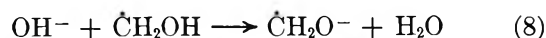
Such a classification of the reactions is also convenient for a comparison of radiolytic generation of radicals with other production methods which have been used in esr experiments. In this sense only the H-atom and e_{aq}^- reactions are unique to radiation chemistry. Reactions of an agent which is most likely OH radical have been studied by esr spectroscopy in flow systems of Ti^{3+} and H_2O_2 ²⁰⁻²² and in photolytic systems containing H_2O_2 .²³ The Ti^{3+} - H_2O_2 system is mechanistically rather complex,²² but at the level of the work here only a few detail differences in reaction paths have been seen for radiolytically produced OH radical as compared with these other sources. Because of the greater radical concentrations available using these other methods of generation, the spectroscopic study of radicals produced from OH is best done by these other techniques in the pH regions available to them. Production of OH by radiolytic means does have the advantage that the strongly alkaline region $\text{pH} > 10$ can be investigated and that no changes in the nature of the chemical agents occur as pH is varied (*cf.* Ti^{3+} in acid and as complexed for $\text{pH} 2-10$ ²⁴⁻²⁶). Electron transfer reactions have been studied by esr spectroscopy in work with Ti^{3+} - H_2O_2 ^{27,28} so that again the radiolytic work is not unique. However, the full pH range is available in the radiolytic work. The major advantages of the use of radiolytic generation (in aqueous systems) of radicals, then, are a mechanistically well-understood initial generation of radicals, the possibility of studying the reactions of e_{aq}^- and H atoms, and the availability of the full pH range with no other changes in conditions.

OH Reactions. Reactions of OH radical will be discussed first because they are the easiest to study without interference from those of the other primary radicals. Both reaction by hydrogen atom abstraction and by addition have been studied. The radicals resulting from abstraction have been observed in the cases of methyl and isopropyl alcohols and several organic acids. A number of these substances and the resultant radicals have been studied by esr spectroscopy using other techniques for OH production. However, it is important to establish that the reactions are the same in all cases. Furthermore, because these radicals are to be expected in studies of other reactions (*e.g.*, $\dot{\text{C}}\text{H}_2\text{CO}_2^-$ from $e_{\text{aq}}^- + \text{H}_2\text{NCH}_2\text{CO}_2^-$), it is important to have accurate spectral parameters. In fact, much of the data from these other studies pertains to other conditions such as nonaqueous solution or strong acid where a different degree of dissociation is expected.²⁹

The reactions with methyl and isopropyl alcohols can be used as an initial illustration of the practicality of studying radiolytically generated radicals in aqueous solutions. In neutral and acid solutions these reactions are expected to be



while in strong base ($\text{pH} \sim 12$) the resulting radicals can dissociate



The pK values reported by Asmus, *et al.*,³⁰ are respectively, 10.7 and 11.6. The results of experiments with N_2O -saturated neutral and basic solutions of the alcohols are shown in Figures 3 and 4. A significant decrease in hyperfine constant and increase of g factor upon dissociation are evident from the figures in both cases. Hyperfine constants for these spectra are given in Table I. The spectra in neutral solution are like those found by Zeldes and Livingston³¹ for aqueous solution and exhibit a splitting by the hydroxyl proton. As the pH is raised, exchange of the OH proton occurs causing first broadening of the doublets corresponding to this splitting and then narrowing to a single line. At still higher pH values where appreciable concentrations of both undissociated and dissociated forms are present the spectrum represents a weighted average over these forms because of the rapid dynamics of the equilibrium. The dynamics are not quite rapid enough, however, to maintain narrow lines for the outer lines (*i.e.*, those which move the most upon dissociation). The broadening does not prevent determination of the positions of at least some of the lines at all pH values. A detailed study of the variation of hyperfine splitting with pH and of the kinetics of the exchange in basic solu-

(20) W. T. Dixon and R. O. C. Norman, *J. Chem. Soc.*, 3119 (1963).

(21) A number of other references can be found in the review by R. O. C. Norman and B. C. Gilbert in "Advances in Physical Organic Chemistry," Vol. 5, V. Gold, Ed., Academic Press, New York, N. Y., 1967, p 53.

(22) R. O. C. Norman and P. R. West, *J. Chem. Soc. B*, 389 (1969).

(23) (a) R. Livingston and H. Zeldes, *J. Chem. Phys.*, **44**, 1245 (1966); this paper describes the technique. Other papers dealing specifically with aqueous solutions are (b) R. Livingston and H. Zeldes, *J. Amer. Chem. Soc.*, **88**, 4333 (1966); (c) R. Livingston and H. Zeldes, *J. Chem. Phys.*, **47**, 4173 (1967); (d) R. Livingston and H. Zeldes, *J. Magnetic Resonance*, **1**, 169 (1969).

(24) R. O. C. Norman and R. J. Pritchett, *J. Chem. Soc. B*, 378 (1967).

(25) R. Poupko, B. L. Silver, and A. Lowenstein, *Chem. Commun.*, 453 (1968).

(26) M. McMillan and R. O. C. Norman, *J. Chem. Soc. B*, 590 (1968).

(27) A. L. Buley and R. O. C. Norman, *Proc. Chem. Soc.*, 225 (1964).

(28) A. L. J. Beckwith and R. O. C. Norman, *J. Chem. Soc. B*, 400 (1969).

(29) For example, although the radical $\dot{\text{C}}\text{H}_2\text{COOH}$ from acetic acid had been reported several times, it was not until the present work that the spectral parameters for the form CH_2CO_2^- were determined (see also ref 7). Also, much of the early work using Ti^{3+} - H_2O_2 did not give hyperfine constants to as great accuracy as is now considered desirable and did not report g factors.

(30) K.-D. Asmus, A. Henglein, A. Wigger, and G. Beck, *Ber. Bunsenges. Phys. Chem.*, **70**, 756 (1966).

(31) H. Zeldes and R. Livingston, *J. Chem. Phys.*, **45**, 1946 (1966).

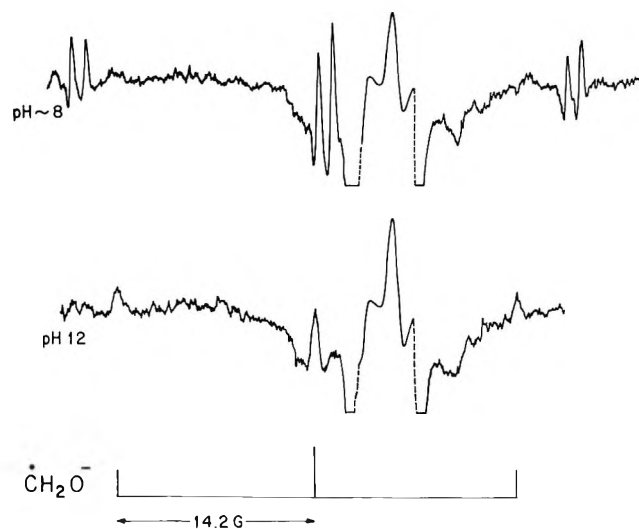


Figure 3. Second-derivative esr spectra of N_2O saturated 0.1 M methanol solution at two pH values taken during irradiation with 2.8-MeV electrons. Magnetic field increases to the right. A portion of the spectrum to the right of the center is recorded at $\sim 100\times$ less gain and shows the signal from the silica cell. A stick spectrum of the basic form, $\dot{C}H_2O^-$, is shown for reference.

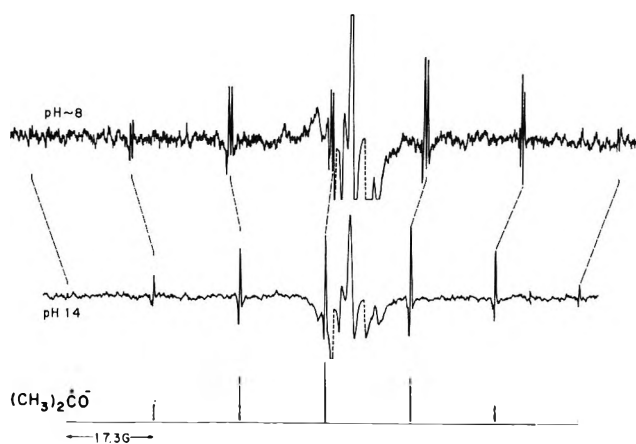


Figure 4. ESR spectrum of an N_2O -saturated 0.1 M solution of isopropyl alcohol at two pH values.

tions of the OH proton is under way.³² In the most basic solutions the lines for each radical all become of the same width. For the radical $(CH_3)_2\dot{C}O^-$ this width is small (~ 0.1 G) and second-order splittings can readily be resolved (Figure 3). For $\dot{C}H_2O^-$ the line width is greater (~ 0.4 G) for some reason not yet understood.³³ The signal-to-noise ratio of these spectra is adequate and demonstrates the practicality of studying radicals with recombination rate constants of $\sim 10^9 M^{-1} \text{sec}^{-1}$.

The absence of lines from the radical $\dot{C}H_2(CH_3)CHOH$ in the experiments with isopropyl alcohol deserves some comment because this radical is relatively prominent in flow experiments with Fe^{2+} ³⁴ or Ti^{3+} ²⁰ and H_2O_2 . Several discussions of the variable ratio of

Table I: Radicals Produced by OH^a (H-Atom Abstraction)

Radical ^b	a_{α}^H	a_{β}^H	a_{OH}^H	a^{Cl}	g
$\dot{C}H_2OH^c$	17.56		1.01		2.00329
$\dot{C}H_2O^-$	14.34				2.00367
$(CH_3)_2\dot{C}OH^c$		19.90	0.48		2.00315
$(CH_3)_2\dot{C}O^-$		17.31			2.00335
$\dot{C}H_2COO^-$	21.20				2.00323
$\dot{C}H(COO^-)_2$	19.95 ^d				2.00341
$-O\dot{C}HCOO^-$	14.17				2.00435
$\dot{C}HCICOO^-$	20.48			3.36 ^e	2.00640

^a Hyperfine constants in gauss, accurate to about ± 0.03 G. Values of g factor accurate to about ± 0.00003 . ^b Radical formed at pH ~ 11 – 12 . ^c Parameters reported previously by Zeldes and Livingston³¹ for aqueous solution are: $\dot{C}H_2OH$, $a_{\alpha} = 17.52$, $g = 2.00335$; $(CH_3)_2\dot{C}OH$, $a_{\beta} = 19.96$, $g = 2.00313$. ^d Splitting for $\dot{C}H(COOH)_2$ at pH 0.9 is 20.44 G. ^e Value for ^{36}Cl ; for ^{37}Cl it is 2.79. The ratio is 0.830 and can be compared with the expected ratio of 0.832.

$\dot{C}H_2(CH_3)CHOH$ to $(CH_3)_2\dot{C}OH$ have been published.^{22,35,36} Because the radiolysis of aqueous solutions of low concentrations of solutes (0.1 M) is very well understood, it is clear that the results reported here should be describable by a mechanism involving only the production of the two abstraction product radicals and their bimolecular recombination. The ratio of production of the two radicals has been found³⁷ to be about 6:1 in favor of $(CH_3)_2\dot{C}OH$. If it is assumed that the recombination reactions all have about the same rate constants (a large departure from this condition seems very unlikely), then our experiments should show a 6:1 ratio of radical concentrations. Such a concentration for $\dot{C}H_2(CH_3)CHOH$ would put its lines at about the noise level in Figure 4 so no inconsistency is present. The spectrum found by Livingston and Zeldes^{23b} for H_2O_2 in 75% isopropyl alcohol and 25% water shows about the expected ratio for the two radicals although experiments in the pure alcohol^{23a} do not seem to show the weaker set of lines. On the basis of these observations we must conclude that while the photolysis of H_2O_2 produces an active species (OH) which behaves in a fashion similar to or identical with radiolytically produced OH, some complications are present in the metal ion systems. At this time an explanation such as that advanced by Norman and West²² and involving for the two types of radicals differing reaction rates with metal ions and H_2O_2 seems

(32) G. P. Laroff and R. W. Fessenden, to be published.

(33) It should be noted that radicals with a small moment of inertia about at least one axis show anomalously broad lines. Examples in addition to $\dot{C}H_2O^-$ are CH_3 and perhaps CH_3CH_2 (ref 3), and $\dot{C}H_2CN$ (ref 23d).

(34) T. Shiga, *J. Phys. Chem.*, **69**, 3805 (1965).

(35) R. E. James and F. Sciglio, *ibid.*, **74**, 1166 (1970).

(36) C. E. Burchill, *ibid.*, **75**, 167 (1971).

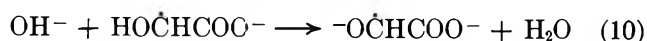
(37) C. E. Burchill and I. S. Ginns, *Can. J. Chem.*, **48**, 1232 (1970).

more reasonable than an active species which is not free $O\dot{H}$.

Other compounds studied which give the expected abstraction product when studied in basic N_2O -saturated solution are acetate, chloroacetate, malonate, and glycolate ($HOCH_2COO^-$) ions. The radicals found are $\dot{C}H_2COO^-$, $\dot{C}HClCOO^-$, $\dot{C}H(COO^-)_2$, and $-O\dot{C}HCOO^-$, respectively. Spectral parameters for these radicals are given in Table I. Because Fischer, *et al.*,³⁸ have found a small change in the α -proton splitting and a large one in the β splitting of the radical $HOOC\dot{C}H-CH_2COOH$ as the carboxyl protons dissociate, it is to be expected that other radicals containing carboxyl groups will also show this trend. Fortunately Fischer, *et al.*,³⁶ have also found only a moderate change in the acid pK values in going to the radical so that there is some hope of estimating whether a particular radical from earlier studies is dissociated or not. Our parameters for $\dot{C}H_2COO^-$ should be compared, therefore, with those of Beckwith and Norman²⁸ who worked near neutral pH. It is not clear why their values of $a = 21.6$ G and $g = 2.0033$ are not closer to those found here. The splitting in acid solutions for (presumably) $\dot{C}H_2COOH$ is reported to be 21.8³⁹ and 21.7 G.⁴⁰

Chloroacetate was studied because of the desire to illustrate by esr the well-known reactions of this compound with the three primary radicals. The spectra found in acid and basic solutions of chloroacetate are shown in Figure 5. The abstraction product $\dot{C}HClCOO^-$ (or $\dot{C}HClCOOH$) is evident in both pH regions. The hyperfine constants for $\dot{C}HClCOO^-$ are given in Table I; no values were determined for the acid form because of low signal-to-noise ratio. The parameters reported by Dixon, *et al.*,³⁹ for $\dot{C}HClCOOH$ ($a^H = 20.9$ G, $a^{Cl} = 3.8$ G) are rather similar to those found here. The high g factor is a result of spin density upon the chlorine. Malonate was studied to establish the spectral parameters of the dissociated form of the radical for comparison with radicals obtained in other reactions. Because Dixon, *et al.*,³⁹ found $\dot{C}H_2COOH$ to be the reaction product of malonic acid in acid solution, an experiment was done at pH 0.9 in addition to that at pH 12. Interestingly the radical found here at both pH values is that obtained directly by hydrogen abstraction. This is the most striking instance we have found of a difference in reaction product between the two methods of radical generation.

Glycolate was of particular interest because of the dissociation of the alcohol proton as shown by pulse radiolysis⁴¹ and also because the same radical can be



formed by electron addition to glyoxylate ion. This

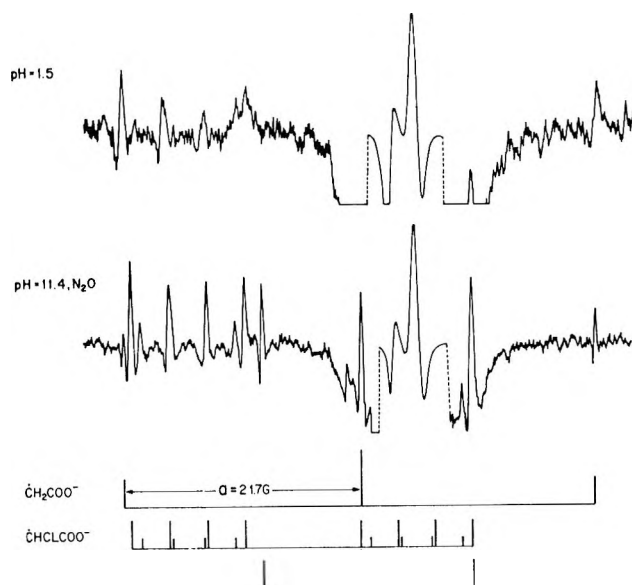
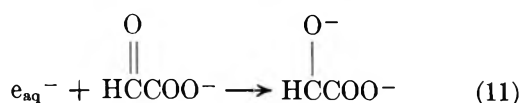


Figure 5. ESR spectra of 10^{-2} M chloroacetic acid at pH 1.5 and of 10^{-2} M chloroacetate saturated with N_2O at pH 11.4. The stick spectra represent the analysis of the pH 11.4 spectrum. The pair of lines in the bottom stick spectrum are from an unknown species.

latter compound also is of importance in studying the reactions of oxalate as discussed below. The pK for reaction 10 is ~ 9 ⁴¹ and in accord with this value no change in the hyperfine splitting (14.17 G) for $-O\dot{C}HCOO^-$ was found over the pH range from 10 to 13. No spectrum was taken in neutral solution, but the α -proton splitting reported for acid conditions is 17.8 G.³⁹ The splitting of 14 G must, therefore, represent that of the doubly dissociated form and has no significant contribution from the form $HO\dot{C}HCOO^-$. The change from 17.8 G in $HO\dot{C}HCOOH$ to the 14.2 G found here parallels the drop of 2.7 G in going from CH_2OH to CH_2O^- and is probably caused mainly by the dissociation of the alcoholic proton.

The lines of $-O\dot{C}HCOO^-$ are very intense because of the slower recombination for this doubly charged radical. (The pulse radiolysis work by Simic, *et al.*,⁴¹ has shown the recombination rate constant to be $1.5 \times 10^7 M^{-1} sec^{-1}$.) As a result sufficient intensity is present to allow a search for lines from ^{13}C -containing radicals and indeed two sets of lines with proper intensity and described by the same a_α and g factor were found with, respectively, $a^C = 6.90$ and 13.56 G. (See Figure 11 for the same radical from electron addition to glyoxylic acid.) No lines of comparable width and corresponding to values of a^C up to 300 G could be found.

(38) H. Fischer, K.-H. Hellwege, and M. Lehnig, *Ber. Bunsenges. Phys. Chem.*, **72**, 1166 (1968).

(39) W. T. Dixon, R. O. C. Norman, and A. L. Buley, *J. Chem. Soc.*, 3625 (1964).

(40) H. Taniguchi, K. Fukui, S. Ohnishi, H. Hatano, H. Hasegawa, and T. Maruyama, *J. Phys. Chem.*, **72**, 1926 (1968).

(41) M. Simic, P. Neta, and E. Hayon, *ibid.*, **73**, 4214 (1969).

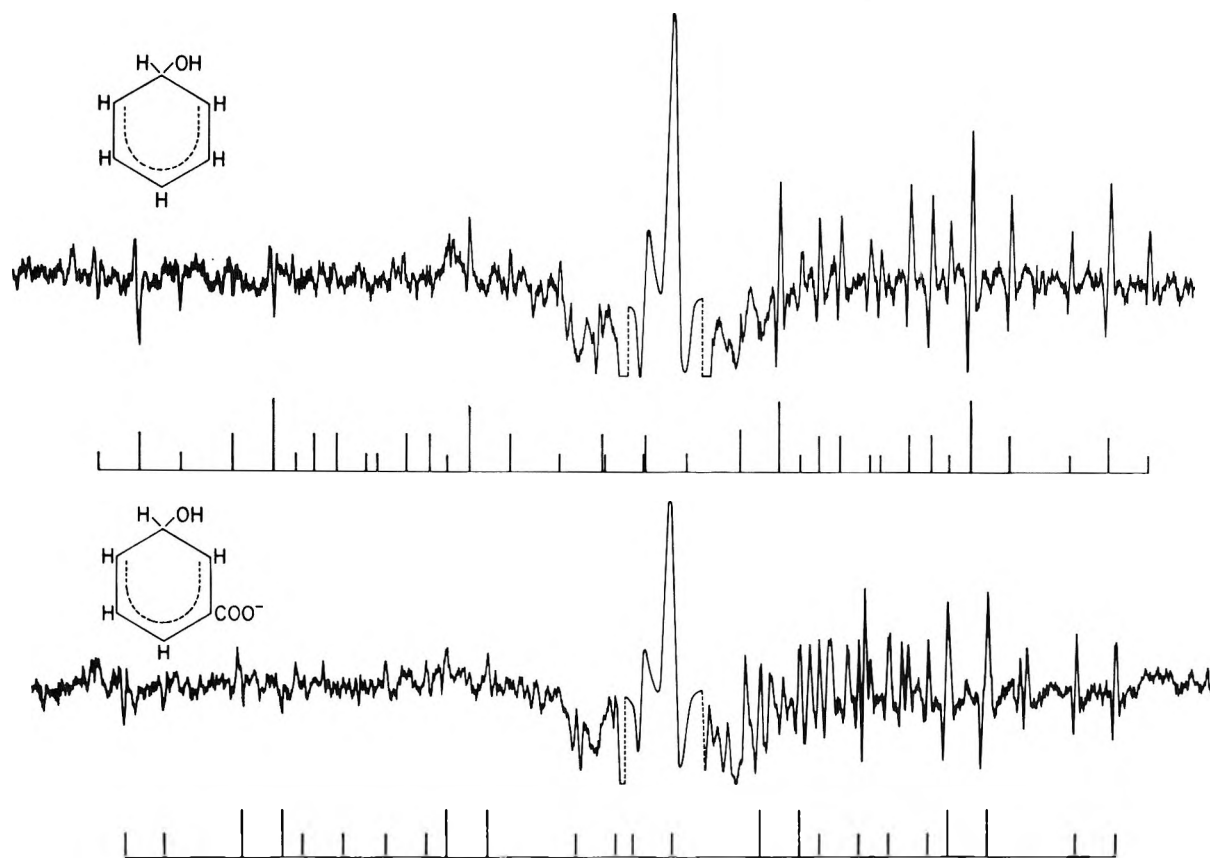
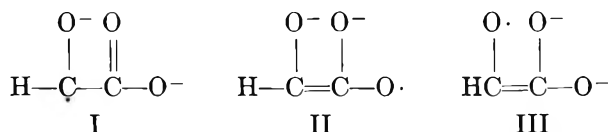


Figure 6. ESR spectra obtained from N_2O -saturated solutions of benzene (saturated, $\sim 10^{-2} M$) and $5 \times 10^{-3} M$ benzoate at about pH 12. Stick spectra are shown for the indicated species. (Only the meta radical is shown in the lower although the other two isomers are present.) Note the large intensity differences between high- and low-field lines and the suggestion of emission lines at several points.

Either of the observed values would be reasonable for the carboxylate carbon (β position), but a larger splitting (~ 35 G) would be expected for the α - or radical carbon. Because similar values have been found in related radicals,³² we reject the suggestion that these lines do not come from the ^{13}C -containing radicals. It must be that the proper electronic description of this radical involves a greater than expected (by us) contribution from all of the structures with the electron located on an oxygen. Structures like II reduce the π -spin density on the α -carbon, and depending on the sign magnitude



of Q_{oc}^C from the theory of Karplus and Fraenkel⁴² structure III could produce a significant negative contribution to the splitting of the α -carbon and partly cancel the main positive contribution from structure I.

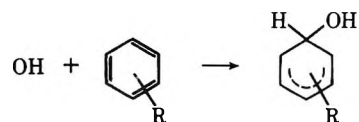
A number of addition reactions of OH radical have been observed by ESR spectroscopy in flow systems. Several authors have reported addition to unsaturated compounds^{20,43-45} and Dixon and Norman⁴⁶ have studied addition to substituted benzenes to form hy-

droxycyclohexadienyl radicals. Previous radiolytic work⁴ demonstrated OH addition to the basic form of



nitromethane. In the work covered here OH addition to benzene and benzoate ion have been studied as well as the addition reaction to nitrosobenzene and the displacement reaction with *p*-nitrophenol to form *p*-benzosemiquinone ion radical.

The spectra of the hydroxycyclohexadienyl radicals from benzene and benzoate ion are shown in Figures 6 and 7. These both show a strong intensity anomaly



and the lines at the lowest fields are inverted. The

(42) M. Karplus and G. K. Fraenkel, *J. Chem. Phys.*, **35**, 1312 (1961).

(43) H. Fischer, *Z. Naturforsch. A*, **19**, 866 (1964).

(44) W. E. Griffiths, G. F. Longster, J. Myatt, and P. F. Todd, *J. Chem. Soc. B*, 530 (1967).

(45) A review of OH addition to vinyl monomers has been published: K. Takakura and B. Ranby, *Advan. Chem. Ser.*, **91**, 125 (1969).

(46) W. T. Dixon and R. O. C. Norman, *J. Chem. Soc.*, 4857 (1968).

Table II: Cyclohexadienyl Radicals^a

Radical (system)	Hyperfine constant ^b				<i>g</i>
	>CHX	Ortho	Meta	Para	
C ₆ H ₇ (aqueous)	48.08	9.06	2.69	13.15	2.00268
C ₆ H ₇ (hydrocarbon) ^c	47.71	8.99	2.65	13.04	(2.0025)
C ₆ H ₆ OH (basic) ^d	34.34	8.92	2.74	13.05	2.00227
C ₆ H ₆ OH (acid)	<i>e</i>	8.85	2.76	13.09	<i>e</i>
<i>O</i> -OOCC ₆ H ₅ OH (basic)	34.71	8.35	2.59, 2.78	12.53	<i>e</i>
<i>M</i> -OOCC ₆ H ₅ OH (basic)	<i>e</i>	8.85, 9.03	2.74	13.08	2.00224
<i>P</i> -OOCC ₆ H ₅ OH (basic)	<i>e</i>	8.29	2.60	...	<i>e</i>

^a Positions labeled with respect to the methylene group >CHX where X is H or OH. ^b In gauss, estimated accuracy ± 0.03 G. ^c Reference 3. ^d Somewhat different parameters were reported by Dixon and Norman.⁴⁶ ^e Because of intensity differences of high- and low-field lines only the high-field lines could be measured; consequently no >CHOH splitting could be obtained, and no *g* factor determined.

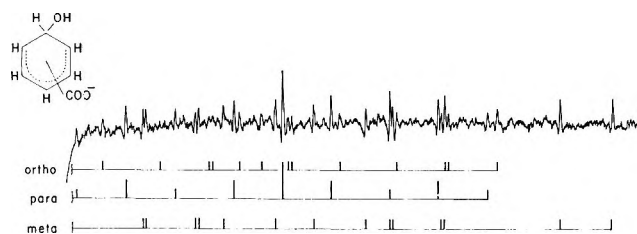


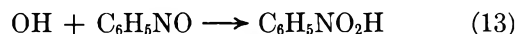
Figure 7. High-field side of the spectrum obtained under high resolution with an N₂O-saturated, 10⁻² M benzoate solution. Present are lines from the three possible isomers.

spectra were analyzed on the basis of the high-field portions of the spectra, and only those lines on the low-field side were measured which were necessary to provide the *g* factor and splitting by the methylene (>CHOH) proton. Figure 7 shows a portion of the high-field half of the spectrum obtained with benzoate ion. The spectra of the three isomers resulting from addition at ortho, meta, and para positions can be seen. The lines from these radicals include essentially all of those visible, and no intense line is unaccounted for. The hyperfine constants are given in Table II. Most striking is the close agreement of the ring proton splittings between the various isomers and with the unsubstituted radical. The meta adduct shows little decrease in spin density over the unsubstituted one because the carboxyl group is at a position of low spin density. In the other two isomers the splittings at para and ortho positions drop by about 4-7% presumably because spin density has been removed to the carboxylate group. The value of the >CHOH splitting of hydroxycyclohexadienyl radical is smaller by 1.5 G than that reported by Dixon and Norman.⁴⁶ This cannot be caused by a dissociation of the OH proton because an identical spectrum was obtained in acid solution. The only other obvious reason for the difference (aside from an error in field scan calibration by them) is that the radical in the Ti³⁺-H₂O₂ experiment is somehow associated with titanium.

The relative rates of OH addition at the three posi-

tions cannot be accurately determined from the results of Figures 6 and 7 without information on the radical lifetimes. A first approximation is to take the line width to be the same for all radicals because no large differences are evident and to say the disappearance rates are the same. Certainly in the mixed system no great differences can exist. Under these assumptions it is concluded that the meta and para adducts are produced at the same rate and the ortho at about half this rate *per position on the ring*. The lower rate in the ortho position may be related to steric factors. The individual identification of the three adduct radicals illustrates in an excellent fashion the usefulness of esr spectroscopy in systems containing closely related radicals.

Asmus, *et al.*,⁴⁷ have studied the reactions of nitrosobenzene. Their results show that this compound reacts with OH by



The latter reaction occurs in basic solution because the *pK* of C₆H₅NO₂H is 4.5.⁴⁸ The spectrum observed when an N₂O-saturated solution of 5 × 10⁻⁴ M nitrosobenzene is irradiated is shown in Figure 8. This spectrum can be totally ascribed to the radical anion C₆H₅NO⁻. This radical has a *pK* of 11.7⁴⁸ and in the dissociated form is known to display the effects of hindered rotation about the C-N bond.^{49,50} The hyperfine splittings determined from the spectrum of Figure 8 are given in Table III and are in accord with those obtained by Russell, *et al.*,⁵⁰ in ethanol solution. To explain the formation of C₆H₅NO⁻ it is necessary to say

(47) K.-D. Asmus, G. Beck, A. Henglein, and A. Wigger, *Ber. Bunsenges. Phys. Chem.*, **70**, 869 (1966).

(48) K.-D. Asmus, A. Wigger, and A. Henglein, *ibid.*, **70**, 862 (1966).

(49) E. J. Geels, R. Konaka, and G. A. Russell, *Chem. Commun.*, **13** (1965).

(50) G. A. Russell, E. J. Geels, F. J. Smentowski, K.-Y. Chang, J. Reynolds, and G. Kaupp, *J. Amer. Chem. Soc.*, **89**, 3821 (1967).

Table III: Radicals from CH_3NO_2 in Acid Solutions^{a,b}

System	Proposed radical	a^{N}	a^{H}	g
$\text{CH}_3\text{NO}_2 + \text{C}_2\text{H}_5\text{OH}$	$\text{CH}_3\dot{\text{N}}\text{O}_2\text{CHOHCH}_3$	28.09	10.19	2.00507
$\text{CH}_3\text{NO}_2 + n\text{-C}_7\text{H}_7\text{OH}$	$\text{CH}_3\dot{\text{N}}\text{O}_2\text{CHOHC}_2\text{H}_6$	28.22	10.19	2.00506
$\text{CH}_3\text{NO}_2 + \text{C}_2\text{H}_5\text{OC}_2\text{H}_5$	$\text{CH}_3\dot{\text{N}}\text{O}_2\text{CH}(\text{CH}_3)\text{OC}_2\text{H}_5$	28.24	9.95	2.00504
$\text{CH}_3\text{NO}_2 + (\text{CH}_3)_2\text{CHOH}$	$\begin{array}{c} \text{O} \\ \\ \text{CH}_3\text{NC}(\text{OH})(\text{CH}_3)_2 \end{array}$	16.64	13.82	2.00545

^a Hyperfine constants in gauss, accurate to about ± 0.03 G. Values of g factor accurate to about ± 0.00003 . ^b These radicals have also been reported by McMillan and Norman.²⁶

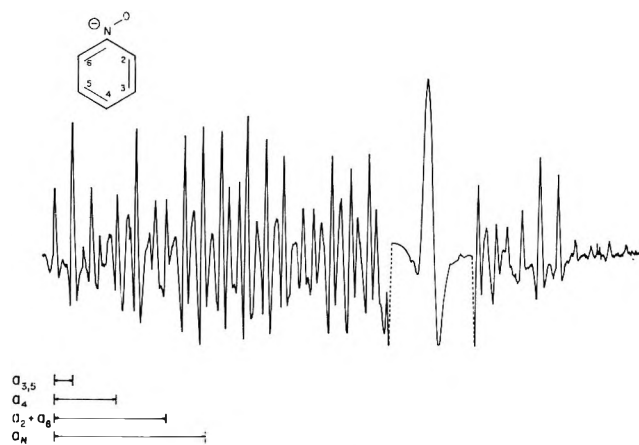
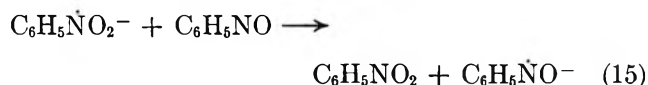


Figure 8. ESR spectrum of $\text{C}_6\text{H}_5\text{NO}^-$ obtained in an N_2O -saturated, 10^{-3} M solution of $\text{C}_6\text{H}_5\text{NO}$ at pH 12.4.

that reactions 13 and 14 are followed by the electron transfer



If this reaction has a rate constant of $>10^7 \text{ M}^{-1} \text{ sec}^{-1}$ (which is very possible), no spectrum of $\text{C}_6\text{H}_5\dot{\text{N}}\text{O}_2^-$ would be expected. Unfortunately in this case we cannot test the proposed mechanism directly by observing the initial intermediate.

A number of experiments with other aromatics have been tried, but in most cases the spectra are complex, consisting of several overlapping spectra, and no assignments have been made. The case of *p*-nitrophenol is an exception. Over the pH range 7–12 this compound (in the form $\text{O}_2\text{NC}_6\text{H}_4\text{O}^-$, $pK = 7.15$ ⁵¹) reacts with OH to form *p*-benzosemiquinone radical ion⁵² ($a = 2.35$ G, $g = 2.00453$) by the net reaction



The spectrum obtained at pH 12 is shown in Figure 9 and the great signal intensity, a result of the long radical lifetime, is apparent. A crude estimate of the radical concentration responsible for the signal of Figure 9 gives 2×10^{-6} M. Because the total OH



Figure 9. ESR spectrum of *p*-benzosemiquinone radical ion obtained from an N_2O -saturated solution of 10^{-3} M *p*-nitrophenol at pH 11.8.

radical production during one pass of the solution through the beam is $\sim 3 \times 10^{-4}$ M, the production of *p*-benzosemiquinone radical ion must represent at least approximately 10% of the product of reaction. It is not possible to say, of course, whether this radical has some precursor such as a hydroxycyclohexadienyl radical which lives of the order of a few microseconds. At lower pH the same lines are present but at lower intensity. It is likely that under these conditions increased protonation leads to a more rapid decay of the *p*-benzosemiquinone ion.^{53,54} Suarez, *et al.*,⁵⁵ have discussed some chemical results related to this reaction.

(51) "Handbook of Chemistry and Physics," Chemical Rubber Co., Cleveland, Ohio, 1966–1967, p D-86.

(52) The parameters found by K. Scheffler and H. B. Stegman [*Ber. Bunsenges. Phys. Chem.*, **67**, 864 (1963)] for alkaline alcohol solution are $a = 2.35$ G and $g = 2.00466$.

(53) I. Yamazaki and L. H. Piette, *J. Amer. Chem. Soc.*, **87**, 986 (1965).

(54) G. E. Adams and B. D. Michael, *Trans. Faraday Soc.*, **63**, 1171 (1967).

H-Atom Reactions. The reactions of hydrogen atoms are evident through the observation of product radicals and also through the decrease in intensity of the H-atom esr lines when solute is added to the solution. In several cases this decrease has been used to show that reaction with solute is occurring. In the present work only with oxalic acid and benzene have the product radicals been studied directly. Further work⁵⁶ is in progress to put this decrease in intensity on a quantitative basis for measuring H-atom reaction rates.

The distinctive spectrum (a 500-G doublet) of the hydrogen atom is observed during irradiation of perchloric acid solutions (Figure 10). The low-field line is inverted as was found in experiments on liquid methane.³ In initial experiments two components of the low-field line were present as is shown in Figure 10. After O₂ was bubbled through the solution, one component remained. On the high-field side a remanent line is also present, but here its position is the same as that of the component removed by O₂. The parameters are for the reactive species $a = 503.2$ G, $g = 2.00210$ and for the other $a = 503.5$ G, $g = 2.00218$. Although the amplitudes of the high- and low-field lines are comparable for both spectra, the low-field lines have somewhat greater peak heights and may in fact have greater area. From the lack of an effect of O₂ on the second pair of lines (the same effect is obtained with isopropyl alcohol) it is evident that the remanent lines are from H atoms in the silica cell. Subsequent experiments with a new cell have shown essentially no signal from the cell. It is interesting that both low-field lines are essentially of the same inverted sense.

A detailed description of the behavior of the hydrogen atom signals is not yet possible. The height of the lines from the solution with no reactive solute is approximately proportional to the electron beam current so that the signal height is not determined only by recombination. Initial signal polarization, polarization upon reaction, and subsequent relaxation may all affect the signal size. Nevertheless, it appears that it is possible to use the decrease in signal height upon addition of solute to measure the rate of reaction with that solute relative to the unknown competing process. Calibration of the competing process can be made with a solute having a known rate constant for reaction with hydrogen atoms. Preliminary experiments showed that $\sim 5 \times 10^{-4}$ M isopropyl alcohol decreased the signals by about 75%. The rate constant of $\sim 5 \times 10^7$ M⁻¹ sec⁻¹⁵⁷ allows the half-time for decay of the hydrogen atom signals in the absence of solute to be determined. The time so determined is ~ 85 μ sec. Once the decay of the signal has been calibrated in this way other compounds can be studied and their rates of reaction determined. A study of the rates H-atom reactions with a number of compounds is under way.⁵⁶

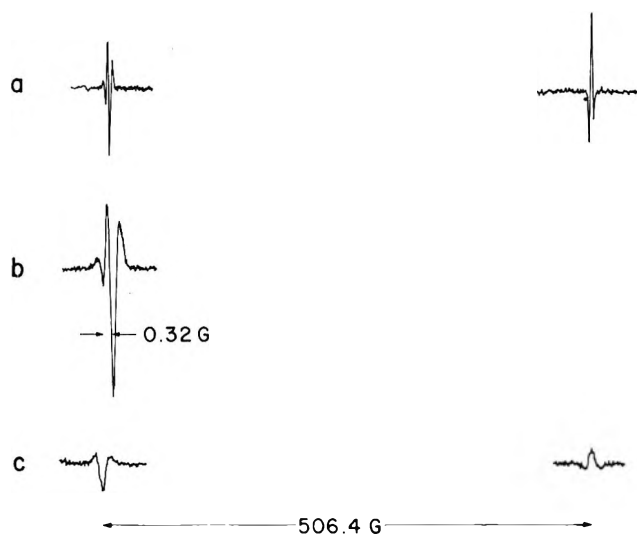


Figure 10. ESR lines of H atoms in an experiment with perchloric acid (pH 1.6) solution (a). Note the inverted sense of the low-field lines. At (b) is given further resolution of the low-field line. No resolution of the high-field line was possible. In (c) are shown the lines present when 0.1 M isopropyl alcohol is added. The 506.4-G spacing is not exactly the hyperfine constant because of higher-order effects.

The reaction of H atoms with aromatics is very fast,⁵⁷ and the product with benzene is expected to be cyclohexadienyl radical. An experiment at pH 2 with a benzene-saturated solution showed signals from both unsubstituted and hydroxycyclohexadienyl radicals formed, respectively, by addition of H and OH to benzene. These spectra were much like those shown in Figures 6 and 7 for basic solution but were weaker. None of the low-field lines of the hydroxycyclohexadienyl radical spectrum could be seen but the ring proton splittings and the displacement of the center of the high-field group had values identical with those in the spectrum of Figure 6 so there is little doubt that the OH is undisassociated at pH 12. One of the stronger low-field lines of the cyclohexadienyl radical could be seen so that it was possible to determine all of the coupling constants. The values found for aqueous solution are very similar to those for the radical in 1,4-cyclohexadiene.³ The parameters are given in Table II.

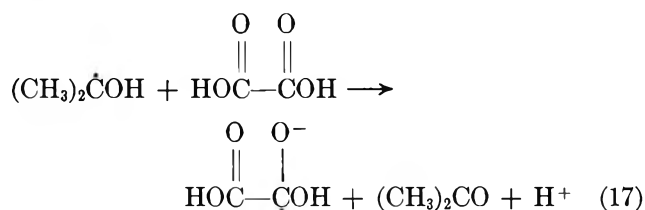
Experiments with nitromethane in acid never gave any significant signal intensity in spite of a demonstrated reaction with hydrogen atoms⁵⁶ much in excess of that expected for abstraction. It seems likely that as a result of some form of exchange of the acid proton the lines for CH₃NO₂H (the expected product) are broadened so much that they cannot be seen.

(55) C. Suarez, F. Louys, K. Günther, and K. Eiben, *Tetrahedron Lett.*, 575 (1970).

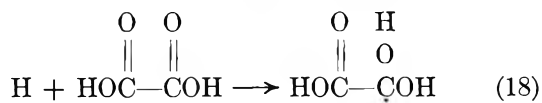
(56) P. Neta, R. W. Fessenden, and R. H. Schuler, *J. Phys. Chem.*, in press.

(57) See the values tabulated by M. Anbar and P. Neta, *Int. J. Appl. Radiat. Isotopes*, 18, 493 (1967).

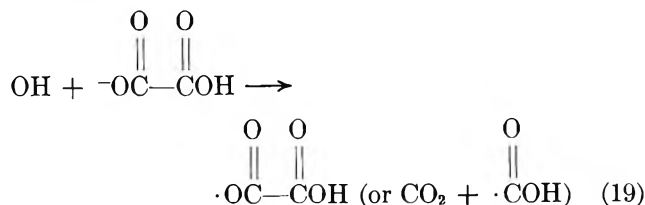
The reactions of oxalic acid in irradiated aqueous solution are complex and involve all of the primary radicals but will be discussed here because the net reaction is reduction. Many experiments on oxalic acid were performed. One of the most useful was on an acid solution of $2 \times 10^{-2} M$ oxalic acid (pH 1.4). Irradiation of the solution with no additive gave a strong single line at $g = 2.00397$ which was reduced in intensity by 70% when $2 \times 10^{-2} M$ *t*-butyl alcohol was added. When $2.6 \times 10^{-2} M$ isopropyl alcohol was added in addition, the signal intensity recovered to approximately 140% of its initial level. The reaction for the final mixture clearly involves electron transfer



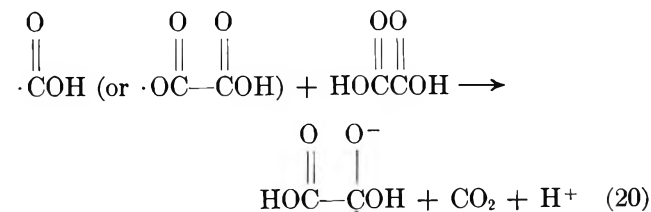
(The state of dissociation of the product radical is not necessarily as shown.) This reaction has been observed by Norman and West²² in $\text{Ti}^{3+}-\text{H}_2\text{O}_2$ systems and also in photolysis by Zeldes and Livingston⁵⁸ and by Arthur and Fessenden.⁵⁹ The g factors from these various experiments are in agreement. The ~50% decrease in the H-atom signals observed when oxalic acid is added at $2 \times 10^{-2} M$ indicates significant reaction, and the reaction giving the same radical (except for the acid dissociation) as in eq 17 seems obvious. The fact



that the signal level drops upon addition of *t*-butyl alcohol shows that OH (which the alcohol scavenges) is also producing the same final product. Because OH is an oxidizing species an intermediate step is needed. The reaction



followed by electron transfer



seems probable. Norman and West²² showed that CO_2^- or HCO_2 can reduce oxalate. Again the state of

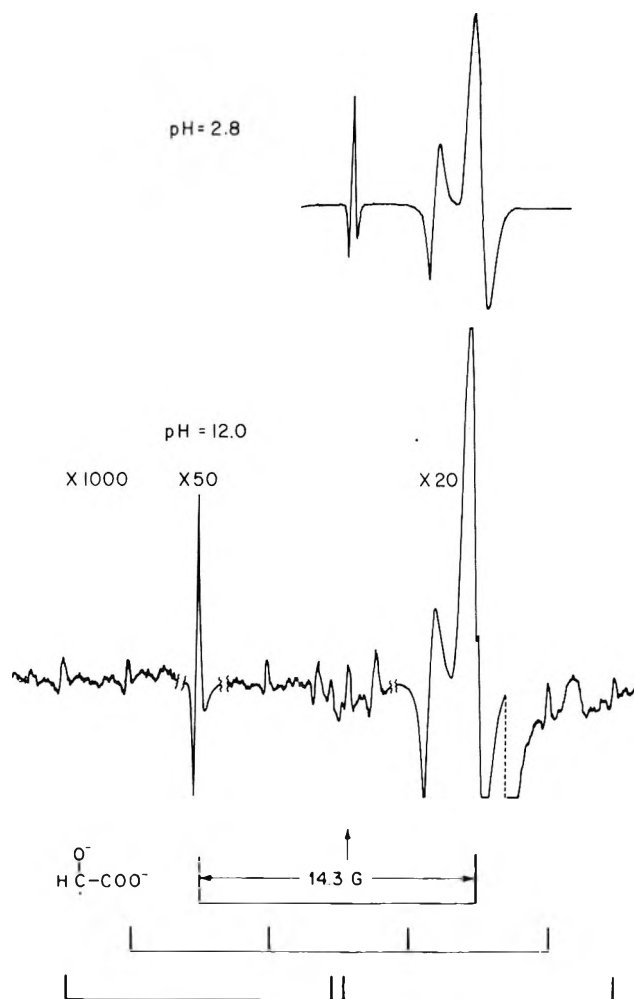
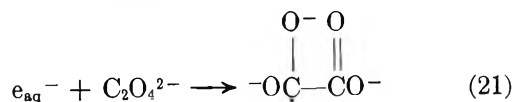


Figure 11. ESR spectra obtained in acid and basic solutions of $10^{-2} M$ glyoxylic acid (HCOCOOH). The lines from the transients approach the intensity of the line from the cell. Note the several different gain settings. The stick spectra are drawn for the indicated radical and for the two corresponding ^{13}C -containing radicals. The arrow marks the position of the line ascribed to $\text{C}_2\text{O}_4^{3-}$.

acid dissociation of the various species is not necessarily as specified. The fact that a larger signal is obtained with isopropyl alcohol than with pure oxalate shows that not all of the H and OH radicals are producing the final radical in the absence of the intermediate step forming $(\text{CH}_3)_2\dot{\text{C}}\text{OH}$.

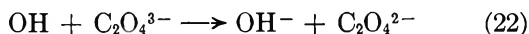
In basic solution the situation seems simpler. Only a weak signal at $g = 2.00403$ is found in $10^{-2} M$ oxalate solutions. This signal is greatly enhanced by the presence of an OH scavenger such as *t*-butyl alcohol or formate (at $10^{-2} M$); when N_2O is added to the solution along with the OH scavenger, no signal remains. The radical must be produced by



(58) H. Zeldes and R. Livingston, *J. Phys. Chem.*, **74**, 3336 (1970).

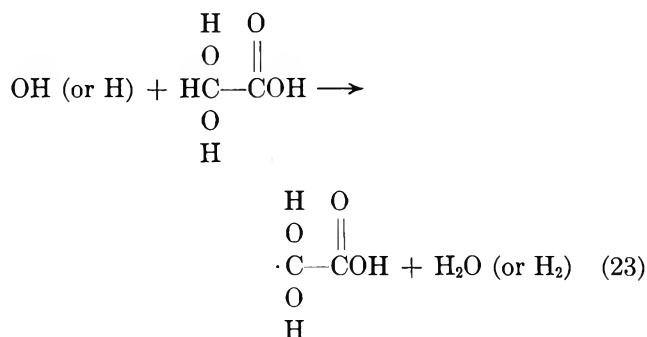
(59) N. L. Arthur and R. W. Fessenden, unpublished results.

and not by electron transfer from CO_2^- . (The photolytic experiments show that $(\text{CH}_3)_2\dot{\text{C}}\text{OH}$ reacts only with HC_2O_4^- or $\text{H}_2\text{C}_2\text{O}_4$.^{58,59}) It is not clear why an OH scavenger is necessary for efficient radical production. Possibly a reaction of OH with the radical destroys it as fast as it is formed. From the great signal



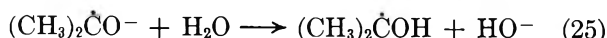
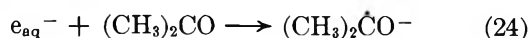
intensity possible in either acid or basic solutions it is clear that the radicals do not recombine rapidly and that the rate constant for this reaction is around 10^6 to $10^7 \text{ M}^{-1} \text{ sec}^{-1}$.

Further confirmation of the identity of the radical giving the line at $g = 2.0040$ is obtained from the observation that a line at the same position is obtained from glyoxylic acid ($\text{HC}(=\text{O})\text{COOH}$) (see Figure 11). The reaction suggested is abstraction from the aldehyde hydrate which is expected to be present in significant concentration. Because this reaction is fast and

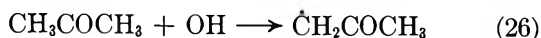


makes use of both H and OH, somewhat more intense signals of the radical are found than when oxalic acid is used. In this case a search for lines from ^{13}C -containing radicals is possible, but none were found. This same negative result was obtained by Zeldes and Livingston⁵⁸ and must be a consequence of a broadening of the lines of the ^{13}C -containing radical by end-to-end proton exchange.

Hydrated Electron Reactions. Only in the cases of acetone, glyoxylic acid, oxalate (mentioned above), and chloroacetate were efforts made to demonstrate reactions of specifically the hydrated electron. With acetone the object was to show that the esr method gives the expected result of e_{aq}^- attachment. In strongly

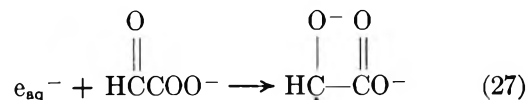


basic solutions of acetone a spectrum identical with that obtained by OH abstraction from isopropyl alcohol was found confirming reaction 24. In neutral solutions the spectrum again agreed with that from isopropyl alcohol demonstrating reaction 25. In both of these cases the OH radical reacted with acetone, but the resultant lines



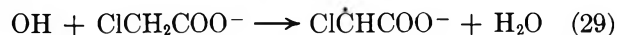
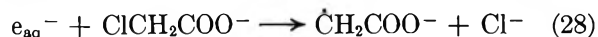
are so weak in our experiments that no hyperfine con-

stants were determined. As well as could be determined, however, these lines are consistent with the known spectrum³¹ of this radical. The other ketonic compound studied was $\text{HC}(=\text{O})\text{COO}^-$. Reaction with e_{aq}^- in this case gives the same product as obtained from glycolate by abstraction of hydrogen.



The spectrum resulting from such an experiment is shown in Figure 11.

Chloroacetate was chosen because this compound has a special place in radiation chemistry through its role in the discovery of the hydrated electron.⁶⁰ When a 10^{-2} M solution of chloroacetate was irradiated at pH 11.4, a spectrum with lines from both $\dot{\text{C}}\text{H}_2\text{COO}^-$ and $\dot{\text{C}}\text{HClCOO}^-$ was found. The parameters for the radi-



cal $\text{Cl}\dot{\text{C}}\text{HCOO}^-$ have been discussed in an earlier section. Those for $\cdot\text{CH}_2\text{COO}^-$ are identical with those found for the radical produced from acetate by OH reaction. With no scavenger for e_{aq}^- present the signals from $\dot{\text{C}}\text{H}_2\text{COO}^-$ are very strong. When the solution is saturated with N_2O , the $\dot{\text{C}}\text{H}_2\text{COO}^-$ signal intensity decreases and a spectrum like that of Figure 5 is found. Some $\dot{\text{C}}\text{H}_2\text{COO}^-$ is still present because of incomplete e_{aq}^- scavenging by N_2O . Another doublet spectrum which has not yet been identified is also present. This spectrum is not that of $-\text{O}\dot{\text{C}}\text{HCOO}^-$, $\dot{\text{C}}\text{H}(\text{COO}^-)_2$, or $-\text{OOC}\dot{\text{C}}(\text{O}^-)\text{CHOHCOO}^-$. As shown in the figure, lines from both $\dot{\text{C}}\text{H}_2\text{COOH}$ and $\dot{\text{C}}\text{HClCOOH}$ are present in acid solutions but are rather weak. Here $\dot{\text{C}}\text{H}_2\text{COOH}$ is formed by



Electron Transfer Reactions. Many of the reduction reactions of the hydrated electron can also be accomplished by alcohol radicals such as $(\text{CH}_3)_2\dot{\text{C}}\text{OH}$ or by CO_2^- . In this work most of the reduction reactions occur in both ways and emphasis was placed upon the product radical rather than the details of the reaction itself. The first example to be discussed in this section is reaction of alcohol radicals with CH_3NO_2 in acid solution. Nitromethane was studied previously in basic solution where long radical lifetimes are found, and it was of interest to compare the behavior. Nitromethane has been studied in acid by Longster, *et al.*,⁶¹ and also by McMillan and Norman²⁶ (who also worked at

(60) E. Hayon and J. Weiss, *Proc. Int. Conf. Peaceful Uses At. Energy, Geneva, 1955*, 29, 80 (1958).

(61) W. E. Griffiths, C. L. Longster, J. Myatt, and P. F. Todd, *J. Chem. Soc. B*, 533 (1967).

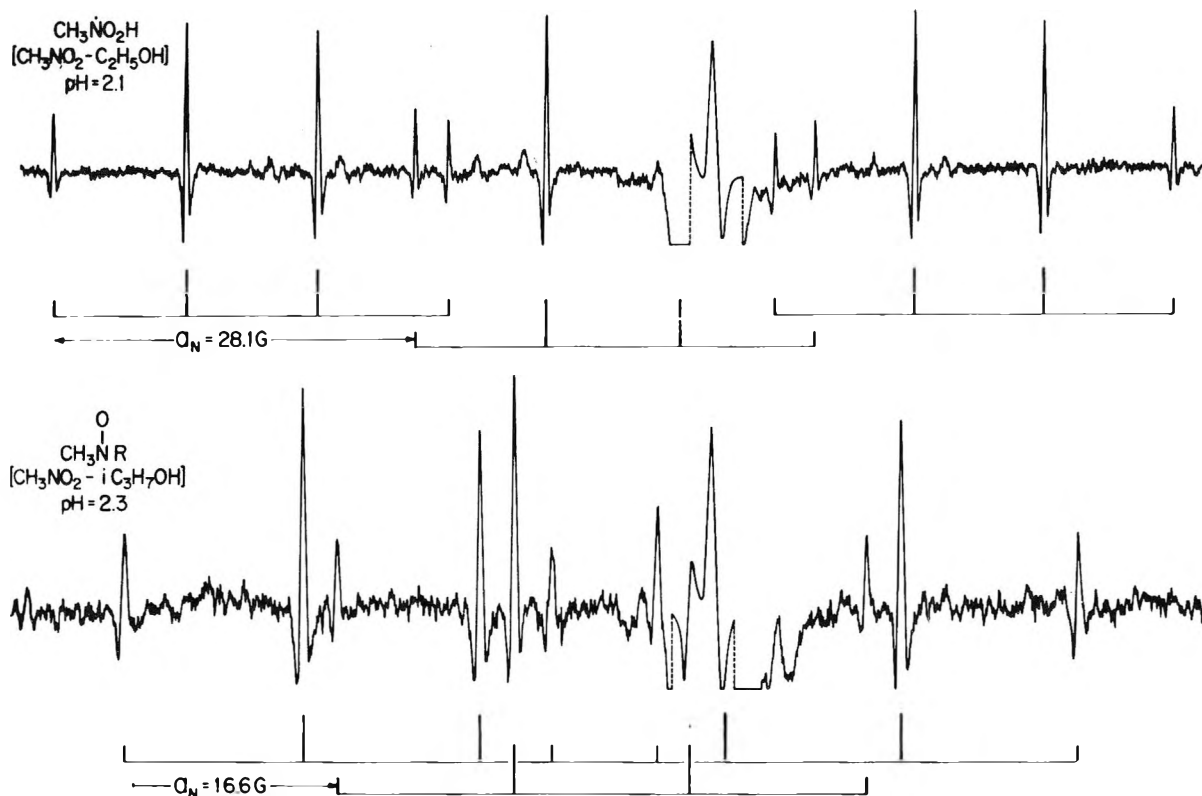


Figure 12. ESR spectra of acid solutions of $5 \times 10^{-3} M$ CH_3NO_2 containing $0.1 M$ ethyl and isopropyl alcohols.

pH 8). Much of our work on this system was performed before we became aware of the latter paper. Our results agree well with those of McMillan and Norman.

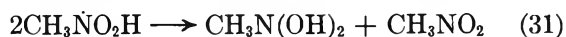
In acid solutions of nitromethane itself we have not been able to find any significant signal intensity. This result is surprising in that the studies⁵⁶ on the kinetics of H-atom disappearance suggest reaction by other than abstraction. Although other explanations for the lack of signals are possible, it is likely that the lines of $\text{CH}_3\text{NO}_2\text{H}$ (pK 4.4)⁶² are broad and unobservable at our radical concentrations—if the lines were narrow they should have been detected. No signals from other than $\dot{\text{C}}\text{H}_2\text{OH}$ were found in solutions containing $0.1 M$ methanol. In solutions of ethanol a strong spectrum (Figure 12) like what might be expected for $\text{CH}_3\dot{\text{N}}\text{O}_2\text{H}$ was found with the parameters $a^{\text{N}} = 28.09 \text{ G}$, $a^{\text{H}} = 10.19 \text{ G}$, $g = 2.00507$. McMillan and Norman found that the parameters varied with the reducing radical and therefore concluded that the species is $\text{CH}_3\dot{\text{N}}\text{O}_2\text{R}$ where R is the alcohol radical. Our results with 1-propanol and diethyl ether are given in Table III and agree with those of McMillan and Norman.²⁶ This agreement is significant and shows that the radicals in their system are not perturbed (as by complexing) by the titanium ions.

Our results also agree with theirs when isopropyl alcohol is present. Instead of a radical with $a^{\text{N}} = 28 \text{ G}$ one with $a^{\text{N}} = 16.64 \text{ G}$ is found (Figure 12).

Here the quartet splitting is 13.82 G . This radical is clearly of a different type and is most probably the radical



formed by reaction of $(\text{CH}_3)_2\dot{\text{C}}\text{OH}$ with CH_3NO produced as a product of radiolysis as suggested by Asmus,



*et al.*⁶² In this case McMillan and Norman²⁶ argue that the tertiary ester $\text{CH}_3\text{NO}_2\text{C}(\text{OH})(\text{CH}_3)_2$ is so labile that electron transfer is preferred to formation of the ester. If so, $\text{CH}_3\dot{\text{N}}\text{O}_2\text{H}$ must also be present (as also required by the proposed formation of CH_3NO) and again one is forced to conclude that $\text{CH}_3\dot{\text{N}}\text{O}_2\text{H}$ cannot be seen under these conditions.

A number of aromatic compounds can be reduced by $(\text{CH}_3)_2\dot{\text{C}}\text{OH}$ (or in base $(\text{CH}_3)_2\dot{\text{C}}\text{O}^-$). Those studied include nitrobenzene and the three nitrophenols. The spectrum of $\text{C}_6\text{H}_5\dot{\text{N}}\text{O}_2^-$ at pH 11.5 is given in Figure 13. The conditions given in the figure caption are typical. The slow decay of the radical is evident through the high steady-state concentration, and it is clear that this

(62) K.-D. Asmus, A. Henglein, and G. Beck, *Ber. Bunsenges. Phys. Chem.*, **70**, 459 (1966).

Hyperfine Constants. The main emphasis of this work has been upon the reaction mechanisms, and many of the hyperfine constants (such as those of the cyclohexadienyl radicals) have already been discussed. The radicals formed by abstraction of hydrogen from alcohols and hydroxy acids deserve some comment, however. The radicals $\dot{\text{C}}\text{H}_2\text{OH}$ and $(\text{CH}_3)_2\dot{\text{C}}\text{OH}$ are well known,^{20, 23a} but the hyperfine constants for the basic forms $\dot{\text{C}}\text{H}_2\text{O}^-$ and $(\text{CH}_3)_2\dot{\text{C}}\text{O}^-$ have not been reported although the spectrum of $\dot{\text{C}}\text{H}_2\text{O}^-$ has been published.⁶ The drop in hyperfine constant upon ionization of the OH group in $(\text{CH}_3)_2\dot{\text{C}}\text{OH}$, $\dot{\text{C}}\text{H}_2\text{OH}$, and $\dot{\text{C}}\text{HOHCOO}^-$ can be related to a drop in spin density on the α -carbon caused by more conjugation with O^- than with OH. However, the situation may be more complex in view of the tendency⁶⁷ of some of the oxy-substituted radicals to be nonplanar at the radical site. Because of the low ^{13}C splittings reported for $-\text{O}\dot{\text{C}}\text{HCO}_2^-$, it is clear that in this case the radical site is planar. The increase in g factor upon ionization of the OH group is consistent with a greater spin density upon the oxygen.

The hyperfine constants for the acid radicals $\dot{\text{C}}\text{H}_2\text{COO}^-$, $\dot{\text{C}}\text{H}(\text{COO}^-)_2$, and $\dot{\text{C}}\text{HClCOO}^-$ are little changed from the undissociated forms, consistent with the results for α_α in succinic acid.³⁸ This concern with the form of the radicals with respect to acid dissociations is one which is not particularly familiar to those concerned mainly with other than aqueous solution. It is, of course, clear that the various forms represent different chemical entities. Some examples of the effect of the exact radical form on reaction rates are the effect of a double negative charge on radical recombination⁴¹ and the absence of reaction of $(\text{CH}_3)_2\dot{\text{C}}\text{OH}$ or CO_2^- with $\text{C}_2\text{O}_4^{2-}$. Acid dissociation also affects hyperfine constants significantly, and nowhere is this better shown than in the spectra of the radicals $\text{H}_2\text{N}\dot{\text{C}}\text{HCO}_2^-$ and $\text{H}_2\text{N}\dot{\text{C}}\text{HCO}_2\text{H}$. Only the latter of these two forms shows equivalent splittings for the two NH protons.⁶⁸ It is clear that with radical production techniques now available for studies of aqueous solutions over a wide range of pH more concern with radical pK's will be necessary.

Conclusions

The results presented here clearly demonstrate the practicality of studying by esr spectroscopy the radicals produced by the reaction of the primary radicals of water radiolysis with various solutes. The intensity of

the esr signals is, of course, dependent on the rate of production of the radicals, their disappearance rate, and the characteristics of the esr spectra (line width and number of hyperfine splittings). With spectra typical of simple organic radicals and reasonably efficient production it is clearly possible to study radicals which disappear bimolecularly with rate constants $\sim 10^9$ to $10^{10} \text{ M}^{-1} \text{ sec}^{-1}$. The unique advantage of esr spectroscopy in allowing ready identification of radicals has been used to advantage in several cases. Of particular importance is the detection of the three isomeric hydroxycyclohexadienyl radicals formed by OH addition to benzoate. In such cases the esr method can stand alone and does not need information from other techniques such as pulse radiolysis with optical detection methods. In many other cases partnership with the optical studies is necessary, and the two methods greatly strengthen each other. In the case of acid nitromethane solutions, for example, no esr spectrum is observed in spite of a demonstrated reaction to form $\text{CH}_3\dot{\text{N}}\text{O}_2\text{H}$. Here the formation and decay rates are defined sufficiently that a necessary conclusion is that the esr lines must be relatively broad.

The esr signal intensity obtained with radiolytic generation of radicals is somewhat less than obtained in typical photolytic or mixing experiments with $\text{Ti}^{3+}-\text{H}_2\text{O}_2$. Thus for some spectroscopic purposes the latter methods may be preferable. However, radiolytic production has its own advantages. Of the three primary radicals from water only OH (at present) can be generated in these other ways. Furthermore the complexity of these other methods (particularly $\text{Ti}^{3+}-\text{H}_2\text{O}_2$) is such that accurate mechanistic and rate information may not always be obtainable. Also the radiolytic method can be applied over the full 0-14 pH range without the worry of the effects of other added substances (such as metal ions).

Acknowledgment. The authors wish to acknowledge some background work on the radiolysis arrangement by L. Kispert in the period between the work of ref 4 and that reported here. Thanks are also due to P. Neta for a number of helpful discussions and to both he and G. P. Laroff for help in obtaining several spectra.

(67) A. J. Dobbs, B. C. Gilbert, and R. O. C. Norman, *Chem. Commun.*, 1353 (1969).

(68) H. Paul and H. Fischer, *Ber. Bunsenges. Phys. Chem.*, **73**, 972 (1969).

Electron Paramagnetic Resonance Studies in Frozen Aqueous Solutions.

Elimination of Freezing Artifacts¹

by John S. Leigh, Jr.,* and George H. Reed

Department of Biophysics and Physical Biochemistry, University of Pennsylvania, School of Medicine, Philadelphia, Pennsylvania 19104 (Received October 12, 1970)

Publication costs assisted by the United States Public Service

Methods for eliminating perturbations on the electron paramagnetic resonance (epr) line shapes of frozen aqueous solutions of paramagnetic species are examined. Solvent-solute segregation which occurs in slowly frozen samples results in high "local" concentrations of paramagnetic species, and the epr spectra exhibit strong dipolar and exchange interactions. These intermolecular effects are only partially removed by rapid freezing techniques. Imbedding the aqueous samples in a polydextran gel prior to freezing results in magnetically dilute samples whose epr line shapes show superior resolution suitable for extracting spin-Hamiltonian parameters. Spectra for aquo complexes of transition metal ions, a metal complex, and a neutral free radical are shown to illustrate the dramatic improvements in spectral resolution for the gel-frozen samples.

Introduction

Solid state electron paramagnetic resonance (epr) spectra of transition metal complexes contain useful information about structures and electronic configurations of the complexes.² For complexes which are formed in aqueous media, preparation of solid samples by freezing the solutions typically produces "magnetically concentrated" specimens which exhibit strong intermolecular magnetic interactions.³ The "slow" freezing of an aqueous salt solution usually promotes ice crystal formation with consequent solute-solvent segregation. The segregated solutes do not freeze until an approximate eutectic composition is reached. This means that "local" concentrations of paramagnetic ions in the frozen samples may be of the order of 1 to 10 *M*.⁴ Furthermore, freezing rates which are sufficiently rapid to overcome the solute segregation effects are difficult to achieve.^{5,6} This paper describes the use of a polydextran gel to achieve magnetic dilution in frozen aqueous solutions. Epr spectra for aquo complexes of paramagnetic ions and an aqueous solution of a nitroxide free radical are presented to illustrate the method.

Experimental Section

Epr spectra were recorded on a Varian E-3 spectrometer operating at 9.2 GHz. Temperature for all measurements was 77°K. Three techniques were used for obtaining frozen samples. (1) Aqueous samples were placed in 3 mm i.d. quartz tubes and frozen by dipping the tube into liquid nitrogen. (2) A special quartz tube as described by Bray and Pettersson⁷ was filled with methylcyclohexane and chilled in a bath of Dry Ice and acetone. The sample was taken up in a syringe fitted with a polyethylene nozzle (drawn to a fine point).⁸ The sample was injected into the cold

methylcyclohexane, and the resulting snow was packed into the bottom (3 mm i.d.) part of the tube. (3) Sephadex G-25-80 (Pharmacia), which had been allowed to swell in distilled water, was poured into a small Büchner funnel (15 mm i.d., 6 mm depth) and excess water was removed by suction. The aqueous sample (~0.5 ml) was poured over the bed of Sephadex and allowed to move into the gel for a minute without suction. Excess moisture was removed by gentle suction, and the moist gels were packed into 3 mm i.d. quartz tubes and frozen in liquid nitrogen.

Results

Epr spectra of MnCl₂ solutions (5×10^{-4} *M*) which were frozen by the three different methods are compared in Figure 1. In Figure 1A the sample was frozen by simply dipping the quartz sample tube in liquid nitrogen. The absence of hyperfine structure is a consequence of strong intermolecular magnetic interactions.³ The spectrum obtained by rapid freezing⁹ is

(1) This work was supported in part by Public Health Service Grant GM 12446 and by Public Health Service Fellowships GM 32,263 (J. S. L.) and GM 34,539 (G. H. R.).

(2) J. S. Griffith, "The Theory of Transition-Metal Ions," Cambridge University Press, London, 1961.

(3) R. T. Ross, *J. Chem. Phys.*, **42**, 3919 (1965).

(4) "International Critical Tables," Vol. IV, E. W. Washburn, Ed., McGraw-Hill, New York, N. Y., 1928, p 254.

(5) C. S. Lindenmeyer, G. T. Onok, K. A. Jackson, and B. Chalmers, *J. Chem. Phys.*, **27**, 822 (1957).

(6) W. B. Hillig in "Growth and Perfection of Crystals," R. H. Doremies, B. W. Roberts, and D. Turnbull, Ed., Wiley, New York, N. Y., 1958, p 350.

(7) R. C. Bray and R. Pettersson, *Biochem. J.*, **81**, 194 (1961).

(8) R. C. Bray, *ibid.*, **81**, 189 (1961).

(9) Bray⁸ has estimated that freezing times of ~10 msec are feasible by this technique. Spectra with markedly better resolution than in Figure 1B have been obtained for us by Dr. Helmut Beinert using a "ram" freezing apparatus.

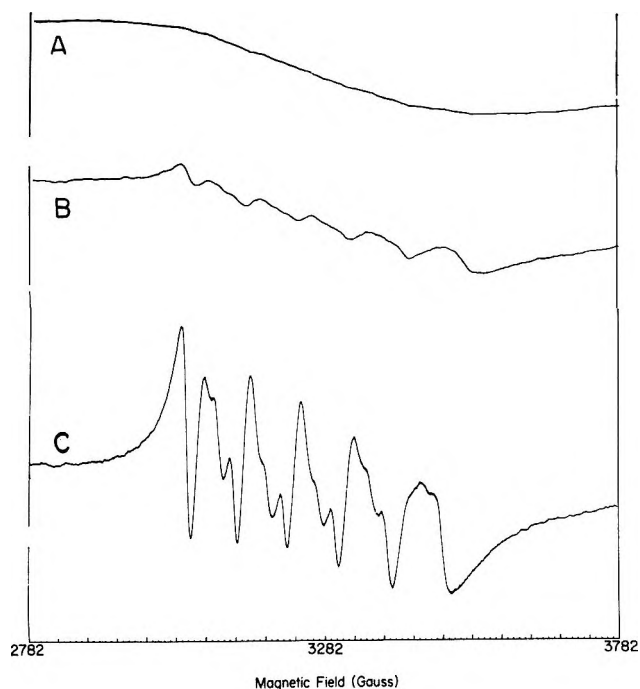


Figure 1. Epr spectra for $5 \times 10^{-4} F$ solution of $MnCl_2$: A, slowly frozen; B, rapidly frozen; C, frozen in Sephadex gel.

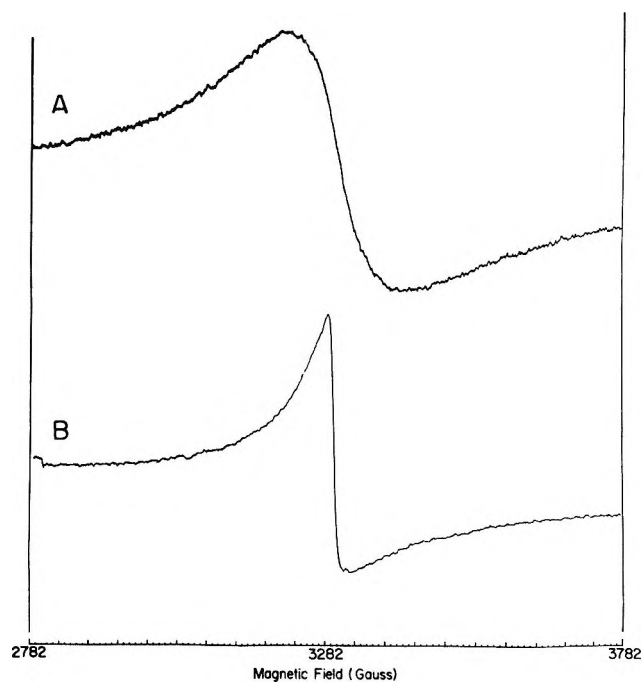


Figure 3. Epr spectra for $1 \times 10^{-3} F$ solution of $Cr(NO_3)_3$: A, slowly frozen; B, frozen in Sephadex gel.

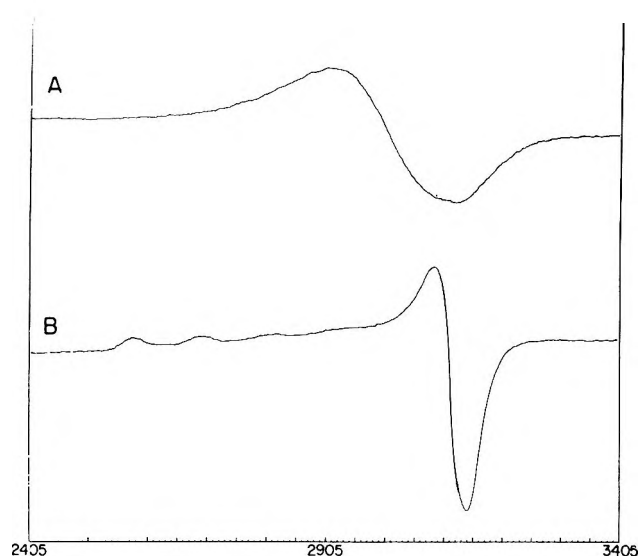


Figure 2. Epr spectra for $5 \times 10^{-4} F$ solution of $Cu(NO_3)_2$: A, slowly frozen; B, frozen in Sephadex gel.

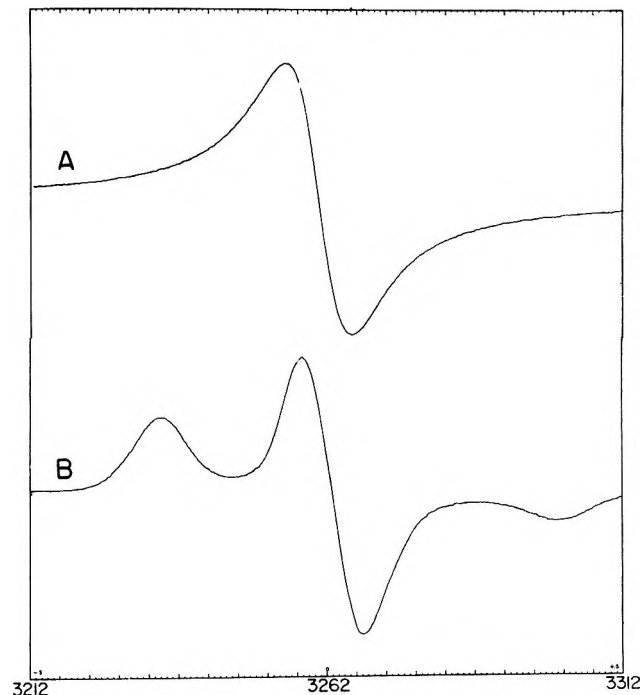


Figure 4. Epr spectra for $1 \times 10^{-3} M$ solution of 2,2,6,6-tetramethylpiperidino-4-oxyl-1: A, slowly frozen; B, frozen in Sephadex gel.

shown in Figure 1B. An improvement in the extent of magnetic dilution is evidenced by the appearance of ^{55}Mn hyperfine structure. Figure 1C illustrates the dramatic improvement in spectral resolution achieved when the sample is imbedded in the polydextran gel prior to freezing. The hyperfine structure including "forbidden" hyperfine transitions is partially resolved, and line widths of less than 20 G are observed. Proton relaxation rate measurements for water in the unfrozen gels gave no evidence for $Mn(II)$ complexation to the dextran matrix.

Some of the spin-Hamiltonian parameters for the aquo-cupric ion can be readily obtained from the gel-frozen spectrum for a $Cu(NO_3)_2$ solution shown in Figure 2B. The resolution in the spectrum 2B should be contrasted to the structureless spectrum (Figure 2A) obtained by the slow freezing method. From the

hyperfine structure in the axially symmetric, powder line shape one calculates $A_{\parallel} = 117$ G. Values for g_{\perp} and g_{\parallel} are estimated to be 2.10 and 2.38, respectively.

Analogous results for the aquo-chromic ion are shown in Figure 3. The solution was made up from the hydrated nitrate salt. Slow exchange of the six hydration waters from the chromic ion¹⁰ precludes any complex formation with the gel. The peak to peak line width of the gel-frozen spectrum (Figure 3B) is only 40 G compared with the 200-G line width of the slowly frozen sample (Figure 3A).

Spectra for frozen aqueous solutions (1 mM) of an uncharged molecule (2,2,6,6-tetramethylpiperidinol-4-oxyl-1) which contains a nitroxide free radical are given in Figure 4. The spectrum for the slowly frozen sample shows the intermolecular interactions brought about by solvent-solute segregation. From the gel-frozen spectrum one can immediately measure $A_z = 33.3$ G. Other components of the A tensor and the g tensor components can, in principle, be estimated by spectral simulations.

The epr spectra for the slowly frozen samples in Figures 1-4 illustrate the effects of dipolar and/or exchange broadening. If during the freezing process the unpaired spins of neighboring molecules are brought into sufficiently close proximity, electron exchange interactions become strong enough to narrow the resonance signal. The slowly frozen spectrum for the Mn(II)-adenosine triphosphate complex (Figure 5A) shows this exchange narrowing phenomenon. Spectra for rapidly frozen samples were broader than that in Figure 5A but exhibited no hyperfine structure. The line width of 260 G in Figure 5A is to be contrasted to the ~ 500 -G hyperfine envelope in the gel-frozen spectrum (Figure 5B).

Discussion

The results presented here indicate that imbedding aqueous solutions in polydextran gels prior to freezing effectively eliminates solvent-solute segregation, and the resulting samples are magnetically dilute. The gel method is faster, more convenient, and gives better results than the rapid freezing method. Ross³ has demonstrated the use of high concentrations of salts or miscible organic liquids to induce glass formation in the frozen aqueous samples. However, for solutions of transition metal complexes the high concentrations of "inert" solutes may directly or indirectly perturb the chemical equilibria and thereby alter the chemistry of

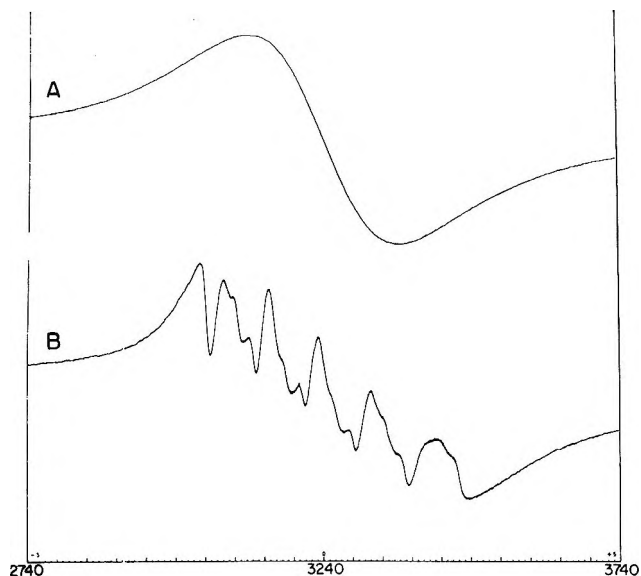


Figure 5. Epr spectra for Mn(II)-adenosine triphosphate, $MnCl_2 = 1 \times 10^{-3} F$, $ATP = 1.1 \times 10^{-3} F$, $pH = 8.0$: A, slowly frozen; B, frozen in Sephadex gel.

the sample. Our preliminary experiments have indicated no complex formation between the gel and transition metal ions. Thus the gel appears to function as a truly inert matrix and chemically distinct samples are obtained by the gel-freezing method.

Epr studies of transition metal complexes with biological macromolecules are often carried out in frozen aqueous solutions.¹¹ While the macromolecules themselves provide for effective magnetic dilution, upon freezing the "local" buffer or salt concentrations may reach levels detrimental to the integrity of the tertiary or quaternary structure of the macromolecule. Polydextran gels with pore sizes sufficient to accommodate the macromolecule could provide protection against high salt concentrations which might otherwise result during freezing process.

Freezing aqueous solutions of paramagnetic species in a polydextran gel provides samples whose epr spectral line shapes are suitable for deriving spin-Hamiltonian parameters. In addition quantitative analyses of paramagnetic components of aqueous samples could be performed through use of an appropriate internal standard signal.

(10) J. P. Hunt and R. A. Plane, *J. Amer. Chem. Soc.*, **76**, 5960 (1954).

(11) H. Beinert and G. Palmer, *Advan. Enzymol.*, **27**, 105 (1965).

Electron Spin Resonance Studies of Biradicals of Nitro Aromatic Radical Anions and Alkali Ions

by C. A. McDowell* and F. Nakano

Department of Chemistry, University of British Columbia, Vancouver 8, British Columbia, Canada
(Received November 9, 1970)

Publication costs assisted by The National Research Council of Canada

Electron spin resonance studies of nitro aromatic radical anions and alkali metal ions in frozen glassy matrices prove the presence of paramagnetic dimers with triplet ground states. The values of the zero-field parameters deduced from the experimental results indicate that the structures of the biradicals have axial symmetry, or higher (probably D_{2d} symmetry), and the spin densities are largely localized on the nitro groups.

Previous electron spin resonance studies have shown the occurrence of spin-spin interactions in rigid glassy solutions of fluorenone-alkali metal ion pairs,¹ the alkali metal ketyls of β -diketones,²⁻⁴ and dipyridal anions and alkali metal ions.^{5,6} Such work has shown that the esr spectra of spin-spin interactions in these glassy solutions can yield important information on the electronic and geometrical structures of the biradical species. In the present communication we report the observation of triplet esr spectra arising from spin-spin interactions in systems such as nitrobenzene-Li-dimethoxyethane (DME), nitrobenzene-Na-DME, *m*-dinitrobenzene-Na-DME, *m*-iodonitrobenzene-Na-DME, and we have also included for comparison purposes some results on the system phthalonitrile-Na-DME. It has, of course, long been known⁷ that nitro aromatic radical anions and alkali metal ions associate forming ion pairs of the type $M-Me^+$. Detailed studies⁸⁻¹⁰ of such systems have elucidated many important details concerning the structures and dynamics of these ion pairs. We were concerned to see if ion clusters of the type $M-Me^+M^-$ could exist for nitro aromatic radical anion and alkali metal ion systems. Our experimental observations reported below indicate that ion clusters of this latter type are in fact possible for these nitro compounds particularly in glassy rigid solutions.

Experimental Section

The 1,2-dimethoxyethane (DME) was purified by fractional distillation and refluxing over metallic sodium for several hours. It was stored over anthracene and sodium and distilled off immediately before use. The chemical reduction was carried out in a glass apparatus which had previously been evacuated. The DME solution of the compound was brought into contact with a film of a highly purified sample of the alkali metal. After the reduction was complete the solution (concentration > 0.1 mg ml⁻¹) was transferred to a

special silica sample tube, frozen at liquid nitrogen temperature, and sealed off under vacuum.

The nitrobenzene was a BDH Analar sample carefully purified by steam distillation and several recrystallizations. After three recrystallizations the freezing point of the compound was 5.96° and without further purification the material was used in the experiments. The *m*-dinitrobenzene, *m*-iodonitrobenzene, and phthalonitrile used were the purest commercially available samples.

All the esr spectra were determined using a variable temperature apparatus to cool the specimen until a rigid glassy matrix was produced. The spectra were recorded using a Varian E3 spectrometer and a laboratory constructed esr spectrometer with 100-KHz of field modulation and a 12-in. Varian magnet.

Results and Discussion

A typical triplet spectra arising from spin-spin interactions in these systems is shown in Figure 1 for the $g = 2$ region. The spectra are, of course, superpositions of the esr signals from the normal one-spin radical anion and the triplet spectra characteristic of a two-spin system for the $\Delta m = \pm 1$ transitions. In the

- (1) N. Hirota and S. I. Weissman, *Mol. Phys.*, **5**, 537 (1962).
- (2) H. van Willigen and S. I. Weissman, *ibid.*, **11**, 175 (1966).
- (3) F. W. Pijpers, H. van Willigen, and J. J. Th. Gerding, *Recl. Trav. Chim., Pays-Bas*, **86**, 511 (1967).
- (4) N. Hirota, *J. Amer. Chem. Soc.*, **89**, 32 (1967).
- (5) I. M. Brown, S. I. Weissman, and L. C. Snyder, *J. Chem. Phys.*, **42**, 1105 (1965).
- (6) J. D. W. van Voorst, W. G. Zijlstra, and R. Sitters, *Chem. Phys. Lett.*, **1**, 321 (1967).
- (7) R. L. Ward, *J. Amer. Chem. Soc.*, **83**, 1296 (1961).
- (8) P. H. H. Fischer and C. A. McDowell, unpublished experiments; see also P. H. H. Fischer, Thesis, University of British Columbia, Vancouver, British Columbia, 1963.
- (9) J. Gendell, J. H. Freed, and G. K. Fraenkel, *J. Chem. Phys.*, **37**, 2832 (1962).
- (10) C. A. McDowell and F. Nakano, unpublished experiments; see also F. Nakano, M.Sc. Thesis, University of British Columbia, Vancouver, British Columbia, 1966.

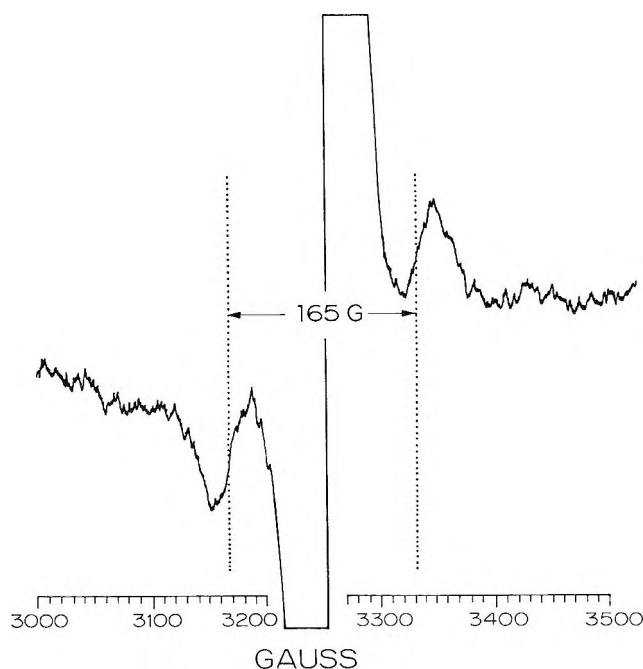


Figure 1. ESR spectrum of spin-spin interactions in ion clusters of the system nitrobenzene-Li-DME in a rigid glassy solution at 77°K. The signals arising from the $\Delta m = \pm 1$ transitions are indicated as being separated by 165 G.

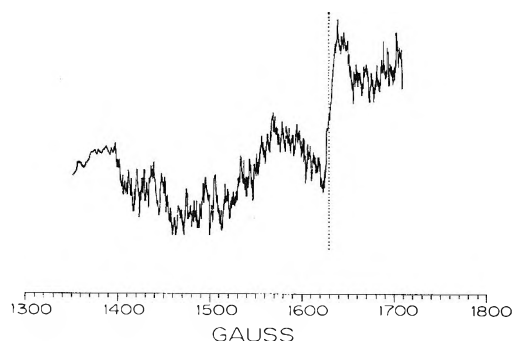


Figure 2. ESR spectra in the $g = 4$ region for the ion clusters in the system nitrobenzene-Na-DME in a rigid glassy solution at 77°K. The $\Delta m = 2$ transition occurs at 1630 G and for this case the $\Delta m = \pm 1$ transitions occur at a mean field of 3250 G.

cases of the nitrobenzene-Na-DME and *m*-dinitrobenzene-K-DME glasses the half-field lines arising from the $\Delta m = 2$ transitions were also observed (see Figure 2) confirming the presence of two spin systems^{11,12} in these ion-pair solutions. Rigid media esr spectra of systems exhibiting spin-spin interaction have usually been found to be characterized by a spin Hamiltonian of the form

$$\mathcal{H} = g\beta HS + DS_z^2 + E(S_x^2 - S_y^2) \quad (1)$$

From the line shapes in the spectra which we observed for the nitro aromatic compounds under study, and the fields at which the $\Delta m = \pm 1$ and the $\Delta m = 2$ transitions occurred, we conclude that for the species examined the value of the E tensor is approximately

zero (see ref 1, 3, 4, and 13). Thus the spin-spin interacting ion clusters in the solutions investigated must have axial or tetrahedral symmetry.

Extensive theoretical analysis and computer calculations of the line shapes for ion cluster triplet species have been reported by several workers.^{1,3,4,13} All of these calculations show that the line shapes of the $\Delta m = 1$ transitions are sensitive to the values of the zero-field parameters D and E , and in particular the line shapes differ greatly for the two cases (i) $E = 0$ and (ii) $E \neq 0$. As mentioned above this type of analysis of the esr spectra arising from spin-spin interactions in glassy solutions has been used to elucidate the geometrical and electronic structures of ion clusters in several systems.

The values for the parameter D derived from our observations are given in Table I.

Table I: Values of the Zero-Field Splitting Parameter D for the Ion Clusters $M^-Me^+M^-$ in Glassy DME Solutions of Nitro Aromatic Compounds and Alkali Metals

Compd	Alkali metal	D , G
Nitrobenzene	Li	165 ± 5
	Na	160 ± 5
<i>m</i> -Dinitrobenzene	Na	157 ± 5
<i>m</i> -Iodonitrobenzene	Na	166 ± 5
Phthalonitrile	Na	166 ± 5

Temperature variations, admittedly over a limited range, seemed to have only a slight effect on the magnitude of the zero-field splitting parameters D . A slight increase in the value of D was observed but this was within the experimental error. The fact that the values of D are nearly the same for all the nitro compounds studied is presumably due to the localization of spin density largely on the nitro groups of the molecules. It may seem peculiar that *m*-iodonitrobenzene gives a triplet spin-spin interaction spectrum very similar to those observed for nitrobenzene and *m*-dinitrobenzene although strict symmetry considerations in this case would seem to preclude $E = 0$. An LCAO calculation using the McLachlan approximation¹⁴ shows that the spin density distribution in the *m*-iodonitrobenzene radical anion is very small at the halogen atom so that the resulting spin density distribution is very similar to that of the nitrobenzene radical anion. Thus if the configuration of the ion clusters $M^-Me^+M^-$ from *m*-

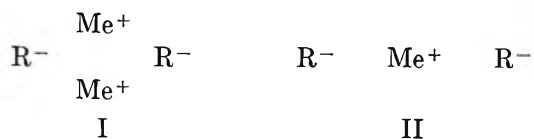
(11) J. H. van der Waals and M. S. de Groot, *Mol. Phys.*, **2**, 333 (1959).

(12) M. S. de Groot and J. H. van der Waals, *ibid.*, **3**, 190 (1960).

(13) W. A. Yager, E. Wasserman, and R. M. R. Cramer, *J. Chem. Phys.*, **37**, 1148 (1962).

(14) A. D. McLachlan, *Mol. Phys.*, **3**, 233 (1960).

iodonitrobenzene in rigid glassy solutions is the same as those from nitrobenzene, as would be expected, then the value of E in that can also be approximately zero. The most likely structure for the ion clusters is $M^-Me^+M^-$ with each M^- radical anion in a plane perpendicular to the other one (see ref 5 and 6). It must be pointed out, however, that an ion quadruplet cluster of type I rather than the triple ion cluster II is also a possible structure.⁴



Acknowledgments. We are indebted to the National Research Council of Canada for generous grants in support of this research work. Our thanks are also extended to Professor J. B. Farmer for his assistance and advice.

Anisotropic Solvent Shifts Determined by Factor Analysis

by Paul H. Weiner¹ and Edmund R. Malinowski*

Department of Chemistry and Chemical Engineering, Stevens Institute of Technology, Hoboken, New Jersey 07030
(Received October 16, 1970)

Publication costs assisted by the Stevens Institute of Technology

The effects of solvents on the proton shift of nonpolar solutes are investigated. A mathematical technique called factor analysis successfully separates solvent anisotropy from other effects of the solvent. Values for solvent anisotropies are deduced. A graphical approach for obtaining solvent anisotropies is also presented.

Introduction

In nmr spectroscopy the chemical shift of a solute molecule depends on the solvent. Many factors (such as van der Waals interactions, reaction field, and solvent anisotropy) are believed to contribute to the solvent effect. Attempts to separate and isolate these effects have not been wholly successful.²⁻⁴ The difficulty arises because it is impossible to change one factor without changing another.

Recently, a preliminary study⁵ indicated that a mathematical technique called factor analysis is applicable to the study of solvent effects in nmr spectroscopy. This technique performs a mathematical separation of the various solvent factors and allows each factor to be tested individually against theoretical models. In the present paper we apply factor analysis for discerning the effect of solvents on the proton shift of nonpolar solutes. This method allows us to isolate solvent anisotropy. Quantitative values for solvent anisotropy are obtained.

Experimental Section

All chemical shifts were referenced to external hexamethyldisiloxane (HMD) and were corrected for bulk susceptibility by the technique described in detail in the earlier work.⁴ All measurements were made at a probe temperature of $39 \pm 1^\circ$. Experimental proton shift

data for the nonpolar solutes in a variety of solvents are shown in Table I. These shifts are accurate to within ± 0.5 Hz. A positive value indicates a downfield shift from external HMD.

Review of Factor Analysis

A detailed discussion of factor analysis as applied to the problem of solvent effects has been presented in a previous paper.⁵ Factor analysis is applicable when a quantity, such as chemical shift, can be expressed as a linear sum of product functions. For example, if $\delta_{i\alpha}$ is the chemical shift of solute i in solvent α , then we seek a solution of the form

$$\delta_{i\alpha} = \sum_j U_{ij}V_{j\alpha} \quad (1)$$

Here U_{ij} refers to the j th solute factor of the i th solute, and $V_{j\alpha}$ refers to the j th solvent factor of the α th solvent. The sum is taken over all factors that contribute to the chemical shift.

(1) Robert-Crooks-Stanley Fellow.

(2) J. Homer, E. J. Hartland, and C. J. Jackson, *J. Chem. Soc. A*, 931 (1970).

(3) N. Lumbroso, T. K. Wu, and B. P. Dailey, *J. Phys. Chem.*, **67**, 2469 (1963).

(4) E. R. Malinowski and P. H. Weiner, *J. Amer. Chem. Soc.*, **92**, 4193 (1970).

(5) P. H. Weiner, E. R. Malinowski, and A. Levinstone, *J. Phys. Chem.*, **74**, 4537 (1970).

Table I: Chemical Shift^a of Nonpolar Solutes Relative to External Hexamethyldisiloxane $\delta^{\text{HMD,X}}(i,\alpha)$

Solvent	Solute ^b					
	CH ₄	CH ₃ CH ₃	Neo-C ₈ H ₁₈	c-C ₆ H ₁₂	c-C ₈ H ₁₆	TMS
CH ₂ Cl ₂	10.7	49.1	53.9	83.8	90.5	-1.4
CHCl ₃	14.6	52.8	57.7	87.0	93.7	1.9
CCL ₄	16.8	55.0	58.7	87.5	94.6	3.0
CH ₂ Br ₂	20.6	57.4	61.0	90.2	96.7	6.8
CHBr ₃	26.0	62.6	65.4	93.7	100.2	10.6
CH ₃ I	18.3	55.0	59.6	89.9	95.4	5.4
CH ₂ I ₂	35.0	69.8	73.5	101.3	107.6	19.9
CH ₂ BrCl	16.6	54.2	58.1	87.7	94.6	3.7
CHBrCl ₂	19.5	56.2	60.5	90.1	96.5	5.7
CBrCl ₃	22.8	59.4	63.2	93.0	99.1	8.0
CH ₃ CCl ₃	16.3	54.6	58.2	88.1	95.1	3.1
CH ₂ ClCCl ₃	16.0	53.6	57.6	87.3	93.8	2.5
CHCl ₂ CCl ₃	16.2	54.1	57.9	87.2	94.0	2.8
CHCl ₂ CHCl ₂	15.4	53.3	56.8	86.9	93.2	2.3
CS ₂	24.3	62.1	64.6	95.2	101.1	11.0
C ₆ H ₆	-17.9	20.5	27.0	56.4	63.7	-27.0
CH ₃ CN	14.0	52.5	57.7	89.7	94.2	1.9
(CH ₃) ₂ CO	1.1	41.5	46.1	77.0	83.4	-8.9
(CH ₃) ₂ SO	18.2	55.1	59.6	88.7	95.1	5.3
C ₆ H ₁₂	8.5	48.5	52.1	80.8	90.5	-2.6
C ₈ H ₁₆	10.9	49.9	53.7	84.9	92.2	-0.5
C ₆ F ₆	-20.9	19.7	24.5	55.6	60.9	-30.3

^a Chemical shifts are in Hz from external HMD and are corrected for bulk susceptibility. Nmr spectrometer was operated at 60 MHz. Positive values indicate downfield shifts from standard.

For factor analysis, a matrix of data is required. Hence, in matrix notation, eq 1 becomes

$$[\delta_{i\alpha}] = [U_{ij}][V_{j\alpha}] \quad (2)$$

A correlation matrix is formed by either premultiplying or postmultiplying the data matrix by its transpose. The correlation matrix is then diagonalized, yielding eigenvalues and eigenvectors, the number of eigenvectors being independent of the premultiplication or postmultiplication procedure of forming the correlation matrix. The number of eigenvectors determines the dimensionality of the space and represents the least number of factors needed to span the solvent effect space. The eigenvalues indicate the relative importance of the various eigenvectors (factors). Furthermore, the eigenvectors, which are abstract quantities, can be rotated mathematically into physically significant parameters. This last step allows us to test theoretical concepts.

Application of Factor Analysis

The matrix of raw data in Table I (involving nonpolar solutes) was subjected to factor analysis. Correlation matrices of size 6×6 and 22×22 were constructed by premultiplication and postmultiplication of the data matrix by its transpose. In both cases we found three eigenvectors which span the solvent effect space and reproduce all data within experimental error, namely ± 0.5 Hz. Thus we conclude that only three fundamental factors are involved. This result corroborates

previous theoretical speculation that three factors are involved, namely gas phase shift, van der Waals effect, and solvent anisotropy. Utilizing factor analysis we are now in a position to test these speculations by attempting to rotate the eigenvectors of the solvent effect space into these three physically significant solvent factors. To rotate into solvent factors we must utilize the 6×6 correlation matrix. (From the 22×22 correlation matrix we can rotate directly into solute factors.)

According to the early work of Buckingham, Schaefer, and Schneider⁶ the solute chemical shift is a linear sum of various contributions. Along this line of reasoning we contend that the shift of a nonpolar solute can be expressed as

$$\delta^{\text{HMD,X}}(i,\alpha) = \delta^{\text{HMD,X}}(i,g) \cdot 1 + \sigma_w(i) \cdot \sigma_w(\alpha) + 1 \cdot \sigma_a(\alpha) \quad (3)$$

where $\delta^{\text{HMD,X}}(i,\alpha)$ is the chemical shift of solute i in solvent α , relative to external HMD; $\delta^{\text{HMD,X}}(i,g)$ is the gas phase shift relative to external HMD (the shifts having been corrected for bulk susceptibility); $\sigma_w(i)$ and $\sigma_w(\alpha)$ refer to the van der Waals effect associated with the solute and solvent, respectively; $\sigma_a(\alpha)$ is the anisotropic shift due to solvent α . Previously,⁴ arguments have been presented to show that the van der Waals term can be expressed as a product function.

(6) A. D. Buckingham, T. S. Schaefer, and W. G. Schneider, *J. Chem. Phys.*, **32**, 1227 (1960).

Notice that eq 3 is the sum of product terms and is of the proper form for factor analysis. However, it is more convenient to express this in another way. For methane as a solute eq 3 takes the form

$$\delta^{\text{HMD},X}(\text{CH}_4,\alpha) = \delta^{\text{HMD},X}(\text{CH}_4,\text{g}) \cdot 1 + \sigma_w(\text{CH}_4) \cdot \sigma_w(\alpha) + 1 \cdot \sigma_a(\alpha) \quad (4)$$

solving eq 4 for $\sigma_w(\alpha)$, and substituting into eq 3, we obtain

$$\delta^{\text{HMD},X}(i,\alpha) = \delta^{\text{HMD},X}(i,\text{g}) \cdot 1 + \left(\frac{\sigma_w(i)}{\sigma_w(\text{CH}_4)} \right) \times \delta^{\text{CH}_4,X}(\text{CH}_4,\alpha) + \left(1 - \frac{\sigma_w(i)}{\sigma_w(\text{CH}_4)} \right) \sigma_a(\alpha) \quad (5)$$

in this expression, $\delta^{\text{CH}_4,X}(\text{CH}_4,\alpha) = \delta^{\text{HMD},X}(\text{CH}_4,\alpha) - \delta^{\text{HMD},X}(\text{CH}_4,\text{g})$, which represents the gas-to-solution shift of methane in solvent α referenced with respect to methane gas. These arguments reveal the nature of the three factors. According to eq 5 we should be able to rotate the eigenvectors resulting from factor analysis into the following physically significant solvent parameters: unity, methane gas-to-solution shift, and solvent anisotropy. From eq 5 we see that the coefficient of the unity vector is the gas phase chemical shift of solute i . The coefficient of the methane gas-to-solution vector is the ratio $\sigma_w(i)/\sigma_w(\text{CH}_4)$. Furthermore we notice that the sum of the last two coefficients in eq 5 is unity.

To perform the rotation we must construct a test eigenvector for each suspected solvent parameter (factor). Unity and methane gas-to-solution shift present no conceptual or experimental problems. For these two suspected factors all necessary data are available. On the other hand, for the solvent anisotropy test vector, data are not readily available. To generate a test vector for solvent anisotropy we proceeded along the following lines of reasoning. All investigators, to date, ascribe a zero value for the solvent anisotropic of carbon tetrachloride because it is nonpolar and symmetric. At present, benzene and carbon disulfide are the only other solvents for which solvent anisotropy values have been assigned. For these two solvents, only general agreement can be found between different investigators. For example, from a graphical approach, Malinowski and Weiner⁴ deduced values of -21 ± 3 Hz for benzene and $+9 \pm 3$ Hz for carbon disulfide. Schug⁷ made a theoretical estimation of -30 Hz for benzene and $+18.1$ Hz for carbon disulfide. Homer⁸ suggested -35 Hz for benzene and $+7$ Hz for carbon disulfide.

In factor analysis⁵ all of the points for a given test factor need not be available in order to apply the rotation part of the scheme. Upon rotation factor analysis will yield predicted values for the missing points. Therefore, the solvent anisotropic shift vector can be tested as a factor even though most of the points are

unknown. In fact since three factors are involved a minimum of three points are required in the test vector.

Factor analysis allows each test vector to be examined separately. Applying the rotation part of the scheme to each of three solvent test factors we obtained the following results. Unity and methane gas-to-solution shift are indeed true factors. This can be seen from the agreement between predicted and experimental values shown in Table II. Since only three speculative points were available for the solvent anisotropy vector a different criteria had to be employed in order to test the validity of the solvent anisotropy vector. These criteria come from eq 5. If the solvent anisotropy vector is correct, then the coefficient of the unity vector should correspond to the solute gas phase shift, and the sum of the other two coefficients for each solute, should equal unity. These criteria were not met for any combination of the anisotropy shifts of benzene and carbon disulfide reported earlier. Since unity and methane gas-to-solution shift were identified as true factors, we proceeded in the following manner. In the solvent anisotropy vector the value for carbon tetrachloride was fixed at zero, and the factor analysis rotation scheme was performed while systematically varying the solvent anisotropic shifts of benzene and carbon disulfide until the coefficient of the unity vector agreed with the experimental gas phase shift, and the sum of the other two coefficients approached unity as predicted by eq 5. In this way the best fit was obtained when $\sigma_a(\text{benzene}) = -24.0$ Hz and $\sigma_a(\text{CS}_2) = +9.0$ Hz. Following this procedure the factor analysis scheme yielded the following equations

$$\begin{aligned} \delta^{\text{HMD},X}(\text{CH}_4,\alpha) &= -8.29f_1 + 0.99f_2 + 0.01f_3 \\ \delta^{\text{HMD},X}(\text{CH}_3\text{CH}_3,\alpha) &= 35.86f_1 + 0.72f_2 + 0.28f_3 \\ \delta^{\text{HMD},X}(\text{neo-C}_5\text{H}_{12},\alpha) &= 41.62f_1 + 0.64f_2 + 0.32f_3 \\ \delta^{\text{HMD},X}(\text{C}_6\text{H}_{12},\alpha) &= 75.79f_1 + 0.49f_2 + 0.55f_3 \\ \delta^{\text{HMD},X}(\text{C}_8\text{H}_{16},\alpha) &= 83.84f_1 + 0.38f_2 + 0.63f_3 \\ \delta^{\text{HMD},X}(\text{TMS},\alpha) &= 12.77f_1 + 0.63f_2 + 0.35f_3 \quad (6) \end{aligned}$$

Here, f_1 = unity, f_2 = methane gas-to-solution shift, and f_3 = solvent anisotropy. The values of the coefficient of the unity terms can be compared to the actual experimental gas phase shift,⁹⁻¹¹ namely (relative to external HMD)¹² methane = -8.4 Hz, ethane =

(7) J. C. Schug, *J. Phys. Chem.*, **70**, 1816 (1966).

(8) J. Homer, *Tetrahedron*, **23**, 4065 (1967).

(9) W. T. Raynes and M. A. Raza, *Mol. Phys.*, **17**, 157 (1969).

(10) F. H. A. Rummens, W. T. Raynes, and H. J. Bernstein, *J. Phys. Chem.*, **72**, 2111 (1968).

(11) H. Spiesscke and W. G. Schneider, *J. Chem. Phys.*, **35**, 722 (1961).

(12) In ref 9, 10, and 11 the shifts are reported with respect to methane gas. A correction factor of -8.4 Hz has been added to each shift to change the reference to external HMD.

Table II: Comparisons between the Suspected Solvent Factors and Their Rotated Vectors

Solvent	Unity ^a		CH ₄ gas-to-solution ^b		Solvent anisotropy ^c	
	Predicted	Test	Predicted	Test	Predicted	Test
CH ₂ Cl ₂	1.005	1.0	19.1	19.1	-1.7	...
CHCl ₃	1.009	1.0	23.1	23.0	0.8	...
CCl ₄	1.014	1.0	25.4	25.2	0.0	0.0
CH ₂ Br ₂	0.992	1.0	28.9	29.0	3.6	...
CHBr ₃	1.002	1.0	34.5	34.4	4.9	...
CH ₃ I	0.990	1.0	26.6	26.7	3.8	...
CH ₂ I ₂	0.974	1.0	43.2	43.4	14.8	...
CH ₂ BrCl	0.996	1.0	25.0	25.0	2.0	...
CHBrCl ₂	1.000	1.0	27.9	27.9	2.7	...
CBrCl ₃	1.010	1.0	31.3	31.4	3.5	...
CH ₃ CCl ₃	1.010	1.0	24.8	24.7	1.2	...
CH ₂ ClCCl ₃	1.007	1.0	24.5	24.4	-0.1	...
CHCl ₂ CCl ₃	1.006	1.0	24.7	24.6	0.4	...
CHCl ₂ CHCl ₂	1.001	1.0	23.8	23.7	0.3	...
CS ₂	0.992	1.0	32.6	32.7	9.0	9.0
C ₆ H ₆	0.977	1.0	-9.7	-9.5	-24.0	-24.0
CH ₃ CN	1.016	1.0	22.5	22.4	2.1	...
(CH ₂) ₂ CO	1.003	1.0	9.5	9.5	-5.9	...
(CH ₂) ₂ SO	0.987	1.0	26.5	26.6	3.6	...
C ₆ H ₁₂	1.001	1.0	16.9	16.9	-1.3	...
C ₈ H ₁₆	1.001	1.0	19.3	19.3	0.5	...
C ₆ F ₆	1.002	1.0	-12.4	-12.5	-27.6	...

^a Unity test vector. ^b Methane gas-to-solution shift test vector. Positive values are downfield shifts. ^c Solvent anisotropy test vector, positive values are downfield shifts. Note only three points are used to define the vector.

36.6 Hz, neopentane = 42.1 Hz, cyclohexane = 75.6 Hz, and tetramethylsilane = 16.4 Hz. Except for TMS, the agreement is excellent. Predictions of the solvent anisotropies for a variety of solvents involved in the analysis are listed in Table II. Notice that halogenated solvents such as methylene iodide and bromoform have large solvent anisotropies. These values should be a guide in the theoretical work involving solvent anisotropy.

Graphical Analysis

We have shown, using factor analysis, that it is possible to obtain values of the solvent anisotropy. Anisotropic shifts can also be obtained by a crude graphical analysis. First we define the solvent-induced chemical shift (SICS) as

$$S(i, \alpha) = \delta^{\text{HMD}, X}(i, \alpha) - \delta^{\text{HMD}, X}(i, g) \quad (7)$$

Considering acetone and carbon tetrachloride as solvents, we see, from eq 4 and 7, that

$$S(i, \text{acetone}) = \left(\frac{\sigma_w(\text{acetone})}{\sigma_w(\text{CCl}_4)} \right) S(i, \text{CCl}_4) + \sigma_a(\text{acetone}) \quad (8)$$

According to eq 8 a plot of $S(i, \text{acetone})$ vs. $S(i, \text{CCl}_4)$ should yield a straight line with a slope equal to $\sigma_w(\text{acetone})/\sigma_w(\text{CCl}_4)$ and an intercept equal to $\sigma_a(\text{acetone})$. From such a plot (see Figure 1) we find that the solvent anisotropy of acetone is approximately -6 Hz, which is in excellent agreement with the value

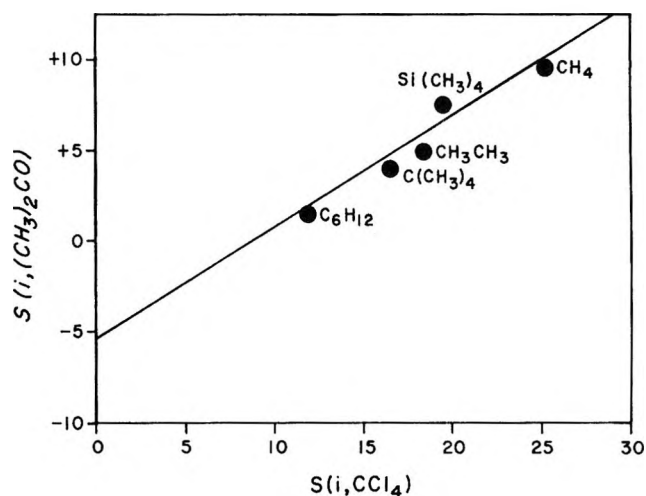


Figure 1. Solvent-induced chemical shifts (SICS) in acetone solvent vs. carbon tetrachloride solvent.

obtained from factor analysis, -5.9 Hz. This graphical method, although admittedly crude, is useful to those who do not have access to computers and lends credence to the conclusions drawn from factor analysis.

Acknowledgment. This investigation was supported in part by the U. S. Army Research Office (Durham) under Contract No. DA-31-124-ARO-D-90. The computations were carried out at the computer center (supported in part by a grant from the National Science Foundation) of Stevens Institute of Technology, for which we record our appreciation.

Nuclear Magnetic Resonance Study of Ion-Exchange Resins.

Macroreticular Resins, Carboxylic Acid Resins, and Line-Width Effects

by Lawrence S. Frankel

Research Laboratories, Rohm and Haas Co., Philadelphia, Pennsylvania 19137 (Received November 11, 1970)

Publication costs assisted by the Rohm and Haas Company

Nuclear magnetic resonance data for a variety of macroreticular ion-exchange resins indicate that water in the pore and gel phase of the resin undergoes rapid solvent exchange independent of temperature. The dominant cause of the water line width from the interior of styrene-divinylbenzene ion-exchange resins is due to susceptibility effects and not to homogeneity effects. The data for the acid form of a carboxylic acid ion-exchange resin are dominated by interactions between water and the undissociated carboxylic acid protons.

Introduction

Several reports have appeared on the nmr spectra of ion-exchange resins.¹⁻¹¹ An especially good survey which indicates the wide scope of information that may be obtained has been presented by Gordon.¹ The nmr spectra will generally show resonances which originate from the interior of the resin and resonances from the region not occupied by the resin (exterior peaks). The resonances from the ion-exchange resin are from the fluid or solvent portion of the resin. The polymer superstructure does not contribute any peaks to the spectrum since its molecular motion is highly restricted. Most of the work has been with gel-type sulfonated styrene-divinylbenzene (DVB) cation resins^{2,6-8} as a function of ionic form. These results show that the chemical shift between the interior and exterior water resonances is dominated by cation hydration effects on water and that all the water in the resin is detected in the nmr experiment.⁴

Application of nmr to resins of fundamentally different physical (macroreticular resins) and chemical (carboxylic acid resins) type have been very limited. Of particular interest is the possibility that the interior water line width may reflect a measure of the homogeneity of the resin.^{1,4}

Experimental Section

The results in Tables II-IV were obtained on a Varian HR-60 spectrometer operating at 56.4 MHz. Variable temperature results were obtained on a Varian A-60 spectrometer (temperature calibration: ethylene glycol or methanol). A Varian HA-100 spectrometer allowed a field strength comparison. This spectrometer was locked on the exterior water signal while the interior line width was measured. The exterior line width was obtained while locked on the interior water signal. A shift of the interior solvent to lower field relative to the exterior solvent will have a negative value.

The fully hydrated resins, studied in exterior immiscible nonswelling solvents, were obtained by a centrifuge technique.^{12a}

All of the resins employed are commercial products of Rohm and Haas Co. A brief description of the resins is given in Table I. The notation Amberlite IR-120 H will be understood to designate the resin, Amberlite IR-120 (Table I) and the ionic form, hydrogen. Unless otherwise stated, the resins are 16-50 mesh size. Prior to use, the resins were treated with copious amounts of an appropriate concentrated ionic solution in an effort to minimize relaxation time effects of paramagnetic ions on the line width.¹

Due to the shape of the spherical resin beads they do not require a susceptibility correction to the chemical shift. However, the exterior solvent does require a susceptibility correction due to the presence of the beads.¹ This correction was evaluated by comparing (A-60 spectrometer) the position of the exterior solvent relative to water alone in a separate matched nmr tube. The following Amberlite resins were examined: 200 H, 200 Na, IRA-900 OH, IRA-910 OH, and IRC-84 H. In no case was the susceptibility cor-

- (1) J. E. Gordon, *J. Phys. Chem.*, **66**, 1150 (1962).
- (2) D. Reichenberg and I. J. Lawrenson, *Trans. Faraday Soc.*, **59**, 141 (1963).
- (3) R. H. Diniu, M. T. Emerson, and G. R. Choppin, *J. Phys. Chem.*, **67**, 1178 (1963).
- (4) J. P. deVilliers and J. R. Parrish, *J. Poly. Sci., Part A*, **2**, 1331 (1964).
- (5) R. H. Dinius and G. R. Choppin, *J. Phys. Chem.*, **68**, 425 (1964).
- (6) D. G. Howery and M. J. Kittay, 158th National Meeting of the American Chemical Society, Sept 1969, New York, N. Y., Division of Colloid and Surface Chemistry, Paper 26.
- (7) T. E. Cough, H. D. Sharma, and N. Subramanian, *Can. J. Chem.*, **48**, 917 (1970).
- (8) R. W. Creekmore and C. N. Reilly, *Anal. Chem.*, **42**, 570 (1970).
- (9) R. W. Creekmore and C. N. Reilly, *ibid.*, **42**, 725 (1970).
- (10) L. S. Frankel, *Can. J. Chem.*, **48**, 2432 (1970).
- (11) L. S. Frankel, *Anal. Chem.*, **42**, 1638 (1970).
- (12) F. Helfferich, "Ion Exchange," McGraw-Hill, New York, N. Y., 1962: (a) p 231; (b) p 86.

Table I: Summary of Amberlite Ion-Exchange Resins Utilized

Amberlite resin	Copolymer	Chemical type	Physical type	Fixed ionic group
IR-120	Styrene-DVB ^a	Strongly acidic	Gel	SO ₃ ⁻
IR-124	Styrene-DVB ^a	Strongly acidic	Gel	SO ₃ ⁻
IRC-84	Cross-linked acrylic	Weakly acidic	Gel	COO ⁻
IRA-400	Styrene-DVB	Strongly basic	Gel	N(CH ₃) ₃ ⁺ ^b
IRA-410	Styrene-DVB	Strongly basic	Gel	N(CH ₃) ₂ (CH ₂ CH ₂ OH) ⁺ ^b
IRA-45	Styrene-DVB	Weakly basic	Gel	Amine
IRA-68	Cross-linked acrylic	Weakly basic	Gel	Amine
200	Styrene-DVB	Strongly acidic	MR ^c	SO ₃ ⁻
252	Styrene-DVB	Strongly acidic	MR	SO ₃ ⁻
IRA-900	Styrene-DVB	Strongly basic	MR	N(CH ₃) ₃ ⁺
IRA-904	Styrene-DVB	Strongly basic	MR	N(CH ₃) ₃ ⁺
IRA-910	Styrene-DVB	Strongly basic	MR	N(CH ₃) ₂ (CH ₂ CH ₂ OH) ⁺
IRA-911	Styrene-DVB	Strongly basic	MR	N(CH ₃) ₂ (CH ₂ CH ₂ OH) ⁺
IRA-93	Styrene-DVB	Weakly basic	MR	Amine

^a IR-120 contains 8% DVB while IR-124 has 12% DVB. ^b These resins are commonly referred to as type I, N(CH₃)₃⁺ and type II, N(CH₃)₂(CH₂CH₂OH)⁺. ^c MR = macroreticular resin.

reaction greater than 2 Hz and does not significantly affect the results or conclusions.

Results and Discussion

Macroreticular Resins. Virtually no nmr data have been reported for macroreticular ion-exchange resins.⁴ Conventional gel resins have a continuous polymeric phase whose average pore size is directly determined by the degree of cross-linking. Macroreticular resins are agglomerates of randomly packed microspheres with large pores or voids occupied by solvent. The sizes of these pores are not primarily directly determined by the degree of cross-linking. The microspheres themselves are usually gels of higher cross-linking than conventional gel resins. Typically, macroreticular resins have a much greater surface area, porosity, and pore size distribution than gel resins.¹³ The total water content of macroreticular resins is distributed between the gel and pores. The macroreticular resins summarized in Table II all give one interior water peak. Separate peaks for pore and gel phase are not observed for any macroreticular resin in any ionic form. Spectra run at high gain with different exterior solvents which do not enter a hydrated resin (benzene, cyclohexane, and 1,2-dichloroethane) did not reveal any additional resonances. The water content of Amberlite 200 H, determined *via* an nmr integral procedure,⁴ was 50%, in satisfactory agreement with a resin drying experiment, 52.7%. Porosity studies as a function of resin hydration indicate that approximately half of the total water in Amberlite 200 H is in the pores, the remainder of the water is in the gel microspheres.¹³ The distribution of water between gel and pore is not sufficiently large enough in one direction so as to escape detection and be consistent with the above water determination

experiment. Although it is difficult to obtain good integrals for Amberlite 200 Na, it is apparent that all the water is being detected.

Table II: Amberlite Macroreticular Resins-Nmr Results

Amberlite resin	Ionic form	δ , Hz	$\Delta\nu_{IN}$, Hz	$\Delta\nu_{EX}$, Hz
200	H	-67	8	6
	Na	12	9	7
252	H	-77	7	7
	Na	14	9	6
IRA-900	Cl	<i>a</i>		
	OH	-13	4	5
IRA-904	Cl	<i>a</i>		
	OH	-8	5	5
IRA-910	Cl	<i>a</i>		
	OH	-16	8	7
IRA-911	Cl	<i>a</i>		
	OH	-17	12	8
IRA-93	Weak base	<i>a</i>		

^a The chemical shift is too small to be measured.

Low-temperature (0°) nmr studies with Amberlite 200 H (exterior solvents, water and 1,2-dichloroethane) and IRA-904 (exterior solvent 1,2-dichloroethane) gave no evidence for separate pore and gel phase water resonances.

Observation of a single peak places kinetic limits on the solvent exchange rate. We assume for ease in calculation that the ratio of ionic groups on the surface of the gel phase ionized in the pores *vs.* those inside the gel is zero and that it is equally probable that any one

(13) K. A. Kun and R. Kunin, *J. Poly. Sci., Part C*, **16**, 1457 (1957).

water molecule be in either pore or gel.¹³ For this model¹⁴ the chemical shift between pore and gel will be approximately twice the observed chemical shift (Table II), 134 Hz. The solvent exchange rate is, therefore, faster than $2 \times 10^3 \text{ sec}^{-1}$ at 25°. It is entirely possible that a rapid proton exchange, and not whole molecule exchange, is mechanistically involved. However, it is pertinent to note that rapid exchange occurs independent of the ionic form of the resin.

The integral ratio of interior water to exterior water, I , for Amberlite 200 H ($I = 0.95$) results in a near equal probability of any water molecule being in either the exterior solvent or the interior of the macroreticular resin. The solvent exchange rate between exterior water and resin water is, therefore, less than 100 sec^{-1} for Amberlite 200 H and less than 20 sec^{-1} for 200 Na. The rate of exchange of water between the exterior and interior water has been reported for the gel resin Dowex 50W-8X by a double resonance technique; $k = 7.3 \times 10^{-1} \text{ sec}^{-1}$.⁹ A comparison with ¹⁸O tracer studies indicates water exchange rather than proton exchange.¹⁵ Although the effect of bead size, cross-linking and counterion have not been reported, it is probably safe to conclude that the rate of exchange between pore and gel water is orders of magnitude faster than for exterior and interior water. The most obvious single factor which might account for this very large kinetic effect is the large difference in surface area. The surface area of Amberlite 200 H is approximately $55 \text{ m}^2/\text{dry g}$, while gel resins give $<0.1 \text{ m}^2/\text{dry g}$.¹³

The chemical shift of Amberlite 200 H measured at 60 MHz, 25° and corrected for susceptibility effects on the exterior solvent was 69.5 Hz. Using the hydrogen ion chemical shift data for HCl reported by Hindman,¹⁶ the molar capacity of the resin is 3.52 M in qualitative agreement with the known value, 4.25 M (17% discrepancy). Recent similar calculations for gel resins show about a 10% negative deviation.^{7,8} We have observed virtually identical results with gel resins. A contributing factor to the low result for Amberlite 200 H can be found in the physical structure of the resin. We have assumed that the chemical shift is due to a continuous distribution of counterions in the resin and have not incorporated the fact that the counterions are virtually all in the gel phase which contains half of the total water in the resin.¹³ Therefore, the chemical shift used to calculate the capacity should be 139.0 Hz (assuming the total water is evenly distributed between pore and gel). Calculating the capacity and then allowing for rapid exchange between pore and gel gives a value of 3.74 M (12% discrepancy).

The data for a variety of other macroreticular resins summarized in Table II are similar to their gel analogs.¹ Only one interior water peak is observed for all of these resins.

Line-Width Effects. Essentially no systematic effort has been directed toward isolating the dominant

cause of the interior water line broadening in styrene-DVB resins. Gordon¹ originally suggested that the interior water line width might provide a measure of the homogeneity of the interior structure of the resin. This is an extremely important property which is at present difficult to evaluate directly.¹⁷ The following properties may contribute to the observed line width: (1) incomplete averaging (restricted motion) of dipole-dipole interactions (this is an intrabead relaxation time effect, and not a homogeneity effect); (2) heterogeneity effects caused by the distribution of resin bead sizes in the sample (interbead effect) (the observed line width is an envelope of peaks of different chemical shifts for different size beads: this would result if either the degree of sulfonation or water content was a function of bead size); (3) surface effects due to cracking and irregularities of the surface; (4) line broadening due to the difference in diamagnetic susceptibility between the two phases (resin interior and exterior solvent); (5) line broadening which reflects a measure of the homogeneity of the resin interior (intrabead effect). Any single resin bead contains a distribution of pore sizes or configurations and, consequently, a distribution of chemical environments in its interior structure.¹⁸ Solvent molecules in different pore configurations may have slightly different resonance frequencies. If there is a slow exchange between these configurations, the observed line width is an envelope of peaks of different chemical shifts for the different configurations, and the line width is a measure of the homogeneity of the resin. Intermediate rates of exchange between different configurations could further complicate this effect. If there is a rapid rate of exchange between the different configurations this effect may be masked.

The line widths of the interior and exterior water resonances are summarized in Tables II and III. The range is comparable to, although somewhat larger than, that observed by Gordon for similar resins.¹ Previous results indicate that the water line width in cation gel resins (measured at 2, 4, 8, and 12% DVB) is independent of cross-linking.¹ We have observed the same independence (measured at 5, 8, 10, and 12% DVB). Therefore, line-width effect 1 is not dominant. Samples of Amberlite IR-120 H, IR-124 Na, and 200 H were separated into the following sieve fractions: 40-50, 35-40, 30-35, 20-30, 16-20, and 16. Since no variation outside of experimental error was observed in the chemical shifts or line widths, line-width effect 2 is not

(14) J. A. Pople, W. G. Schneider, and H. J. Bernstein, "High Resolution Nuclear Magnetic Resonance," McGraw-Hill, New York, N. Y., 1961, Chapter 10.

(15) D. W. McCall and D. C. Douglass, *J. Phys. Chem.*, **69**, 2001 (1965).

(16) J. C. Hindman, *J. Chem. Phys.*, **36**, 1000 (1962).

(17) Jacob A. Marinsky, Ed., "Ion Exchange," Marcel Dekker, New York, N. Y., 1966, Chapter 6.

(18) W. Rieman III and H. F. Walton, "Ion Exchange in Analytical Chemistry," Pergamon Press, New York, N. Y., 1970, p 13.

Table III: Gel Resins—Nmr Results

Amberlite resin	Ionic form	δ , Hz	$\Delta\nu_{IN}$, Hz	$\Delta\nu_{EX}$, Hz
IR-120	H	-78	5	7
	Na	15	6	9
IR-124	Na	21	8	10
IRA-68	Free base	-12	8	8
IRA-400	Cl	<i>a</i>		
	OH	-24	6	8
IRA-410	Cl	<i>a</i>		
	OH	-30	5	8
IRA-45	Free base	<i>a</i>		

^a The chemical shift is too small to measure.

dominant.⁷ A sample of Amberlite IR-120 H was heated to 120° for various times up to 1000 min. The hot resin was immediately plunged into cold water. Samples of the starting resin and the 1000-min sample were compared under a low-power microscope. While the starting resin is virtually flawless, essentially all of the resin beads of the 1000-min sample showed some bead fracture. In no case did the line width vary, which is not consistent with line-width effect 3. The line width of Amberlite IR-120 H in a variety of inert solvents (by inert, we mean that the solvent will not enter a hydrated bead) is summarized in Table IV. The following Amberlite resins have also been studied in most of these solvents: IR-120 Na; IRA-400 Cl; IRA-410 Cl; IRA-45; 200 Na; 200 H; IRA-900 Cl; IRA-910 Cl; and IRA-93. The general trends observed for all of these resins are not significantly different from the data for Amberlite IR-120 H in Table IV. The volume susceptibility of cation styrene-DVB resins has been estimated to be approximately 0.70×10^{-6} and depends somewhat on cross-linking and ionic form.¹ The susceptibilities of the inert solvents are summarized in Table IV. The interior water line width depends on the nature of the exterior medium

Table IV: The Line Width of Interior Water and Exterior Solvent for Amberlite IR-120 and IRC-84 as a Function of the Exterior Solvent

Exterior solvent	Solvent susceptibility ^a	IRC-84		IR-120 H	
		$\Delta\nu_{IN}$, Hz	$\Delta\nu_{EX}$, Hz	$\Delta\nu_{IN}$, Hz	$\Delta\nu_{EX}$, Hz
1,2-Dichloroethane	0.757	30	4	5	4
Water	0.721	29	6	5	7
Carbon disulfide	0.69			7	
Cyclohexane	0.63	34	25	12	24
Toulene	0.62			11	25
Benzene	0.62	34	26	11	25
<i>n</i> -Hexane	0.586			15	
Air				38	

^a Volume susceptibility taken from ref 14.

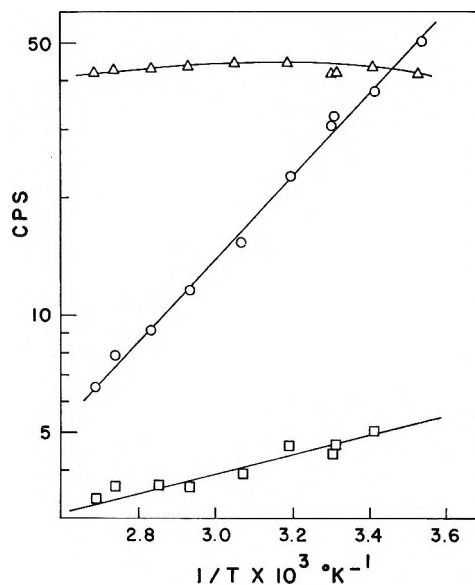


Figure 1. Summary of data for Amberlite IRC-84. The chemical shift (Δ), interior line width (O), and exterior line width (\square), as a function of reciprocal temperature.

and qualitatively parallels the susceptibility difference with the exterior medium.

Both the interior and exterior line width of Amberlite IR-120 H were studied as a function of temperature (5–90°). Very small effects which are close to experimental error were observed: $\Delta\nu_{IN} = 5.5 \pm 1$, $\Delta\nu_{EX} = 7.0 \pm 1$. At 100 MHz, the same sample used in the variable temperature experiment had an interior line width of 9 Hz and an exterior line width of 14 Hz. The variation of the chemical shift with temperature was virtually identical with that recently reported.^{7,8} These three experiments, medium dependence, temperature dependence, and field strength dependence, are in agreement with line-width effect 4. No experimental evidence has been obtained which is in any way contrary to this effect. It is difficult to conceive of an unambiguous positive experiment to test line-width effect 5. The independence on cross-linking and the dependence on exterior medium is not what one would expect for this effect. The fact that resins of grossly different physical structure (gel *vs.* macroreticular) give comparable line widths would also not be anticipated. In conclusion, it is believed that the difference in susceptibility between the two phases (line-width effect 4) is the dominant cause of the interior water line width for styrene-DVB resins. The results obtained for the exterior line widths (Table IV) indicate that they are also due to susceptibility effects as previously explained by Gordon.¹

Carboxylic Acid Resins. The data for the carboxylic acid gel cation-exchange resin Amberlite IRC-84 are summarized in Figure 1 as plots of the log of $\Delta\nu_{IN}$, $\Delta\nu_{EX}$, and δ *vs.* reciprocal temperature. The line-width data have been corrected for the natural line

width of pure water and are entirely reversible with temperature. The water content and the capacity of the resin studied were 48% and 10.6 mequiv/dry g. The water content determined from the nmr integral at 80.5 and 89.5° was 49%. Good integrals can only be obtained at elevated temperatures due to the increased line width at lower temperature. Resins of this type are less than 1% dissociated.^{12b} Ion hydration effects on the chemical shift (<2 Hz) are much too small to account for the experimental value, 42 Hz. The susceptibility correction for the exterior solvent is less than 1.0 Hz and is not the cause of the chemical shift. Dispersion interactions with the polymer matrix can effect the chemical shift; however, it seems quite unlikely that this would account for this large an effect, in view of the results obtained for other systems.¹ In the sodium form, the interior line width is comparable to other resins, $\Delta\nu_{IN} = 4$ Hz, $\Delta\nu_{EX} = 6$ Hz. Sieve cut samples, 16–20, 20–30, 30–40, did not give significantly different line widths or chemical shifts. Medium effects are summarized in Table IV. The exterior line-width variation with solvent is similar to Amberlite IR-120 H and other resins and presumably has the same origin. The relative variation of the interior line width is almost an order of magnitude less than that typically observed. A sample of Amberlite IRC-84, heated as previously described, and immediately

plunged into cold water, did not show any spectral data variation. The data in Figure 1 show that: (1) the chemical shift is virtually independent of temperature in opposition to the results for Amberlite IR-120 H;^{7,8} (2) the exterior water line width shows a comparable effect to Amberlite IR-120 H; (3) the interior water line width gives a reasonable activation energy plot, $E_A = 4.9$ kcal, which is considerably greater than Amberlite IR-120 H. The high-temperature line width of Amberlite IRC-84 is comparable to Amberlite IR-120 H. It is apparent that the observation of a line width at one temperature does not independently imply anything about the homogeneity of the resin.⁴

Line-width effects 2–4 are not consistent with the variable temperature results and other results just described. Line-width effect 5 is unlikely because: (1) a smaller temperature dependence would be expected for no exchange conditions; (2) the line width of the sodium form indicates that the results are unique for the hydrogen form. Line-width effect 1 is unlikely because the sodium form is comparable to other resins, and there is no apparent reason why incomplete dipole-dipole interactions should be important in high water content resins. The dominant cause of the chemical shift and line width probably results from an interaction between the carboxylic acid group and water. The details of this interaction are still obscure.

Infrared Study of the Surface of Titanium Dioxides.

I. Hydroxyl Groups

by Michel Primet, Pierre Pichat, and Michel-Vital Mathieu

Institut de Recherches sur la Catalyse, C.N.R.S., Villeurbanne, 69, France
(Received June 22, 1970)

Publication costs assisted by the Institut de Recherches sur la Catalyse, C.N.R.S.

The stretching frequencies of the OH groups of anatase and rutile have been tentatively related to the positions of these groups in the crystal lattices. Exchange of these OH groups with D₂O vapor or D₂ gas has been examined by infrared spectrometry. All the hydroxyl groups are found to be exchangeable with D₂O. Depending on the temperature, D₂ acts as either an exchange or a reducing agent. In order to explain the results of the dehydroxylation-rehydroxylation cycles, the formation of incompletely coordinated titanium atoms is proposed. This formation is confirmed by the ionization of perylene.

Introduction

The present papers complete our study of the surface properties of the titanium dioxides by means of infrared spectrometry.¹⁻⁷ In this part, an attempt is made to relate the hydroxyl groups previously observed² to the possible positions on the most likely cleavage planes of the crystals. Then we examine the deuteration of these groups with heavy water vapor or deuterium gas in order to find out whether they are on the surface or in the bulk. Finally, mechanisms are proposed to explain the dehydroxylation-rehydroxylation experiments.

Experimental Section

Materials. Miscellaneous data on the titanium dioxides used in this work are summarized in Table I and Figure 1. The surface areas were measured by the BET method using N₂ at 78°K. The losses of weight were registered with a Sartorius Balance, Type Electrono 1, Model Vacuum. The size of the particles, as determined by electron microscopy, was 80-120, 100-250, and ca. 500 Å for A₁, A₃, and R₁ samples, respectively. It should be noticed that the particles are not spherical and that some of them are cubic.

Oxygen (99.98%) and deuterium (99.98%) were supplied by the Air Liquide Co. (France), and dried by passage through traps cooled to 78°K and containing Linde 5A-type zeolite. Deuterium oxide (Commissariat à l'Énergie Atomique, France) of purity 99.78% was used, *in vacuo*, without further treatment other than the removal of permanent gases.

Techniques. Most of the experimental procedures have been described elsewhere.^{7,8} To reduce the light scattering, the TiO₂ samples were pressed into thin wafers 18 mm in diameter and 20-50 mg in weight. Infrared spectra were recorded on a Perkin-Elmer Model 125 grating spectrophotometer after the cooling

of the solid to room temperature. This instrument was continuously flushed with air from which the H₂O and CO₂ were removed. The reference beam was attenuated. The spectral slit width was less than 2 cm⁻¹. The spectrometer was calibrated against known standards.

The experimental conditions of the epr measurements for the ions perylene⁺ 9 and Ti³⁺ 10 have already been given.

Results and Discussion

(A) *Positions of the OH Groups in the Lattices of Anatase and Rutile.* We have recently carried out an infrared study of the dehydration of anatase and rutile.² The stretching frequencies of the OH groups observed after evacuation at 200° are listed in Table II (1st row). These groups are removed by evacuation at the temperature given in the second row of Table II. Figure 2 shows typical changes of the intensities of the OH infrared bands as a result of dehydroxylation. For anatase A₃, the 3410-cm⁻¹ band is due to the presence of rutile in this sample (Table I), and the band at ca. 3660 cm⁻¹ is likely to be ascribable to the superposition of the

(1) M. Primet, P. Pichat, M. V. Mathieu, and M. Prettre, *C. R. Acad. Sci. Ser. B*, **265**, 681 (1967).

(2) M. Primet, P. Pichat, and M. V. Mathieu, *ibid.*, **267**, 799 (1968).

(3) M. Primet, J. Bandiera, C. Naccache, and M. V. Mathieu, *J. Chim. Phys.*, **67**, 535 (1970).

(4) M. Primet, J. Bandiera, C. Naccache, and M. V. Mathieu, *ibid.*, **67**, 1030 (1970).

(5) M. Primet, M. Che, C. Naccache, M. V. Mathieu, and B. Imelik, *ibid.*, **67**, 1629 (1970).

(6) M. Primet, J. Basset, M. V. Mathieu, and M. Prettre, *J. Phys. Chem.*, **74**, 1860 (1970).

(7) M. Primet, Thesis, Lyon, France, 1970.

(8) M. V. Mathieu and P. Pichat in "La Catalyse au Laboratoire et dans l'Industrie," Masson et Cie, 1967, pp 319-323.

(9) Y. Kodratoff, C. Naccache, and B. Imelik, *J. Chim. Phys.*, **65**, 562 (1968).

(10) M. Che, C. Naccache, B. Imelik, and M. Prettre, *C. R. Acad. Sci. Ser. C*, **264**, 1901 (1967); M. Che, Thesis, Lyon, France, 1968.

Table I: TiO₂ Samples

Solid	Preparation	Crystalline structure	Metallic impurities (traces)	Loss (% of the weight at 25°)	
				Between 25 and 200°	Between 25 and 400°
Anatase A ₁	II ^{a,b}	Crystallized	Mg, Si, Al, Fe	1.85	2.85
Anatase A ₂	II ^{a,c}	Very badly crystallized	Na, Mg, Al, Sn, Si	4.85	5.85
Anatase A ₃ (Degussa, Frankfurt am Main)	I ^{a,b}	Crystallized anatase with 10–15% of rutile	Mg, Si, Al, Sn, Cu	0.40	0.50
Rutile R ₁ (British Titan Products)	III ^{a,d}	Crystallized	Na, Mg, Fe, Al, Sn, Pb, Cu	0.32	0.40
Rutile R ₂	IV ^a	Very badly crystallized	Na, Mg, Fe	3.80	4.30

^a Preparation: method of the flame reactor (I); hydrolysis of TiCl₄ with NaOH (II, IV) or NH₄OH (III). ^b J. Long and S. J. Teichner, *Rev. Hautes Temp. Refract.*, **2**, 47 (1965); J. Long and S. J. Teichner, *Bull. Soc. Chim. Fr.*, 2625 (1965). ^c See ref 10. ^d See ref 12.

Table II: Stretching Frequencies of the OH and OD Groups of the TiO₂ Samples

$\nu(\text{OH}), \text{cm}^{-1}$	Anatase A ₁ , A ₂		Rutile R ₁ , R ₂			Anatase A ₃			
	3715	3665	3685	3655	3410	3715	3685	3660	3410
$T, ^\circ\text{C}$	400	350	400	350	200–250	400	400	350	200–250
$\nu(\text{OD}), \text{cm}^{-1}$	2740	2705	2720	2695	2515	2740	2720	2700	2515

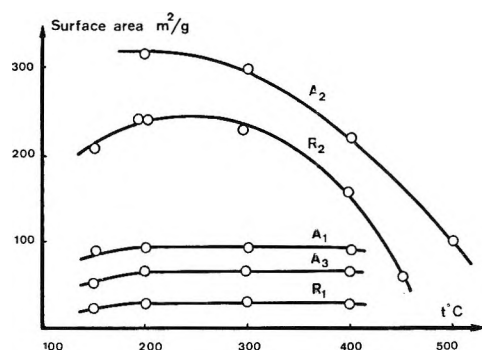


Figure 1. Surface area of the various TiO₂ samples according to the temperature of the vacuum treatment.

3665-cm⁻¹ band of anatase and the 3655-cm⁻¹ band of rutile.

Previous to our study, Yates,¹¹ Lewis, and Parfitt¹² suggested that the OH groups they found for titanium dioxides were probably due to different cleavage planes or to different positions on these planes, but without detailed information. Besides, none of these authors noticed a 3410-cm⁻¹ band in the case of rutile. It therefore seemed of interest to examine whether the stretching frequencies we observed could be related to particular positions of the OH groups in the crystal lattices.

We have supposed that the most likely cleavage planes of the titanium dioxides are the 001 plane for the anatase and the 110 plane for the rutile, since these planes correspond to the highest atomic density and to the greatest interreticular distance.

Having made this assumption, the five OH frequen-

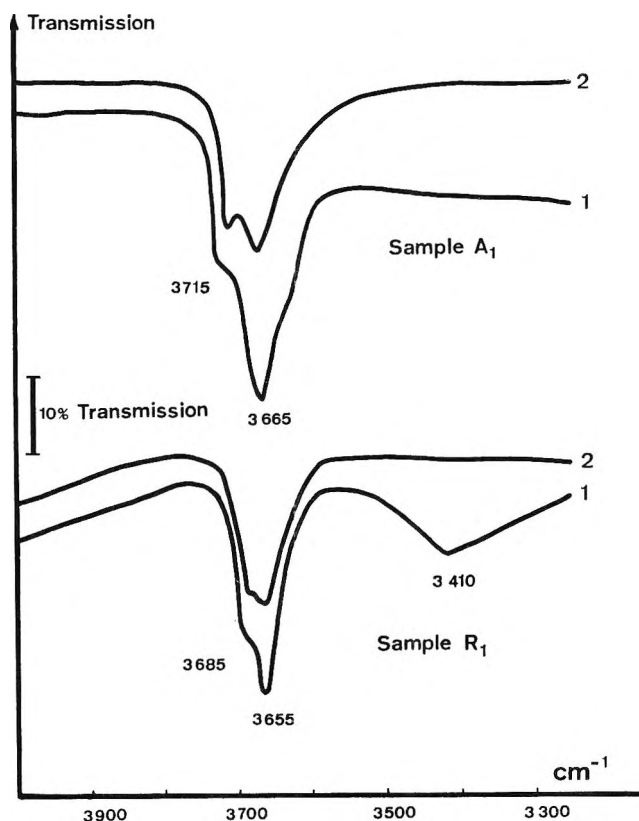


Figure 2. OH bands of the anatase A₁ or the rutile R₁ after evacuation for 20 hr: 1, at 200°; 2 at 300°. For clarity, the spectra have been translated along the transmission axis.

(11) D. J. C. Yates, *J. Phys. Chem.*, **65**, 746 (1961).

(12) K. E. Lewis and G. D. Parfitt, *Trans. Faraday Soc.*, **62**, 204 (1966).

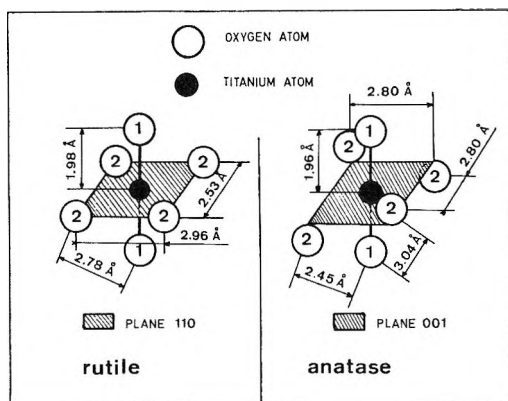


Figure 3. Interatomic distances in anatase and rutile.

cies can be assigned by putting all hydroxyl groups in the place of the oxygen atoms labeled 1 of Figure 3. Depending on the degree of dehydroxylation these surface OH groups in position 1 occur in two configurations, one in which they are on adjacent sites and one in which they are isolated from each other. The OH groups responsible for the bands at 3715 cm^{-1} (anatase) and 3685 cm^{-1} (rutile) are presumed to be isolated. The bands at 3665 cm^{-1} (anatase) or 3655 and 3410 cm^{-1} (rutile) are assumed to originate from OH groups bonded to each other by hydrogen bridges and situated in adjacent unit cells.

The following arguments show that the observed frequencies are in reasonable agreement with these tentative models and assignments.

The low-frequency bands (3665 , 3655 , and 3410 cm^{-1}) are removed from the spectra by evacuation at elevated temperature before the high-frequency bands (3715 and 3685 cm^{-1}); see Table II and Figure 2. This suggests that the former are involved in hydrogen bonding and are therefore more favorably situated for removal from the surface as water.¹³

Moreover, the OH stretching vibrations situated above 3700 cm^{-1} are generally assigned to "free" hydroxyl groups in the case of metallic oxides of high surface area.¹³ The very similar behavior of the bands at 3715 and 3685 cm^{-1} during the dehydroxylation² strongly suggests that the OH groups responsible for this latter band are isolated as well, although their stretching vibration is 30 cm^{-1} lower. This difference shows that the force constant of the O-H bond is greater for anatase than for rutile and this fact implies that the hydroxylic hydrogen atom is more protonic for the former than for the latter, since in the case of the hydracids the force constant of the X-H bond increases with the ionic character of the bond. The environment of the OH groups in the two allotropic forms can explain this hypothesis. For anatase, the oxygen atoms labeled 2 (Figure 3) are closer to the OH groups labeled 1 (2.45 \AA) than for rutile (2.78 \AA). These electronegative oxygen atoms are more likely to increase the electron density of the hydroxylic oxygen by polar-

izing the OH bond and hence the hydrogen atom tends toward a proton-like state.

The neighboring OH groups are separated by 2.80 \AA for anatase or 2.96 and 2.53 \AA for rutile (Figure 3). Therefore, one or two infrared bands are expected in the case of anatase and rutile, respectively, which is in agreement with our spectra. In order to find out whether the distances (O...O) concord with the OH frequencies, we have listed these distances in Table III along with the differences $\Delta\nu_{\text{obsd}}$ between the wave numbers of the isolated OH groups (3715 or 3685 cm^{-1}) and those of the hydrogen-bonded OH groups (3665 or 3655 and 3410 cm^{-1}). The same differences have been calculated for crystals, using a correlation diagram¹⁴⁻¹⁶ and are given in the 3rd column, $\Delta\nu_{\text{calcd}}$. It should be noted that $\Delta\nu_{\text{obsd}}$ are much lower than $\Delta\nu_{\text{calcd}}$ but this is usually the case if solids of high surface area are compared to crystals.¹³ In addition $\Delta\nu_{\text{calcd}}$ are for straight hydrogen bonds, whereas the hydrogen bonds in TiO_2 are probably bent. Nevertheless it is interesting to note that the ratios $\Delta\nu_{\text{calcd}}/\Delta\nu_{\text{obsd}}$ (4th column) are nearly constant.

Table III: Frequencies Shifts of the Hydrogen-Bonded OH Groups According to the (O...O) Distance

Samples	(O...O) distance, Å	$\Delta\nu_{\text{obsd}}$, cm^{-1}	$\Delta\nu_{\text{calcd}}$, ^a cm^{-1}	$\Delta\nu_{\text{obsd}}/\Delta\nu_{\text{calcd}}$
Rutile	2.96	30	150 ^b	5
Anatase	2.80	50	260 ^c	5.2
Rutile	2.53	275	1360 ^d	4.9

^a These values are obtained from the spectra of crystalline compounds presenting hydrogen bond lengths close to those found for TiO_2 . ^b See ref 14. ^c See ref 15 and 16. ^d See ref 16.

(B) *Deuteration of the OH Groups. 1. With D₂O Vapor.* The action on a rutile sample of D₂O in air at a very low relative pressure has been examined by Lewis and Parfitt¹² but the exchange of the OH groups of several TiO_2 samples by pure deuterium oxide has not been studied previously.

At room temperature with increasing doses of D₂O vapor, all the infrared bands due to OH groups decrease in intensity, whereas the corresponding set of OD bands appears (Table II, 3rd row). In these experimental conditions, no difference was found between the OH groups. With an excess of D₂O vapor, an addi-

(13) L. H. Little, "Infrared Spectra of Adsorbed Species," Academic Press, London and New York, N. Y., 1966, Chapter X.

(14) K. Nakamoto, M. Margoshes, and R. E. Rundle, *J. Amer. Chem. Soc.*, **77**, 6480 (1955).

(15) O. Glemser and E. Hartert, *Z. Anorg. Allg. Chem.*, **283**, 22 (1958).

(16) G. C. Pimentel and C. H. Sederholm, *J. Chem. Phys.*, **24**, 41 (1956); G. C. Pimentel and A. L. McClellan, "The Hydrogen Bond," Reinold, London and New York, N. Y., 1960, Chapter III.

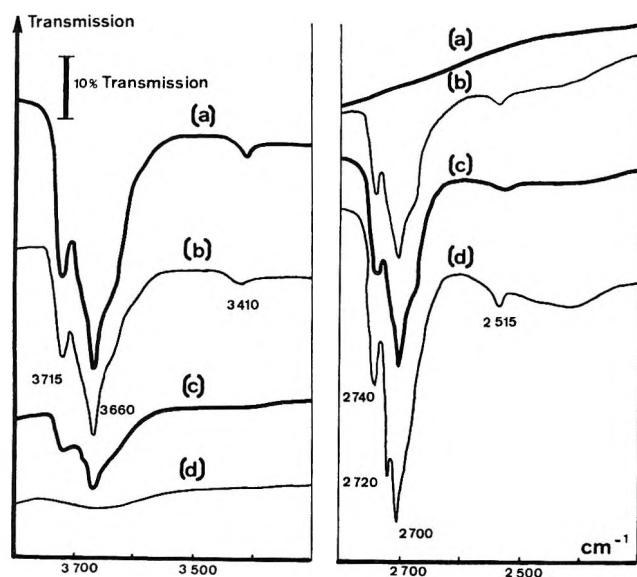


Figure 4. Exchange of the hydroxyl groups. Infrared absorption spectra of $\text{TiO}_2 \text{ A}_3$, heated in 100 Torr of H_2 at 200° for 10 hr, outgassed at 200° for 8 hr, heated in 100 Torr of D_2 for 10 hr at: (a) 25° ; (b) 100° ; (c) 200° ; and (d) 250° . For clarity, the spectra have been translated along the transmission axis.

tional OD stretching band is observed at 2675 cm^{-1} which is the equivalent of the 3630-cm^{-1} band due to adsorbed water molecules² and is similarly removed by evacuation at 100° . In each case, the value of the ratio $\nu(\text{OH})/\nu(\text{OD})$ is 1.355.

Three or four successive deuteration at 25° are necessary to complete the exchange, the solid being desorbed for 1 hr at 150° before each new addition of D_2O . It may be concluded that all the OH groups are accessible to D_2O vapor.

2. *With D_2 .* Yates,¹¹ Lewis, and Parfitt¹² have already studied the exchange of the OH groups of TiO_2 samples with D_2 at 350 and 250° , respectively. We were interested in finding out at what temperature the exchange begins and whether the mechanism of exchange is the same at low and high temperatures. The possible reduction of the solid was followed by epr measurements.

When a 50-mg TiO_2 sample, previously treated at 200° under H_2 then under vacuum, is exposed to deuterium gas (100 Torr) at various temperatures, OD stretching bands appear in the spectrum of the solid from 100° (Figure 4b). Their frequencies are the same as those observed with D_2O exchange. At 150° , it becomes possible to detect HD molecules in the gas phase by means of mass spectrometry. Finally, at 200° , most of the OH groups are exchanged.

Thus, between 100 and 200° , the exchange of D_2 with the hydroxyl groups of titanium dioxide is an activated process similar to the one observed for alumina¹⁷ and all the different types of OH groups seem to be exchanged at the same rate. Deuterium gas is the actual ex-

change agent, since the sample has been previously reduced by H_2 , so that the formation of D_2O is excluded.

Between 250 and 300° , the solid is reduced by D_2 as is shown by the detection of the epr signal of the Ti^{3+} ion. The absorption of the resulting D_2O molecules produces the appearance of broad bands in the OD stretching region ($2500\text{--}2100 \text{ cm}^{-1}$) (Figure 4d). Moreover, the exchange of OH groups is completed by heavy water. A slight reduction was observed by Yates¹¹ in the case of only one among four of his TiO_2 samples, but this reduction was merely determined by a color change.

These results confirm that the OH groups are easily exchangeable.

(C) *Dehydroxylation-Rehydroxylation Cycles.* Previously, Lewis and Parfitt¹² rehydrated a rutile sample with humid air, but it was impossible to "decide whether reformation of OH groups actually takes place."

In order to attempt to answer this uncertainty, increasing doses of pure water vapor were added on completely dehydroxylated samples (evacuated at 400°). Dehydroxylation-rehydroxylation cycles were also carried out.

Results

The rehydroxylation depends on the crystallinity of the solids.

Solids with a High Percentage of Amorphous Phase. Initial groups are not restored on amorphous anatase or rutile after exposure to 20 Torr of H_2O , even at 400° . On the spectra there occur only broad bands of hydrogen-bonded OH groups which are removed by evacuation between 150 and 200° .

Crystallized Solids. At room temperature, initial OH bands readily reappear in an inverted order relative to that of their removal. So in the case of anatase, the 3715-cm^{-1} band occurs before the 3665-cm^{-1} band, but later, the intensity of the second one becomes the greatest. For rutile, the 3685 , 3655 , and 3410-cm^{-1} bands are observed.

By evacuation the rehydrated solids are completely dehydroxylated at a lower temperature than the initial titanium dioxides, $300\text{--}350^\circ$ instead of $350\text{--}400^\circ$. Reformed OH groups on a twice dehydrated sample are removed by outgassing at 300° . If the dehydration-rehydration cycles are repeated ten times, no more specific OH groups are reformed. As for the amorphous titanium dioxides only broad bands of hydrogen-bonded OH groups occur on the spectra and they are eliminated by evacuation at 150° .

Discussion

The existence of only a small number of well defined crystalline sites on titanium dioxides with a high percentage of amorphous phase may account for the fact

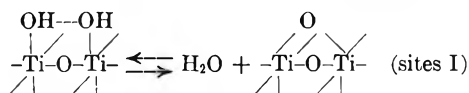
(17) J. L. Carter, P. J. Lucchesi, P. Corneil, D. J. C. Yates, and J. H. Sinfelt, *J. Phys. Chem.*, **69**, 3070 (1965).

that the reformation of initial groups does not take place. The specific sites are likely to be destroyed during the dehydroxylation.

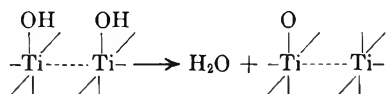
The dehydroxylation of crystallized TiO_2 is only partly reversible. Similar phenomena have already been observed for rutile and hematite.¹⁸ The decrease in surface area of the TiO_2 during the dehydration-rehydration cycles does not seem a sufficient explanation of this incomplete rehydroxylation, since only a 20% decrease is measured after ten cycles.

This leads to the assumption that dehydroxylation eliminates some of the dissociative adsorption sites of water molecules. To understand this change of the surface properties, the mechanisms of dehydration and rehydration need to be examined.

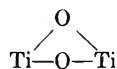
As has been shown, dehydroxylation first removes the hydrogen-bonded OH groups responsible for the bands at 3410, 3655 (rutile), and 3665 cm^{-1} (anatase). The following scheme may account for this removal



At higher temperature, a migration of protons or hydroxyl groups could allow the removal of isolated OH groups and formation of incompletely coordinated titanium atoms (sites II)



Whereas the sites I would be able to chemisorb H_2O molecules with subsequent reformation of the initial OH groups (probably with proton or hydroxyl migration), the sites II would fix only coordination-bonded water molecules which would be removed by evacuation at 150°. After each new dehydroxylation, the number of incompletely coordinated titanium atoms increases at the expense of the following type of bridge.



If our assumption of the formation of incompletely coordinated titanium atoms is correct, the dehydroxylated TiO_2 will present an electron-acceptor surface.

To check this character of the surface we investigated the adsorption of electron-donor molecules. Adsorption of CO^3 and NO^5 at room temperature is described elsewhere. Here the ionization of perylene is briefly reported.

Perylene has been chosen for its relatively low ionization potential (6.8 eV) which allows this compound to be ionized by oxidizing surface centers, giving rise to a paramagnetic species.¹⁹ Perylene is not ionized by anatase A_3 which has undergone only one dehydration treatment, but after three dehydration-rehydration cycles, the epr signal of the perylene cation is observed and its intensity grows with the number of cycles, giving proof of an increasing number of electron-acceptor sites.

Conclusions

1. The five stretching frequencies of the OH groups of anatase and rutile have been tentatively related to the positions of these groups in the crystalline lattices. Assuming that the cleavage planes are the 001 plane (anatase) or the 110 plane (rutile), it is suggested that the isolated hydroxyl groups have stretching frequencies at 3715 (anatase) or 3685 cm^{-1} (rutile). The bands at 3665 (anatase), 3655, and 3410 cm^{-1} (rutile) are assigned to OH groups bonded to each other by hydrogen bridges corresponding to 2.80, 2.96, and 2.53 Å ($\text{O} \cdots \text{O}$) distances, respectively.

2. All the OH groups of the TiO_2 studied are accessible to D_2O vapor.

3. Between 100 and 200° they are almost completely exchanged with D_2 gas. Between 250 and 300°, D_2 reduces the titanium dioxides with formation of D_2O and Ti^{3+} .

4. Partial rehydroxylation could be explained by the formation of an increasing number of incompletely coordinated titanium atoms during the dehydroxylation-rehydroxylation cycles. These incompletely coordinated titanium atoms are supposed to be the electron-acceptor sites responsible for the perylene ionization.

(18) T. Morimoto, M. Nacao, and F. Tokuda, *J. Phys. Chem.*, **73**, 243 (1969).

(19) D. M. Brouwer, *J. Catal.*, **1**, 372 (1962).

Infrared Study of the Surface of Titanium Dioxides.

II. Acidic and Basic Properties

by Michel Primet, Pierre Pichat, and Michel-Vital Mathieu*

Institut de Recherches sur la Catalyse, C.N.R.S., Villeurbanne, 69, France
(Received June 22, 1970)

Publication costs assisted by Institut de Recherches sur la Catalyse, C.N.R.S.

For samples of anatase and rutile, the adsorption of three acidic compounds (CH_3COOH , $\text{C}_6\text{H}_5\text{OH}$, CO_2) and three basic compounds (NH_3 , $\text{C}_5\text{H}_5\text{N}$, $(\text{CH}_3)_3\text{N}$) has been studied. $\text{C}_6\text{H}_5\text{OH}$ is too weak an acid to react with the basic OH groups, but CO_2 forms bicarbonate species. Some OH groups of anatase show a protonic character toward $(\text{CH}_3)_3\text{N}$, but not toward NH_3 and $\text{C}_5\text{H}_5\text{N}$. No acidic character has been detected for the same groups of rutile. The adsorptions of ammonia and pyridine give evidence of two types of Lewis acid sites. The strongest ones are created by the removal of the isolated OH groups and their acidic force is similar to that found for a δ -alumina. The weakest ones are due to the removal of molecular water.

Introduction

It is well known that the hydroxyl groups of some metal oxides are at the origin of the acidic or basic properties of these solids. Besides, in some cases, the removal of these groups creates Lewis acid sites.

Actually the formation of the radical ions (TCNE^- and $(\text{TNB})^-$) during the adsorption of tetracyanoethylene and trinitrobenzene on an anatase sample has been assumed to be partly due to the presence of OH^- ions.¹ On the other hand, Hermann and Boehm² found that the surface of TiO_2 is amphoteric in character and that some of the OH groups of anatase react as a relatively strong acid.

Moreover it is possible to predict that the incompletely coordinated titanium atoms remaining after the dehydroxylation (see part I, the preceding paper³) can behave as Lewis acid centers. Precisely, Kiselev and Uvarov⁴ have shown, by means of infrared spectrometry, that diethylenetriamine and pyridine are adsorbed on the aprotic acid centers of a rutile sample, but no attempt has been made to find out the origin of these centers.

It therefore seemed of interest to specify the acidic and basic properties of the titanium dioxides by using infrared spectrometry to determine the structure of the species created during the adsorption of several acids and bases.

Experimental Section

Most of the experimental procedures and information about the titanium dioxides used in the present work have been given in the preceding paper.³ All the solid samples were oxygen (160 Torr) treated at 400° for 16 hr, then evacuated (10^{-5} Torr) at the indicated temperature for 8 hr.

Acetic acid (Prolabo R.P., France) was dried by mixing with acetic anhydride. Phenol (Prolabo R.P.)

was purified by successive distillations. CO_2 (99.98%) was supplied by the Air Liquide Co. (France) and dried by successive distillations. Pyridine and trimethylamine (Merck, spectra grade) were dried over Linde 5A-type zeolite at 25°. Ammonia (99.96%) supplied by the Air Liquide Co. was stored over sodium wire.

Results and Discussion

Adsorption of Acidic Compounds. A. 1. Acetic Acid. When acetic acid (10 Torr) is added at room temperature to a 200°-evacuated anatase A₃ sample (for the designation of the TiO_2 samples, see Table I), the spectrum of the surface OH groups is strongly changed. A very broad absorption band occurs due to the hydrogen-bonded OH which is removed by evacuation at 200° leaving a completely dehydroxylated surface. After this evacuation, the spectrum presents the characteristic bands of acetate species at 1555 (ν_{CO} asym), 1450 (δ_{CH} , asym), 1410 (ν_{CO} sym), and 1340 cm^{-1} (δ_{CH_3} sym)⁵ and is quite similar to the one obtained in the same conditions but with an initially totally dehydroxylated catalyst (400°-evacuated). The formation of acetates can thus be interpreted by assuming a dissociative adsorption of the acetic acid on the Ti-O-Ti bridges created during the dehydroxylation.³ Similar infrared bands have been pointed out for a rutile sample by Kiselev and Uvarov.⁴

The dehydroxylation of the solids during the desorption of the acetic acid can be explained in two ways, either by formation of hydrogen bonds between the

(1) M. Che, C. Naccache, and B. Imelik, *J. Catal.*, in press.

(2) M. Hermann and H. P. Boehm, *Z. Anorg. Allg. Chem.*, **368**, 73 (1969).

(3) Part I of the present paper: M. Primet, P. Pichat, and M. V. Mathieu, *J. Phys. Chem.*, **75**, 1216 (1971).

(4) A. V. Kiselev and A. V. Uvarov, *Surface Sci.*, **6**, 399 (1967).

(5) K. Itoh and H. J. Bernstein, *Can. J. Chem.*, **34**, 170 (1956).

Table I: TiO₂ Samples

Solid	Preparation	Crystalline structure
Anatase A ₁	I ^a	Crystallized
Anatase A ₂	II ^a	Very badly crystallized
Anatase A ₃ (Degussa, Frankfurt am Main)	I ^a	Crystallized anatase with 10–15% of rutile)
Rutile R ₁ (British Titan Products)	III ^a	Crystallized
Rutile R ₂	IV ^a	Very badly crystallized

^a Preparation: method of the flame reactor (I); hydrolysis of TiCl₄ with NaOH (II, IV) or NH₄OH (III).

acetic acid molecules and the surface OH groups with further removal of these hydroxyl groups as in the case of basic adsorbates (to be discussed later), or by an acid-base reaction between this acid and the basic OH groups, if they exist. The reaction of the acetic is too strong and does not allow the specification of the character of the surface OH groups. Thus the adsorption of a weaker acid, phenol, was studied.

2. *Phenol.* The adsorption of phenol has little effect on the OH groups of a 200°-evacuated TiO₂ if the pressure remains lower than 1 Torr. Under the vapor pressure at room temperature, broad bands of hydrogen-bonded OH groups are substituted for the bands of the initial surface OH groups. All of these OH groups are removed by evacuation at 200°, except those accounting for the 3410-cm⁻¹ band³ (rutile) which do not react with phenol.

The adsorbed phenol gives two bands at 1592 and 1490 cm⁻¹ due to ring vibrations (Figure 1B, curve b). These bands are slightly shifted relative to that of phenol vapor.⁶

From the above results, it may be concluded that the phenol is fixed on the surface hydroxyl groups by hydrogen bonds. An acid-base reaction between the phenol and these OH groups will produce phenate species and no such species is detected in the case of a hydroxylated surface.

On the contrary, a 1448-cm⁻¹ band which occurs with completely dehydroxylated TiO₂ (Figure 1A, curve b and 1B, curve c) under a weak pressure of phenol at 25° is assigned to the creation of a phenate species, since we found a similar band at 1428 cm⁻¹ in the spectrum of the sodium phenate. This 1448-cm⁻¹ band appears and progressively grows with the temperature if a 200°-evacuated TiO₂ is heated in a phenol atmosphere, while simultaneously the dehydroxylation of the surface takes place. These conditions of appearance suggest that the phenate species are due to the dissociative adsorption of the phenol on the Ti-O-Ti bridges created during the dehydroxylation. The same type of adsorption has been demonstrated for benzylic and isobutylic alcohols on γ -alumina.⁷ The

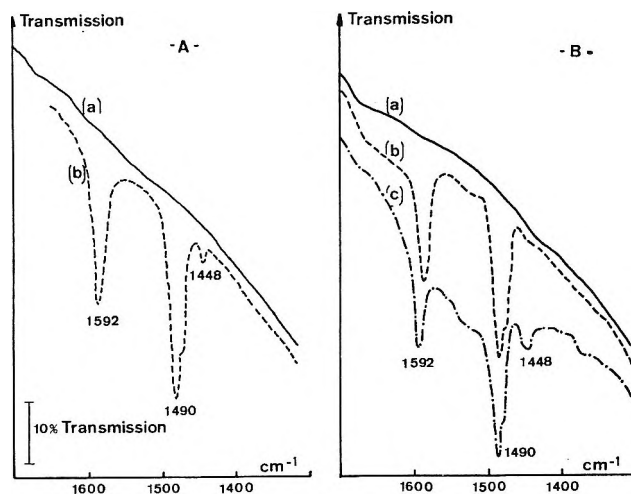


Figure 1. Phenol adsorption: A (a) infrared spectra of rutile R₁, dehydroxylated at 380°; (b) after admitting 1 Torr of phenol at 25°; B, (a) infrared spectra of rutile R₁, evacuated at 200°; (b) after admitting 1 Torr of phenol at 25°, (c) sample (b) after evacuation at 200°, then admitting 1 Torr of phenol at 25°. Note: for clarity, in Figures 1–7, the spectra have been translated along the transmission axis.

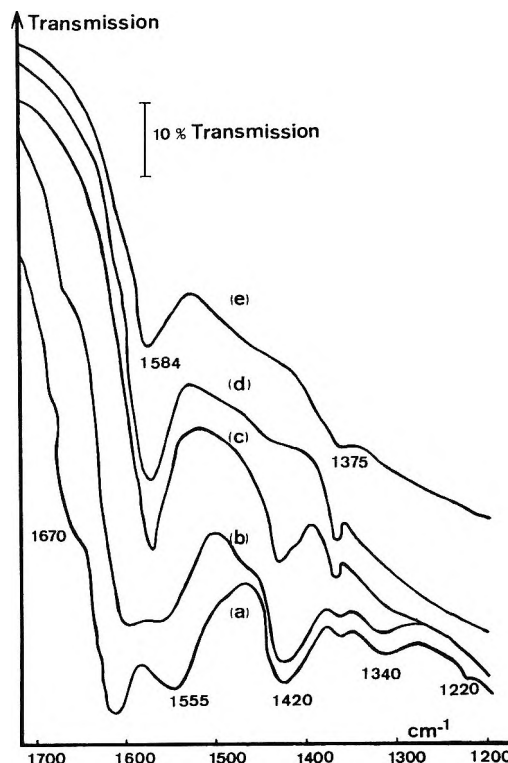


Figure 2. CO₂ adsorption. Infrared spectra after admitting 100 Torr of CO₂ at 25° on a TiO₂ A₃ previously evacuated at (a) 25, (b) 100, (c) 250, (d) 300, and (e) 400°.

1592, 1490, and 1448-cm⁻¹ bands are removed by evacuation at ca. 250°.

(6) J. C. Evans, *Spectrochim. Acta*, **16**, 1382 (1960); S. Pinchas, D. Sadeh, and D. Samuel, *J. Phys. Chem.*, **69**, 2259 (1965).

(7) H. Knozinger, H. Buhl, and E. Röss, *J. Catal.*, **12**, 121 (1968).

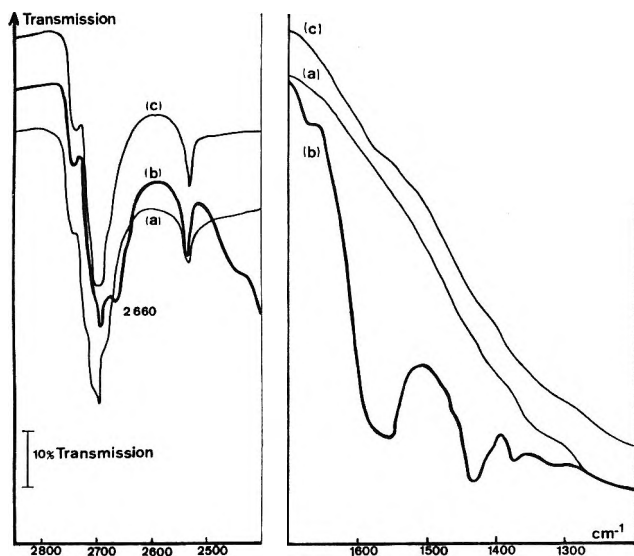


Figure 3. CO_2 adsorption. Infrared spectra of $\text{TiO}_2 \text{ A}_2$ deuterated with D_2O at 25° and (a) evacuated at 200° ; (b) after admitting 350 Torr of CO_2 at 25° ; (c) sample (b) evacuated at 25° .

Therefore, phenol seems to be too weak an acid to react with the basic surface OH groups if they exist.

3. Carbon Dioxide. At room temperature, CO_2 (100–300 Torr) is reversibly adsorbed on titanium dioxide. The intensity of the observed infrared bands increases with the adsorbate's pressure and the nature of the created species varies with the temperature of the initial treatment of the catalyst.

When the solid is completely dehydroxylated, the bands are similar to those reported by Yates.⁸ But in the case of a sample evacuated below 100° (Figure 2, curves a and b), CO_2 produces another set of bands at 1670 (shoulder), 1555, 1420, 1340, and 1220 cm^{-1} .

Carboxylate groups and carbonate groups of different types absorb in the same region, as well as bicarbonate groups.⁹ As this set of bands is only present on the spectra of hydroxylated TiO_2 , one may assume that it is due to bicarbonate species. If this assumption is correct, the stretching and bending vibrations of the OH groups of the bicarbonate species should be observed. The weak band at 1220 cm^{-1} may be assigned to the $\delta(\text{OH})$ vibration.¹⁰ If it exists, the $\nu(\text{OH})$ band is not distinguishable from the combination bands of the gaseous CO_2 which are centered at 3609 and 3716 cm^{-1} . To avoid this overlapping of infrared bands, deuterated samples have been used. When carbon dioxide is adsorbed on such samples, a new OD band appears at 2660 cm^{-1} (Figure 3); its intensity increases with the pressure of the reagent at the expense of the bands of the free or weakly bonded OD groups. This band disappears by outgassing at 25° . The 1220-cm^{-1} band does not occur on a deuterated solid; hence its assignment to a bicarbonate $\delta(\text{OH})$ vibration is strengthened.

The corresponding OH band to the 2660-cm^{-1} band would be at *ca.* 3605 cm^{-1} as the ratio $\nu(\text{OH})/\nu(\text{OD})$ is

1.355 for the TiO_2 studied here.³ This last wave number needs to be compared to the frequencies of the OH stretching vibration in bicarbonates. In alkaline bicarbonates,¹¹ where OH groups are hydrogen-bonded, this vibration occurs near 2600 cm^{-1} ; the corresponding frequency of the free OH group can be calculated from the hydrogen bond length with a correlation diagram.¹² For example, a 2.61 \AA ($\text{C}\cdots\text{O}$) distance in $(\text{KHCO}_3)_2$ gives¹³ 3670 cm^{-1} for the stretching frequency of the free hydroxyl group. This value differs very little from that calculated for the adsorbed species on TiO_2 (3605 cm^{-1}). The same frequency has been found by Parkyns¹⁴ for bicarbonate species on alumina.

The influence of CO_2 on the OD bands of the deuterated solid and the formation of new OD groups give support to the assumption of the creation of bicarbonate species. However, the 1555-cm^{-1} band is shifted from the most common region of absorption of bicarbonates,¹¹ but these alkaline bicarbonates are bonded together into rings or chains,^{13,15} which is probably not the case on TiO_2 . On the other hand, the surface affects the adsorbed species and that may also account for the observed shift.

The formation of bicarbonate species indicates the presence of basic OH groups on anatase or rutile. This basic character of the surface is rather weak, since these bicarbonate species are destroyed by mere outgassing at 25° . On the contrary, acetic acid reacts too strongly so that the intermediate species are not detected.

(B) Adsorption of Basic Compounds. 1. Ammonia.

(a) Adsorption on the OH Groups. The initial OH bands of a 200° -evacuated TiO_2 disappear after the introduction at room temperature of ammonia (Figure 4, curve b). The formation of $\text{OH}\cdots\text{N}$ hydrogen bonds is shown by a broad band at *ca.* 3250 cm^{-1} . This band is removed by evacuation above 150° (Figure 4, curve c) and the solid is more dehydroxylated than before the adsorption. This fact has already been pointed out in the case of ammonia and alumina¹⁶ or $\text{Cr}_2\text{O}_3\text{-WO}_3$.¹⁷

On the other hand, ammonium bands were not noticed in the present case. These data are in disagreement with that of Hermann and Boehm² who found a

(8) D. J. C. Yates, *J. Phys. Chem.*, **65**, 746 (1961).

(9) L. H. Little, "Infrared Spectra of Adsorbed Species," Academic Press, London and New York, N. Y., 1966, pp 74–83.

(10) D. L. Bernitt, *J. Chem. Phys.*, **42**, 3553 (1965).

(11) A. Novak, P. Saumagne, and L. D. C. Bok, *J. Chim. Phys.*, **60**, 1385 (1963).

(12) K. Nakamoto, M. Margoshes, and R. E. Rundle, *J. Amer. Chem. Soc.*, **77**, 480 (1955).

(13) I. Nitta, Y. Tommie, and Hoe Koo, *Acta Crystallogr.*, **5**, 292 (1952).

(14) N. D. Parkyns, *J. Chem. Soc. A*, 410 (1969).

(15) R. L. Lass and R. F. Scheurmann, *Acta Crystallogr.*, **15**, 77 (1962).

(16) A. E. Hirschler, *J. Catal.*, **6**, 1 (1966).

(17) G. France and M. V. Mathieu, *Bull. Soc. Chim. Fr.*, 2891 (1970).

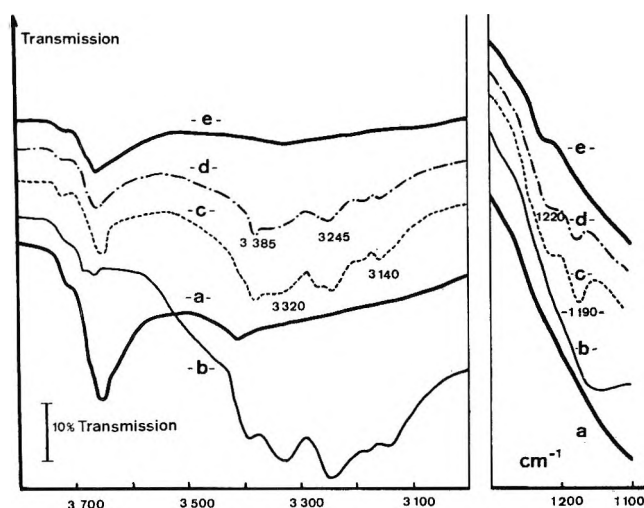


Figure 4. Ammonia adsorption. Infrared spectra of 200°-evacuated TiO₂ A₃ (a), after admitting 40 Torr of NH₃ for 1 hr at 25° (b), then outgassing for 8 hr at 150° (c), at 200° (d), and at 250° (e).

band at *ca.* 1400 cm⁻¹, characteristic of ammonium ions, for ammonia chemisorbed on an anatase sample.

(b) *Lewis Acidity.* After desorption at 150° of ammonia fixed on OH groups, several bands are still detected in the infrared spectra of crystallized 200 or 400°-evacuated titanium dioxides (Figure 4 curves c and d). These bands are removed by evacuation between 200 and 300° as indicated in Table II and shown in Figure 4, curve e.

Table II: Vibrational Frequencies (in cm⁻¹) of NH₃

Modes ^a	Gas ^b	Ammine complexes ^c	Adsorbed NH ₃ on well crystallized TiO ₂
ν_3	3443.9–3443.6	3412–3200	3385–3320 ^d
ν_1	3337.2–3336.2	3330–3115	3245–3140 ^d
ν_4	1627.4–1626.1	1655–1550	1595 (250–300°)
ν_2	968.3–932.5	1361–1170	1190 (200°)– 1220 (300°)

^a G. Herzberg, "Infrared and Raman Spectra of Polyatomic Molecules," Van Nostrand, New York, N. Y., 1956, p 295.

^b W. S. Benedict and E. K. Plyler, *Can. J. Phys.*, **35**, 1235 (1957). ^c A. D. Allen and C. V. Senoff *Can. J. Chem.*, **45**, 1337 (1967). ^d It is difficult to determine precisely the order and temperature of removal of these bands between 250 and 300°, because of their broadness and weak intensity.

For a 200°-evacuated TiO₂, the 1190-cm⁻¹ band is produced on adding ammonia at 25°. Another band at 1220 cm⁻¹ appears on heating under vacuum and can also be observed at room temperature if the solid is initially completely dehydroxylated.

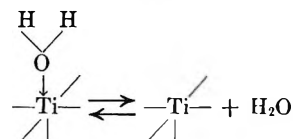
These last two bands (1190 and 1220 cm⁻¹) are absent from the spectra of ammonia adsorbed on badly crystallized anatase A₂ or rutile R₂. Moreover, no

ammonia remains on the surface of these solids after evacuation at 150°.

The observed frequencies in the case of ammonia adsorbed on crystallized titanium dioxides are situated in the absorption regions of ammonia complexes (Table II). This fact and the temperature of desorption of ammonia strongly suggest the existence of bonds between the nitrogen atom of ammonia and electron-acceptor sites (Lewis type acid sites).

Since two bands occur in the region of NH₃ symmetric bending vibration and four in the NH stretching vibration region, it may be concluded that two types of Lewis sites exist. The first type (sites III) would be responsible for the 3385, 3245, and 1190-cm⁻¹ bands, the second type (sites II) for the 3330, 3140, and 1220-cm⁻¹ bands. In agreement with these frequencies and the stabilities of the respective surface species, sites II are supposed to be more acidic than sites III.

The sites III exist on a 150°-evacuated TiO₂. We may assume that they are created by molecular water removal according to the following scheme.



These titanium atoms are incompletely coordinated and can therefore fix either a water molecule or an ammonia molecule.

The sites II exist on a 400°-evacuated TiO₂, but not on a 200°-evacuated TiO₂. On this last solid, they are created by partial desorption of the ammonia which produces a dehydroxylation. Therefore, they must be the sites created by the removal of the isolated OH groups and responsible for perylene ionization (sites II of the preceding paper³). Their acid force is similar to that found for a δ -alumina.¹⁸

2. *Pyridine.* Figures 5 and 6 show the infrared bands found when pyridine is adsorbed on 200 or 400°-evacuated titanium dioxides. The frequencies of the vibrational modes 19b and 8a after desorption of the pyridine between 200° and the indicated temperature are listed in Table III. These modes have been chosen because they are affected the most by the bonding of the nitrogen atom.¹⁹

The adsorption of pyridine on the OH groups is similar to that of ammonia, *i.e.*, OH...N bonds are created. No pyridinium species (band at *ca.* 1540 cm⁻¹¹⁹ is detected (Figure 5).

It may be deduced from the comparison (Tables III and IV) of the frequencies of chemisorbed pyridine and coordinated pyridine that pyridine is also bonded to electron-acceptor surface sites.

(18) P. Pichat, M. V. Mathieu, and B. Imelik, *J. Chim. Phys.*, **66**, 845 (1969); P. Pichat, Thesis, Lyon, France, 1966.

(19) E. P. Parry, *J. Catal.*, **2**, 371 (1963).

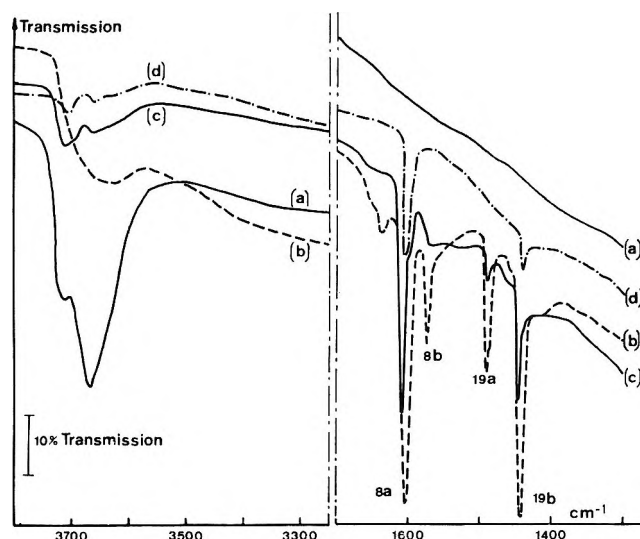


Figure 5. Pyridine adsorption. Infrared spectra of $\text{TiO}_2 \text{ A}_1$ 200°-evacuated (a), after admitting pyridine (vapor pressure) for 1 hr at 25°, then outgassing for 8 hr at 25° (b), at 250° (c), and 300° (d).

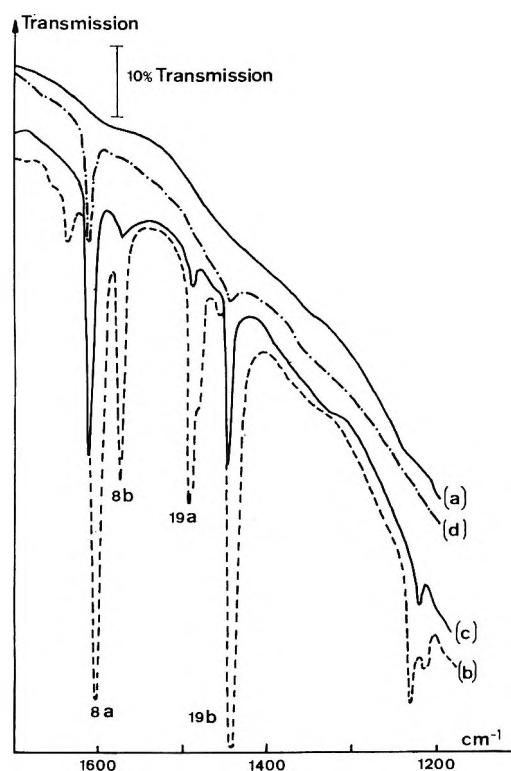


Figure 6. Pyridine adsorption. Infrared spectra of $\text{TiO}_2 \text{ A}_1$ 400°-evacuated (a), after admitting pyridine (vapor pressure) for 1 hr at 25°, then outgassing for 8 hr at 25° (b), at 250° (c), and 400° (d).

This interaction of pyridine with the aprotic acid centers of rutile has been briefly pointed out by Kiselev and Uvarov,⁴ but no attempt has been made to determine the origin of these centers.

The adsorbed pyridine is more stable on the completely (400°-evacuated) than on the partly (200°-

Table III: Vibrational Frequencies (in cm^{-1} , Modes 19b and 8a) of the Adsorbed Pyridine on Titanium Dioxides

Catalyst	Temperature of evacuation, °C	19b	8a
Anatase A ₃	200	1440	1600
		↓	↓
		1445 (300°)	1610 (300°)
Anatase A ₃	400	1440	1605
		↓	↓
		1445 (400°)	1610 (450°)
Rutile R ₁	200	1440	1600
		↓	↓
		1445 (350°)	1610 (450°)
Rutile R ₁	400	1440	1605
		↓	↓
		1445 (500°)	1610 (500°)
Anatase A ₁	200	1440	1600
		↓	↓
		1445 (350°)	1610 (350°)
Anatase A ₁	400	1440	1605
		↓	↓
		1445 (400°)	1610 (450°)
Rutile R ₂ and Anatase A ₂	200 and 400	1440 (200°)	1600
			↓
			1605 (200°)

Table IV: Vibrational Frequencies (in cm^{-1}) of Pyridine

Modes	19b	8a
Liquid ^a	1439	1579
in metallic complexes ^b	{ 1440	{ 1592
	{ 1461	{ 1615
+ AlCl ₃ or AlBr ₃ or SnCl ₄ ^c	{ 1450	{ 1610
	{ 1458	{ 1628

^a See ref 18. ^b F. Fratesi and R. Freymann, *C. R. Acad. Sci. Paris Ser. B*, 266, 327 (1968). ^c A. Terenin, V. Filimonov, and D. Bystrov, *Z. Elektrochem.*, 62, 1080 (1958).

evacuated) dehydroxylated crystallized TiO_2 . Besides, the desorption above 200° of pyridine adsorbed on a 200°-evacuated solid produces a dehydroxylation of the surface and the 19b and 8a bands of the remaining pyridine become narrower and are situated at slightly higher frequencies. These results suggest that pyridine, like ammonia, is adsorbed on two types of electron-acceptor sites: sites III and sites II created by the elimination of molecular water and isolated OH groups, respectively. Pyridine is more strongly fixed on sites II than on sites III.

The absence of sites II and III on the surface of badly crystallized anatase or rutile is confirmed by the far weaker stability of the adsorbed species and the lower frequencies of 19b and 8a modes (last line of Table III).

3. *Trimethylamine.* Trimethylamine was chosen as a stronger base to check whether the titanium dioxides show a protonic acidity.

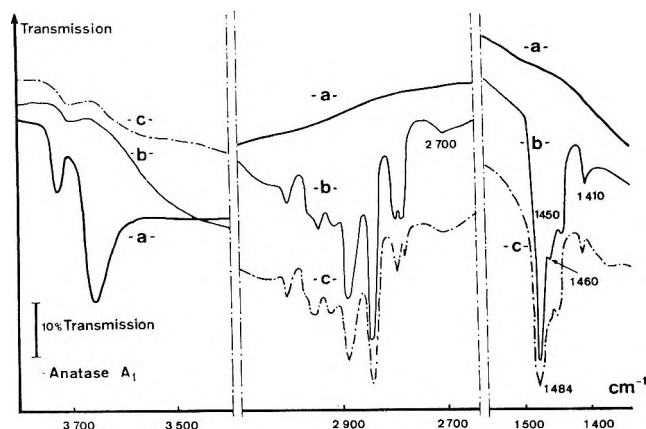


Figure 7. Trimethylamine adsorption. Infrared spectra of $\text{TiO}_2 \text{ A}_1$, evacuated at 200° (a), after admitting 30 Torr of trimethylamine for 1 hr at 25° , then outgassing for 8 hr at 25° (b), and 150° (c).

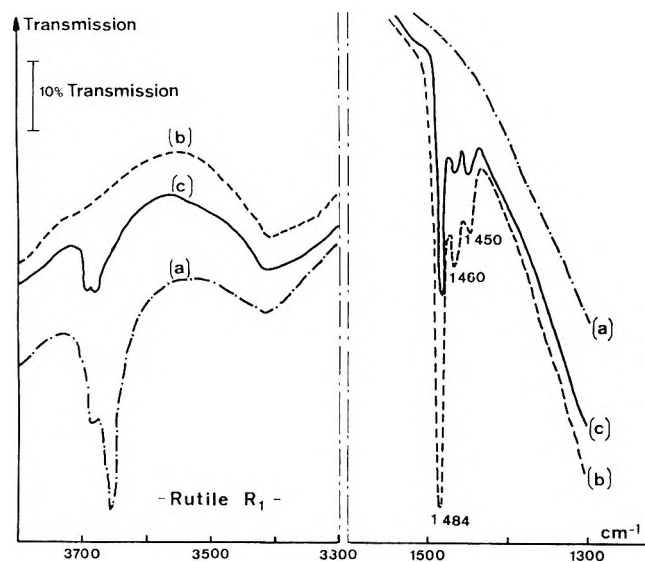


Figure 8. Trimethylamine adsorption. Infrared spectra of $\text{TiO}_2 \text{ R}_1$, evacuated at 200° (a), after admitting 30 Torr of trimethylamine for 1 hr at 25° , then outgassing for 8 hr at 25° (b), and 150° (c).

Like ammonia or pyridine, part of the trimethylamine is hydrogen bonded to the rutile or anatase OH groups with subsequent removal of a fraction of these groups during the desorption at 150° (Figures 7 and 8). The remaining trimethylamine produces infrared bands

at 1484, 1460, and 1450 cm^{-1} (Figures 7 and 8) due to the bending vibrations of the methyl groups.²⁰ It is removed by evacuation at 250° . The comparison with the adsorption of ammonia or pyridine suggests that trimethylamine is chemisorbed on Lewis acid sites.

In addition, two bands are recorded at 2700 and 1410 cm^{-1} (Figure 7) for 200° -evacuated anatase. They are removed by evacuation at 200° with a simultaneous and slight increase in the intensity of the OH bands. They are less intense for samples evacuated at higher temperatures. They do not occur for completely dehydroxylated anatase, but the addition of a little quantity of water vapor makes them appear. Since similar bands have been found in the spectrum of the trimethylamine chlorhydrate and assigned to the stretching and bending vibrations of the NH^+ group,²¹ it may be concluded that some OH groups of anatase show a protonic acidity.

This 1410-cm^{-1} band is not observed for rutile (Figure 8). Actually this result is not unexpected, since according to the hydroxyl stretching frequencies the isolated OH groups of anatase are more protonic than those of rutile, as was pointed out in part I of this series.³

Conclusions

1. The OH groups of anatase and rutile show a basic character toward compounds, like CO_2 , with a $\text{p}K_{\text{ab}}$ lower than 6.5.
2. Some OH groups of anatase have a sufficient acidic character to react with trimethylamine, but not with ammonia and pyridine.
3. Apart from their amphoteric (anatase) or basic (rutile) character, these OH groups possess the property of easily forming hydrogen bonds with the studied compounds. A partial or total dehydroxylation of the surface occurs during the subsequent desorption of these hydrogen-bonded compounds.
4. Two types of Lewis acid sites have been found. The strongest ones are created by the removal of the isolated OH groups, the weakest ones by the removal of molecular water.

(20) J. R. Barcelo and J. Bellanato, *Spectrochim. Acta*, **8**, 27 (1956).

(21) J. Bellanato, *ibid.*, **16**, 1344 (1960).

The Aggregation of Arylazonaphthols. II.

Steric Effects on Dimer Structure in Water

by Alan R. Monahan,* Nicholas J. Germano, and Daniel F. Blossey

Research Laboratories, Xerox Corporation, Xerox Square, Rochester, New York 14603 (Received October 12, 1970)

Publication costs assisted by The Xerox Corporation

The absorption spectra of three ionic arylazonaphthol dyes (3'-alkyl-4'-chloro-6'-sulfophenylazo-2-hydroxy-3-naphthoic acids) in aqueous acidic solution (pH 3.15) are analyzed in terms of monomer-dimer equilibria in the 10^{-6} to 10^{-4} mol l.⁻¹ concentration range. From the changes in the absorption spectra with dye concentration, the dimerization constant ($K_{eq} = c_d/c_m^2$), the pure monomer spectrum, and the pure dimer spectrum are calculated for each dye. The dimerization constants are $(6.83 \pm 0.80) \times 10^4$, $(5.55 \pm 0.39) \times 10^4$, and $(3.40 \pm 0.71) \times 10^3$ l. mol⁻¹ for the (I) methyl-, (II) ethyl-, and (III) isopropyl-, 3'-substituted dyes, respectively. Each dimer spectrum consists of an intense H-band hypsochromic to the monomer band, and a weaker J-band, bathochromic to the monomer band. The J-band strength, relative to the H-band, increases with increasing size of the substituent thus indicating steric effects in the dimer structure. As calculated from the relative strengths of the split bands in the dimer spectrum, the twist angle between equivalent molecular axes of the molecules in the dimer increases from $64 \pm 1^\circ$ in dye I, to $72 \pm 0^\circ$ in dye II, to $88 \pm 1^\circ$ in dye III. Both in-plane and parallel-plane structural models are considered for the dimer with the in-plane model giving the most consistent results.

Introduction

It has been known for many years that most ionic organic dyes in aqueous solution deviate from strict Beer's law behavior.¹ These departures from normal solution spectra behavior are generally interpreted as being due to the formation of dimers and higher order aggregates. Thus, by measuring the changes in the observed extinction coefficient with changes in the dye concentration, the dye aggregation processes can be observed directly by spectrophotometric techniques.² For example, the absorption spectra of most ionic hydroxy azo dyes in water show a decrease in the strength of the main absorption band accompanied by a hypsochromic shift (shift to higher energy) in the peak maxima with increasing dye concentration.^{2,3} The spectral changes of azo dyes with the degree of dye aggregation are generally small and cause only minor alterations in the absorption spectra of the azo dyes. This is in marked contrast to the phthalocyanines² and cyanine dyes⁴ which are known to form new, easily resolved absorption bands upon aggregation. The differences between the degree of spectral change upon aggregation for the azo and cyanine are due in part to the differences between the absorptive strengths of the main absorption band of the isolated dye molecules. Azo dyes⁵ have transition dipole strengths on the order of 10^{-35} erg cm³ and cyanine dyes⁶ on the order of 10^{-34} erg cm³. From molecular exciton theory,⁷ the energy splitting of the bands in the dimer spectrum is roughly proportional to the absorptive strength of the monomer band which would explain the relatively small changes between the

monomer and dimer spectra of azo dyes as opposed to the large changes for cyanine dyes.

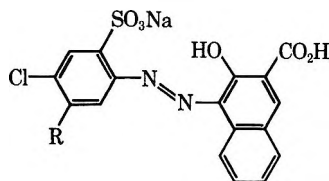
Since the spectral changes upon aggregation are dependent in many ways on the properties of the isolated molecule, the degree of spectral change is not a direct indication of the degree of aggregation. In fact, both ionic arylazonaphthol dyes⁵ and cyanine dyes^{4a} have equilibrium constants for dimer formation, $K_{eq} = c_d/c_m^2$, on the order of 10^4 l. mol⁻¹ in spite of the fact that their spectral changes are quite different. Thus, the spectral changes with dye concentration must be converted into association constants to fully evaluate the affinity for aggregation of the dye molecules. Also, in order to interpret the spectra in terms of structural dimer models,⁷ the pure monomer and pure dimer spectra must be separated. For cases where there is small overlap between the monomer and dimer bands, as is the case for the cyanine dyes, this separation is accomplished quite easily. In the case of azo dyes, however, the monomer and dimer bands are completely over-

- (1) S. E. Sheppard, *Proc. Roy. Soc., Ser. A*, **82**, 256 (1909).
- (2) S. E. Sheppard and A. L. Geddes, *J. Amer. Chem. Soc.*, **66**, 2003 (1944).
- (3) E. Coates, *J. Soc. Dyers Colour.*, **85**, 355 (1969).
- (4) (a) W. West and S. Pearce, *J. Phys. Chem.*, **69**, 1894 (1965);
(b) W. West, S. P. Lovell, and W. Cooper, *Photogr. Sci. Eng.*, **14**, 52 (1970).
- (5) A. R. Monahan and D. F. Blossey, *J. Phys. Chem.*, **74**, 4014 (1970).
- (6) E. S. Emerson, M. A. Conlin, A. E. Rosenoff, K. S. Norland, H. Rodriguez, D. Chin, and G. R. Bird, *ibid.*, **71**, 2396 (1967).
- (7) M. Kasha, H. R. Rawls, and M. Ashraf El-Bayoumi, *Pure Appl. Chem.*, **11**, 371 (1965).

lapping which makes their separation more difficult. A computer program, which was outlined in a previous paper,⁵ has been developed to separate the monomer and dimer contributions to the spectra and calculate the equilibrium constants for dimerization.

In this study, the effect of varying the alkyl substituent on the aryl portion of an ionic arylazonaphthol was investigated. The ionic arylazonaphthols have been chosen because their aggregation processes have not been studied before due to their small spectral changes with aggregation, and a more detailed knowledge of the aggregate structure is desired in view of the importance of these dyes in the dyeing of polymers⁸ and in color reproduction.⁹ The object of this study was to determine the magnitude to which a structural variation in the dye molecule changes the stability and structure of the dimer. Similar studies have been carried out on chlorophylls¹⁰ and cyanine dyes.^{4a,6} Emerson, *et al.*,⁶ have shown that methyl substitution in the center of a cyanine dye results in an aggregate band hypsochromic (H-band) to the monomer band. Conversely, ethyl substitution results in a bathochromic (J-band) shift upon aggregation.

In this paper we report studies of the monomer-dimer equilibria of three molecules of the structure



in aqueous acidic solution (pH 3.15) where R = CH₃, C₂H₅, and *i*-C₃H₇. The methyl-, ethyl-, and isopropyl-substituted dyes will be referred to in the following as dye I, dye II, and dye III, respectively. The visible absorption spectra of the three dyes in aqueous solution were measured in the concentration range of 10⁻⁶ to 10⁻⁴ mol l.⁻¹. The spectra were analyzed using previously reported computer techniques⁵ which separate the monomer and dimer contributions to the spectra at each concentration. The calculated monomer and dimer spectra were then analyzed in terms of molecular exciton theory⁷ to determine possible dimer structures. Analyses of the results suggest dimer structures which are consistent with dimer stability, which is defined in terms of the standard free energy for dimer formation.

Experimental Section

Preparation of the Dyes. The three dyes were prepared by standard preparative procedures¹¹ from 2-hydroxy-3-naphthoic acid (Pfister) and the corresponding 2-amino-4-alkyl-5-chlorobenzenesulfonic acids. The 4-methyl- and ethylamines were commercial samples supplied by Eastman Organic Chemicals and American Cyanamid, respectively. The isopropylaminochlorobenzenesulfonic acid was prepared from cumene.¹² The structure of the isopropyl compound

was confirmed by direct comparison with the infrared and nmr spectra of the methyl and ethyl analogs. *Anal.* Calcd for C₉H₁₂ClNO₃S: C, 43.3; H, 4.9; Cl, 14.1; N, 5.6; S, 12.9. Found: C, 43.0; H, 5.1; Cl, 14.1; N, 5.4; S, 12.3. The amines were recrystallized twice from a sodium acetate deionized water solution and 2-hydroxy-3-naphthoic acid was recrystallized twice from isopropyl alcohol.

After coupling at pH 9, each dye was washed several times with distilled water and recrystallized twice from an isopropyl alcohol-water mixture to a constant extinction coefficient. The disodium salts of the dyes were obtained in each synthesis. The compounds were dried under vacuum for 12 hr at 60°.

Anal. Calcd for dye I: C₁₈H₁₁N₂Na₂O₆SCl: C, 46.5; H, 2.4; N, 6.0; Na, 9.9; S, 6.9; Cl, 7.6. Found: C, 46.3; H, 2.6; N, 6.2; Na, 9.6; S, 6.8; Cl, 7.4.

Anal. Calcd for dye II: C₁₉H₁₃N₂Na₂O₆SCl: C, 47.7; H, 2.7; N, 5.9; Na, 9.6; S, 6.7; Cl, 7.4. Found: C, 48.0; H, 2.4; N, 6.2; Na, 9.6; S, 7.0; Cl, 7.7.

Anal. Calcd for dye III: C₂₀H₁₅N₂Na₂O₆SCl: C, 48.8; H, 3.1; N, 5.7; Na, 9.3; S, 6.5; Cl, 7.2. Found: C, 48.8; H, 3.3; N, 5.9; Na, 9.6; S, 6.5; Cl, 7.5.

Preparation of Solutions. The spectroscopic measurements were performed using dye-water solutions having a pH of 3.15 ± 0.05 (~10⁻³ M HCl). The pH was chosen such that both the hydroxy and carboxylate groups of the dye molecules would be protonated whereas the sulfonic group would be ionized. For calculation of the proper conditions for protonation of the carboxylate group, the dissociation constant of β-naphthoic acid was used. The dissociation constant for β-naphthoic acid¹³ is 7 × 10⁻⁵ and is an upper limit for the dissociation constant of the carboxylate group on the dye molecules because of the electronic character of the other substituents on the naphthol group.¹⁴ Therefore, at pH ~3, the fraction of carboxylate groups protonated to those ionized is at least 100:1. The hydroxy group is also protonated because to ionize the hydroxy portion of the molecule, a pH of about 10 would be required.³ The sulfonate group is definitely ionized because, as Reeves and Kaiser¹⁵ have recently shown, the azo dye sulfonates can be converted into protonated species only at very low pH (0.1 to 3 M aqueous H₂SO₄).

(8) E. J. G. Bailey, *J. Soc. Dyers Colour.*, **85**, 571 (1969).

(9) J. A. C. Yule, "Principles of Color Reproduction," Wiley, New York, N. Y., 1967, p 193.

(10) R. Sauer, J. R. Lindsay Smith, and A. J. Schultz, *J. Amer. Chem. Soc.*, **88**, 2681 (1966).

(11) H. Zollinger, "Azo and Diazo Chemistry," Interscience, New York, N. Y., 1961, pp 311-360.

(12) F. H. Adams, U. S. Patent 2,598,483 (1952).

(13) "Handbook of Chemistry and Physics," 48th ed, The Chemical Rubber Co., Cleveland, Ohio, 1967-1968, p D-90.

(14) C. D. Ritchie and R. E. Uschold, *J. Amer. Chem. Soc.*, **90**, 2821 (1968).

(15) R. L. Reeves and R. S. Kaiser, *J. Phys. Chem.*, **73**, 2279 (1969).

For each dye, five solutions were prepared in the 10^{-6} to 10^{-4} M concentration range. The water was obtained from a Millipore Super-Q system (18 megohms) and acidified to pH 3.15 using HCl. The pH of all solutions was within ± 0.05 pH unit before and after spectrophotometric analysis. Spectra were run on a Cary Model 14R automatic spectrophotometer using 0.1-, 1-, 5-, and 10-cm matched quartz cells.

Results

Concentration Dependence. The concentration dependence of the absorption spectra of dye I is shown in Figure 1. Isosbestic points occur at 17,700 and 20,100 cm^{-1} . At the most dilute concentration of 3.26×10^{-6} M, the main peak (monomer peak) occurs at 19,500 cm^{-1} . Successively higher concentrations result in a blue shift of this peak and a measurable decrease in apparent extinction coefficient. The concentration dependencies of the spectra of dye II and dye III are qualitatively similar to dye I in that both show dilute solution maxima near 19,500 cm^{-1} . However, isosbestic points appear at 17,900 and 20,600 cm^{-1} for dye II and at 18,100 and 21,600 cm^{-1} for dye III. The shift of these isosbestic points with molecular structural changes is due to the differences in physical size of the substituents (see Discussion).

Monomer-Dimer Equilibrium. The monomer-dimer equilibrium of dye II in aqueous solution has been reported previously for pH 6.00 and the same concentration range.⁵ Under these conditions, the carboxylate group, as well as the sulfonate group, is ionized. In this paper, the three dyes are analyzed at pH 3.15 so that both structural and pH dependencies could be compared. It has already been noted that at pH 3.15, the carboxylate group is protonated whereas the sulfonate group is ionized. The calculation of the pure monomer spectrum, pure dimer spectrum, and equilibrium constant is accomplished using a computer procedure which was reported previously.⁵ In the analysis, it is initially assumed that the monomer concentration c_m and dimer concentration c_d follow the law of mass action

$$K_{\text{eq}} = c_d/c_m^2 \quad (1)$$

where K_{eq} is the association (equilibrium) constant for dimer formation. If the total concentration c_t is small enough that no higher aggregates are present, then

$$c_d = (c_t - c_m)/2 \quad (2)$$

Assuming that eq 1 and 2 hold, a best-fit monomer spectrum and dimer spectrum can be calculated for a given K_{eq} . By varying K_{eq} systematically, the best ϵ_m , ϵ_d , and K_{eq} are established where ϵ_m and ϵ_d are extinction coefficients of monomer and dimer, respectively. To make the calculation self-consistent, the best ϵ_m and ϵ_d are used to calculate K_{eq} at each concentration and thereby establish limits of errors on K_{eq} and any resulting parameters.

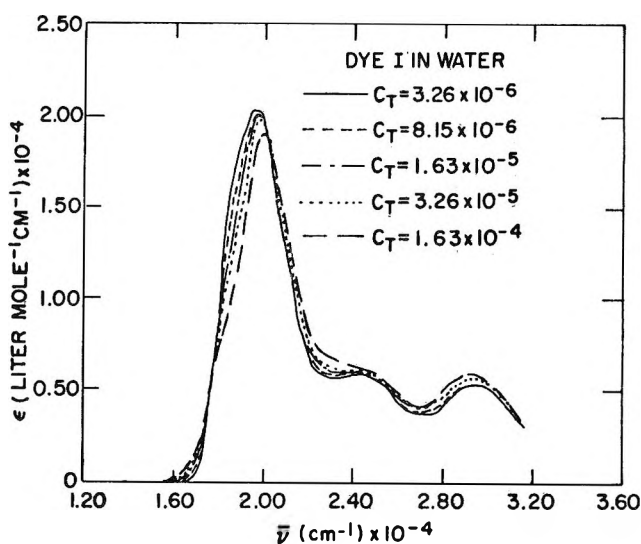


Figure 1. Concentration-dependent spectra of dye I in water. All spectra obtained at 22°.

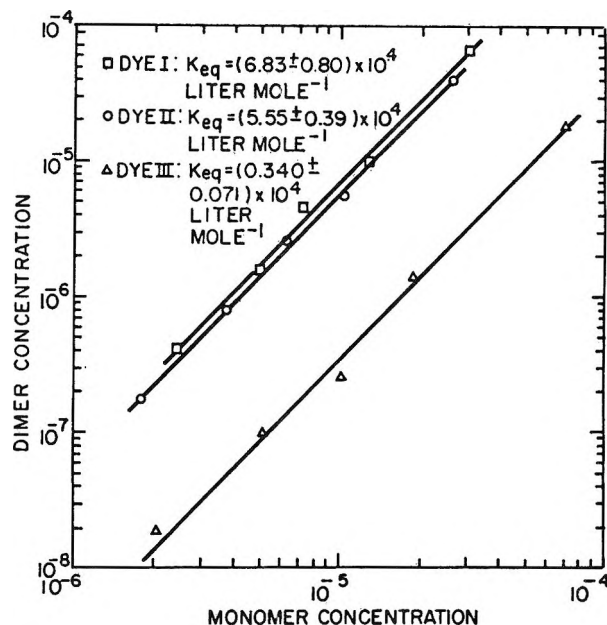


Figure 2. Plot of $\log c_d$ vs. $\log c_m$ for three dyes in water. Solid lines drawn with theoretical slopes of 2.

The results of this analysis for dyes I, II, and III are shown in Table I. Each dye was measured at five concentrations in the 10^{-6} to 10^{-4} l. mol $^{-1}$ concentration range. For each concentration, the total concentration c_t , monomer concentration c_m , dimer concentration c_d , and equilibrium constant K_{eq} are listed. The fit of the concentrations c_m and c_d to eq 1 is demonstrated graphically in Figure 2. The solid lines are drawn with a theoretical slope of 2.

Discussion

Substituent Effects on Dimer Structure. Analysis of a homologous series of ionic arylazonaphthol dyes allows direct interpretation of steric effects on dimer structure.

Table I: Monomer-Dimer Equilibrium of Dyes in Water (pH 3.15) at 22°

Dye I: $K_{eq} = (6.83 \pm 0.80) \times 10^4 \text{ l. mol}^{-1}$					
Total dye concentrations, mol l. ⁻¹ ($\times 10^6$)	3.26	8.15	16.3	32.6	163.0
Monomer concentrations, mol l. ⁻¹ ($\times 10^6$)	2.44	5.01	7.35	12.9	30.8
Dimer concentrations, mol l. ⁻¹ ($\times 10^6$)	0.408	1.57	4.48	9.87	66.1
Equilibrium constants, l. mol ⁻¹ ($\times 10^{-4}$)	6.82	6.27	8.29	5.97	6.96
Dye II: $K_{eq} = (5.55 \pm 0.39) \times 10^4 \text{ l. mol}^{-1}$					
Total dye concentrations, mol l. ⁻¹ ($\times 10^6$)	2.14	5.35	16.5	21.4	107.0
Monomer concentrations, mol l. ⁻¹ ($\times 10^6$)	1.79	3.80	6.40	10.4	26.7
Dimer concentrations, mol l. ⁻¹ ($\times 10^6$)	0.173	0.777	2.55	5.49	40.1
Equilibrium constants, l. mol ⁻¹ ($\times 10^{-4}$)	5.40	5.39	6.24	5.05	5.62
Dye III: $K_{eq} = (3.40 \pm 0.71) \times 10^3 \text{ l. mol}^{-1}$					
Total dye concentrations, mol l. ⁻¹ ($\times 10^6$)	2.09	5.40	10.8	21.6	108.0
Monomer concentrations, mol l. ⁻¹ ($\times 10^6$)	2.05	5.21	10.3	18.9	72.5
Dimer concentrations, mol l. ⁻¹ ($\times 10^6$)	0.0188	0.0973	0.249	1.37	17.7
Equilibrium constants, l. mol ⁻¹ ($\times 10^{-4}$)	0.447	0.359	0.234	0.384	0.337

The three substituent groups, methyl, ethyl, and isopropyl, are equivalent in terms of electronic interaction with the ring structure but are different in terms of physical size. Thus, *if steric bulk appreciably affects dimer stability, the three dyes should show an inverse relationship between substituent size and dimer stability which indeed they do.* The equilibrium constants and free energy for dimer formation are given in Table II. Note that the equilibrium constant for dimer formation decreases as the steric size of the alkyl substituent increases.

Table II: Equilibrium Constants and Free Energies for Dimer Formation

Dye	K_{eq} , l. mol ⁻¹	$-\Delta G^\circ_{298}$, kcal (mol dimer) ⁻¹
I	$(6.83 \pm 0.80) \times 10^4$	6.60 ± 0.07
II	$(5.55 \pm 0.39) \times 10^4$	6.47 ± 0.05
III	$(3.40 \pm 0.71) \times 10^3$	4.65 ± 0.10

The relative stability of the dimer species of the three dyes is reflected in their free energies of dimer formation which indicate that the dimer of dye I is more stable than the dimer of either dye II or dye III and that the dimer of dye II is more stable than the dimer of dye III.

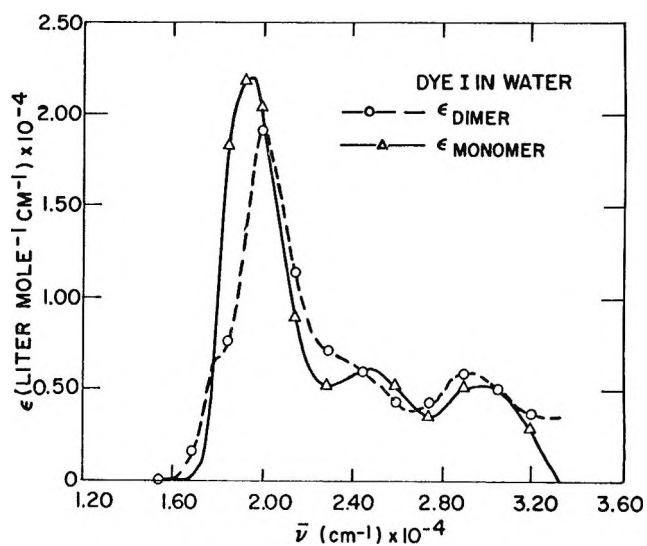


Figure 3. Calculated absorption spectra of pure monomer and dimer species of dye I in water. The symbols on curves in this figure and following figures for notation purposes only.

The calculated pure monomer and dimer spectra for the three dyes are shown in Figures 3, 4, and 5. The spectra are interpreted in terms of molecular exciton theory which predicts that the energy levels of the monomer species are split in the dimer species.⁷ The splitting is a function of the geometrical structure of the

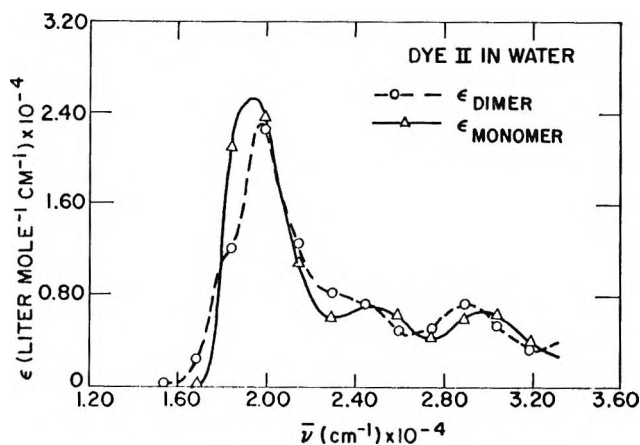


Figure 4. Calculated absorption spectra of pure monomer and dimer species of dye II in water.

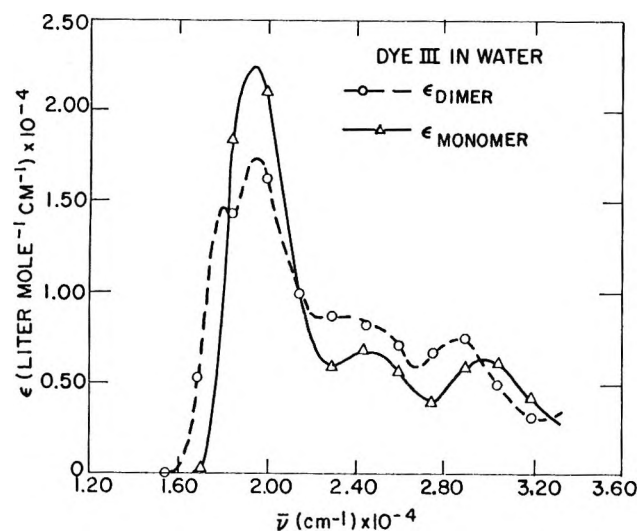


Figure 5. Calculated absorption spectra of pure monomer and dimer species of dye III in water.

dimer. Each of the dimer spectra in Figures 3, 4, and 5 show a strong H-band on the high-energy side of the monomer band and a weaker J-band on the low-energy side of the monomer band. The peak positions and splittings of the spectra for the monomer and dimer species are summarized in Table III.

Table III: Spectral Peak Positions and Splitting, cm^{-1} , for Monomer and Dimer Species

Dye	Monomer	Dimer		Splitting $\Delta\bar{\nu}$, $\bar{\nu}_H - \bar{\nu}_J$
		$\bar{\nu}_H$	$\bar{\nu}_J$	
I	19,500	19,900	18,000	1,900
II	19,400	19,700	18,000	1,700
III	19,400	19,300	18,000	1,300

The resolution of the instrument is about 100 cm^{-1} for the spectral range of interest so that the numbers in Table III are accurate within this limit.

The amount of information available in the pure monomer and dimer spectra is not enough to specify exactly the dimer structures, but insight can be gained by examining the simpler models. The inputs are the monomer oscillator strength f_m , the dimer J-band strength f_J , the dimer H-band strength f_H , and the splitting $\Delta\bar{\nu}$. From these inputs, it is possible to calculate an angle α between dipoles of the adjacent molecules in the dimer and a separation distance R between the molecules. If more structural variables are included, then the problem becomes insolvable. The splitting $\Delta\bar{\nu}$ from molecular exciton theory⁷ is given by

$$\Delta\bar{\nu} = \frac{2DG}{hcR^3} \text{ cm}^{-1} \quad (3)$$

where D is the monomer dipole strength and G is a geometry factor which, for the simplest dimer models, is only dependent on the angle α . The two models which allow transitions to both J- and H-bands are a parallel-plane twist angle model and an in-plane oblique angle model. The angle for both models is the angle α which is defined as the angle between the transition dipoles of the two molecules in the dimer. For these two simple dimer configurations, the geometry factor G of eq 3 is given by

$$G = \cos \alpha \quad (\text{parallel-plane model}) \quad (4a)$$

$$G = \cos \alpha + 3 \sin^2 \left(\frac{\alpha}{2} \right) \quad (\text{in-plane model}) \quad (4b)$$

The models are chosen so that there are only two variables R and α whereby a solution is tractable. The angle α is independent of the model chosen and is given by

$$\alpha = 2 \tan^{-1} (\bar{\nu}_H f_J / \bar{\nu}_J f_H)^{1/2} \quad (5)$$

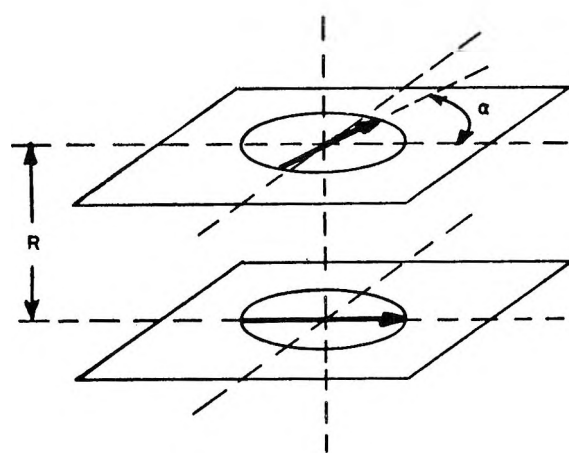
where $\bar{\nu}_H$, $\bar{\nu}_J$, f_H , and f_J are the peak positions and oscillator strengths for the H-band and J-band in the dimer spectra. Equation 5 is the same regardless of the dimer structural model chosen. The oscillator strengths of the bands and the calculated structural parameters for the dimer are given in Table IV. The two dimer models which allow transitions to both excited dimer states and depend only on R and α are considered for the three dyes. Schematic diagrams of the two models are shown in Figure 6. A hypochromic effect is noted for each of the dye systems upon dimerization. This is a common feature for many dye dimers.¹⁶

Independent of the model, the dimer structure shows a pronounced steric effect. The ratio of f_J to f_H increases as the substituent size increases. From eq 5, this also implies that the angle between the transition dipoles of the molecules in the dimer increases as the substituent size increases; indeed, the angle increases

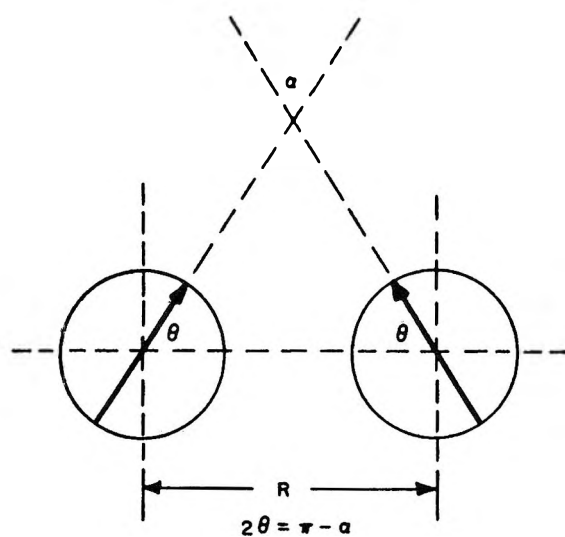
(16) K. K. Rohatgi, *J. Mol. Spectrosc.*, **27**, 545 (1968).

Table IV: Oscillator Strengths and Dimer Structure

	Dye I	Dye II	Dye III
Monomer strength, f_m	0.34 ± 0.02	0.38 ± 0.02	0.34 ± 0.00
Dimer J-band strength, f_J	0.08 ± 0.01	0.09 ± 0.01	0.15 ± 0.00
Dimer H-band strength, f_H	0.23 ± 0.01	0.21 ± 0.01	0.18 ± 0.00
f_J/f_H	0.35	0.43	0.83
α , deg	64 ± 1	72 ± 0	88 ± 1
R , Å			
(i) In-plane oblique angle model	6.3 ± 0.1	6.6 ± 0.1	7.4 ± 0.0
(ii) Parallel-plane twist angle model	4.4 ± 0.1	4.0 ± 0.0	2.1 ± 0.0



PARALLEL PLANE DIMER MODEL



IN-PLANE DIMER MODEL

Figure 6. Schematic diagrams for parallel-plane and in-plane dimer geometries.

from 64° for the methyl substituent to 72° for the ethyl substituent to 88° for the isopropyl substituent at the 3' position on the dye molecule. The model must account for this marked substituent effect on the dipole twist angle as well as the reduced stability of the dimer

in going from dye I to dye III. It seems reasonable that a larger twist angle and reduced dimer stability as reflected in a smaller K_{eq} or larger ΔG indicates a reduction in the binding of the two dye molecules in the dimer. For this reason, the separation distances obtained for the in-plane oblique transition dipole model are the most reasonable since R and α increase as K_{eq} decreases. The values of R are severely model dependent; and, since the exact model is not known, only the trends are significant and valuable in choosing the most consistent model.

pH Effects on Dimer Structure. The monomer-dimer equilibrium of dye II in aqueous solution at pH 6.00 has been previously reported.⁵ For approximately neutral conditions, both the carboxylate and sulfonate groups are ionized, whereas at pH 3.15, the carboxylate group is protonated and the sulfonate group is ionized. By comparing the results at these two values of pH, a qualitative picture of Coulombic repulsion effects on dimer structure should evolve. The pH dependencies of several monomer and dimer parameters are shown in Table V.

Table V: pH Dependence of Dye II Aggregation Parameters

	pH 3.15 (dye II ⁻)	pH 6.00 (dye II ²⁻)
$K_{eq} \times 10^{-4}$, l. mol ⁻¹	5.55 ± 0.39	1.25 ± 0.00
$-\Delta G^\circ_{295}$, kcal (mol dimer) ⁻¹	6.47 ± 0.05	5.58 ± 0.00
Monomer strength, f_m	0.38 ± 0.02	0.35 ± 0.00
Dimer J-band strength, f_J	0.09 ± 0.01	0.07 ± 0.00
f_J/f_H	0.43	0.32
α , deg	72 ± 1	63 ± 0
Splitting $\Delta\bar{\nu}$, cm ⁻¹	1700 ± 100	2200 ± 100
R , Å		
(i) In-plane oblique angle model	6.6 ± 0.1	5.7 ± 0.0
(ii) Parallel-plane twist angle model	4.0 ± 0.0	4.3 ± 0.0

The equilibrium constants and free energies for dimer formation are reasonable in that the doubly ionized molecule has a less stable dimeric state than the singly ionized molecule. From separation distance R , the parallel plane model is most consistent with the pic-

ture of the doubly ionized molecule having a less stable dimeric state than the singly ionized molecule.

Since the pH and steric dependencies suggest different dimer models, an intermediate case is probably the most likely. The trends in K_{eq} and α are certainly meaningful in this study since they are independent of the dimer model. However, R is strongly dependent on the geometry factor G and is not dependable for data interpretation. Taking all things into account, the in-plane oblique angle dimer model gives the most satisfactory results in that it is consistent with the picture of

sterically hindered dimer formation. The parallel-plane twist angle dimer model is most consistent with the pH dependencies, but interpretation is not as straightforward as with the substituent effects. The inconsistencies point up inadequacies in the simple molecular exciton theory when used to evaluate aggregate structure.

Acknowledgment. The authors would like to thank Allen F. DeLuca for solution preparations and spectrophotometric measurements.

Photophysical Processes of *m*-Difluorobenzene

by Terry L. Brewer

University of Texas, Austin, Texas 78712 (Received September 30, 1970)

Publication costs assisted by the Camille and Henry Dreyfus Foundation

The absorption and fluorescent spectra (of *m*-difluorobenzene) are reported. The O-O band is at 263.5 nm. The quantum yield of fluorescence has been found to increase with increasing wavelength and reaches a maximum of 0.16 ± 0.02 at the O-O band. Vibrational relaxation studies using butane as the quenching gas indicate that relaxation is a multicollisional process. The amount of energy lost per collision within a large error is 66 cm^{-1} . The present data in conjunction with other data indicate that internal conversion from the first excited singlet to the ground state is at most a minor process.

Introduction

Benzene, although the most thoroughly studied of the single-ring aromatics, is a poor theoretical standard for comparative fluorescent studies in aromatic compounds, since the relatively long radiative lifetime of the first singlet-singlet transition makes it a poor competitor with radiationless processes. This is exemplified in the comparison of the fluorescent yield of benzene with the yields from alkyl-substituted benzenes with allowed first singlet-singlet transitions.¹ However, when fluorobenzene is brought into the comparison it becomes obvious that factors other than radiative lifetimes are important in determining relative quantum yields of fluorescence. Fluorobenzene has a relatively short radiative lifetime of 100 nsec (*ca.* $1/4$ the lifetime of benzene), but its fluorescent quantum yield of 0.21 is only slightly higher than that of benzene.² It thus becomes important to know the effect of additional fluorines attached to the benzene ring.

The fluorescence of *m*-difluorobenzene has been previously studied.³ However, its unusual wavelength dependence and quantum yields suggest further investigation.

Experimental Section

Chemicals. The *m*-difluorobenzene was purified by use of preparative gas chromatography and degassed by three freeze-thaw cycles before use. The butane was Matheson Co. instrument grade, which was degassed *via* the freeze-thaw process before use.

Equipment. The optical train consisted of a 1000-W xenon point source lamp, a Bausch and Lomb monochromator with grating of 600 lines mm^{-1} . Slit widths were set at 0.5 mm. This gave a band pass of 8 Å. The wavelength settings were checked with a 500-W, high-pressure mercury arc. The light from the monochromator was collimated by a lens and passed through the T-shaped cell 4-cm long with windows of 2 cm in diameter. The windows were optically flat Suprasil quartz. The center of the side window was 1.3 cm from one end of the cell. At the end of the optical train was an RCA 935 phototube operated at 90 V with

(1) W. A. Noyes, Jr., and C. S. Burton, *Ber. Bunsenges. Phys. Chem.*, **72**, 146 (1968).

(2) K. Nakamura, *J. Chem. Phys.*, **53**, 998 (1970).

(3) F. W. Ayers, F. Grein, G. P. Semeluk, and I. Unger, *Ber. Bunsenges. Phys. Chem.*, **72**, 282 (1968).

current measured by a Keithley Model 410 micromicroammeter in connection with a Hewitt-Packard Model 680 recorder. The fluorescence was measured by a 1P28 photomultiplier tube at the side window. A 6-mm diameter area of the 1P28 was exposed to the cell. The current from the photomultiplier was read with the same equipment used for the 935 phototube. The light beam transversing the cell was reasonably parallel and had a diameter of 1 cm. The system was calibrated by benzene vapor at 253 nm with a fluorescent yield assumed to be 0.18 at 15–20 Torr.⁴ The standardization was carried out so that the per cent transmittance was the same for both benzene ($P \leq 10$ Torr) and *m*-difluorobenzene ($P = 1$ Torr).

The fluorescent and absorption spectra were obtained with a Czerny-Turner 0.75-m scanning spectrometer as previously described.²

Procedure. In experiments where mixing of different gases was required, a 1200-ml mixing chamber was used. The gases were allowed to mix from 1 to 14 hr depending upon the pressure.

All experiments were carried out in the gas phase with a *m*-difluorobenzene pressure of 1 Torr.

Results

The absorption spectrum of *m*-difluorobenzene was found to be essentially the same as that reported by Sponer⁵ in which she gives the O–O band as 37,909 cm^{-1} . Due to the large amount of fine structure no attempt has been made to analyze the spectrum further. Some of the more intense bands are listed in Table I. The maximum extinction coefficient occurs in the O–O band and is 820 $\text{l. mol}^{-1} \text{cm}^{-1}$ at 5 mm pressure. From the integrated area of the absorption, the radiative lifetime for *m*-difluorobenzene is calculated to be 120 nsec. This same entity calculated from Sponer's work is 97 nsec. Due to the larger experimental uncertainty in the present experimental system, the latter value is preferable.

Table I: Bands in the Absorption Spectra of *m*-Difluorobenzene

Band, cm^{-1}	Vibrational energy, cm^{-1} ^a
37,202.4	–748.3
37,721.6	–229.1
37,850.1	–100.6
37,950.7	0
38,654.8	704.1
38,910.5	959.8
39,215.7	1265.0
39,651.1	1700.4
39,880.4	1930.7
40,306.3	2455.6

^a The minus signs indicate excess vibrational energy in the ground state.

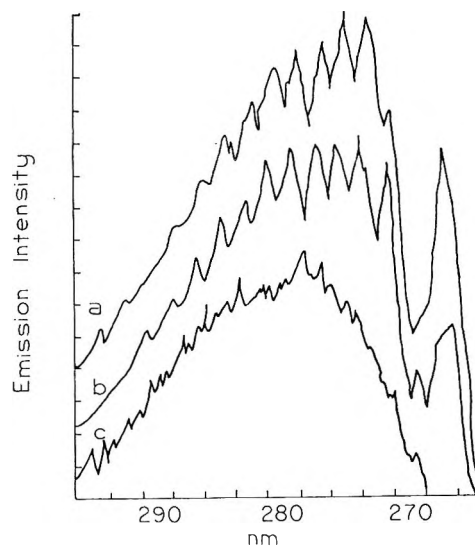


Figure 1. The fluorescence spectra of *m*-difluorobenzene (1 Torr pressure). The different excitation wavelengths are: 2640 Å, curve a; 2600 Å, curve b; 2500 Å, curve c. The emission intensity scale is different for each curve.

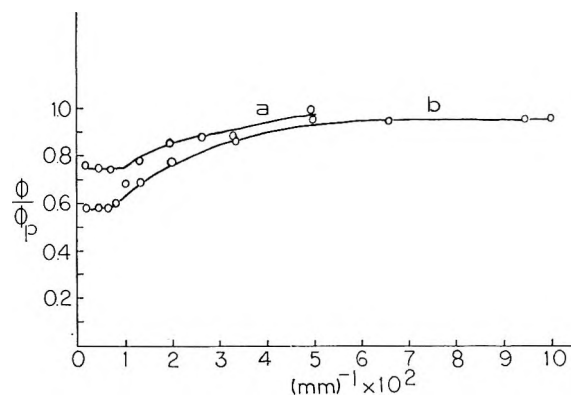


Figure 2. The enhancement of the fluorescent quantum yield with added butane. The excitation wavelengths are: 2540 Å, curve a; and 2500 Å, curve b. Φ = fluorescent yield without quenching gas; Φ_p = fluorescent at pressure p of quenching gas.

The fluorescent spectra are shown in Figure 1. The intensities of the various bands within any one spectrum are relative, but different scales are used for different spectra. The structural features of the spectrum decrease as the wavelength decreases, which is an expected result of vibrational redistribution. The prominent, highest energy band of the curve occurs at a longer wavelength than the O–O absorption band.

Figure 2 shows the results of vibrational relaxation studies with butane as the quenching gas. The graph shows only relative changes in $1/\Phi$, with $1/P$ and not absolute values. Each point in the graphs is the average of three runs, each with an experimental scatter of $\pm 15\%$. In addition to the two wavelengths shown,

(4) W. A. Noyes, Jr., W. A. Mulac, and D. A. Harter, *J. Chem. Phys.*, **44**, 2100 (1966).

(5) H. Sponer, *ibid.*, **49**, 1705 (1968).

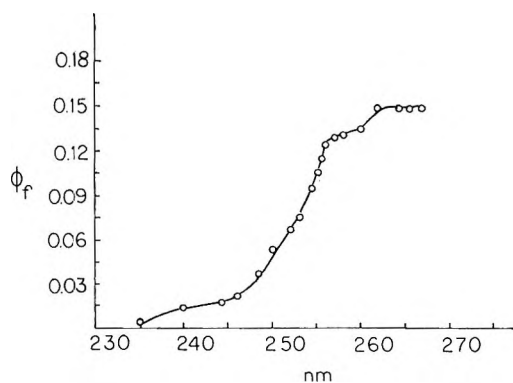


Figure 3. The wavelength dependence of the fluorescent quantum yield.

the Φ_f vs. pressure at 264 nm was also determined. The yield decreased by 12% at 25 mm and then leveled off. Although this decrease is small, it is believed to be real.

The wavelength dependence of the fluorescent quantum yield is consistent with the trend found in other aromatics.^{6,7} As Figure 3 shows, above a certain minimum energy, the yield drops off rapidly and finally reaches zero about 235 nm. One interesting feature of this curve, not found in similar data with benzene, is the sudden increase in the fluorescence quantum yield near the O-O band. The enhancement observed is beyond relative errors and is in the opposite direction expected for "round-the-corner" effects.⁸

The maximum fluorescent quantum yield for *m*-difluorobenzene in the gas phase at 1 mm pressure and room temperature is 0.16 ± 0.02 . This maximum yield occurs only from excitation in the O-O band. This value does not include the inherent error due to the uncertainty in the benzene quantum yield of 0.18 which was used as a standard.

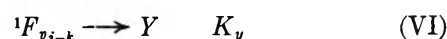
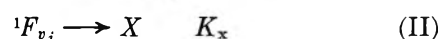
Discussion

The low fluorescent yield found for *m*-difluorobenzene is consistent with values for other fluoroaromatics and reflects the large increase of radiationless transition rates compared with benzene.^{2,8,9} Even though the radiative constant ($k_r = 1/\tau_r = 1.03 \times 10^7 \text{ sec}^{-1}$) for difluorobenzene is about four times that for benzene, the fluorescent quantum yield is lower than that of benzene. This is in opposition to the trend found for alkyl substitution where the increased fluorescent yields are in line with the increase in radiation rates. Thus, the peculiarities of the fluorobenzenes are the large values of the nonradiative decay rate constants (which may include isomerization^{3,10,11}). This may be due to a combination of heavy-atom effects and possible changes in the shapes of the potential surfaces compared with benzene.^{12,13} The heavy-atom effect due to fluorine alone as reported by other researchers for other systems^{14,15} would seem to be too small to account for the large change in rate constants observed here.

Below 255 nm radiationless processes become in-

creasingly important and the fluorescent quantum yield drops sharply and finally reaches zero. A similar behavior has been found for most other substituted benzenes and can be at least partially explained by invoking rearrangement processes.⁵ Although this argument seems applicable to the present case too, no positive statement can be made with regard to the processes occurring below 255 nm since chemical and isomerization reactions were not investigated. Between 255 and 252 nm of the fluorescent yield appears to be independent of wavelength. The increase at 262 nm is probably due to a decrease in the radiationless rate constant at the O-O band without a proportionate decrease in the radiative rate constant. In addition, toluene¹⁴ and the xylenes,¹⁶ which all have large extinction coefficients for their O-O bands, exhibit an increase similar to *m*-difluorobenzene. The fact that this phenomenon is real is further suggested by the fluorescent quenching effects of butane. Collisions between 264-nm excited *m*-difluorobenzene and butane will cause vibrational activation of the difluorobenzene and thus, according to Figure 4, lower the fluorescent yield. This result is also corroborated by similar results found for the xylenes¹⁶ and fluorobenzene.¹⁷

When butane is added to *m*-difluorobenzene, excited to an upper vibrational level of its first excited singlet, it will act mainly as a heat sink and cause vibrational relaxation. If each collision caused vibrational relaxation to the thermal state the following mechanism would hold



(6) D. Phillips, J. Kemaire, C. S. Burton, and W. A. Noyes, Jr., *Advan. Photochem.*, **5**, 341 (1968).

(7) C. L. Braun, S. Kato, and S. Lipsky, *J. Chem. Phys.*, **39**, 1645 (1963).

(8) D. Phillips, *J. Chem. Phys.*, **46**, 4679 (1967).

(9) G. P. Semeluk, R. D. Stevens, and I. Unger, *Can. J. Chem.*, **47**, 3177 (1970).

(10) J. L. Dunham, G. P. Semeluk, and I. Unger, *ibid.*, **46**, 3177.

(11) S. H. Ng, G. P. Semeluk, and I. Unger, *Ber. Bunsenges. Phys. Chem.*, **74**, 29 (1970).

(12) S. Leach, "Transitions Non Radiatives Dans Les Molecules," Societe de Chimie Physique, Paris, 1969, pp 27-30.

(13) A. C. Verma and H. D. Best, *Chem. Phys. Lett.*, **4**, 577 (1970).

(14) C. S. Burton and W. A. Noyes, Jr., *J. Chem. Phys.*, **49**, 1705 (1968).

(15) J. B. Birks, "Photophysics of Aromatic Molecules," Wiley, New York, N. Y., 1970, p 264.

(16) W. A. Noyes, Jr., and D. A. Harter, *J. Amer. Chem. Soc.*, **91**, 7585 (1969).

(17) K. Nakamura, The University of Texas at Austin, private communication, 1970.

where $v_{j-k} = v_0$. The superscript 1 indicates the first excited singlet. The subscript v is symbolic of excess vibration energy. Based on this scheme, a plot of $(\Phi_f)^{-1}$ vs. $(B)^{-1}$ should give a straight line according to (1) if the assumption is made that $[B]k_B \gg k_{v_{j-k}}$

$$\frac{1}{\Phi_f} = [(K_f + K_v)/k_f][1 + K_x/[B]K_B + K_{v_{j-k}}] \quad (1)$$

which seems valid, at least, at the higher pressures where the collisional frequency is high. As Figure 3 shows, the one collision deactivation model does not fit the data either at 254 or 250 nm. Thus complete vibrational deactivation must involve more than one collision. Kemper and Stockburger,¹⁸ among others, have shown collisional vibrational relaxation to involve two processes. First, the vibrational energy initially localized in a few modes is distributed randomly over all the degrees of freedom. The process may be first order in which case collisions would not be the rate-determining steps, or it may be second order with a rate determined by the collisional frequency. Secondly, the total vibrational energy is lost in a stepwise fashion. Thus, processes (3) and (6) must be repeated n times (each time replacing j by $j - k$). The analysis of this mechanism has been carried out by several authors.^{19,20} The quantum yield is dependent on the quotient of two n th degree polynomials in $[B]$ with n equal to the number of collisions necessary for vibrational relaxation. The shapes of the graphs in Figure 3 are in qualitative agreement with such a complex function. As the figure indicates, more collisions are necessary for vibrational relaxation at 2500 than 2540 Å, which is intuitively expected. A rigorous approach to calculating the energy lost per collision involves the slope at the limit $P \rightarrow 0$. The experimental error in the low-pressure region is too large for meaningful calculations. A simpler approach based on hard spheres, assuming each collision to remove the same amount of energy, permits energy removed per collision to be obtained by dividing the excess vibrational energy by the collisional frequency (at the pressure $\Phi_{264\text{nm} + v} = \Phi_{264\text{nm}}$ multiplied by the singlet lifetime). This lifetime will change with vibrational level and therefore a mean lifetime must be used. Thus using a mean lifetime of 10^{-8} sec and a collision frequency of 1.6×10^7 collisions per

molecule per sec at 1 mm pressure (calculated from an assumed $\sigma_{AB} = 6 \times 10^{-8}$ cm) the amount of energy lost per collision for the 250-nm excitation is 66 cm^{-1} and for 254 nm is 56 cm^{-1} . The agreement between the two values may be fortuitous in light of the large error involved.

The triplet yield of *m*-difluorobenzene, reported for O-O band excitation, is 0.79 by the biacetyl method.³ Cundall's value is 0.53 at 253 nm.²¹ Extrapolating this value to the 264-nm region (assuming the increase in triplet yield parallels the increase in fluorescence) gives a triplet yield of 0.81. These results taken with the results reported here give

$$\Phi_f + \Phi_t = 0.96$$

where Φ_t is the triplet state yield at 264 nm. The result indicates that internal conversion from *m*-difluorobenzene's first singlet to the ground state, as found in other single ring aromatics, is of minor importance.

Finally, comparison should be made between these results and earlier work.³ Below 260 nm there is fairly good agreement. The present work does not show the need to assume two excited singlet states between 250 and 276 nm. There is no major absorption at wavelengths longer than the O-O band (263.5 nm). Experimental difficulties such as "round-the-corner" effect, band pass, and monochromator settings (as mentioned by the authors) may be the major source of the discrepancy. The "round-the-corner" effect, in itself, could reasonably explain the maxima and minima reported by Unger.

Acknowledgment. I wish to thank Dr. W. A. Noyes, Jr., for many thoughtful discussions on this research. Financial support came in part from the U.S. Air Force, Air Research and Development Command, Office of Scientific Research, and the Camille and Henry Dreyfus Foundation through grants to Dr. W. A. Noyes, Jr.

(18) H. F. Kemper and M. Stockburger, *J. Chem. Phys.*, **53**, 268 (1970).

(19) M. Boudart and J. T. Dubois, *ibid.*, **23**, 223 (1954).

(20) W. A. Noyes, Jr., and F. C. Henriques, Jr., *ibid.*, **7**, 767 (1939).

(21) J. B. Birks, "Photophysics of Aromatic Molecules," Wiley, New York, N. Y., 1970, p 293.

Relaxation Processes of Cholesteryl Methyl Ether

by P. F. Mountain

Chemistry Department, University of Aston, Birmingham, England

and S. Walker*

Department of Chemistry, Lakehead University, Thunder, Ontario, Canada (Received October 8, 1970)

Publication costs assisted by Lakehead University

The dielectric constants and losses have been determined over a wide microwave frequency range for cyclohexane and *p*-xylene solutions of cholesteryl methyl ether at 25°. The considerable difference in the relaxation times of the molecule and the mobile group produced some separation of the two absorption processes; this enabled a reasonable estimate of the weight factor (C_2) governing that process and provided a lower limit for C_2 for aromatic methoxy compounds of 0.4. In the literature considerable divergence exists for the C_2 values for anisole which ranges between 0.2 and 0.8. The results establish that the C_2 value of <0.4, which have been obtained by three independent investigations recently on the pure liquid anisole and its more concentrated solutions, are not representative as to what appertains in dilute solution.

Introduction

When the weight factors governing the molecular and intramolecular processes are of the same order and the ratio of the molecular (τ_1) to the intramolecular dielectric relaxation time (τ_2) of a nonrigid molecule is less than 8, the Cole-Cole plot¹ remains in its normal form, but as the ratio τ_1/τ_2 (giving the notation k) becomes progressively greater, separation into two distinct absorption regions occurs. If a complete separation occurs, then τ_1 , τ_2 , and C_2 may be evaluated directly without the uncertainty which sometimes arises from a Budó-type analysis.^{2,3} A case in point is the methoxy relaxation time in anisole; a large variance in this parameter determined by the conventional methods has been reported in the literature^{4,5} and C_2 values range between 0.2 and 0.8. Cholesteryl methyl ether (see Figure 1), a large molecule with a long relaxation time, was therefore examined to obtain a lower limit for the C_2 value of anisole, since the presence of a mesomeric effect in anisole would involve a moment opposed in direction to the molecular moment⁵ and thus lead to a smaller C_1 value and hence, since $C_2 = 1 - C_1$, a larger C_2 . It remained a possibility with the anisole and substituted anisoles that the computer analyses on the Budó-type of equation, although mathematically satisfactory, had no significance in terms of molecular behavior. The present work was therefore aimed at making a good estimate of the C_2 governing group relaxation and it was hoped that it would prove possible to achieve some separation of the molecular and group relaxation time absorption peaks.

Experimental Section and Evaluation of Data

The dielectric constant and loss have been determined by a bridge technique (35.1–6.7 GHz) and a coaxial line method (2.46–0.87 GHz). The apparatus and procedure employed are reported elsewhere.^{6–8}

The static dielectric constant, ϵ_0 , was measured with a heterodyne beat apparatus at 2 MHz.

The dipole moments were obtained from the Debye equation

$$\mu = 0.012812[3T(\epsilon_0 - \epsilon_\infty) / \{(\epsilon_0 + 2)(\epsilon_\infty + 2)c\}]^{1/2} \quad (1)$$

in which c is the concentration in moles per milliliter.

The dielectric constant and loss data are presented in Table I, while the relaxation times and dipole moments

Table I: Dielectric Constant and Loss Data for Cholesteryl Methyl Ether in Cyclohexane and *p*-Xylene Solvents at 25°

Frequency, GHz	Cyclohexane		<i>p</i> -Xylene	
	ϵ'	ϵ''	ϵ'	ϵ''
35.11	2.080	0.0142	2.292	0.0198
23.98	2.085	0.0151	2.307	0.0239
16.20	2.096	0.0151	2.311	0.0255
9.313	2.094	0.0143	2.316	0.0239
6.70	2.102	0.0137		
2.455	2.111	0.0191	2.335	0.0292
1.90	2.115	0.0207	2.339	0.0308
1.50	2.116	0.0210		
1.30			2.348	0.0334
1.10	2.119	0.0217		
0.87	2.120	0.0226	2.354	0.0348

- (1) K. S. Cole and R. H. Cole, *J. Chem. Phys.*, **9**, 341 (1941).
- (2) A. Budó, *Phys. Z.*, **39**, 706 (1938).
- (3) M. D. Magee and S. Walker, *J. Phys. Chem.*, **74**, 2378 (1970).
- (4) D. B. Farmer, A. Holt, and S. Walker, *J. Chem. Phys.*, **44**, 4116 (1966).
- (5) D. B. Farmer and S. Walker, *Can. J. Chem.*, **47**, 4645 (1969).
- (6) W. F. Hassell, M. D. Magee, S. W. Tucker, and S. Walker, *Tetrahedron*, **20**, 2137 (1964).
- (7) D. B. Farmer and S. Walker, *ibid.*, **22**, 111 (1965).
- (8) E. H. Grant and S. E. Keefe, *Rev. Sci. Instrum.*, **39**, 1800 (1968).

Table II: Relaxation Times (in Picoseconds) and Weight Factor (C_2) from Computer Analysis, Dipole Moment (μ), Square of the Refractive Index Sodium D line (n^2_D), Static Dielectric Constant (ϵ_0), and Dielectric Constant at Infinite Frequency (ϵ_∞) for Cholesteryl Methyl Ether Solutions of Concentration c (Moles/Liter) and Mole Fraction (f_2) at 25°

Solvent	f_2	c	ϵ_0	ϵ_∞	n^2_D	Computer		C_2	μ
						τ_1	τ_2		
Cyclohexane	0.05457	0.4220	2.159	2.074	2.068	270	8.0	0.39	1.32
<i>p</i> -Xylene	0.08034	0.5476	2.403	2.280	2.241	225	8.6	0.37	1.32

are given in Table II, together with the static and high-frequency dielectric constants.

Purification of Materials. The cholesteryl methyl ether was kept under vacuum over phosphorus pentoxide for several days. The cyclohexane and *p*-xylene solvents were distilled from sodium in a 20-plate column and stored over sodium in stoppered amber bottles.

Discussion

Some consideration of the accuracy of the measured ϵ' and ϵ'' values would be preferable since their variation is small for the systems examined here. It is, however, difficult to attach error limits for ϵ' and ϵ'' for each wave band although an attempt was made to do this in an early publication.⁹ Much depends on the experience and skill of the experimenter. With respect to the data obtained for cholesteryl methyl ether, justification that it is satisfactory may be gained from (i) the dipole moment value of 1.32 D for cholesteryl methyl ether in cyclohexane differs from those of the aliphatic ethers in the literature^{10,11} by no more than the probable error. This implies that the Cole-Cole plot in Figure 2 is probably satisfactory since the dipole moment is highly dependent on the value of ϵ_∞ which is obtained by extrapolating the Cole-Cole plot to infinite frequency. Further, the same result was obtained when the solute was examined in the other noninteracting solvent, *p*-xylene (ii) the sequence of points in the plots in Figures 2 and 3 which always appear in the correct order with increasing frequency, (iii) the fact that the molecular relaxation time of cholesteryl methyl ether in *p*-xylene at 25° of $\sim 225 \times 10^{-12}$ sec from the dielectric data is of the same order as that of the slightly smaller rigid molecule 5 α -cholestan-3-one in *p*-xylene at 25° which has a value of 216×10^{-12} sec.¹² Thus the indications are that the ϵ' and ϵ'' accuracy is of a higher order than we quoted in an early paper⁹ and that the derived parameters ϵ_∞ , μ , and τ_1 are satisfactory, although the accuracy of τ_1 may be not better than $\pm 20\%$.⁹

The ϵ'' vs. $\log \omega$ plot for cholesteryl methyl ether in *p*-xylene at 25° is given in Figure 4, and a reasonable separation into two absorptions may be observed. It is apparent from Figure 3 that since the ϵ''_{\max} value for the molecular absorption peak (the one at lower frequency) is greater than that of the intramolecular process then $C_1 > C_2$; thus values of $C_2 > 0.5$ can be rejected. From the ratio of the two peak heights $C_2 = 0.43$. If separa-

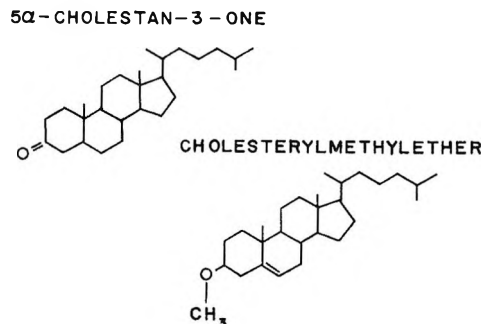


Figure 1. Structural formulas of cholesteryl methyl ether and the similar sized rigid ketone 5 α -cholestan-3-one.

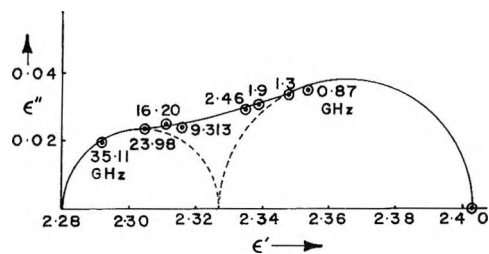


Figure 2. Cole-Cole plot of cholesteryl methyl ether in *p*-xylene at 25°.

tion of the two absorption regions were complete then for both the molecular and group dispersion in Figure 2

$$\epsilon''_{\max} = 1/2(\epsilon_0 - \epsilon_\infty') \quad (2)$$

where ϵ_∞' is $\epsilon_{\infty 1}$ and $\epsilon_{\infty 2}$ for each dispersion, respectively, and $\epsilon_{\infty 1}$ is equivalent to ϵ_0 for the group dispersion. An estimate of each dispersion has been made by approximating the absorptions to correspond with the case of complete separation as on the dotted lines in Figure 2. From these dispersions the C_2 value is 0.3g.

Further, a computer analysis for C_1 , τ_1 , τ_2 in the Budó equation

$$\frac{\epsilon''}{\epsilon_0 - \epsilon_\infty} = (1 - C_2) \frac{\omega\tau_1}{1 + \omega^2\tau_1^2} + C_2 \frac{\omega\tau_2}{1 + \omega^2\tau_2^2} \quad (3)$$

(9) M. D. Magee and S. Walker, *Trans. Faraday Soc.*, **62**, 3093 (1966).

(10) C. P. Smyth, "Dielectric Behavior and Structure," McGraw-Hill, New York, N. Y., 1955.

(11) A. L. McLellan, "Tables of Experimental Dipole Moments," W. H. Freeman and Co., San Francisco, Calif., 1963.

(12) B. J. Cooke, M.Sc. Thesis, Lakehead University, 1969.

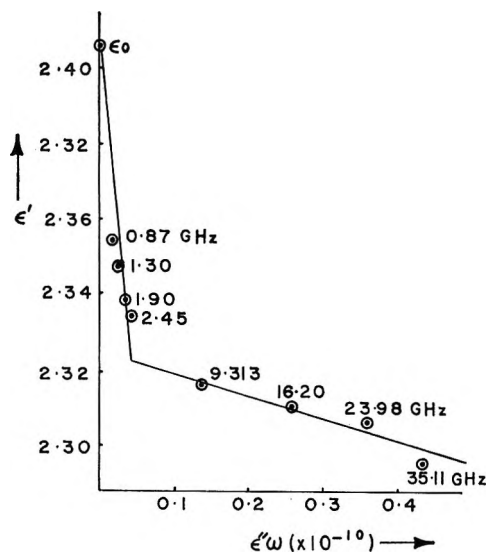


Figure 3. ϵ' vs. $\epsilon'' \omega$ plot of cholesteryl methyl ether in *p*-xylene at 25°.

yielded C_2 values of ~ 0.4 (see Table II). It is interesting to note that the τ_2 values are, within the error of analysis, the same as the value for anisole. However, since τ_2 involves the frictional coefficient for molecular rotational diffusion and this should increase between anisole and cholesteryl methyl ether, since the size of the molecule increases, then this would result in an increase in the τ_2 for cholesteryl methyl ether and, hence, it is difficult to make a meaningful comparison of τ_2 between the two molecules since the frictional constants are not known.

The C_2 value of ~ 0.4 for the steroid thus provides a reasonable estimate of a lower limit for that of anisole, and thus the value of 0.7 ± 0.15 obtained by Farmer and Walker⁵ on a study of anisole would not be opposed to this. However, careful studies by Vaughan, Roeder, and Provder,¹³ and Garg and Smyth¹⁴ on pure liquid anisole produced a C_2 value of 0.25. A more recent examination by Kranbuehl, Klug, and Vaughan¹⁵ indicated that in concentrated solutions C_2 varied between 0.4 to 0.1 and decreased with increasing concen-

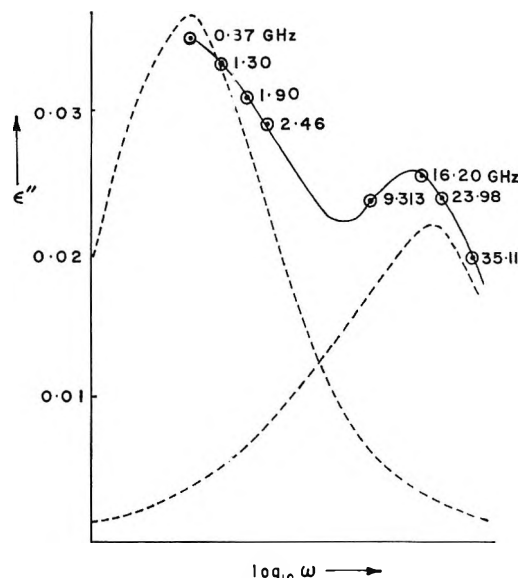


Figure 4. ϵ'' vs. $\log \omega$ plot of cholesteryl methyl ether in the *p*-xylene solution at 25°. The full line represents experimental points and the dotted the molecular and methoxy group absorptions. The molecular absorption is based on a relaxation time of 193×10^{-12} sec while the methoxy absorption curve was obtained by subtracting the molecular absorption from the total absorption.

tration. It seems that for anisole the C_2 obtained from studies on the pure liquid and concentrated solutions is not representative as to what appertains in more dilute solution. Thus it would seem that, for methoxy compounds at least, data should be obtained from work on dilute solutions and that for the anisole and cholesteryl methyl ether systems the C_2 values are in the correct sequence when the mesomeric factor in the former molecule is taken into account.

Acknowledgment. We wish to thank Mr. B. K. Morgan for invaluable technical assistance.

(13) W. E. Vaughan, S. B. W. Roeder, and T. Provder, *J. Chem. Phys.*, **39**, 701 (1963).

(14) S. K. Garg and C. P. Smyth, *ibid.*, **46**, 373 (1967).

(15) D. E. Kranbuehl, D. D. Klug, and W. E. Vaughan, *ibid.*, **50**, 5266 (1969).

Dielectric Properties of Some Diols

by Eiji Ikada¹

Institute for Chemical Research, Kyoto University, Uji, Kyoto-Fu, 611, Japan (Received July 21, 1970)

Publication costs borne completely by The Journal of Physical Chemistry

The dielectric properties of the four diols, 2-methyl-2,4-pentanediol, dipropylene glycol, 2-ethyl-1,3-hexanediol, and thiodiglycol, were studied to correlate the dielectric properties with the molecular structures. The measurements of the dielectric constant and loss were carried out over the audio- and radiofrequency range at temperatures from -70 to 60° . All of these diols except thiodiglycol showed the Davidson-Cole-type dispersions. No significant difference concerning the molecular structure in the shape of the dielectric relaxations was observed for these rather complicated diols. The dielectric behavior of diols was discussed in contrast with those of polyamino compounds.

Introduction

Owing to the dipole-dipole association, the static dielectric constants of hydrogen-bonding molecules are larger than those of the normal polar liquids, and the strong interaction between the molecules leads to large values of relaxation time in breaking and reforming of hydrogen bond accompanying reorientation of the dipoles.² The dielectric relaxation of the monohydroxyl compounds generally shows the Debye-type dispersion involving a single relaxation time and the relaxation mechanism is reasonably explained in terms of breaking and reforming of OH---O hydrogen bond.³ For the dielectric behavior of the diols and triols,⁴ however, the situation seems to be much more complicated in comparison with that of the monohydroxyl compounds. The liquid structure of the polyhydroxyl molecules has not yet been clarified and remained unsolved, although it is no doubt that the hydrogen bond takes part in the cluster formation of liquid diols.⁵

The dielectric dispersions of the polyhydroxyl compounds do not exhibit the Debye type, but the Davidson-Cole-type dispersion.

Meanwhile, the present author has studied the dielectric behavior of the polyamino molecules such as ethylenediamine oligomers $\text{H}_2\text{NC}_2\text{H}_4(\text{HNC}_2\text{H}_4)_{n-1}\text{NH}_2$, ($n = 1, 2, 3$, and 4),⁶ monoethanolamine, diethanolamine, and aminoethylethanolamine.⁷ It was found that the dielectric behavior of these amines was considerably different from that of the hydroxyl compounds such as alcohols and diols. In contrast with the Davidson-Cole-type dispersion of the polyhydroxyl compounds, neither ethylenediamine oligomers nor aminoethylethanolamine showed this type of dispersion in spite of the hydrogen-bonding molecules, but showed the existence of the two large dispersion regions which were analyzed as the superposition of the relaxations of the Debye or the Cole-Cole and the Davidson-Cole type. The shape of the complex loci in the dielectric relaxation of ethylenediamine oligomers differs with each oligomer. The larger the molecule of ethylenediamine oligomers,

the more the shape of the complex loci differs from that of the Davidson-Cole-type dispersion. The shape of the complex locus in aminoethylethanolamine, however, more closely resembles the shape of the Davidson-Cole-type dispersion than those of ethylenediamine oligomers do.

Moriamez, *et al.*, also analyzed the dielectric dispersions of diol molecules such as 2-methyl-2,4-pentanediol⁸ and 2-ethyl-1,3-hexanediol⁹ in terms of the superposition of the Debye-type dispersions. In view of these situations, it is definite that the relaxation mechanism is different with the liquid involving the different type of the hydrogen bond.

On the other hand, Denny¹⁰ studied the dielectric properties of the three isoalkyl halides and found that the dielectric dispersion of these compounds having no hydrogen bonds showed also the Davidson-Cole-type dispersions. In these compounds the hydrogen bond does not exist. This fact, therefore, shows that the hydrogen bond is not a necessary condition for the Davidson-Cole-type dispersion.

The purpose of the present study was to investigate the dielectric relaxation of the complicated diols and to

(1) Correspondence should be addressed to Faculty of Engineering, Kobe University, Kobe, Japan.

(2) G. C. Pimentel and A. B. McClellan, "The Hydrogen Bond," W. H. Freeman and Co., San Francisco, Calif., 1960, p 15.

(3) See, *e.g.*, C. P. Smyth, "Dielectric Behavior and Structure," McGraw-Hill, New York, N. Y., 1955, p 105.

(4) D. W. Davidson and R. H. Cole, *J. Chem. Phys.*, **19**, 1484 (1951).

(5) G. E. McDuffie, Jr., and T. A. Litovitz, *ibid.*, **37**, 1699 (1962).

(6) E. Ikada, *Bull. Inst. Chem. Res., Kyoto Univ.*, **45**, 352 (1967).

(7) E. Ikada, Y. Hida, H. Okamoto, Z. Hagino, and N. Koizumi, *ibid.*, **46**, 239 (1968).

(8) Cl. Moriamez, M. Moriamez, and R. Arnoult, "Spectroscopy and Relaxation at Radio Frequency," North-Holland Publishing Co., Amsterdam, 1962, p 47.

(9) Cl. Moriamez and M. D. Allab, "Magnetic and Electric Resonance and Relaxation," North-Holland Publishing Co., Amsterdam, 1963, p 338.

(10) D. J. Denny, *J. Chem. Phys.*, **27**, 259 (1957).

compare these results with those of the polyamino compounds.

Experimental Section

Materials. Commercial reagents of thiodiglycol, 2-methyl-2,4-pentanediol, dipropylene glycol, and 2-ethyl-1,3-hexanediol were repeatedly distilled in a 70 × 2-cm glass bead-packed column operated at a high reflux ratio under reduced pressure. Refractive indices were measured by a Pulfrich refractometer, and densities were measured by the Lypkin-type pycnometer. Physical constants of these diols are collected in Table I.

Table I: Physical Constants of Diols

Sample	Mp, °C	Bp, °C
2-Methyl-2,4-pentanediol	Glassy	89.5 (9 mm)
Dipropylene glycol	Glassy	113.7 (8 mm)
2-Ethyl-1,3-hexanediol	Glassy	124.5 (7 mm)
Thiodiglycol	-10.2	115.5 (9 mm)

Refractive Indices n_D				
Temp, °C	2-Methyl-2,4-pentanediol	Dipropylene glycol	2-Ethyl-1,3-hexanediol	Thiodiglycol
20	1.4276	1.44092	1.45076	1.521084
30	1.42415	1.43770	1.44734	1.51770
40	1.42065	1.43459	1.44353	1.51464
50	1.41735	1.43067	1.44012	...

Densities (g/ml)				
Temp, °C	2-Methyl-2,4-pentanediol	Dipropylene glycol	2-Ethyl-1,3-hexanediol	Thiodiglycol
20	0.92109	1.02147	0.93971	1.18723
30	0.91390	1.01389	0.93253	1.17425
40	0.91390	1.01389	0.93253	1.17425
50	0.89965	0.99856	0.91771	1.15989

Dielectric Measurements. Dielectric constant and dielectric loss were measured by a transformer ratio-arm bridge (Ando Electric Co. TR-1A) over the frequency range from 7.5 Hz to 5 MHz. Dielectric measurements at higher frequencies up to 250 MHz were made by the use of a Boonton 250 A RX meter.

The dielectric cell was a platinum concentric cell of which vacuum capacitance was determined by the standard liquids.¹¹ The measurement of cell temperature was made by the calibrated thermometer and an Au-Co vs. Cu thermocouple.

Results

Static Dielectric Constants. The observed static dielectric constants of the diols are listed in Table II. The variation of dielectric constants was experimentally represented by the straight lines with respect to the reciprocal of absolute temperature except that of 2-ethyl-1,3-hexanediol which increased more slowly with decreasing temperature, tending to approach a limiting

Table II: Static Dielectric Constants of Diols

Temp, °C	2-Methyl-2,4-pentanediol	Dipropylene glycol	2-Ethyl-1,3-hexanediol	Thiodiglycol
60	20.10	15.66	15.24	22.74
50	21.50	16.73	16.08	24.09
40	22.91	17.88	17.00	25.49
30	24.36	19.02	17.91	26.98
20	25.86	20.38	18.73	28.61
10	27.67	21.83	19.75	30.56
0	29.44	23.38	20.88	32.37
-10	31.38	25.08	21.84	34.46
-20	33.42	26.88	22.88	36.52
-30	35.71	28.85	23.90	...
-40	38.05	30.86	25.00	...
-50	40.78	33.08
-60	43.96	34.50
-70	47.80

value at lower temperature. The observed values are expressed by

$$\epsilon_0 = a + \frac{b}{T} \quad (1)$$

where ϵ_0 is the static dielectric constants, a and b are the empirical constants, and T is the absolute temperature. Numerical values of a and b are listed in Table III in comparison with those of other hydrogen-bonding liquids.

Table III: Numerical Constants of a and b of the Equation $\epsilon_0 = a + (b/T)$ with the Values of the Other Hydrogen-Bonding Liquids

Molecules	a	b
2-Methyl-2,4-pentanediol ^a	-22.38	1.415×10^4
Dipropylene glycol ^a	-18.94	1.155×10^4
Thiodiglycol ^a	-21.23	1.463×10^4
Ethylene glycol ^b	-28.75	2.070×10^4
Diethanolamine ^c	-7.20	9.658×10^3
Diethylenetriamine ^d	-7.36	5.874×10^3

^a The difference between the observed and the calculated dielectric constants is within $\pm 2\%$. ^b N. Koizumi and T. Hanai, *J. Phys. Chem.*, **60**, 1496 (1956). ^c Reference 7. ^d Reference 6.

Dielectric Dispersion. These diols exhibited the dielectric dispersions in the glassy state over the measuring frequency range. Thiodiglycol solidified at the melting point and the dielectric constants reduced to the small values of the order of the magnitude of induced polarization. The primary dispersions of the three diols were observed at the lower frequency region. The complex loci of the dielectric dispersion of 2-

(11) A. A. Maryott and E. R. Smith, *Natl. Bur. Stand. Circ.*, **514**, 1 (1951).

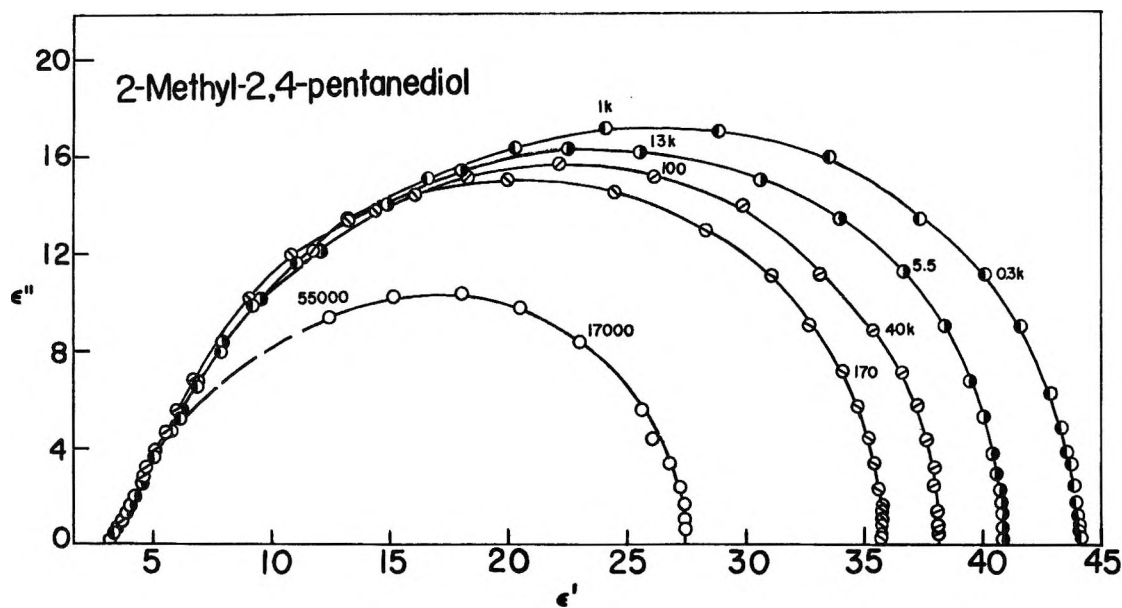


Figure 1. Complex dielectric constant loci for 2-methyl-2,4-pentanediol. Data points are: \bullet , -60° ; \circ , -50° ; \odot , -40° ; \ominus , -30° ; \circ , 5° . The numbers beside data points denote frequency in kHz.

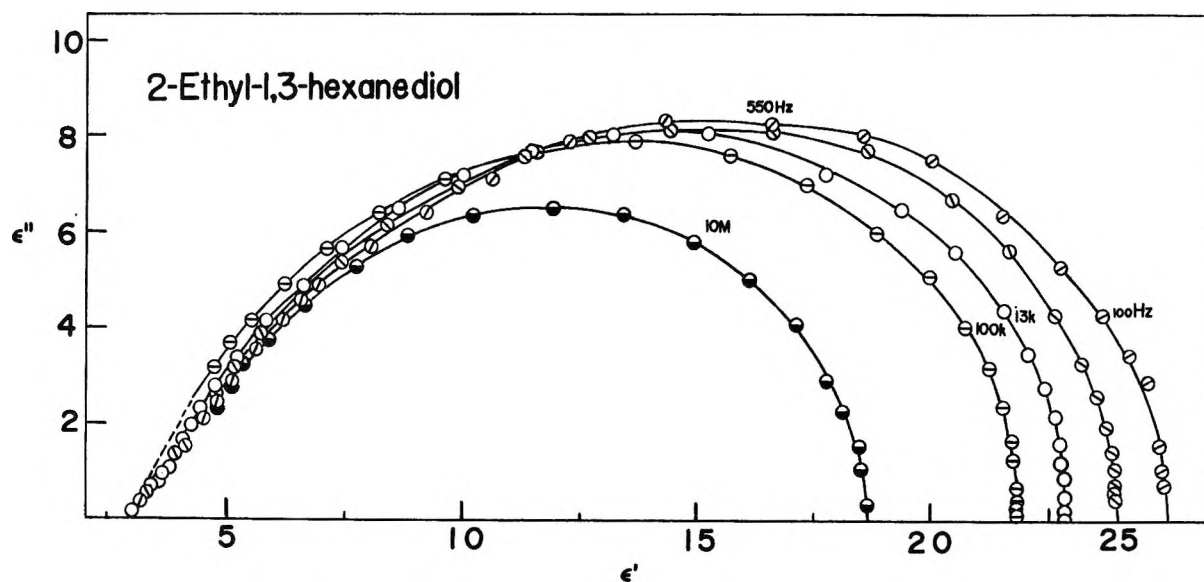


Figure 2. Complex dielectric constant loci for 2-ethyl-1,3-hexanediol. Data points are: \odot , -40° ; \ominus , -30° ; \circ , -20° ; \oplus , -10° ; \bullet , 5° .

methyl-2,4-pentanediol and 2-ethyl-1,3-hexanediol are shown in Figures 1 and 2, respectively. Further at the high frequency region, the small residual dispersions were observed for 2-methyl-2,4-pentanediol and 2-ethyl-1,3-hexanediol.

These principal dispersions are expressed by the Davidson-Cole skewed arc equation⁴

$$\epsilon^* = \epsilon' - j\epsilon'' = \epsilon_\infty + \frac{\epsilon_0 - \epsilon_\infty}{(1 + j\omega\tau_0)^\beta} \quad (2)$$

where ϵ^* is the complex dielectric constant, ϵ_0 is the static dielectric constant, and ϵ_∞ is the limiting high frequency dielectric constant, τ_0 is the relaxation time,

and β is the distribution parameter of relaxation times.

The real and imaginary parts of complex dielectric constants are given by

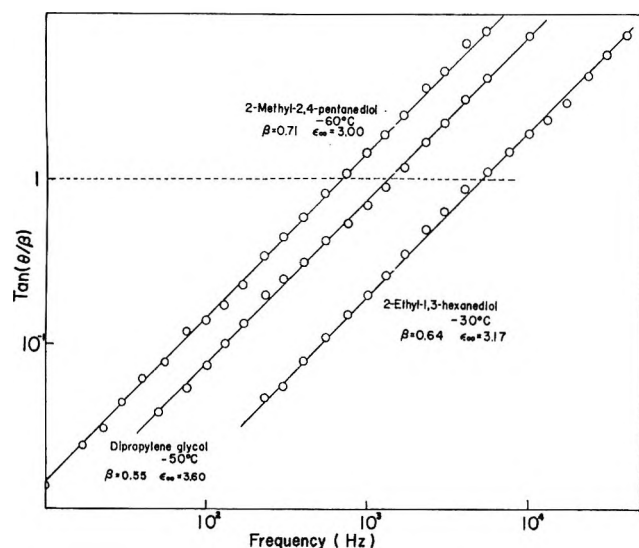
$$\begin{aligned} \epsilon' - \epsilon_\infty &= (\epsilon_0 - \epsilon_\infty)(\cos \phi)^\beta \cos \beta\phi \\ \epsilon'' &= (\epsilon_0 - \epsilon_\infty)(\cos \phi)^\beta \sin \beta\phi \end{aligned}$$

where $\tan \phi = \omega\tau_0$. Putting $\theta = \tan^{-1} [\epsilon''/(\epsilon' - \epsilon_\infty)]$, then $\tan \theta = \tan \beta\phi$, or $\omega\tau_0 = \tan (\theta/\beta)$.

For the Davidson-Cole-type dispersion, plots of $\log \tan (\theta/\beta)$ against \log frequency should give a straight line with the slope of unity. The values of the distribution parameter β and the limiting high frequency dielec-

Table IV: Relaxation Times and Distribution Parameters β of Diols

	2-Methyl-2,4-pentanediol		Dipropylene glycol		2-Ethyl-1,3-hexanediol	
	β	τ_0	β	τ_0	β	τ_0
20	0.71	1.16×10^{-8}
10	0.68	4.58×10^{-9}	0.72	...
5	0.85	4.42×10^{-9}
-10	0.71	5.04×10^{-7}
-20	0.67	1.86×10^{-7}	0.70	3.04×10^{-6}
-30	0.85	2.56×10^{-7}	0.62	1.08×10^{-6}	0.64	3.14×10^{-5}
-40	0.74	1.58×10^{-6}	0.59	8.90×10^{-8}	0.57	5.34×10^{-4}
-50	0.73	1.32×10^{-5}	0.55	1.16×10^{-4}
-60	0.71	2.26×10^{-4}	0.53	3.70×10^{-3}
-65	0.69	9.64×10^{-4}
-70	0.67	1.11×10^{-2}

Figure 3. Frequency plot to determine relaxation time τ_0 .

tric constant ϵ_∞ were selected to satisfy this condition as is shown in Figure 3. The relaxation time was determined from the frequency where the logarithm of $\tan(\theta/\beta)$ corresponds to unity on this straight line. The values of β and τ_0 are listed in Table IV.

Discussion

Static Dielectric Constant. Trouton's constants¹² were calculated as 45.5 for dipropylene glycol, 41.5 for 2-methyl-2,4-pentanediol, and 29.0 for 2-ethyl-1,3-hexanediol which can be regarded as a measure of molecular association. These values are larger than those of ethylenediamine oligomers showing that hydrogen bonds play a more important role in the liquid structure of diols.

For the hydrogen-bonding liquids, regularity and strength of the short-range order has been discussed in terms of Kirkwood's correlation factor g in the following equation¹³

$$\epsilon_0 = \epsilon_\infty + \frac{\epsilon_0}{2\epsilon_0 + \epsilon_\infty} \left(\frac{\epsilon_\infty - 2}{\epsilon} \right)^2 \frac{4\pi N_0 \mu_0^2}{3kT} g \quad (3)$$

where ϵ_0 is the static dielectric constant, ϵ_∞ is the high frequency dielectric constant, μ_0 is the dipole moment *in vacuo*, N_0 is the number of molecules per cubic centimeter, and g is Kirkwood's correlation factor.

It is necessary to know the value of the dipole moment *in vacuo* in order to evaluate g factor. The values of the dipole moment of the diols are considerably dependent on the solvent. The dipole moment of 2-methyl-2,4-pentanediol was observed as 2.9 D in benzene solution and as 2.2 D in dioxane solution;¹⁴ it is rather difficult to estimate experimentally the Kirkwood's correlation factor of polyhydroxyl compounds. Lin and Dannhauser¹⁵ introduced a reduced dielectric constant $(\epsilon_0)_R$ by rearranging eq 3

$$(\epsilon_0)_R = \frac{4\pi N \mu_0^2}{9kT} g = \frac{(\epsilon_0 - \epsilon_\infty)(2\epsilon_0 + \epsilon_\infty) M}{\epsilon_0(\epsilon_\infty + 2)^2 \rho}$$

$$T \times (\epsilon_0)_R = \frac{4\pi N \mu_0^2}{9f} g = 6.08 \times 10^{39} \mu_0^2 \cdot g$$

where N is Avogadro's number, M is the molecular weight, and ρ is the density. The values of $T \times (\epsilon_0)_R$ of diols were plotted against temperature and compared with that of diethylenetriamine in Figure 4. This plot shows that the molecular association of diols due to the hydrogen bond changes more markedly with temperature than that of diethylenetriamine in this temperature range. The coefficient b in eq 1 of the amino compounds and polyhydroxyl molecules are compared in Table III. As is seen in Table III, these

(12) Trouton's constant was calculated by dividing the heat of vaporization by the boiling point. The values of heat of vaporization and the boiling point at atmospheric pressure were adopted from the following references. The heat of vaporization of dipropylene glycol and 2-ethyl-1,3-hexanediol: K. Dolittle, "Technology of Solvents and Plasticizers," Wiley, New York, N. Y., 1954, pp 678-680. The heat of vaporization of 2-methyl-2,4-pentanediol: C. Marsden, "Solvents Manual," Cleaver Hume, London, 1954, p 224. The boiling points: G. O. Curme and F. Johnston, "Glycols," Reinhold, New York, N. Y., 1952.

(13) G. Oster and J. G. Kirkwood, *J. Chem. Phys.*, **11**, 175 (1943).

(14) L. G. Wesson, "Tables of Electric Dipole Moments," The Technology Press (MIT), Cambridge, Mass., 1948, p 32.

(15) R. Lin and W. Dannhauser, *J. Phys. Chem.*, **67**, 1805 (1963).

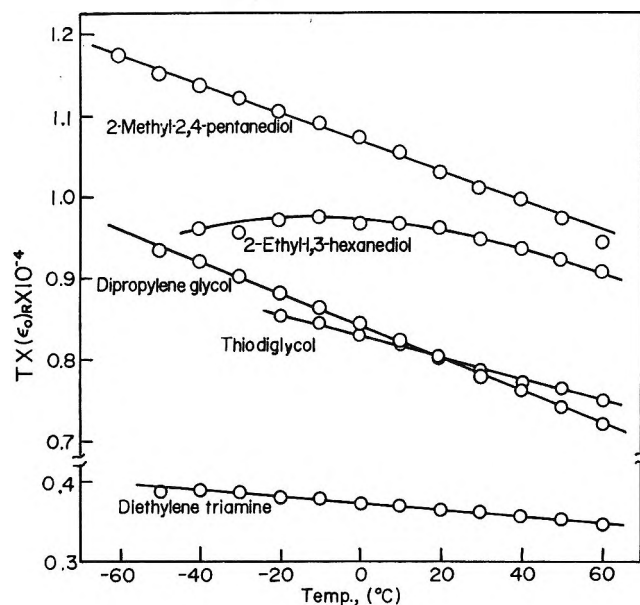


Figure 4. Plots of $T(\epsilon_0)_R$ against temperature.

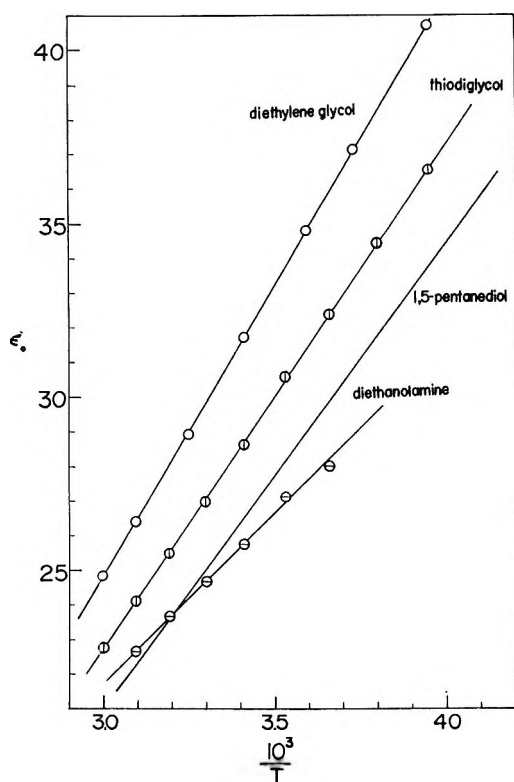


Figure 5. Comparison of the static dielectric constants of various $\text{HOC}_2\text{H}_1\text{XC}_2\text{H}_4\text{OH}$ molecules.

coefficients increase in the order of ethylenediamine oligomers, ethanolamines, and diols.

It is supposed that this order results from the difference in the relative contribution of the hydrogen bond in cluster formation of these compounds. The static dielectric constants of various $\text{HOC}_2\text{H}_1\text{XC}_2\text{H}_4\text{OH}$ molecules are compared in Figure 5, where $\text{X} = -\text{O}-$ corresponds to diethylene glycol,¹⁶ $\text{X} = -\text{S}-$ to thiodi-

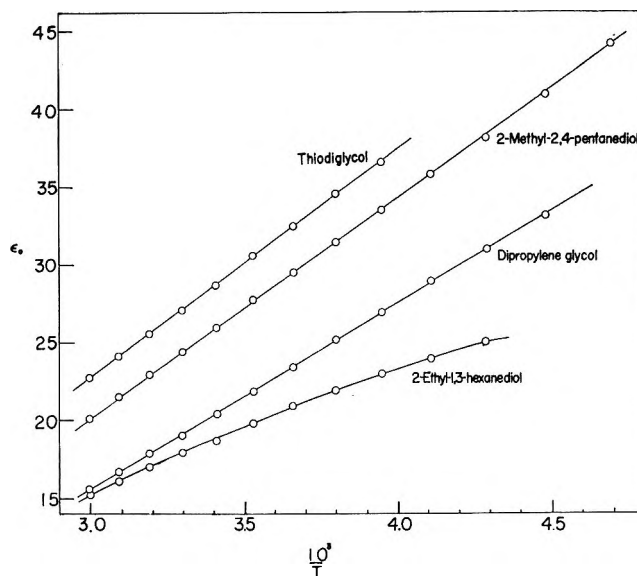


Figure 6. Static dielectric constants of diols plotted against the reciprocal of absolute temperature.

glycol, $\text{X} = -\text{NH}-$ to diethanolamine,⁷ and $\text{X} = -\text{CH}_2-$ to 1,5-pentanediol.¹⁷

Of these substituents, ether oxygen of diethylene glycol and imino group of diethanolamine are capable of hydrogen bonding. It seems that the electronegativity¹⁸ of X group has no direct correlation with the values of the static dielectric constants of these diols. In other words, the X group of these diols does not contribute much to the value of the static dielectric constant. The steric hindrance in the diol molecule is a more important factor for the effective cluster formation which is characteristic of the polyhydroxyl compound as pointed out by McDuffie, *et al.*⁵

As is seen in Figures 5 and 6, the static dielectric constants of diethylene glycol are larger than those of dipropylene glycol since two methyl groups on each end carbon of the latter molecule give the steric hindrance for the intermolecular hydrogen bond. The same effect is recognized in the dielectric constants of 2-ethyl-1,3-hexanediol which has the large ethyl group on the carbon chain. The deviation of the static dielectric constant from the linear relationship would be related with this steric hindrance as seen in Figure 6.

On the other hand, according to Davidson's data of the isomeric pentanediol, the static dielectric constants of the vicinal diols (1,2- and 2,3-pentanediol¹⁷) increase more rapidly at lower temperature. This result is contrasted with the temperature dependence of 2-ethyl-1,3-hexanediol.

Dielectric Dispersion. In the glassy state, ethylenediamine oligomers⁶ and aminoethylethanolamine⁷

(16) N. Koizumi and T. Hanai, *J. Phys. Chem.*, **60**, 1496 (1956).

(17) D. W. Davidson, *Can. J. Chem.*, **39**, 2139 (1961).

(18) L. Pauling, "Nature of the Chemical Bond," Cornell University Press, Ithaca, N. Y., 1940, Chapter 2.

showed considerably complicated dielectric dispersions. The shapes of the complex loci of these dispersions apparently resembled the shape of the Davidson–Cole-type dispersion. The detailed analysis, however, clarified that the dispersion of the above amino molecules could not be represented by the Davidson–Cole-type dispersion.

Unfortunately, the dielectric dispersion of diethanolamine, which is also a kind of diol and amino compound, could not be observed over the measuring frequency range, because this molecule solidified at the melting point. It has been known that the dielectric dispersions of the polyhydroxyl compounds in the liquid or supercooled state are generally of the Davidson–Cole-type dispersion with an exception of 1,5-pentanediol.¹⁷ These structurally complicated diols such as 2-ethyl-1,3-hexanediol and dipropylene glycol also showed the Davidson–Cole-type dispersion. The structural difference in the diols seems to produce no significant difference in the relaxation mechanism of diols. Further, it seems that the principal dielectric dispersions of all the diols studied are better represented by the Davidson–Cole-type dispersion than by the superposition of the Debye-type dispersion as reported by Moriamez, *et al.*^{8,9} This point is an important difference between the dispersions of polyhydroxyl and polyamino compounds. Koizumi and Hanai¹⁶ reported that the large glycol such as tetraethylene glycol shows the Davidson–Cole-type dispersion. On the other hand, the dispersion of tetraethylenepentamine was not of the Davidson–Cole-type but was analyzed by the superposition of two different types of dispersion.

The relaxation times of diols increase more rapidly with decreasing temperature. The Arrhenius plots of relaxation time did not show straight lines, but were adequately represented by the following equation⁴ as is shown in Figure 7

$$\log \tau_0 = A + \frac{B}{T - T_\infty}$$

where T_∞ is the characteristic temperature and A and B are the empirical constants. The values of A , B , and T_∞ are given in Table V together with those of pentanediols. One can recognize the good coincidence of the characteristic temperature T_∞ for the relaxations of the polyhydroxyl compounds with the different molecular structures as is seen in Table V.

It can be supposed that this characteristic temperature which is considered as the freezing temperature of dipolar reorientation is related to the relaxation mechanism of the polyhydroxyl compounds. Davidson and Cole⁴ and Berberian and Cole¹⁹ studied the dielectric properties of the hydrogen-bonded compounds and isoamyl bromide, respectively, and found that there was good agreement between the empirical constants T_∞ calculated from the temperature dependence of the relaxation times and T_∞ calculated from the tempera-

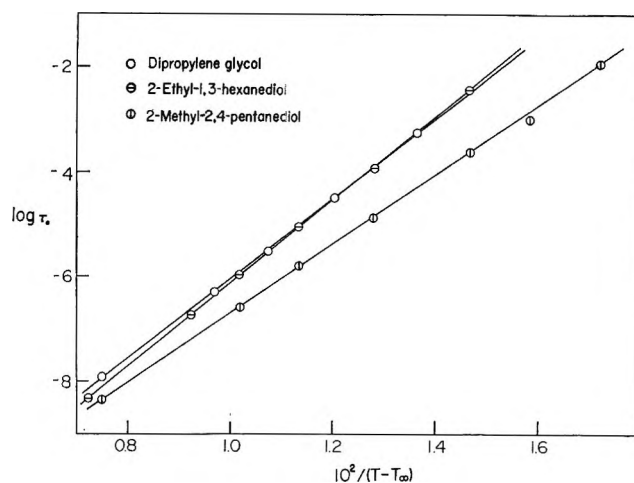


Figure 7. Relaxation times as a function of the reciprocal of $(T - T_\infty)$.

Table V: Numerical Values for the Equation $\log \tau_0 = A + [B/(T - T_\infty)]$

Molecule	A	B	T_∞ , °K
2-Methyl-2,4-pentanediol ^a	-13.24	653	145
Dipropylene glycol ^a	-14.07	793	145
2-Ethyl-1,3-hexanediol ^a	-13.64	758	160
2,4-Pentanediol ^b	-15.33	985	143
2,3-Pentanediol ^b	-15.28	985	145

^a The difference between the observed and the calculated values of $\log \tau_0$ is within $\pm 3\%$. ^b Reference 17.

ture dependence of viscosity and between B and B_η in the equation

$$\log \eta = A_\eta + [B_\eta/(T - T_\infty)]$$

It is supposed from these situations that the mechanism of dielectric relaxation in the polyhydroxyl compounds and isoalkyl halides is closely associated with that of the viscous flow because both dipolar relaxation and viscous flow are governed by the rotational diffusion process.

Davidson¹⁶ reported that the dielectric properties of the isomeric pentanediols depend on the regularity of the hydrogen bonding. It seems that irregularity of the liquid structure with the random intermolecular hydrogen bonding is an important factor for the Davidson–Cole-type dispersion in the polyhydroxyl compounds. The same type of dispersions for isoalkyl halides may be related with the structural irregularity of the supercooled liquids. These irregularly hydrogen-bonded clusters characteristic of the polyhydroxyl compounds may not be formed in the weakly hydrogen-bonded ethylenediamine oligomers. Thus the relaxa-

(19) J. G. Berberian and R. H. Cole, *J. Amer. Chem. Soc.*, **90**, 3100 (1968).

tion of the weakly hydrogen-bonded molecules such as ethylenediamine oligomers are different from that of the strongly hydrogen-bonded polyhydroxyl compounds. The dielectric relaxation of aminoethylethanolamine is an intermediate case between those of ethylenediamine oligomers and the polyhydroxyl molecules. The

dielectric dispersions of the polyhydroxyl compounds depend on the liquid structure rather than the molecular structure.

Acknowledgment. The author wishes to thank Professor N. Koizumi for many helpful discussions.

Perchlorodiphenylmethyl Stable Free Radical. X-Ray

Analysis of a Disordered Mixed Crystal^{1a}

by J. Silverman,* L. J. Soltzberg,^{1b} N. F. Yannoni, and A. P. Krukoniis

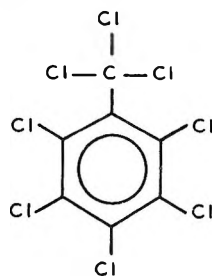
Air Force Cambridge Research Laboratories, Bedford, Massachusetts 01730 (Received August 28, 1970)

Publication costs assisted by Air Force Cambridge Research Laboratories

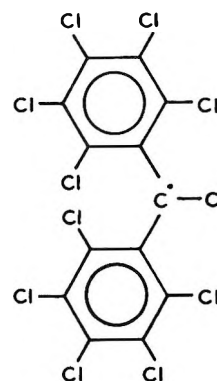
A single crystal originally believed to be pure perchlorodiphenylmethyl free radical, $(C_6Cl_5)_2\dot{C}Cl$, is monoclinic, space group $P2_1/c$, with $a = 9.71$, $b = 13.29$, $c = 14.67$ Å, $\beta = 97.1^\circ$. The X-ray structure determination was supplemented by the analytical techniques of elemental microanalysis, esr spectroscopy, mass spectrometry, and neutron activation analysis in order to characterize a crystalline disorder present in the specimen. While about 37% of the molecules in the crystal are the expected free radical, the crystal also contains about 36% of a related molecule with bromine, probably $(C_6Cl_5)_2CBrCl$, and also a third species, possibly $(C_6Cl_5)_2CHCl$. Although the elements of disorder in the structure limit the accuracy of the determination, the main features of the free-radical structure as well as the deformations in the similarly overcrowded molecules are revealed. The "composite molecule" obtained in the X-ray analysis has approximately twofold symmetry with the phenyl rings rotated by 47 and 43° with respect to the trigonal plane of the central carbon atom. The five chlorine atoms of each phenyl ring deviate from planarity in zigzag fashion.

Introduction

Ballester and coworkers² have succeeded in synthesizing a novel series of alkaromatic chlorocarbons, perchlorotoluene being the first example. Many of these



compounds have very severe intramolecular steric strain and for this reason act readily as the synthetic precursors for the formation of stable free-radical species in the solid. One of these radicals is analogous to the well known hydrocarbon free radical, diphenylmethyl, namely perchlorodiphenylmethyl (PDM; shown below with the unpaired electron indicated by a dot). PDM was synthesized³ in 1964, and an esr study⁴ has been reported on the molecule in solution.



PDM

(1) (a) Presented before the American Crystallographic Association, Ottawa, Canada, Aug 1970; (b) National Research Council Postdoctoral Research Associate, Jan–Sept 1969.

(2) M. Ballester, *Pure Appl. Chem.*, **15**, 123 (1967); *Bull. Soc. Chem. Fr.*, **7** (1966), and references therein.

(3) M. Ballester and J. Riera, *J. Amer. Chem. Soc.*, **86**, 4505 (1964).

(4) H. R. Falle, G. R. Luckhurst, A. Horsfield, and M. Ballester, *J. Chem. Phys.*, **50**, 258 (1969).

Considerable interest is attached to a crystal structure determination of the PDM molecule for two reasons. First, no structural results have been reported on any of these new alkaromatic perchlorocarbons, and second, structural information on the conformation of free radicals in the solid state remains relatively sparse,⁵ particularly when the unpaired electron is localized on a carbon atom.⁶ We have now completed three-dimensional X-ray structure work on crystals originally thought to be pure PDM. Certain anomalies in our X-ray results received further clarification through the auxiliary analytical techniques of elemental microanalysis, esr, mass spectrometry, and neutron activation analysis. It is shown that the free-radical species occurs in our sample in the presence of two other molecules in a disordered, mixed crystal. While this unexpected result obscures somewhat the structural information on the free radical, the quite unusual mixed crystal is well characterized by integration of the analytical and X-ray techniques.

Experimental Section

(a) *X-Ray Analysis.* Our bright red-orange crystals contain four molecules per unit cell in the monoclinic space group $P2_1/c$. Cell dimensions are: $a = 9.71 \pm 0.02$; $b = 13.29 \pm 0.03$, $c = 14.67 \pm 0.03$ Å; $\beta = 97.1 \pm 0.5^\circ$. Intensities were measured by densitometry of integrated precession camera films taken with Zr-filtered Mo $K\alpha$ radiation. Data taken about three axes yielded 700 observed independent reflections after cross correlation. Corrections for Lorentz and polarization factors were applied, but no absorption corrections were made ($\mu = 16.4 \text{ cm}^{-1}$ for $\lambda 0.7107$ Å). The data crystal was a pinacoidal prism whose cross section in the X-ray beam ranged from 0.16 to 0.22 mm.

Attempts to solve the structure by Patterson (vector map) methods failed, and we turned to direct (probability) methods and solved the structure by the symbolic addition procedure.⁷ The initial E map, based on 152 signed E 's ≥ 1.4 , showed ten peaks corresponding to the phenyl chlorine atoms. The initial positions for the carbon atoms were derived from these chlorine peaks. In addition, the E map showed two peaks arranged tetrahedrally about the central methyl carbon atom which were equally likely candidates for the anticipated 11th chlorine atom. Further examination of difference Fourier maps and preliminary least-squares refinement results revealed that three distinct electron-density maxima are "attached" to the methyl carbon atom. The two tetrahedrally arranged peaks are each about 1.9 Å from this carbon atom and each has an electron content of 0.7 of a full chlorine atom; a third peak, roughly equivalent to 0.3 of a chlorine atom, is found in a trigonal configuration with respect to, and 1.7 Å away from, the methyl carbon. The obvious supposition that a higher molecular weight impurity was present received further support from careful dens-

ity measurements ($D_m = 2.03 \text{ g cm}^{-3}$) which, based on four molecules per unit cell, gave an experimental molecular weight of 578 ± 10 as compared with 546 calculated for PDM.

(b) *Results of Auxiliary Measurements.* At this point in the analysis, the following auxiliary techniques were used in order to clarify the X-ray results. Elemental analysis gave a surprising result: 5% of the sample by weight is neither carbon, chlorine, nor hydrogen, although for the remaining 95%, the ratio of carbon to chlorine is very close to C_{13}/Cl_{11} . A routine esr experiment on a single crystal showed a free-radical signal at a g value close to that reported for PDM⁴ and provided a crude estimate of about 50% fraction of free radical. The mass spectrum, in addition to exhibiting many peaks plausibly explained in terms of a parent PDM molecule, showed a small peak starting at m/e 585. This peak was about 7% as intense as the strongest spectral peak (found at m/e 471 and assigned to $C_{13}Cl_9^+$). While the small peak came at nine mass units greater than an anticipated impurity, $C_{13}Cl_{12}$ (not found in the spectrum), its isotopic peak distribution did correspond to that of a 12-chlorine species! Consistency among these diverse observations evolved from the tentative identification of the m/e 585 species as $C_{13}Cl_{10}Br^+$ presumed to derive from a $C_{13}Cl_{11}Br$ parent.⁸ Hoping to confirm the presence of bromine, we had a neutron activation analysis performed on other crystals from the same batch. These crystals provided zero-level Weissenberg photographs identical with that of the data crystal. The neutron activation analysis showed that the total sample of 100 μg (several crystals) contained 6% bromine by weight, in substantial agreement with the missing 5% in the elemental analysis. The partial atomic occupancy factors derived from the X-ray study (see next section) were also in good agreement with the presence of this amount of bromine.

Characterization of the Mixed Crystal

Keeping these results in mind, we completed the X-ray structural analysis by means of full-matrix least-squares refinement. Isotropic thermal parameters were assigned to each atom. For the three partially occupied sites attached to the methyl carbon C^* , we

(5) A general review is found in the article by P. Anderson in "Selected Topics in Structure Chemistry," P. Anderson, O. Bastiansen, and S. Furberg, Ed., Universitetsforlaget, Oslo, 1967, p 125. More recent free-radical structure determinations are reported by D. E. Williams, *J. Amer. Chem. Soc.*, **89**, 4280 (1967); *ibid.*, **91**, 1243 (1969); *Mol. Phys.*, **16**, 145 (1969).

(6) The only example we know of is tri-*p*-nitrophenylmethyl: P. Anderson and B. Klewe, *Acta Chem. Scand.*, **21**, 2599 (1967).

(7) J. Karle and I. L. Karle, *Acta Crystallogr.*, **21**, 849 (1966).

(8) We noted that the $C_{13}Cl_{10}Br^+$ species can mask as a 12-chlorine fragment because the isotopic peak distribution for a Cl_n species becomes very similar to that for $Cl_{n-2}Br$ as n gets larger. See J. H. Beynon, R. A. Saunders, and A. E. Williams, "The Mass Spectra of Organic Molecules," Elsevier, Amsterdam, 1968, pp 375, 376.

creases slightly despite the drop in R and because the physical basis for a Gaussian (ellipsoidal) model of the thermal motion may be lacking. In any case the molecular conformation does not change significantly after anisotropic refinement.

The general reasonableness of the molecular dimensions, the plausibility of the conformational features, and the good quality of the X-ray photographs indicate that the molecules have very similar shape and comfortably occupy crystallographically identical sites within the same crystal. Hence the configuration of the molecular hybrid obtained from the X-ray analysis yields some quantitative information on the sought for conformation of the free radical despite the low accuracy in bond lengths and angles inevitable for such a complex disorder. A general picture of the deformations arising from the severe overcrowding present in all three molecules is also obtained.

The ten ring carbon-chlorine distances range from 1.65 to 1.76 Å (mean value = 1.71 Å); for the 12 carbon-carbon distances in the rings, the range is 1.35–1.50 Å (mean value = 1.40 Å). Standard deviations for an individual bond can be estimated statistically from the scatter about these mean values and are 0.037 and 0.047 Å for the C-Cl and C-C bonds, respectively. These values are well within the estimated standard deviations of 0.06 and 0.07 Å obtained from the least-squares matrix inversion. The C*-Cl* distance of 1.75 Å associated with the free radical cannot be distinguished from the ring (aromatic) carbon-chlorine distances at the level of accuracy of the determination. The two C*-X distances are 1.88 and 1.90 Å, and, as expected from the mixed identity of these atoms, are intermediate between the range found for C-Cl aliphatic distances,¹² 1.75–1.84 Å, and the typical value for the corresponding C-Br bond,¹³ 2.00 Å.

The severe internal overcrowding of the present molecule(s) is somewhat analogous to that found in octachloronaphthalene¹⁴ in which adjacent Cl...Cl contacts range from 2.998 to 3.078 Å and severe distortions from planarity are found for the chlorine atoms. In the present composite molecule, the ortho Cl...Cl contacts range from 2.95 to 3.15 Å. The deviations from planarity of the phenyl chlorines are quite marked and follow a similar zigzag pattern in both rings (see Figure 2, upper half). Least-squares planes passed through the ring carbon atoms indicate that these atoms are planar to within experimental error. The deviations from these planes (Figure 2, lower half) suggest that the deformations of the six ring substituents have a "boat-shaped" character.

A noteworthy feature of the conformation is that the five-atom groups Cl6, C6, C1, C*, X1 and Cl6a, C6a, C1a, C*, X2 are coplanar to within ± 0.1 and ± 0.2 Å, respectively. Very severe steric repulsion is found in the final conformation as it relates to species II and III due to the unusually close approaches of 2.76 Å between

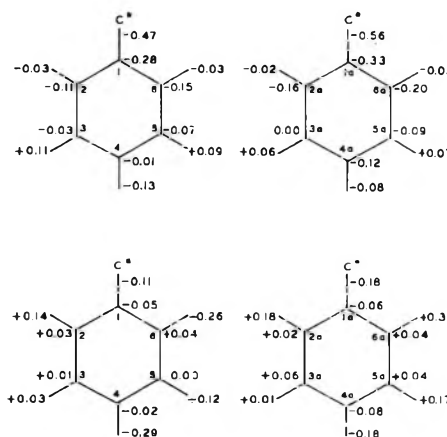


Figure 2. Least-squares planarity analysis. Displacements in Å from planes passed through the five chlorine atoms of each ring (upper half) and from planes through the six carbon atoms of each benzene ring (lower half).

Cl6 and X1 and 2.83 Å between Cl6a and X2 (sums of the van der Waals radii for Cl...Cl and Cl...Br are 3.6 and 3.75 Å, respectively). The configuration of species II and III is apparently constrained sterically by these contacts as far as further out-of-plane rotation of the phenyl rings is concerned and largely by Cl2, Cl2a contacts with the π clouds of the opposite benzene rings as far as further rotation toward the trigonal plane. The PDM species itself is less overcrowded with Cl* intramolecular contacts at about 3.15 Å on both sides (Figure 1). While further rotation from the trigonal plane of the phenyl rings of this species would provide steric relief, the tendency is presumably balanced by intermolecular packing forces and/or conjugation effects. It is emphasized that the statistical averaging over the atomic positions of the three molecules is likely to be spatially broadest for atoms Cl6 and Cl6a for reasons discussed above. The mean positions obtained for these atoms in the X-ray analysis may well have exaggerated the differences just described between the degree of overcrowding of the free radical and that of the other species.

Many values of the bond angles such as the large angles at C1 and C1a of 129 and 126° can be rationalized in terms of steric interactions. However, the high standard deviations, 4–5°, preclude detailed comment.

The two phenyl rings are related to each other by an axis of approximate twofold symmetry through atom C*, which relates the positions of corresponding atoms (2 with 2a, etc.) to within 0.27 Å. Various aspects of the configuration such as the deformations from planarity also reflect this approximate twofold character. With reference to a hypothetical completely

(12) I. L. Karle and J. Karle, *Acta Crystallogr., Sect. B*, **25**, 1097 (1969).

(13) E. M. Gopalakrishna, A. Cooper, and D. A. Norton, *ibid.*, **25**, 2473 (1969).

(14) G. Gafner and F. H. Herbstein, *Nature*, **200**, 130 (1963).

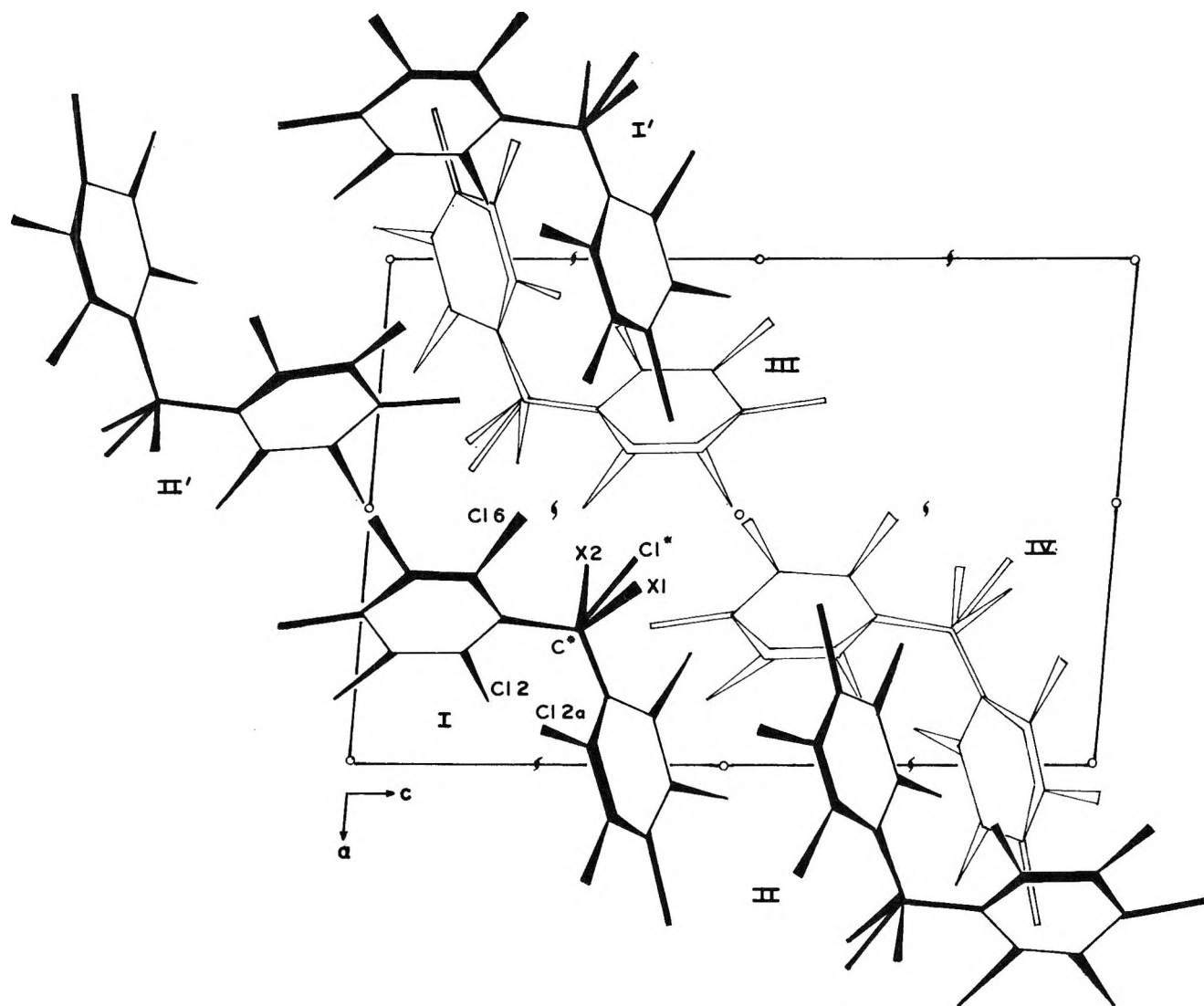


Figure 3. View of the crystal structure in projection down the b axis. Molecules in lighter outline are separated from those in darker relief by approximately $\pm b/2$.

planar molecule, the benzene rings are rotated about the C^*-Cl and C^*-Cl_1a bonds by 47 and 43°, respectively. The two rings make a dihedral angle of 72° with each other. The rotation angles are substantially less than the value of 64° for the free-radical species inferred from the solution esr data;⁴ the usual tendency is indeed toward greater molecular planarity in the solid, particularly when bulky groups can rotate about single bonds (see final reference cited in footnote 5).

Figure 3 is a projection of the crystal structure down the b axis. The packing is quite efficient with many close but no unusual intermolecular approaches. The shortest are 3.29 Å, $X2 \cdots Cl_4$; 3.34 Å, $X1 \cdots Cl_5$; 3.34 Å, $Cl^* \cdots Cl_4a$; and 3.41 Å, $X2 \cdots Cl_6$. The closest $Cl \cdots C$ contact is 3.53 Å and there are no close $C \cdots C$ approaches.

A structure analysis on a pure crystal of the free radical would establish whether any differences in the

PDM conformation or its crystal structure result from the presence of the two other species. We do not plan further work along these lines in the foreseeable future.

Acknowledgment. We are much indebted to Dr. J. Stauffer of the Arthur D. Little Co. for taking the mass spectrum, to Professor S. J. Weininger of Worcester Polytechnic Institute for helpful discussions on these spectra, to Professor T. Tuttle of Brandeis University for the esr measurement, and to Capt. F. C. Damm of the Air Force Nuclear Engineering Center at Wright Patterson AFB for the neutron activation analyses. We are grateful to Professor M. Ballester of the University of Barcelona for supplying us with the crystals and for useful discussions, and to Dr. L. Spialter of the Aerospace Research Laboratories (OAR) for proposing the structure determination, maintaining an active interest during its course, and for suggesting and arranging for the neutron activation analysis.

Cohesive Energies of the Alkali Hydrides and Deuterides

by R. C. Bowman, Jr.

Monsanto Research Corporation, Mound Laboratory,¹ Miamisburg, Ohio 45342 (Received December 21, 1970)

Publication costs assisted by the Monsanto Research Corporation

The effect of isotopic substitution on cohesive energies of alkali hydrides has been estimated using Born-Mayer equations. Second-neighbor interactions and van der Waals terms were included in the calculations. Vibrational contributions were obtained from Debye lattice theory. Theoretical cohesive energies are in excellent agreement with experimental values. Differences between calculated hydride and deuteride cohesive energies are slightly larger than experimental differences. Estimates of compressibilities and Debye temperatures are also given.

Introduction

Since the hydride ion possesses a noble gas electron configuration, the alkali hydrides can be considered members of the alkali halide family. In fact, these hydrides have many ionic properties similar to those found in the alkali halides. However, some past studies on LiH as discussed by Pretzel, *et al.*,² and Magee³ indicate that there may be extensive covalent bonding in the alkali hydrides.

The Born theory of solids provides a means of estimating covalency in "ionic" crystals. When the bonds have large covalent contributions,⁴ the cohesive energies determined from the Born model are significantly smaller than values deduced from thermochemical cycles. Although this analysis is not very sensitive in detecting departures from ideal ionicity, it does predict lower limits of the covalent contributions to alkali hydride cohesion.

While the crystal properties of alkali hydrides have been estimated for a variety of Born-type models,^{3,5-9} the majority of these calculations are based on simple models which only include electrostatic static interactions between point charges and repulsive forces between nearest neighbors (NN). The important contributions^{4b} of next-nearest-neighbor (NNN) repulsions, van der Waals (VDW) potentials, and lattice vibrations have been consistently omitted. The alkali hydride cohesive energies reported in this paper were determined from a Born-Mayer model^{4b} with NNN-VDW terms. The most recent data were used in the calculations where the VDW coefficients were obtained from crystal optical absorption spectra. The lattice vibrational energies were estimated using the Debye theory of lattices.

Because of a large mass ratio between hydride and deuteride ions, alkali hydride cohesive energies should be particularly sensitive to isotopic substitution. Although calorimetric measurements¹⁰ show a small, but discernible, isotopic effect for the alkali hydrides, no previous Born-type calculation has explicitly considered the role of isotopic substitution. In the present

calculations, special attention was given to include systematically all relevant isotopic contributions.

Besides the cohesive energies, the compressibilities and Debye temperatures have been estimated for the alkali hydrides and deuterides. These results are compared, whenever possible, with values deduced by other workers.

A Digital PDP-8/I computer was used for the actual computations.

Theoretical Considerations

The cohesive energy of an ionic crystal is the sum of the lattice energy, W_L , and the internal energy associated with lattice vibrations, W_{VIB} . In terms of the Born theory, W_L is expressed as a sum of two-body interaction energies using adjustable parameters deduced from crystal data. For cubic solids, which include all alkali hydrides, these parameters are found by fitting the Born lattice energy model to the solid-state equation of state and its volume derivative.^{4b} In the present study, the thermodynamical condition of the alkali hydride crystals are specified as room temperature and atmospheric pressure. W_{VIB} , which represents the sum of zero point and heat capacity energies, can be estimated¹¹ from well-known Debye models.

(1) Mound Laboratory is operated by Monsanto Research Corp. for the U. S. Atomic Energy Commission under Contract No. AT-33-1-GEN-53.

(2) F. E. Pretzel, G. N. Rupert, C. L. Mader, E. K. Storms, G. V. Gritton, and C. C. Rushing, *J. Phys. Chem. Solids*, **16**, 10 (1960).

(3) C. G. Magee in "Metal Hydrides," W. H. Mueller, J. P. Blackledge, and G. G. Libowitz, Ed., Academic Press, New York, N. Y., 1968, Chapter 6.

(4) (a) M. F. C. Ladd and W. H. Lee, *J. Inorg. Nucl. Chem.*, **11**, 264 (1959); (b) M. P. Tosi, *Solid State Phys.*, **16**, 1 (1964).

(5) J. Sherman, *Chem. Rev.*, **11**, 93 (1932).

(6) E. C. Baughan, *Trans. Faraday Soc.*, **55**, 736 (1959).

(7) T. R. P. Gibb, Jr., in "Progress in Inorganic Chemistry," Vol. III, F. A. Cotton, Ed., Interscience, New York, N. Y., 1962, pp 315-511.

(8) L. Dass and J. C. Saxena, *J. Chem. Phys.*, **43**, 1747 (1965).

(9) D. W. Hafemeister and J. D. Zahrt, *ibid.*, **47**, 1428 (1967).

(10) S. R. Gunn and L. G. Green, *J. Amer. Chem. Soc.*, **80**, 4782 (1958).

When VDW and NNN terms are included in the Born-Mayer model, the lattice energy is given by

$$W_L = -(\alpha_r e^2/r) - (C_r/r^6) - (D_r/r^8) + 6b \left[\beta_{+-} \exp\left(\frac{r_+ + r_- - r}{\rho}\right) + \beta_{++} \exp\left(\frac{2r_+ - sr}{\rho}\right) + \beta_{--} \exp\left(\frac{2r_- - sr}{\rho}\right) \right] \quad (1)$$

Here, α_r is the Madelung constant, e is the electronic charge, r is the interionic separation between nearest neighbors, C_r and D_r are dipole-dipole and dipole-quadrupole VDW coefficients, respectively, β_{12} are constants of order unity which are qualitatively related to the electronic configuration of the ions, r_+ and r_- are ionic radii, b and ρ are Born-Mayer repulsive parameters, and sr is the separation between NNN ions. Since all alkali hydrides crystallize in a NaCl lattice structure, α_r and s equal 1.75756 and $\sqrt{2}$, respectively.

The present calculations are based upon the "static lattice" approximation of equation of state in which the Born-Mayer parameters can be determined using only the lattice parameter, $2r_0$, and isothermal compressibility, K . A trivial, but important, reason for choosing this version of the equation of state is the nearly complete absence of reported crystal data (other than lattice parameters) for all alkali hydrides except LiH and LiD. A more fundamental difficulty arises from the very high Debye temperatures possessed by the alkali hydrides.² Detailed thermodynamic analysis¹² has shown that conventional Hildebrand or Mie-Grüneisen formulations of the equation of state are invalid in temperature regions much lower than the Debye temperature. Since room temperature lies within this temperature range for the alkali hydrides, the use of these more involved formulations cannot be justified. Therefore, the static lattice version has been used for the alkali hydrides. The calculated cohesive energies are expected to be reasonable as careful studies on the alkali halides by Tosi^{4b} indicate the energies determined from the static lattice approximation agree within a couple per cent with values obtained from more elaborate models.

Methods for evaluating the equation of state and its volume derivative from a given Born-Mayer model have been adequately described elsewhere.^{4b,13} Only the final equations are presented here. When b is eliminated from eq 1 by use of the static lattice equations, the lattice energy can be rewritten as

$$W_L = -\frac{\alpha_r e^2(1 - \chi_1)}{r_0} - \frac{C_r(1 - 6\chi_1)}{r_0^6} - \frac{D_r(1 - 8\chi_1)}{r_0^8} \quad (2)$$

where

$$\chi_1 = \rho\sigma/r_0\gamma \quad (3)$$

$$\tau = \beta_{+-} \exp\left(\frac{r_+ + r_- - r_0}{\rho}\right) + \beta_{++} \exp\left(\frac{2r_+ - sr_0}{\rho}\right) + \beta_{--} \exp\left(\frac{2r_- - sr_0}{\rho}\right) \quad (4)$$

$$\gamma = \beta_{+-} \exp\left(\frac{r_+ - r_- - r_0}{\rho}\right) + s \left[\beta_{++} \exp\left(\frac{2r_0 - sr_0}{\rho}\right) + \beta_{--} \exp\left(\frac{2r_- - sr_0}{\rho}\right) \right] \quad (5)$$

The Born-Mayer parameter ρ is obtained by solving the equation

$$K^{-1} = \frac{-1}{18r_0^3} \left[\frac{\alpha_r e^2}{r_0} (1 - \chi_2) + \frac{6C_r}{r_0^6} (6 - \chi_2) + \frac{8D_r}{r_0^8} (8 - \chi_2) \right] \quad (6)$$

where

$$\chi_2 = \rho\sigma/r_0\gamma \quad (7)$$

$$\sigma = \frac{r_0}{\rho} \left(\frac{r_0}{\rho} - 1 \right) \beta_{+-} \exp\left(\frac{r_+ + r_- - r_0}{\rho}\right) + \frac{sr_0}{\rho} \left(\frac{sr_0}{\rho} - 1 \right) \left[\beta_{++} \exp\left(\frac{2r_+ - sr_0}{\rho}\right) + \beta_{--} \exp\left(\frac{2r_- - sr_0}{\rho}\right) \right] \quad (8)$$

The VDW coefficients C_r and D_r represent summations over two-body VDW interactions between the various ions. When the ionic crystal is comprised of two Bravais lattices, the van der Waals coefficients are given by¹⁴

$$C_r = c_{+-} S_R^{(6)}(\mathbf{r}_-) + 1/2(c_{++} + c_{--}) S_R^{(6)}(0) \quad (9)$$

$$D_r = d_{+-} S_R^{(8)}(\mathbf{r}_-) + 1/2(d_{++} + d_{--}) S_R^{(8)}(0) \quad (10)$$

where the lattice sums, $S_R^{(n)}(\mathbf{r})$ are known and have been tabulated by Tosi.^{4b} The two-body VDW coefficients c_{12} and d_{12} are determined from the Mayer¹⁴ equations

$$c_{12} = 3\alpha_1\alpha_2 E_1 E_2 / 2(E_1 + E_2) \quad (11)$$

$$d_{12} = \frac{27\alpha_1\alpha_2 E_1 E_2}{8e^2(E_1 + E_2)} \left(\frac{\alpha_1 E_1}{n_1} + \frac{\alpha_2 E_2}{n_2} \right) \quad (12)$$

Here, E is the average excitation energy, α is the ionic polarizability, and n is the number of outer-shell electrons.

(11) L. D. Landau and E. M. Lifshitz, "Statistical Physics," Addison-Wesley, Reading, Mass., 1958, pp 187-190.

(12) F. G. Fumi and M. P. Tosi, *J. Phys. Chem. Solids*, **23**, 395 (1962).

(13) M. Born and K. Huang, "Dynamical Theory of Crystal Lattices," Clarendon Press, Oxford, 1954, Section 3.

(14) J. E. Mayer, *J. Chem. Phys.*, **1**, 270 (1933).

Table I: Experimental Data^a

	LiH	NaH	KH	RbH	CsH
r_0 (10^{-8} cm)	2.042 2.034	2.440 2.434	2.854 2.848	3.024	3.194
r_+ (10^{-8} cm)	0.90	1.21	1.51	1.65	1.80
r_- (10^{-8} cm)	1.30	1.30	1.30	1.30	1.30
K (10^{-12} dyn/cm ²)	2.88 2.85				
α_+ (10^{-24} cm ³)	0.029	0.255	1.201	1.797	3.137
α_- (10^{-24} cm ³)	1.86	1.86	1.86	1.86	1.86
E_+ (10^{-12} erg)	118.4	107.8	63.3	71.0	66.0
E_- (10^{-12} erg)	10.7	13.9	11.8	10.3	9.36
c_{++} (10^{-60} erg cm ⁶)	0.075	5.26	68.5	180	487
c_{--} (10^{-60} erg cm ⁶)	22.3	17.3	20.3	23.2	23.2
c_{+-} (10^{-60} erg cm ⁶)	0.828	7.03	31.5	48.8	85.6
C_r (10^{-60} erg cm ⁶)	25.7	66.8	288.0	505	1030
d_{++} (10^{-76} erg cm ⁸)	0.025	3.53	127	535	2460
d_{--} (10^{-76} erg cm ⁸)	45.2	35.0	41.2	46.9	51.8
d_{+-} (10^{-76} erg cm ⁸)	0.98	9.48	61.1	125	304
D_r (10^{-76} erg cm ⁸)	24.1	73.7	442	1000	2870

^a In the rows for r_0 and K , the upper values are for the hydrides while the lower values pertain to the deuterides. For the other rows, single values represent both hydrides and deuterides.

Data

The data used in the cohesive energy calculations are summarized in Table I. The r_0 values are from the compilation by Magee.³ The alkali radii r_+ are taken from the work of Fumi and Tosi¹⁵ on the alkali halides. The hydride (deuteride) radius r_- is the average deduced from differences between r_0 and the Fumi-Tosi r_+ for all alkali hydrides. The only experimental compressibilities reported for the alkali hydrides pertain to LiH and LiD. The recent values obtained by Stephens and Lilley¹⁶ are used in the present calculations.

The van der Waals coefficients, as well as the polarizabilities and excitation energies required to determine them, are also listed in Table I. The alkali polarizabilities α_+ are from the study by Tessman, *et al.*,¹⁷ while α_- was calculated from LiH refractive index data¹⁸ using the familiar Clausius-Mossotti equation. Following the procedure developed by Mayer,¹⁴ E_- is estimated for each salt from the exciton band in the corresponding ultraviolet absorption spectrum.^{2,19} Instead of the arbitrary alkali energies E_+ suggested by Mayer, semiquantitative values were determined from free ion polarizabilities²⁰ using an analysis due to Ruffa.²¹ Deuteride VDW coefficients are taken equal to the corresponding hydride values since nuclear mass substitution has negligible effect upon α or E values.

β_{12} coefficients cannot be determined from the traditional Pauling^{4b,22} formula which predicts $\beta_{--} = 0$ and implies repulsion between hydride ions vanishes. Recognizing the general property that overlap repulsive forces between two cations with high electron densities are stronger than repulsive forces between two anions with diffuse electron distributions, the β_{12} coefficients are set equal to the following values: $\beta_{++} = 1.25$,

$\beta_{+-} = 1.0$, and $\beta_{--} = 0.75$ in the present calculations. A careful examination of the results for LiH, NaH, and KH indicates that W_L is insensitive ($\approx 0.1\%$) for a wide choice of β_{12} coefficients (excluding the Pauling values which gave $\Delta W_L \approx 0.5\%$).

Cohesive Energy

The cohesive energy of alkali hydrides has been determined from thermochemical data by a number of workers^{3,6-8} using the familiar Born-Haber cycle. Traditionally, the cohesive energy has been described as the energy difference between the dispersed ions and the crystal lattice at absolute zero. Because room temperature crystal data were used in the present Born-Mayer calculations, the experimental cohesive energy W_{BH} is found from a modified Born-Haber cycle in which the energy difference is between the crystal lattice at room temperature and dispersed ions at absolute zero. In this case, W_{BH} is given by

$$W_{BH} = Q - S - I - \frac{1}{2}D - E + 2\Delta H^\circ \quad (13)$$

Here, Q is the enthalpy of formation of alkali hydride (deuteride) crystals from alkali metal and hydrogen (deuterium) molecules; S is enthalpy of sublimation of

(15) F. G. Fumi and M. P. Tosi, *J. Phys. Chem. Solids*, **25**, 45 (1964).

(16) D. R. Stephens and E. M. Lilley, *J. Appl. Phys.*, **39**, 177 (1968).

(17) J. R. Tessman, A. H. Kahn, and W. Shockley, *Phys. Rev.*, **92**, 890 (1953).

(18) E. Staritzky and D. I. Walker, *Anal. Chem.*, **28**, 1055 (1956).

(19) W. Rauch, *Z. Phys.*, **111**, 650 (1939).

(20) L. Pauling, *Proc. Roy. Soc., Ser. A*, **114**, 181 (1927).

(21) A. F. Ruffa, *Phys. Rev.*, **130**, 1412 (1963).

(22) L. Pauling, *Z. Krist.*, **67**, 377 (1928).

the alkali metal; I is the ionization potential of the metal; D is the dissociation enthalpy of the hydrogen (deuterium) molecules; E is the electron affinity of the hydrogen (deuterium) atom; and ΔH° represents the enthalpy change in cooling monatomic alkali and hydrogen gases from room temperature to absolute zero and is taken equal to $-5R\Delta T/2$. Reliable values of these quantities are available for most of the alkali hydrides. The S and I values are the same as those used by Tosi^{4b} for the alkali halides. Calorimetric values of Q for LiH, NaH, KH, and the corresponding deuterides are reported by Gunn and Green¹⁰ while Herold²³ obtained Q for RbH and CsH from dissociation-pressure measurements. Values for E and D were also taken from Gunn and Green.¹⁰ The resultant experimental cohesive energies W_{BH} are presented in Table II, column 2. Since uncertainties in the various data amount to a few tenths kilocalories per mole, the total uncertainty in W_{BH} should not be larger than ~ 1 -2 kcal/mol. However, the uncertainties between corresponding hydride and deuteride W_{BH} are expected to be about a factor of 10 smaller.

Table II: Cohesive Energies^a of the Alkali Hydride and Deuterides

	W_{BH}	W_{L}	W_{VIB}	W_{C}	$\Delta = \frac{W_{\text{BH}} - W_{\text{C}}}{W_{\text{C}}}$
LiH	-216.2	-224.4	6.0	-218.4	2.2
LiD	-217.2	-225.1	5.0	-220.1	2.9
NaH	-189.5	-195.2	5.3	-189.9	0.4
NaD	-190.3	-195.7	4.5	-191.2	0.9
KH	-167.1	-172.7	4.9	-167.8	0.7
KD	-167.4	-173.1	4.3	-168.8	1.4
RbH	-160.6	-165.5	4.8	-160.7	0.1
CsH	-153.7	-159.6	4.7	-154.9	1.2

^a All quantities are in kcal/mol.

Before W_{L} can be calculated, ρ must be obtained by solving eq 6 using compressibilities determined independently. As mentioned previously, experimental compressibilities among the alkali hydrides are available for only LiH and LiD. To circumvent this difficulty in the present study, the alkali hydrides (deuterides) are assumed to be described by a constant ρ determined from known¹⁶ LiH (LiD) compressibility. Although this important approximation has not been rigorously justified, previous independent studies^{3,5-9} strongly support the use of a constant ρ for the alkali hydrides. From the data in Table I, ρ is determined to be $\rho_{\text{H}} = 0.463 \text{ \AA}$ and $\rho_{\text{D}} = 0.462 \text{ \AA}$ for the hydrides and deuterides, respectively. The W_{L} values calculated with these ρ choices are given in column 3 of Table II. Careful analysis of the calculation procedure indicates an uncertainty of 1-2% arises in W_{L} from the assump-

tion that ρ determined from LiH (LiD) data represents all the alkali hydrides (deuterides).

Determination of the alkali hydride vibration energies W_{VIB} listed in column 4 of Table II requires¹¹ knowledge of the corresponding Debye temperatures θ_{D} . Since experimental Debye temperatures are not available for the alkali hydrides, the well-known Blackman²⁴ equation

$$\theta_{\text{D}} = \hbar(5r_0/K\mu)^{1/2}/k \quad (14)$$

is used to determine θ_{D} from the compressibility and reduced mass μ . Although experimental compressibilities are not available for most alkali hydrides, K can be calculated by solving eq 6 for ρ values determined from lithium hydride data. The theoretical K and θ_{D} values used to estimate W_{VIB} are given in Table III along with results from other workers.

Table III: Compressibilities and Debye Temperatures of the Alkali Hydrides

	$K, 10^{-12} \text{ cm}^2/\text{dyn}$			$\theta_{\text{D}}, ^\circ\text{K}$	
	Present study ^a (eq 6)	Sherman ^b	Hafemeister and Zahrt ^c	Present (eq 14)	Experimental
LiH	2.88 ^d	2.32	3.39 ^e	1190	815, ^f (920), ^f 850 ^g 1091 ^c
LiD	2.85 ^d			895	(614, 744) ^f
NaH	4.55	3.78	5.42	991	
NaD	4.51			702	
KH	6.75	6.16	7.90	869	
KD	6.71			627	
RbH	7.88	6.67	9.15	827	
CsH	8.92	7.83	10.60	793	

^a Theoretical K determined using ρ values obtained from experimental LiH compressibility in footnote *d* of this table. ^b Reference 5. ^c Reference 9. ^d Reference 16. ^e Calculated using eq 32 and ρ data from Hafemeister and Zahrt (ref 9). ^f Reference 2. ^g V. N. Kostyukov, *Russ. J. Phys. Chem.*, **35**, 865 (1961).

The theoretical cohesive energy W_{C} , which equals the sum of W_{L} and W_{VIB} , is listed in column 5 of Table II. The differences between W_{C} and W_{BH} are summarized in column 6 of Table II.

Discussion

As is evident from Table II, W_{C} is in excellent agreement with W_{BH} for all alkali hydrides and deuterides where Δ is much smaller than combined experimental and theoretical uncertainties ($\sim 3\%$). These results indicate a constant ρ determined from LiH (LiD) compressibility data and give an adequate description of alkali hydride (deuteride) short-range forces when NNN and VDW terms are included in the Born-Mayer model.

(23) A. Herold, *Ann. Chim. (Paris)*, **6**, 536 (1951).

(24) M. Blackman, *Proc. Roy. Soc., Ser. A*, **181**, 58 (1942).

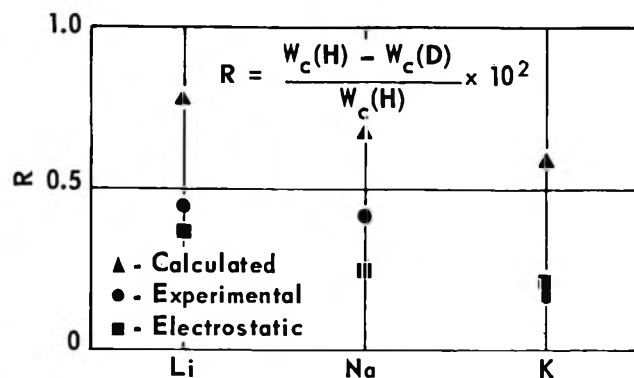


Figure 1. Effect of isotopic substitution on alkali hydride cohesive energies.

Since extensive covalent bonding leads to large negative Δ 's,⁴ the present slight positive Δ 's substantiate the basic ionic nature of the alkali hydrides. This conclusion agrees with recent analysis²⁵ of electrical conductive studies on molten LiH.

The effect of isotopic substitution on alkali hydride cohesive energies is shown in Figure 1 where the percentage differences R between hydride and deuteride energies are given for Li, Na, and K salts. The electrostatic differences result from changed lattice parameters, while differences in W_C and W_{BH} include effects in short-range forces and vibrational energies. The

isotope effect is small ($<1\%$) and decreases with increasing alkali mass. Differences in W_C are systematically higher than differences for W_{BH} , although the values are in qualitative agreement. The difficulty in determining accurate values of W_{VIB} , which is unimportant in calculating absolute cohesive energies, gives a large uncertainty ($\sim 25\%$) in R for W_C and is probably the major cause for higher W_C differences.

The compressibilities calculated using ρ values determined from lithium hydride data are given in Table III along with compressibilities found by other workers.^{5,9} The compressibilities determined from the NNN-VDW Born-Mayer model are intermediate to the other values and appear to be in reasonable agreement with corresponding alkali halide values.^{4b} The Debye temperatures found using the Blackman formula (eq 4) are also shown in Table III; they are higher than the few available experimental values.

Although the present study indicates that NNN-VDW Born-Mayer model gives an adequate description of the alkali hydrides and deuterides, it would be interesting to perform more refined calculations when accurate compressibility data become available for these salts.

(25) M. A. Bredig, *J. Chem. Phys.*, **46**, 4166 (1967); C. E. Johnson, S. E. Wood, and E. J. Cairns, *ibid.*, **46**, 4168 (1967).

The Thermodynamic Properties of Liquids, Including Solutions.

IV. The Entropy of Mixing

by Maurice L. Huggins

Arcadia Institute for Scientific Research, 135 Northridge Lane, Woodside, California 94062 (Received October 1, 1970)

Publication costs borne completely by The Journal of Physical Chemistry

An equation for the combinatorial entropy for a mixture of rigid molecules, not necessarily of the same size, is derived, assuming perfect randomness of mixing. An equation for the additional entropy resulting from the concentration dependence of the randomness of orientation of the parts of a flexible molecule is next deduced. Finally, an equation to correct the previous combinatorial entropy calculation for nonrandomness is obtained. The last two of these three entropies of mixing result in contributions to the interaction parameter χ for solutions of chain polymers. Equations for these contributions are presented.

Introduction

This paper reports an attempt to arrive at a quantitative theoretical treatment of the entropy of mixing. In part, the development follows old treatments; in part it is new.

The combinatorial entropy—that related to the randomness of placing the molecules in the total volume—is considered first, making the usual assumption of perfect randomness and assuming the molecules to be rigid, but not necessarily of the same size.

Next, the effect of flexibility is treated. In a non-rigid molecule there is some randomness of orientation of one or more bonds or segments relative to other bonds or segments to which they are attached. If this orientational randomness changes as the concentration—hence the environment of these bonds or segments—changes, there is a contribution to the entropy of mixing.

Finally, theory and equations for a correction to the previously calculated combinatorial entropy are presented. This correction allows for the fact that the distribution of molecules (and of intermolecular contacts) is not perfectly random.

The total theoretical entropy of mixing is obtained by adding together these three parts. The last two involve parameters that can be determined from heat of mixing or volume of mixing measurements. For a ditonic system (one containing two kinds of segments) these parameters are (1) the ratio ($r_\sigma = \sigma_\beta^0/\sigma_\alpha^0$) of the contacting surface areas of the two segment types, and (2) an equilibrium constant, $K = \sigma_{\alpha\beta}^2/4\sigma_{\alpha\alpha}\sigma_{\beta\beta}$, relating the total contact areas of the three types.

For polymer solutions, the segment orientation entropy and the combinatorial entropy correction combine to give χ_s , the entropy part of the interaction parameter χ .

*The Combinatorial Entropy for Rigid Molecules, Assuming Perfect Randomness.*¹⁻⁴ Let x_1 and x_2 be mole fractions of the two types of molecules in a solution and let N_{Av} represent Avogadro's number. Consider the molecules ($N_1 = x_1N_{Av}$ of kind 1 and $N_2 = x_2N_{Av}$ of kind 2) to be added randomly to a vessel having a volume equal to the molal volume of the solution, from a stock in which their relative numbers are always the same as in the final solution. To a high degree of approximation the relative numbers in the volume being filled are, before and after each addition, also the same as in the final solution. If v_1 and v_2 are the volumes per molecule of the two types, with $v_1 = \bar{V}_1/N_{Av}$ and $v_2 = \bar{V}_2/N_{Av}$

$$V = N_1v_1 + N_2v_2 \quad (1)$$

For the i th added molecule of the first type the filled volume is $[(i-1)/N_1]V$ and the available volume is

$$\left[\frac{N_1 - (i-1)}{N_1} \right] V \approx \left(1 - \frac{i}{N_1} \right) V$$

For the j th added molecule of the second type, the available volume is very close to $[(1-j)/N_1]V$.

The entropy of placing the molecules of type 1 is

$$S_1 = k_B \ln \left(\frac{\prod_{i=1}^{N_1} \left(1 - \frac{i}{N_1} \right) V}{N_1!} \right) =$$

$$k_B \left[N_1 \ln \left(\frac{V}{v_1} \right) + \ln \prod_{i=1}^{N_1} \left(1 - \frac{i}{N_1} \right) - \ln (N_1!) \right] =$$

$$k_B [(N_1 \ln N_1 - N_1 \ln \phi_1) -$$

$$N_1 + (N_1 - N_1 \ln N_1)] = -k_B N_1 \ln \phi_1 \quad (2)$$

where k_B is the Boltzmann constant and ϕ_1 is the volume fraction of component 1. The entropy of placing the molecules of type 2 is, similarly

$$S_2 = k_B \ln \left(\frac{\prod_{j=1}^{N_2} \left(1 - \frac{j}{N_2} \right) V}{N_2!} \right) = -k_B N_2 \ln \phi_2 \quad (3)$$

The total combinatorial entropy, for random mixing of rigid molecules, is

$$S_{rm} = S_1 + S_2 = -k_B (N_1 \ln \phi_1 + N_2 \ln \phi_2) \quad (4)$$

or per mole

$$\bar{S}_{rm} = -R(x_1 \ln \phi_1 + x_2 \ln \phi_2) \quad (5)$$

where R is the gas constant per mole.

If the molecules are of the same size, the mole fractions are the same as the volume fractions, hence

$$\bar{S}_{rm} = -R(x_1 \ln x_1 + x_2 \ln x_2)$$

$$\bar{S}_{rm}^E = -R \left[x_1 \ln \left(\frac{\phi_1}{x_1} \right) + x_2 \ln \left(\frac{\phi_2}{x_2} \right) \right] \quad (6)$$

from which, if the heat of mixing is zero, Raoult's law can be derived.

In dealing with polymer solutions, it is customary to use the relationship²⁻⁹

$$\frac{\Delta \bar{G}_1}{RT} = \frac{\Delta \bar{H}_1 - T \Delta \bar{S}_1}{RT} =$$

$$\ln \phi_1 + \left(1 - \frac{\bar{V}_1}{\bar{V}_2} \right) \phi_2 + \chi \phi_2^2 \quad (7)$$

where \bar{V}_1 and \bar{V}_2 are the partial molal volumes of the two components and χ is a concentration-dependent parameter, the sum of an enthalpy component and an entropy component

$$\chi = \chi_h + \chi_s \quad (8)$$

From eq 5 it is readily shown that

- (1) M. L. Huggins, *J. Phys. Colloid Chem.*, **52**, 248 (1948).
- (2) M. L. Huggins, *J. Polym. Sci.*, **16**, 209 (1955).
- (3) M. L. Huggins, "Physical Chemistry of High Polymers," Wiley, New York, N. Y., 1958.
- (4) M. L. Huggins, *J. Amer. Chem. Soc.*, **86**, 3535 (1964).
- (5) M. L. Huggins, *J. Phys. Chem.*, **46**, 151 (1942).
- (6) M. L. Huggins, *Ann. N. Y. Acad. Sci.*, **41**, 1 (1942).
- (7) P. J. Flory, *J. Chem. Phys.*, **10**, 51 (1942).
- (8) P. J. Flory, *ibid.*, **12**, 425 (1944).
- (9) P. J. Flory, "Principles of Polymer Chemistry," Cornell University Press, Ithaca, N. Y., 1953.

$$\frac{-\Delta\tilde{S}_1}{R} = \ln \phi_1 + \left(1 - \frac{\bar{V}_1}{\bar{V}_2}\right)\phi_2 \quad (9)$$

hence the combinatorial entropy, for rigid molecules mixed with perfect randomness, does not contribute to χ_s .

This statement and the equations preceding it are not strictly accurate, because the theoretical development did not allow for the fact that all of the unoccupied space is not available for the center of the molecule being placed. Any location that would cause overlapping with a placed molecule—two parts of molecules occupying the same space—is ruled out. Neglect of this limitation may result in significant differences between the actual entropy and that calculated at high concentrations of the larger species, if there is a large difference between the sizes of the two kinds of molecules and especially if the larger ones are rodlike or otherwise elongated. This effect has been discussed elsewhere.¹

The Segment Orientation or Flexibility Entropy. Many types of molecules are not rigid. One or more parts (e.g., segments or interatomic bonds) of such a molecule can change orientation relative to other parts. There is thus some randomness of orientation and, for a solution containing such molecules, if the degree of randomness changes with the concentration, there is a corresponding contribution to the entropy of mixing.^{2-4,6}

For simplicity, let us consider a mixture of rigid solvent molecules (type 1) and flexible solute chain molecules (type 2), each composed of n rigid segments connected together by $n - 1$ flexible joints. The theoretical treatment can obviously be readily extended to systems containing more than one type of solvent and/or solute molecule and more than one type of segment in either solvent or solute molecules or both.

In this theory¹⁰ it is assumed that a liquid behaves thermodynamically like a hypothetical one composed of rigid molecules with mutually contacting surfaces. The thermodynamic properties are then related to the kinds of chemical segments of which the molecules are composed, the average contacting surface area per segment of each kind, and the average energy of segment-segment interaction per unit area for each type of contact. For the present the surface area and energy parameters are determined empirically from the experimental thermodynamic data. It is hoped that it will be possible, after enough of these parameters have been collected, to relate their magnitudes to structural arrangements and interatomic energy-distance relationships, at least in simple cases.

Let ν^0 and $\nu^0(1 - k_s)$ designate the average randomness of orientation of a segment in the chain polymer molecule, relative to the orientation of the preceding segment in the chain, when this molecule is in infinitely dilute solution in a given solvent and when it is in pure polymer, respectively. At intermediate concentrations, assume the average orientation randomness to be

$\nu^0(1 - k_s p)$, where p is the probability that a contacting unit area of the segment surface makes contact with a polymer segment surface, rather than with a solvent molecule surface. The segment orientation entropy is then

$$S_{or} = k_B \ln [\nu^0(1 - k_s p)]^{(n-1)N_2} \quad (10)$$

If the solvent molecule is (or can be treated for this purpose as) a single rigid segment (type α) and each of the n segments in the polymer is (or can be treated as) a rigid segment (type β), then the probability p is related to the average areas of $\beta\beta$ and $\alpha\beta$ contacts between segment surfaces¹⁰ by the equation

$$p = \frac{2\sigma_{\beta\beta}}{2\sigma_{\beta\beta} + \sigma_{\alpha\beta}} \quad (11)$$

These contact areas are related to the contacting areas ($\sigma_\alpha, \sigma_\beta$) of the two types by the equations

$$\sigma_{\alpha\beta} = \frac{-2(\sigma_\alpha + \sigma_\beta)}{K'} [1 - (1 + K' z_\alpha z_\beta)^{1/2}] \quad (12)$$

$$\sigma_{\beta\beta} = \frac{\sigma_\beta}{2} + \frac{(\sigma_\alpha + \sigma_\beta)}{K'} [1 - (1 + K' z_\alpha z_\beta)^{1/2}] \quad (13)$$

$$z_\alpha = \sigma_\alpha / (\sigma_\alpha + \sigma_\beta) \quad (14)$$

$$z_\beta = \sigma_\beta / (\sigma_\alpha + \sigma_\beta)$$

$$K' = 4 \left(\frac{1}{K} - 1 \right) \quad (15)$$

and

$$K = \sigma_{\alpha\beta}^2 / 4\sigma_{\alpha\alpha}\sigma_{\beta\beta} \quad (16)$$

K is an equilibrium constant, assumed in this theory to govern the relative areas of contact of the three types. For complete randomness $K = 1$, $K' = 0$, and

$$\frac{(\sigma_\alpha + \sigma_\beta)}{K'} [1 - (1 + K' z_\alpha z_\beta)^{1/2}] = -\frac{z_\alpha z_\beta}{2} \quad (17)$$

With these relationships

$$p = 1 - z_\alpha g_K \quad (18)$$

where

$$g_K = \frac{-2}{z_\alpha z_\beta K'} [1 - (1 + K' z_\alpha z_\beta)^{1/2}] \quad (19)$$

For perfect randomness

$$K = g_K = 1 \quad (20)$$

and

$$p = z_\beta \quad (21)$$

Substituting eq 18 into eq 10 and replacing $n - 1$ by n , one obtains for the excess entropy of mixing per mole

(10) M. L. Huggins, *J. Phys. Chem.*, **74**, 371 (1970).

$$\tilde{S}_{\text{or}}^E = \tilde{S}_{\text{or}} - \tilde{S}_{\text{or}, N_1=0} = RnN_2 \ln \left[1 + \left(\frac{k_s}{1 - k_s} \right) z_\alpha g_K \right] \quad (22)$$

In this development the randomness of orientation of the first segment in each polymer molecule, relative to neighbor molecules, has been neglected. This may be roughly compensated by the replacement of $n - 1$ by n . When n is large, both approximations certainly introduce only negligible error in the final result.

For nonpolymeric systems containing nonspherical molecules whose orientational randomness varies with the concentration, eq 22, with $n = 1$, may be assumed to hold.

Differentiating with respect to N_1 to obtain $\Delta \tilde{S}_1$ and dividing by $-k_B \phi_2^2$ (see eq 7-9), one obtains for the segment orientation entropy part of the interaction parameter χ

$$\chi_{s,\text{or}} = \frac{-k_s' z_\beta}{r_\sigma \phi_2^2} \left[\frac{\frac{z_\beta - z_\alpha}{(1 + K' z_\alpha z_\beta)^{1/2}} + z_\alpha g_K}{1 + k_s' z_\alpha g_K} \right] \quad (23)$$

where

$$k_s' = k_s / (1 - k_s) \quad (24)$$

and

$$r_\sigma = \sigma_\beta^0 / \sigma_\alpha^0 \quad (25)$$

For random mixing

$$\chi_{s,\text{or}} = \frac{-k_s' z_\beta^2}{r_\sigma \phi_2^2 (1 + k_s' z_\alpha)} \quad (26)$$

Combinatorial Entropy Correction for Imperfect Randomness. If the free energy of interaction between a molecule (or a molecular segment) and its neighbors in a solution depends on the kind of neighbors, the mixing of molecules (or of segments) is not random. The magnitude of the departure of the combinatorial entropy of a solution from that calculated on the assumption of perfect randomness should be a function of the equilibrium constant K . Let us deduce the relationship, for a ditonic system containing only two kinds of segments, α and β . The total contacting surface areas of the two types are designated σ_α and σ_β , as before.

Consider the formation of contacts of the three types by unit areas of the α and β surfaces. The correction to the combinatorial entropy is assumed to be the actual entropy for making these contacts minus that calculated on the assumption of perfect randomness. If this assumption is correct

$$S_{\text{cc}}^E = S_{\text{cc}} = \frac{-k_B}{2} \times \ln \left[\frac{(p_{\alpha \rightarrow \alpha})^{\sigma_{\alpha\alpha}} (p_{\alpha \rightarrow \beta})^{\sigma_{\alpha\beta/2}} (p_{\beta \rightarrow \beta})^{\sigma_{\beta\beta}} (p_{\beta \rightarrow \alpha})^{\sigma_{\alpha\beta/2}}}{(p'_{\alpha \rightarrow \alpha})^{\sigma'_{\alpha\alpha}} (p'_{\alpha \rightarrow \beta})^{\sigma'_{\alpha\beta/2}} (p'_{\beta \rightarrow \beta})^{\sigma'_{\beta\beta}} (p'_{\beta \rightarrow \alpha})^{\sigma'_{\alpha\beta/2}}} \right] \quad (27)$$

Here, $p_{\alpha \rightarrow \alpha}$ is the probability that a unit α surface contacts another unit α surface to make an $\alpha\alpha$ contact, $p_{\alpha \rightarrow \beta} = 1 - p_{\alpha \rightarrow \alpha}$ is the probability that a unit α surface contacts a unit β surface to make an $\alpha\beta$ contact, $p_{\beta \rightarrow \beta}$ is the probability that a unit β surface makes a $\beta\beta$ contact, $p_{\beta \rightarrow \alpha} = 1 - p_{\beta \rightarrow \beta}$ is the probability that a unit β surface makes an $\alpha\beta$ contact; also $\sigma_{\alpha\alpha}$ is the total number of unit $\alpha\alpha$ contacts, $\sigma_{\beta\beta}$ is the total number of unit $\beta\beta$ contacts, and $\sigma_{\alpha\beta}$ is the total number of unit $\alpha\beta$ contacts.

The primed letters in the denominator indicate that the probabilities and numbers are calculated on the assumption of perfect randomness ($K = 1$). The factor $1/2$ is inserted to avoid counting each contact twice.

The contact areas and probabilities are related through the equations

$$\sigma_{\alpha\alpha} = \sigma_\alpha p_{\alpha \rightarrow \alpha} / 2 \quad p_{\alpha \rightarrow \alpha} = 2\sigma_{\alpha\alpha} / \sigma_\alpha \quad (28)$$

$$\sigma_{\beta\beta} = \sigma_\beta p_{\beta \rightarrow \beta} / 2 \quad p_{\beta \rightarrow \beta} = 2\sigma_{\beta\beta} / \sigma_\beta \quad (29)$$

$$\sigma_{\alpha\beta} = (\sigma_\alpha p_{\alpha \rightarrow \beta} + \sigma_\beta p_{\beta \rightarrow \alpha}) / 2 \quad (30)$$

The contact areas are also related¹⁰ to the equilibrium constant K through the equations

$$\sigma_{\alpha\alpha} = \frac{\sigma_\alpha}{2} (1 - z_\beta g_K) \quad (31)$$

$$\sigma_{\beta\beta} = \frac{\sigma_\beta}{2} (1 - z_\alpha g_K) \quad (32)$$

$$\sigma_{\alpha\beta} = \sigma_\alpha z_\beta g_K = \sigma_\beta z_\alpha g_K \quad (33)$$

where z_α , z_β , and g_K are given by eq 14 and 19.

Since g_K is unity for perfect randomness of contacts (see eq 20)

$$\sigma'_{\alpha\alpha} = \sigma_\alpha z_\alpha / 2 \quad (34)$$

$$\sigma'_{\beta\beta} = \sigma_\beta z_\beta / 2 \quad (35)$$

$$\sigma'_{\alpha\beta} = \sigma_\alpha z_\beta = \sigma_\beta z_\alpha \quad (36)$$

$$p'_{\alpha \rightarrow \alpha} = p'_{\beta \rightarrow \alpha} = z_\alpha \quad (37)$$

$$p'_{\beta \rightarrow \beta} = p'_{\alpha \rightarrow \beta} = z_\beta \quad (38)$$

Substitution into eq 27 leads to the result

$$S_{\text{cc}}^E = \frac{-k_B}{4} [\sigma_\alpha (1 - z_\beta g_K) \ln (1 - z_\beta g_K) + \sigma_\beta (1 - z_\alpha g_K) \ln (1 - z_\alpha g_K) + \sigma_\beta z_\alpha g_K \ln (z_\alpha z_\beta g_K^2) - \sigma_\alpha z_\alpha \ln z_\alpha - \sigma_\beta z_\beta \ln z_\beta - \sigma_\alpha z_\beta \ln (z_\alpha z_\beta)] \quad (39)$$

If there are $n_{1\alpha}$ α -type and $n_{1\beta}$ β -type segments per molecule of type 1 and $n_{2\alpha}$ α -type and $n_{2\beta}$ β -type segments per molecule of type 2

$$\sigma_\alpha = (n_{1\alpha} N_1 + n_{2\alpha} N_2) \sigma_\alpha^0 \quad (40)$$

$$\sigma_\beta = (n_{1\beta} N_1 + n_{2\beta} N_2) \sigma_\beta^0 \quad (41)$$

For 1 mol of solution

$$\frac{N_1}{x_1} = \frac{N_2}{x_2} = \frac{R}{k_B} \quad (42)$$

hence the k_B in eq 39 can be replaced by the molar gas constant R and one can make the substitutions

$$\sigma_\alpha = (n_{1\alpha}x_1 + n_{2\alpha}x_2)\sigma_\alpha^0 \quad (43)$$

$$\sigma_\beta = (n_{1\beta}x_1 + n_{2\beta}x_2)\sigma_\alpha^0 r_\sigma \quad (44)$$

Then

$$\begin{aligned} \bar{S}_{cc}^E = & -\frac{R\sigma_\alpha^0}{4} \{ (n_{1\alpha}x_1 + n_{2\alpha}x_2) \times \\ & [(1 - z_\beta g_K) \ln(1 - z_\beta g_K) - \\ & z_\alpha \ln z_\alpha - z_\beta \ln(z_\alpha z_\beta)] + (n_{1\beta}x_1 + \\ & n_{2\beta}x_2)r_\sigma [(1 - z_\alpha g_K) \ln(1 - z_\alpha g_K) + \\ & z_\alpha g_K \ln(z_\alpha z_\beta g_K^2) - z_\beta \ln z_\beta] \} \quad (45) \end{aligned}$$

with z_α , z_β , and g_K calculated from eq 14, 19, 43, and 44.

The variables involved, other than the volume fractions, are the equilibrium constant K and the contacting segment surface ratio r_σ , both of which are obtainable from measurements of excess enthalpies (or, in some cases, excess volumes) and the contacting segments surface area σ_α^0 , which cannot be obtained from such measurements. Since the magnitude of σ_α^0 depends on the arbitrary choice of the unit area, this parameter really defines the average unit area of a segment surface that acts *independently* in the imaginary process of making contacts with other segments.

It is readily shown that S_{cc}^E equals zero if $K = 1$ and so $g_K = 1$.

For the special case of a mixture of polymer molecules containing only β segments and solvent molecules each containing only a single α segment, the combinatorial entropy correction contribution to χ_s is

$$\begin{aligned} \chi_{s,cc} = & -\frac{1}{\phi_2^2} \left(\frac{\partial S_{cc}}{\partial N_1} \right)_{N_2} = \frac{\sigma_\alpha^0}{4\phi_2^2} \left\{ \ln \left(\frac{z_\alpha}{1 - z_\beta g_K} \right) + \right. \\ & \left. \left[\frac{z_\beta(z_\beta - z_\alpha)}{(1 + K'z_\alpha z_\beta)^{1/2}} + z_\alpha z_\beta g_K \right] \ln \left[\frac{(1 - z_\alpha g_K)(1 - z_\beta g_K)}{z_\alpha z_\beta g_K^2} \right] \right\} \quad (46) \end{aligned}$$

The Total Excess Entropy of Mixing and the Total Entropy Part of χ . The total excess entropy of mixing per mole of solution, for nonrandom mixtures of rigid molecules, is obtained by adding the contributions given by eq 5 and 45.

For a solution of flexible polymer molecules, with

each mer considered as a β segment, in a solvent composed of molecules, each of which is treated as a rigid α segment, the total χ_s is obtained by adding the contributions given by eq 23 and 46, with

$$z_\alpha = 1 - z_\beta = \frac{x_1}{x_1 + n_2 r_\sigma x_2} = \frac{1}{1 + (n_2 r_\sigma - 1)x_2} \quad (47)$$

The parameters needed are r_σ and K , obtainable from excess enthalpies, plus the segment orientation parameter k_s and (if there is nonrandom mixing) σ_α^0 . There does not appear to be any valid way of reducing the number of parameters to be determined by experiment. (Of course, the assumption of random mixing, which is not in general justifiable, fixes the value of K at 1 and requires S_{cc} and $\chi_{s,cc}$ to be zero, thus eliminating the need for σ_α^0 .)

It should be noted that the parameters required for a given system, since they are properties of segments and segment-segment interactions, need not necessarily be determined experimentally for that system. They can be determined from measurements on other systems containing the same kinds of segments and segment-segment contacts. Thus, one can hope to obtain the parameters for high polymer solutions entirely from measurements on simple systems of low molecular weight.

The validity of the theory here presented can of course only be judged by the degree of agreement achieved when it is applied to good experimental data for actual systems. Applications to two polymer-solvent systems have already been made, with gratifying results.

For the rubber + benzene system it has been shown¹¹ that the difference between the experimental magnitudes of χ and χ_h equals (over the whole concentration range, within the probable experimental error, as judged by the scatter of the data) $\chi_{s,rm} + \chi_{s,or} + \chi_{s,cc}$, calculated using r_σ , and K' parameters deduced from the concentration dependence of the excess enthalpies and volumes of mixing.

A similar result has been obtained, for volume fractions up to $1/2$, for the poly(ethylene oxide) + CCl_4 system.^{11,12} The apparent disagreement at higher concentrations can be attributed to additional entropy factors, peculiar to some polymeric systems, for which no quantitative theory has yet been developed.

Applications to a number of mixtures of compounds of low molecular weight have also been made. The results will be reported in future papers.

(11) M. L. Huggins, *Polymer*, in press.

(12) M. L. Huggins, *Macromolecules*, in press.

The Electrical Conductance of Gaseous Mixtures of Aluminum

Trichloride and Sodium Tetrachloroaluminate

by E. W. Dewing

Alcan Research and Development Ltd., Arvida, Quebec, Canada (Received October 2, 1970)

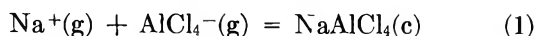
Publication costs assisted by Alcan Research and Development Ltd.

It has been shown that the presence of NaAlCl₄ in gaseous AlCl₃-Al₂Cl₆ mixtures imparts electrical conductances of 10⁻¹¹ to 10⁻⁶ ohm⁻¹ cm⁻¹ in the range 500-900°. From the variation of conductance with temperature, total pressure, and concentration of NaAlCl₄, it is postulated that the mechanism of ionization is NaAlCl₄ + AlCl₃ = NaAlCl₃⁺ + AlCl₄⁻, with $\Delta H \simeq 70$ kcal. The results are not consistent with the positive ion being Na⁺, NaAl₂Cl₆⁺, Na₂AlCl₄⁺, or Na₂Cl⁺.

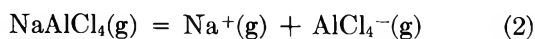
Introduction

Gases, in general, are electrical insulators, except at very high temperatures or at field strengths high enough that a plasma is formed. However, on the basis of calculations¹ of the energy of formation of the gaseous AlCl₄⁻ ion it can be deduced that NaAlCl₄(g) should be ionized to a detectable extent at temperatures of the order of 1000°K. The object of this work was to verify the prediction.

Wood and D'Orazio¹ estimate ΔH for



as -138 ± 7 kcal. Since the enthalpy of sublimation of NaAlCl₄ is about 38 kcal,^{2,3} ΔH for



is $\simeq +100$ kcal. ΔS may be estimated as +30 cal deg⁻¹, so that

$$\Delta G = 100,000 - 30T \quad (3)$$

At 1000°K, for example, ΔG is +70 kcal, so that $K_p = 10^{-15}$. If p_{NaAlCl_4} is 0.1 atm, the total partial pressure of ions becomes 10⁻⁸ atm which, as will be seen later, would give rise to an electrical conductivity of the order of 10⁻⁸ ohm⁻¹ cm⁻¹. This, although low, is measurable.

Gaseous NaAlCl₄ cannot be obtained in pure form since it can exist only in the presence of an excess of AlCl₃,^{2,3} the latter itself being partially dimerized to Al₂Cl₆. There is, therefore, a strong possibility that the ionization process will not be as simple as reaction 2, but that the Na⁺ ion will attach itself to one of the other species present and thereby displace the equilibrium to the right, giving rise to a conductivity higher than indicated above.

Experimental Section

A preliminary experiment with two small, parallel plate electrodes showed that there was indeed sufficient

conductance to measure. The problem was to get quantitative values when glass (including Vycor), from which the apparatus had to be constructed, had a resistivity of the same order as the gas, and when aluminum chloride and the entrained NaAlCl₄ would condense in any cool regions to which they had access, possibly leading to current leakage.

The approach adopted was to use a concentric electrode arrangement; in this way the glass walls of the apparatus could not offer a direct short circuit. They did, however, give rise to extensive end corrections in addition to those inevitable when the electrodes were not of infinite length. (See Figure 1.) The central electrode could be moved axially upward, thereby changing the length of the central region in which uniform current flow was occurring without changing appreciably the end effects. Since the current flowing through the system is given by

$$i = 2\pi lV/[\rho \ln(r_2/r_1)] + \text{end currents} \quad (4)$$

where l is the length of the central uniform region, V is the applied voltage, ρ is the resistivity, and r_1 and r_2 are the radii of the central and outer electrodes, respectively, ρ can be deduced from the slope of a plot of current vs. position of the central electrode.

A 0-180-V dc power supply was used, and with an X-Y recorder it was demonstrated that current-voltage curves were linear and passed through the origin. Subsequently all measurements were made at about 180 V. The position of the central rod was also varied. Despite some drift in readings during the course of the experiment it was demonstrated that over the range used the current was linearly dependent on displacement, implying that the end effects were being satisfactorily eliminated. The chief problem was that a

(1) R. H. Wood and L. A. D'Orazio, *Inorg. Chem.*, **5**, 682 (1966).

(2) E. W. Dewing, *J. Amer. Chem. Soc.*, **77**, 2639 (1955).

(3) E. W. Dewing, unpublished work. Vapor pressure measurements were made by a gas-transference method.

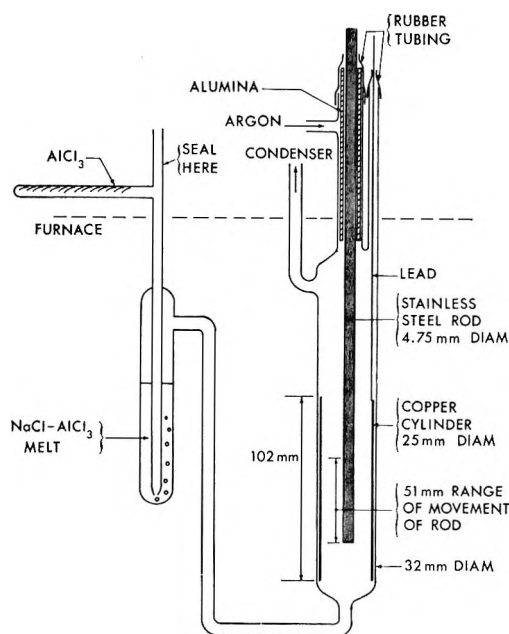


Figure 1. Apparatus for measuring electrical resistivity of gaseous aluminum chloride containing evaporated NaAlCl_4 .

small systematic change in conditions during the course of the experiment (*e.g.*, condensation of NaAlCl_4) could seriously change the slope of the plot. More rapid measurements were obtained by placing the rod in two positions only ("up" and "down," separated by 51 mm) with stops so that these positions could be readily found. The current was recorded, and the rod held at each position in turn for about 5 sec. A series of values for the change in current was thus obtained, and drift in the end corrections could be eliminated.

The region of the apparatus where the electrical leads entered was kept free of condensed chloride by purging with argon.

In view of the importance of the NaAlCl_4 in giving rise to the ionization its concentration in the gas had to be controlled. This was done by bubbling a stream of AlCl_3 through a NaCl-AlCl_3 melt held at a known temperature. For this work the limitation was accepted that the temperature of the melt should be the same as that at which the resistivity was measured. At first it was assumed that the saturated vapor pressure would be established, but it became apparent that this was not the case, so that it was necessary to collect the distilled AlCl_3 and analyze it for Na.

Two forms of apparatus, differing in detail, were used. The first is shown in Figure 1. It was made in Pyrex or Vycor, as appropriate to the temperature, and was operated at atmospheric pressure. Argon was used to purge out the cool region where the central electrical lead entered, and this argon left by the condenser with out descending to the region where the measurement was made. To purge the apparatus initially argon was passed down the vertical tube into the bubbler before it was filled. After filling, this vertical tube was sealed

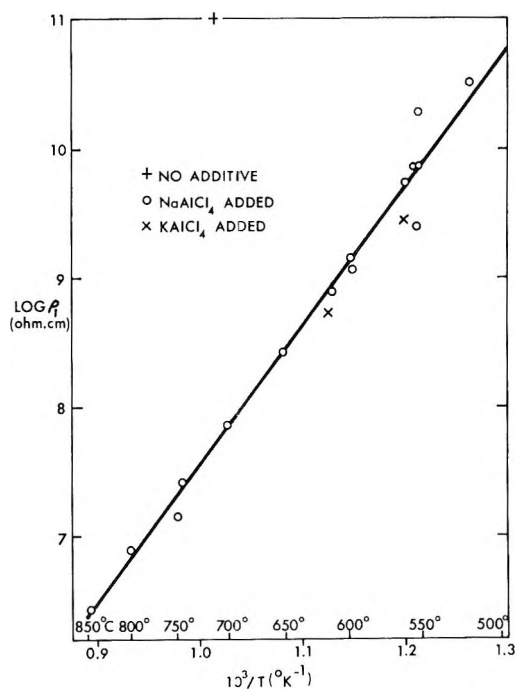


Figure 2. Electrical resistivity of gaseous aluminum trichloride (corrected to 1 atm).

off and AlCl_3 was passed through the apparatus by subliming it with a gas burner.

A later form of apparatus, used at pressures below atmospheric, was similar except that (a) both leads and the argon purge entered *via* a rubber stopper at the top of the 32-mm tube, and (b) a trap was interposed between the bubbler and the AlCl_3 entry to avoid the risk of blowing the melt into the solid AlCl_3 while changing the pressure in the apparatus. The pressure was set by attaching the exit of the condenser to a water pump, and it was measured with a mercury manometer and barometer.

Results

Each experiment was run until the observed resistance became substantially constant. There was a tendency, particularly with a new Pyrex apparatus, for the measured resistance to be low for the first few minutes; this was presumably due to some material extracted from the glass by reaction with the aluminum chloride.

The resistivity of AlCl_3 itself without added NaAlCl_4 was checked at 550° and at 711° . At the lower temperature it was unmeasurable, and at the higher 1×10^{11} ohm cm was found. Comparison with Figure 2 shows that this is higher by a factor of 2000 than when NaAlCl_4 was added. It cannot be ruled out that traces were not still present, derived from the Vycor, so that this value represents a lower limit of the true resistivity.

Table I gives the results obtained. The resistivities have been corrected to 1 atm on the basis that they

Table I: Electrical Resistivity of Gaseous Aluminum Chloride after Bubbling through NaCl–AlCl₃ Melt

Temp., °C	P_{total} , atm	Resistivity, ohm cm	ρ_1 , ohm cm	p_{NaAlCl_4} , atm	p_{AlCl_3} , atm	$p_{\text{Al}_2\text{Cl}_6}$, atm	p_{ions} , atm
559	0.988	5.23×10^9	5.29×10^9	0.0090 ^a	0.516	0.463	1.06×10^{-10}
61	0.988	7.58×10^8	7.67×10^8	0.0188 ^a	0.673	0.297	7.30×10^{-10}
650	1.001	2.66×10^8	2.66×10^8	0.0307 ^a	0.769	0.201	2.11×10^{-9}
596	1.001	1.11×10^9	1.11×10^9	0.0153 ^a	0.637	0.348	5.05×10^{-10}
597	0.986	1.37×10^9	1.39×10^9	0.0155 ^a	0.633	0.338	4.03×10^{-10}
700	0.986	7.12×10^7	7.22×10^7	0.0545 ^a	0.823	0.108	7.76×10^{-9}
748	0.986	1.39×10^7	1.41×10^7	0.0895 ^a	0.838	0.0582	3.97×10^{-8}
744	0.991	2.53×10^7	2.56×10^7	0.0861 ^a	0.843	0.0620	2.19×10^{-8}
796	0.991	7.70×10^6	7.77×10^6	0.145 ^a	0.816	0.0296	7.21×10^{-8}
845	0.991	2.64×10^6	2.67×10^6	0.215 ^a	0.761	0.0154	2.10×10^{-7}
553	0.988	6.95×10^9	7.06×10^9	0.0082 ^a	0.496	0.484	7.93×10^{-11}
552	0.426	7.48×10^9	1.75×10^{10}	0.0068 ^a	0.271	0.148	3.20×10^{-11}
55C	0.730	1.03×10^{10}	1.42×10^{10}	0.0075 ^a	0.396	0.327	3.94×10^{-11}
55C	0.762	9.71×10^9	1.27×10^{10}	0.0076 ^a	0.408	0.347	4.41×10^{-11}
55C	0.987	7.06×10^9	7.16×10^9	0.0079 ^a	0.486	0.493	7.82×10^{-11}
55C	0.482	5.51×10^9	1.14×10^{10}	0.0068 ^a	0.294	0.181	4.91×10^{-11}
518	0.987	3.12×10^{10}	3.16×10^{10}	0.00048 ^a	0.382	0.604	1.77×10^{-11}
55C	0.993	1.33×10^{10}	1.34×10^{10}	0.0056	0.489	0.499	4.18×10^{-11}
55C	0.457	5.65×10^9	1.24×10^{10}	0.0067 ^a	0.283	0.167	4.52×10^{-11}
55C	0.193	6.53×10^9	3.38×10^{10}	0.0045	0.145	0.0438	1.66×10^{-11}
555	0.097	3.63×10^9	3.73×10^{10}	0.0032	0.0813	0.0125	1.50×10^{-11}
550	0.108	4.23×10^9	3.92×10^{10}	0.0031	0.0885	0.0164	1.43×10^{-11}
551	0.983	2.42×10^9	2.46×10^9	0.0079	0.488	0.487	2.28×10^{-10}

^a Estimated from eq 5 and Figure 3.

are proportional to the total pressure; the corrected values are designated ρ_1 and those measured at close to 1 atm are plotted in Figure 2.

Towards the end of the work some measurements were made of the amount of NaAlCl₄ entering the gas stream. The condenser was cut off after a run, weighed, washed out, and weighed again; the washings were analyzed for sodium. The equilibrium partial pressure of NaAlCl₄ over NaCl–AlCl₃ melts with a total pressure of 1 atm was known from previous work³ to be given by

$$\log p_{\text{NaAlCl}_4}^0 = -4474/T + 3.449 \quad (5)$$

Figure 3 shows, on an empirical basis, the degree of saturation achieved as a function of total pressure at 550°. In compiling Table I it has been assumed that the same relation holds at other temperatures.

The dimerization constant for AlCl₃ ($p_{\text{AlCl}_3}^2/p_{\text{Al}_2\text{Cl}_6} = -6749/T - 2.013 \log T + 13.747$) was based on the work of Smits and Meijering.⁴

Two measurements were made with a KCl–AlCl₃ melt instead of NaCl–AlCl₃. Figure 2 shows that similar results were obtained.

Discussion

Before the chemistry of the ionization can be discussed it is necessary to have values for the partial pressures of the ions present. To derive these from the observed conductances needs a knowledge of the ionic mobilities. Although the theory involved is clear, there is in practice insufficient data to make any but a rough estimate.

The key to the problem is the Nernst–Einstein equation which relates the equivalent conductance, Λ , of a charged particle to its diffusion coefficient, D

$$\Lambda = \frac{F^2 D}{RT} \quad (6)$$

where F is the faraday and R here has the value 8.314 J deg⁻¹ mol⁻¹. If the partial pressure of all ions taken together is p_{ions} , then

$$\Lambda = \frac{RT}{p_{\text{ions}} \rho} \quad (7)$$

where R now has the value 82.06 cm³ atm⁻¹ deg⁻¹ mol⁻¹. Hence

$$p_{\text{ions}} = \frac{R}{F^2} \left(\frac{RT^2}{PD} \right) \frac{P}{\rho} \quad (8)$$

where P is the total pressure. The quantity ρ/P has already been defined as ρ_1 , the resistivity corrected to 1 atm. Hence

$$p_{\text{ions}} = 8.93 \times 10^{-10} \left(\frac{RT^2}{PD} \right) \frac{1}{\rho_1} \quad (9)$$

From the work of Brokaw⁵ and Svehla⁶ the term in

(4) A. Smits and J. C. Meijering, *Z. Phys. Chem. Abt. B*, **41**, 98 (1938).

(5) R. S. Brokaw, NASA Technical Report R-81, Washington, D. C., 1960.

(6) R. A. Svehla, NASA Technical Report R-132, Washington, D. C., 1962.

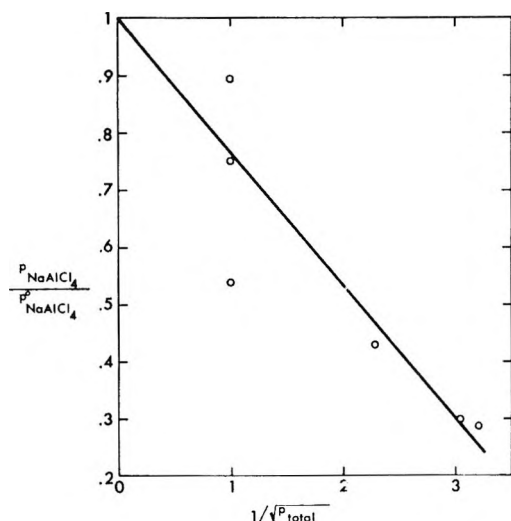


Figure 3. Degree of saturation of AlCl_3 gas stream with NaAlCl_4 as a function of total pressure.

brackets may be estimated. For self- and interdiffusion of the molecules AlCl_3 , Al_2Cl_6 , and NaAlCl_4 the values vary little with temperature over the range 600–1600°K, and lie in the range $0.47\text{--}0.83 \times 10^9$. Since the exact nature of the ions involved and their force constants is unknown, the best that can be done is to take

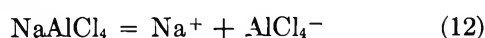
$$\frac{RT^2}{PD} = 0.63 \times 10^9 \quad (10)$$

and hence

$$p_{\text{ions}} = 0.56/p_1 \quad (11)$$

The resulting values have been listed in Table I.

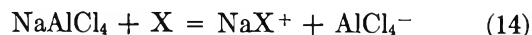
Owing to scatter in the experimental results and the uncertainty in deriving partial pressures from them the task of deciding the mechanism of ionization is not quite as simple as it might have been. Basically there are two criteria which a proposed mechanism must satisfy. (a) It must fit the observed pressure dependence of the resistivity at constant temperature within the experimental accuracy. (b) The entropy derived from the temperature dependence of the resistivity must be reasonable. Since it has already been demonstrated that the presence of NaAlCl_4 is necessary for conductance, and in view of the thermodynamic calculation of the stability of the AlCl_4^- ion, it may be assumed that the latter is present. The reaction could therefore be simply



with

$$\begin{aligned} K_p &= p_{\text{Na}^+} \cdot p_{\text{AlCl}_4^-} / p_{\text{NaAlCl}_4} \\ &= p_{\text{ions}}^2 / 4p_{\text{NaAlCl}_4} \end{aligned} \quad (13)$$

since $p_{\text{Na}^+} = p_{\text{AlCl}_4^-} = p_{\text{ions}}/2$, or, in general it could be



with

$$\begin{aligned} K_p &= p_{\text{NaX}^+} \cdot p_{\text{AlCl}_4^-} / (p_{\text{NaAlCl}_4} \cdot p_{\text{X}}) \\ &= p_{\text{ions}}^2 / (4p_{\text{NaAlCl}_4} \cdot p_{\text{X}}) \end{aligned} \quad (15)$$

For reaction 12 ΔS should be around $+30 \text{ cal deg}^{-1}$, while for reaction 14 it should be approximately zero. X could plausibly be AlCl_3 , Al_2Cl_6 , or NaAlCl_4 .

For each of the four proposed mechanisms the equilibrium constant was calculated for each experiment, and hence ΔG . These values were then fitted by least-squares regression analysis to the equation

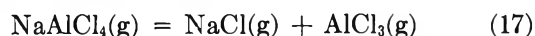
$$\Delta G = \Delta H - T\Delta S + a \log P \quad (16)$$

The criterion that the observed pressure dependence of resistivity be accounted for satisfactorily is equivalent to requiring that the coefficient a be statistically not significant.

Table II shows the results of these calculations. The significance of a is assessed in terms of its statistical F value and the corresponding probability of its having arisen by chance.

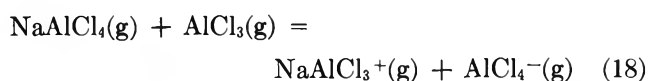
Of the four reactions, 12 can be ruled out on the grounds of both entropy and pressure dependence, and (14) with $\text{X} = \text{Al}_2\text{Cl}_6$ on the ground of entropy. Of the two remaining, $\text{X} = \text{AlCl}_3$ is favored on both grounds, although the pressure dependence for it is higher than is desirable.

Without going into details (which require more auxiliary data than can be presented here) it can be seen qualitatively that $\text{X} = \text{NaCl}$ is also not admissible. p_{NaCl} is governed by the equilibrium



which, since $\Delta H \simeq 50 \text{ kcal}$,² has a high temperature dependence. This would give a correspondingly large value of ΔS for the reaction producing Na_2Cl^+ .

It is therefore postulated that the ionization reaction is



with $\Delta H \simeq 70 \text{ kcal}$. If the estimate for $\Delta H \simeq 100 \text{ kcal}$ for reaction 2 is accepted, this means that ΔH for $\text{Na}^+(\text{g}) + \text{AlCl}_3(\text{g}) = \text{NaAlCl}_3^+(\text{g})$ is $\simeq -30 \text{ kcal}$. That these magnitudes are at least plausible can be seen from a simple electrostatic energy calculation. With an Al-Cl distance of 2.14 Å (as in AlCl_3) and an Na-Cl distance of 2.36 Å (as in NaCl) the energy of attachment of an Na^+ ion to one apex of an AlCl_4^- ion is 97 kcal; the energy of attachment to a neutral AlCl_3 is 32 kcal. (The calculation is based on the assumption that repulsion and polarization terms cancel out, an assumption Margrave⁷ has shown to be justified for the alkali chlorides.)

Table II: Expected and Observed Values of ΔS and Pressure Dependence of ΔG for Various Ionization Mechanisms

Reaction	ΔS , cal deg ⁻¹		ΔH , kcal, observed ^a	Coefficient a	
	Expected	Observed ^a		F statistic	Probability
$\text{NaAlCl}_4 = \text{Na}^+ + \text{AlCl}_4^-$	+30	7.6 ± 3.1	76.5 ± 2.8	33	$\ll 0.001$
$\text{NaAlCl}_4 + \text{AlCl}_3 = \text{NaAlCl}_3^+ + \text{AlCl}_4^-$	0	4.6 ± 3.1	72.9 ± 2.8	5.6	0.03
$\text{NaAlCl}_4 + \text{Al}_2\text{Cl}_6 = \text{NaAl}_2\text{Cl}_6^+ + \text{AlCl}_4^-$	0	33.1 ± 3.3	96.5 ± 2.9	0.57	0.5
$2\text{NaAlCl}_4 = \text{Na}_2\text{AlCl}_4^+ + \text{AlCl}_4^-$	0	-9.9 ± 4.3	53.7 ± 3.9	11.6	0.002

^a Error limits are statistical standard errors.

The ion NaAlCl_3^+ would be analogous to LiAlF_3^+ reported in mass spectra,⁸ and also to the neutral KMgCl_3 .⁹

This work has been largely exploratory in character. It would be possible to improve experimental precision in the future, but, from a thermodynamic point of view, the major source of uncertainty lies in the deriva-

tion of partial pressures from the measured resistivities. An improvement in the numerical factor in eq 11 would be most desirable.

(7) J. L. Margrave, *J. Phys. Chem.*, **58**, 258 (1954).

(8) R. F. Porter and E. E. Zeller, *J. Chem. Phys.*, **33**, 858 (1960).

(9) E. E. Schrier and H. M. Clark, *J. Phys. Chem.*, **67**, 1259 (1963).

The Thermochemistry, Thermodynamic Functions, and Molecular Structures of Some Cyclic Hydrocarbons

by Richard H. Boyd,* Shiv N. Sanwal, Shahrokh Shary-Tehrany, and Donal McNally

Department of Chemical Engineering and Division of Materials Science and Engineering, University of Utah, Salt Lake City, Utah 84112 (Received October 13, 1970)

Publication costs assisted by the U. S. Air Force Office of Scientific Research

The following heats of combustion (kilocalories per mole) have been measured *via* oxygen bomb calorimetry; adamantane (I) (c), -1441.95 ± 0.68 ; tricyclo[5.2.1.0^{2,6}]decane (II) (c), -1460.04 ± 0.60 ; 1,2,3,4-tetrahydronaphthalene (III) (l), -1342.61 ± 0.51 ; 1,2,3,4,5,6,7,8-octahydroanthracene (IV) (c), -1902.99 ± 0.69 . Vapor pressure curves have been measured for the above compounds and for bicyclo[2.2.1]heptane (V) and bicyclo[2.2.2]octane (VI) which when combined with literature values for the heats of combustion lead to the following gas phase heats of formation (kilocalories per mole); I, -30.65 ± 0.98 (-32.4 ± 0.6 , selected value); II, -14.38 ± 0.90 ; III, 5.29 ± 0.81 ; IV, -9.01 ± 0.99 ; V, -12.42 ± 0.70 ; VI, -23.75 ± 0.30 . The heats of formation and strain energies have been calculated by energy minimization using transferable valence potentials and compared with experimental values with satisfactory results. The ideal gas phase thermodynamic functions have been calculated. In a number of cases comparison with experimental entropies is possible. Calculated geometries are also reported.

Introduction

Transferable bond energy or group contribution schemes have proved to be highly successful in the prediction of the heats of formation of many organic molecules. The concept of transferable potential functions for bond deformation (stretching, bending, and twisting) has been very useful in vibrational spectroscopy. The synthesis of these two approaches in the simultaneous prediction of molecular geometries and

heats of formation of strained molecules appears promising.¹⁻⁸ This synthesis has been made possible by the

(1) K. B. Wiberg, *J. Amer. Chem. Soc.*, **87**, 1070 (1965).

(2) N. L. Allinger, M. A. Miller, F. A. Van Catledge, and J. A. Hirsch, *ibid.*, **89**, 4345 (1967).

(3) N. L. Allinger, J. A. Hirsch, M. A. Miller, I. Tyminski, and F. A. Van Catledge, *ibid.*, **90**, 1199 (1968).

(4) E. J. Jacob, H. Thompson, and L. S. Bartell, *J. Chem. Phys.*, **47**, 3736 (1967).

Table I: Vapor Pressure Results

Compound	$\log P(\text{mm}) = (A/T) + B + C \log T$			Temp range, °K
	A	B	C	
Norbornane (c)	-2097.5	8.479	0.0	284-327
Bicyclo[2.2.2]octane (c)	-2416.4	8.628	0.0	323-363
Tricyclo[5.2.1.0 ^{2,6}]- decane (l)	-2273.7	7.782	0.0	358-417
Adamantane (c)	-2746.8	8.617	0.0	366-443
(c) ^a	-4054.4	29.220	-6.666	313-443
Tetralin (l)	-2797.9	11.954	-1.187	370-446
Octhracene (l)	-2383.9	6.786	0.0	437-498

^a Combined data of ref 11 and this work.

advent of large fast digital computers and the development of algorithms for finding the geometry of minimum deformation energy. It is also possible to extend such calculations to yield vibrational frequencies of the molecule^{5,6} so that from these and the calculated moments of inertia, the gas phase thermodynamic functions can be calculated.^{5,6} With these developments it is important to be able to test proposed sets of transferable valence force (bond deformation) potentials by comparison of calculated and experimental heats of formation (or strain energies), geometries, and thermodynamic functions. It is the purpose of the present work to provide experimental gas phase heats of formation of several important potentially strained cyclic hydrocarbons. It is also our purpose to calculate the heats of formation (and strain energies), geometries, and gas phase thermodynamic functions for comparison with experimental values. The compounds studied are bicyclo[2.2.1]heptane (or norbornane), bicyclo[2.2.2]octane, tricyclo[5.2.1.0^{2,6}]decane (or tetrahydrodicyclopentadiene), tricyclo[3.3.1.1^{3,7}]decane (or adamantane), 1,2,3,4-tetrahydronaphthalene (or tetralin), and 1,2,3,4,5,6,7,8-octahydroanthracene (or octhracene).

Experimental Section

Compounds Studied. Norbornane and adamantane were purchased from the Aldrich Chemical Co. and were purified by three sublimations through a temperature gradient with the center portion retained. Tetrahydrodicyclopentadiene (Aldrich Chemical Co.) and octhracene (Aldrich Chemical Co.) were purified by multiple-pass zone-refining and then sublimed through a temperature gradient. Heat of fusion curves of the latter two compounds taken with a Perkin-Elmer DSC1B differential scanning calorimeter indicated a purity in excess of 99.9 mol %. Tetralin was purified by fractional distillation and gas-liquid partition chromatographic analysis showed only a single peak. Bicyclo[2.2.2]octane was synthesized by catalytic hydrogenation (reduced Adams PtO catalyst, 1 atm) of the parent diene (City Chemical Co). It was purified by several temperature gradient sublimations.

Vapor Pressure Measurements. The vapor pressure of tetralin was determined by a semimicro ebulliometer method.⁹ It was fit by least squares to the equation

$$\log P (\text{mm}) = (A/T) + B + C \log T \quad (1)$$

The heat of vaporization was calculated assuming no vapor imperfection and negligible liquid volume as

$$\Delta H_{\text{vap}} = R(-2.30259A + CT) \quad (2)$$

The vapor pressures of norbornane, bicyclo[2.2.2]octane, tetrahydrodicyclopentadiene, and adamantane were measured in a glass Bourdon gauge that was nulled against a mercury manometer. The temperature ranges and accuracy were more limited than with the ebulliometer method, and therefore the vapor pressures of these compounds were fit by least squares to eq 2 with $C = 0.0$ and the heats of vaporization calculated by eq 3 with $C = 0.0$. The vapor pressure results are summarized in Table I. The vapor pressure of adamantane has been measured previously¹⁰ at temperatures lower than used here. Table II also lists the three constant equations for the combined data in which we improved the fit by weighting our two lowest points less than the others.

Heats of Fusion and Heat Capacities. Octhracene and tetrahydrodicyclopentadiene are liquids in the temperature range of the vapor pressure measurements, but solids at the temperature of the heat of combustion measurement. Heats of fusion were measured with the differential scanning calorimeter. Heat capacities of

(5) R. H. Boyd, "Division of Physical Chemistry Abstracts," 152nd National Meeting of the American Chemical Society, New York, N. Y., Sept 11-16, 1966.

(6) R. H. Boyd, *J. Chem. Phys.*, **49**, 2574 (1968).

(7) C. F. Shieh, D. McNally, and R. H. Boyd, *Tetrahedron*, **25**, 3653 (1969).

(8) S. Chang, D. McNally, S. Shary-Tehrany, M. J. Hickey, and R. H. Boyd, *J. Amer. Chem. Soc.*, **92**, 3109 (1970).

(9) A. Weissberger, "Technique of Organic Chemistry, Vol. I. Physical Methods, Part I," Interscience Publishers, New York, N. Y., 1959, p 439.

(10) W. K. Bratton, I. Szilard, and C. A. Cupas, *J. Org. Chem.*, **32**, 2019 (1967).

Table II: Heats of Fusion and Heat Capacities

Compound	T, °K	C _P , cal/(mol °K)	Δ <i>H</i> _{fusion} , kcal/mol
Tricyclo[5.2.1.0 ^{2,6}]-decane			
(c)	329	57.7	
(c)	342	59.8	
(l)	372	66.9	
(l)	390	69.6	
	352		0.705 ± 0.01
Octhracene			
(c)	327	78.3	
(c)	336	81.9	
(l)	372	89.8	
(l)	390	94.5	
	346		4.28 ± 0.05

these two compounds were also determined for correction of the heat of vaporization to room temperature. The results are summarized in Table II.

Heat of Combustion Calorimetry. The calorimeter previously described^{11,12} was used with the following modification. The Mueller bridge was replaced by a Leeds and Northrup 7556 potentiometer in the configuration of Figure 1 as suggested by Daneman.¹³ The 10-V power supply was constructed at the University of Utah and is based on a General Electric RA3A reference amplifier. It is stable to the load changes of the experiment, line voltage variations, and temperature drift over a period of 1 min to better than 1 ppm. The divider on the 10-V supply connected to the "standard cell check" position on the potentiometer provides a convenient check of the ratio of the voltages of the two power supplies without resetting the potentiometer. The "standard cell adjust" rheostat is used to adjust the ratio to constancy each minute during a run. The *R*₁ resistor is manganin wire and is immersed in oil and mounted in the thermostated bath of the calorimeter. The resistance of the thermometer (~25 Ω) is calculated as

$$R_z = V_z R_1 / (V_{\text{Sec}}(R_3 + R_2) / R_3 - V_z) \quad (3)$$

A resolution of 0.05 μV = 10⁻⁵ Ω = 10⁻⁴° is obtained. Our experience has been that this arrangement is an acceptable alternative to the G-2 Mueller bridge but does not offer any significant advantage over it in our application. Of the compounds listed in the Introduction, norbornane and bicyclo[2.2.2]octane were not burned since reliable values of their heats of combustion have been published.^{14,15} Tetralin (a liquid) and all of the solids were enclosed in Mylar bags to avoid weight loss due to volatilization. The complete heat of combustion results for adamantane, and typical results for the others are shown in Table III.

Summary of Results. The heats of combustion and derived heats of formation are listed in Table IV along

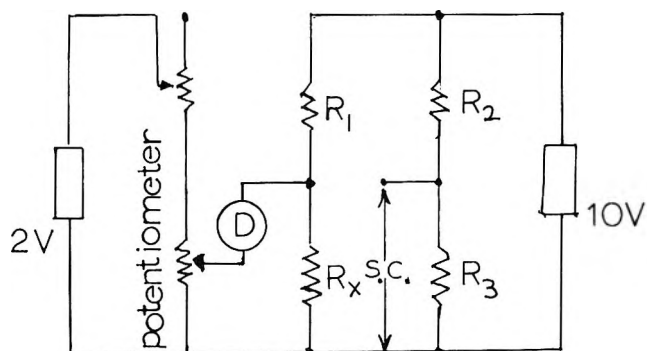


Figure 1. Potentiometer circuit for resistance thermometry. *R*₁ = 1999.1 ohms, *R*₂ = 1012.6 ohms, *R*₃ = 118.4 ohms, *R*_z = ~25 ohms, SC = standard cell connection on potentiometer.

with the heats of vaporization derived from eq 2 at the temperature or temperature interval indicated. The heats of vaporization were corrected to room temperature from the indicated temperature or temperature interval midpoint using the calculated vapor enthalpies of the next section along with the condensed phase heat capacities and heats of fusion of Table II, or the literature enthalpies for norbornane,¹⁶ bicyclo[2.2.2]octane,¹⁷ adamantane,¹⁸ and tetralin.¹⁹ Values of the heat of combustion (-1439.89 ± 0.17 kcal/mol) and heat of vaporization (-14.18 ± 0.04 kcal/mol) of adamantane have recently been published by Månsson, *et al.*²⁰ The mean of their result and ours for the heat of combustion is slightly outside the uncertainty intervals of the two experiments, but the agreement is reasonably satisfactory. The heats of vaporization are in good agreement. We have selected a value of -32.4 ± 0.6 kcal/mol for the gas phase heat of formation by weighting according to the uncertainty intervals.

Discussion

Our primary interest is in comparing the measured properties with those calculated using the methods and parameters presented previously by us.⁶⁻⁸ We have made some adjustments in the bending constants associated with hydrogen and carbon pendant to an aro-

(11) R. H. Boyd, R. L. Christensen, and R. Pua, *J. Amer. Chem. Soc.*, **87**, 3554 (1965).

(12) R. H. Boyd, K. R. Guha, and R. Wuthrich, *J. Phys. Chem.*, **71**, 2187 (1967).

(13) H. L. Daneman, Leeds and Northrup Co., private communication.

(14) A. F. Bedford, A. E. Beezer, C. T. Mortimer, and H. D. Springall, *J. Chem. Soc.*, 3823 (1963).

(15) E. F. Westrum, Jr., and S. W. Wong, *Thermodynamik Symposium*, IUPAC, Heidelberg, Germany, 1967.

(16) E. F. Westrum, Jr., and W. K. Wong, private communication.

(17) W. K. Wong and E. F. Westrum, Jr., *J. Phys. Chem.*, **74**, 1303 (1970).

(18) E. F. Westrum, Jr., *J. Phys. Chem. Solids*, **18**, 83 (1961).

(19) J. P. McCullough, H. L. Finke, J. F. Messerly, S. S. Todd, T. C. Kincheloe, and G. Waddington, *J. Phys. Chem.*, **61**, 1105 (1957).

(20) M. Månsson, N. Rapport, and E. F. Westrum, Jr., *J. Amer. Chem. Soc.*, **92**, 7296 (1970).

Table III: Combustion Data, ^a 25°

M_s (air vs. stainless steel)	M_f	M_m	ΔR	Q_f	Q_m	Q_i	Q_{std}	$-\Delta E_c$
Adamantane: $d = 1.07 \text{ g cm}^{-3}$ ^b (6 combustions), $\sigma = 3.8$								
0.162584	0.002264	0.035250	0.211273	9.5	193.5	0.58	0.75	10,565.8
0.151024	0.002297	0.025873	0.192330	9.6	142.0	0.62	0.69	10,573.6
0.157454	0.002296	0.025259	0.199405	9.6	138.6	0.62	0.73	10,571.5
0.146413	0.002145	0.026354	0.187181	8.9	144.6	0.62	0.68	10,572.3
0.152042	0.002271	0.028688	0.195101	9.5	157.5	0.62	0.71	10,567.1
0.164324	0.002154	0.017858	0.202707	9.0	98.0	0.62	0.76	10,562.9
							Av	10,568.9
Tricyclo[5.2.1.0 ^{2,6}]decane: $d = 0.95 \text{ cm}^{-3}$ ^c (6 combustions), $\sigma = 3.0$								
0.142521	0.002446	0.029010	0.186431	10.2	159.3	0.62	0.65	10,701.5
							Av	10,700.6
Tetralin: $d = 0.97 \text{ g cm}^{-3}$ ^d (6 combustions), $\sigma = 2.4$								
0.177666	0.002082	0.036899	0.221425	8.7	202.5	0.62	0.82	10,139.9
							Av	10,141.4
Octhracene: $d = 1.10 \text{ g cm}^{-3}$ ^d (6 combustions), $\sigma = 2.0$								
0.141371	0.002254	0.027133	0.176035	9.4	148.9	0.62	0.74	10,199.1
							Av	10,200.8

^a σ = standard deviation; M_s = weight of sample (g in air vs. stainless steel); M_f = weight of fuse (g in air vs. stainless steel); M_m = weight of "Mylar" (g in air vs. stainless steel); ΔR = corrected temperature rise (ohms); Q_f = energy of combustion of cotton fuse (calories); Q_m = energy of Mylar combustion (calories); Q_i = electrical energy of ignition (calories); Q_{std} = correction to standard states (Washburn); $-\Delta E_c$ = energy of combustion (standard state); $(\epsilon\Delta R - Q_f - Q_m - Q_i - Q_{std})/M_s$ (cal g⁻¹ in air vs. stainless steel) where ϵ , the energy equivalent of the calorimeter, was 9103.9 ± 2.7 cal/ohm. ^b W. Nowacki, *Helv. Chim. Acta*, 28, 78 (1945). ^c Measured on sample pellet. ^d R. C. Weast, Ed., "Handbook of Chemistry and Physics," 50th ed. Chemical Rubber Co., Cleveland, Ohio, 1969.

Table IV: Summary of Thermochemical Data, ^a 25° (kcal/mol)

	ΔH_c°	ΔH_{vap}	ΔH_f°
Norbornane			
(c)	-1046.24 ± 0.52^b	9.59 ± 0.20 (284–326°K)	-22.01 ± 0.52
(g)	-1055.83 ± 0.70		-12.42 ± 0.70
Bicyclo[2.2.2]octane			
(c)	-1195.49 ± 0.10^c	11.40 ± 0.20 (298°K) 11.06 ± 0.20 (323–363°K)	-35.15 ± 0.10
(g)	-1206.89 ± 0.30		-23.75 ± 0.30
Adamantane			
(c)	-1441.95 ± 0.68	14.45 ± 0.3 (298°K) 14.23 ± 0.2 (325°K)	-45.10 ± 0.68
(g)	-1456.40 ± 0.98		-30.65 ± 0.98
Tricyclo[5.2.1.0 ^{2,6}]- decane			
(c)	-1460.04 ± 0.60	12.65 ± 0.3 (298°K)	-27.03 ± 0.60
(l)		10.40 ± 0.2 (359–443°K)	
(g)	-1472.69 ± 0.90		-14.38 ± 0.90
Tetralin			
(l)	-1342.61 ± 0.51	13.20 ± 0.3 (298°K) 11.92 ± 0.2 (380°K)	-7.91 ± 0.51
(g)	-1355.81 ± 0.81		5.29 ± 0.81
Octhracene			
(c)	-1902.99 ± 0.69	19.66 ± 0.3 (298°K)	-28.67 ± 0.69
(l)		10.91 ± 0.2 (438–499°K)	
(g)	-1922.65 ± 0.99		-9.01 ± 0.99

^a The uncertainty intervals for the condensed phases are the combined uncertainty intervals (for 95% confidence of the deviation of the sample mean from the population mean) for the sample and benzoic acid combustions. The uncertainty interval for the heats of vaporization are estimates. ^b From ref 14. ^c From ref 15.

matic ring to bring the calculated vibrational frequencies into better agreement with the assignments of Pitzer and Scott²¹ for benzene and toluene. The parameters not included in ref 8 are summarized in Table V. Equation 9 of ref 8 expresses the calculated or predicted heat of formation of a hydrocarbon, C_aH_b , in terms of intrinsic group contributions to the atomization energy, E_1^* , the deformational energy (bond stretching, bending, and twisting) and nonbonded energies ($DE + NB$), enthalpy, $H_{298}^\circ - H_0^\circ$ and zero-point energy, ZPE , as

$$\Delta H_f^\circ (\text{calcd, 298}) = -\sum E_1^*(\text{group}) + (DE + NB)_{\text{calcd}} + (H_{298}^\circ - H_0^\circ) + ZPE + 170.890a + 52.090b - \frac{5}{2}(a + b)RT_{298}$$

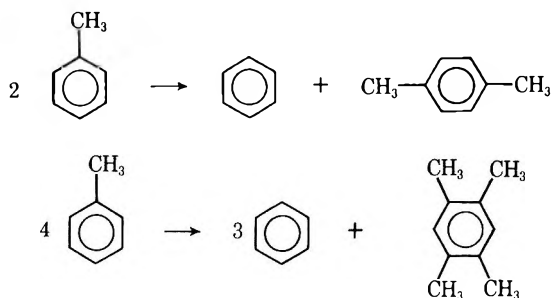
This equation can also be expressed somewhat less esoterically as

$$\Delta H_f^\circ (\text{calcd, 298}) = \sum \Delta H_f^\circ(\text{group, 298}) + (DE + NB)_{\text{calcd}} - \sum (DE + NB)_{\text{group}} + (H_{298}^\circ - H_0^\circ) - \sum (H_{298}^\circ - H_0^\circ)_{\text{group}} + ZPE - \sum ZPE(\text{group}) \quad (4)$$

The term $(DE + NB)_{\text{calcd}} - \sum (DE + NB)_{\text{group}}$ represents the excess energy or strain energy due to the deformation of bonds or to nonbonded interactions over that in the reference compounds used to work out the groups. The terms involving enthalpies (thermal energies) and zero-point energy take into account any failure of group contributions to account for these in the compound in question. The overall strain energy may be defined as the excess energy from all three of the above effects or as

$$SE(\text{calcd, 298}) = \Delta H_f^\circ(\text{calcd, 298}) - \sum \Delta H_f^\circ(298, \text{group}) \quad (5)$$

Experimental strain energies may be defined by using eq 5 with $\Delta H_f^\circ(\text{calcd, 298})$ replaced by $\Delta H_f^\circ(\text{exptl, 298})$. Heats of formation and strain energies were calculated from eq 4 and 5 using $(DE + NB)_{\text{calcd}}$, $(H_T^\circ - H_0^\circ)_{\text{calcd}}$, and $ZPE(\text{calcd})$ values from energy minimization calculations⁶ carried out in the present study. For the alkanes, the parameters and group contributions of ref 8 were used. Our previous work^{6,7} on aromatic systems included nonbonded interactions only where sterically important, whereas in this work, they have been included between all atoms not interacting through a bond angle (except the $C \cdots C$ interaction within an aromatic ring). Consequently the group contributions have to be modified slightly. Table VI summarizes these new group contributions. They were arrived at from calculations and data on benzene and toluene and the $-CH_3$ contributions of ref 8 by assuming that the reactions



involve no overall change in enthalpy function, zero-point energy, and $DE + NB$ and that the enthalpy of reaction is zero. This leads to group values for predicting the heats of formation, enthalpies, etc., of un-

Table V: Aromatic Ring Parameters for Conformational Calculations^a

Bond Stretching		k_r , mdyn/Å	R_0 , Å
C—H (pendant to aromatic)		5.05	1.09
C \cdots C (aromatic)		7.65	1.39
C—C (pendant to aromatic)		4.40	1.50
Bond Bending		k_θ , 10^{-11} erg/rad	θ_0 , deg
(aromatic)		1.00	120
(pendant to aromatic)		0.70	120
(pendant to aromatic)		0.50	120
Out-of-Plane Bending		k_δ , 10^{-11} erg/rad	δ° , deg
(pendant to aromatic)		0.80	0
(pendant to aromatic)		0.29	0
$U = U_0/2[b + \cos 3\phi]$			
out-of-plane aromatic ring twisting		$U_0 = -0.080$ (10^{-11} erg/molecule)	
C—C twisting (pendant to aromatic)		$b = -1.0$ $U_0 = 0.001$ (10^{-11} erg/molecule)	
		$b = 1.0$	

^a For other parameters, see ref 8. Nonbonded interactions (ref 8) were used between all atoms not sharing a bond angle interaction except in an aromatic ring, where the $C \cdots C$ nonbonded interaction was deleted.

(21) K. S. Pitzer and D. W. Scott, *J. Amer. Chem. Soc.*, **65**, 803 (1943).

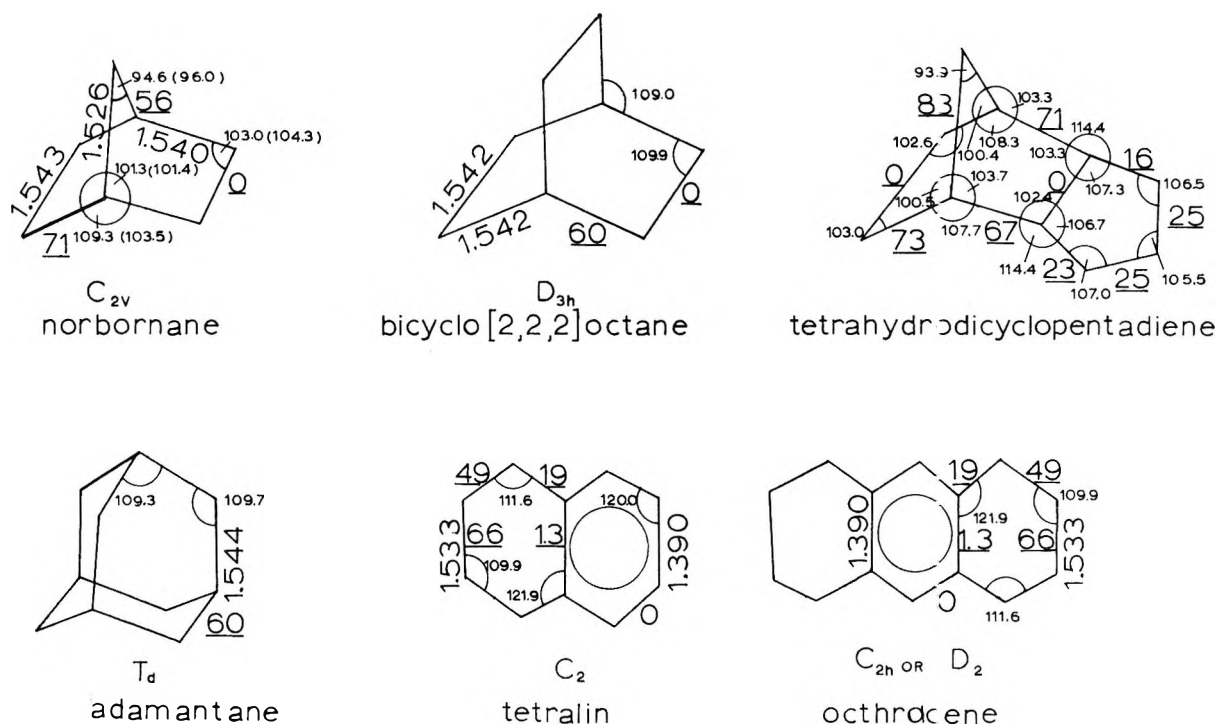


Figure 2. Calculated structures of cyclic hydrocarbons. Angles with larger size lettering are torsional angles based on eclipsed positions as zero. Smaller lettering angles are bond angles.

strained substituted aromatics. Thus, for example, the $\Sigma\Delta H_f^\circ(\text{group})$ values are in good agreement with the experimental ΔH_f° for *p*-xylene but slightly lower than experimental for *o*-xylene and 1,2,4,5-tetramethylbenzene because of the slight strain associated with the crowding of the methyl groups. Energy minimization calculations, in principle, would lead to the appropriate correction terms for $\Sigma\Delta H_f^\circ(\text{group})$ (see eq 4) to bring it into agreement with experiments in crowded aromatics. The strain effects are small enough however that the combined uncertainties of the calculation could mask the improvement.

Table VII lists the experimental and calculated heats of formation and strain energies. The agreement be-

tween experimental and calculated values is gratifying and lends further support to the general approach of conformational energy calculations. The heats of formation of the three most strained cycloalkanes in Table VII are quite sensitive to the choice of energy parameters used. Adamantane is seen from the table to be appreciably strained. Schleyer, *et al.*,²² have made an extensive discussion of this strain. We suffice here to say that qualitatively it can be attributed to the gauche conformations of the skeletal bonds. In the present scheme the gauche energy is represented by nonbonded interactions and is primarily due to $C\cdots C$ repulsions. Cyclohexane is also slightly strained for the same

Table VI: Group Contributions in Aromatic Compounds^a to the Heat of Formation, the Intrinsic Bond Energies in the Hypothetical Motionless State (E_1^*), Deformation and Nonbonded Energies ($DE + NB$), Enthalpies ($H_{228}^\circ - H_0^\circ$) and Zero-Point Energies (ZPE) (kcal/mol)

	ΔH_f° (group, 298)	E_1^* (group)	$(DE + NB)_{\text{group}}$	$(H_{228}^\circ - H_0^\circ)_{\text{group}}$	ZPE (group)
	22.07	1307.17	-0.56	2.91	57.40
	24.32	1247.89	-1.07	2.33	52.06
	28.82	1129.31	-2.09	1.17	41.38

^a See ref 8 for aliphatic groups used.

Table VII: Comparison of Calculated Heats of Formation and Strain Energies (SE) with Experimental, 25° (kcal/mol)

Compound	ΔH_f° (calcd)	ΔH_f° (exptl)	SE (calcd)	SE (exptl)
Norbornane	-11.7	-12.4	17.5	16.8
Bicyclo[2.2.2]-octane	-22.3	-23.8	11.4	10.5
Adamantane	-33.3	-32.4	4.9	5.8
Tetrahydrodicyclopentadiene	-12.2	-14.4	25.0	23.8
Tetralin	5.3	5.3	1.8	1.3
Octhracene	-7.3	-9.0	3.9	2.8
<i>p</i> -Xylene	3.7	4.3	-0.4	0.2

(22) P. v. R. Schleyer, J. E. Williams, and K. R. Blanchard, *J. Amer. Chem. Soc.*, **92**, 2377 (1970).

Table VIII: Calculated Ideal Gas State Thermodynamic Functions (cal/°K)

T , °K	$(G^\circ - H_0^\circ)/T$	$(H^\circ - H_0^\circ)/T$	S°	C_p°	ZPE , kcal/mol
Norbornane, C_{2v} , $\sigma = 2$					
200	54.85	10.64	65.49	16.28	107.52
298.15	59.70	14.06	73.76 (74.0 ± 0.6) ^a	26.14	
300	59.79	14.13	73.92	26.35	
350			78.47 (78.8 ± 0.8) ^a		
400	64.45	18.58	83.03	37.36	
500	69.11	23.38	92.49	47.44	
Bicyclo[2.2.2]octane, D_{3h} , $\sigma = 6$					
200	55.53	12.37	67.91	19.58	125.89
298.15	61.22	16.57	77.79 (77.6 ± 0.6) ^b	39.98	
300	61.32	16.65	77.98	31.21	
400	66.81	21.87	88.69	43.75	
500	72.29	27.44	99.74	55.27	
Adamantane, T_d , $\sigma = 12$					
200	54.48	11.80	66.28	20.98	149.29
298.15	60.14	17.17	77.32 (78.0 ± 0.7) ^c	35.59	
300	60.25	17.28	77.53	35.88	
400	66.11	23.90	90.01 (90.4 ± 0.6) ^c	51.44	
500	72.20	30.87	103.07	65.54	
600	78.43	37.66	116.09	77.32	
800	91.00	49.96	140.96	95.36	
1000	103.30	60.39	163.69	108.17	
Tetrahydrodicyclopentadiene, d,l pair					
200	63.17	13.81	76.98	22.81	148.19
298.15	69.60	18.96	88.56	36.56	
300	69.72	19.07	88.79	36.84	
400	76.06	25.43	101.49	52.09	
500	82.46	32.21	114.68	66.05	
Benzene, ^d D_{6h} , $\sigma = 12$					
298.15	53.09 (52.93)	11.71 (11.41)	64.80 (64.34)	19.91 (19.52)	62.74
400	56.94 (56.69)	14.67 (14.41)	71.61 (71.10)	26.63 (26.74)	
500	60.54 (60.24)	17.66 (17.50)	78.20 (77.74)	32.37 (32.80)	
Toluene, ^d C_{2h} , $\sigma_{ex} = 2$, free methyl rotation, $\sigma_i = 3$, $\sigma = 2 \times 3 = 6$					
298.15	62.20 (61.98)	14.48 (14.44)	76.68 (76.42)	24.50 (24.80)	79.98
400	66.96 (66.74)	18.96 (18.17)	85.02 (84.91)	32.48 (33.25)	
500	71.38 (71.20)	21.67 (21.94)	93.05 (93.13)	39.42 (40.54)	
<i>p</i> -Xylene, ^d D_{2h} , $\sigma_{ex} = 4$, free methyl rotation, $\sigma_i = 3$, $\sigma = 4 \times 3 \times 3 = 36$					
298.15	66.04 (66.26)	17.27 (17.97)	83.32 (84.23)	29.24 (30.32)	96.83
400	71.71 (72.15)	21.51 (22.32)	93.23 (94.47)	38.52 (39.70)	
500	76.97 (77.59)	25.77 (26.66)	102.75 (104.25)	46.85 (48.06)	
Tetralin, C_{2v} , $\sigma = 2$, d,l pair					
200	62.54	14.12	76.67	23.14	120.56
298.15	69.07	19.02	88.10	35.03	
300	69.19	19.12	88.32	35.27	
380			97.80 (98.9 ± 0.8) ^a		
400	75.45	24.71	100.16	47.51	
500	81.58	30.41	112.00	58.56	
600	87.62	35.90	123.52	67.87	
Octracene 1:1 mixture of C_{2h} , $\sigma = 2$, and D_{2v} , $\sigma = 4$, d,l pair					
200	70.68	19.54	90.23	33.33	178.24
298.15	79.82	26.85	106.67	50.39	
300	79.99	26.99	106.99	50.73	
400	88.87	35.19	124.06	68.64	
500	97.62	43.57	141.20	85.02	
600	106.29	51.67	157.97	98.87	

^a From the crystal entropy of Westrum and Wong,¹⁶ and the vapor pressure and heat of vaporization of the present work. ^b Experimental value based on the crystal entropy of Westrum and Wong,¹⁷ and the vapor pressure and heat of vaporization reported in the present work. ^c Experimental value based on the crystal entropy of Westrum,¹⁸ and the vapor pressure and heat of vaporization of the present work. ^d Values in parentheses are from F. D. Rossini, "Selected Values of Physical and Thermodynamic Properties of Hydrocarbons and Related Compounds," Carnegie Press, Pittsburgh, Pa., 1953. ^e Experimental value based on the liquid entropy of ref 19 and the vapor pressure and heat of vaporization of the present work.

reason as is apparent when ΔH_f° groups for defining the strain energy are based solely on trans conformations of linear alkanes^{8,22} and zero-point energy effects are taken into account.⁸

Tetralin and octhracene are interesting because of the possibility of both bond angle and rotational angle strain due to fusion of the cyclohexane ring to the aromatic ring. However, the free rotation of the methyl groups in toluene and *p*-xylene²¹ indicates that the inherent barrier to rotation of a pendant carbon-to-aromatic ring bond is very small. This could alleviate the overall strain considerably; the calculations of Table VII which assume an essentially zero inherent barrier (the nonbonded interactions can still contribute) at these bonds verify this. There is a small but real strain present. However, it would have been substantially higher (about 1.6 kcal/fusion bond) if the full inherent barrier⁸ (2.1 kcal/mol) of an aliphatic C-C-C-C bond had been used.

The calculated vibrational frequencies and moments of inertia have been used to calculate the gas phase thermodynamic functions of the compounds studied, and the results are summarized in Table VIII. Also included in Table VIII are the calculated zero-point energies used in the heat of formation calculations (Table VII). Benzene and toluene are included to indicate the reliability of the calculated results. The entropies are rather sensitive to the calculated skeletal frequencies and when a comparison with the experiment is possible, provide a good overall check on the method. The determination of experimental gas phase entropies requires accurate crystal entropies, vapor pressures, and heats of vaporization. The gas phase entropy is particularly sensitive to the latter. An error of 0.3 kcal/mol at room temperature causes an error of 1.0 cal/(°K mol) in the entropy. In compounds having ΔH_{vap} equal to 10 kcal/mol or higher accurate data is required, and errors of this magnitude can be expected. In the most favorable cases (benzene, toluene) the experimental values have uncertainties of at least 0.3 cal/(°K mol).

For three of the cycloalkanes, a comparison can be made (see Table VIII), and the agreement is excellent. For bicyclo[2.2.2]octane the calculated entropy is based on the D_{3h} symmetry which results from the energy minimization calculation and provides some confirmation of the nontwisted conformation. The agreement for tetralin seems to lie slightly outside the estimated experimental error and could possibly indicate that the calculated C_2 symmetry (symmetrical puckering of the saturated ring) is in error. A nonsymmetrical structure might change the vibrational frequencies only slightly but would decrease the symmetry number to one and lead to better agreement of the entropy with the experiment. However, the calculations seem to show real preference for the symmetrical structure, and we are inclined to believe it is the actual one and that the discrepancy lies in the calculated frequencies and experimental error. Similarly, the entropy of octhracene is sensitive to the calculated symmetrical puckering of the saturated rings. There are two calculated structures of equal energy depending on the sense of the ring puckering of the saturated rings. However, there is no experimental entropy to verify or refute this point.

The calculated geometries are summarized in Figure 2. The calculated angles of norbornane are of interest since some are fairly distorted. An electron diffraction study of this compound has been made,²³ and the results are included in the figure.

Acknowledgments. The authors are indebted to the U. S. Army Research Office (Durham) and the U. S. Air Force Office of Scientific Research (Contract FO4460-68-C-0002, Project Themis) for financial support of this work. We are also indebted to Professor E. F. Westrum, Jr., for generously sharing his thermochemical results prior to publication.

(23) J. F. Chiang, C. F. Wilcox, Jr., and S. H. Bauer, *J. Amer. Chem. Soc.*, **90**, 3149 (1968).

The Self-Diffusion of Water in Uranyl Nitrate Hexahydrate

by M. L. Franklin and Ted B. Flanagan*

Chemistry Department, University of Vermont, Burlington, Vermont 05401 (Received December 7, 1970)

Publication costs assisted by the National Science Foundation

The self-diffusion of water in uranyl nitrate hexahydrate (UNH) has been investigated by following the course of isotopic exchange with D_2O . The extent of exchange exhibits a square-root dependence upon time. This suggests that the slow step is solid-state diffusion. The rate of diffusive exchange of UNH with $H_2^{18}O$ is comparable to that with D_2O and therefore the entire water molecule diffuses. The pressure and temperature dependences of diffusive exchange have been examined. The temperature dependence can be expressed as $D = 4 \times 10^{-3} \exp(-7600/RT)$. Possible mechanisms for diffusive exchange in UNH are considered.

Introduction

In 1961, Barrer¹ pointed out that there was a notable lack of measurements of the self-diffusion of water in nonzeolitic crystalline hydrates. The situation is unchanged today with regard to direct measurements of diffusion but nmr techniques have recently given some information about translational diffusion in hydrates.^{2,3} The availability of such data from nmr increases the desirability of having direct diffusional data for purposes of comparison. The only detailed study of diffusion of water in crystalline hydrates (nonzeolitic) has been made by Kraft.⁴ He surrounded light water hydrates with D_2O vapor and noted their increase of weight as a function of time. Potassium aluminum alum was investigated in some detail and Kraft found

$$D = 0.56 \times 10^{-7} \exp(-6000/RT)$$

This gives $D = 2 \times 10^{-12} \text{ cm}^2 \text{ sec}^{-1}$ (25°). He did not observe exchange with magnesium sulfate heptahydrate and copper sulfate pentahydrate. He noted that uranyl nitrate hexahydrate exchanged about 100 times as fast as potassium alum.

Wei and Bernstein⁵ found exchange of D_2O with boehmite powder (α -alumina monohydrate), but in this case, exchange of protons and deuterons takes place rather than water molecule entities. In connection with their detailed nmr studies, O'Reilly and Tsang² have measured an approximate diffusion constant for water in potassium ferrocyanide trihydrate powder by weighing material stored in a desiccator over D_2O . They obtained a value of D of $3 \times 10^{-11} \text{ cm}^2 \text{ sec}^{-1}$ at room temperature assuming that the particles were uniform spheres and that isotropic diffusion occurred.

In UNH the uranyl group is surrounded equatorially by a near-hexagon of four oxygen atoms from two non-equivalent bidentate nitrate groups and two equivalent water oxygens.⁶ The additional four water molecules are structural water since they are not coordinated to the uranyl group but are hydrogen bonded to nitrate ions and to other water molecules. The hydrogen

bond of the structural water to the nitrate oxygen is weak.⁶

Because Kraft observed that diffusive exchange does occur in UNH and because its structure is known in detail,⁶ this hydrate was chosen for a detailed investigation. In addition to determining the time course and temperature dependence of exchange it was of interest to investigate its pressure dependence since this dependence has not been hitherto examined in the hydrates.

Experimental Section

Materials. UNH single crystals were grown using a modification of the procedure of Taylor and Mueller.⁶ A slightly acidified aqueous solution of the salt was allowed to evaporate slowly at room temperature until single crystals had grown. Crystals of a convenient size ($\sim 2 \text{ mm}$ = dimension along the c axis and about 8 mg weight) were chosen, removed, and stored in a desiccator over an H_2SO_4 (50% by weight) solution. This solution maintained a vapor pressure sufficient to prevent dehydration and yet low enough to avoid deliquescence of the hydrate. The powder was prepared by grinding crystals of UNH in a water-saturated atmosphere (to prevent dehydration) into a fine powder. The powder was stored as described and small samples (5 to 10 mg) were employed for each run.

D_2O ($\sim 98\%$, Columbia Southern Chemical Corp.) was inserted into the vacuum system and after approximately 30 exchange runs the D_2O ($\sim 10 \text{ ml}$) was replaced. $H_2^{18}O$ (11.8% ^{18}O) was obtained from Merck Sharp and Dohme, Canada.

Apparatus. A quartz helix balance (Worden Quartz

- (1) R. M. Barrer and B. E. F. Fender, *J. Phys. Chem. Solids*, **21**, 12 (1961).
- (2) D. E. O'Reilly and T. Tsang, *J. Chem. Phys.*, **47**, 4072 (1967).
- (3) S. P. Gabuda and A. G. Lundin, *Sov. Phys.*, **28**, 555 (1969).
- (4) H. Kraft, *Z. Phys.*, **110**, 303 (1938).
- (5) Y. K. Wei and R. B. Bernstein, *J. Phys. Chem.*, **63**, 738 (1959).
- (6) J. C. Taylor and M. H. Mueller, *Acta Crystallogr.*, **19**, 536 (1965).

Products, Houston, Texas) of sensitivity 1 cm/mg was used to monitor the exchange reaction. It was mounted with a water jacket ($\pm 0.1^\circ$) within a conventional high-vacuum system. All helix balances employed were calibrated prior to use. The temperatures of the sample and D_2O supply were maintained by well stirred water-ice-methanol baths to temperatures $\sim -20^\circ$, and below this by CO_2 -acetone baths. These temperatures were generally held to $\pm 0.3^\circ$.

Procedure. In order to avoid dehydration of the UNH samples the system was evacuated while simultaneously cooling the sample to -78° . After approximately 10 min, a pressure of 10^{-6} Torr was generally obtained. Following this procedure the sample was adjusted to the desired temperature and D_2O was admitted to the reaction vessel to initiate the exchange run. Dehydration did not occur prior to admitting the D_2O . This was shown by noting that in several blank runs rehydration did not occur following the preliminary procedure. It has been shown that rehydration occurs rapidly under the blank conditions employed.⁷

The weight change, ΔM_∞ , of the sample following complete diffusive exchange with D_2O is

$$\Delta M_\infty = (0.1117)W(\% H_2O/100)$$

where W is the weight of the sample and $\% H_2O$ refers to the weight per cent of exchangeable water in the hydrate. For a 5-mg sample of UNH the helix movement following dehydration is 0.0802 cm. Since the helix can be read to ± 0.001 cm, the error in the final reading at complete exchange is $\pm 1.3\%$ and correspondingly greater percentage errors at smaller percentage exchange. For the experiments with $H_2^{18}O$ (11.8% ^{18}O) the total movement of the helix is 0.0094 cm (5 mg sample) so that the error in the final reading is $\pm 10.6\%$.

Results

Figure 1 shows a typical diffusive exchange run on a single crystal of habit shown in Figure 2. The temperature of the run is 25° and the vapor pressure of water employed relative to that of liquid water is $p_r = 0.18$. At this and at lower temperatures, only four of the six water molecules undergo diffusive exchange—the structural water molecules. The exchange of these structural water molecules goes to completion. At 35° only the four structural water molecules are lost during dehydration *in vacuo* but in contrast to diffusive exchange, at lower temperatures, *e.g.*, -30° only three water molecules are lost.⁷ The diffusion times for individual single crystals (~ 8 mg) are long; for example, 24 hr is required at 35° for M_t/M_∞ to reach 50%, where M_t is the weight of the sample at time t and M_∞ the weight at $t = \infty$.

The fraction of exchange, M_t/M_∞ , can be seen to follow a $t^{1/2}$ relationship (Figure 1) which is a character-

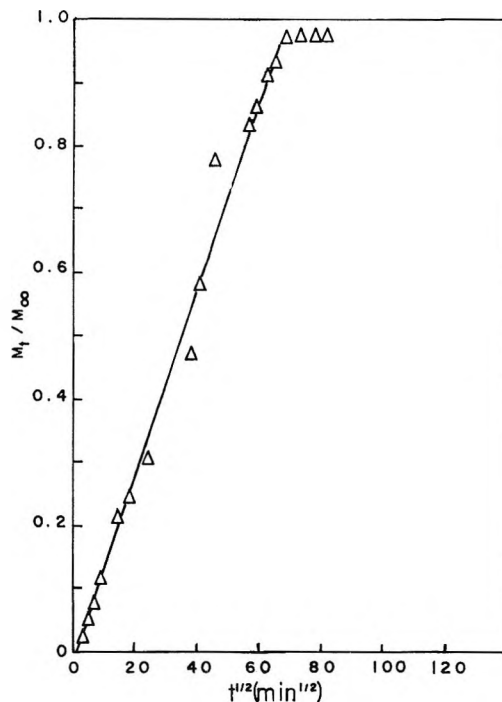


Figure 1. Representative diffusive exchange run on a single crystal of UNH (4.6 mg, $p_r = 0.18$, 25°).

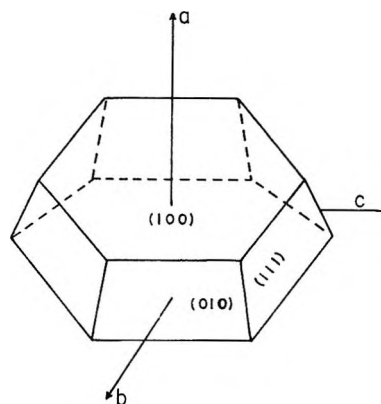


Figure 2. Typical habit of single crystals employed for diffusive exchange runs.

istic of many diffusion-controlled solid reactions.¹ The relationships were found to be linear to about 50%.

A single crystal was coated with water-impermeable plastic on the $\{100\}$ faces. If diffusion is isotropic, the diffusion problem reduces from three to two dimensions. The appropriate equation for two-dimensional diffusion in a parallelepiped of sides a_1 and a_2 ¹ is

$$M_t/M_\infty = 1 - \sum_{m=0}^{\infty} \sum_{n=0}^{\infty} \frac{64}{\pi^4} \frac{1}{(2m+1)^2(2n+1)^2} \times \exp\left\{-\frac{D\pi^2}{4} \left[\frac{(2m+1)^2}{a_1^2} + \frac{(2n+1)^2}{a_2^2} \right] t\right\} \quad (1)$$

(7) M. L. Franklin and T. B. Flanagan, to be submitted for publication.

which, at small times, reduces to

$$M_t/M_\infty = 2\left(\frac{Dt}{\pi}\right)^{1/2}\left(\frac{1}{a_1} + \frac{1}{a_2}\right) \quad (2)$$

The habit of this coated crystal was approximated by a parallelepiped of active sides a_1 and a_2 where these are the dimensions of the crystal along the b and c axes, respectively (Figure 2). The calculated value of D is $8 \times 10^{-10} \text{ cm}^2 \text{ sec}^{-1}$ (0° , $p_r = 0.4$). Other single crystals, which were uncoated, gave similar diffusion constants with the assumption that diffusion does not occur in the a direction. The water molecules lie in sheets parallel to the (100) planes and so diffusion might be expected to be anisotropic; *i.e.*, diffusion in directions perpendicular to the (100) planes is insignificant compared to diffusion parallel to these planes. The direct experimental evidence for complete anisotropy which is based on the measured values of D for coated and uncoated crystals is tenuous because of some irreproducibility in these runs using individual single crystals. The long linear region in the M_t/M_∞ plots, however, supports the assumption of anisotropic diffusion.¹

A series of consecutive diffusive exchange runs were made on the same single crystal of UNH. Two points of interest emerged. The rates of these consecutive runs were comparable and an isotope effect was noted. The first proves that diffusive exchange does not disrupt the diffusive path lengths of the single crystal. The isotope effect was in the direction such that H_2O diffuses into a crystal containing D_2O faster than the reverse process. A comparable isotope effect has been observed and examined extensively in another hydrate system.⁷ It will not be discussed here save to mention that an isotope effect supports bulk diffusion as the slow step because significant isotope effects would not be expected if exchange of entire water molecules occurred as the slow step at the surface.

As would be expected, diffusive exchange occurs much faster for powder than for single crystals as shown in Figure 3. The powder consists of roughly cubic particles of average size about 0.005 cm. Using eq 2 this gives $D = 5 \times 10^{-10} \text{ cm}^2 \text{ sec}^{-1}$ ($p_r = 0.35$, 0°) in good agreement with the value found for the single crystals. Since the diffusional behavior of powder is similar to that observed for the single crystals except for the convenience of shorter diffusion times exhibited by the former, the powder was extensively employed for the determination of the diffusion parameters.

Pressure Dependence. The pressure dependence of the rate of diffusive exchange was examined at -29° for powder and at 0° for single crystals. These relatively low temperatures were used because the rate of exchange is slow at these temperatures and consequently self-dilution is not a factor. Self-dilution describes the error introduced by the dilution of the D_2O with

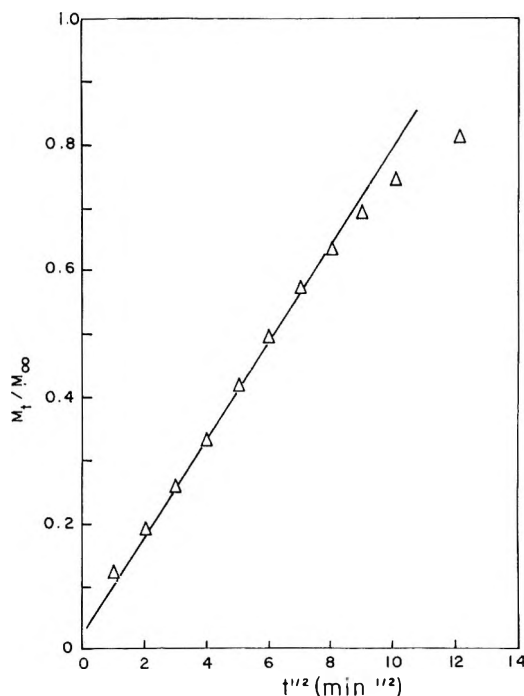


Figure 3. Representative diffusive exchange run with UNH powder ($p_r = 0.35$, 0°).

H_2O in the gas phase (Appendix). Figure 4 shows that the rate of diffusive exchange decreases with pressure for both the single crystal and powder. The pressure range is quite limited because above $p_r = 0.7$ and below $p_r = 0.1$ the samples deliquesced and dehydrated, respectively.

Temperature Dependence. The temperature dependence of diffusive exchange was examined at a constant value of p_r . Other possibilities would have been to hold p or p/p_s constant, where p_s is the equilibrium vapor pressure of the hydrate. Kraft⁴ chose to hold p/p_s constant. Investigators employing nmr techniques coated the crystals with plastic in order to prevent dehydration;² under these conditions the water vacancy \leftrightarrow water vapor equilibrium is presumably not established. Surface exchange—the precursor to bulk exchange—must proceed *via* adsorbed water; it is therefore reasonable to maintain p_r constant. Since UNH would dehydrate and deliquesce at the extremes of the temperature range employed, it would not have been feasible to maintain p constant. A value of $p_r = 0.4$ was chosen for convenience because this is halfway between the two limiting values of p_r which can be employed. The Arrhenius plot for the diffusive exchange is shown in Figure 5 as $\log k$ vs. $1/T$ where k is the slope of M_t/M_∞ against $t^{1/2}$ plots. The energy of activation for diffusion, E_d , is twice that determined from the slope of the line in Figure 5 and from this value and the diffusion constant for the single crystals D can be expressed as

$$D = 4 \times 10^{-3} \exp(-7600/RT) \quad (3)$$

Diffusive Exchange with H_2^{18}O . In order to deter-

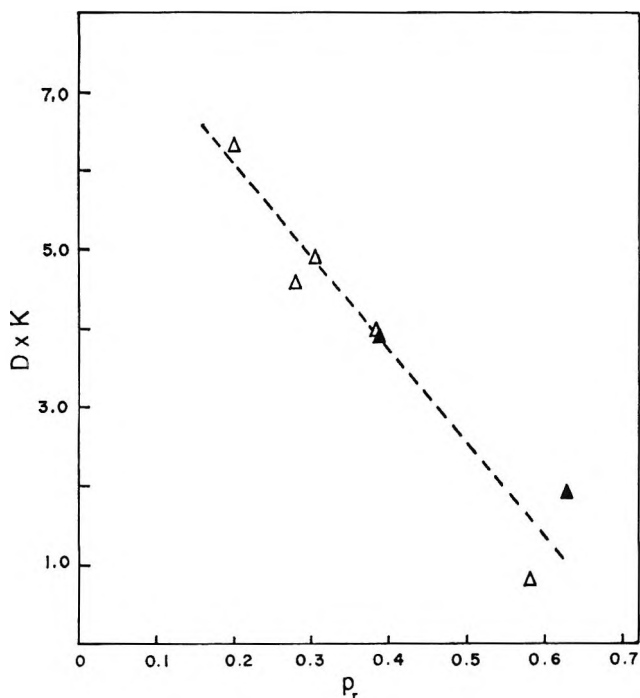


Figure 4. Pressure dependence of diffusive exchange plotted as DK against p_r where D is the diffusion coefficient and K is a constant: Δ , UNH powder, -29° ; \blacktriangle , UNH single crystals (0°) normalized to the powder data at $p_r = 0.4$.

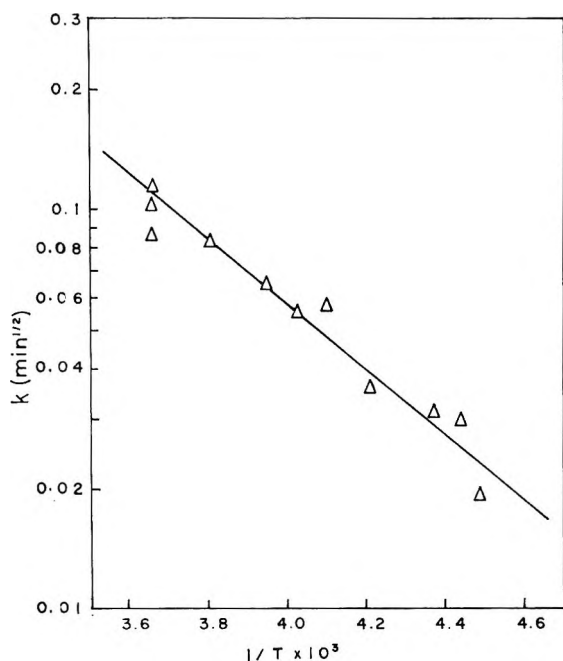


Figure 5. Arrhenius plot for diffusive exchange for UNH powder plotted as $\log k$ against $1/T$, where k is the slope of M_t/M_∞ against $t^{1/2}$.

mine whether the entire water molecule diffuses, in contrast to only the hydrogen isotopes, a run was performed with $H_2^{18}O$. The rates of diffusive exchange are comparable for the two water isotopes (Figure 6) which proves that the entire water molecule diffuses.

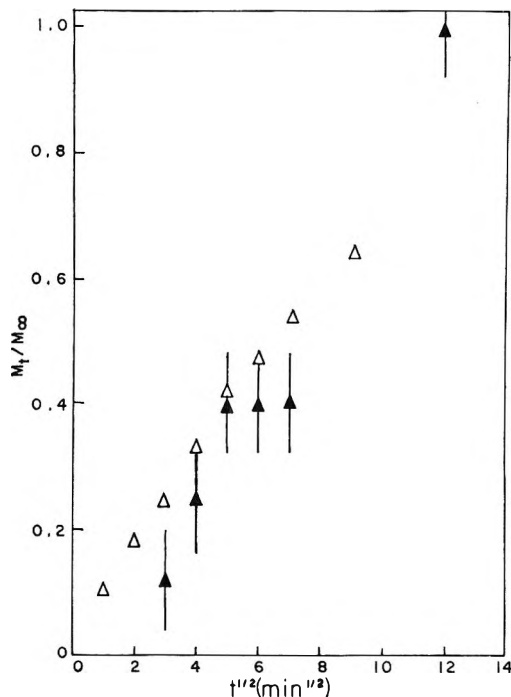


Figure 6. Comparison of diffusive exchange with $H_2^{18}O$ and D_2O with UNH under powder ($p_r = 0.35$, 0°): \blacktriangle , $H_2^{18}O$; Δ , D_2O .

Discussion

When solid-state diffusion is carried out using a gas-solid technique like that employed here, it must be established that the rate-determining process is solid-state diffusion rather than a surface step. Intuitively solid-state diffusion would be expected to be the slow step in a system such as this since diffusion is relatively slow in comparison to, for example, gas-metal systems (where D for hydrogen in face-centered cubic metals is typically $\sim 10^{-7} \text{ cm}^2 \text{ sec}^{-1}$ (25° , H in $\alpha\text{-Pd/H}^8$) and consequently slow surface steps can often be an experimental problem. If a surface step were slow, the interior of the hydrate would be expected to be uniform with respect to its isotopic distribution. The rate of exchange would then be first order with respect to time. This dependence is not observed (Figure 1) and, therefore, diffusion within the solid is rate controlling.

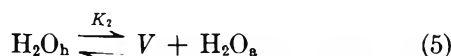
It is not unexpected that only the four structural water molecules, *i.e.*, those not directly coordinated to the uranyl ions, undergo diffusive exchange. These are the only waters which are lost upon dehydration *in vacuo* above -20° and below $\sim 140^\circ$.⁷ Equilibrium is therefore not established between the two types of water ($\leq 35^\circ$). More surprising, perhaps, is the fact that there is no proton-deuteron exchange between the structural and coordinated water within the solid. Below about -20° only three water molecules are lost upon dehydration⁷ but all four undergo exchange; this

(8) J. W. Simons and T. B. Flanagan, *J. Phys. Chem.*, **69**, 3773 (1965).

suggests that the four structural water molecules are in equilibrium but the fourth cannot leave the lattice *in vacuo* below -20° .

It is generally believed that vacancies are the defects responsible for diffusion in molecular solids.⁹ Since the bonding of the water molecules in crystalline hydrates resembles that in molecular solids, it seems likely that water vacancies are the defect by which diffusion occurs. A possible role of vacancies in the kinetics of dehydration of crystalline hydrates has been noted by Garner,¹⁰ who suggested that prenucleation corresponds to the formation and aggregation of vacancies.

The diffusion constant found in the present work must reflect both the concentration and mobility of water vacancies. If an equilibrium concentration of vacancies exists within the hydrate at each temperature and pressure, then



where H_2O_a , H_2O_b , and H_2O_g represent the total water, $\text{H}_2\text{O} + \text{D}_2\text{O}$, in the following regions: adsorbed on the surface, in UNH as exchangeable water, and in the gas phase, respectively. The concentration of vacancies is therefore

$$V = K_1 K_2 \text{H}_2\text{O}_b / p_{\text{D}_2\text{O}} \quad (6)$$

Experimentally p_r has been maintained constant for the temperature dependence studies and therefore $p_{\text{D}_2\text{O}} = p_r p_0$ where p_0 is the vapor pressure of pure D_2O . Since the temperature dependence of p_0 and K_1 should be comparable, eq 6 reduces to

$$V = B \exp(-\Delta H_f / RT) \quad (7)$$

where B is a constant and ΔH_f is the enthalpy of formation of water vacancies according to eq 5.

If an equilibrium vacancy concentration is attained at each temperature, the observed value of E_d should be $\Delta H_f + E_m$ where E_m is the activation energy for mobility of a vacancy. Jost⁹ has pointed out that the energy to form a vacancy in a molecular solid can be taken as the lattice energy and this can be approximated by the latent heat of sublimation. In the case of crystalline hydrates the heat of dehydration is analogous to the latent heat of sublimation of molecular crystals but it is not as reliable an estimate of ΔH_f as ΔH_s is for molecular crystals because when the water is returned to the surface following formation of a vacancy it does not form a new layer of crystal lattice but rather forms an adsorbed layer.

In metals, the energy of vacancy migration is generally assumed to be of the same order as, but less than, that for vacancy formation.¹¹ Sherwood¹² has assumed that the same situation holds for molecular solids. Garner¹⁰ has also suggested that the activation

energy for water vacancy migration should be of the same order of magnitude as the heat of dehydration. Sherwood¹³ has collected the meager data available for diffusion in molecular crystals and he noted that generally E_d is of the order of twice the latent heat of sublimation. An important exception is ice. Delibaltas, *et al.*,¹⁴ have found that E_d is 15.7 kcal/mol and Gränicher¹⁵ has again equated ΔH_f to the latent heat of sublimation, *i.e.*, 12.2 kcal/mol. This leaves only 3.5 kcal/mol for the migration energy of activation. Delibaltas, *et al.*,¹⁴ have pointed out that this is surprisingly small since 3 hydrogen bonds must be broken for a water molecule to jump into an adjacent vacancy.

If E_d is about twice ΔH_f then E_d should be 25.4 kcal/mol, because the enthalpy for dehydration of UNH to the dihydrate is 12.7 kcal/mol H_2O .¹⁵ For potassium alum the corresponding value for E_d would be 26.2 kcal/mol since the enthalpy of dehydration per mole of water is 13.1 kcal.¹⁷ O'Reilly and Tsang² report two values for E_d for potassium ferrocyanide trihydrate, *i.e.*, 5.2 (proton relaxation) and 10.4 kcal/mol (deuteron line width); no explanation is offered for the discrepancy but the average of these two values is again too small if E_d is to be equal to twice the enthalpy of dehydration.

The disagreement can be resolved if it is assumed that an equilibrium vacancy concentration does not exist at each temperature, then $E_d = E_m$, and, if E_m is considerably less than the enthalpy of dehydration, agreement with the observed value of E_d could be obtained. Under these conditions diffusive exchange would occur only *via* the "grown-in" vacancies. This hypothesis is, however, untenable because the available vacancies would soon be destroyed and diffusive exchange would not go to completion. Vacancies must be both created and destroyed at the surface for a vacancy mechanism to control diffusive exchange.

An equilibrium concentration of vacancies which obtains only near the surface is a possible alternative to the assumption of a uniform vacancy equilibrium. Diffusive exchange would then be proportional to the concentration and mobility of vacancies in the vicinity of the surface. In this case a steady-state treatment can be applied to the vacancy concentration at and

- (9) W. Jost, "Diffusion," Academic Press, New York, N. Y., 1952.
 (10) G. P. Acock, W. E. Garner, J. Milstead, and H. J. Willavoys, *Proc. Roy. Soc.*, **189**, 508 (1946).
 (11) P. Shewmon, "Diffusion in Solids," McGraw-Hill, New York, N. Y., 1963.
 (12) J. N. Sherwood and D. J. White, *Phil. Mag.*, **15**, 745 (1967).
 (13) J. N. Sherwood, *Proc. Brit. Ceram. Soc.*, **9**, 233 (1967).
 (14) P. Delibaltas, O. Dengal, D. Helmreich, N. Riehl, and H. Simon, *Phys. Kondens. Mater.*, **5**, 166 (1966).
 (15) H. Gränicher, *Z. Kristallogr. Kristallgeometrie, Kristallphys., Kristallchem.*, **110**, 450 (1958).
 (16) W. H. Smith, *J. Inorg. Nucl. Chem.*, **30**, 1761 (1968).
 (17) D. A. Young, "Decomposition of Solids," Pergamon Press, Oxford, 1966.

adjacent to the surface, and this again leads to the result that $E_d = \Delta H_f + E_m$. In fact, this alternative is not likely in view of the experimental result that the rate of diffusive exchange is unchanged in a single crystal which has previously undergone exchange.

The flux of H_2O within the crystal is equal and opposite to the flux of D_2O ; therefore the rate of creation is equal to the rate of destruction of vacancies. The loss of H_2O from the surface hydrate layer does not occur simultaneously with the addition of D_2O to the resulting vacancy because otherwise vacancies would not be formed internally and they are necessary for diffusive exchange. The creation and destruction of vacancies at the surface are therefore separate events. The fact that their rates become equal almost immediately, *i.e.*, there is no observable dehydration or rehydration of the crystal, indicates that vacancy equilibrium is attained. This is consistent with the observation that the rate of diffusive exchange decreases with increase of pressure (Figure 4). The observed pressure dependence indicates that the equilibrium concentration of vacancies is governed by eq 6. Since the rate does not change during these runs until $M_t/M_\infty \leq 0.6$ the vacancy concentration rapidly adjusts to the ambient pressure. This behavior is reasonable if the relative time scales of vacancy mobility and diffusive exchange are considered. The equilibrium fraction of vacancies is of the order of $N_v/N = \exp(-\Delta G_f/RT) \cong \exp(-\Delta H_f/RT) = 7 \times 10^{-6}$ (0°) if ΔH_f is taken as 7100 cal/mol (see below). Diffusion of a water molecule into a given lattice site requires that a vacancy be at the latter site (probability = N_v/N), whereas the diffusion of a vacancy to a given site requires that the latter site be occupied (probability $\cong 1$). Therefore the time scale for vacancy diffusion is $\sim 1.4 \times 10^5$ times faster than that for diffusive exchange (0°). This supports the assumption that water vacancy diffusion is extremely rapid compared to the observed rates of diffusive exchange.

The basic problem therefore remains—how are the observed values of E_d to be reconciled with estimates of $\Delta H_f + E_m$? It is of interest to reexamine the estimated values of ΔH_f and E_m specifically for the case of crystalline hydrates. For UNH, four hydrogen bonds (one of these is weak, the H bond to the nitrate oxygen) must be broken to form a vacancy. The strength of these H bonds can be roughly estimated from the heat of dehydration of UNH to the dihydrate.¹⁶ Three H bonds must be broken for this process since only two of the bonds involve bonds to removable water molecules. This requires 12.7 kcal and therefore an average of 4.2 kcal/bond is found. (This neglects any modifications in the heat of dehydration upon cooling to $0^\circ K$ and differences between ΔH and ΔE but these corrections are generally small.¹⁸) In order to form a vacancy plus a gaseous water molecule 16.8 kcal/mol is required, and when this water is returned to an adsorbed layer,

9.7 kcal/mol is recovered, the latent heat of vaporization of liquid water. The formation of a vacancy therefore requires 7.1 kcal/mol. It is not unreasonable to expect the adsorbed water to be liquid-like.¹⁹ The maximum energy for mobility of a vacancy can be estimated from the energy required to break three hydrogen bonds (one weak), *i.e.*, 12.5 kcal/mol. It is difficult to estimate how much smaller this may be when the relaxation of water molecules around the vacancy is considered. Because of their asymmetry, the uranyl ions and the coordinated nitrate ions are not expected to relax.¹⁷ In any case, E_d still remains significantly larger than $\Delta H_f + E_m$ for UNH and similar considerations would lead to the same impasse for potassium alum⁴ and potassium ferrocyanide trihydrate.²

The value of D_0 observed here, $3 \times 10^{-3} \text{ cm}^2 \text{ sec}^{-1}$, is similar to that which has been found for ice.¹⁴ It can be compared to a theoretical value calculated by¹¹

$$\gamma a^2 \nu \exp[(\Delta S_m + \Delta S_f)/R] \quad (8)$$

where γ is a geometric factor taken as 1, a is the jump distance which is 2.7 Å in UNH,⁶ ΔS_m is assumed to be 1,¹¹ ΔS_f is taken as the entropy of dehydration of UNH to liquid water,²⁰ and ν for the low-energy translational mode of water in UNH has been determined by Rush and coworkers²¹ from neutron scattering to be $5 \times 10^{12} \text{ sec}^{-1}$. D_0 is then $180 \times 10^{-3} \text{ cm}^2 \text{ sec}^{-1}$. In view of the uncertainty in the value of ΔS_f this agreement is not bad and indicates that a vacancy mechanism may obtain with a surprisingly low value for E_d .

The unresolved problem of the anomalously small value of E_d observed here for UNH and elsewhere for ice¹⁴ deserves further investigation.

Acknowledgments. The authors are grateful for financial support by NSF Grant GP-9560. The authors thank Dr. M. H. Mueller for assistance in identification of the faces of the UNH single crystals employed in this research.

Appendix

The most serious source of potential error can be termed "self-dilution" and arises from the dilution of the surrounding water vapor isotope with that from the sample in the nonstirred system which has been employed. An exact solution of the diffusion problem is impossible because of the complex geometries involved. In all cases, however, the sample dimensions were small compared to the reaction vessel and it can be assumed that the sample is a continuous point source in

(18) D. Eisenberg and W. Kauzmann, "The Structure and Properties of Water," Oxford University Press, New York, N. Y., 1969.

(19) H. A. Resing, *Advan. Mol. Relaxation Processes*, 1, 109 (1968).

(20) W. M. Latimer, "Oxidation Potentials," 2nd ed, Prentice-Hall, Englewood Cliffs, N. J., 1952.

(21) J. J. Rush, J. R. Ferraro, and A. Walker, *Inorg. Chem.*, 6, 546 (1967).

an infinite medium. Crank²² gives the solution for this problem as

$$C(r,t) = \frac{1}{8(\pi D)^{3/2}} \int_0^t \varphi(t') \times \exp\left[\frac{-r^2}{4D(t-t')}\right] \frac{dt'}{(t-t')^{3/2}} \quad (1A)$$

where $C(r,t)$ is the concentration of diffusing substance at any distance, r , from the source at time, t . The diffusing substance is generated at the rate $\varphi(t)$, where

$$\varphi(t) = K \frac{d(M_t/M_\infty)}{dt} = \frac{KS t^{-1/2}}{2}$$

K converts the fraction reaction per second to molecules of water per second and S is the observed slope (in seconds^{-1/2}). Substituting this into eq 1A gives

$$C(r,t) = \frac{KS}{16(D\pi)^{3/2}} \int_0^t \frac{\exp\left[\frac{-r^2}{4D(t-t')}\right] dt'}{t'^{1/2}(t-t')^{3/2}} \quad (2A)$$

If $y = 1/(t-t')$ and $b = r^2/4D$, eq 2A reduces to

$$C(r,t) = \frac{KS}{16(D\pi)^{3/2}} \int_{1/t}^\infty \frac{\exp[-by]}{(t-1/y)^{1/2} y^{1/2}} dy \quad (3A)$$

which can be further reduced to

$$C(r,t) = \frac{KS}{16(D\pi)^{3/2}} \int_{1/t}^\infty \frac{\exp[-by]}{(ty-1)^{1/2}} dy$$

if x is substituted for ty , eq 3 simplifies to

$$C(r,t) = \frac{KS}{16(D\pi)^{3/2}} \int_1^\infty \frac{\exp[-xb/t]}{(x-1)^{1/2} t} dx = \frac{KS}{16(D\pi)^{3/2} t} \int_1^\infty \frac{\exp(-xb/t)}{(x-1)^{1/2}} dx \quad (4A)$$

The integral 4A can be evaluated as

$$C(r,t) = \frac{KS}{8D\pi t^{1/2}} \exp\left[\frac{-r^2}{4Dt}\right] \quad (5A)$$

A maximum value for this effect can be estimated from the data on powder at 0°; *i.e.*, this is the highest temperature used in the Arrhenius plot to evaluate E_d (Figure 5). For a typical sample $K = 3.6 \times 10^{16}$ molecules H₂O and $S = 10^{-3}$ sec^{-1/2} at 2.0 mm of D₂O pressure. The value of D for H₂O(g) is estimated as 102 cm² sec⁻¹ from $D = 1/2\lambda\bar{c}$ and $\lambda = kT/(\nu_2\pi\sigma^2p) = 4.6 \times 10^{-3}$ cm. Inserting these values into eq 5A taking $r = \lambda$ and $t = 60$ sec, $c(\lambda, 60) = 3.9 \times 10^{14}$ molecules H₂O cm⁻³ compared with 7×10^{16} molecules of H₂O + D₂O in the gas phase under these conditions of temperature and pressure. A value of r has been taken equal to λ because molecules one mean free path away from the surface will be those which will collide with the surface to undergo exchange. Self-dilution is concluded to be insignificant under these conditions because the concentration of H₂O in the gas phase is only 0.5% of the total. At lower temperatures and longer times the effect will be even smaller.

Experimental tests for the importance of self-dilution have been made by moving the position of the D₂O reservoir closer to the sample, *i.e.*, the diffusion path of the H₂O from sample to bath is thereby reduced and the diffusion should therefore be faster as the concentration gradient is increased. There was no effect upon the measured exchange rate noted for a fivefold change in the overall bath to sample distance.

(22) J. Crank, "Mathematics of Diffusion," Clarendon Press, Oxford, 1956.

Transient Phenomena Caused by Temperature Change on Capacitance of Rutile Film¹

by Masaki Yamazaki* and Hiroshi Nozaki

*Institute of Industrial Science, University of Tokyo, Roppongi 7-Chome, Minatoku, Tokyo, Japan
(Received August 11, 1970)*

Publication costs borne completely by The Journal of Physical Chemistry

An electrolytic rutile film containing barium was formed on the surface of a titanium electrode. By evaporating silver on the rutile film, a capacitor-like Ti-TiO₂-Ag sandwich was fabricated. It has been found that the capacitance of the rutile film sandwich shows transient phenomena when the temperature is rapidly increased or decreased. Thus, the measurements of the capacitance were made not only as a function of temperature but also as a function of time. The capacitance was measured under the condition that the temperature was rapidly increased with a given rate and then was fixed to be constant at a given point. The capacitance varied up to a certain nonequilibrium value when the temperature was being increased, then the capacitance decayed exponentially to an equilibrium value after the temperature was fixed to be constant. The rate of decay depends on the fixed temperature, so that the relaxation times (τ) of the transients were examined as a function of the various fixed temperatures between 25 and 100°; the relaxation times at 50, 75, and 100° were 54, 44, and 36 min, respectively. Arrhenius plots of $\log 1/\tau$ vs. $1/T$ indicate that the energy of activation for the transients is about 1.7 kcal/mol.

1. Introduction

Thin insulating films of controlled thickness can be formed on a number of metals including aluminum, tantalum, titanium, zirconium, niobium, hafnium, and tungsten by anodization of the metals in a suitable electrolyte, and anodic oxide films formed in this way have been widely used in electrolytic capacitors.^{2,3} On the other hand, we formed a titanium oxide film by applying an alternating current to a titanium electrode in an aqueous solution of barium hydroxide.⁴ The oxide film was found to be rutile which contains barium.

Many studies have been made of electrical properties of metal-insulator-metal sandwiches which were fabricated with oxide films, particularly studies of electrical conductivity, since under certain conditions a large permanent increase in the conductivity of the thin film metal-insulator-metal sandwiches can be induced by the application of an electric field.⁵⁻⁷ In those cases, measurements have always been made under the condition that systems (samples) were completely in thermal equilibrium with respect to an external system (thermostat). At a single frequency, the capacitance (dielectric constant) was only a function of temperature. However, when the capacitance of the rutile film sandwich is examined under the condition that the temperature is rapidly varied, transient phenomena are found. To the authors' knowledge, these transients of the capacitance caused by the change of temperature have not yet been reported. In this work, we report the capacitance of the rutile film as a function of temperature and time.

The present paper is concerned primarily with experi-

mental results, and further work is necessary for the theoretical explanation of the phenomena. We will first show experimental procedures and experimental conditions, then go on to describe the observed transient phenomena.

2. Experimental Section

2.1. Sample Preparation. The electrode, 1 × 20 × 40 mm, was prepared from Kobe Seiko Co. KS-50 titanium (H₂, <0.01%; O₂, <0.20%; N₂, <0.05%; Fe, <0.20%). The surface of the electrode was first treated in 16 wt % H₂SO₄ solution at 25°, using an alternating current (50 Hz) at 50 mA/cm² for 2 hr. Then, the oxide film was formed on the surface of the electrode; the electrode was electrolyzed by applying the alternating current (50 Hz) in a saturated solution of barium hydroxide first for 1 hr at 40 mA/cm², and next for 2 hr at 70 mA/cm². The oxide film obtained was washed in water, and the heat treatment was done in air at 150° for 8 hr in order to increase stability of the measurements of the capacitance. Capacitor-like Ti-

(1) Presented in part at the Annual Meeting of the Japan Society of Applied Physics, Tokyo, March 1970.

(2) L. Young, "Anodic Oxide Films," Academic Press, London and New York, 1961.

(3) D. A. Vermilyea, *Advan. Electrochem. Electrochem. Eng.*, **3**, 211 (1963).

(4) M. Yamazaki and H. Nozaki, *J. Electrochem. Soc.*, **118**, 400 (1971).

(5) T. W. Hickmott, *J. Appl. Phys.*, **33**, 2669 (1962); **35**, 2118 (1964).

(6) J. G. Simmons and R. R. Verderber, *Proc. Roy. Soc., Ser. A*, **301**, 77 (1967).

(7) J. G. Simmons, *Phys. Rev.*, **155**, 657 (1967).

TiO₂-Ag samples were fabricated by the vacuum evaporation of silver onto the oxide film through a mask with slits of 5 × 5 mm². Three samples (1, 2, and 3) were made in this way.

To ascertain the composition, the oxide film was examined by electron diffraction and by X-ray microanalysis. The surface of the oxide film was observed with an electron microscope.

2.2. Apparatus. In order to eliminate the nonreproducible time-dependent change of the capacitance,⁸ the capacitance of the samples was measured at 1000 Hz with an impedance bridge, Yokokawa Electric Model 4255 A. The samples were put in a thermostat which was devised to control a rapid change of temperature by using a silicone fluid as the bath liquid. The control of the temperature of the thermostat was carried out with a bimetal thermoregulator, and the temperature was measured with a thermocouple, with an accuracy of ±0.1°.

2.3. Experimental Conditions. The temperature of the samples was varied over the range from 25 to 100°. Since the capacitance depends on temperature and time, it is necessary to give experimental conditions. These experimental conditions are shown in Figure 3A and Figure 4A, which are expressed by plots of temperature vs. time.

3. Results and Discussion

3.1. Electrolytic Rutile Film. Electron diffraction patterns, shown in Figure 1, indicate that the oxide film is composed of TiO₂ (rutile), though the patterns are somewhat obscure. X-Ray microanalysis showed barium to be present in the rutile film.⁴ It is not clear, at present, whether the barium affects the transients of the capacitance. According to the electron microscope, the rutile film was polycrystalline. The thickness of the rutile film was 1.5 ~ 2.5 μ, which was estimated from the capacitance at the equilibrium.

3.2. Transient Phenomena of the Capacitance. The measurements of the capacitance of the samples were made under the condition that the temperature was rapidly increased from 20 to 100° and then slowly decreased from 100 to 20°. Then, anomalous phenomena as shown in Figure 2 were observed. If these phenomena are based on the process that the samples are not in thermal equilibrium with respect to the thermostat, the usual anticlockwise curves should be obtained. Thus, it is obvious from Figure 2 that the phenomena are not brought about by a time lag of attaining thermal equilibrium between the samples and thermostat. In general, atmospheres and counterelectrodes have an effect on an electrical conductivity of thin film metal-insulator-metal sandwiches.^{5,6} However, the observed phenomena are independent of the particular atmosphere chosen, and these phenomena were also observed when gold, copper, aluminum, and indium were used as counterelectrodes.

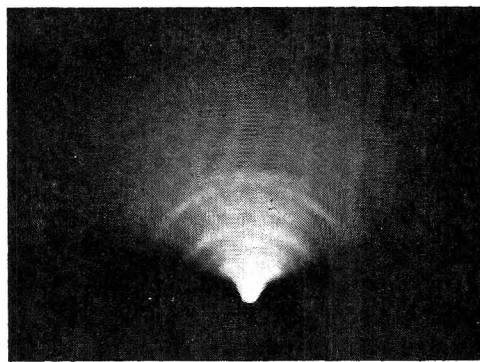


Figure 1. Reflection electron diffraction patterns of the electrolytic oxide film, which indicate that the oxide film is rutile.

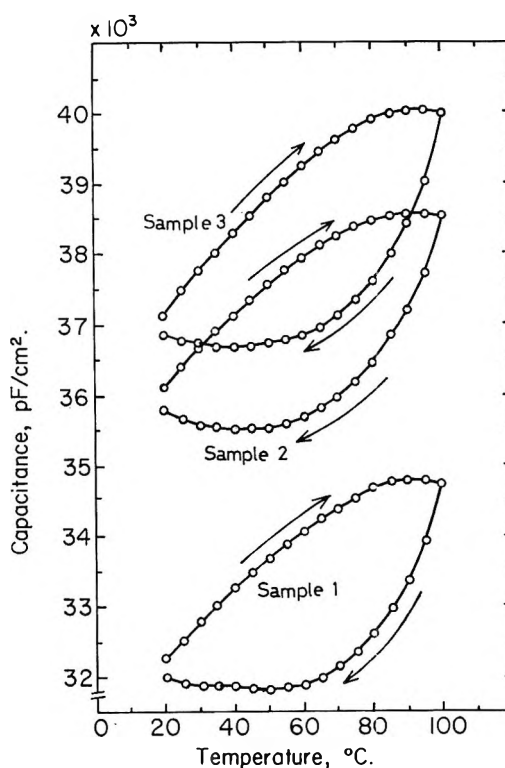


Figure 2. Anomalous curves of the capacitance vs. temperature obtained under the condition that the temperature is rapidly increased from 20 to 100° and then slowly decreased from 100 to 20°.

To clarify the phenomena described above, the capacitance of sample 1 was investigated under the controlled temperature vs. time conditions shown in Figure 3A. The results are shown in Figure 3B, where the values of the capacitance are plotted against time corresponding to the conditions Figure 3A. Comparison of the curves a and a' with the curves d and d' in Figure 3 indicates that the capacitance varies rapidly when the temperature is rapidly increased and then it decays to the equilibrium value after the temperature is fixed at

(8) Y. Kumagai, S. Nishimatsu, and Y. Shibata, *Oyo Butsuri*, **33**, 649 (1964).

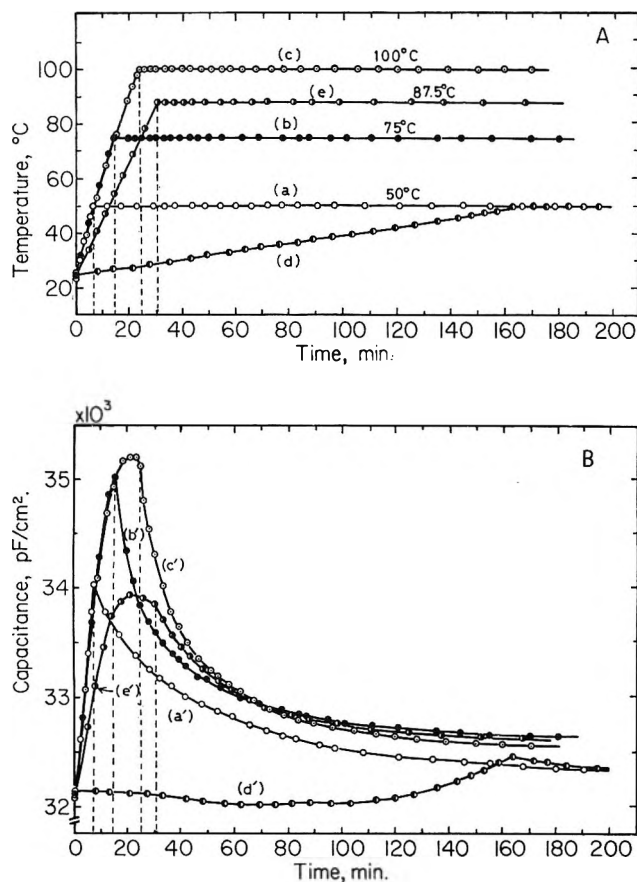


Figure 3. A. Experimental conditions for sample 1, plots of temperature vs. time. B. Plots of capacitance vs. time where (a'), (b'), (c'), (d'), and (e') correspond to (a), (b), (c), (d), and (e), respectively.

50°, but that the capacitance merely gives values corresponding to equilibrium at each temperature when the temperature is slowly increased to 50°. Furthermore, after sufficiently long time in a and d, the capacitance gives the same values at 50° in the both cases. The curves c, c', e, and e' show that the curves c' and e' reach maximum values and then begin to decrease before the maximum temperatures (100° and 87.5°) are attained. The increase and decrease of the capacitance are determined by competition between the increase of the capacitance caused by temperature increase and the decrease of the capacitance caused by decay process to equilibrium. When the rate of temperature increase is rapid enough in comparison with the decay rate of the transients, the capacitance increases, and *vice versa*. The rate of decay becomes larger with increasing temperature as will be seen in Figure 6 and Table I. Thus, the capacitance occasionally decreases as shown in (c') and (e') despite the fact that the temperature is being increased. If one wishes to get a larger value of the capacitance than the maximum value of the capacitance in (c') or (e'), one should increase the temperature in (c) or (e) more rapidly.

Similar results obtained under the various conditions for sample 2 are shown in Figure 4. The results in

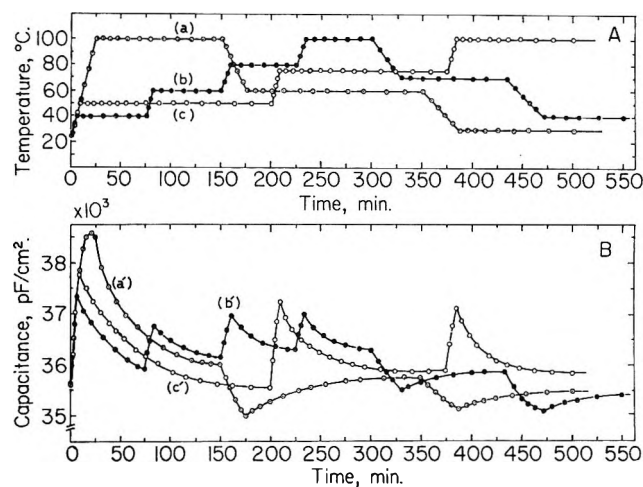


Figure 4. A. Experimental conditions for sample 2, plots of capacitance vs. time. B. Plots of capacitance vs. time where (a'), (b'), and (c') correspond to (a), (b), and (c), respectively.

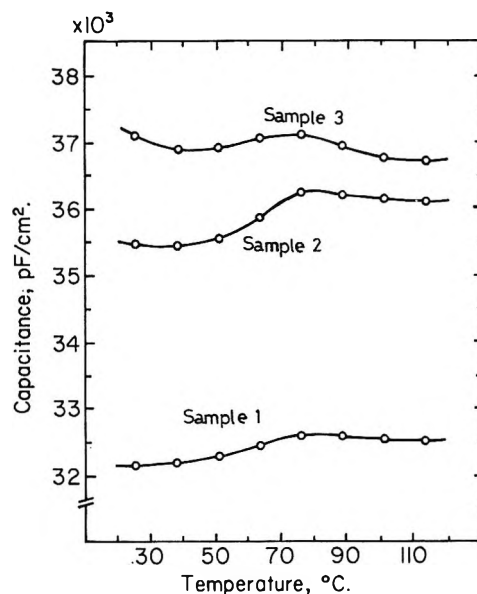


Figure 5. Temperature dependence of the capacitance of rutile film at 1 kHz.

Figure 4 indicate that the transients can occur over the whole range of temperature from 25° to 100°. Moreover, when the temperature is decreased and then fixed at a given point, we observe transient phenomena which are converse in comparison with those in the case of temperature increase. This fact will provide important information to explain the transient phenomena.

The temperature dependence of the capacitance is shown in Figure 5, corresponding to equilibrium which is attained after a sufficiently long time. These results are approximately in agreement with measurements made by other workers.⁹

It is premature to give a conclusive explanation for the above-mentioned phenomena at present. In semi-

(9) L. J. Berberich and M. E. Bell, *J. Appl. Phys.*, 11, 681 (1940).

conductors and insulators, it is well known that it is possible to obtain departure from the thermal equilibrium concentrations of electrons and holes in several ways: by injecting carriers into the sample through a metal contact or by charged particle bombardment or by the creation of electron-hole pairs by light. In those cases, recombination of the excess electrons and holes take place,¹⁰ showing transient conductivity. However, transients which are concerned with the capacitance (dielectric constant) have not been discussed. It is considered that the transients of the capacitance are based on the process of temperature-induced disorder in the film. A disordered system may be caused by a sudden change of temperature. Once disordered, the system tends to return to equilibrium at the fixed temperature. Then the capacitance will show the transients, since the disordered system in oxides frequently has a higher dielectric constant than the ordered system.¹¹ It is not easy to explain why the transients have the long relaxation times and regularity as mentioned below.

3.3. Rate of Decay and Energy of Activation. To estimate the rate of decay for the transients, the values of $\log(C - C_\infty)$ at the fixed temperatures 50, 75, and 100° in Figure 3B were plotted against time, where C is the capacitance at arbitrary time after fixing temperature and C_∞ is the capacitance corresponding to equilibrium at the fixed temperature. These plots yielded approximately straight lines, which are shown in Figure 6. From Figure 6, the rate of decay of the capacitance is approximately expressible in an equation

$$C = C^*e^{-k(t-t^*)} + C_\infty[1 - e^{-k(t-t^*)}] \quad (t \geq t^*) \quad (1)$$

where t is arbitrary time, t^* is the time when the temperature was fixed to be constant, C^* is the capacitance at $t = t^*$, and k is a rate constant. Equation 1 can be derived also from a differential equation

$$\frac{d(C - C_\infty)}{dt} = -k(C - C_\infty) \quad (t > t^*) \quad (2)$$

$$C = C^* \text{ at } t = t^*$$

which indicates that the decay of the transients follows first-order kinetics. The relaxation time for the eq 1 is reasonably given by

$$\tau = \frac{\int_{t^*}^{\infty} k(C - C_\infty) dt}{k(C^* - C_\infty)} = \frac{1}{k} \quad (t \geq t^*) \quad (3)$$

As k has the dimension time^{-1} , the relaxation time (τ) has the dimension time (min).

The values of $C^* - C_\infty$ are dependent on the rate of temperature increase and on the fixed temperature, and the deviations of the capacitance from eq 1 are considerably large near $t = t^*$, as can be seen in Figure 6. However, the deviations become smaller with time. Ultimately, the rate of decay becomes independent of

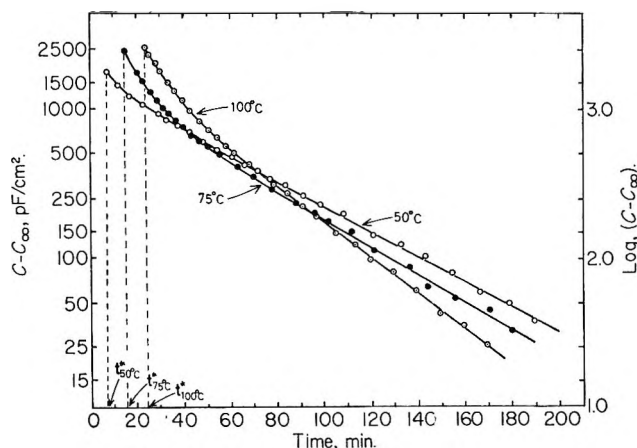


Figure 6. Plots of $\log(C - C_\infty)$ vs. time at the fixed temperatures 50°, 75°, and 100° in Figure 3.

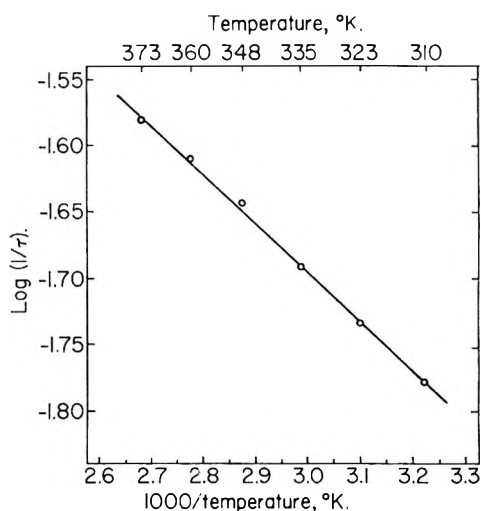


Figure 7. Arrhenius plot for sample 1, $\log 1/\tau$ vs. $1/T$.

the rate of temperature increase and depends only on the fixed temperature. In this region the relaxation time can reasonably be defined as a function of the fixed temperature. Relaxation times estimated from the slopes of the straight lines in Figure 6 are 54, 44, and 36 min at 50, 75, and 100°, respectively. The relaxa-

Table I: Relaxation Times of Samples 1, 2, and 3 at Several Fixed Temperatures

Sample	Relaxation times (min)					
	$T_{37.6}^\circ$	T_{50}°	$T_{62.5}^\circ$	T_{75}°	$T_{87.5}^\circ$	T_{100}°
1	60	54	49	44	40	36
2	59	54	48	43	39	36
3	59	53	47	43	39	35

(10) For example, W. Shockley, "Electrons and Holes in Semiconductors," Von Nostrand, Princeton, N. J., 1950.

(11) H. Fröhlich, "Theory of Dielectrics," Clarendon Press, Oxford, 1958.

tion times obtained in similar way for samples 1, 2, and 3 at several temperatures are given in Table I.

If it is assumed that the decay process involves an activated state, then the temperature dependence of the relaxation time can be reasonably expressed by¹²

$$\log 1/\tau = -(\Delta E/2.30R_gT) + \text{constant} \quad (4)$$

where T is the fixed temperature in degrees Kelvin, R_g

is the gas constant, and ΔE is the energy of activation for the transients. An Arrhenius plot of $1/\tau$ vs. $1/T$ for sample 1 is given in Figure 7. The energy of activation is about 1.7 kcal/mol, which is estimated from the slope in Figure 7. However, the physical meaning of this energy is not quite clear at present.

(12) S. Glasstone, K. J. Laidler, and H. Eyring, "Theory of Rate Processes," McGraw-Hill, New York, N. Y., 1941.

Isotope Effects in the Substitution Reaction of 2.8-eV

Tritium Atoms with Methane¹

by C. C. Chou and F. S. Rowland*

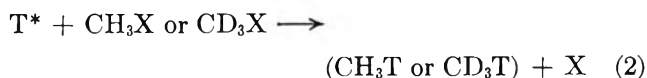
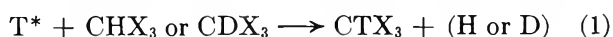
Department of Chemistry, University of California, Irvine, California 92664 (Received July 27, 1970)

Publication costs assisted by Division of Research, United States Atomic Energy Commission

The relative yields of the substitution reactions of 2.8-eV tritium atoms decrease by a factor of 7.2 for CH_3T from CH_4 to 1.0 for CD_3T from CD_4 in competitive experiments. The ratio of the intramolecular competition for substitution of T-for-H vs. T-for-D in partially deuterated methanes is approximately 1.0. The results are consistent with a primary replacement isotope effect of 1.6 ± 0.2 favoring the substitution of H over D and a secondary isotope effect of 1.6 ± 0.2 per H/D favoring bond formation to a methyl group with more H atoms in it. The characteristics are discussed of the pseudocomplexes existing during the simultaneous presence near the central C atom of five hydrogenic substituents including the energetic tritium atom. The substitution process is inadequately described by a three-particle T-H-R model and instead involves appreciable motion of all of the hydrogenic substituents.

Introduction

Hydrogen isotope effects have been extensively studied for the reactions of energetic tritium atoms recoiling from nuclear reactions and have provided important information concerning mechanisms and other characteristics of these reactions.²⁻⁷ In addition to an isotope effect in the abstraction of H or D by energetic T atoms, three different kinds of isotope effects have been demonstrated that are involved in determining the yields of substitution reactions by these atoms: (a) primary replacement; (b) secondary; and (c) moderator. The first two of these are concerned with intrinsic differences in reaction yield, under equivalent conditions, for isotopic molecules, as illustrated for primary replacement⁵⁻⁷ and secondary isotope effects⁴ by reactions 1 and 2, respectively.⁸ The moderator isotope effect is



concerned with the possibility of nonequivalent energy losses in nonreacting collisions with RH or RD for the energetic tritium atoms²⁻⁴ and therefore for variations in the number of possibly reactive hot collisions available at each energy as the tritium atom loses its excess kinetic energy.

The reactivity integrals of CH_3T from CH_4 and CD_3T from CD_4 were indicated through measurements made separately with CH_4 and CD_4 to be about equal for

(1) This research has been supported by A.E.C. Contract No. AT-(04-3)-34, Agreement No. 126.

(2) E. K. C. Lee, J. W. Root, and F. S. Rowland, *Chem. Eff. Nucl. Transform., Proc. Symp.*, 1964, 1, 55 (1965).

(3) R. Wolfgang, *Progr. React. Kinet.*, 3, 97 (1965).

(4) E. K. C. Lee, G. Miller, and F. S. Rowland, *J. Amer. Chem. Soc.*, 87, 190 (1965).

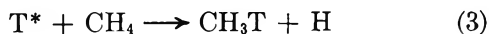
(5) T. Smail and F. S. Rowland, *J. Phys. Chem.*, 72, 1845 (1968).

(6) T. Smail and F. S. Rowland, *ibid.*, 74, 456 (1970).

(7) T. Smail and F. S. Rowland, *ibid.*, 74, 1859 (1970).

(8) A fourth kind of isotope effect, the primary substitution isotope effect (as exemplified by $\text{H}^* + \text{CD}_3 \rightarrow \text{CHD}_3 + \text{D}$ vs. $\text{T}^* + \text{CD}_3 \rightarrow \text{CD}_3\text{T} + \text{D}$), has not yet been measured.

reactions 3 and 4, thereby demonstrating that direct



“billiard-ball” transfer of the energy of the tritium atom to a struck H or D atom was not an important control mechanism for such reactions.⁹ In these experiments, however, all three isotope effects listed as (a) to (c) above are involved, although the reactivity integrals themselves reflect directly the composite of the primary replacement and secondary isotope effects, as indicated in reactions 3 and 4. A more accurate value for the relative magnitude of the reactivity integrals¹⁰ of CH₄ and CD₄ was obtained through competitive experiments carried out in CH₄-CD₄ mixtures, indicating an intermolecular isotope effect in reactions 3 and 4 of 1.33 ± 0.04 for the ratio $(\text{CH}_3\text{T}/\text{CH}_4)/(\text{CD}_3\text{T}/\text{CD}_4)$.² Such direct competition experiments eliminate the moderator effect as a factor but do not discriminate between primary replacement and secondary isotope effects.

The occurrence of reactions 3 and 4 has also been demonstrated for 2.8-eV tritium atoms formed by photolysis of TBr at 1849 Å.¹¹⁻¹³ We report here information about the relative yields with 2.8-eV tritium atoms of reactions 3 and 4 in intermolecular competition; of reactions 5 and 6 in intramolecular competition; and similar reactions with other inter- and intramolecular systems containing protonated and deuterated methanes.¹⁴



Experimental Section

The deuterated methanes were all obtained from Merck Sharp and Dohme and were purified by adsorption-desorption cycles on activated charcoal. The stated minimum atomic isotopic purities were 99% for CD₄ and 98% for the other deuterated methanes. Research grade CH₄ (Matheson) was used.

The details of synthesis of TBr, sample preparation and irradiation, and radio gas chromatographic analysis have been described elsewhere.¹² Most photolyses were carried out for 1 min—a time period for which the product ratios do not vary with time. Analytical separation of isotopic methanes was performed by recycle gas chromatography^{14,15} on two identical charcoal columns (100 ft × ³/₁₆ in.) at 50°. The quality of the isotopic separations is a function of the number of H vs. D atom differences in the molecules being separated. In general, the separation of pairs of methanes differing by two or three H/D changes (*e.g.*, CH₃T vs. CHD₂T) is very satisfactory. The separation of pairs of isotopic methanes differing only by a single H/D pair is not complete, as shown in Figure 1, but is sufficient to allow semiquantitative comparisons.¹⁶ For the separa-

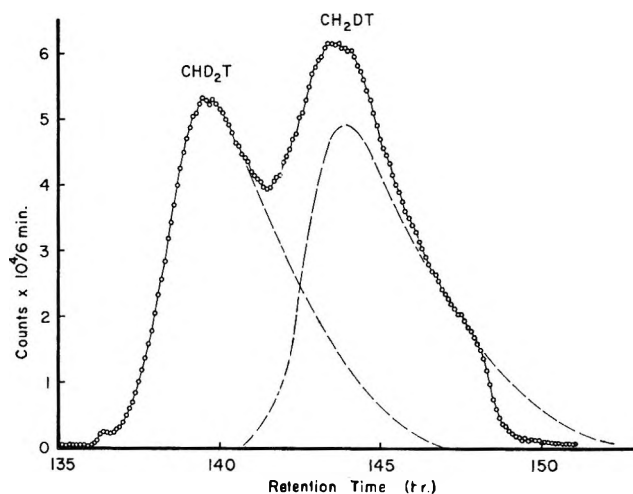


Figure 1. Recycle separation of CHD₂T and CH₂DT. Separation on activated charcoal at 50°, total path length in the column, 1200 ft. The sudden decrease in count rate at 148 hr is an artifact introduced by peak-chopping in the process of recycling.

tion of CHD₂T and CH₂DT, the columns were recycled six times each, for a total separation path length of 1200 ft. Further recycling was not feasible in this case because the two peaks had spread so broadly that they extended almost the entire length of one column.

In earlier experiments with CH₄ and CD₄ it was found that spurious reactions producing additional HT were sometimes important.¹¹⁻¹⁴ These effects play a small part in the HT yields quoted later but do not affect the yields of tritiated methanes, the prime goal of these experiments.

The data on relative yields from different parent molecules were obtained by photolysis of mixtures of pairs of methanes, with summation over the product yields of both tritiated methane products from partially deuterated molecules. For example, photolysis of a mixture of CH₄ and CH₂D₂ gave three tritiated methanes (CH₃T, CH₂DT, CHD₂T), each sufficiently separated to permit (a) estimation of the yield of the first *vs.* the sum of the other two and (b) assurance that the CHD₂T/CH₂DT ratio was 1.0 ± 0.2 , in agreement

(9) R. J. Cross and R. Wolfgang, *J. Chem. Phys.*, **35**, 2000 (1961).

(10) A much improved estimate of the absolute magnitude of the CH₄ reactivity integral was obtained by D. Seewald and R. Wolfgang, *ibid.*, **47**, 143 (1967).

(11) C. C. Chou and F. S. Rowland, *J. Amer. Chem. Soc.*, **88**, 2612 (1966).

(12) C. C. Chou and F. S. Rowland, *J. Chem. Phys.*, **50**, 5133 (1969).

(13) C. C. Chou and F. S. Rowland, *ibid.*, **50**, 2763 (1969).

(14) C. C. Chou, Ph.D. Thesis, University of California, Irvine, Calif., 1968.

(15) J. W. Root, E. K. C. Lee, and F. S. Rowland, *Science*, **143**, 676 (1964).

(16) More complete separations for the isotopic methanes have been reported using capillary columns and relatively small sample injections. See F. Bruner and G. P. Cartoni, *J. Chromatogr.*, **18**, 390 (1965); F. Bruner, G. P. Cartoni, and A. Liberti, *Anal. Chem.*, **38**, 298 (1966); F. Bruner, G. P. Cartoni, and A. Liberti, *ibid.*, **41**, 1122 (1969).

with the result found for CH_2D_2 in the absence of CH_4 .

Results

Intermolecular and Intramolecular Competitions. The results from intermolecular competitions with CH_4 - CD_4 mixtures are summarized in Table I, showing that substitution into CH_4 is favored by a factor of 7.2 with no systematic variation for mole fraction ratio of CH_4/CD_4 or for $\text{Br}_2/\text{methane}$. Similar measurements with CH_2D_2 vs. CH_4 and CH_3D vs. CD_4 have then given the relative yields summarized in Table II. In these experiments, the total yield of the substitution reaction with 2.8-eV tritium atoms falls steadily with increasing deuteration. Measurement of the intramolecular isotope effect in the replacement of H vs. D, however, gives *per bond* substitution ratios with a value of approximately unity, as indicated in Table III for intramolecular measurements with CH_2D_2 and CHD_3 , each taken separately. The relatively large error limits on the intramolecular competitions reflect the incomplete separation of peaks differing only in one H/D pair, as shown in Figure 1.

Table I: Intermolecular Isotope Effects in Reactions of 2.8-eV Tritium Atoms with Isotopic Methanes

Pressure of reactants, Torr			Product ratios	
CH_4	CD_4	Br_2	(HT/CH_4) (DT/CD_4)	$(\text{CH}_3\text{T}/\text{CH}_4)$ $(\text{CD}_3\text{T}/\text{CD}_4)$
192	184	32	1.45	7.17
107	254	34	1.43	6.92
216	152	30	1.61	7.23
115	98	6	1.95	7.15
111	98	6	2.03	7.30
			$(\text{CH}_3\text{T} + \text{CH}_2\text{DT})/(\text{CH}_3\text{D})$ $(\text{CD}_3\text{T})/(\text{CD}_4)$	$(\text{CH}_2\text{DT})/$ (CH_3T)
CH_3D	CD_4	Br_2	5.58	2.4 ± 0.7
66.8	31.6	6.1		
			$(\text{CH}_3\text{T})/(\text{CH}_4)$ $(\text{CHD}_2\text{T} + \text{CH}_2\text{DT})/(\text{CH}_3\text{D}_2)$	$(\text{CHD}_2\text{T})/$ (CH_3DT)
CH_4	CH_2D_2	Br_2	2.3	1.0 ± 0.2
31.6	72.3	6.1		

Table II: Relative Yields in Intermolecular Competition for the Substitution Reactions of 2.8-eV Tritium Atoms with Isotopic Methanes

CH_4	CH_3D	CH_2D_2	CD_4
7.2 ± 0.2	5.6 ± 0.3	3.1 ± 0.3	(1.0)

The *per bond* abstraction yields have also been recorded in all experiments and are consistently 1.4–2.0 times as high for HT as for DT in all molecules. The primary concern of our experiments has been the substitution process, and the abstraction yields (of HT) are more sensitive to experimental difficulties. Conse-

Table III: Relative Yields of Protium and Deuterium Substitution for 2.8-eV Tritium Atom Reactions with Partially Deuterated Methanes

Target molecule	Product molecules	Ratio of product yields, T-for-H/T-for-D
CH_2D_2	CHD_2T or CH_2DT	1.06 ± 0.1
CHD_3	CD_3T or CHD_2T	0.4 ± 0.1 (per bond: 1.2 ± 0.3)

quently, we have not considered the abstraction isotope effects in more detail.

Discussion

Primary Replacement or Secondary Isotope Effect? No energetic tritium atom experiment with methane has yet been entirely free from the general question, "Is the observed effect caused by the isotopic difference in the primary replacement process or in the secondary effect of the residual methyl group?" Even in the intramolecular comparisons, *e.g.*, of CHD_2T and CH_2DT from CH_2D_2 , both the replaced atoms (H and D) and the residual methyl radicals (CHD_2 and CH_2D) with which combination occurs are isotopically different and therefore potentially contributory to the observed overall isotope effect. If the observed intermolecular isotope effect of 7.2 between CH_4 and CD_4 were attributed entirely to the primary replacement effect of H and D and if this effect were assumed to be applicable in the same ratio for CH_2D and CHD_2 residual radicals, then a $\text{CHD}_2\text{T}/\text{CH}_2\text{DT}$ ratio of 7.2 would be expected for the intramolecular isotope effect in CH_2D_2 . Since this prediction is notably in disagreement with the actual observation given in Table III, the hypothesis of the sole importance of a primary replacement effect is seriously in error; secondary effects are nontrivial in magnitude and must be evaluated in detail.

We can estimate the magnitude of the secondary isotope effect by a comparison of the T-for-D reaction, *per bond*, between CH_2D_2 and CD_4 , in which we observe that the yield from the former is about 3 times as large as that from the latter, after correction for the number of C–D bonds in each molecule. A secondary isotope effect factor of 3 between CH_2D and CD_3 indicates a multiplicative factor of about 1.7 ± 0.2 per H/D change in the residual radicals. A similar comparison of yields from T-for-H in CH_4 vs. CH_2D_2 indicates a secondary isotope effect of about 1.5 ± 0.2 for each H/D variation in the residual CH_3 and CHD_2 radicals. The entire set of data is consistent with a secondary isotope effect of 1.6 ± 0.2 per H/D over the range from CH_4 to CD_4 .

If this secondary isotope effect were the only isotope effect operating in this system, one would then anticipate for CH_2D_2 that T-for-D (forming CH_2DT with residual CH_2D) should have a higher yield than T-for-H (forming CHD_2T with residual CHD_2) by a factor of

about 1.6 ± 0.2 . However, the measured ratio of $\text{CHD}_2\text{T}/\text{CH}_2\text{DT}$ is essentially unity, implying that the secondary isotope effect is being counterbalanced by a primary replacement isotope effect which *also* affects the total yields—the identity of the replaced atom (H *vs.* D) must also be important, with a quantitative effect just sufficient to counteract the D replacement preference of the secondary effect. Therefore, we estimate the primary replacement isotope effect as 1.6 ± 0.2 favoring the replacement of H over D for 2.8-eV tritium atoms in methane.

A consistent conclusion can thus be drawn from all of the data of Tables II and III: the probability of tritium substitution into a methane molecule by 2.8-eV T atoms increases with the number of H atoms (*vs.* D) in the molecule by a factor of 1.6 ± 0.2 per H/D, but with little isotopic preference for replacement of either H or D intramolecularly. The primary replacement isotope effect favors the replacement of H over D by 1.6 ± 0.2 ; the secondary isotope effect favors combination with more protonated methyl radicals (and therefore for replacement of D rather than H) by 1.6 ± 0.2 per H/D variation. These quantitative estimates, of course, do not apply to the reactions of 2.8-eV T atoms but rather to the weighted spectrum of energies for which substitution occurs for the multiple collisions usually made above the substitution threshold by T atoms which initially possess 2.8-eV kinetic energy.

Primary Replacement Isotope Effects. The primary replacement isotope effect has been measured earlier for very high-energy (192,000-eV) tritium atoms recoiling from the ${}^3\text{He}(n,p)\text{T}$ nuclear reaction and substituting into CHX_3 *vs.* CDX_3 molecules with $\text{X} = \text{CH}_3$,⁶ CD_3 ,⁶ or F .⁷ All of these data for higher energy tritium atoms are consistent with a preference for H replacement of 1.30 ± 0.05 . Our 2.8-eV estimated value of 1.6 ± 0.2 shows the same qualitative preference for replacement of H *vs.* D, while the quantitative increase is quite reasonable considering the much lower initial energy of T from TBr photolysis than from nuclear recoil. The easier replacement of H than D is qualitatively in the wrong direction for reactive collisions dominated by atom-atom collisions (*e.g.*, “billiard ball” collisions) between T and H or D, confirming the inapplicability of this especially simple model to the system of T plus methane.⁹ In contrast, the response of an H atom to changes in the direction or magnitude of the force field will be more rapid than that of a D atom. If the initial interaction of T with methane has the effect of perturbing the electron distribution, then the quicker motion of the H atom in this varying force field may very well facilitate bond formation—and therefore the overall process of substitution—for the newly collided tritium atom.

Secondary Isotope Effects. The earlier measurements with nuclear recoil tritium atoms showed a preference of 1.33 ± 0.04 for the replacement of F in CH_3F *vs.*

CD_3F for an average multiplicative effect of 1.10 ± 0.02 per H/D⁴ and a preference of 1.45 ± 0.05 for replacement of F in CHF_3 *vs.* CDF_3 with only one H/D difference.⁷ The ratio of $\text{CH}_3\text{T}/\text{CD}_3\text{T}$ from equimolar $\text{CH}_3\text{F}/\text{CD}_3\text{F}$ is higher for 2.8-eV initial energy—about 1.7 ± 0.1 .¹⁷ The current estimate of 1.6 ± 0.2 per H/D is consistent with the other 2.8-eV measurement and larger than those observed for the nuclear recoil systems. The existence of a secondary isotope effect indicates that the motions of atoms *not* being replaced are important in facilitating successful substitution reactions.

All of the motions of these atoms through the entire course of reaction must of course conserve total energy, total linear momentum, and total angular momentum. With these normal energetic and inertial restrictions, motion by heavy atoms or groups is intrinsically limited to slower velocities than those possible for the lighter species such as H or D atoms. A special example of the conservation laws—the slower rotation of $-\text{CX}_3$ groups than $-\text{CH}_3$ groups when $m_x \gg m_H$ —has been described as “rotational inertia” and postulated as important in many hot-atom substitutions.³ Our concept of these photochemical isotope effects in methane is also an application of the conservation laws and differs from the rotational inertia concept in that (a) the atomic motions of the residual atoms are not uniformly coordinated as implied for the rotation of a methyl group and (b) the atom to be replaced is still rather strongly bonded as the relaxation motion of the residual atoms commences, *i.e.*, the reactions are “concerted” and not “sequential.” The more rapid relaxation of protonated than deuterated species is a natural consequence of these conservation laws under most circumstances.

Combined Isotope Effects. It is clear that the isotope effects measured in different systems do not hold individually and cumulatively over wide variations in the nature of the experimental target and in initial tritium energies: the primary replacement isotope effect for H/D in $\text{CHF}_3(\text{CDF}_3)$ ⁷ and the secondary isotope effect for 3H *vs.* 3D in $\text{CH}_3\text{F}(\text{CD}_3\text{F})$ ⁴ are 1.35 ± 0.05 and 1.33 ± 0.04 , respectively, while the cumulative overall isotope effect for substitution into CH_4 (CD_4) is only 1.33 ± 0.04 ,² all three systems involving the energetic T atoms from nuclear recoil.

The difference between CH_4/CD_4 isotope effects with 2.8- and 192,000-eV tritium atoms is quite striking: $(\text{CH}_3\text{T}/\text{CH}_4)/(\text{CD}_3\text{T}/\text{CD}_4) = 7.2$ and 1.33, respectively. Unfortunately, significant observations about the relative importance of primary replacement and secondary isotope effects cannot now be obtained for 192-keV tritium atoms because our analytical separation of $\text{CHD}_2\text{T}/\text{CH}_2\text{DT}$ is not complete enough for accurate measurement of the small variations expected in yields from CH_2D_2 at these energies.

(17) C. C. Chou and F. S. Rowland, unpublished results.

The Substitution Mechanism in Methane near Threshold Energies. The existence of cumulative H/D effects of 1.6 ± 0.2 for all H or D atoms in the methane molecule implies the intimate participation in the substitution process of all four of the original hydrogen substituents. In the terminology of Bunker,¹⁸ the substitution process is >3-centered, rather than a 3-centered reaction in which the only pairs of atoms that attract strongly during the reaction are those whose bonds are being made or broken. The observation of substitution into methane for initial tritium energies as low as 1.9 eV with an apparent threshold in the vicinity of 1.6 eV¹³ indicates that the saddle point for substitution must be only about 35–40 kcal/mol above the energy for separated tritium atom and methane molecule. The mere existence of this substitution reaction more than 60 kcal/mol below the dissociation energy of C–H bonds in methane is in itself ample proof that the reaction is “concerted,” involving simultaneous formation of the C–T bond and breakage of the C–H or C–D bond. Such a “concerted” reaction can be described in terms of a 3-centered reaction with three nonparticipating hydrogen atoms, but the requirement of participation by these other H or D atoms invites a more suitable description in terms of some transitory structure in which the electron densities between the C atom and the five substituent hydrogen atoms are all somewhat different from that in the normal C–H bonds of methane.

The trajectory calculations of Polanyi, *et al.*, have treated both substitution and abstraction reactions through potential energy surfaces allowing only 3-centered reactions of T, H, and R.¹⁹ A variety of surfaces in which all six atoms of T + CH₄ have had some freedom of motion has been considered by Bunker and Pattengill, without satisfactory success in simulating the ratio of substitution to abstraction for 2.8-eV T atoms.^{18,20} In particular, none of these six-particle surfaces has yet generated a sufficiently large yield of substitution reactions, while the authors have definitely concluded that 3-centered calculations are inadequate for description of these substitution processes. Yet more elaborate calculations seem to offer some possibility for more definitive statements concerning the orientations of the five hydrogenic substituents during the substitution process.

A 2.8-eV tritium atom has an initial velocity of 1.3×10^6 cm/sec and therefore travels Å distances in $\sim 10^{-14}$ sec. No good measurements or securely based estimates are available for the kinetic energies of the replaced H or D atoms following such substitutions. A head-on two-body T–H collision would transfer at most 75% of the kinetic energy of the tritium to the H atom, while collisions at angles other than head-on would result in lesser energy transfer to the departing atom. The failure of the “billiard ball” approximation implies that this atom–atom model is very poor for tritium–methane collisions⁹ and that energy transfer

to the H or D atom will be much less than calculated from two-atom collisions. Moreover, the prevalence of high vibrational energies in nuclear recoil T-for-H reactions^{2,3} suggests that the replaced atom normally has far less kinetic energy than did the original incoming tritium atom. The time scale for removal of a replaced H or D atom (velocity of 0.1-eV D atom = 3×10^5 cm/sec) to distances of 1 Å or more is probably several times longer than the time for T atom approach and hence is long enough for several vibrations of a normal C–H bond with vibrational frequency of $\sim 8 \times 10^{13}$ sec⁻¹ and presumably also for vibrations of the perturbed carbon–hydrogen bonds in a reacting methane system. In addition, uncertainties exist in the paths followed by colliding atoms within these arbitrarily indicated 1-Å limits, and some calculated trajectories show multiple atom–atom collisions before departure of any of the interacting atoms.^{18–20} Thus, for a period of several C–H vibrations or more, five hydrogenic substituents are close enough to the C atom that one should expect appreciable concentrations of electron density between each hydrogen atom and the central carbon atom. We shall describe this fleeting coexistence of five carbon–hydrogen interactions as a pseudocomplex and estimate its lifetime as $3\text{--}7 \times 10^{-14}$ sec.

The word “complex” often conveys connotations of particular theories in chemical kinetics, and we have added the qualifier “pseudo” primarily to differentiate it from other prior connotations—for example, although excess internal energy may well be partially distributed among the internal degrees of freedom of this pseudocomplex, we see no reason to believe that it has been equilibrated among them. We also have no information about the possible existence or nonexistence of shallow minima in potential energy surfaces for five hydrogen atoms around a carbon atom and do not wish to imply either the presence or absence of such minima with our terminology.

“Complexes” in Hot Tritium Atom Reactions at Saturated Carbon Positions? Since there is general agreement that the substitution reactions of energetic tritium atoms proceed through a single elementary exchange reaction, there *must* be some time interval during which all four of the original substituents and the tritium atom are all within 1 or 2 Å of the central carbon atom. At present, the time scale of this interval and the interrelations among these atoms during this period are rather uncertain. In our view, the current results are reasonably consistent with the earlier speculations that “recoil tritium reactions with saturated positions of aliphatic molecules involve momentarily a transition complex including the recoil tritium atom and all of the

(18) D. Bunker and M. Pattengill, *J. Chem. Phys.*, **53**, 3041 (1970).

(19) P. J. Kuntz, E. M. Nemeth, J. C. Polanyi, and W. H. Wong, *ibid.*, **52**, 4654 (1970).

(20) D. L. Bunker and M. Pattengill, *Chem. Phys. Lett.*, **4**, 315 (1969).

previously bonded substituents. The lifetime of this complex is very short—it may only exist for one vibration or so, and equilibration of energy among the vibrational coordinates of the complex does not occur,"²¹ and "this complex involves too many groups for stable bonding and decomposes in a competitive manner. The lifetime of such a 'complex' is rather uncertain, but must be long enough for reasonably normal isotope effects on decomposition to be in effect."²²

A contrasting view has been expressed for the reactions of tritium atoms with kinetic energy from nuclear recoil.^{3,23} "There appears to be no data supporting the supposition that hot displacement reactions do go through such quasi-equilibrated intermediates. For instance, if HT and CH₂T were produced from methane by decomposition of a common activated complex in which the incident and the CH₄ atoms have become indistinguishable, their ratio HT/CH₂T would be expected on a purely statistical basis to be 2:3. Even allowing for possible isotope effects, the observed ratio of 9:1 hardly supports such a mechanism.²⁴ Instead, all results are consistent with the hypothesis that the displacement reaction is a fast, direct, localized event occurring on a time scale comparable to a bond vibration ($\sim 10^{-14}$ sec)."

Our view is that substantial distribution—but not full equilibration—of energy occurs on a time scale appreciably faster than deexciting collisions in condensed phases (therefore, $< 10^{-12}$ sec and perhaps $\sim 10^{-13}$ sec), since secondary unimolecular decompositions involving reaction several bonds removed from the newly bonded tritium atom are observed in liquid-phase experiments.^{25,26} Searches for decomposition reactions occurring from not-yet-equilibrated radicals have thus far been unsuccessful in chemical activation studies at pressures to 115 atm.²⁷ These results have led to estimates that internal equilibration times are much shorter than some rotation and vibration rates in the molecules involved, implying that "equilibration" does not require the actual intramolecular transfer of energy through many degrees of freedom of each radical, but only that an ensemble of such radicals has distribution of energy among these slow rotational or vibrational degrees of freedom that is indistinguishable from a thermal distribution.^{28,29}

The time scale for isotope effects is not well specified, but high-temperature limits on k_H/k_D often become simply the relative rates of motion through the saddle point of H vs. D,³⁰ so that a time scale of $\sim 10^{-13}$ sec or faster may easily be quite long enough for a preference for loss of H vs. D to be observed. In the current experiments, the reactions are initiated by tritium atoms possessing precisely limited kinetic energies and velocities. Moreover, the time scale of interaction is much more dependent upon the *exit* velocity of the replaced atom and the details of the close interaction than upon the initial velocity of the T atom. We believe that

the five-bonded carbon system exists for several C-H vibrations or more and therefore is very appropriately described as a pseudocomplex. Very probably, the substitution reactions of 10-eV tritium atoms (with only twice the initial velocity of 2.5-eV tritium atoms) *also* involve the slow exit of the replaced hydrogen atom and are *also* adequately described as pseudocomplexes which last at least 2 or 3 vibrations of the C-H or C-D bonds.

Pseudocomplexes and Potential Energy Surfaces. Several questions should eventually be answerable for the understanding of such pseudocomplexes. What are the relative orientations of the five substituents? How rapidly does the potential energy of the complex change with variations in the positions and angles of the substituents? What are the patterns of motion into and out of the complex? Experiments such as ours can provide very little except qualitative information in answer to such questions.

For the substitution reactions initiated by energetic tritium atoms, it is not obvious that there is a *single* set of bond angles and bond distances that can describe a configuration which will occur at some point in the path of every substitution reaction. Rather, the relatively high probabilities of hot reaction per collision almost certainly indicate that the requirements for reaction permit a range of values for one or several geometric parameters.³ This same loosening of geometric restrictions has been discussed in some detail for the abstraction of H atoms from RH by energetic tritium atoms.^{31,32} Nevertheless, the abstraction reactions occurring near threshold energy—for example, those

(21) J. K. Lee, B. Musgrave, and F. S. Rowland, *Can. J. Chem.*, **38**, 1756 (1960).

(22) E. K. C. Lee and F. S. Rowland, *J. Amer. Chem. Soc.*, **85**, 2907 (1963).

(23) M. Henschman, D. Urch, and R. Wolfgang, *Chem. Eff. Nucl. Transform., Proc. Symp.*, **1960**, **2**, 83 (1961).

(24) This statistical calculation relies on the entirely unsupported assumption that all reactions must proceed through a common "complex" with all hydrogen atoms in indistinguishable positions. The saddle point for abstraction has been almost universally assumed not to have five indistinguishable H positions, but instead to exist in the linear T-H-CH₃ form. See ref 19, 33, 36, and 38. In contrast, the saddle point for substitution was assumed by Eyring, *et al.*,³⁶ and by others since to have five hydrogen atoms partially bonded to the central carbon atom.

Much of the CH₂T—we believe almost all (see ref 26)—arises from the secondary unimolecular decomposition of excited CH₃T* formed in the hot substitution reactions and is therefore not really a direct hot product and would be inappropriate for use in a hot calculation.

(25) E. K. C. Lee and F. S. Rowland, *J. Chem. Phys.*, **36**, 554 (1962).

(26) Y.-N. Tang and F. S. Rowland, *J. Phys. Chem.*, **72**, 707 (1968).

(27) D. W. Placzek, B. S. Rabinovitch, and F. H. Dorer, *J. Chem. Phys.*, **44**, 279 (1966); I. Oref, D. Schuetzle, and B. S. Rabinovitch, *ibid.*, **54**, 575 (1971).

(28) R. A. Marcus, *ibid.*, **49**, 2617 (1968), and earlier articles.

(29) D. G. Truhlar and A. Kuppermann, *ibid.*, **52**, 3841 (1970).

(30) See, for example, B. S. Rabinovitch and D. W. Setser, *Advan. Photochem.*, **3**, 1 (1964).

(31) E. Tachikawa and F. S. Rowland, *J. Amer. Chem. Soc.*, **90**, 4767 (1968).

(32) E. Tachikawa and F. S. Rowland, *ibid.*, **91**, 559 (1969).

observed in thermal systems—presumably pass near a particular set of bond lengths and bond angles at the saddle point of the potential energy surface leading to abstraction.

The potential energy surface must also include pathways to substitution, with another saddle point.³³ Near the threshold energy for substitution, very little excess energy can be available and passage over the potential energy surface at these energies must occur with similar orientations for all reactions. As with abstraction, when the kinetic energy rises, the energy requirements become more relaxed and substitution can occur through structures less and less similar to that of the substitution saddle point on the potential energy surface. Successful reactions initiated by high kinetic energy atoms are then under the simultaneous influence both of the energetics as embodied in the potential energy surface and of the dynamics of the motions which determine the accessible paths along this potential energy surface.

Retention and Inversion of Configuration. The problem of motion into and out of pseudocomplexes is chiefly a qualitative question of retention *vs.* inversion of the relative orientations of the three residual substituents during the substitution process. While some theoretical calculations have been performed on the bonding characteristics as a hydrogen atom approaches a methane molecule,^{34–37} no systematic searches for potential energy saddle points without geometric restrictions to the region of search appear to have been made.

All experiments with energetic tritium atoms from nuclear recoil have shown that the substitution mechanism of T-for-H has occurred very predominantly by a retention mechanism, and the most recent experiments using *dl*- and *meso*-(CHFCl)₂ as the target molecules have led to an estimate of $\geq 99\%$ retention of configuration during substitution.³⁸ All such experiments have required at least one asymmetric carbon atom with three heavy (*i.e.*, not H or D) substituent groups in addition to the H atom being replaced, and the argument is quite plausible that the presence of each additional heavy substituent will make the attainment of the trigonal-bipyramidal inversion structure just that much more difficult. Whether this limitation is dynamic or energetic or partially both is a moot point.

The yields of the T-for-H substitution reaction with various alkanes and halocarbons correlate quite well with the cumulative electronegativity of the various residual substituents, and methane does not appear to

have an anomalously high yield when compared with this correlation.³⁹ The argument is thus quite plausible that the substitution into methane occurs predominantly—and perhaps exclusively—by the same mechanism applicable for the case of three heavy substituents, *i.e.*, with retention of configuration for the residual substituents. Nonetheless, if a mechanistic change were to occur *vs.* substituent mass, CH₄ is obviously the most likely molecule in which this second mechanism might occur.

The correlation of yield with the electronegativity of substituents is essentially an energetic requirement, involving the deviations of potential energy surfaces from a single standard pattern. It is quite apparent that secondary isotope effects—*i.e.*, the substituted effect for D instead of H atoms—involving a decrease in yield of 30% for tritium atoms from nuclear recoil will not fit an electronegativity correlation in which three F atoms cause a decrease of only 44% in yield and that different explanations must be applied to D and F substituent effects. Qualitatively, the chief effect of F is assumed to be through its perturbation of the potential energy surface by its electronegativity. Replacement of H by a D atom, on the other hand, will not alter the potential energy surface but does involve slower motion by D than H in responding to force constant changes involved with the surface. The secondary isotope effect is thus chiefly a dynamic influence of hydrogenic species upon the trajectories across the potential energy surface.

(33) A path *must* exist for net substitution with an activation energy equivalent to that for the abstraction reaction, the "double abstraction" pathway. The products (HT + CH₃) could be formed either by reaction of T with CH₄ or of H with CH₃T, with an equal potential energy barrier for each path. Thus, a substitution reaction could theoretically proceed from T + CH₄ over the barrier and almost to completion to HT + CH₃ and then switch and follow the other abstraction path in the reverse direction over the second abstraction barrier to H + CH₃T. However, this pathway over the potential energy surfaces is probably strongly forbidden for the dynamic pathways open to real interacting systems.

(34) The initial calculation of this type showed an activation energy of 37 kcal/mol for a trigonal-bipyramidal complex and a 17 kcal/mol basin of stability for this CH₅ complex: E. Gorin, W. Kauzmann, J. Walter, and H. Eyring, *J. Chem. Phys.*, **7**, 633 (1939).

(35) F. O. Rice and E. Teller, *ibid.*, **6**, 489 (1938).

(36) J. J. Kaufman, J. J. Harkins, and W. S. Koski, *Int. J. Quantum Chem.*, **15**, 261 (1967).

(37) Empirical assumptions have also been required for the three-dimensional trajectory calculations of ref 18–20.

(38) All of these experiments are summarized in the accompanying article: G. F. Palino and F. S. Rowland, *J. Phys. Chem.*, **75**, 1299 (1971).

(39) Y.-N. Tang, E. K. C. Lee, E. Tachikawa, and F. S. Rowland, *ibid.*, **75**, 1290 (1971).

A Study of the Roles of Chemical Factors in Controlling the Yields of Substitution Reactions by Energetic Tritium Atoms. Electronegativity, Electron Density, and Bond Energy¹

by Yi-Noo Tang, Edward K. C. Lee, Enzo Tachikawa, and F. S. Rowland*²

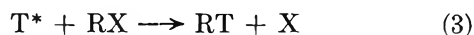
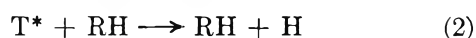
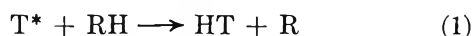
Department of Chemistry, University of California, Irvine, California 92664 (Received July 27, 1970)

Publication costs assisted by Division of Research, United States Atomic Energy Commission

The relative yields of the T-for-H substitution reactions by nuclear recoil tritium atoms have been measured for various halomethane and alkane molecules under equivalent conditions of tritium atom flux. After the application of corrections for secondary decomposition of primary products, the yield of the T-for-H reaction with CH₃X decreases smoothly with the increasing electronegativity of the substituent X, as measured by the nmr shifts. No evidence was found in support of the hypothesis that halogen substituents interfered sterically with the T-for-H substitution reaction. The relative yields of the T-for-X reaction in CH₃X increase as much as a factor of 7.5 from CH₃F to CH₃I. The most important factor in controlling this variation in yield with the substituent X is the bond dissociation energy of the C-X bond. The sensitivity of both T-for-H and T-for-X substitution reactions to "chemical" factors such as electronegativity and bond strength demonstrates that models for these reactions based only on geometric physical factors such as atomic masses and sizes, bond angles, angle of attack, etc., are seriously inadequate.

Introduction

The energetic reactions of recoil tritium atoms with saturated hydrocarbons and halocarbons fall chiefly into the two categories of abstraction, as in (1), and substitution, including replacement of H (or D) or of heavier groups, as in (2) and (3).³⁻⁵ Explanations and



(X = CH₃, F, Cl, Br, OH, etc.)

theories concerning the mechanistic nature of the reactions of energetic tritium atoms have largely been based upon the yields of reactions 1-3, or more often upon the ratios of yields from these reactions, both in intramolecular and intermolecular competition with one another. A substantial number of such observations have been correlated and rationalized through considerations which are predominantly physical in nature and which have been collectively characterized as an "impact model."^{5,6} This model has involved, among other considerations, steric factors such as the obstruction of substitution by methyl groups,⁶⁻⁸ or by halogen atoms,^{9,10} and inertial factors dependent chiefly upon the mass of the substituent groups.^{4,9,10}

On the other hand, the yields of the abstraction reaction (1) have been demonstrated to be very sensitive to more "chemical" effects, since they show an excellent correlation with the bond dissociation energies of re-

lated alkanes and cyclanes¹¹⁻¹³ and are generally quite responsive to the substituent influences of halogens, etc.^{14,15} Our own recoil tritium experiments with certain individual molecules have earlier led us to speculate that the inductive effect of electronegative substituents might be playing an important role in the substitution

(1) This research was supported by A.E.C. Contracts No. AT-(11-1)-407, with the University of Kansas, and AT-(11-1)-34, Agreement No. 126, with the University of California. Part of the work was presented at the 150th National Meeting of the American Chemical Society, Atlantic City, N. J., Sept 1965. Part of the work was submitted in partial fulfillment of the Ph.D. requirements of the University of Kansas (by Y. N. T.) and of the University of California, Irvine, Calif. (by E. T.).

(2) To whom reprint requests should be addressed at the University of California, Irvine, Calif. 92664.

(3) F. Schmidt-Bleek and F. S. Rowland, *Angew. Chem., Int. Ed. Engl.*, **3**, 769 (1964).

(4) R. Wolfgang, *Progr. React. Kinet.*, **3**, 97 (1965).

(5) R. Wolfgang, *Ann. Rev. Phys. Chem.*, **16**, 15 (1965).

(6) D. Urch and R. Wolfgang, *J. Amer. Chem. Soc.*, **83**, 2982 (1961).

(7) M. Henchman, D. Urch, and R. Wolfgang, *Can. J. Chem.*, **38**, 1722 (1960).

(8) A. Odell, A. Rosenberg, R. D. Fink, and R. Wolfgang, *J. Chem. Phys.*, **40**, 3730 (1964).

(9) R. A. Odum and R. Wolfgang, *J. Amer. Chem. Soc.*, **83**, 4668 (1961).

(10) R. A. Odum and R. Wolfgang, *ibid.*, **85**, 1350 (1963).

(11) W. Breckenridge, J. W. Root, and F. S. Rowland, *J. Chem. Phys.*, **39**, 2374 (1963).

(12) J. W. Root, W. Breckenridge, and F. S. Rowland, *ibid.*, **43**, 3694 (1965).

(13) E. Tachikawa and F. S. Rowland, *J. Amer. Chem. Soc.*, **90**, 4767 (1968).

(14) E. Tachikawa, Y.-N. Tang, and F. S. Rowland, *ibid.*, **90**, 3584 (1968).

(15) E. Tachikawa and F. S. Rowland, *ibid.*, **91**, 559 (1969).

reactions as well but did not furnish any evidence permitting clear discrimination among the possible controlling factors for these reactions.¹⁶⁻¹⁸ In assessing the results of some experiments with aromatic molecules, we have also suggested that the bond dissociation energies of C-X bonds might be quite important in determining the yields of reaction 3 for X = halogens.¹⁹ This paper presents the results of a series of experiments designed to evaluate the possible influences of the more "chemical" factors such as electronegativity, electron density, and bond energy, upon the substitution reactions, including both (2) and (3). Our experiments have led us to the eventual conclusion that such "chemical" factors are quite important in controlling the course of these substitution reactions and are, in many cases, actually the dominant influence.²⁰

Certain steric aspects of the substitution reactions of recoil tritium atoms, included in the description of the "impact model," are rather generally agreed upon—for example, replacement of H by energetic T at an sp³ asymmetric carbon atom occurs predominantly with retention of configuration in both solid^{21,22} and gas phases,²³⁻²⁵ when other substituents are heavy atoms or groups (*i.e.*, not H or D).²⁶ Similarly, replacement of olefinically bonded H atoms also occurs with a strong preference for the original *cis-trans* isomer among the tritium-labeled products, again in both solid²⁷ and gas²⁸ phases. Our early comment²⁷ that "it seems quite probable that many true 'hot' atom reactions will also follow mechanisms which involve economy of atomic motion" and parallel, more extensive comments by Urch and Wolfgang^{6,28} have been amply confirmed by many subsequent experiments; many processes such as Walden-inversion type substitution reactions with heavy substituents simply do not occur in measurable yield. Wolfgang has expressed this as a general principle, in an atomic analogy to the Franck-Condon principle by which the absence of certain reactions is attributable to the rapid time-scale of reaction: "Hot atom reactions requiring nuclear motions which are slow relative to the time of collision tend to be forbidden."^{2,10}

Furthermore, the relatively high collision yields—as well as the general multiplicity of hot products—certainly indicate that restrictions on the orientation of reaction partners are much less severe for collisions involving atoms possessing substantial excess kinetic energy than for the corresponding thermal reactions. In contrast to the severe energy limitations of thermal reaction mechanisms, the molecular orientation and the angle of approach providing the minimum energy at the moment of bimolecular collision are no longer factors of overwhelming importance when abundant extra kinetic energy is available. Our experiments have implicitly accepted this aspect of steric considerations—that many angles, orientations, and points of impact in collision can successfully lead to hot reaction—and have been aimed toward comparisons of the factors

which *then* determine whether a particular collision leads to product A, to product B, or to nonreactive scattering.

Early estimates of the magnitude of steric obstruction of T-for-H substitution by alkyl groups in hydrocarbons indicated a reduction in yield of the substitution product of 45% per alkyl group.^{6,7} Now, however, there is essential agreement that the cumulative alkyl-substituent effects on these T-for-H substitution reactions, for steric or other reasons, fall in the range from 0 to 10% per alkyl group.^{3-5,8,29-32}

Comparisons of Primary Yields of Hot Reactions. The basic goal in these experiments, as in many previous ones, is the measurement of either the absolute or relative yields of two or more hot reactions under exactly equivalent (and appropriate) experimental conditions. Two chief difficulties have confronted such experiments: (a) the attainment of "equivalent conditions" and (b) the failure of all of the molecules formed in the primary reactions to survive long enough to be measured. The most important problem in trying to equalize conditions for intercomparison of different samples is control over the number and distribution *vs.* energy of the hot collisions potentially available to an energetic atom prior to thermalization.³³ The cumulative absolute yield from a particular hot-atom reaction

(16) Y.-N. Tang, E. K. C. Lee, and F. S. Rowland, *J. Amer. Chem. Soc.*, **86**, 1280 (1964).

(17) Y.-N. Tang and F. S. Rowland, *ibid.*, **87**, 3304 (1965).

(18) Y.-N. Tang and F. S. Rowland, *ibid.*, **90**, 574 (1968).

(19) R. M. White and F. S. Rowland, *ibid.*, **82**, 4713 (1960).

(20) F. S. Rowland, E. K. C. Lee, and Y.-N. Tang, *J. Phys. Chem.*, **73**, 4204 (1969).

(21) F. S. Rowland, C. N. Turton, and R. Wolfgang, *J. Amer. Chem. Soc.*, **78**, 2354 (1956); H. Keller and F. S. Rowland, *J. Phys. Chem.*, **62**, 1373 (1958).

(22) J. G. Kay, R. P. Malsan, and F. S. Rowland, *J. Amer. Chem. Soc.*, **81**, 5050 (1959).

(23) M. Henchman and R. Wolfgang, *ibid.*, **83**, 2991 (1961).

(24) Y.-N. Tang, C. T. Ting, and F. S. Rowland, *J. Phys. Chem.*, **74**, 675 (1970).

(25) G. F. Palino and F. S. Rowland, *ibid.*, **75**, 1299 (1971).

(26) No asymmetric carbon atom experiments have been conducted except with three heavy substituents. The question of substitution in molecules such as CH₄ remains moot insofar as any actual laboratory experiments are concerned. See C. C. Chou and F. S. Rowland, *ibid.*, **75**, 1283 (1971).

(27) R. M. White and F. S. Rowland, *J. Amer. Chem. Soc.*, **82**, 5345 (1960).

(28) D. Urch and R. Wolfgang, *ibid.*, **83**, 2997 (1960).

(29) J. W. Root and F. S. Rowland, *ibid.*, **84**, 3027 (1962).

(30) T. Smail and F. S. Rowland, *J. Phys. Chem.*, **72**, 1845 (1968).

(31) T. Smail and F. S. Rowland, *ibid.*, **74**, 456 (1970).

(32) C. T. Ting and F. S. Rowland, *ibid.*, **74**, 445 (1970).

(33) Direct comparison of absolute observed radioactivities, *i.e.*, number of counts in particular radio gas chromatographic peaks, implies satisfactorily equivalent neutron fluxes during sample irradiation. Under favorable conditions, such control is feasible to an accuracy of $\pm 1\%$. Our consideration here assumes that the total number of tritium atoms available in the system is accurately controlled and monitored. With gas samples, this includes estimate not only of the number of tritium atoms formed but also of the fraction actually stopped in the gas phase, *i.e.*, estimates of the "recoil loss" into the walls of the sample bulb.

is a function not only of the other hot reactions available to the energetic atom at all energies but also of the rate of energy loss for the atom in nonreactive collisions.³⁻⁵ These energy processes in nonreactive collisions control the number of additional collisions available and, in addition, the distribution of these collisions along the energy scale. Since the number and/or distribution of hot collisions in one system are only fortuitously equal to those in another system, differences in absolute yields, while often suggestive, may arise from variations in more than one parameter. Wolfgang, *et al.*, for example, have demonstrated that the rate of energy loss in nonreactive collisions is almost twice as great in *n*-butane as in methane,³⁴ an observation that would be reflected, if other conditions were also to remain unchanged, in an absolute yield about half as large for reactions carried out in excess *n*-butane *vs.* the same reaction in excess methane.

Comparisons of absolute yields thus require control both over the number of hot collisions available to the energetic atom and over the distribution of these collisions with energy, since not all hot reactions can be expected to have the same energy dependence. Measurement of the relative yields in an intramolecular system, however, ensures that each hot reaction was summed over the identical, albeit unknown, tritium atom spectrum; intermolecular comparisons are similarly free from problems if the two molecules are present in an intimate mixture such that both are exposed to the identical spectrum of collision energies. (The assurance, however, is not that the hot reactions in these competitions are occurring in the same energy range but merely that they have originated in the same total spectrum of tritium atom energies.) Cross-comparisons among several binary mixtures are also possible if one component is common to all. In the latter case, it is no longer guaranteed that the tritium atom spectrum of a binary mixture of A with C is identical with that of B with C. However, if C is the major component in each mixture and especially if the reactions being compared can be assumed in first approximation to have a rather similar dependence of reaction cross section *vs.* energy (*e.g.*, substitution of T-for-H in RH and in R'H), then variations in ratios of product yield should be minimized insofar as any dependence upon the spectra of tritium energies in collision is concerned. Most of our experiments have consequently been conducted in binary or ternary mixtures, permitting determination of relative yields from different reactions for identical tritium atom collision spectra; cross-comparisons have also been carried out for series of mixtures involving a common component as the major ingredient of each.

The other major experimental complication in the comparison of product yields is the instability of many hot reaction products toward secondary isomerization or decomposition by reason of the high internal excita-

tion energies left on the molecules during the substitution process.^{3-5, 16-18, 31, 35-39} In extreme cases involving product molecules with low activation energies toward further reaction, such secondary loss can be almost total: the CH₂TNC* molecules formed by the substitution of T-for-H in CH₃NC are not observed under the gas-phase condition because of the easy isomerization (activation energy: 38 kcal/mol) to CH₂T-CN,³⁶ while only about 2% of the T-for-CH₃ substitution products from 1,3-dimethylcyclobutane are stabilized prior to decomposition (to CH₂=CHT and propylene).³² For this reason, some estimate and/or correction for the magnitude of loss by secondary reaction seems appropriate before the observed product yields can be considered to be representative of the original primary yields. Since such secondary decompositions can be reduced (but not usually eliminated) by more rapid collisional deexcitation of the highly excited molecules, the primary yields are usually observed to be less depleted in higher density media, particularly in the condensed phases. Most of our comparison experiments have been carried out in the liquid phase in order to minimize alteration of primary product yield through secondary reaction, while avoiding the possible influences of crystal structure upon both reaction and deexcitation. Because the change of phase between gas and liquid could be accompanied by effects on the processes of energetic substitution other than increased rates for collisional deexcitation (*e.g.*, "cage" effects), confirmation of liquid-phase results through gas-phase experiments appropriately corrected for secondary decomposition is often quite desirable.

Experimental Section

A series of recoil tritium experiments has been performed utilizing standard techniques for sample preparation, irradiation, and radic gas chromatography.^{16-18, 40, 41} These techniques are quite similar to those previously described in detail earlier and involve the production of tritium by neutron irradiation of ³He in gaseous samples and ⁶Li in liquid-phase samples.

Methyl fluoride can be readily irradiated in the gas phase and in the liquid phase at room temperature when it is present as a relatively minor component in a binary or tertiary mixture with CH₃Cl as the major

(34) The measurement of energy loss is given in terms of α values:³⁻⁵ $\alpha_{\text{CH}_4}/\alpha_{\text{H}_2} = 1.6$; $\alpha_{n\text{-C}_4\text{H}_{10}}/\alpha_{\text{H}_2} = 3.4$, R. T. K. Baker, M. Silbert, and R. Wolfgang, *J. Chem. Phys.*, **52**, 1120 (1970).

(35) E. K. C. Lee and F. S. Rowland, *J. Amer. Chem. Soc.*, **85**, 897 (1963).

(36) C. T. Ting and F. S. Rowland, *J. Phys. Chem.*, **72**, 763 (1968).

(37) A. J. Johnston, D. Malcolm-Lawes, D. S. Urch, and M. J. Welch, *Chem. Commun.*, 187 (1966).

(38) R. Cipollini and G. Stoecklin, *Radiochim. Acta*, **9** (1968).

(39) R. T. K. Baker and R. Wolfgang, *J. Phys. Chem.*, **65**, 1842 (1969).

(40) Y.-N. Tang, Ph.D. Thesis, University of Kansas, 1964.

(41) J. K. Lee, E. K. C. Lee, B. Musgrave, Y.-N. Tang, J. W. Root, and F. S. Rowland, *Anal. Chem.*, **34**, 741 (1962).

component. However, capillaries in which liquid CH_3F was the major component always exploded when warmed to room temperature and hence could not be irradiated at the ambient temperature of the neutron facility (about 20°). Iodine crystals and LiF were included in each capillary as radical scavenger and tritium source, respectively.

The primary interest in these experiments lay with those mixtures involving CH_3Cl , $c\text{-C}_4\text{H}_8$, or $c\text{-C}_4\text{F}_6$. However, some additional experiments were performed to permit estimation of the excitation-decomposition properties of CH_3Br , as shown in Table I. The CH_3Br system requires further study for clarification of its details, especially since the low yield of CH_2TI in the liquid phase indicates that very few CH_2T radicals are scavenged by I_2 under these conditions. Some preferential reaction with brominated species (*e.g.*, $\text{CH}_2\text{T} + \text{CH}_3\text{Br} \rightarrow \text{CH}_2\text{TBr} + \text{CH}_3$) appears to occur under the liquid-phase conditions.

Table I: Radioactive Products from Recoil Tritium Reactions with Methyl Bromide

	Gas pressure, cm				Liq.	Liq.
	4.5	25.9	71.4			
CH_3Br						
^3He	2.2	2.2	2.2			
I_2	Yes	Yes	Yes	Yes	Yes	
LiF				Yes	Yes	

	Relative product yield (HT = 100)				
	(100)	(100)	(100)	(100)	(181)
HT					
CH_3T	49	56	57	81	}
CH_2TBr	21	28	36	103	
CH_2TI	55	61	54	2	
				2	

Methyl fluoride was also irradiated as a high-pressure ($\sim 5\text{--}10$ atm), I_2 - or Br_2 -scavenged gas, following condensation in a capillary at a low temperature. Many such capillaries exploded on warming (prior to irradiation), and the ratios of product yields were not completely consistent in the survivors. The relative yields in the presence of I_2 scavenger are approximately: CH_2TF , 100; CH_3T , 38; CH_2TI , 13; CHTFI , 9. The small yield of CHTFI relative to CH_2TF suggests that decomposition of excited CH_2TF^* by C-H bond break occurs only to about 9% in the gas phase (and presumably even less in the liquid phase). Discussions of the secondary reactions involved with several other molecules included in this investigation have already been published on the basis of studies in both gas and liquid phases: CH_3Cl ,¹⁶ $c\text{-C}_4\text{H}_8$,³⁵ CH_2Cl_2 ,¹⁸ C_2H_6 ,³⁷⁻³⁹ CH_2F_2 ,^{41,42} and CHF_3 .⁴³

Results and Discussion

In our experiments, we have measured the yields of the various hot substitution reactions with a variety of molecules and are thereby able to study the trends in

the yields found for two different variable-parameter sequences: (1) the T-for-H substitution reaction in CH_3X as X is changed and (2) the T-for-X substitution reaction in CH_3X as X is changed. Trends in the absolute yields at about 1 atm of pressure have previously

Table II: Primary Yields for T-for-H Reaction of Energetic Tritium Atoms, As Estimated from Liquid-Phase Experiments in Methyl Chloride

Molecule, RH	Yield for T-for-H Reaction per C-H Bond vs. T-for-H in Liquid CH_3Cl as Standard			Absolute yield ^a
	Measured yield of RT, %	Cor-rection factor	Estimated primary yield, %	
CH_3F	68 ± 2	1.04 ^c	71 ± 2	4.0
CH_3Cl	(63)	(75/63) ^d	75 ± 3	2.8
CH_3Br	80 ± 6	$\sim 1.02^e$	82 ± 6	3.2
CH_2F_2	53 ± 2	1.20 ^f	64 ± 4	2.8
CH_2ClF	47 ± 4			
CH_2Cl_2	46 ± 5	1.37 ^g	63 ± 5	1.5
CHF_3	47 ± 3	1.20 ^h	56 ± 3	2.9
CHClF_2	47 ± 6			
CH_4	^b			7.7
C_2H_6	83 ± 2			
C_3H_8	81 ± 2	$\sim 10\%^i$	91 ± 5	
$i\text{-C}_4\text{H}_{10}$	80 ± 2			

^a % Absolute yield, in per cent *per bond*, measured in gas phase near 1 atm of pressure.¹⁰ ^b Could not be measured in the liquid phase at 20° . ^c The correction factor is less than 1.09 on the basis of gas-phase measurements of CH_2TFI from CH_3F (see Experimental Section). Assuming that liquid-phase collision frequencies would reduce decomposition still further, we estimate a correction factor only half as large, 1.04 ± 0.02 . ^d We have estimated ~ 3 units of CH_2T radicals arise from decomposition of CH_3T^* and not from CH_2TCl^* and have subtracted this from the 78 given in ref 16. ^e See Table I, which shows $\text{CH}_2\text{TI}/\text{CH}_2\text{TBr}$ as 0.02 in I_2 -scavenged liquid. ^f The ratio of CTF products to CHTF_2 is 0.10 ± 0.03 in the liquid phase.⁴¹ However, the excited CHTF_2^* molecule may also decompose by the isotopically alternate route to $\text{TF} + \text{CHF}$. No measurements appear to have been made of isotope effects for HX elimination from dihalomethanes. They have, however, been measured for the 1,2 elimination of HX from haloethanes and have shown a preference for elimination of HX over DX by a factor of 1.4 with molecules excited by radical-radical combination. If the same isotopic factors were to hold for dihalomethanes, then HX elimination would be favored over TX by a factor of 1.7, and the 0.10 ± 0.03 correction factor would require another 0.06 ± 0.02 for TF elimination. In the absence of actual experimental information on dihalomethanes, we have estimated decomposition at 0.20 ± 0.06 for a correction factor of 1.20 ± 0.06 . ^g Reference 18. The ratio of $\text{CHTClBr}/\text{CHTCl}_2$ in Br_2 -scavenged CH_2Cl_2 is 0.37. ^h Decomposition to $\text{CF}_2 + \text{TF}$ cannot be measured. Since both CHF_3^* and CH_2F_2^* decompose by elimination of HF with similar pyrolytic parameters, we have assumed that equal fractions of CTF_3^* and CHTF_2^* decompose under these conditions and have used the same 1.20 ± 0.06 correction factor for each. ⁱ Experiments show small yields of scavengeable alkyl-*t* radicals, in the order of ~ 0.1 times the parent yield.

(42) Y.-N. Tang and F. S. Rowland, *J. Amer. Chem. Soc.*, **89**, 6420 (1967).

(43) T. Smail and F. S. Rowland, *J. Phys. Chem.*, **74**, 1859 (1970).

been reported for both of these sequences (see Table II) and have been rationalized, respectively, by these separate mechanistic considerations:¹⁰ (1) steric hindrance by larger halogen atoms and (2) increasing reactivity with increasing collision size of the halogens. Our explanations, taking into account the new data available, do not agree in either case with these earlier hypotheses.

Measurements have also been carried out for the study of T-for-X in $\text{CH}_{4-n}\text{X}_n$ as n is varied and will be reported in a separate paper. Some results for T-for-H in $\text{CH}_{4-n}\text{X}_n$ are included with the present data.

Intermolecular Competition in Liquid CH_3Cl . A series of binary and ternary mixtures has been irradiated, each of which has contained methyl chloride as the major component of the mixture. The relative specific activities of the product molecules in these mixtures are given in Table II, expressed as a yield *per bond* relative to that of CH_2TCl from the substitution of T-for-H.⁴⁴ Anticipating the subsequent intercalibration of CH_3Cl and $c\text{-C}_4\text{H}_8$ as standards (see Table III), the observed yield of CH_2TCl from liquid CH_3Cl has been assigned the standard value 63. Table II also lists the absolute percentage yields *per bond* for these reactions in gas-phase experiments with the individual molecules.¹⁰

III. The decomposition of cyclobutane has been very thoroughly studied, and it has been shown that the excited $c\text{-C}_4\text{H}_7\text{T}^*$ molecules have an average excitation energy of about 5 eV, but with a broad distribution such that from 46 to 60% are collisionally stabilized and survive in the 0.1–1.0-atm range and 82% are stabilized in the liquid-phase experiments.³⁵ The decomposition of $c\text{-C}_4\text{H}_7\text{T}^*$ goes cleanly to $\text{CH}_2=\text{CHT}$ (plus an unlabeled C_2H_4) and the yields in Table III are listed with the sum of $c\text{-C}_4\text{H}_7\text{T} + \text{C}_2\text{H}_3\text{T}$ as the standard, set as 100. In experiments with Br_2 present as the scavenger molecule, $\text{CH}_2=\text{CHT}$ is initially formed but is then removed by chemical reaction and is not measured; in these cases, the normalization has been carried out relative to the yield of $c\text{-C}_4\text{H}_7\text{T}$ alone, with the $\text{CH}_2=\text{CHT}$ yield assumed to have the value appropriate for the total pressure in the system. Such binary comparisons with $c\text{-C}_4\text{H}_8$ have previously been used for CH_4 , CH_3F , and CH_3Cl .

Intermolecular Competition in Gaseous $c\text{-C}_4\text{F}_6$. A third set of data has been obtained for energetic tritium atom reactions in the gas phase in a system dominated by bulk quantities of perfluorocyclobutene: $c\text{-C}_4\text{F}_6$, 71; RH, 5; and O_2 , 1.5 cm. These conditions of measurement have been used for standardized comparisons of the abstraction yields from C–H bonds, and the same experiments have frequently permitted simultaneous measurement of the yields of T-for-H and T-for-X products.^{13,15} The data are given in Table IV. Since these experiments involve a moderator without C–H bonds and whose chemical structure probably leads to very different moderator properties, no special utility arises from normalization to values obtained in hydrogenous moderators such as CH_3Cl or $c\text{-C}_4\text{H}_8$. We have instead listed the yields per bond relative to the abstraction of H from CH_4 as 1.00. This is the same standard used in reporting the yields of HT formed by abstraction from various C–H bonds in excess $c\text{-C}_4\text{F}_6$ ^{13,15} and readily permits comparison of the relative yields in this particular system (*e.g.*, from CH_4 , $\text{HT} = 1.00$ and $\text{CH}_3\text{T} = 1.56$; $\text{HT}/\text{CH}_3\text{T} = 0.64 \pm 0.02$). Simple estimates for decomposition of CH_2TX^* molecules are included in Table IV, using the same correction factors applied in Table II. However, there is no assurance at all that decomposition in $c\text{-C}_4\text{F}_6$ and in $c\text{-C}_4\text{H}_8$ should be comparable since both the tritium atom spectra and the probabilities for collisional deexcitation could be very different for two such unlike molecules.

(44) The omission of CH_3I from Table II arises from a severe experimental complication: this molecule captures electrons very efficiently and thereby quenches the operation of a gas proportional counter during the passage of the methyl iodide peak. The quenching effect is so strong that even 10^{-2} times the amount normally used with CH_3F or a hydrocarbon is sufficient to introduce serious errors into the measurement of CH_2TI activity. Measurement of CH_3T from CH_3I is, of course, unaffected and CH_3I is included in Table V. A lower limit on CH_2TI yield in excess perfluorocyclobutene is also given in Table V.

Table III: Primary Yields for T-for-H Reaction of Energetic Tritium Atoms, Estimated from Competition with Cyclobutane in the Gas Phase

Molecule	Observed yield, %	Estimated correction factor for CH_2TX^* decomposition	Original primary yield, %
CH_3F	58 ± 2	$(12.1 + 1.2)/(12.1)^a$	64 ± 3
CH_3Cl	40 ± 1	$(37 + 32)/(37)^b$	75 ± 3
CH_3Br	33 ± 1	$(36 + 49)/(36)^c$	78 ± 5
CH_4	83 ± 3	1.20 ^d	100 ± 5
$c\text{-C}_4\text{H}_8$	(60)	(100/60) ^e	(100)

^a The absolute yields of CH_2TF and CH_2TFI are given in ref 10 as 12.1 and 1.2%, respectively. ^b The relative yields at 1 atm are given in ref 16 as 30, 37, and 34 for CH_3T , CH_2TCl , and CH_2TI in I_2 -scavenged samples. The comparable figures in ref 10 are 32, 37, and 36. We have assumed that decomposition of CH_3T^* will be small and have arbitrarily assigned it as 3 units. Averaging 34 and 36 for CH_2TI , and subtracting 3, we obtain 32 as the yield of CH_2TI from decomposition of CH_2TCl by C–Cl bond break. ^c The yield of CH_2TI in Table I at 1 atm has been arbitrarily assigned as 5 units from decomposition of CH_3T^* and the remainder from decomposition of CH_2TBr^* . ^d The competitive data were measured in ref 35. The most recent value for $\text{CH}_2\text{T}/\text{CH}_3\text{T}$ in methane is 0.20, given in the Seewald-Wolfgang paper cited in ref 34. In ref 16, a slightly smaller factor (0.12) was used, based on the data of ref 6. ^e See ref 35.

Intermolecular Competition with $c\text{-C}_4\text{H}_8$. Competition experiments have also been carried out in the gas phase with CH_3Br –cyclobutane mixtures, as shown in Table

Table IV: Yields for T-for-H and T-for-X Products from Recoil Tritium Reactions with Halomethanes in Gas-Phase Perfluorocyclobutene-Moderated Systems

Standard T* + CH₄ → HT + CH₃; 1.00 per Bond

Molecule ^a	Observed yields, per bond		
	T-for-H	Corrected ^c	T-for-X
CH ₄	1.56 ± 0.04	1.9 ± 0.1	(1.56)
CH ₃ F	0.87 ± 0.04	1.0 ± 0.1	0.84 ± 0.05
CH ₂ F ₂	0.66 ± 0.04		0.20 ± 0.03
CHF ₃	0.48 ± 0.04		0.05 ± 0.02
CH ₃ Cl	0.68 ± 0.05	1.3 ± 0.1	2.0 ± 0.1
CH ₃ Br	0.43 ± 0.10	1.0 ± 0.3	3.6 ± 0.1
CH ₃ I	≥ 0.6 ^b		6.3 ± 0.2

^a Gas pressures: *c*-C₄F₆, 71; RH, 5; O₂, 1.5; and ³He, 1.5 cm.

^b Quenching correction uncertain.⁴⁴ ^c Corrected for estimated secondary decomposition of products (see Table III).

The column of "corrected data" in Table IV is thus of semiquantitative significance, at most.

Factors Affecting the Substitution of T-for-H in CH₃X. Our gas-phase measurements of the observed yields of stabilized tritiated products, as well as the absolute yield data of ref 10 quoted in Table II, both demonstrate marked differences in the per bond yields of the T-for-H products. The decrease in this yield with increasing size of X in CH₃X served as the basis for the postulate of steric hindrance of T-for-H substitution by halogen atoms:¹⁰

"Hot tritium atom substitution for H per C-H bond drops by a factor of 2-3 in the sequence CH₄, CH₃F, CH₃Cl. (No further decrease is observed in going to CH₃Br.) These observations are entirely in accord with the impact model previously described.^{2,4} H abstraction was postulated to proceed primarily by attack approximately axial with the C-H bond. It is thus relatively insensitive to the nature of neighboring substituents on the carbon atom. On the other hand, displacement results from attack more nearly normal to the axis of the C-H bond. It is thus sensitive to steric hindrance by neighboring atoms or groups, the extent of the inhibition depending on the number and size of such atoms. These effects seem clearly evident in both the mono- and dihalomethanes."

"Although there are considerable variations in the strengths of the C-H bonds involved, there seems to be no obvious correlation with any trend in abstraction or displacement. These results tend to confirm further the hypothesis that bond energy effects do not determine the course of the primary reactions of hot hydrogen atoms, and that instead steric effects are dominant."

However, examination of the uncorrected data shows that the maximum fluctuation of a factor of 5 in T-for-H yields of Table III yields among all compounds in the gas phase has been reduced to less than a factor of 2 in

the liquid-phase relative yields in Table II, while the trend of decreasing yield with increasing size of halogen substituent has disappeared. Clearly, the variations found in the gas phase are much more strongly affected by secondary decompositions than they are by substituent effects on the primary reactions themselves.^{16,18,38} Moreover, the reduction in the spread of yields makes corrections for secondary decomposition necessary even for the liquid-phase results.

Correction factors for the decomposition of CH₂TCl*, CH₂TBr*, and CH₂TF* in the liquid phase can be applied through the published data on the former^{16,45-48} and from the data given above for the latter two. These corrected estimates of original primary yield for the substitution of energetic tritium for H in the methyl halides in liquid CH₃Cl competition are also given in Table II. Substitution into these molecules is roughly equivalent for all C-H bonds with differences of only 10-30% in primary yields. However, a small trend for increased primary substitution of T-for-H with larger halogen atoms appears. This mild trend is in the opposite direction anticipated from the steric obstruction hypothesis, while fitting possible alternative hypotheses that T-for-H substitution is favored either by less electronegative substituents or by weaker C-X bonds in CH₃X.

Similar corrections, of larger magnitude, can be made to the observed gas-phase data, as shown in Tables III and IV. Both sets of gas-phase measurements clearly indicate that substitution in CH₃F has a lower yield than substitution into CH₄ or other alkanes and that CH₃Cl and CH₃Br fit plausibly between these two outer values. All of the values in Tables II-IV are consistent with a trend in relative yields CH₄ > CH₃Br > CH₃Cl > CH₃F, although the limits of error are too high for exact placement in the sequence measured *vs.* *c*-C₄F₆.

When methane is included in this series of CH₃X compounds, the trend of increased substitution of T-for-H no longer correlates with the bond dissociation energy but does correlate with generalized functions of the electronegativity of the substituents, as shown in Figure 1, in which the proton nmr shift is used as one measure of electronegativity.⁴⁹ Similar correlations with

(45) The greater decomposition of CH₂TCl* *vs.* CH₂TF* is expected since the C-Cl bond rupture has a much lower energy (84 ± 2 kcal/mol)^{39,46} than that of either the C-H (101 ± 4 kcal/mol) or C-F (108 ± 3 kcal/mol) bonds of the latter. The lesser decomposition of CH₂TBr* is somewhat surprising, since equal excitation energies would produce more decomposition in the bromide, because of the weakness of the C-Br bond (70 ± 2 kcal/mol) than the C-Cl bond. However, the assumption of equivalent excitation energies following T-for-H substitution has been shown to be unjustified for comparisons of *c*-C₄H₈ and CH₄,^{47,48} and could also be inapplicable for CH₂TCl* and CH₂TBr*. The comparison appears to be worthy of further study.

(46) J. A. Kerr, *Chem. Rev.*, **66**, 465 (1966).

(47) Y.-N. Tang and F. S. Rowland, *J. Phys. Chem.*, **72**, 707 (1968).

(48) E. K. C. Lee and F. S. Rowland, *J. Amer. Chem. Soc.*, **85**, 2907 (1963).

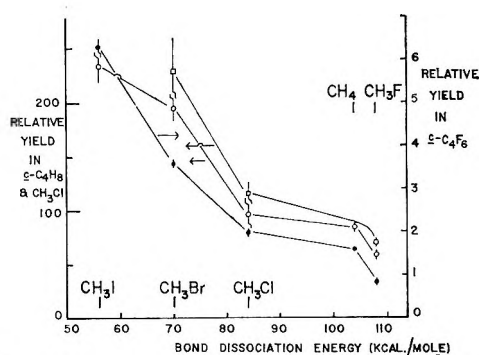


Figure 1.

other measures of electronegativity (including other nmr parameters) have comparable success.⁵⁰ Tables II and IV both include some data for CH_2Cl_2 , CH_2F_2 , and CHF_3 , which are also plotted in Figure 1. The line connecting the data points is drawn as a straight line only for convenience, since there is at this time no theoretical reason predicting either a straight or a curved line, and the yield data are in any event insufficiently accurate to distinguish among such possible choices.

In summary, the basic experimental conclusion from these T-for-H experiments is that they show no evidence in support of the earlier hypothesis of steric hindrance of T-for-H substitution in CH_3X .¹⁰ Instead, a milder trend in influence of the substituent X is found in the opposite direction, correlating well with a postulate that more electronegative substituents reduce the probability of T-for-H substitution. If any steric hindrance to the substitution reaction is actually present, the effects are masked by the more important electronegativity trend. The absence of any appreciable steric hindrance to T-for-H substitution by halogen atoms is consistent with the revised interpretation that such effects are small or nonexistent for alkyl substituents.²⁹⁻³²

The Substitution of T-for-X in CH_3X . The observations of the absolute yields of CH_3T from gas-phase CH_3X demonstrate definite correlations with changes in X in a sequence of CH_3X molecules, as shown in the first row of data in Table V, taken from ref 10. This correlation has been explained as the consequence of another kind of steric effect, the size of the replaced atom X.¹⁰

"There is clearly a moderate trend favoring substitution of heavier halogen atoms, $\text{F} < \text{Cl} < \text{Br}$ [in the series CH_3X]. Such a trend has already been observed in substituted benzoic acids by White and Rowland.¹⁹ There are two obvious explanations for this effect: (1) the weakening of the C-X bond with increasing atomic number of the halogen; (2) the larger collision cross section of the higher halogens which may well be reflected in a larger reaction cross section. White and Rowland favor the first explanation; we tend toward the second."

Comparisons of the relative probabilities of T-for-X reactions with equivalent tritium atom spectra can readily be made by determining the yield of CH_3T from CH_3X in direct competition with cyclobutane. Experimental results for such measurements are shown in the second row of data of Table V. The data of Table IV listed again in the third row of Table V show the same ordering of yields in dilute gas solution in *c*- C_4F_6 ; the yield of CH_3T from CH_3I is especially high in the perfluorocyclobutene sequence. A comparable set of numbers for the liquid-phase competitions with CH_3Cl can only be obtained by an indirect method—by multiplying the T-for-H numbers of Table II by the ratios of yield of T-for-H and T-for-X found in experiments with the pure molecules, thereby assuming that these relative yields will not be changed very much by the differences in the tritium fluxes. These values (fourth row in Table V) are in semiquantitative agreement with the relative values found with the other sets of numbers. All of the new measurements agree well with the correlation observed by Odum and Wolfgang from the absolute yields in the pure compounds.

No corrections have been made in the data of Table V for the possible decomposition of CH_3T^* formed by the substitution of T-for-X in these methyl halides. Calculations of the expected pressure dependence of the decomposition of CH_3T^* , based on RRKM calculations for CH_4 ,⁵¹ indicate that very little difference is anticipated even over wide ranges of variation in pressure. However, if all of the CH_2T radicals scavenged in the CH_4 systems are presumed to arise from the decomposition of CH_3T^* , then an estimate can be made that about 17% of the originally excited CH_3T^* molecules decompose following T-for-H substitution.⁵² In the CH_3X systems, CH_2T radicals can arise from either the decomposition of CH_2TX^* or CH_3T^* and the observed yield of scavengeable CH_2T radicals cannot be unequivocally assigned to either parent molecule, except as an upper limit. Comparisons of the decomposition of CH_2TCl^* formed by T-for-H in CH_3Cl and by T-for-Cl in CH_2Cl_2 indicate that more excitation energy is deposited in the latter case;^{16,17} hence decomposition of CH_3T^* might be greater following T-for-X substitution than the 17% found after T-for-H substitution. Nevertheless, since the changes in Table V are substantially larger than the estimated (15–50%) corrections for secondary decom-

(49) Proton nmr shifts are taken from J. W. Emsley, J. Feeney, and L. H. Sutcliffe, "High Resolution Nuclear Magnetic Resonance," Pergamon Press, London, 1966; and from C. J. Creswell and A. L. Allred, *J. Amer. Chem. Soc.*, **85**, 1723 (1963).

(50) The yield for T-for-H from *c*- C_4H_8 is higher than would be expected from the correlation shown in Figure 1. However, unlike with the other molecules involved in this study, the possible range of motions of two substituents (the C atoms) on a cyclobutane carbon atom is greatly restricted by the existence and maintenance of the four-membered ring.

(51) B. S. Rabinovitch and D. W. Setser, *Advan. Photochem.*, **3**, 1 (1964).

(52) D. Seewald and R. Wolfgang, *J. Chem. Phys.*, **47**, 143 (1967).

Table V: Relative Yields of T-for-X Products from Recoil Tritium Atom Reactions with CH₃X

Molecule, CH ₃ X	CH ₃ -F	CH ₃ -H	CH ₃ -Cl	CH ₃ -Br	CH ₃ -I
Absolute yield, % gas ^a	4.4	7.7	7.1	12.0	
T-for-X in <i>c</i> -C ₄ H ₈ competition	59 ± 3 ^b	85 ± 3 ^c	97 ± 16 ^d	196 ± 12 ^e	234 ± 14 ^e
T-for-X in <i>c</i> -C ₄ F ₆ competition ^f	0.84 ± 0.05	1.56 ± 0.04	2.0 ± 0.1	3.6 ± 0.1	6.3 ± 0.2
Estimated T-for-X in CH ₃ Cl solution	70 ± 2 ^g		117 ± 10 ^h	230 ± 25 ⁱ	
D(C-X), kcal/mol ^j	108 ± 3	104 ± 1	84 ± 2	70 ± 2	56 ± 1
van der Waals radius, Å	1.35	1.20	1.80	1.95	2.15

^a Reference 10. ^b See ref 48. ^c See ref 35. ^d See ref 16. ^e This work. ^f Table IV. ^g In CH₃F: T-for-H, 68 ± 2 × 1.04 (ref 48) ≅ 71 ± 2. ^h In CH₃Cl: T-for-H, (63) × 1.85 (ref 16) ≅ 117 ± 10. ⁱ In CH₃Br: T-for-H, (74) × 3.2 (Table I) ≅ 230 ± 25. ^j Reference 46.

position and because these corrections would tend to cancel out in *relative* yield measurements (especially if the excitation energies of CH₃T* are approximately equivalent from different CH₃X molecules), we assume that the trend shown in Table V would be qualitatively unchanged after suitable correction of the original primary yields for secondary decomposition. The consistently larger values for reactions *vs.* CH₃Cl than for those *vs.* *c*-C₄H₈ reflect some increased stabilization of CH₃T* in the liquid phase but again suggest that secondary decomposition is not perturbing the qualitative ordering of the results.

This trend of increasing yields for replacement of the halogen atom correlates well with both the increasing radius of the halogen atom¹⁰ and with the weakening of the C-X bond.^{19,53} Inclusion of the data for the T-for-H reaction in CH₄ results in fair agreement with the bond dissociation energies but not with the van der Waals radii of the X substituents, as summarized in Table V and Figure 2. The replacement of H is apparently somewhat more frequent than indicated by a smooth correlation with bond dissociation energy, while atomic size alone would predict a yield even lower than from CH₃F.⁵⁴

The observation of a factor of 7.5 increase in the relative yields from CH₃F to CH₃I casts very serious doubt on yield explanations based solely on an increased collision radius of the struck halogen atom. The relative surface areas of the I and F atoms vary only by a factor of 2.5, while the effective radii for T-I and T-F collisions must vary by much less than 2.5. Since the detailed mechanism of substitution of T-for-X is essentially unknown, even the implied postulate that T-for-X substitution reactions begin with T-X collisions could very well be either wrong or misleading, *e.g.*, if T-for-X were to occur by a Walden inversion mechanism, then the X atom would be completely shielded from the approaching T atom throughout the reaction.

Since the halogen atom data correlate well with both collision size and bond energy parameters, no definitive

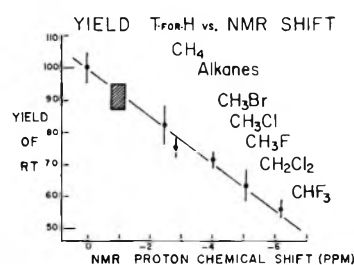


Figure 2.

separation can be made of the contribution of each factor. However, we believe that both (a) the large magnitude of the variation in yield with X and (b) the agreement with the CH₄ data indicate that the more important controlling factor in these T-for-X reactions is the change in bond dissociation energy of the C-X bond. In the sequence of CH₃X compounds in Table V, the substitution reaction shifts from several kcal/mol endothermicity with CH₃F to almost 50 kcal/mol exothermicity with CH₃I. This very substantial change in energetics could result in either (a) a lowered threshold for replacement of I < Br < Cl < F and/or (b) a relaxation of the restrictions upon possible collision parameters when the exiting X atom requires much less energy to detach it from its original bond. Either energetic factor could probably account for the entire variation in yield, while a smaller contribution from collision size might also be included as a factor in the overall control of the dynamics of the reaction.

The effect on T-for-X substitution yields of the weak-

(53) The trend is strongly in the wrong direction for the hypothesis that atom-atom energy transfer between T and X is an important factor, direct transfer of energy from mass 3 to mass 127 should be very inefficient, yet T-for-I is a high probability process. Energy transfer clearly involves highly inelastic molecular collisions.

(54) It should be noted that the substituent H does *not* fit in smoothly with the halogens in a bond energy correlation of the yields from substituted benzoic acids,¹⁹ being high in yield by about a factor of 3-5. However, as pointed out in both ref 10 and 19, the reactions in solid benzoic acids were not scavenged and the substitution reactions may have included T atoms down to thermal kinetic energies.

ening of the C-X bond can essentially be described as a smooth variation in the characteristics of the potential energy surface. The most important aspect of this variation is probably a lowered energy and somewhat shifted location for the substitution saddle point as the reaction becomes more and more exothermic. Since the breaking of a C-I bond will require eventually less energy than the breaking of a C-F bond, the initial trajectories for T-for-I substitution need not be as limited as in those in which the strengthening C-T bond must be accompanied by substantial loosening of the C-F bond. Even in the case of CH_3F , however, the threshold energy for F replacement is only about 35 kcal/mol⁵⁵ indicating that the C-T bond forming and C-F bond breaking occur simultaneously. The somewhat anomalous position of H on Figure 2 probably reflects a dynamic effect in addition to the effect on the potential energy surface. The more rapid response of H to changing force fields of this surface could facilitate the substitution process and result in higher yields than would be obtained for substitution on a (hypothetical) surface of the same shape but with X much heavier than H.²⁶

Dynamics of Substitution Reactions. Although an initially plausible description was offered based on the various components of the "impact model,"^{5,6,10} the detailed dynamics of T-for-H and T-for-X displacement reactions are essentially unknown. Some initial trajectory calculation studies have been made which illustrate several crude characteristics of hot reactions,⁵⁶⁻⁵⁸ but the potential energy surfaces used to date have not been realistic even for CH_4 . In the more elaborate six-particle study of $\text{T} + \text{CH}_4$, in fact, the apparent yield of the substitution reaction was far below the known experimental values.^{57,58}

The results obtained in these experiments offer some additional information that needs to be encompassed in any detailed, general prescription of the substitution dynamics. First, the essential absence of steric obstruction of the substitution of T-for-H by either alkyl or

halogen substituents places certain geometric limitations upon the potentially successful trajectories of approach of the energetic tritium atoms to the reactant molecules. These limitations are not particularly severe, however, involving mostly the denial of high-angle approaches (crudely, $>90^\circ$ relative to the C-H axis of the H atom to be replaced), for which bulky substituents could be obstructions.

Second, during the critical dynamic period during the possible exit of one H atom and possible bond formation for the recoil T atom, seemingly small changes in the "chemical" environment apparently are very influential in determining whether the collision ends with no C-H bond and/or no C-T bond. A highly electronegative substituent such as F could well serve as a sink for electron density released by the gradual displacement and departure of the H atom, leaving less electron density in the vicinity of the incipient C-T bond, with a consequent reduction in the probability that such a bond would actually form. This redistribution of electron density would of course be reflected in the potential energy surface itself. Formulations of the substitution process that emphasize only physical characteristics such as atomic masses, atomic sizes, bond angles, angles of attack, etc., appear to be inadequate for explanation of the full range of data now available. Adequate treatments will require inclusion of some direct bond energy effects in substitution as well as abstraction, in addition to the secondary influences of the electronegativities of the neighboring substituent atoms *not* being replaced.

(55) C. C. Chou, D. Wilkey, and F. S. Rowland, presented at the 160th National Meeting of the American Chemical Society, Chicago, Ill., Sept 1970.

(56) P. J. Kuntz, E. M. Nemeth, J. C. Polanyi, and W. H. Wong, *J. Chem. Phys.*, **52**, 4654 (1970).

(57) D. L. Bunker and M. Pattengill, *Chem. Phys. Lett.*, **4**, 315 (1969).

(58) D. L. Bunker and M. Pattengill, *J. Chem. Phys.*, **53**, 3041 (1970).

Complete Retention of Configuration during the Replacement of Hydrogen by Energetic Tritium in *dl*- and *meso*-(CHFCl)₂¹

by G. F. Palino and F. S. Rowland*

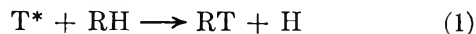
Department of Chemistry, University of California, Irvine, California 92664 (Received July 27, 1970)

Publication costs assisted by Division of Research, U. S. Atomic Energy Commission

The stereochemistry of the substitution of energetic tritium for H has been studied with *dl*- and *meso*-(CHFCl)₂. In the gas phase, the direct substitution reactions proceed with >99% retention of configuration at the asymmetric carbon atoms. No positive evidence has been found for the existence of a direct gas-phase substitution mechanism for T-for-H with inversion of configuration. The "inversion" products are formed from radical combination reactions in experiments without scavenger in the gas phase or with I₂ as scavenger in the liquid phase. Comparison of the relative T-for-H yields indicates that substitution in CH₄ is consistent with results for other molecules such as Si(CH₃)₄, (CH₃)₃CH, etc. By this indirect comparison, the inversion mechanism is postulated to occur with negligible yield for CH₄ despite the small mass of each substituent.

Introduction

The substitution for the hydrogen atom of a C-H bond by an energetic tritium atom from nuclear recoil, as in eq 1, has been demonstrated to occur in good yield with a large variety of organic molecules.²⁻⁵ Previous studies have shown that this displacement reaction occurs with higher collisional efficiency than



thermal reactions⁶ and with nearly complete retention of configuration at the symmetric carbon atom in both the crystalline⁷⁻⁹ and gaseous phases.¹⁰⁻¹²

The results of the experiments in crystalline samples with glucose^{7,8} and with L-(+)-alanine,⁹ although quite suggestive that substitution occurs chiefly with retention of configuration, might not be directly applicable to gaseous-phase experiments since the crystalline structure surrounding the reactant molecule could exert a "template" effect hampering the formation of any molecule except one with the configuration of the original reactant molecule. The possibility of "cage effects" in the solid and liquid phases may also further complicate the interpretation of results.^{13,14} On the other hand, the tritium-labeled molecules formed in gas-phase experiments, while free from the possible configurational constraints of surrounding molecules, do frequently undergo extensive secondary decomposition. The surviving molecules in such experiments must preferentially represent those formed with lower excitation energies and could conceivably not represent accurately the primary distribution of configurations formed by the initial hot reactions with energetic tritium atoms.

Most previous experiments have involved numerous chemical manipulations and separations involving optically active molecules, followed by degradation procedures permitting determination of the intramolecular

distribution of the substituted tritium atoms. Such experiments of necessity require very high specific radioactivities and consequently also involve more extensive radiation damage during the longer irradiation periods necessary for production of these higher activities. The use of target molecules with more than one asymmetric center obviates the necessity for resolution of optical isomers from a racemic mixture, since inversion at one optical center will produce the meso compound from *dl* mixture, etc. The use of volatile target compounds permits the ready application of gas chromatography to the separation problem. Such gas chromatographic separation techniques were first applied to the similar problem of retention or inversion of configuration during the substitution of energetic ³⁸Cl into *dl*- and *meso*-2,3-dichlorobutane (DCB).¹³⁻¹⁶

(1) This research was supported by A.E.C. Contract No. AT-(04-3)-34, Agreement No. 126.

(2) R. Wolfgang, *Progr. React. Kinet.*, **3**, 97 (1965).

(3) R. Wolfgang, *Ann. Rev. Phys. Chem.*, **16**, 15 (1965).

(4) *Chem. Eff. Nucl. Transform., Proc. Symp., 1964*, **1**, 2 (1965).

(5) F. Schmidt-Bleek and F. S. Rowland, *Angew. Chem., Int. Ed. Engl.*, **3**, 769 (1964).

(6) M. Henchman, D. Urch, and R. Wolfgang, *Can. J. Chem.*, **38**, 1722 (1960).

(7) F. S. Rowland, C. N. Turton, and R. Wolfgang, *J. Amer. Chem. Soc.*, **78**, 2354 (1956).

(8) H. Keller and F. S. Rowland, *J. Phys. Chem.*, **62**, 1373 (1958).

(9) J. G. Kay, R. P. Malsan, and F. S. Rowland, *J. Amer. Chem. Soc.*, **81**, 5050 (1959).

(10) M. Henchman and R. Wolfgang, *ibid.*, **83**, 2991 (1961).

(11) Y.-N. Tang, C. T. Ting, and F. S. Rowland, *J. Phys. Chem.*, **74**, 675 (1970).

(12) C. T. Ting and F. S. Rowland, *ibid.*, **74**, 445 (1970).

(13) C. M. Wai, C. T. Ting, and F. S. Rowland, *J. Amer. Chem. Soc.*, **86**, 2525 (1964).

(14) F. S. Rowland, C. M. Wai, C. T. Ting, and G. Miller, *Chem. Eff. Nucl. Transform., Proc. Symp., 1964*, **1**, 333 (1965).

(15) C. M. Wai and F. S. Rowland, *J. Phys. Chem.*, **71**, 2752 (1967).

(16) C. M. Wai and F. S. Rowland, *ibid.*, **74**, 434 (1970).

The recent experiments involving recoil tritium reactions with *dl*- and *meso*-2,3-DCB, performed at low radiolytic conversion, have again demonstrated that the T-for-H substitution reaction occurs very preferentially with retention of configuration.¹¹ However, a precise determination of the limiting values for the per cent retention-inversion at the asymmetric carbon atoms was not possible without a determination of the intramolecular distribution of the tritium atoms. Estimates of the upper limits upon inversion were placed at $\leq 7\%$ for reaction with *dl*-2,3-DCB and $\leq 20\%$ for reaction with *meso*-2,3-DCB. The observation of clearly defined "opposite isomer" peaks—but of mechanistically doubtful origin^{11,16}—made it desirable to perform additional gas-phase experiments on a system which required neither extensive chemical handling nor determination of the intramolecular tritium distribution. The target molecules chosen for this study were *dl*- and *meso*-(CHFCI)₂, which contain hydrogen bonded only to the asymmetric carbon atoms and which can be readily separated and analyzed by conventional radio gas chromatography. Experiments have been carried out with these molecules and a variety of free radical scavengers in both the gaseous and liquid phases.

Experimental Section

A mixture of *dl*- and *meso*-(CHFCI)₂ was obtained from Peninsular ChemResearch, Inc., and subjected to preliminary preparative purification on a Carbowax 20M column, eliminating most of the minor impurities. None of our experiments differentiated in any way between *l*- and *d*-(CHFCI)₂ and all descriptions assume that we were dealing at all times with an optically inactive *dl* mixture. Final purification and isolation of the *dl* and *meso* isomers was performed in a two-step procedure using a 50-ft 20% Carbowax 300 column operating at 62° and a helium flow rate of 60 cm³/min. A purity of >99.6% was obtainable for each isomer. A minor unidentified impurity (<0.4%) with a gas chromatographic retention time intermediate between the *dl* and *meso* peaks on the Carbowax column was the chief impurity remaining in each of the purified diastereomers. Substitution of energetic tritium for hydrogen also took place into this impurity compound during irradiation but in amounts roughly comparable to the mole fractions of each component and therefore involving only very small (<0.4%) corrections to the observed tritium activities in the molecules of interest. Identification of the diastereomers was made from boiling point differences (as reflected in relative retention times on several gas chromatographic columns known to separate alkyl halides chiefly in the order of their boiling points) and by comparison of ir and nmr spectral data with the available literature.¹⁷

Gaseous and liquid samples using ³He and LiF, respectively, as the source of recoil tritium²⁻⁵ were prepared in standard manner and were irradiated for 12

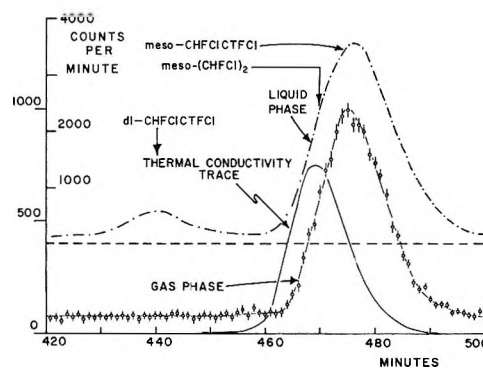


Figure 1. Radio gas chromatograms of CHFCICTFCl molecules from the reactions of recoil tritium with *meso*-(CHFCI)₂: —, thermal conductivity trace, O₂-scavenged gas phase; ○, radioactivity, O₂-scavenged gas phase; - - -, radioactivity, I₂-scavenged liquid phase, with — as the zero base line.

min in the rotating Lazy Susan of a TRIGA reactor operating at a power level of 250 kW and a neutron flux of approximately 1×10^{12} n/(cm² sec). All other chemicals used in sample preparation are commercially available and were used without further purification.

The irradiated samples were analyzed by conventional radio gas chromatography:¹⁸ the peaks of interest (*i.e.*, *dl*- and *meso*-CHFCICTFCl) were satisfactorily separated on the 50-ft Carbowax column, operating at a helium flow rate of 30 cm³/min and at a temperature of 60°, as shown in Figure 1. The minor impurity peak can be seen as a slight shoulder on the leading edge of both the mass (453 min) and radioactivity (458 min) records of the gas-phase experiment. The radioactivity peak of *meso*-CHFCICTFCl is shown emerging approximately 5 min (474 min *vs.* 469 min) later than that of *meso*-(CHFCI)₂. A time differential of about 1 min exists in the data recording of the thermal conductivity and proportional counter detectors, but the major source of the difference in retention times is a hydrogen isotope effect of about 0.8%, giving a longer retention time for the tritiated isomer. A comparable isotope effect exists for the tritiated and ordinary *dl* compounds. While such isotope effects have been regularly observed in our radio gas chromatographic procedures,¹⁹ this is the first time we have reported an isotope effect for an alkyl halide.

Results

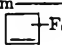
Scavenger Experiments. The pertinent results relating to the stereochemistry of the T-for-H substitution reaction with *dl*- and *meso*-(CHFCI)₂ are summarized in Tables I and II. A direct comparison of the re-

(17) E. G. Bissell and D. B. Fields, *J. Org. Chem.*, **29**, 1591 (1964).

(18) J. K. Lee, E. K. C. Lee, B. Musgrave, Y.-N. Tang, J. W. Root, and F. S. Rowland, *Anal. Chem.*, **34**, 741 (1962).

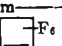
(19) J. W. Root, E. K. C. Lee, and F. S. Rowland, *Science*, **143**, 676 (1964).

Table I: Relative Yield of Diastereomers from Reactions of Recoil Tritium with *meso*-(CHFCI)₂

Phase	Sample composition, cm			³ He	Relative yield of <i>dl</i> -(CHFCI) ₂ meso = 100.0
	meso	Scavenger			
Gas	15.2			1.4	9.4 ± 0.5
Gas	14.5	O ₂ (4.5)		1.4	0.7 ± 0.4
Gas	15.3	$\left\{ \begin{array}{l} \text{O}_2 (4.7) \\ \text{C}_2\text{H}_4 (3.3) \end{array} \right\}$			-0.6 ± 0.8
Gas	13.9		H ₂ S (4.9)	70.7	1.2
Gas	13.5	$\left\{ \begin{array}{l} \text{O}_2 (5.3) \\ 1,3\text{-C}_4\text{H}_6 \\ (4.8) \end{array} \right\}$	66.2	1.2	0 ± 4
Liquid			I ₂		LiF

^a Observed relative yield 9.4 ± 0.2. Corrected for 3.7% macroscopic isomerization.

Table II: Relative Yield of Diastereomers from Reactions of Recoil Tritium with *dl*-(CHFCI)₂

Phase	Sample composition, cm			³ He	Relative yield of <i>meso</i> -(CHFCI) ₂ <i>dl</i> = 100.0
	<i>dl</i>	Scavenger			
Gas	12.9			1.3	18.1 ± 1.2
Gas	12.9	O ₂ (5.1)		1.3	2.1 ± 1.4
Gas	12.9	O ₂ (5.2)	60.0	1.3	5 ± 4
Liquid		I ₂		LiF	19.6 ± 0.3 ^a

^a Observed relative yield 21.3 ± 0.3. Corrected for 1.7% macroscopic isomerization.

sults obtained with an O₂-scavenged gas-phase sample and an I₂-scavenged liquid-phase sample, both with the *meso* compound as substrate, is shown in Figure 1. The replacement reaction is observed to occur exclusively (>99%) with retention of configuration at the asymmetric center in each of the gas-phase experiments with adequate scavengers to eliminate thermal radical processes. Within the statistical counting errors, the addition of 1 atm of *c*-C₄F₆ in both O₂- and H₂S-scavenged samples failed to produce a statistically significant yield of the inversion product. Measurable yields, however, of the "inversion products" were found in the unscavenged gaseous systems and in I₂-scavenged liquid-phase experiments. It is possible that slight "inversion" peaks were present in the samples scavenged by O₂ alone. However, any inversion product should be consistently present in all samples and its clear absence in one or more samples is sufficient to invalidate the direct inversion mechanism. Small inversion peaks in O₂-scavenged samples may indicate a slight inefficiency in scavenging, as observed with 2,3-DCB.¹¹

In the gaseous experiments, the macroscopic level (<0.3%) of the other diastereomer did not appear to increase as the result of radiation damage during the neutron irradiation, and therefore no corrections to the

data for macroscopic amounts of the opposite isomer were possible because of the difficulty in obtaining an accurate measurement of this quantity. The I₂-scavenged liquid-phase samples did show measurable macroscopic isomerization during irradiation, and the observed isomeric yields are corrected for this isomerization in Tables I and II.

Competition Experiments. Competition experiments were also performed in which equimolar mixtures of *meso*-(CHFCI)₂ and CH₄ (~5 cm each) were mixed with 70 cm of perfluorocyclobutene acting as a bath molecule to standardize the tritium atom flux. The substitution yields in each molecule were measured and the labeled *meso* compound was found to have a yield of 33 ± 3, per C-H bond, relative to CH₃T from CH₄ as 83. Recent experiments have shown that the substitution yield in an individual C-H bond correlates rather successfully with the proton nmr shift of the H atom replaced; CHF₃, which has an nmr shift very similar to that of (CHFCI)₂, has a substitution yield of 56 relative to 100 for CH₃T from CH₄, with both values corrected for secondary decomposition.^{20,21} Since the correction for decomposition of CH₃T is 20% (83 → 100), it seems quite probable that the original primary yield for the formation of CHFCICTFCl is approximately 56 ± 5 and the observed 33 ± 4 represents about 60% stabilization under these gas-phase experimental conditions.

Photochemical Experiments. Some experiments were also attempted with tritium atoms possessing 2.8 eV of initial energy from the photolysis of TBr.²² However, these experiments showed that the yield for the substitution of 2.8-eV tritium atoms into (CHFCI)₂ was negligibly small—the *dl* and *meso* peaks summed together represented about 0.1% of the observed organically bound tritium. Moreover, since the *meso*/*dl* ratio of radioactivities was essentially identical (~5) from either the *meso* or *dl* parent molecules and since numerous other labeled organic molecules were formed in the photolytic system, we believe that even this very small fraction of observed CHFCICTFCl activity arose from incomplete scavenging of the reactants for radical-radical reactions. The threshold energy for substitution of T-for-H into these molecules is apparently high enough that the direct one-step substitution has an undetected yield for tritium atoms with an initial kinetic energy of 2.8 eV. The threshold energy for the substitution of T-for-H in solid cyclohexane has been estimated as ~1 eV,²³ while the threshold for replacement of D in CD₄ is about 1.6 eV.²⁴ Both of these cross

(20) F. S. Rowland, E. K. C. Lee, and Y.-N. Tang, *J. Phys. Chem.*, **73**, 4024 (1969).

(21) Y.-N. Tang, E. K. C. Lee, E. Tachikawa, and F. S. Rowland, *ibid.*, **75**, 1290 (1971).

(22) C. C. Chou and F. S. Rowland, *J. Chem. Phys.*, **50**, 5133 (1969).

(23) M. Menzinger and R. Wolfgang, *J. Amer. Chem. Soc.*, **89**, 5992 (1967).

(24) C. C. Chou and F. S. Rowland, *J. Chem. Phys.*, **50**, 2762 (1969).

sections rise rapidly with increasing kinetic energy above the threshold.

Discussion

Evidence for Retention of Configuration. The results of these gas-phase experiments with *dl*- and *meso*-(CHFCl)₂ confirm that the predominant mechanism of energetic substitution of T-for-H involves a retention of configuration at the sp³ carbon atom and are completely consistent with the results of earlier experiments as summarized in Table III. Our measurement

Table III: Results of Stereochemical Experiments Involving Recoil Tritium Reactions at Asymmetric Carbon Positions

A. Experiments with Crystalline Materials	
(1) T* + glucose → glucose- <i>t</i> + H	(ref 7)
Yield 12%; retention of configuration.	
(2) T* + glucose → galactose- <i>t</i> + H	(ref 8)
Yield <0.02%; no inversion observed at no. 4 carbon atom.	
(3) T* + L-(+)-alanine → alanine- <i>t</i> + H	(ref 9)
At asymmetric CH position	
Yield L-(+) 19 D-(-) 0 ± 1 } 95 ± 5% retention	
B. Experiments with Gases	
(4) T* + 2-butanol → 2-butanol- <i>t</i> + H	(ref 10)
At asymmetric CH position: 90 ± 10% retention.	
(5) T* + 2,3-dichlorobutane →	
2,3-dichlorobutane- <i>t</i> + H (ref 11)	
(a) From <i>dl</i> parent, <i>meso/dl</i> = 0.012 ± 0.003.	
Estimated at asymmetric CH position	
≥93% retention.	
(b) From <i>meso</i> parent, <i>dl/meso</i> = 0.046 ± 0.005.	
Estimated at asymmetric CH position	
≥80% retention.	
(6) T* + 1,3-dimethylcyclobutane →	
1,3-dimethylcyclobutane- <i>t</i> + H (ref 12)	
(a) From <i>cis</i> parent, <i>trans/cis</i> = 0.010 ± 0.002.	
Estimated at asymmetric CH position	
>94% retention.	
(b) From <i>trans</i> parent, <i>cis/trans</i> = 0.007 ± 0.001.	
Estimated at asymmetric CH position	
>96% retention.	
(7) T* + (CHFCl) ₂ → CHFClCTFCl + H	(this work)
(a) From <i>dl</i> parent, <i>meso/dl</i> = 0.021 ± 0.014.	
>97.6% retention.	
(b) From <i>meso</i> parent, <i>dl/meso</i> = -0.006 ± 0.008.	
>99.5% retention.	

of the yield of product corresponding to an inversion mechanism is, however, substantially more accurate than in any previous experiment and leads to the conclusion that retention of configuration is not only the predominant mechanism in energetic substitutions by tritium atoms but it appears to be the *exclusive* mech-

anism in this system. Only the recent gas-phase experiments with 2,3-dichlorobutane¹¹ and 1,3-dimethylcyclobutane¹² (1,3-DMC) have shown convincing positive evidence for the presence of small radioactivity yields corresponding to the inversion products. We discount immediately the observation of the labeled *cis*-1,3-DMC-*t* from T* + *trans*-1,3-DMC (and *vice versa*) as evidence for direct, one-step inversion processes, for these isomerizations as well as the decompositions to two molecules of propylene are well known thermally and the parent *trans*- and *cis*-1,3-DMC-*t* molecules formed by T-for-H substitution have been shown to have sufficient energy to undergo both the isomerization and the decomposition (with observation of propylene-*t* as a product).¹² We also believe that the "inversion" products found in the 2,3-DCB experiments are not the result of single-step substitutions with inversion but rather arise from radical combination processes with inversion occurring in one of the radicals. The earlier experiments on hot ³⁸Cl reactions with 2,3-DCB showed that prevention of radical-radical reactions is very difficult in that system:¹⁶ for example, they persist strongly in the presence of both O₂ and CH₂=CH₂ and were not fully suppressed with a scavenger mixture of O₂ and 1,2-butadiene. The exact nature of these difficult to suppress radical-radical reactions is not known, but they may involve atomic Cl as one constituent. We believe therefore that there does not exist any positive evidence in any gaseous system for the existence of an inversion pathway for single-step substitution by energetic T atoms.

The failure to detect experimentally any inversion in gas-phase experiments is strongly suggestive that no direct inversion reactions occur but should be viewed more conservatively since most studies of T-for-H substitutions provide evidence for substantial secondary decomposition of primary products.^{2-5,25,26} Some of the experiments, notably the study of T* + CH₃NC,²⁶ show that essentially all substitutions are accompanied by 2-3-eV excitation energy. If, in a hypothetical mechanism, the direct gas-phase substitutions of T-for-H with inversion were always accompanied by the deposition with the product molecule of vibrational energies greater than certain minimum energies, then *all* of the inversion products would also undergo secondary decomposition, and not be in disagreement with the experimental observations.

The yields of the other radioactive products from hot tritium reactions in (CHFCl)₂ have not been quantitatively evaluated, and positive identification has not been made for some of the compounds observed by radio gas chromatography. Several products are apparently haloethylenes, presumably resulting from the

(25) E. K. C. Lee and F. S. Rowland, *J. Amer. Chem. Soc.*, **85**, 897 (1963).

(26) C. T. Ting and F. S. Rowland, *J. Phys. Chem.*, **72**, 763 (1968).

elimination of HF or HCl from the primary products formed by the original substitution of tritium for H, F, or Cl in the target molecule (at least 11 such di- or trihaloethylenes are readily possible by this mechanism). The minimum energy for essentially complete decomposition of CHFCICTFCl in the time available can be estimated by analogy with other fluoro- and chloroethanes as about 7–8 eV, although no kinetic parameters are yet available for either (CHFCI)₂ molecule. Since energies in the 7–8-eV range have been found in other T-for-H substitutions, the existence of high vibrational energy inversion processes without observable gas-phase survival is not an implausible hypothesis.

The present experimental situation to date can then be summarized. All gas-phase studies of T-for-H substitution at an asymmetric C–H position show that the reaction occurs with retention of configuration about the carbon atom. Any direct substitution of T-for-H with inversion of configuration must occur with a much higher threshold energy and follow a mechanistic path leading to very high internal excitation energy and secondary decomposition, for none of the stabilized product molecules has been detected.

Inversion Products in Condensed-Phase and Unscavenged Gas-Phase Experiments. From Tables I and II and Figure 1, it is evident that a significant yield of the inversion product occurs both in the I₂-scavenged liquid-phase and in the unscavenged gas-phase experiments. In both cases, the yield of the labeled *meso*-CHFCICTFCl is greater from the *dl*-(CHFCI)₂ parent than is that of the labeled *dl* isomer from the *meso* parent. As indicated above, the CHFCICTFCl molecule from the T-for-H substitution reaction is sufficiently excited to undergo secondary decomposition unless collisionally stabilized, and a crude estimate of 40% decomposition can be made for the gas-phase experiments by analogy with related systems. In the liquid phase, less decomposition is anticipated, but still 15–25% of the molecules may decompose.^{2–5,25,26}

The decomposition paths for (CHFCI)₂ do not appear to have been established experimentally, but both C–Cl bond break and HF elimination mechanisms are probably present for the recoil activated molecules. After decomposition by C–Cl bond break in the liquid phase, the resultant Cl atom and CHFCICTF (or CHFCITFCl) radical may be held in close proximity by the surrounding cage of solvent molecules. The recombination of Cl with the radical may then occur in competition with racemization of the radical, as postulated earlier for ³⁸Cl + CH₃CHCHClCH₃.^{13,14}

In addition, if a higher energy inversion mechanism were also to exist, the higher density and shorter collision times of the liquid systems could result in stabilization of some molecules which were originally formed with 7–8 eV of vibrational energy. The observed liquid-phase yields represent the sum of the contribu-

tions from either or both of these postulated processes.

In the gas phase without the surrounding cage of solvent molecules, recombination of a radical with the lost Cl atom is less probable per decomposed molecule, but a much larger fraction of labeled molecules actually decompose, and the overall effect on diastereomer production is about the same. The *meso* compound is thermodynamically a little more stable, and the *meso*/*dl* ratio from such radical processes may approach the value of 5 found in the photochemical studies.

Stereochemistry of Substitution at Carbon Atoms with Light Substituents. All of the experiments to date have required three unlike substituents other than H or D on the asymmetric carbon atom and must therefore involve retention *vs.* inversion with three heavy (*i.e.*, not H or D) substituents. Can the observed experimental results be generalized to molecules with one or more light substituents? And in the limiting case, what can be said about the stereochemistry of the substitution process with CH₄?

It is quite clear that no laboratory experiment (excluding computer laboratories) on the stereochemistry of T* + CH₄ will be feasible for many years. However, trajectory calculations have been performed for the specific case of T* + CH₄ and are not subject to the ordinary laboratory limitations on stereochemical feasibility, although they are still seriously restricted by computational difficulties.^{27–29} In the first study of T* + CH₄,²⁷ the trajectories were considered essentially as three-body point-mass calculations for T, H, and R of mass 15, and substitution processes corresponding to inversion processes were prominently observed. Since the methyl radical in this case had no structure, bonding of the incoming T atom to it was possible from all angles, independent of the (unspecified) location of the existing bonds.

In a later study of T* + CH₄, the trajectory calculations involved six atoms moving separately but with a more complex potential function for the H atom ("target" H) nearest to the T atom than for the other three ("backside") H atoms.^{28,29} By the nature of this simplified potential energy surface, substitutions by the Walden inversion kind of mechanism are not permitted to occur. The reaction of trajectories in this study which led to the formation of HT by abstraction was consistent with the results of laboratory experiments; however, the fraction of substitution reactions leading to CH₃T was much too low in comparison with the experimental results. A much larger number of events was observed, designated as "tracking errors of the second kind," in which the tritium atom successively

(27) P. J. Kuntz, E. M. Nemeth, J. C. Polanyi, and W. H. Wong, *J. Chem. Phys.*, **52**, 4654 (1970).

(28) D. L. Bunker and M. Pattengill, *Chem. Phys. Lett.*, **4**, 315 (1969).

(29) D. L. Bunker and M. Pattengill, *J. Chem. Phys.*, **53**, 3041 (1970).

approached closely to one and then another H atom, etc., until the accumulated errors involved in switching between the "target" potential function and the "back-side" potential function finally destroyed the accuracy of the calculation and caused the trajectory to be terminated. These terminated trajectories, ending with the tritium atom shifting around near two or three H atoms, have led to the speculation that similar trajectories calculated with a more elaborate and satisfactory potential might then disclose the existence of a substantial fraction of Walden inversion substitutions.^{28, 29}

In the absence of direct experiments on the stereochemistry of $T^* + CH_4$, indirect comparisons can be made of the observed yields of the T-for-H reaction with CH_4 and with other target molecules. As indicated above, these T-for-H yields correlate well with the proton nmr shifts of the C-H bonds involved,^{20, 21} *i.e.*, with the electronegativity of the other C-atom substituents. Since this correlation successfully includes such molecules as CH_4 , $Si(CH_3)_4$, $(CH_3)_3CH$, CH_3F , and CHF_3 , it seems reasonable to us to conclude that the mechanisms of T-for-H substitution for each are all similar or at least vary in some smooth manner with the electronegativity of the substituents. The substitution yield, per C-H bond, is not much larger (about 20%) in CH_4 than in the tertiary C-H of isobutane^{20, 30} and is slightly less than that in $Si(CH_3)_4$.²⁰

One reasonable hypothesis is that the existence of an inversion mechanism for molecules with light substituents would most reasonably be accompanied by a decrease in yield *not* in substitution with retention but in some other process, most probably inelastic scattering. In other terminology, the trajectories with angles, energies, etc., such that (hypothetically) inversion is observed with CH_4 would not lead to substitution at all for tertiary C-H in isobutane, presumably because the three heavy CH_3 groups moved too slowly for possible formation of a new C-T bond in the time available. Instead, the trajectories might involve substantial energy transfer to the C-H bonds but eventually would terminate with nonreactive scattering of the tritium atom. If this hypothesis is correct, then the yield of CH_3T from CH_4 should be anomalously high (*vs.* tertiary C-H) to the extent that the inversion mechanism was supplementing the established yield by the retention mechanism. Therefore, since the CH_3T yield is apparently *not* anomalously high but in fact fits neatly into the place estimated from pnmr shifts, we postulate that with *all* C-H bond systems, the yield from the inversion mechanism for T-for-H substitution is negligibly small when compared to that from the retention mechanism. An obvious corollary to this hypothesis is that the improved trajectory calculations for $T + CH_4$ now in progress will show that no substantial yield of inversion reactions lies concealed within the "trajectories of the second kind."²⁹

Alternate hypotheses are certainly feasible, although

somewhat less plausible to us. In particular, it is possible that the inversion mechanism occurs especially easily with the four light substituents of CH_4 and then rapidly disappears as heavier substituents replace the H atoms. If the methane inversion yield were not large (up to $\sim 10\%$ of reaction yield), then the incremental yield might not be detectable within the accuracy of the electronegativity correlation, and no experimental inconsistencies would result. It is also possible that the substitution-with-retention mechanism is adversely affected by small mass substituents unable to absorb as much energy of the incoming tritium atom as CH_3 or C_2H_5 groups,³¹ with the result that the cross section for higher energy reactions drops off more rapidly for CH_4 than for other molecules. In this case, the increased yield for substitution-with-inversion would be approximately balanced by a decrease in substitution-with-retention and again no experimental inconsistency would result. While such a balancing of an increase in one mechanism and a decrease in another such that no appreciable deviation is observed seems improbable to us, it is certainly not impossible and could be the actual situation. We have reached an experimental impasse with this problem which will not be easily removed since its resolution requires retention-inversion experiments with CH_4 or some other molecule containing several small mass substituents.

Some Aspects of the Retention Mechanism. Any current model for the description of T-for-H substitutions must include rationalization of (a) the observed dependence of yield upon the electronegativity of substituents, (b) the high vibrational energy of labeled product molecules, and (c) the retention of configuration during the process. The high vibrational energies suggest that the attached groups (and especially the T atom itself) are usually appreciably displaced from equilibrium molecular positions at the time of separation of the replaced H atom from the residual molecule. Some motion of both light and heavy substituents may be necessary to reach these unusual positions, and the time scale for such motion is in the 10^{-14} to 10^{-13} sec range. The process of substitution of T-for-H could conceivably occur in a time as short as $\sim 10^{-14}$ sec, and the failure to observe inversion would then rationally follow, for the heavy substituents could not move fast enough to make an electron orbital available near the tritium atom. However, the substitution of ^{38}Cl -for-Cl also goes with complete retention of configuration, and the inertial motions of originally thermal Cl atoms

(30) An experimental study of the stereochemistry of the gas-phase substitution of T for CH_3 in $CH_3CFCICHFCI$ has not been successful since secondary decomposition of the resulting $CTFCICHFCI^*$ is apparently nearly complete. (Secondary decomposition of methylcyclobutane-*t* is 98% complete after the T-for- CH_3 reaction with 1,3-dimethylcyclobutane in the gas phase.¹²)

(31) See C. C. Chou and F. S. Rowland, *J. Phys. Chem.*, **75**, 1283 (1971), for details of experiments with isotopic methanes.

are *not* fast compared with H, CH₃, etc.¹⁶ Furthermore, the hot substitutions of recoil T for heavier groups (such as CH₃, F, Cl, etc.) also proceed in good yield,²⁻⁵ and the escape of the replaced heavy atom must take place on a time scale of almost 10⁻¹³ sec, long enough for several vibrations of each C-H bond in the reacting molecule. We postulate that the failure to observe an inversion mechanism is more involved with the difficulties in getting several groups into simultaneous rapid motion than it is in the great rapidity of the T/H time scale. In this view, the reaction *is* fast, ($\sim 10^{-13}$ sec), but some heavy groups *do* move appreciably while the substitution is occurring—the dynam-

ical requirements for simultaneous rapid acceleration of several heavy substituents are severe, apparently severe enough to reduce the probability of such a reaction to the negligible level. The substitution of T-for-H with retention certainly also requires the acceleration of one or more additional groups to account for the high vibrational energies but is enough less restrictive to permit substitution to occur. This conceptual approach suggests that the substitution of tritium for CH₃, F, or other heavy group will probably also be found to proceed with retention of configuration,³⁰ even though this time scale cannot approach the 10⁻¹⁴-sec time scale conceivable for T-for-H substitution.

The Prediction of Osmotic and Activity Coefficients in Mixed-Electrolyte Solutions

by P. J. Reilly,* R. H. Wood,

Department of Chemistry, University of Delaware, Newark, Delaware 19711

and R. A. Robinson

Department of Chemistry, State University of New York, Binghamton, New York 13901 (Received August 21, 1970)

Publication costs assisted by Office of Saline Water, U. S. Department of the Interior

The equations of Reilly and Wood for the prediction of free energy have been used to derive expressions for the osmotic and activity coefficients of many-component charge-asymmetric mixtures of electrolytes. Two levels of approximation are available with the equations. In the first level of approximation only data on single-salt solutions are used. In the full equations data on common ion mixtures of electrolytes are used. The first level of approximation is used to predict activity coefficients in mixtures of hydrochloric acid with alkaline earth perchlorates. A comparison with the experimental results of Stokes and Stokes and of Weeks show that the predictions are superior to those of the ionic strength principle. The full equations are applied to mixtures of three cations with a common anion. The results are compared with experimental measurements on the following systems: LiCl-NaCl-KCl, LiCl-NaCl-CsCl, and LiCl-NaCl-BaCl₂ reported in this paper; NaCl-KCl-BaCl₂ reported by Robinson and Bower; and HCl-CsCl-BaCl₂ reported by Lietzke, Hupf, and Stoughton. In all cases the predictions agree with the experimental measurements to within the experimental error.

Introduction

In a recent paper¹ the authors presented an equation for the prediction of the excess free energy of any mixed-electrolyte solution. The equation used Friedman's² approach to mixed electrolytes and predicts the free energy, heat content, volume, etc., of any mixture of electrolytes from measurements on pure solutions and common ion mixtures. The equation correctly accounts for all pairwise interactions.

The purpose of this paper is to derive the corresponding equations for the osmotic and activity coeffi-

cients and to show how these equations can be used to predict the properties of mixtures with more accuracy than has previously been possible.

As an example of their use the equations are used to predict the trace activity coefficient of any electrolyte in a solution of another electrolyte. If the trace elec-

* Correspondence to be addressed to University of Lethbridge, Lethbridge, Alberta, Canada.

(1) P. J. Reilly and R. H. Wood, *J. Phys. Chem.*, **73**, 4292 (1969).

(2) H. L. Friedman, "Ionic Solution Theory," Interscience, New York, N. Y., 1962.

trolyte and the supporting electrolyte have a common ion, the situation is the same as that investigated by Harned³ and the equation is of the same form as the Harned equation. Stokes and Stokes⁴ and also Weeks⁵ have obtained experimental data on the more general case with no common ion. Even using only the terms involving single-salt solutions the equation predicts the experimental results much more accurately than the principle of ionic strength.

As a further test the full equations (including terms involving two-salt mixtures) were used to predict the properties of mixtures containing three cations and a common anion. The difference between the predictions and the measured values was less than the experimental error in the measurements.

Results and Discussion

The derivations of the equations for the osmotic and activity coefficients of many-component electrolyte solutions are given in the Appendix. Given the equations of Reilly and Wood, the derivation is straightforward, although tedious. Equation A-6 gives the osmotic coefficient and A-9 the activity coefficient for a general mixture in terms of the osmotic and activity coefficients of pure electrolyte solutions at the same ionic strength (ϕ^0 and γ^0) and interactions between pairs of electrolytes (g_{MN^X}). The symbols in these equations are defined in eq A-1a to A-1e. Ionic strength (I) and equivalents per kilogram of solvent (E) are the basic concentration scales. Equations A-6 and A-9 can be used for any mixture of electrolytes. In this paper the equations will be applied to two types of mixtures: (1) mixtures of two salts without a common ion (MX with NY); (2) mixtures of three salts with a common anion (LX, MX, and NX). Specific equations will be derived for these cases but first it is useful to derive the equations for the simplest possible case: two salts with a common ion (MX and NX). If the mixture is formed at constant ionic strength by adding y kg of solvent containing the salt MX to $(1 - y)$ kg of solvent containing the salt NX then, the final solution contains a mixture of the three ions in 1 kg of solvent. The concentrations of the three ions are

$$m^M = \frac{2Iy}{Z^M(Z^M - Z^X)}$$

$$m^N = \frac{2I(1 - y)}{Z^N(Z^N - Z^X)}$$

$$m^X = -\frac{2Iy}{Z^X(Z^M - Z^X)} - \frac{2I(1 - y)}{Z^X(Z^N - Z^X)}$$

If these values are used to calculate the quantities required for eq A-6, then eq 1 results.

$$\frac{[Z^M - (Z^M - Z^N)y]}{Z^M Z^N Z^X} (1 - \phi) =$$

$$\frac{y}{Z^M Z^X} (1 - \phi^0_{MX}) + \frac{(1 - y)}{Z^N Z^X} (1 - \phi^0_{NX}) + \frac{y(1 - y)I}{2} \left\{ g_{MN^X} + I \frac{\partial}{\partial I} (g_{MN^X}) \right\} \quad (1)$$

Substitution into eq A-9 gives

$$\ln \gamma_{\pm}^{MX} = \ln \gamma^0_{MX} + (1 - y) \times \left[1 - \phi^0_{MX} - \frac{Z^M}{Z^N} (1 - \phi^0_{NX}) \right] - \frac{1}{2} Z^M Z^X (1 - y) I \left[g_{MN^X} + y I \frac{\partial}{\partial I} (g_{MN^X}) \right] \quad (2a)$$

and

$$\ln \gamma_{\pm}^{NX} = \ln \gamma^0_{NX} + y \left[-\frac{Z^N}{Z^M} (1 - \phi^0_{MX}) + 1 - \phi^0_{NX} \right] - \frac{1}{2} Z^N Z^X y I \left[g_{MN^X} + (1 - y) I \frac{\partial}{\partial I} (g_{MN^X}) \right] \quad (3a)$$

Equations 2a and 3a can be used to describe the trace activity coefficient of one salt in a solution of the other. If the value of y becomes zero, eq 2a gives

$$(\ln \gamma_{\pm}^{MX})_{\text{trace}} = \ln \gamma^0_{MX} + \left[1 - \phi^0_{MX} - \frac{Z^M}{Z^N} (1 - \phi^0_{NX}) \right] - \frac{1}{2} Z^M Z^X I g_{MN^X} \quad (2b)$$

while a value of 1 for y converts eq 3a to

$$(\ln \gamma_{\pm}^{NX})_{\text{trace}} = \ln \gamma^0_{NX} + \left[-\frac{Z^N}{Z^M} (1 - \phi^0_{MX}) + 1 - \phi^0_{NX} \right] - \frac{1}{2} Z^N Z^X I g_{MN^X} \quad (3b)$$

These equations are of the same form as the Harned relations. It is interesting that in this case the trace activity coefficient depends on the activity coefficient of the pure electrolyte in a solution of the same ionic strength. This result is due to the common ion and does not apply to a trace activity if there is no common ion. This is because when both ions are present in trace amounts (no common ion), they will never interact with each other because of their very small concentrations.

Equations for the MX, NY System. The trace activity coefficient of the salt MX in a solution of the salt NY is obtained by applying eq A-9 to a mixture of the two salts and then reducing the concentration of MX to zero. The result is

(3) See for example H. S. Harned and B. B. Owen, "The Physical Chemistry of Electrolytic Solutions," 3rd ed, Reinhold, New York, N. Y., 1958.

(4) J. M. Stokes and R. H. Stokes, *J. Phys. Chem.*, **67**, 2442 (1963).

(5) I. A. Weeks, *Aust. J. Chem.*, **20**, 2367 (1967).

$$\begin{aligned} \frac{(Z^M - Z^X)}{Z^M Z^X} (\ln \gamma_{\pm}^{MX})_{\text{trace}} = & \\ \frac{(Z^M - Z^Y)}{Z^M Z^Y} (1 - \phi_{MY}^0 + \ln \gamma_{MY}^0) + & \\ \frac{(Z^N - Z^X)}{Z^N Z^X} (1 - \phi_{NX}^0 + \ln \gamma_{NX}^0) - & \\ \frac{(Z^N - Z^Y)}{Z^N Z^Y} (1 - \phi_{NY}^0 + \ln \gamma_{NY}^0) - & \\ \frac{(Z^M - Z^X)}{Z^N Z^Y} (1 - \phi_{NY}^0) - & \\ \frac{I}{2} \{ (Z^M - Z^Y) g_{MN}^Y + (Z^N - Z^X) g_{XY}^N \} & \quad (4) \end{aligned}$$

While equations similar to eq 2 and 3 have been applied to common ion mixtures, very little work has been done on systems of the type described by eq 4. The literature contains some data on metal perchlorate-hydrochloric acid systems^{4,5} and it is of interest to see how the predictions of eq 4 compare with the experimental data. The data provide a severe test of the equation since the mixture is not symmetric—the cations involved being magnesium, calcium, strontium, and barium. The trace activity coefficient of hydrochloric acid in an alkaline earth perchlorate solution is given by

$$\begin{aligned} (\ln \gamma_{\pm}^{HCl})_{\text{trace}} = (1 - \phi_{HClO_4}^0 + \ln \gamma_{HClO_4}^0) + & \\ \frac{3}{4} (1 - \phi_{NCl_2}^0 + \ln \gamma_{NCl_2}^0) - & \\ \frac{3}{4} (1 - \phi_{N(ClO_4)_2}^0 + \ln \gamma_{N(ClO_4)_2}^0) - & \\ \frac{1}{2} (1 - \phi_{N(ClO_4)_2}^0) + & \\ \frac{I}{4} \{ 2g_{H,N}^{ClO_4} + 3g_{Cl,C lO_4}^N \} & \quad (4a) \end{aligned}$$

while the trace activity coefficient of the alkaline earth perchlorate in hydrochloric acid is given by

$$\begin{aligned} (\ln \gamma_{\pm}^{N(ClO_4)_2})_{\text{trace}} = (1 - \phi_{NCl_2}^0 + \ln \gamma_{NCl_2}^0) + & \\ \frac{4}{3} (1 - \phi_{HClO_4}^0 + \ln \gamma_{HClO_4}^0) - & \\ \frac{4}{3} (1 - \phi_{HCl}^0 + \ln \gamma_{HCl}^0) - & \\ 2(1 - \phi_{HCl}^0) + \frac{I}{3} \{ 3g_{H,N}^{Cl} + 2g_{Cl,C lO_4}^H \} & \quad (4b) \end{aligned}$$

Weeks has measured the activity coefficient of HCl in $HClO_4$ so that $g_{Cl,C lO_4}^H$ can be calculated. Unfortunately the properties of the other common ion mixtures are not known. It is still of interest to see how accurate the equations are when the term involving measurements on mixtures (the last term) is dropped from the equation and only the properties of single-salt solutions are used to predict the activity coefficients of the mixtures. This is equivalent to assuming the excess free energy of mixing is zero (Young's rule)⁶ at

constant molal ionic strength for common ion mixtures specified by eq 4.

Tables I-VIII give the approximate values of the

Table I: Trace Activity Coefficient of Hydrochloric Acid in Magnesium Perchlorate Solution⁵

Ionic strength	Activity coeff		
	Exptl ^a	Calcd ^b	Calcd ^c
0.01	0.904	0.910	0.905
0.04	0.835	0.841	0.842
0.1	0.782	0.790	0.796
0.2	0.742	0.754	0.767
0.3	0.721	0.732	0.756
0.4	0.706	0.721	0.755
0.5	0.695	0.715	0.757
0.6	0.689	0.712	0.763
0.7	0.684	0.713	0.772
0.8	0.681	0.712	0.783
1.0	0.677	0.718	0.809
1.5	0.677	0.747	0.897
2.0	0.689	0.789	1.009
2.5	0.706	0.850	1.147
3.0	0.724	0.926	1.316

^a The trace activity coefficient as reported by Weeks.⁵ ^b Calculated from eq 4a using only the osmotic and activity coefficients of the single-salt solutions, *i.e.*, the first 4 terms of eq 4a. ^c Activity coefficient of the pure electrolyte at the same ionic strength. (Except where noted the properties of pure electrolyte solutions, required for these computations, were taken from R. A. Robinson and R. H. Stokes, "Electrolyte Solutions," 2nd ed (revised), Butterworths, London, 1970.)

Table II: Trace Activity Coefficients of Hydrochloric Acid in Calcium Perchlorate Solution⁴

Ionic strength	Activity coeff		
	Exptl ^a	Calcd ^b	Calcd ^c
0.1	0.782	0.789	0.796
0.3	0.726	0.731	0.756
0.6	0.704	0.712	0.763
1.0	0.712	0.717	0.809
1.4	0.734	0.737	0.876
2.0	0.788	0.786	1.009
3.0	0.913	0.911	1.316
3.3	0.956	0.960	1.434

^a The trace activity coefficients as reported by Stokes and Stokes.⁴ ^b Calculated from eq 4a using only the osmotic and activity coefficients of the single salt solutions, *i.e.*, the first 4 terms of eq 4a. ^c Activity coefficient of the pure electrolyte at the same ionic strength.

trace activity coefficients from eq 4a and 4b (without the last term) together with the actual trace activity coefficients. It is possible to use the equations in this paper to give quite an accurate first approximation for the activity coefficient of a salt in a mixture even if the

(6) T. F. Young and M. B. Smith, *J. Phys. Chem.*, **58**, 716 (1954).

Table III: Trace Activity Coefficient of Hydrochloric Acid in Strontium Perchlorate Solution⁵

Ionic strength	Activity coeff		
	Exptl ^a	Calcd ^b	Calcd ^c
0.01	0.904	0.908	0.905
0.04	0.835	0.842	0.842
0.1	0.782	0.794	0.796
0.2	0.747	0.759	0.767
0.3	0.728	0.742	0.756
0.4	0.718	0.734	0.755
0.5	0.712	0.729	0.757
0.6	0.710	0.727	0.763
0.7	0.709	0.729	0.772
0.8	0.710	0.729	0.783
1.0	0.714	0.737	0.809
1.5	0.748	0.766	0.897
2.0	0.792	0.809	1.009
2.5	0.845	0.864	1.147
3.0	0.912	0.912	1.316
3.5	0.989	1.042	1.518

^a The trace activity coefficient as reported by Weeks.⁵ ^b Calculated from eq 4a using only the osmotic and activity coefficients of the single-salt solutions, *i.e.*, the first 4 terms of eq 4a. ^c Activity coefficient of the pure electrolyte at the same ionic strength.

Table IV: Trace Activity Coefficient of Hydrochloric Acid in Barium Perchlorate Solution⁵

Ionic strength	Activity coeff		
	Exptl ^a	Calcd ^b	Calcd ^c
0.01	0.904	0.909	0.905
0.04	0.835	0.840	0.842
0.1	0.782	0.793	0.796
0.2	0.747	0.754	0.767
0.3	0.723	0.736	0.756
0.4	0.718	0.725	0.755
0.5	0.712	0.720	0.757
0.6	0.708	0.716	0.763
0.7	0.705	0.712	0.772
0.8	0.705	0.716	0.783
1.0	0.709	0.721	0.809
1.5	0.735	0.744	0.897
2.0	0.778	0.784	1.009
2.5	0.828	0.848	1.147
3.0	0.880	0.893	1.316
3.5	0.941	0.965	1.518
4.0	1.000	1.047	1.762

^a The trace activity coefficient as reported by Weeks.⁵ ^b Calculated from eq 4a using only the osmotic and activity coefficients of the single-salt solutions, *i.e.*, the first 4 terms of eq 4a. ^c Activity coefficient of the pure electrolyte at the same ionic strength.

only information available is in the standard tables of osmotic and activity coefficients of single-electrolyte solutions. The equations also show that for more accurate predictions only the common ion mixtures of electrolytes need be measured.

There are a number of other approximations available for estimating the activity coefficients in a mixed-electrolyte solution.

Table V: Trace Activity Coefficient of Magnesium Perchlorate in Hydrochloric Acid Solution⁵

Ionic strength	Activity coeff		
	Exptl ^a	Calcd ^b	Calcd ^c
0.01	0.814	0.815	0.819
0.04	0.700	0.709	0.714
0.1	0.620	0.632	0.640
0.2	0.567	0.582	0.595
0.3	0.544	0.558	0.577
0.4	0.533	0.553	0.573
0.5	0.529	0.550	0.569
0.6	0.530	0.548	0.565
0.7	0.534	0.551	0.566
0.8	0.540	0.553	0.567
0.9	0.549	0.567	0.576
1.0	0.560	0.577	0.583
1.5	0.634	0.647	0.633
2.0	0.737	0.752	0.706
2.5	0.867	0.888	0.802
3.0	1.020	1.076	0.925

^a The trace activity coefficient as reported by Weeks.⁵ ^b Calculated from eq 4b using only the osmotic and activity coefficients of the single-salt solutions, *i.e.*, the first 4 terms of eq 4b. ^c Activity coefficient of the pure electrolyte at the same ionic strength (ionic strength principle).

Table VI: Trace Activity Coefficient of Calcium Perchlorate in Hydrochloric Acid Solution⁴

Ionic strength	Activity coeff		
	Exptl ^a	Calcd ^b	Calcd ^c
0.01	0.817	0.814	0.819
0.04	0.705	0.708	0.711
0.1	0.627	0.629	0.634
0.25	0.564	0.560	0.566
0.5	0.543	0.542	0.540
0.7	0.547	0.539	0.530
1.0	0.572	0.561	0.535
2.0	0.740	0.716	0.606
3.0	1.040	1.006	0.743
4.0	1.553	1.497	0.944

^a The trace activity coefficient as reported by Weeks.⁵ ^b Calculated from eq 4b using only the osmotic and activity coefficients of the single-salt solutions, *i.e.*, the first 4 terms of eq 4b. ^c Activity coefficient of the pure electrolyte at the same ionic strength.

The simplest approximation is the ionic strength principle⁷ which gives the trace activity coefficient the same value as the activity coefficient of the pure electrolyte at the same ionic strength. Tables I–VIII give the values of the activity coefficient indicated by the ionic strength principle. Using only osmotic and activity coefficients from single-salt solutions eq 4a and 4b are consistently better than the ionic strength principle.

(7) G. N. Lewis and M. Randall, "Thermodynamics and Free Energies of Chemical Substances," McGraw-Hill, New York, N. Y., 1923.

Table VII: Trace Activity Coefficient of Strontium Perchlorate in Hydrochloric Acid Solution⁵

Ionic strength	Activity coeff		
	Exptl ^a	Calcd ^b	Calcd ^c
0.01	0.810	0.814	0.817
0.04	0.689	0.708	0.705
0.1	0.602	0.628	0.620
0.2	0.547	0.577	0.559
0.3	0.522	0.551	0.528
0.4	0.510	0.544	0.515
0.5	0.504	0.540	0.504
0.6	0.502	0.535	0.494
0.7	0.504	0.536	0.489
0.8	0.506	0.536	0.485
0.9	0.514	0.548	0.488
1.0	0.521	0.556	0.489
1.5	0.577	0.612	0.507
2.0	0.661	0.700	0.537
2.5	0.772	0.814	0.582
3.0	0.912	0.971	0.638

^a The trace activity coefficient as reported by Weeks.⁵ ^b Calculated from eq 4b using only the osmotic and activity coefficients of the single-salt solutions, *i.e.*, the first 4 terms of eq 4b. ^c Activity coefficient of the pure electrolyte at the same ionic strength.

Table VIII: Trace Activity Coefficient of Barium Perchlorate in Hydrochloric Acid Solution⁵

Ionic strength	Activity coeff		
	Exptl ^a	Calcd ^b	Calcd ^c
0.01	0.809	0.813	0.817
0.04	0.690	0.707	0.705
0.1	0.555	0.627	0.619
0.2	0.535	0.572	0.556
0.3	0.507	0.547	0.524
0.4	0.491	0.538	0.508
0.5	0.482	0.533	0.494
0.6	0.477	0.526	0.481
0.7	0.475	0.526	0.473
0.8	0.475	0.523	0.465
0.9	0.477	0.534	0.464
1.0	0.480	0.539	0.462
1.5	0.519	0.587	0.462
2.0	0.584	0.665	0.472
2.5	0.674	0.767	0.480
3.0	0.793	0.903	0.513
3.5	0.946	1.072	0.539

^a The trace activity coefficient as reported by Weeks.⁵ ^b Calculated from eq 4b using only the osmotic and activity coefficients of the single-salt solutions, *i.e.*, the first 4 terms of eq 4b. ^c Activity coefficient of the pure electrolyte at the same ionic strength.

Another approximation is that of Guggenheim.⁸ Since this equation treats only cation-anion pairs and ignores cation-cation and anion-anion pairs, it is not capable of precision at high ionic strengths. The restrictions imposed by this equation on the ion-size parameter are also unnecessary and are absent from the equations presented in this paper. More recently Guggenheim⁹ has proposed an equation which includes

pairs formed by two ions of the same charge type but this equation is only valid for mixtures of univalent electrolytes and in addition it approximates the properties of pure electrolytes with a linear deviation function at high concentrations.

Scatchard¹⁰ proposed equations for mixtures of electrolytes but the amounts of pure electrolytes to be taken to make the mixture are not specified. The prediction of the properties of the mixture will depend on the amounts of pure electrolytes chosen. A later equation of Scatchard¹¹ defines the components exactly. Before these equations can be tested, the same approximations will have to be made and the appropriate expressions for activity and osmotic coefficients derived.^{11a}

Equations for the LX, MX, NX System. This section will be concerned with the case of a mixture of three cations and one anion. The simplest case is a mixture of univalent ions. Equation A-6 applied to the osmotic coefficient of a mixture of LiCl, NaCl, and CsCl becomes

$$\phi = \frac{E^{Li}}{I} \phi_{LiCl}^0 + \frac{E^{Na}}{I} \phi_{NaCl}^0 + \frac{E^{Cs}}{I} \phi_{CsCl}^0 + \frac{E^{Li} E^{Na}}{I} \left[g_{Li,Na}^{Cl} + I \frac{\partial}{\partial I} (g_{Li,Na}^{Cl}) \right] + \frac{E^{Li} E^{Cs}}{I} \left[g_{Li,Cs}^{Cl} + I \frac{\partial}{\partial I} (g_{Li,Cs}^{Cl}) \right] + \frac{E^{Na} E^{Cs}}{I} \left[g_{Na,Cs}^{Cl} + I \frac{\partial}{\partial I} (g_{Na,Cs}^{Cl}) \right] \quad (5)$$

This equation shows how the osmotic coefficient of a mixture containing three cations and one anion can be predicted from the osmotic coefficients of the pure electrolytes and measurements on two-salt mixtures. In the case of a mixture of equal amounts of all three cations eq 5 can be reformulated in terms of the osmotic coefficients of the pure electrolytes (ϕ_{LiCl}^0 , etc.) and the osmotic coefficients of 50:50 mixtures of two salts ($\phi_{LiCl-NaCl}$, etc.). The result is

$$9\phi_{LiCl-NaCl-CsCl} = 4[\phi_{LiCl-NaCl} + \phi_{LiCl-CsCl} + \phi_{NaCl-CsCl}] - \phi_{LiCl}^0 - \phi_{NaCl}^0 - \phi_{CsCl}^0 \quad (6)$$

In order to test the prediction for univalent cations, the isopiestic method already used for mixtures of two salts¹² was easily extended to mixtures of three salts.

- (8) E. A. Guggenheim, "Thermodynamics," 3rd ed, North-Holland, Amsterdam, 1957; *Phil. Mag.*, **19**, 588 (1935).
- (9) E. A. Guggenheim, *Trans. Faraday Soc.*, **62**, 3446 (1966).
- (10) G. Scatchard, *J. Amer. Chem. Soc.*, **83**, 2636 (1961).
- (11) G. Scatchard, *ibid.*, **90**, 3124 (1968).
- (11a) NOTE ADDED IN PROOF. This has been done. See G. Scatchard, R. M. Rush, and J. S. Johnson, *J. Phys. Chem.*, **74**, 3786 (1970).
- (12) R. A. Robinson, *ibid.*, **65**, 662 (1961).

Table IX: Isopiestic Measurements on Binary and Ternary Salt Mixtures at 25°

(A) The binary system: NaCl-CsCl. $m_{\text{NaCl}} = m_{\text{CsCl}} = m/2$			(D) The ternary system: LiCl-NaCl-KCl. $m_{\text{LiCl}} = m_{\text{NaCl}} = m_{\text{KCl}} = m/3$		
m_{ref}^a	m	ϕ	m_{ref}^a	m	ϕ
2.7093	3.0000	0.9268	2.9349	2.8950	1.0553
2.7221	3.0140	0.9277	(3.0534)	3.0000	1.0677
2.7671	3.0620	0.9308	3.0903	3.0342	1.0709
			3.1660	3.0963	1.0802

At $m = 3$, $\phi_{\text{LiCl}}^0 = 1.2847$,^b $\phi_{\text{NaCl}}^0 = 1.0453$,^c $\phi_{\text{KCl}}^0 = 0.9367$.^c
 $(\phi_{\text{LiCl}}^0 + \phi_{\text{NaCl}}^0 + \phi_{\text{KCl}}^0)/3 = 1.0889$. $\phi_{\text{LiCl-NaCl}} = 1.1683$,^d
 $\phi_{\text{LiCl-KCl}} = 1.0659$, $\phi_{\text{NaCl-KCl}} = 0.9783$.^{a,f} Hence, $\phi_{\text{LiCl-NaCl-KCl}}$
calculated by eq 6 = 1.0648.

(B) The ternary system: LiCl-NaCl-CsCl. $m_{\text{LiCl}} = m_{\text{NaCl}} = m_{\text{CsCl}} = m/3$			(E) The ternary system: LiCl-NaCl-CsCl. $m_{\text{LiCl}} = 0.3256 m$, $m_{\text{NaCl}} = 0.3244 m$, $m_{\text{CsCl}} = 0.3500 m$				
m_{ref}^a	m	ϕ	m_{ref}^a	m	ϕ	ϕ , calcd 1	ϕ , calcd 2
2.9003	2.9751	1.0126					
(2.9250)	3.0000	1.0143	4.5088	4.7102	1.1045	1.2117	1.1073
3.0242	3.1011	1.0209	4.9910	5.2325	1.1359	1.2586	1.1397

At $m = 3$, $\phi_{\text{LiCl}}^0 = 1.2847$,^b $\phi_{\text{NaCl}}^0 = 1.0453$,^c $\phi_{\text{CsCl}}^0 = 0.8809$.^b
 $(\phi_{\text{LiCl}}^0 + \phi_{\text{NaCl}}^0 + \phi_{\text{CsCl}}^0)/3 = 1.0703$. $\phi_{\text{LiCl-NaCl}} = 1.1683$,^d
 $\phi_{\text{LiCl-CsCl}} = 0.9917$,^b $\phi_{\text{NaCl-CsCl}} = 0.9268$. Hence, $\phi_{\text{LiCl-NaCl-CsCl}}$
calculated by eq 6 = 1.0151.

$\phi(\text{calcd 1}) = 0.3526 \phi_{\text{LiCl}}^0 + 0.3244 \phi_{\text{NaCl}}^0 + 0.3500 \phi_{\text{CsCl}}^0$.
 $\phi(\text{calcd 2})$ by means of eq 5, using data for the binary systems
LiCl-NaCl,^d LiCl-CsCl,^b and NaCl-CsCl.^g

(C) The binary system: LiCl-KCl. $m_{\text{LiCl}} = m_{\text{KCl}} = m/2$			(F) The ternary system: LiCl-NaCl-BaCl ₂ . $I_{\text{LiCl}} = 0.3339I$, $I_{\text{NaCl}} = 0.3328I$, $I_{\text{BaCl}_2} = 0.3333I$				
m_{ref}^a	m	ϕ	m_{ref}^a	I	ϕ	ϕ , calcd 1	ϕ , calcd 2
2.9868	2.9360	1.0636	1.8776	2.1371	1.0295	1.0383	1.0308
(3.0495)	3.0000	1.0659	2.8743	3.1888	1.1215	1.1383	1.1217
3.0816	3.0328	1.0677	2.9834	3.2973	1.1337	1.1494	1.1315

$\phi(\text{calcd 1})$ by eq 7 using only the osmotic coefficients of the
single-salt solutions.
 $\phi(\text{calcd 2})$ by eq 7 using osmotic coefficients of the single-salt
solutions and also the terms for the binary mixtures LiCl-NaCl,^d
LiCl-BaCl₂,^b NaCl-BaCl₂.^h

^a In all cases, sodium chloride was the reference salt. Values in parentheses are interpolated. ^b R. A. Robinson, unpublished.
^c R. A. Robinson and R. H. Stokes, "Electrolyte Solutions," 2nd ed (revised), Butterworths, London, 1970. ^d R. A. Robinson,
R. H. Wood, and P. J. Reilly, *J. Chem. Thermodyn.*, in press. ^e R. A. Robinson, *J. Phys. Chem.* **65**, 662 (1961). ^f R. M. Rush and
R. A. Robinson, *J. Tenn. Acad. Sci.*, **43**, 22 (1968). ^g R. M. Rush, Oak Ridge National Laboratory Report 4402. ^h See Table X.

All salts were recrystallized twice from water. Isopiestic vapor pressure measurements using sodium chloride as the reference salt gave values of the osmotic coefficient of the mixed-salt solutions. The results of these measurements are given in Table IX. For the ternary system LiCl-NaCl-CsCl at $m = 3.000$, $\phi = 1.0143$ in good agreement with the prediction of eq 6, $\phi(\text{calcd}) = 1.0151$ (Table IXB). Similar results are obtained for this system using eq 5 at $m = 4.7102$ and 5.2325 (Table IXE). Equation 6 also predicts the LiCl-NaCl-KCl system accurately at $m = 3.000$ (Table IXD). The choice of eq 5 or 6 for prediction of these mixtures is a matter of convenience.

Robinson and Bower¹³ have reported measurements of the osmotic coefficients of NaCl-KCl-BaCl₂ mixtures using the isopiestic method. For this mixture eq A-6 becomes

$$\phi = \frac{2E^{\text{Na}}}{m} \phi_{\text{NaCl}}^0 + \frac{2E^{\text{K}}}{m} \phi_{\text{KCl}}^0 + \frac{3E^{\text{Ba}}}{2m} \phi_{\text{BaCl}_2}^0 +$$

$$\frac{E^{\text{Na}}E^{\text{K}}}{m} \left[g_{\text{Na,K}^{\text{Cl}}} + I \frac{\partial}{\partial I} (g_{\text{Na,K}^{\text{Cl}}}) \right] +$$

$$\frac{3}{2} \frac{E^{\text{Na}}E^{\text{Ba}}}{m} \left[g_{\text{Na,Ba}^{\text{Cl}}} + I \frac{\partial}{\partial I} (g_{\text{Na,Ba}^{\text{Cl}}}) \right] +$$

$$\frac{3}{2} \frac{E^{\text{K}}E^{\text{Ba}}}{m} \left[g_{\text{K,Ba}^{\text{Cl}}} + I \frac{\partial}{\partial I} (g_{\text{K,Ba}^{\text{Cl}}}) \right] \quad (7)$$

In order to test this equation it is necessary to have values of the bracketed terms in eq 7. These were derived from the measurements of Robinson and

(13) R. A. Robinson and V. E. Bower, *J. Res. Nat. Bur. Stand.*, **69A**, 365 (1965).

Table X: Isopiestic Equilibrium in NaCl–BaCl₂ Solutions

Concn of NaCl, <i>m</i>	Concn of BaCl ₂ , <i>m</i>	Ionic strength	Osmotic coeff	$g_{\text{NaBa}}^{\text{Cl}} + I \frac{\partial}{\partial I} (g_{\text{NaBa}}^{\text{Cl}})$
0.3591	0.1045	0.6726	0.9006	+0.01894
0.2213	0.2037	0.8324	0.8818	+0.02637
0.0794	0.3060	0.9974	0.8629	+0.05489
0.4033	0.0736	0.6241	0.9078	+0.03194
0.2797	0.1628	0.7681	0.8901	+0.02581
0.1453	0.2597	0.9244	0.8719	+0.03680
0.7382	0.1644	1.2314	0.9232	+0.00966
0.4910	0.3378	1.5044	0.9112	+0.00551
0.2610	0.4999	1.7607	0.8994	−0.00118
0.9479	0.1963	1.5368	0.9366	+0.00178
0.6389	0.4092	1.8665	0.9289	+0.00044
0.3356	0.6193	2.1935	0.9202	−0.00270
1.1653	0.2730	1.9843	0.9557	−0.00444
0.7442	0.5586	2.4200	0.9513	−0.00557
0.2721	0.8790	2.9091	0.9462	−0.00924
1.4141	0.1421	1.8404	0.9599	−0.01046
0.9784	0.4356	2.2852	0.9572	−0.00530
0.5259	0.7414	2.7501	0.9536	−0.00620
1.3930	0.3219	2.3587	0.9758	−0.00612
1.0035	0.5821	2.7498	0.9754	−0.00725
0.4308	0.9647	3.3249	0.9748	−0.01014
1.2466	0.4905	2.7181	0.9850	−0.00421
0.7037	0.8501	3.2540	0.9867	−0.00409
0.3073	1.1124	3.6445	0.9882	−0.00113
1.5471	0.3006	2.4489	0.9853	−0.00305
1.0496	0.6303	2.9405	0.9868	−0.00467
0.5733	0.9452	3.4089	0.9887	−0.00315
1.8885	0.1878	2.4519	0.9941	−0.00970
1.3509	0.5407	2.9730	0.9979	−0.00798
0.7850	0.9136	3.5258	1.0010	−0.01013
0.3184	1.2206	3.9802	1.0038	−0.01487
1.0177	0.7670	3.3187	1.0010	−0.00844
0.7602	0.9375	3.5727	1.0019	−0.01140
0.4557	1.1377	3.8688	1.0038	−0.01414
0.3008	1.2396	4.0196	1.0048	−0.01662
1.9192	0.1845	2.4727	0.9956	−0.01046
1.3574	0.5542	3.0200	0.9989	−0.01045
0.8234	0.9060	3.5414	1.0018	−0.01350
0.3348	1.2274	4.0170	1.0048	−0.02127
1.7350	0.4108	2.9674	1.0088	−0.01158
1.1799	0.7744	3.5031	1.0130	−0.01360
0.5922	1.1591	4.0695	1.0176	−0.02035
1.7263	0.5781	3.4606	1.0302	−0.01278
1.0073	1.0448	4.1417	1.0378	−0.01749
0.2911	1.5106	4.8229	1.0449	−0.02542
2.0250	0.4451	3.3603	1.0349	−0.01212
1.3969	0.8514	3.9511	1.0422	−0.01588
0.6356	1.3458	4.6730	1.0499	−0.02247

Table XI: Isopiestic Equilibria in KCl–BaCl₂ Solutions

Concn of KCl, <i>m</i>	Concn of BaCl ₂ , <i>m</i>	Ionic strength	Osmotic coeff	$g_{\text{KBa}}^{\text{Cl}} + I \frac{\partial}{\partial I} (g_{\text{KBa}}^{\text{Cl}})$
0.6309	0.09985	0.9305	0.8873	+0.00359
0.4178	0.2482	1.1624	0.8767	+0.00230
0.1967	0.3994	1.3949	0.8704	+0.00111
0.3099	0.3280	1.2939	0.8709	−0.01122
0.2308	0.3814	1.3750	0.8698	−0.00860
0.1411	0.4423	1.4680	0.8680	−0.01551
0.5789	0.1491	1.0262	0.8828	−0.00344
0.4185	0.2603	1.1994	0.8758	−0.00367
0.2048	0.4060	1.4228	0.8706	−0.00484
0.6644	0.09088	0.9370	0.8876	−0.00456
0.5072	0.2007	1.1093	0.8794	−0.00256
0.3186	0.3302	1.3092	0.8733	−0.00234
0.7074	0.06345	0.8978	0.8894	−0.01288
0.6163	0.1269	0.9970	0.8850	−0.00134
0.5063	0.2028	1.1147	0.8808	+0.00462
0.4067	0.2712	1.2203	0.8775	+0.00616
0.8081	0.1856	1.3649	0.8877	−0.01010
0.5648	0.3514	1.6190	0.8833	−0.01508
0.3064	0.5228	1.8848	0.8764	−0.01975
0.6330	0.6110	2.4660	0.9047	−0.02381
0.4063	0.7535	2.6668	0.9124	−0.02504
0.2358	0.8588	2.8122	0.9200	−0.02774
1.3606	0.1526	1.8184	0.9005	−0.01848
1.1475	0.2965	2.0370	0.8990	−0.02133
1.0259	0.3772	2.1575	0.8993	−0.02228
0.8270	0.5066	2.3468	0.9020	−0.02308
1.9274	0.2142	2.5700	0.9168	−0.02406
1.4671	0.5127	3.0052	0.9220	−0.02776
0.8579	0.8894	3.5261	0.9406	−0.03391
0.3443	1.1881	3.9086	0.9696	−0.04104
1.3394	0.6012	3.1430	0.9261	−0.02769
0.6887	0.9968	3.6791	0.9504	−0.03442
0.2503	1.2482	3.9949	0.9779	−0.04198
1.8961	0.2554	2.6623	0.9183	−0.02459
1.1888	0.7051	3.3041	0.9317	−0.02839
0.5955	1.0604	3.7767	0.9574	−0.03403
1.6329	0.5589	3.3096	0.9320	−0.02714
1.2541	0.7931	3.6334	0.9425	−0.03105
0.3002	1.3455	4.3367	0.9934	−0.04432
1.8855	0.5384	3.5007	0.9381	−0.02764
0.5746	1.3145	4.5181	0.9921	−0.04110
0.2539	1.4896	4.7227	1.0153	−0.04527
2.5365	0.1524	2.9937	0.9308	−0.02616
2.2111	0.3630	3.3001	0.9340	−0.02725
1.7890	0.6282	3.6736	0.9423	−0.03012
1.1054	1.0339	4.2071	0.9689	−0.03150
2.3901	0.2521	3.1464	0.9334	−0.02237
1.5011	0.8090	3.9281	0.9519	−0.03165
0.4287	1.4251	4.7040	1.0069	−0.04177
2.3016	0.3635	3.3921	0.9373	−0.02657
1.3772	0.9332	4.1768	0.9609	−0.03533
0.9462	1.1832	4.4958	0.9806	−0.03884

Bower¹⁴ on the NaCl–BaCl₂ and KCl–BaCl₂ systems, and the measurements of Robinson¹² on NaCl–KCl. The results of the calculation for the NaCl–BaCl₂ and KCl–BaCl₂ systems are given in Tables X and XI. The values of

$$g_{\text{Na,Ba}}^{\text{Cl}} + I \frac{\partial}{\partial I} (g_{\text{Na,Ba}}^{\text{Cl}})$$

were calculated from eq 1. Note that this quantity is a function of the ionic strength but not a function of the

mole fraction of sodium chloride. This treatment of the data is very similar to the method of Robinson and Covington¹⁵ because their deviation function is given by

(14) R. A. Robinson and V. E. Bower, *J. Res. Nat. Bur. Stand.*, **69A**, 19, 439 (1965).

(15) R. A. Robinson and A. K. Covington, *ibid.*, **72A**, 239 (1968).

$$\Delta/(y_{\text{Na}}y_{\text{Ba}}) = I \left[g_{\text{Na,Ba}}^{\text{Cl}} + I \frac{\partial}{\partial I} (g_{\text{Na,Ba}}^{\text{Cl}}) \right]$$

The osmotic coefficients of the three-salt mixtures are given in Table XII together with values of the calculated osmotic coefficients. Again the values of ϕ (calcd) were calculated using only data on single-salt solutions (the first three terms on the right-hand side of eq 7).

Table XII: Osmotic Coefficients of Three-Salt Solutions

Concn, m			Ionic strength	Osmotic coeff		
NaCl	KCl	BaCl ₂		Exptl ^a	Calcd 1 ^b	Calcd 2 ^c
0.4708	0.4708	0.3559	2.0093	0.9179	0.9255	0.9197
0.3110	0.3110	0.5654	2.3182	0.9175	0.9257	0.9199
0.1740	0.1740	0.7449	2.5827	0.9205	0.9269	0.9224
0.1127	0.1127	0.8250	2.7004	0.9220	0.9278	0.9245
1.1980	1.1980	0.2126	3.0338	0.9718	0.9859	0.9713
1.0281	1.0281	0.4292	3.3438	0.9772	0.9944	0.9768
0.5509	0.5509	1.0022	4.1084	0.9976	1.0175	0.9980
0.3521	0.3521	1.2443	4.4371	1.0110	1.0281	1.0120

^a Results of R. A. Robinson and V. E. Bower, *J. Res. Nat. Bur. Stand.*, **69A**, 365 (1965). ^b Calculated by eq 7 using only the osmotic coefficients of the single-salt solutions, *i.e.*, the first 3 terms of eq 7. ^c Calculated by eq 7 using the osmotic coefficients of the single-salt solutions and also the terms for the binary mixtures. NaCl-KCl of Table IX, ref 4 and 5, NaCl-BaCl₂ of Table X, KCl-BaCl₂ of Table XI.

An examination of Table XII shows that single-salt data give a useful approximation. Using all of the terms in eq 7, the calculated osmotic coefficients are equal to the measured values within experimental error. Similar results are obtained for the LiCl-NaCl-BaCl₂ system reported in Table IXF.

Lietzke, *et al.*,¹⁶ have made some measurements in the system HCl-CsCl-BaCl₂ and it is interesting to compare the experimental and measured activity coefficients.

Substitution into eq A-9 yields the following expression for the activity coefficient of hydrochloric acid in the mixture.

$$\ln \gamma_{\pm}^{\text{HCl}} = \ln \gamma_{\text{HCl}}^0 + \left(1 - \frac{E^{\text{H}}}{I} \right) (1 - \phi_{\text{HCl}}^0) - \frac{E^{\text{Cs}}}{I} (1 - \phi_{\text{CsCl}}^0) - \frac{3}{4} \frac{E^{\text{Ba}}}{I} (1 - \phi_{\text{BaCl}_2}^0) + \frac{1}{2} E^{\text{Cs}} \left[g_{\text{H,Cs}}^{\text{Cl}} + E^{\text{H}} \frac{\partial}{\partial I} (g_{\text{H,Cs}}^{\text{Cl}}) \right] + \frac{3}{4} E^{\text{Ba}} \left[g_{\text{H,Ba}}^{\text{Cl}} + E^{\text{H}} \frac{\partial}{\partial I} (g_{\text{H,Ba}}^{\text{Cl}}) \right] + \frac{3}{4} E^{\text{Cs}} E^{\text{Ba}} \frac{\partial}{\partial I} (g_{\text{Cs,Ba}}^{\text{Cl}}) \quad (8)$$

The terms, due to common ion mixtures, in eq 5, have all been measured. The very precise measurements of

Harned and coworkers include hydrochloric acid-cesium chloride¹⁷ and hydrochloric acid-barium chloride.¹⁸ The data for the cesium chloride-barium chloride system can be obtained from measurements by Lindenbaum quoted by Lietzke.¹⁶ Only the data at 25° were treated because only at this temperature were precise measurements of all the quantities in the equation available. The results of this test are in Table XIII.

Table XIII: Activity Coefficient of Hydrochloric Acid in a Mixture of Cesium and Barium Chlorides¹⁶ at 25°

Concn, m			Activity coeff		
HCl	CsCl	BaCl ₂	Exptl ^a	Calcd 1 ^b	Calcd 2 ^c
0.1231	0.2963	0.0313	0.692	0.694	0.757
0.1235	0.1908	0.0627	0.688	0.702	0.757
0.1263	0.0972	0.0949	0.695	0.708	0.757
0.2454	0.1905	0.0209	0.725	0.714	0.757
0.2459	0.1490	0.0419	0.718	0.716	0.758
0.2445	0.0645	0.0621	0.722	0.724	0.757
0.3471	0.1107	0.0101	0.752	0.732	0.756
0.3609	0.0750	0.0208	0.750	0.735	0.757
0.3591	0.0351	0.0311	0.750	0.739	0.756
0.2507	0.5432	0.0624	0.693	0.689	0.806
0.2487	0.3869	0.1257	0.665	0.699	0.811

^a Results of M. H. Lietzke, H. B. Hupf, and R. W. Stoughton, *J. Inorg. Nucl. Chem.*, **31**, 3481 (1969). Corrected by M. H. Lietzke, private communication and interpolated to 25°. ^b Calculated by eq 8 using: HCl-CsCl data from H. S. Harned and O. E. Shupp, *J. Amer. Chem. Soc.*, **52**, 3892 (1930); HCl-BaCl data from H. S. Harned and C. G. Geary, *ibid.*, **59**, 2032 (1937), and H. S. Harned and R. Gary, *ibid.*, **76**, 5924 (1954); CsCl-BaCl₂ data from S. Lindenbaum quoted by M. H. Lietzke, H. B. Hupf, and R. W. Stoughton, *J. Inorg. Nucl. Chem.*, **31**, 3481 (1969). ^c Activity coefficient of pure HCl at the same ionic strength.

It seems likely that for strong electrolytes the equation is as accurate as the data now available. It is expected that deviations will be found at the higher concentrations when electrolytes with strong interactions are measured.

Appendix

Reilly and Wood¹ have shown that for a solution containing m_i^{M} moles of cation M_i with charge Z_i^{M} , m_j^{X} moles of anion X_j with charge Z_j^{X} , etc., in each kilogram of solvent the excess free energy is given by

$$G = \sum_{l=1}^{l=i} \sum_{m=1}^{m=j} \frac{E_l^{\text{M}} E_m^{\text{X}} Z_{lm} G_{0,M_l X_m}^0}{2EI} + \frac{RT}{4E} \sum_{k=2}^{k=i} \sum_{l=1}^{l=k-1} \sum_{m=1}^{m=j} E_k^{\text{M}} E_l^{\text{M}} E_m^{\text{X}} Z_{km} Z_{lm} g_{M_k M_l X_m}^{\text{M}} + \frac{RT}{4E} \sum_{k=1}^{k=i} \sum_{l=2}^{l=j} \sum_{m=1}^{m=l-1} E_k^{\text{M}} E_l^{\text{X}} E_m^{\text{X}} Z_{kl} Z_{km} g_{X_l X_m}^{\text{M}} \quad (\text{A-1})$$

(16) M. H. Lietzke, H. B. Hupf, and R. W. Stoughton, *J. Inorg. Nucl. Chem.*, **31**, 3481 (1969).

where

$$E_l^M = Z_l^M m_l^M \tag{A-1a}$$

$$E_l^X = -Z_l^X m_l^X \tag{A-1b}$$

$$E = \sum_{k=1}^{k=i} E_k^M = \sum_{l=1}^{l=j} E_l^X \tag{A-1c}$$

$$Z_{km} = Z_k^M - Z_m^X \tag{A-1d}$$

$$2I = \sum_{k=1}^{k=i} Z_k^M E_k^M - \sum_{l=1}^{l=j} Z_l^X E_l^X \tag{A-1e}$$

$G_{M_l X_m}^0$ is the excess free energy of pure $M_l X_m$ while $g_{M_k M_l X_m}$ and $g_{X_l X_m M_k}$ are parameters in the equations describing the excess free energy of mixing of M_k and M_l in the presence of X_m ; and X_l and X_m in the presence of M_k , respectively.¹⁹ These parameters are discussed in ref 1.

The free energy of the pure electrolyte ($G_{M_l X_m}^0$) is the value of free energy of the pure salt in a solution of the same ionic strength as that of the mixed-electrolyte solution. The excess free energy is related to the osmotic and activity coefficients of the salt by the relation²

$$G_{M_l X_m}^0 = RTm^0(1 - \phi_{M_l X_m}^0 + \ln \gamma_{M_l X_m}^0) \tag{A-2}$$

where

$$m^0 = m_l^M + m_m^X \tag{A-2a}$$

$$= -\frac{2I}{Z_k^M Z_l^X}$$

Differentiation of eq 2 with respect to m^0 gives²

$$\frac{\partial}{\partial m^0} [G_{M_l X_m}^0] = RT \ln \gamma_{M_l X_m}^0 \tag{A-3}$$

a relationship which will be used several times in this paper.

The free energy of the mixed-electrolyte solution is related to its osmotic coefficient and the activity coefficients of the ions in it by eq A-4

$$G = RT \left\{ m(1 - \phi) + \sum_{l=1}^{l=i} m_l^M \ln \gamma_l^M + \sum_{m=1}^{m=j} m_m^X \ln \gamma_m^X \right\} \tag{A-4}$$

where

$$m = \sum_{l=1}^{l=i} m_l^M + \sum_{m=1}^{m=j} m_m^X \tag{A-4a}$$

The Osmotic Coefficient of the Solution. The osmotic coefficient is obtained from the free energy and its differential with respect to the total salt concentration, the quantity of solvent being allowed to vary.

If the mass of solvent in the solution is allowed to vary, it is obvious that the ratio of any function of the concentration (in molal units) of the electrolytes to m is constant. Hence

$$\frac{\partial}{\partial m} (m_l^M) = \frac{m_l^M}{m} \quad \frac{\partial}{\partial m} (m_m^X) = \frac{m_m^X}{m}$$

Differentiating eq 4 with respect to m at constant E_k^M/E , etc., and remembering that²⁰

$$-\frac{\partial}{\partial m} [m(1 - \phi)] = \sum_{l=1}^{l=i} m_l^M \frac{\partial}{\partial m} (\ln \gamma_l^M) + \sum_{m=1}^{m=j} m_m^X \frac{\partial}{\partial m} (\ln \gamma_m^X)$$

the following is obtained

$$\frac{\partial G}{\partial m} = \frac{RT}{m} \left\{ \sum_{l=1}^{l=i} m_l^M \ln \gamma_l^M + \sum_{m=1}^{m=j} m_m^X \ln \gamma_m^X \right\}$$

Hence

$$G - m \left(\frac{\partial G}{\partial m} \right) = \frac{\partial (G/m)}{\partial (1/m)} = RTm(1 - \phi) \tag{A-5}$$

Differentiation of eq A-1 according to eq A-5, using eq A-2 and A-3, gives

$$RTm(1 - \phi) = -\frac{RT}{E} \sum_{l=1}^{l=i} \sum_{m=1}^{m=j} \frac{E_l^M E_m^X Z_{lm}}{Z_l^M Z_m^X} (1 - \phi_{M_l X_m}^0) - \frac{RT}{4E} \sum_{k=2}^{k=i} \sum_{l=1}^{l=k-1} \sum_{m=1}^{m=j} E_k^M E_l^M E_m^X Z_{km} Z_{lm} \times \left\{ g_{M_k M_l X_m} + I \frac{\partial}{\partial I} (g_{M_k M_l X_m}) \right\} - \frac{RT}{4E} \sum_{k=1}^{k=i} \sum_{l=2}^{l=j} \sum_{m=1}^{m=l-1} E_k^M E_l^X E_m^X Z_{kl} Z_{km} \times \left\{ g_{X_l X_m M_k} + I \frac{\partial}{\partial I} (g_{X_l X_m M_k}) \right\} \tag{A-6}$$

which expresses the osmotic coefficient of the mixed-electrolyte solution in terms of the osmotic coefficients of the pure electrolytes and the excess free energy of mixing of common ion mixtures.

The Activity Coefficient of Any Salt in a Mixed-Electrolyte Solution. The derivation of the activity coefficient of any salt in the mixture requires differentiation of the free energy with respect to the total salt concentration also, but in this case the only variable quantity is the concentration of the salt whose activity coefficient is required. Since the equation for the free energy is based on molal concentrations, these requirements are easily satisfied.

If the ionic strength of the solution is varied by

(17) H. S. Harned and O. E. Schupp, *J. Amer. Chem. Soc.*, **52**, 3892 (1930).

(18) H. S. Harned and C. G. Geary, *ibid.*, **59**, 2032 (1937); H. S. Harned and R. Gary, *ibid.*, **76**, 5924 (1954).

(19) The mixing is carried out at a constant ionic strength equal to that of the multicomponent mixture.

(20) See for example ref 8, p 348.

adding a quantity of the salt $M_p X_q$, then the ionic strength is given by

$$2I = 2\bar{I} + 2I^*$$

where the overscore indicates the initial value.

Since all the concentrations are expressed in molal units the following relations apply

$$m_p^M = \bar{m}_p^M + \frac{2I^*}{Z_p^M Z_{p,q}} \quad m_l^M = \bar{m}_l^M \quad (l \neq p)$$

$$m_q^X = \bar{m}_q^X - \frac{2I^*}{Z_q^X Z_{p,q}} \quad m_l^X = \bar{m}_l^X \quad (l \neq q)$$

$$E = \bar{E} + \frac{2I^*}{Z_{p,q}}$$

$$m = \bar{m} - \frac{2I^*}{Z_p^M Z_q^X}$$

Differentiation of the free energy relationship (eq A-4) with respect to m yields

$$\frac{\partial G}{\partial m} = RT \left\{ \frac{\partial}{\partial m} [m(1 - \phi)] + \sum_{l=1}^{l=i} m_l^M \frac{\partial \ln \gamma_l^M}{\partial m} + \sum_{m=1}^{m=j} m_m^X \frac{\partial \ln \gamma_m^X}{\partial m} + \frac{\partial m_p^M}{\partial m} \ln \gamma_p^M + \frac{\partial m_q^X}{\partial m} \ln \gamma_q^X \right\}$$

Using eq A-6 to cancel the three leading terms gives

$$\begin{aligned} \frac{\partial G}{\partial m} &= RT \left\{ \frac{\partial m_p^M}{\partial I^*} \frac{\partial I^*}{\partial m} \ln \gamma_p^M + \frac{\partial m_q^X}{\partial I^*} \frac{\partial I^*}{\partial m} \ln \gamma_q^X \right\} \\ &= RT \left\{ -\frac{Z_q^X}{Z_{p,q}} \ln \gamma_p^M + \frac{Z_p^M}{Z_{p,q}} \ln \gamma_q^X \right\} \\ &= RT \ln \gamma_{\pm}^{M_p X_q} \end{aligned} \quad (A-7)$$

Equation A-1 may now be differentiated with respect to m using the relations above, *i.e.*

$$\begin{aligned} RT \ln \gamma_{\pm}^{M_p X_q} &= -\frac{Z_p^M Z_q^X}{Z_{p,q}} \sum_{m=1}^{m=j} \frac{E_m^X Z_{p,m} G^0_{M_p X_m}}{2EI} - \\ &\quad \frac{Z_p^M Z_q^X}{Z_{p,q}} \sum_{l=1}^{l=i} \frac{E_l^M Z_{l,q} G^0_{M_l X_q}}{2EI} + \\ &\quad \frac{Z_p^M Z_q^X}{Z_{p,q} E^2} \sum_{l=1}^{l=i} \sum_{m=1}^{m=j} \frac{E_l^M E_m^X Z_{l,m} G^0_{M_l X_m}}{2I} + \\ &\quad \frac{Z_p^M Z_q^X}{2I^2} \sum_{l=1}^{l=i} \sum_{m=1}^{m=j} \frac{E_l^M E_m^X Z_{l,m} G^0_{M_l X_m}}{2E} + \\ &\quad RT Z_p^M Z_q^X \sum_{l=1}^{l=i} \sum_{m=1}^{m=j} \frac{E_l^M E_m^X Z_{l,m}}{2EI Z_l^M Z_m^X} \ln \gamma^0_{M_l X_m} - \\ &\quad \frac{RT}{4E} \frac{Z_p^M Z_q^X}{Z_{p,q}} \sum_{l=1}^{l=p-1} \sum_{m=1}^{m=j} E_l^M E_m^X Z_{p,m} Z_{l,m} g_{M_p M_l}^{X_m} - \\ &\quad \frac{RT}{4E} \frac{Z_p^M Z_q^X}{Z_{p,q}} \sum_{k=p+1}^{k=i} \sum_{m=1}^{m=j} E_k^M E_m^X Z_{k,m} Z_{p,m} g_{M_k M_p}^{X_m} - \end{aligned}$$

$$\begin{aligned} &\frac{RT}{4E} \frac{Z_p^M Z_q^X}{Z_{p,q}} \sum_{k=2}^{k=i} \sum_{l=1}^{l=k-1} E_k^M E_l^M Z_{k,q} Z_{l,q} g_{M_k M_l}^{X_q} + \\ &\frac{RT}{4E^2} \frac{Z_p^M Z_q^X}{Z_{p,q}} \sum_{k=2}^{k=i} \sum_{l=1}^{l=k-1} \sum_{m=1}^{m=j} E_k^M E_l^M E_m^X Z_{k,m} Z_{l,m} g_{M_k M_l}^{X_m} - \\ &\frac{RT}{8E} \frac{Z_p^M Z_q^X}{Z_{p,q}} \sum_{k=2}^{k=i} \sum_{l=1}^{l=k-1} \sum_{m=1}^{m=j} E_k^M E_l^M E_m^X Z_{k,m} Z_{l,m} \times \\ &\quad \frac{\partial}{\partial I} (g_{M_k M_l}^{X_m}) - \\ &\frac{RT}{4E} \frac{Z_p^M Z_q^X}{Z_{p,q}} \sum_{l=2}^{l=j} \sum_{m=1}^{m=l-1} E_l^X E_m^X Z_{p,l} Z_{p,m} g_{X_l X_m}^{M_p} - \\ &\frac{RT}{4E} \frac{Z_p^M Z_q^X}{Z_{p,q}} \sum_{k=1}^{k=i} \sum_{m=1}^{m=q-1} E_k^M E_m^X Z_{k,q} Z_{k,m} g_{X_q X_m}^{M_k} - \\ &\frac{RT}{4E} \frac{Z_p^M Z_q^X}{Z_{p,q}} \sum_{k=1}^{k=i} \sum_{l=q+1}^{l=j} E_k^M E_l^X Z_{k,l} Z_{k,q} g_{X_l X_q}^{M_k} + \\ &\frac{RT}{4E^2} \frac{Z_p^M Z_q^X}{Z_{p,q}} \sum_{k=1}^{k=i} \sum_{l=2}^{l=j} \sum_{m=1}^{m=l-1} E_k^M E_l^X E_m^X Z_{k,l} Z_{k,m} g_{X_l X_m}^{M_k} - \\ &\frac{RT}{8E} \frac{Z_p^M Z_q^X}{Z_{p,q}} \sum_{k=1}^{k=i} \sum_{l=2}^{l=j} \sum_{m=1}^{m=l-1} E_k^M E_l^X E_m^X Z_{k,l} Z_{k,m} \times \\ &\quad \frac{\partial}{\partial I} (g_{X_l X_m}^{M_k}) \end{aligned} \quad (A-8)$$

The equation above may be simplified by using eq A-2 and collecting terms. Equation A-8 then becomes

$$\begin{aligned} \frac{Z_{p,q}}{Z_p^M Z_q^X} \ln \gamma_{\pm}^{M_p X_q} &= \sum_{l=1}^{l=i} \sum_{m=1}^{m=j} \frac{E_l^M E_m^X}{E^2} \times \\ &\quad \left\{ \frac{Z_{p,m}}{Z_p^M Z_m^X} [1 - \phi^0_{M_p X_m} + \ln \gamma^0_{M_p X_m}] + \right. \\ &\quad \left. \frac{Z_{l,q}}{Z_l^M Z_q^X} [1 - \phi^0_{M_l X_q} + \ln \gamma^0_{M_l X_q}] - \right. \\ &\quad \left. \frac{Z_{l,m}}{Z_l^M Z_m^X} \left[\left(1 + \frac{Z_{p,q} E}{2I} \right) (1 - \phi^0_{M_l X_m}) + \ln \gamma^0_{M_l X_m} \right] \right\} - \\ &\quad \sum_{l=1}^{l=i} \sum_{m=1}^{m=j} \frac{E_l^M E_m^X Z_{p,m} Z_{l,m}}{4E} g_{M_p M_l}^{X_m} + \\ &\quad \sum_{k=2}^{k=i} \sum_{l=1}^{l=k-1} \sum_{m=1}^{m=j} \frac{E_k^M E_l^M E_m^X}{4E^2} \times \\ &\quad \left\{ Z_{k,m} Z_{l,m} \left[g_{M_k M_l}^{X_m} - \frac{Z_{p,q} E}{2} \frac{\partial}{\partial I} (g_{M_k M_l}^{X_m}) \right] - \right. \\ &\quad \left. Z_{k,q} Z_{l,q} g_{M_k M_l}^{X_q} \right\} - \\ &\quad \sum_{k=1}^{k=i} \sum_{l=1}^{l=j} \frac{E_k^M E_l^X Z_{k,l} Z_{k,q}}{4E} g_{X_l X_q}^{M_k} + \\ &\quad \sum_{k=1}^{k=i} \sum_{l=2}^{l=j} \sum_{m=1}^{m=l-1} \frac{E_k^M E_l^X E_m^X}{4E^2} \left\{ Z_{k,l} Z_{k,m} \left[g_{X_l X_m}^{M_k} - \right. \right. \\ &\quad \left. \left. \frac{E_{p,q} Z}{2} \frac{\partial}{\partial I} (g_{X_l X_m}^{M_k}) - Z_{p,l} Z_{p,m} g_{X_l X_m}^{M_p} \right] \right\} \end{aligned} \quad (A-9)$$

where

$$g_{M_p M_p}^{X_m} = g_{X_q X_q}^{M_k} = 0$$

Acknowledgment. Two of the authors (P. J. R. and R. H. W.) gratefully acknowledge the support of their

work by the Office of Saline Water, U. S. Department of the Interior.

NOTES

Isotope Effects in the Diffusion of ^{14}C -Substituted Molecules in the Liquid Phase. II. The Relative Diffusion Rates of Benzene-1- ^{14}C and Benzene-1,2- ^{14}C

by Lee B. Eppstein* and John G. Albright

Department of Chemistry, Texas Christian University,
Fort Worth, Texas 76129 (Received August 10, 1970)

Publication costs assisted by the Albright-Welch Foundation

The search for an adequate description of transport phenomena in liquid systems has created an increased theoretical and experimental interest in the properties of isotopic mixtures. The application of isotopically substituted tracers has become established as a standard technique for the study of diffusion phenomena in liquid systems. In this note the intradiffusion coefficient will be operationally defined as the observed diffusion coefficient of a trace component which is an isotopically substituted form of a component present in the bulk liquid. The term self-diffusion coefficient will be used to describe a hypothetical intradiffusion coefficient of a trace component which is chemically and physically equivalent to one of the components of the bulk liquid.

The application of the velocity-correlation method allows the calculation of the self-diffusion coefficient from the Van Hove correlation function.¹ Brown and March² have shown that for a classical liquid with a total potential energy independent of mass the Van Hove function $S(k, \omega, M, T)$ has the form $M^{1/2}f(k, M^{1/2}\omega, T)$, where f is the same function for different isotopes. These authors used this information to show the self-diffusion coefficient, D_{self} , is "rigorously" proportional to $M^{-1/2}$

$$D_{\text{self}} = \frac{1}{M^{1/2}} h(T) \quad (1)$$

where $h(T)$ is a function related to the specific intermolecular force law. Steele³ has shown that in the case of deuterium-substituted compounds the function $h(T)$ is not independent of the isotopic composition of the species.

The experimental work previously reported⁴⁻⁷ has been primarily concerned with the study of the relative mobilities of isotopic ionic species in both aqueous and molten salt media. The ratio of the mobilities of ^6Li and ^7Li in various solutions has been shown to be smaller than the square root of the inverse ratio of the masses.⁴⁻⁶ However, the relative mobilities of ^6Li and ^7Li in molten lithium chloride have been shown to approach the square root of the inverse ratio of the masses.⁸ The ratio of the mobilities of ^6Li and ^7Li in aqueous solutions of acetic and nitric acids has been shown to be dependent upon the acid concentration.^{4b}

Diffusion data for isotopic mixtures of nonelectrolytes are limited. Lyons and Birkett⁹ have used the modified Rayleigh-Philpot-Cook interferometric method to measure the binary-diffusion coefficients of deuterated hydrocarbons in mixtures with their unsubstituted parent compounds. Mills and coworkers¹⁰⁻¹⁵ have used the diaphragm cell to study the tracer-diffusion coefficients of ^{14}C -substituted molecules in both aqueous and nonaqueous solutions. Eppstein¹⁶ has suggested a coherent correlation of the form

$$\frac{D^+}{D^0} = \left(\frac{M^0}{M^+} \right)^{1/2} \quad (2)$$

* Address correspondence to this author at the Bio-Medical Division, Lawrence Radiation Laboratory, Livermore, Calif. 94550

(1) P. A. Egelstaff, "An Introduction to the Liquid State," Academic Press, New York, N. Y., 1967, Chapter 11.

(2) R. C. Brown and H. N. March, *Phys. Chem. Liquids*, **1**, 141 (1968).

(3) W. A. Steele, *J. Chem. Phys.*, **33**, 1619 (1960).

(4) (a) F. Lantelme and M. Chemla, *Bull. Soc. Chim. Fr.*, 1314 (1968); (b) M. Perie, J. Perie, and M. Chemla, *J. Chim. Phys.*, **66**, 48 (1969).

(5) R. W. Kunze and R. M. Fuoss, *J. Phys. Chem.*, **66**, 930 (1962).

(6) A. K. Brewer, *et al.*, *J. Res. Nat. Bur. Stand.*, **38**, 137 (1947).

(7) A. Lunden and V. Ljubimou, *Z. Naturforsch. A*, **23**, 1558 (1968).

(8) S. Jordan, R. Leuke, and A. Klemm, *ibid.*, **23**, 1563 (1968).

(9) J. D. Birkett and P. A. Lyons, *J. Phys. Chem.*, **69**, 2782 (1965).

(10) R. Mills, *ibid.*, **67**, 600 (1963).

(11) R. Mills and H. Ellerton, *ibid.*, **70**, 4089 (1966).

(12) J. G. Albright and R. Mills, *ibid.*, **69**, 3120 (1965).

(13) J. G. Albright, *ibid.*, **70**, 2299 (1966).

(14) R. Mills, *ibid.*, **69**, 3116 (1965).

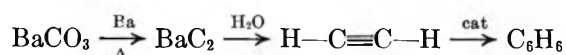
(15) J. F. Tilley and R. Mills, *Trans. Faraday Soc.*, **63**, 2931 (1967).

(16) L. B. Eppstein, *J. Phys. Chem.*, **73**, 269 (1969).

where D^+ and D^0 are, respectively, the values at infinite dilution of the tracer- and mutual-diffusion coefficients of species with molecular weights of M^+ and M^0 . In the present work the correlation in eq 2 has been tested by the comparison of the observed tracer-diffusion coefficients of benzene- $1-^{14}\text{C}$ and benzene- $1,2-^{14}\text{C}$ at high dilution in unsubstituted benzene. The diaphragm cell method has been used in these experiments since only the relative diffusion rates are necessary for this test. The absolute values of the diffusion coefficient have been based upon the calibration constant of the cell obtained with the diffusion of 0.8 M urea into H_2O . The absolute values of the tracer-diffusion coefficients determined in this work have been compared to the value of the self-diffusion coefficient of benzene previously reported by Mills.¹⁰ An additional comparison has been made to mutual-diffusion data of Birkett and Lyons⁹ for the perdeuteriobenzene-benzene system.

Experimental Section

Matheson Coleman and Bell "Chromato-quality" benzene (99.8+ mol %) was used without further purification. The urea used for the calibration of the diaphragm cell was recrystallized from a warm aqueous solution; special care was taken to avoid heating the mother liquor above 60°. The crystals were separated from the mother liquor by centrifugal drainage and were dried *in vacuo*. This material was tested for the presence of biuret with concentrated KOH and dilute CuSO_4 solution. Benzene- $1-^{14}\text{C}$ and benzene- $1,2-^{14}\text{C}$ were used as supplied by Mallinckrodt Nuclear. These compounds were synthesized by the following route



The benzene- $1-^{14}\text{C}$ was prepared by diluting the BaCO_3 to an activity of 2.0 mCi/mmol. The acetylene produced from this material was used without further dilution to form benzene with an activity of 12mCi/mmol. Assuming a random distribution of the ^{14}C , the molecular weight of this compound is 80.30. The benzene- $1,2-^{14}\text{C}$ was prepared from 0.2 mmol of acetylene having a specific activity of 122.8 mCi/mmol, 98.9% ^{14}C . This acetylene was diluted with 9.7 mmol of unlabeled acetylene and the mixture was used to produce the 1,2-labeled benzene. Assuming a random distribution of the ^{14}C the molecular weight of this compound is 82.23.

The labeled benzenes were purified by the methods of preparative gas chromatography. The radiochemical purity of the benzenes as determined from chromatographic data is greater than 99 mol %; *i.e.*, only a single peak was observed in these chromatograms.¹⁷

BBOT (2,5-bis[2-(5-*tert*-butylbenzoxazolyl)]thiophene), Packard Instrument Co., and reagent grade toluene, Matheson Coleman and Bell, were used in the

scintillation stock solutions without further purification.

A Stokes-type¹⁸ diaphragm cell which used a bottom plug similar to the design of Albright and Mills¹² was fabricated from a glass sealing tube with a 40-mm medium-porosity frit (Corning No. 39580). Each cell compartment contained a volume of *ca.* 17 cm^3 and the ratio of the compartment volumes was 1.0057. This assembly was permanently attached to a brass mounting plate which could be kinematically positioned in the water thermostat. Leveling screws on the mounting plate were adjusted so that the diaphragm was within 1° of horizontal when the cell was positioned in the thermostat. During the diffusion measurements the thermostat was maintained at a temperature of $25.00 \pm 0.005^\circ$ and the stirring rods were rotated at 59 rpm. The cell constant was determined with the diffusion of 0.8 M urea into H_2O . The effective diaphragm cell diffusion coefficient was calculated from the diffusion data of Gosting and Akeley¹⁹ with the technique presented by Gordon²⁰ and Stokes.²¹ Urea concentrations were calculated from refractive indices determined with a Phoenix-Brice differential refractometer (Phoenix Precision Instruments) by using the data of Gosting and Akeley¹⁹

$$\Delta n = 8.613(10^{-3})C - 4.43(10^{-5})C^2 + 1.83(10^{-6})C^3 \quad (3)$$

where C is the molar concentration. Equation 3 was solved by the method of false positions using a Hewlett-Packard 9100-A programmable calculator.

Relative radiotracer concentrations were determined using liquid-scintillation counting techniques. The sample chamber was maintained at a constant temperature in an air thermostat. Two sample cells are mounted on a pneumatically powered sliding mechanism which alternately places each cell before the EMI 6097-S11 photomultiplier tube. The output of the photomultiplier tube was counted electronically with AEC modular-type equipment manufactured by Canberra Industries (Model 1405 pre-amp, Model 1411 DDL amplifier, Model 1430 single-channel analyzer, Model 1473 scaler, and Model 1491 timer). Scintillation stock solutions were prepared by dissolving 4 g of BBOT in 1 l. of toluene. Stock solution (70 g) was added to 4 g of benzene solutions from the experiment. All solutions were prepared by weight and the counting procedures previously described by Albright¹³ were followed.

The experimental results are shown in Table I.

(17) Private communication, Dr. J. W. Woods, Mallinckrodt Nuclear Corp., St. Louis, Mo.

(18) R. H. Stokes, *J. Amer. Chem. Soc.*, **72**, 763 (1950).

(19) L. J. Gosting and D. F. Akeley, *ibid.*, **74**, 2058 (1952).

(20) A. R. Gordon, *Ann. N. Y. Acad. Sci.*, **46**, 285 (1945).

(21) R. H. Stokes, *J. Amer. Chem. Soc.*, **72**, 2243 (1950).

Table I: Observed Tracer-Diffusion Coefficients for Benzene-1-¹⁴C and Benzene-1,2-¹⁴C

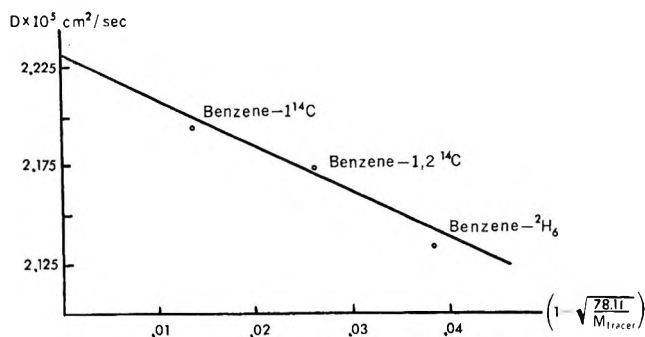
$D_L^a \times 10^{-5}$, cm ² /sec	$D_H^a \times 10^{-5}$, cm ² /sec
2.208	2.175
2.198	2.186
2.195	2.160
2.193	2.178
2.195	2.171
2.194	2.179
Av 2.197 ± 0.005	Av 2.175 ± 0.008

^a Subscripts refer to heavy and light tracers.

Mills¹⁰ has reported a value of 2.247×10^{-5} cm²/sec for the self-diffusion coefficient of benzene. Mills²² has recently completed an extensive study of the self-diffusion coefficients of benzene and CCl₄. In this more recent work a value of 2.107×10^{-5} cm²/sec for the self-diffusion of benzene has been obtained. This value is in good agreement with our value of 2.197×10^{-5} cm²/sec for benzene-1-¹⁴C. In order to test the relation suggested in eq 2 the mean values of the tracer-diffusion coefficients of the ¹⁴C-substituted species and the limiting mutual-diffusion coefficient of benzene-*d*₆ in benzene⁹ were plotted, in Figure 1, against the quantity $[(78.11/M_{\text{tracer}})^{1/2} - 1]$ and were fitted to an empirical expression of the form

$$D_{\text{tracer}} = a + ab \left(\left[\frac{78.11}{M_{\text{tracer}}} \right]^{1/2} - 1 \right) \quad (4)$$

where *a* and *b* are adjustable parameters. The values of the parameters *a* (2.231×10^{-5} cm²/sec) and *b* (1.051) were determined by the method of least squares. Finally, it is noted that the parameter *a* can be used as an approximation of the true self-diffusion coefficient, and as the parameter *b* approaches unity, eq 6 takes the form of eq 2. This result is interesting since theory applies only in the case of true self-diffusion and hence cannot directly predict the effect of varying the isotopic composition of the tracer component.

**Figure 1.**

Acknowledgment. The authors wish to express their gratitude to the Robert A. Welch Foundation (Grant No. P-225), Texas Christian University Research Foundation (Grant No. C-6971), and Petroleum Research Fund (Grant No. 971-G2) for their financial support of this research. They also wish to express their appreciation to Dr. James Woods of Mallinckrodt Nuclear for his many suggestions concerning the preparation of the labeled benzene samples.

(22) (a) Dr. R. Mills, private communication; (b) Abstracts, 160th National Meeting of the American Chemical Society, Chicago, Ill., Sept 1970, No. PHYS 201.

On the Photolysis of Ethylene at 1216 Å

by Y. Inel, A. Siddiqi, and G. G. Meisels*

Department of Chemistry, University of Houston, Houston, Texas 77004 (Received September 8, 1970)

Publication costs assisted by the U. S. Atomic Energy Commission

Ethylidene (CH₃CH) is a primary species in the photolysis of diazoethane,¹⁻³ methylketene,⁴ and methyldiazirene,⁵ and these systems have been studied to investigate its reactions. It has also been suggested that ethylidene is an intermediate in the photolysis of solid ethylene at 1470 Å as evidenced by the formation of methylcyclopropane.⁶ This product was not observed in the gas-phase photolysis at the same wavelength, and this was ascribed to a rapid isomerization of the ethylidene structure to an excited ethylene incapable of the addition reaction to ethylene typical of a carbene structure.⁶ Moreover, it was suggested that the rate of isomerization may depend on internal energy. While the vacuum ultraviolet photolysis of ethylene at 1236 Å has been reported,⁷ analysis for small yields of C₄ hydrocarbons was not made. We have therefore photolyzed ethylene at 1216 Å and report our findings here.

Photolyses were carried out using the conventional vacuum apparatus and lamp design described previously.⁸ Phillips research grade ethylene containing 2% oxygen was introduced into a cylindrical reaction vessel and irradiated using a Lyman α resonance lamp

(1) R. K. Brinton and D. H. Volman, *J. Chem. Phys.*, **19**, 1394 (1951).

(2) H. M. Frey, *J. Chem. Soc.*, 2293 (1962).

(3) C. L. Kibby and G. B. Kistiakowsky, *J. Phys. Chem.*, **70**, 1793 (1966).

(4) D. P. Chong and G. B. Kistiakowsky, *ibid.*, **68**, 1793 (1964).

(5) H. M. Frey and I. D. R. Stevens, *J. Chem. Soc.*, 1700 (1965).

(6) E. Tschuikow-Roux, J. R. McNesby, W. M. Jackson, and J. L. Faris, *J. Phys. Chem.*, **71**, 1531 (1967).

(7) H. Okabe and J. R. McNesby, *J. Chem. Phys.*, **36**, 69 (1962).

(8) P. S. Gill, Y. Inel, and G. G. Meisels, *ibid.*, in press.

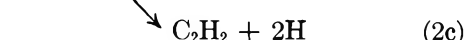
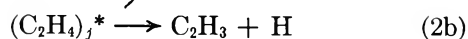
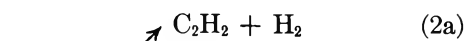
[argon (90%) and hydrogen (10%)⁹] with a lithium fluoride window. Initially, the lamp emitted small amounts of the two argon resonance lines at 1048 and 1067 Å. After several hours of use these lines disappeared; there were no other significant impurity lines. The lamp emitted in the range of 10^{13} quanta/sec. All runs were carried out at room temperature.

The reaction products were transferred directly¹⁰ from the reaction vessel to a gas chromatograph with flame ionization detector. They were separated at room temperature on a combination of 20 ft \times 0.25 in. o.d. dimethylsulfolane (10% w/w on Chromosorb P, 60–80 mesh) and 10 ft \times 0.25 in. o.d. squalene (10% w/w on Chromosorb P, 60–80 mesh). The identification of products was confirmed on 30 ft \times 0.25 in. o.d. dimethylsulfolane (33% w/w on Chromosorb P, 60–80 mesh) and on a 9 ft \times $\frac{1}{8}$ in. column of Poropak N, 100–120 mesh, programmed at 4°/min. Retention times were calibrated with all C₁ through C₄ hydrocarbons except for cycloalkenes. Methylcyclopropane was a single peak without overlap on all columns.

The reaction products in the 1216-Å photolysis of C₂H₄ with 2% oxygen added include acetylene, allene, methylcyclopropane, and small amounts of propylene and 1,3-butadiene. Butenes and methylacetylene may also be produced. C₅–C₆ products were observed at increased pressures or lamp intensities. It should be noted here that a possible minor lamp impurity at shorter wavelength such as at 1048–1067 Å cannot be invoked to account for the observation of methylcyclopropane since this compound is not a significant product ($\Phi < 0.01$) of ethylene photolysis in the ionization region.^{7,11}

The product distribution remains constant for different irradiation times. Neither allene nor methylcyclopropane are formed as products of secondary photolysis (Figure 1) and their yields are not affected by a fourfold change in lamp intensity (Figure 2) or by using neon as an inert additive (Figure 3).

The most important product of ethylene photolysis at 1216 Å (10.2 eV) in the presence of oxygen is acetylene, in accordance with observations at other wavelengths.¹² It may be formed with the simultaneous elimination of two hydrogen atoms or a hydrogen molecule



where reaction 2c may be considered as a very rapid loss of a hydrogen atom from excited vinyl radicals formed in step 2b. The subscript indicates that the dissociation may occur from several states formed either

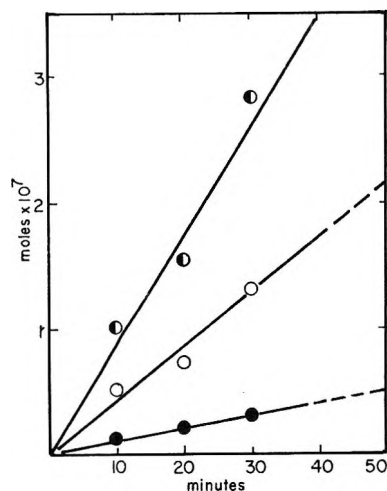


Figure 1. Product formation as a function of irradiation time at constant lamp intensity: ●, acetylene; ○, methylcyclopropane $\times 100$; ●, allene $\times 10$.

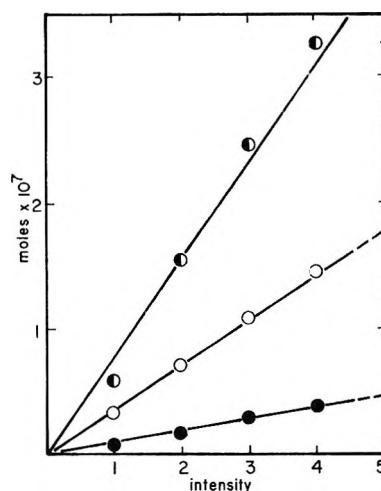


Figure 2. Product formation as a function of lamp intensity (arbitrary units) at constant photolysis time: ●, acetylene; ○, methylcyclopropane $\times 100$; ●, allene $\times 10$.

by excitation into different manifolds at these high energies or by subsequent internal conversion or possibly intersystem crossing.^{13,14} Reaction 2c is favored by a ratio of ca. 3:1. Vinyl radicals formed in step 2b should react rapidly with oxygen and would therefore not lead to the hydrocarbon products observed in our experiments.

(9) H. Okabe, *J. Opt. Soc. Amer.*, **54**, 478 (1964).

(10) G. G. Meisels and W. H. Wahl, *Rev. Sci. Instrum.*, **36**, 508 (1965).

(11) R. Gordon, Jr., and P. Ausloos, *J. Chem. Phys.*, **47**, 1799 (1967).

(12) For reviews see: (a) W. Sieck in "Fundamental Processes in Radiation Chemistry," P. Ausloos, Ed., Interscience, New York, N. Y., 1968, Chapter 3, p 152; (b) G. G. Meisels, "Fundamental Processes in Radiation Chemistry," Interscience, New York, N. Y., 1968, Chapter 6, p 387.

(13) R. J. Cvetanovic, *Progr. React. Kinet.*, **2**, 39 (1964).

(14) For a summary, see J. G. Calvert and J. N. Pitts, Jr., "Photochemistry," Wiley, New York, N. Y., 1966.

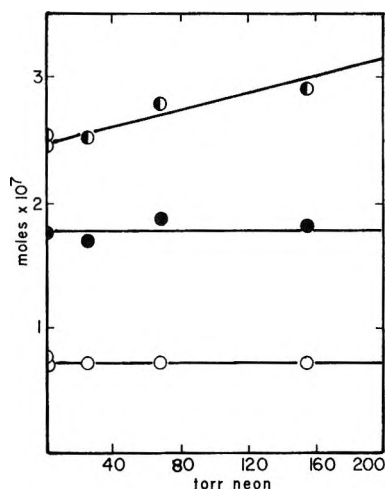
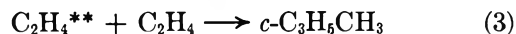


Figure 3. Effect of neon as an inert additive on product formation in 20-min photolyses: ●, acetylene, displaced vertically by 10^{-7} mol; ○, methycyclopropane $\times 100$; ●, allene $\times 100$.

The addition of inert gases increases the quantum yield of acetylene (Figure 3). At the same time there is little effect on the other minor products, and in any event their yield would be too small to counterbalance such a change. The increase in acetylene yield could result from an effect of collisional energy degradation on the competition between reactions 2b and 2c.

Methycyclopropane and allene are minor products, accounting for only *ca.* 1% of the hydrocarbon products. Both are formed as a consequence of the absorption of single quanta since there is no intensity effect, and the yield of either one is unaffected by the addition of inert gases. The probability that these products are a result of lamp emission at other wavelengths is small because they could not exceed 3% of the intensity of the 1216-Å line. Moreover, the additive oxygen has an absorption window at the Lyman α line and would therefore selectively absorb incident light at other wavelengths. Neither yield is substantially affected by variations of the oxygen concentration. We suggest, therefore, that a small finite amount of direct addition of excited ethylene yielding methycyclopropane occurs



Our results do not permit us to speculate on the structure of $\text{C}_2\text{H}_4^{**}$.

Tschuikow-Roux, *et al.*,⁶ did not observe methycyclopropane as a product of the gas-phase photolysis at 1470 Å (xenon resonance). A possible explanation of this could be the higher energy employed in this investigation which was only *ca.* 0.5 eV below the ionization potential of ethylene. The density of states is much greater at this energy and only a small fraction of the total excitation processes must be channeled into a specific state which eventually adds to ethylene to account for our results.

Acknowledgments. We are indebted to Professor G. K. Walters and Mr. A. C. Conrad, Department of Physics, Rice University, for use of the vacuum uv monochromator. This investigation was supported in part by the United States Atomic Energy Commission for whose assistance we are sincerely grateful. This is Document ORO-3606-19.

An Improved Numerical Method for Evaluating Second-Order Rate Constants

by G. R. Howe

Department of Chemistry, Brock University,
St. Catharines, Ontario, Canada (Received October 19, 1970)

Publication costs borne completely by The Journal of Physical Chemistry

The integrated rate equation for a second-order reaction of stoichiometry $A + B \rightarrow \dots$ which is first order both in A and B is given by¹

$$\frac{1}{B_0 - A_0} \ln \frac{A_0 B}{B_0 A} = kt \quad (1)$$

where the symbols have their conventional meanings. Commonly k is determined by measuring A_0 and B_0 and then subsequently measuring B at various times t . A , at time t , is then determined from the stoichiometry

$$A = A_0 - B_0 + B \quad (2)$$

The value of k is then found by application of eq 1.¹

There are a number of disadvantages inherent in this method, arising from the much greater weighting given to A_0 and B_0 as compared with subsequent B values. Frequently one of the initial values may be determined very accurately, *e.g.*, by weighing (say A_0), but the measurement of B_0 is less accurate, *e.g.*, by titration, and is only as accurate as each of the other B values. Yet B_0 is involved in determining each experimental point. An error in B_0 consequently leads to a systematic error² in the value for k obtained, no matter how many experimental observations are made. In addition, B_0 is often more prone to error than other B measurements, as it is often determined under different experimental conditions, *e.g.*, prior to mixing the reacting solutions. Alternatively, a sample may be analyzed as close as possible to the start of the reaction but not actually at zero time due to the time necessary for mixing, stirring,

(1) A. A. Frost and R. G. Pearson, "Kinetics and Mechanism," 2nd ed, Wiley, New York, N. Y., and London, 1961, Chapter 2.

(2) "Systematic error" in this context means systematic (constant) with respect to one particular run, though, of course, it is random with respect to a series of kinetic runs.

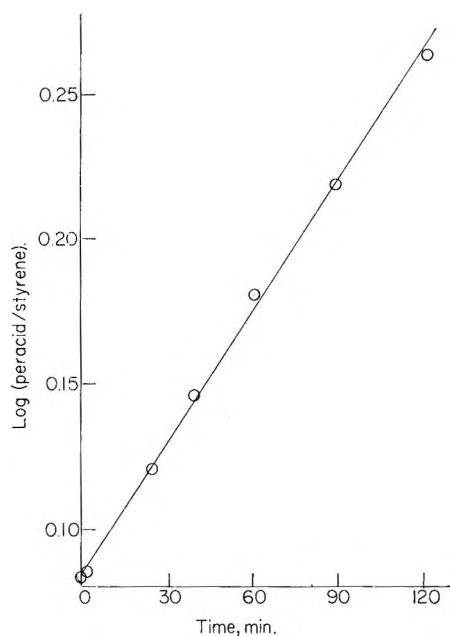


Figure 1. Log (peracid/styrene) vs. time.

etc.; this latter error is of obvious importance in fast reactions.

To overcome these difficulties a method has been developed for analyzing such reactions, where A_0 and t are known accurately, k and B_0 are treated as unknowns, and all B values are given equal weighting. In such a case no transformation of eq 1 can be made to reduce it to a linear regression form; one has to apply a Newton-Raphson technique.³

From (1) we may write

$$B = \frac{E(B_0 A_0 - B_0^2)}{A_0 - B_0 E} \quad (3)$$

where $E \equiv \exp(B_0 - A_0)kt$. From Taylor's theorem we may approximate

$$B_{\text{obsd}} - \frac{E(B_0 A_0 - B_0^2)}{A_0 - B_0 E} = \left| \frac{\partial B}{\partial B_0} \right| \Delta B_0 + \left| \frac{\partial B}{\partial k} \right| \Delta k \quad (4)$$

B_{obsd} is the measured value of B at time t , the other expressions are evaluated using approximations for B_0 and k , and ΔB_0 and Δk are incremental improvements in B_0 and k evaluated by least-mean-square solution² of the linear regression eq 4. Analytical expressions for the derivatives in a form suitable for computation are given by

$$\left| \frac{\partial B}{\partial B_0} \right| = \frac{EA_0 - 2B_0 E + EB + A_0 Bkt}{A_0 - B_0 E} \quad (5)$$

$$\left| \frac{\partial B}{\partial k} \right| = Bt(B_0 - A_0)[1 + BE/(A_0 - B_0 E)] \quad (6)$$

Given an initial approximation for B_0 , an initial approximation for k may be evaluated using eq 1 in the usual way; these may then be used in eq 4 to determine ΔB_0

and Δk . Hence a new B_0 and k can be calculated, and the process reiterated to any desired degree of self-consistency. All the observed values of B in this method are given equal weighting, and while the number of degrees of freedom is decreased by 1 (to allow for the extra variable) this is negligible if a reasonable number (say ≥ 6) of experimental points are determined. In addition, it is unnecessary to make any actual initial determination of B_0 ; the initial approximation can easily be made by graphic extrapolation or may even be guessed quite satisfactorily.

The usefulness of this method may be illustrated by some results recently obtained in this laboratory⁴ for the *m*-chloroperbenzoic acid oxidation of styrene in benzene: this reaction has the stoichiometry and rate equation as in (1) and (2). The initial styrene concentration is determined very accurately by weighing; the peracid concentration is followed by iodometric titration. The figure shows the conventional straight-line plot of log (peracid/styrene concentration) vs. time. The least-mean square value of the slope gives a value for k of $0.248 M^{-1} \text{ min}^{-1}$ with standard deviation of 0.0028. Application of the method described above gives a k value of $0.268 M^{-1} \text{ min}^{-1}$ with standard deviation of 0.0026. This illustrates the point very well: one would reasonably expect³ the correct value for k to lie within 0.242–0.254 (*i.e.*, ± 2 standard deviations) from using the conventional method. This arises of course from consideration of *random* error and fails to allow for the *systematic* error² induced by the incorrect value of B_0 . (Subsequent improvement in the technique for measuring B_0 confirmed the accuracy of the result given by the second method of calculation.)

The complete numerical method has been incorporated into a FORTRAN 4 subroutine; copies are available from the author upon request.

(3) E. M. Pugh and G. W. Winslow, "The Analysis of Physical Measurements," Addison-Wesley, London, 1966.

(4) G. R. Howe and R. R. Hiatt, unpublished observations.

Mass Spectrometric Study of the Reaction of Oxygen Atoms with Nitrosyl Chloride

by M. R. Dunn, C. G. Freeman, M. J. McEwan, and L. F. Phillips*

Chemistry Department, University of Canterbury, Christchurch, New Zealand (Received December 17, 1970)

Publication costs borne completely by The Journal of Physical Chemistry

The reaction of O atoms with ONCl does not appear to have been studied previously for its own sake, although it has been postulated as a secondary process in

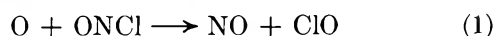
two accounts of the reaction of N atoms with ONCl.^{1,2} We now report a study of the O + ONCl reaction in a fast-flow system, using a mass spectrometer to monitor the concentrations of reactants and products. The reaction resembles that of O atoms with NO₂, in that it is accompanied by a visible "air afterglow" luminescence, which contracts toward the inlet jet when the ONCl flow exceeds the flow of O atoms. However, the ONCl reaction is about two orders of magnitude slower than the NO₂ reaction and is correspondingly less suitable as a gas-phase titration for estimating O atom concentrations.

Experimental Section

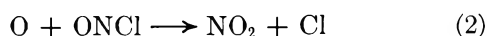
The apparatus, materials, and experimental procedures were as previously described.^{2,3} As before the walls of the flow system were normally poisoned with phosphoric acid to inhibit recombination of Cl atoms. Atomic oxygen was generated by passing oxygen, either pure or mixed with argon, through a microwave discharge, or, in the absence of O₂, by titrating N atoms with NO. Because H reacts much more rapidly than O with ONCl,⁴ it was necessary to ensure that H atoms were not produced in significant amounts during passage of the various gases through the discharge. Preliminary measurements of the O atom rate were made using Matheson ultrahigh-purity oxygen, but difficulty was experienced in obtaining a steady and adequate concentration of O atoms throughout the measuring process. Most studies were therefore made with gas from a cylinder of commercial O₂ (selected for low N₂ content), which was passed through a trap at Dry Ice temperature. Presumably, catalytic impurities were responsible for the more reproducible O atom production.⁵ The rates thus measured did not differ significantly from the few results obtained using ultrahigh-purity oxygen; this is in accordance with predictions based on the vapor pressure of ice at -78°. When the oxygen was saturated with water vapor at 0° the apparent rate of the O + ONCl reaction increased by an order of magnitude. As nitric oxide is a major product of the reaction, we were obliged to use the NCl⁺ peak at mass 49 to monitor ONCl concentrations.^{2,4}

Results and Discussion

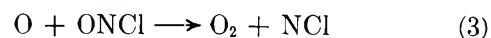
The products at long reaction times (*ca.* 300 msec) were NO, Cl₂, and O₂. At short reaction times, with an excess of O¹⁶NCl, an increase in peak height at mass 51 showed that long-lived ClO radicals³ were formed. This observation implies that a large proportion of the primary reactions follow the equation



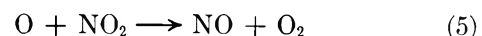
since the alternative processes



and



would not lead to the production of significant amounts of ClO. (The reaction O + NCl → N + ClO is endothermic by 20–30 kcal and is therefore very slow.) All three primary processes can account for the observed "air afterglow" emission, which depends upon the reaction sequence



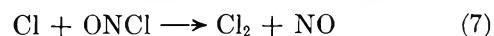
An increase at mass 46, due to NO₂ produced by reaction 2, was searched for over a wide range of conditions, but no such increase was ever observed. The steady-state concentration of NO₂, as fixed by reactions 2 and 5, is $k_2[\text{ONCl}]/k_5$. The detection limit for NO₂ was about 5×10^{-6} Torr. Using $k_5 = 5 \times 10^{-12}$ cm³ molecule⁻¹ sec⁻¹⁶ this implies that, with 0.02 Torr of ONCl, k_2 must be less than 1.3×10^{-15} . This turns out to be considerably less than our measured value of the primary rate constant, and so we consider that reaction 2 is relatively unimportant. Since NO₂ could also be produced by the reaction of NO with ClO,⁷ this upper limit for k_2 is a conservative one.

The stoichiometry of the reaction at 300 msec was investigated by treating excess ONCl with a known concentration of atomic oxygen. In a freshly poisoned system the mean ratio of ONCl to O atoms destroyed was 0.95 ± 0.14 for Ar-O₂ mixtures and 1.17 ± 0.19 for O atoms from the N + NO reaction. Lower values were obtained for this ratio when the wall coating had not been renewed for a few days, the smallest such value being 0.58.

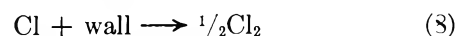
The observed stoichiometry can be accounted for by primary reaction 1, followed by the fast reactions



($k_6 > 1.3 \times 10^{-11}$ cm³ molecule⁻¹ sec⁻¹)³ and



($k_7 = 3 \times 10^{-12}$ cm³ molecule⁻¹ sec⁻¹)⁸, where in an unpoisoned system reaction 7 has to compete with wall recombination of Cl atoms



However, the same stoichiometry results from reaction 2, followed by (5) and (7) (or (5) and (8) in the un-

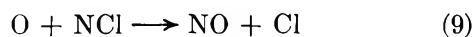
- (1) J. C. Biordi, *J. Phys. Chem.*, **73**, 3163 (1969).
- (2) M. R. Dunn, C. G. Freeman, M. J. McEwan, and L. F. Phillips, *ibid.*, in press.
- (3) C. G. Freeman and L. F. Phillips, *ibid.*, **72**, 3025 (1968).
- (4) M. R. Dunn, M. M. Sutton, C. G. Freeman, M. J. McEwan, and L. F. Phillips, *ibid.*, in press.
- (5) R. L. Brown, *ibid.*, **71**, 2492 (1967).
- (6) F. S. Klein and J. T. Herron, *J. Chem. Phys.*, **41**, 1285 (1964).
- (7) J. A. Coxon, *Trans. Faraday Soc.*, **64**, 2118 (1968).
- (8) W. G. Burns and F. S. Dainton, *ibid.*, **48**, 52 (1952).

Table I: Primary Rate for the O + ONCl Reaction

[Ar] ^a	[O ₂]	10 ³ [O] ₀	10 ³ [ONCl] ₀	10 ³ [ONCl] _t	t	10 ¹⁴ k ^b	[O] ₀ / [ONCl] ₀
0.269	0.118	8.88	0.725	0.469	26.6	2.62	12.2
		7.62	0.631	0.493	17.7	2.55	12.1
		6.35	0.959	0.772	24.6	1.99	6.6
		5.08	0.582	0.549	15.6	2.02	8.7
		2.66	1.78	1.50	42.9	2.28	1.5
0.220	0.133	1.84	2.41	2.00	32.4	4.95	0.8
		1.60	1.91	1.65	25.6	5.33	0.8
		1.45	0.777	0.718	22.3	3.18	1.9
0.238	0.109	4.22	1.92	1.49	43.4	2.05	2.2
0.380	0.211	4.27	2.96	2.63	19.8	2.02	1.4
		4.28	2.20	1.93	19.8	2.17	2.0
		3.92	2.96	2.28	33.2	3.08	1.3
		2.68	1.30	0.93	36.3	5.19	2.1
		2.71	1.76	1.38	36.5	3.63	1.5
0.403	0.229	3.56	1.79	1.33	48.5	2.58	2.0
		3.21	1.99	1.81	23.1	1.80	1.6
		2.27	0.361	0.270	35.2	5.07	6.4
0.386	0.204	3.40	1.28	0.880	28.1	5.68	2.7
		3.52	1.59	1.15	54.4	2.53	2.2
		3.11	1.26	0.835	43.2	4.60	2.5

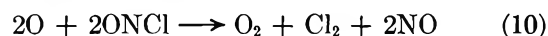
^a Concentrations are given in Torr, times *t* in milliseconds. The results at [Ar] = 0.269 Torr were obtained using ultrahigh-purity oxygen. $k(\text{mean} \pm \text{std dev}) = (3.3 \pm 1.3) \times 10^{-14} \text{ cm}^3 \text{ molecule}^{-1} \text{ sec}^{-1}$. ^b A correction for back-diffusion of reactant, amounting to 2–5% of the time value, has been applied in calculating these rate constants.

poisoned system), and also from reaction 3 followed by



plus reaction 7 or 8. As noted above, our failure to detect NO₂ in the products indicates that reaction 2 is relatively unimportant. Reaction 3 is probably exothermic; a linear Birge–Sponer extrapolation yields a value of 92 kcal mol⁻¹ for the dissociation energy of NCl, and if this is correct the reaction is exothermic to the extent of 23 kcal, compared with 27 kcal for reaction 1. The true dissociation energy is likely to be lower than the value derived from a linear extrapolation, but probably not low enough to make reaction 3 endothermic and therefore slow. A better reason for eliminating (3) is that the ground state of NCl is almost certainly a triplet,⁹ in which case reactions 3 and 9 are both forbidden by the Wigner spin-conservation rule.

The rate constant of reaction 1 was determined from the rate of disappearance of ONCl in the presence of excess O atoms, on the assumption that the stoichiometry could be represented as



The mean of 20 determinations (see Table I) gave $k_1 = 3.3 \times 10^{-14} \text{ cm}^3 \text{ molecule}^{-1} \text{ sec}^{-1}$, with a standard deviation of 1.0×10^{-14} . In conjunction with our upper limit for k_2 , this value implies that at least 95% of primary reactions in this system obey eq 1.

Acknowledgments. This work was supported by the New Zealand Universities Research Committee and by Grant AF-AFOSR-1265-67 from the United States Air Force Office of Scientific Research.

(9) R. Colin and W. E. Jones, *Can. J. Phys.*, **45**, 301 (1967).

COMMUNICATIONS TO THE EDITOR

Dielectric Measurements with Time Domain Reflectometry When Large Conductivities Are Involved

Publication costs assisted by the Physics Laboratory RVO-TNO

Sir: Recently Fellner-Feldegg has introduced time domain reflectometry (TDR) into the field of dielectric measurements.¹⁻³ This technique is based upon measurement of the reflected part of a voltage step V_0 , applied to a transmission line partly filled with a polar dielectric. From the curve $V_0P(t)$, representing the reflected part of the voltage step traveling from the air-dielectric interface, the dielectric permittivity $\epsilon(i\omega)$ can be determined using numerical methods.⁴ However, to obtain knowledge about the possibility of a direct determination of $\epsilon(i\omega)$, the reverse procedure is carried out,^{5,6} calculating $P(t)$ in the time domain from a known behavior of $\epsilon(i\omega)$ in the frequency domain.

When low-frequency conductivity was predominant, Fellner-Feldegg^{1,3} suggested a relation for $P(t)$. From this relation dP/dt at $t = 0$, a linear function of the conductivity σ , is calculated. This suggests that σ can be measured from TDR experiments *via* a measurement of the slope of the reflected voltage at $t = 0$.

It is the purpose of this letter to show that: (A) it is possible, using however questionable approximations, to derive a relation for $P(t)$ which is close to Fellner-Feldegg's formula; (B) his relation for $P(t)$ in the time domain cannot be derived from known results in the frequency domain; and (C) his relation for $P(t)$ cannot be used for a determination of σ .

(A) Because Laplace methods are used, s is written instead of $i\omega$ where necessary. Then $P(t)$ and $\epsilon(s)$ are related by the equation

$$P(t) = \mathcal{L}^{-1}\left\{\frac{\rho(s)}{s}\right\} \quad (1)$$

and $\rho(s)$ is given by

$$\rho(s) = \frac{\sqrt{s} - \sqrt{s \cdot \epsilon(s) + \sigma/\epsilon}}{\sqrt{s} + \sqrt{s \cdot \epsilon(s) + \sigma/\epsilon}} \quad (2)$$

\mathcal{L}^{-1} denotes the inverse Laplace transform. $\rho(s)$ is the reflection coefficient in the frequency domain and ϵ the dielectric permittivity of the vacuum. Because $\rho(s)$ is a complicated function of s , $P(t)$ can only be calculated numerically from eq 1 and 2.

The question is how much eq 2 must be simplified in order that the inverse Laplace transformation can be

found in closed form. The formula quoted by Fellner-Feldegg suggests the following form

$$\rho(s) = \frac{\sqrt{s} - \sqrt{s \cdot \epsilon_\infty + \sigma/\epsilon}}{\sqrt{s} + \sqrt{s \cdot \epsilon_\infty + \sigma/\epsilon}} \quad (3)$$

where $\epsilon(s)$ is replaced by the high-frequency limit ϵ_∞ . This approximation however cannot be used since the inverse transformation is not known in closed form.^{7,8} The rather crude approximation which has to be made before a formula for $P(t)$ can be obtained is the complete neglect of $\epsilon(s)$ from eq 2, *i.e.*

$$\rho(s) = \frac{\sqrt{s} - \sqrt{s + \sigma/\epsilon}}{\sqrt{s} + \sqrt{s + \sigma/\epsilon}} \quad (4)$$

From eq 4 the following relation for $P(t)$ is obtained⁹

$$P(t) = -1 + e^{-zt}[I_0(xt) + I_1(xt)] \quad (5)$$

$$x = \sigma/2\epsilon \quad (6)$$

I_0 and I_1 are modified Bessel functions. The behavior of $P(t)$ according to eq 5 is for very small and very large times, respectively

$$\lim_{t \rightarrow 0} P(t) = 0 \quad \lim_{t \rightarrow \infty} P(t) = -1 \quad (7)$$

The value for $P(\infty)$ is correct, but the value for $P(0)$, which should be $\rho(\infty)$, is not, due to the complete neglect of $\epsilon(s)$ in eq 4. However, eq 5 is very close to Fellner-Feldegg's relation, which is discussed under (B).

(B) The formula given by Fellner-Feldegg is (including the term -1)

$$P(t) = -1 + [1 + \rho(\infty)]e^{-yt}[I_0(yt) + I_1(yt)] \quad (8)$$

$$y = \sigma/2\epsilon\epsilon_\infty \quad (9)^{10}$$

(1) H. Fellner-Feldegg, *J. Phys. Chem.*, **73**, 616 (1969).

(2) T. A. Whittingham, *ibid.*, **74**, 1824 (1970).

(3) Hewlett-Packard Application Note No. 118, March 1970.

(4) This can be done by using a fast Fourier transform technique.

(5) H. Fellner-Feldegg and E. F. Barnett, *J. Phys. Chem.*, **74**, 1962 (1970).

(6) M. J. C. van Gemert and J. G. de Graan, to be submitted for publication.

(7) M. Abramowitz and I. A. Stegun, "Handbook of Mathematical Functions," 7th ed, Dover Publications, New York, N. Y., 1968.

(8) A. Erdélyi, W. Magnus, F. Oberhettinger, and F. G. Tricomi, "Tables of Integral Transforms," Vol. I and II, McGraw-Hill, New York, N. Y., 1954.

(9) B. M. Oliver, *Hewlett-Packard J.*, **15**, No. 6, (1964).

(10) Fellner-Feldegg has included a factor 4π in eq 9 which is incorrect as can be concluded by comparing his results,³ p 4, with the results given by Ramo and Whinnery,¹¹ p 307.

(11) S. Ramo and J. R. Whinnery, "Fields and Waves in Modern Radio," 7th ed, Wiley, London, 1952.

The values for $P(0)$ and $P(\infty)$ are now correctly given. However, due to the factor $1 + \rho(\infty)$, this relation for $P(t)$ must be considered as an *ad hoc* solution because it is not derived from eq 3 or some other approximation from eq 2. The consequence is that the value for y must now be adapted to the experiment. Thus, eq 9 cannot be used to relate any curve $P(t)$ with the dielectric parameters ϵ_∞ and σ .

(C) It is clear from the discussion of eq 8 and 9 that although y can be determined from an experiment (by measuring dP/dt at $t = 0$), no value for σ can be found from it since eq 9 is invalid.

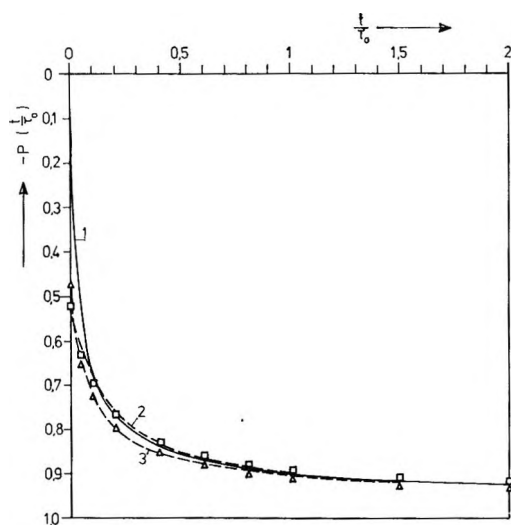


Figure 1. Some curves for the step response of the reflection coefficient $P(t)$: 1, $P(t)$ calculated from eq 5 and 6; 2, $P(t)$ from exact calculations for a Debye dielectric with $\epsilon_0 = 20$, $\epsilon_\infty = 10$ and $\sigma\tau_0/\epsilon = 113$; 3, $P(t)$ from exact calculations for a Debye dielectric with $\epsilon_0 = 80$, $\epsilon_\infty = 8$, and $\epsilon\sigma\tau_0 = 113$; \square , calculated from eq 8 with $y\tau_0 = 12$; Δ , calculated from eq 8 with $y\tau_0 = 20$.

The statements given above are illustrated in Figure 1 where the curves $P(t)$, calculated from eq 5 and 8 are compared with the exact curves, obtained numerically from eq 1 and 2, using a Debye function for $\epsilon(s)$.⁶ The value for x has been calculated according to eq 6, but instead of using eq 9 the value for y has been adapted (by hand) to give a good fit of eq 8 with the results of the exact transformations. Because $P(t/\tau_0)$ is calculated,⁶ the parameters x and y are multiplied by τ_0 , the dielectric relaxation time involved in $\epsilon(s)$.

From the above discussions it can be concluded that: (a) eq 5 describes the behavior of $P(t)$ reasonably well for $t/\tau_0 > 0.1$ (and for large values of $\sigma\tau_0/\epsilon$), but it is clear that this equation cannot be used when small values of t/τ_0 are important; (b) although eq 8 can be adapted to give a good fit with the exact results, no link exists between this equation and the dielectric parameters ϵ_∞ and σ . This means that eq 8 cannot be used for a determination of σ .

Acknowledgments. Discussions with Dr. G. P. de Loor are gratefully acknowledged.

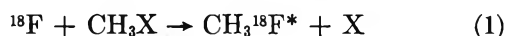
PHYSICS LABORATORY RVO-TNO M. J. C. VAN GEMERT
 OUDE WAALSDORPERWEG
 DEN HAAG
 THE NETHERLANDS

RECEIVED NOVEMBER 6, 1970

Bond Energy Effects in Substitution Reactions of Fluorine-18 Atoms with Methyl Halides¹

Publication costs assisted by the Division of Research, U. S. Atomic Energy Commission

Sir: The chemically energetic ¹⁸F atoms formed in nuclear reactions are capable of substitution for H, F, Cl, and CH₃, in gas-phase reactions.²⁻⁵ Earlier investigations of the relative yields of halogen reactions such as (1) have served as the basis for theories concerning the nature of these energetic processes. Among the factors



postulated to influence the progress of these reactions are steric,⁵ translational inertia,⁶ and liquid "cage" effects.⁷⁻¹⁰ Each of these is essentially a physical factor concerned with mass, atomic radius, solid angles, etc. Our present experiments have sought additional information about reaction 1 with X = F, Cl, Br, and I and lead to the conclusion that the relative yields of these substitution reactions increase markedly with decreasing C-X bond strength. This evidence for the importance of more chemical influences in halogen atom reactions parallels closely the developing descriptions of energetic tritium atom reactions.¹¹⁻¹⁴

Earlier experiments have demonstrated that the ob-

- (1) This research was supported by A.E.C. Contract No. AT-(11-1)-34, Agreement No. 126.
- (2) N. Colebourne, J. F. J. Todd, and R. Wolfgang, *Chem. Eff. Nucl. Transform., Proc. Symp.*, 1964, 1, 149 (1965).
- (3) N. Colebourne, J. F. J. Todd, and R. Wolfgang, *J. Phys. Chem.*, 71, 2875 (1967).
- (4) Y.-N. Tang and F. S. Rowland, *ibid.*, 71, 4576 (1967).
- (5) L. Spicer, J. F. J. Todd, and R. Wolfgang, *J. Amer. Chem. Soc.*, 90, 2425 (1968).
- (6) L. Spicer and R. Wolfgang, *ibid.*, 90, 2426 (1968).
- (7) Y.-N. Tang, T. Smail, and F. S. Rowland, *ibid.*, 91, 2130 (1969).
- (8) J. E. Willard, *Ann. Rev. Phys. Chem.*, 6, 141 (1955).
- (9) F. S. Rowland, C. M. Wai, C. T. Ting, and G. Miller, *Chem. Eff. Nucl. Transform., Proc. Symp.*, 1964, 1, 333 (1965).
- (10) A. E. Richardson and R. Wolfgang, *J. Amer. Chem. Soc.*, 92, 3480 (1970).
- (11) R. Wolfgang, *Progr. React. Kinet.*, 3, 99 (1965).
- (12) F. Schmidt-Bleek and F. S. Rowland, *Angew. Chem., Int. Ed. Engl.*, 3, 769 (1964).
- (13) F. S. Rowland, E. K. C. Lee, and Y.-N. Tang, *J. Amer. Chem. Soc.*, 73, 4024 (1969).
- (14) Y.-N. Tang, E. K. C. Lee, E. Tachikawa, and F. S. Rowland, *J. Phys. Chem.*, in press.

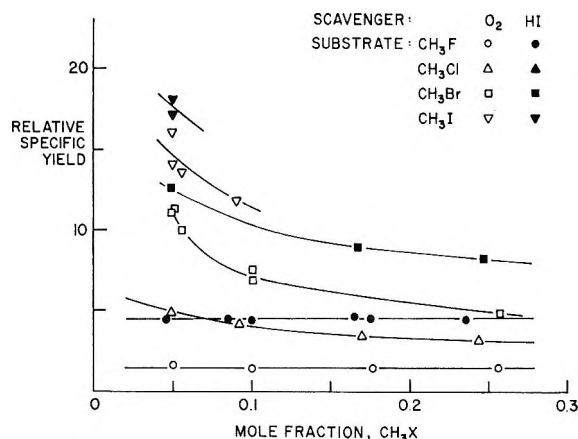
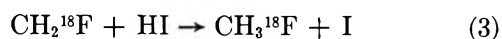
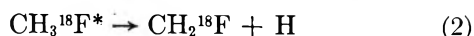


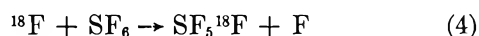
Figure 1. Relative specific yield $[(\text{CH}_3^{18}\text{F}/\text{CH}_3\text{F})(\text{SF}_5^{18}\text{F}/\text{SF}_6)]$ for ^{18}F -for- X in CH_3X vs. mole fraction in SF_6 : open symbols, O_2 -scavenged; solid symbols, HI -scavenged; \circ , CH_3F ; Δ , CH_3Cl ; \square , CH_3Br ; ∇ , CH_3I . Ratio $\text{CH}_3\text{X}/\text{scavenger} = 10$.

served gas-phase yields can often lead to serious underestimates of the primary yields of substitution reactions because of the extensive secondary decomposition involved.^{4,7,10} We have accordingly also determined upper limits for the secondary decomposition products from (2) through reaction with HI ,^{15,16} as in (3). These



are only upper limits because decomposition of the ^{18}F -H substitution product $\text{CH}_2^{18}\text{FX}^*$ also leads to CH_3^{18}F in the presence of HI : elimination of HX , insertion of CH^{18}F into HI , decomposition of the resulting $\text{CH}_2^{18}\text{FI}^*$ to $\text{CH}_2^{18}\text{F} + \text{I}$, and abstraction of H from another HI molecule.¹⁵

The experimental procedures have followed standard techniques involving the formation of ^{18}F by the $^{19}\text{F}(n,2n)^{18}\text{F}$ reaction on SF_6 in a Kaman A711 neutron generator.^{15,16} The major component in each gas mixture has been SF_6 , in order to ensure essentially equivalent ^{18}F fluxes through moderation in nonreactive collisions with SF_6 . Although the yields of all ^{18}F reactions have been measured on an absolute basis,¹⁶ the yields of reaction 1 with the minor component, CH_3X , have been expressed on a per-molecule basis relative to that of the low-yield substitution reaction 4 with SF_6 .



Otherwise duplicate samples were scavenged either with O_2 or with HI . The sample temperature during irradiation was approximately 10° . All samples were analyzed by radio gas chromatography, as described previously.^{15,16}

The relative yields of the substitution reactions increase from CH_3F to CH_3I by a factor of 8 for CH_3^{18}F stabilized at about 4 atm of pressure, as shown in Figure 1. Even if all incremental CH_3^{18}F with H were

attributed to decomposition by (3)—and much certainly arises from $\text{CH}_2^{18}\text{FX}^*$ decomposition—the primary yield of CH_3^{18}F from CH_3I is more than 4 times the yield from CH_3F . The trend in increased yield obviously parallels both the increase in size of the halogen substituent and the decrease in C-X bond energy. Usual estimates of atomic radii indicate about a factor of 2 increase in collision radius between F-F and F-I ,¹⁷ insufficient by itself to account for the actual observed change.

Substitutions of ^{18}F -for- X initiated only by “hot” ^{18}F atoms should exhibit a yield of CH_3^{18}F proportional to the mole fraction of CH_3X , or a relative specific yield $[(\text{CH}_3^{18}\text{F}/\text{CH}_3\text{X})/(\text{SF}_5^{18}\text{F}/\text{SF}_6)]$ that is independent of CH_3X concentration in excess SF_6 . On the other hand, a thermally initiated reaction (e.g., a “scavenger” reaction) should—in the absence of other competing thermal reactions¹⁸—trap the same amount of ^{18}F , independent of concentration of the scavenger molecule, and thus show increasing relative specific yields at lower concentrations. The data for CH_3F are clearly indicative that the thermoneutral $^{18}\text{F-F}$ substitution is entirely a hot process. However, the progressively rising relative specific yields with decreasing mole fraction of CH_3X from the other molecules indicate that these exothermic $^{18}\text{F-X}$ substitution reactions (e.g., $^{18}\text{F-I}$ is about 48 kcal/mol exothermic) can be initiated both by hot and by near-thermal ^{18}F atoms. This trend in relative specific yields with the change from CH_3F to CH_3I is further evidence that the energetics of the substitution—and not the size of the halogen atom being replaced—is the more important factor in the determination of the $^{18}\text{F-X}$ reaction yields.

The division of reactions into “hot” and “thermal” groups is necessarily rather arbitrary and imprecise. In each of these systems, there is necessarily an eventual preferred reaction path for true thermal ^{18}F atoms (if such could be introduced into the system) and this reaction route is most probably the abstraction of H for the molecular mixtures involved here. In systems with a high mole fraction of SF_6 , moderating collisions are much more probable than reactive collisions, and the median energy of ^{18}F at reaction is probably not very much above the corresponding value in a true thermal system. The implication of Figure 1 is that: (a) substitution of ^{18}F -for- I and ^{18}F -for- Br can occur well down into the energy region in which H^{18}F formation is also observed; and (b) the activation energy for these replacement reactions must be no more than several kilocalories per mole.

(15) T. Smail and F. S. Rowland, *J. Phys. Chem.*, **74**, 1866 (1970).

(16) T. Smail, G. Miller, and F. S. Rowland, *ibid.*, **74**, 3474 (1970).

(17) E. A. Moelwyn-Hughes, “Physical Chemistry,” Pergamon Press, New York, N. Y., 1961, p 25.

(18) The competing thermal reactions in this system are presumably abstraction of H from CH_3X with the formation of H^{18}F and reaction with the scavenger molecule, O_2 or HI .

For such a situation, division of the reaction into hot and thermal processes is especially arbitrary. It is not clear yet whether real "scavengers" exist for near-thermal ^{18}F atom systems—it seems likely that several reactions (abstraction of H by ^{18}F ; addition to multiple bonds; perhaps ^{18}F -for-I) have sufficiently high reaction probabilities that no trace ingredient can successfully compete with such reactions with a major component. The O_2 or HI scavenger molecules serve very well in reacting preferentially with radical intermediates; whether they function with any success as scavengers for ^{18}F is a moot point.

The incremental absolute yield of CH_3^{18}F detected by comparison of scavenger experiments with HI *vs.* O_2 is little changed from CH_3F to CH_3I and is therefore *fractionally* less important in the overall CH_3^{18}F yields for the heavier halogen atoms. While this "decomposition" yield has not yet been distributed between $\text{CH}_3^{18}\text{F}^*$ and $\text{CH}_2^{18}\text{FX}^*$ decompositions, the indication is that substitution for X in molecules with weaker C-X bonds leaves less excitation energy with the $\text{CH}_3^{18}\text{F}^*$ product, on the average, and is consistent with the hypothesis that these reactions are often initiated by ^{18}F atoms quite near the thermal energy range.

Other factors, including collision radii, may also contribute to the variations in substitution yields, and more detailed elaborations of the bond energy dependence can be suggested. However, the overall conclusion still remains that substitution reactions initiated by ^{18}F atoms are influenced strongly by the same chemical factors which are reflected in changes in the bond strengths of C-X bonds.

DEPARTMENT OF CHEMISTRY
UNIVERSITY OF CALIFORNIA
IRVINE, CALIFORNIA 92664

THOMAS SMAIL
R. SUBRAMONIA IYER
F. S. ROWLAND*

RECEIVED JANUARY 4, 1971

Hexafluoroacetone Imine Filter for 185 nm

Publication costs assisted by the National Science Foundation

Sir: The isolation of the 185-nm line from the 254-nm line when using low-pressure mercury arcs has long proved a troublesome photochemical problem. Glasgow and Willard¹ have most recently developed a complex filter utilizing a flow of ozonized oxygen for this purpose. The ratio of the extinction coefficients of ozone for 254:185 nm is found¹ to be about 10:1. We wish to report on a very simple chemical filter consisting of a cell of gaseous hexafluoroacetone imine (hexafluoroisopropylideneimine). Hexafluoroacetone imine has a lower extinction coefficient than ozone at 185 nm, and the 254:185 nm extinction coefficient ratio is 23:1.

The imine² (purchased from Hynes Chemical Research Corp., Durham, N. C.) boils at 16° and we

have found the vapor to be stable up to at least 200°. The colorless liquid was distilled in a vacuum system with the middle fraction being retained; no special precautions were found to be needed and no impurities were detected by gas chromatography. In our preliminary photochemical experiments³ with the imine the decadic extinction coefficients at 254 and 185 nm were found to be 87 and 3.7 l. mol⁻¹ cm⁻¹ at 25°. Thus 100 Torr in a 5-cm long Suprasil cell will transmit 79% of the incident 185-nm radiation, but only 0.5% at 254 nm.

Hexafluoroacetone imine is photochemically stable, presumably due to very efficient self-quenching.³ The most abundant product of the photolysis at 254 nm is CF_3CN , and its quantum yield at 25° and 100 Torr is $<10^{-3}$. HBr was used as an actinometer. The imine filter is thus very photostable and only occasionally requires replacement, depending on the intensity of the light used.

Acknowledgment. The authors thank the National Science Foundation for support of this work. S. T. thanks Rutgers University for a Faculty Fellowship.

(1) L. C. Glasgow and J. E. Willard, *J. Phys. Chem.*, **74**, 4290 (1970).

(2) For properties see W. J. Middleton and C. G. Krespan, *J. Org. Chem.*, **30**, 1398 (1965).

(3) S. Toby and G. O. Pritchard, to be submitted for publication.

DEPARTMENTS OF CHEMISTRY
RUTGERS UNIVERSITY
NEW BRUNSWICK, NEW JERSEY 08903

SIDNEY TOBY*

UNIVERSITY OF CALIFORNIA
SANTA BARBARA, CALIFORNIA 93106

GLYN O. PRITCHARD

RECEIVED JANUARY 28, 1971

Kinetics of Isopropyl Alcohol Radicals by Electron Spin Resonance-Flow Techniques

Publication costs assisted by Texas A & M University

Sir: The interpretation of the kinetic behavior of radicals R_1 and R_2 from 2-propanol offered by Burchill in a previous communication¹ cannot be a suitable alternative. If the decays of substrate radicals are clearly determined by reaction 1, then a case analogous to transient equilibrium would hold and both R_1 and R_2 would decay with the same specific rates. The decays of both R_1 and R_2 would parallel the decay of Ti(III) on first-order plots, with $[\text{R}_1]/[\text{R}_2]$ remaining constant after equilibrium had been established. This is clearly not the case, as shown by Figures 2-4 and the data in Table I of our previous paper.²

(1) C. E. Burchill, *J. Phys. Chem.*, **75**, 167 (1971).

(2) R. E. James and F. Sicilio, *ibid.*, **74**, 1166 (1970).

Furthermore, all hydroxyalkyl radicals would exhibit the same $k(\text{decay})$ value, that set by reaction 1. We have unpublished data showing that a number of radicals have different k values. In addition, the upward concavity (*i.e.*, faster decay at shorter times) commonly observed in first-order plots of decays of alkyl radicals in the Ti(III)- H_2O_2 system is not in accord with the transient equilibrium concept.

The explanation by Burchill of a concentration inversion due to different reactivities of R_1 and R_2 toward H_2O_2 is diametrically opposed to the thesis that reaction 1 is rate determining. Either reaction 1 is rate determining, as he insists, so that $-\text{d}[\text{R}]/\text{d}t = k_1[\text{Ti(III)}][\text{H}_2\text{O}_2]$, or reaction 1 is not rate determining, so that the kinetic decreases of R_1 and R_2 are influenced by their reactivities with H_2O_2 . Both of these postulates cannot be valid. In addition, Burchill's predicted first-order dependency on $[\text{Ti(III)}]$ is not realized. As seen in Table I, ref 2, $k(\text{R} + \text{H}_2\text{O}_2)$ is relatively independent of $[\text{Ti(III)}]_0$.

Burchill contended that our mechanism would require radical concentrations four orders of magnitude greater than those observed. Reaction of Ti(III) with $\cdot\text{OH}$ to produce Ti(IV) and OH^- (reaction 13 in ref 2) explains both the stoichiometry and the disparity in radical concentrations. Reaction 13 also accounts for the low concentrations of S_1 and S_2 , Ti(IV)-complexed forms of $\cdot\text{OH}$ or $\cdot\text{O}_2\text{H}$, in the absence of substrate.² Any $\cdot\text{OH}$ reacting by (13) cannot be available for abstraction or direct formation of S_1 or S_2 . The effective competition of reaction 13 for the initially produced $\cdot\text{OH}$ radical is supported by gc analyses of nonfractionated distillates of effluent solutions from kinetic runs. It was found that concentrations of the predominant organic product, acetone, were less than 0.0010 M .

Acknowledgment. This research was supported by the Robert A. Welch Foundation, Grant A-177.

DEPARTMENT OF CHEMISTRY
TEXAS A & M UNIVERSITY
COLLEGE STATION, TEXAS 77843

R. E. JAMES
F. SICILIO*

RECEIVED JANUARY 11, 1971

Trifluoroacetic Acid. The Nature of Association in Diluted Solutions in Inert and Slightly Basic Solvents

Publication cost assisted by Laboratoire de Spectrochimie Moléculaire, Faculté des Sciences de Paris

Sir: It is well known that trifluoroacetic acid in the vapor phase forms cyclic dimers;¹⁻³ nevertheless the autoassociation of this acid in inert and slightly basic solvents is still disputed.^{4,5} Recently, Murty and

Pitzer thought they had provided evidence for linear association of this acid in nonpolar solvents.⁵ Since we are in disagreement with their experimental results, we present a critical study which is extended to other slightly basic solvents.

Trifluoroacetic acid (Baker Chemicals), after drying over phosphorus pentoxide, was distilled under vacuum in an all-glass apparatus, without ground joint to prevent any trace of grease. The solvents were dried over a 4-A molecular sieve.

The spectra were measured using a Beckman IR 12 and a Perkin-Elmer 225 spectrophotometer. Spectral slit width is about 2 cm^{-1} . The gain was checked every 10 cm^{-1} in solvent absorption regions to secure a good spectrophotometer response. When compensation was used, the base line was first verified by putting a fixed path length cell in the reference beam and a variable path length cell in the measure beam. The thickness of the latter was then fixed using the more intense absorption band of the solvent. For benzene under a thickness of 0.5 cm correct compensation was only obtained with a Perkin-Elmer 225 spectrophotometer owing to its source of high energy.

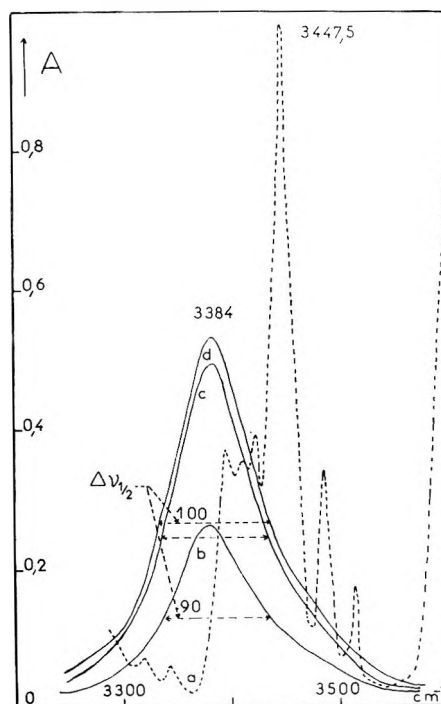


Figure 1. Benzene (---) and trifluoroacetic acid-benzene solutions (—): CF_3COOH concentration (b) $3.5 \times 10^{-3} M$; (c) $7 \times 10^{-3} M$; (d) $2.15 \times 10^{-2} M$. Cell thickness: (a) 0.5 cm; (b) and (c) 0.5 cm; (d) 0.2 cm.

- (1) C. Ling, S. D. Christian, H. E. Affsprung, and R. W. Gray, *J. Chem. Soc. A*, 293 (1966); *J. Phys. Chem.*, **70**, 901 (1966).
- (2) N. Fuson, M. L. Josien, E. A. Jones, and J. R. Lawson, *J. Chem. Phys.*, **20**, 1627 (1952).
- (3) J. R. Barcelo and C. Otero, *Spectrochim. Acta*, **18**, 1231 (1962).
- (4) L. W. Reeves, *Can. J. Chem.*, **39**, 1711 (1961).
- (5) T. S. R. Murty and K. S. Pitzer, *J. Phys. Chem.*, **73**, 1426 (1969).

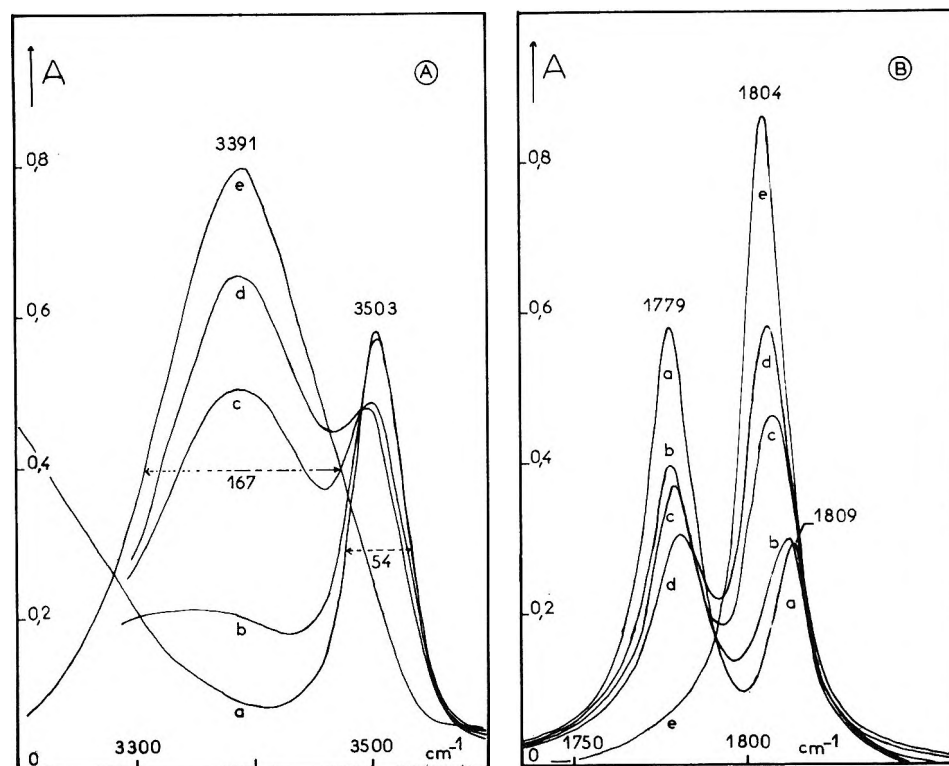


Figure 2. Trifluoroacetic acid $2.15 \times 10^{-2} M$ solution in carbon tetrachloride-1,2-dichloroethane solvent mixtures. Proportion of 1,2-dichloroethane: (a) 0; (b) 5; (c) 20; (d) 30; (e) 100%. A, hydroxyl stretching vibration region, $l = 0.5$ cm; B, carbonyl stretching vibration region, $l = 0.0627$ cm.

Table I: Spectral features of Trifluoroacetic Acid Monomer and Dimer Bands in Diluted Solutions

	CH ₃ OH $\nu(\text{OH}), \text{cm}^{-1}$	CF ₃ COOH				
		ν, cm^{-1}	$\Delta\nu_{1/2}, \text{cm}^{-1}$	$\epsilon, \text{cm}^2 M^{-1}$	$\nu_{\text{monomer}}(\text{C}=\text{O}), \text{cm}^{-1}$	$\nu_{\text{dimer}}(\text{C}=\text{O}), \text{cm}^{-1}$
1 Gas phase	3685 ^a	3587 ^c			1826 ^c	1781 ^c
2 <i>n</i> -Hexane	3654 ^b	3524	44	48	1815	1780
3 <i>n</i> -Heptane	3652 ^a	3520	72	82	1814	1780
4 Carbon tetrachloride	3644	3504	54	12	1809	1779
5 Carbon disulfide	3629 ^a	3477	109	17	1807	1779
6 1,2-Dichloroethane	3619	3391	167	74	1804	1782
7 <i>tert</i> -Butyl chloride	3615	3318	209	95		
8 Benzene	3612 ^b	3384	95	125		
9 Nitromethane	3606	3211	380	116	1799	
10 1,3,5-Trimethylbenzene	3596 ^a	3325	118	15	1803	
11 Acetonitrile	3543				1793	
12 Tetrahydrofuran	3486				1781	

^a A. R. M. Cole, L. H. Little, and A. J. Michell, *Spectrochim. Acta*, **21**, 1169 (1965). ^b A. Allerhand and P. v. R. Schleyer, *J. Amer. Chem. Soc.*, **85**, 371 (1963). ^c See ref 2.

All of the cells were equipped with calcium fluoride windows.

Used solvents and observed absorption band characteristics are summarized in Table I. Some spectra are presented for illustration in Figures 1 and 2. Figure 2 also shows the application of mixed solvents technique to the study of association with 1,2-dichloroethane. This solvent is well suited to simultaneously examine the $\nu(\text{OH})$ and $\nu(\text{C}=\text{O})$ vibrations of trifluoroacetic acid.

The spectrum of trifluoroacetic acid in diluted carbon

tetrachloride solution (Figures 2A and B, curve a) agrees with those reported by Fuson, *et al.*,² Reeves,⁴ and Barcelo;³ it corresponds with the assumption of an equilibrium between monomers and cyclic dimers like other carboxylic acids in the gas phase.¹ The monomer $\nu(\text{OH})$ stretching vibration is observed at 3504 cm^{-1} , that of dimer corresponding to a wide absorption at quite lower frequency. In the carbonyl stretching region, only two bands are observed at 1809 and 1779 cm^{-1} and assigned to the monomer and cyclic dimer.

We were unable to see the other band at 1792 cm^{-1} observed by Murty and Pitzer although we studied solutions of same concentration.

In benzene, Figure 1, only the hydroxyl stretching region might be observed for diluted solutions, due to solvent absorption between 1750 and 1850 cm^{-1} . As shown by curve a, the solvent presents several absorption bands in this region including one at 3447.5 cm^{-1} which is particularly intense. The spectra of trifluoroacetic acid in the concentration range 3.5×10^{-3} to $2.15 \times 10^{-2}\text{ M}$ run with compensation for solvent absorptions show only one band located at 3384 cm^{-1} . The sharp band observed at 3455 cm^{-1} by Murty and Pitzer⁵ was probably due to a wrong compensation of benzene absorption at 3447.5 cm^{-1} . When the acid concentration increases, the 3384-cm^{-1} band becomes slightly wider and the molar absorption coefficient decreases. The integrated intensity remains approximately constant and indicates that in the concentration range studied, most of the acid molecules form a monomer-solvent complex. Benzene is indeed a solvent well known for its basic properties⁶ and it may be expected to form a hydrogen-bonded complex with a strongly proton-donor compound.

As Murty and Pitzer claimed they obtained results in 1,2-dichloroethane similar to those in benzene, we have run spectra of a $2.75 \times 10^{-2}\text{ M}$ trifluoroacetic acid solution in pure 1,2-dichloroethane and in mixtures of 1,2-dichloroethane and carbon tetrachloride (Figures 2A and B). When the proportion of 1,2-dichloroethane increases the intensity of the associated band at 1779 cm^{-1} decreases and a new band at 1804 cm^{-1} appears near the monomer acid band in the carbon tetrachloride solution. The relative intensity of the two bands is reversed for a mixture with 30% 1,2-dichloroethane and the band at 1804 cm^{-1} stays alone in the latter solvent. (Nevertheless the band foot is wider at lower frequencies; this may be explained by a very small amount of cyclic dimer of acid corresponding to a band at 1782 cm^{-1} in 1,2-dichloroethane.) In the hydroxyl stretching vibration region (Figure 2A), the band at 3504 cm^{-1} and lower frequency absorption progressively disappears while an intermediate band at 3391 cm^{-1} appears with the increase in 1,2-dichloroethane proportion and is the only one observed in that pure solvent. This behavior must be related to the formation of a monomer-solvent complex with a $\nu(\text{OH})$ band 113 cm^{-1} lower and a $\nu(\text{C}=\text{O})$ band only 7 cm^{-1} lower than the bands of acid monomer in carbon tetrachloride. Our assumption is supported by a study of trifluoroacetic acid autoassociation in 1,2-dichloroethane. When the acid concentration is increased a band appears at 1782 cm^{-1} due to cyclic dimer. This band is only noticeable for a concentration of $4 \times 10^{-2}\text{ M}$ but appears in carbon tetrachloride at 1779 cm^{-1} in a concentration a hundred times smaller. This might be correlated with the already implied formation of

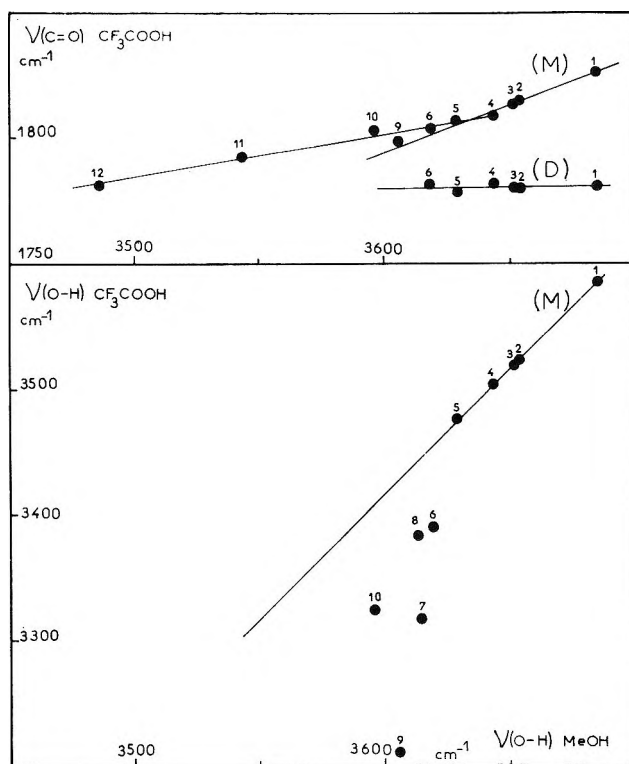


Figure 3. Trifluoroacetic acid monomer (M) and dimer (D) $\nu(\text{OH})$ and $\nu(\text{C}=\text{O})$ frequencies in different solvents (numbers see Table I) vs. methanol $\nu(\text{OH})$ frequency.

hydrogen-bonded complexes between alcohols and chlorinated aliphatic solvents.⁷

This study has been extended to some more active solvents. Observed band characteristics for dilute acid solutions in these solvents are summarized in Table I and Figure 3. In solvents 7–12 we were unable to see the dimer $\nu(\text{C}=\text{O})$ band even at a 1 M acid concentration but at this same concentration the intensities of solvent associated monomer and dimer bands are equal in 1,2-dichloroethane. Figure 3 shows $\nu(\text{C}=\text{O})$ monomer and dimer, and $\nu(\text{OH})$ monomer frequencies vs. methanol $\nu(\text{OH})$ frequency in diluted solutions in the same solvents. Points corresponding to solvents 1–5 are located on a straight line and it can be assumed that in these solvents perturbations are related to environmental effects. However, as soon as the solvents present basic properties the trifluoroacetic acid $\nu(\text{OH})$ frequency is much more strongly lowered than that of methanol, thus proving formation of a monomer-solvent complex. Although Bellamy, *et al.*,⁸ have implied in similar groups a solvent independent linear relation, such deviations have already been observed.^{9–11}

(6) M. Tamres, *J. Amer. Chem. Soc.*, **74**, 3375 (1952).

(7) P. J. Krueger and H. D. Mettee, *Can. J. Chem.*, **42**, 288 (1964).

(8) L. J. Bellamy, H. E. Hallam, and R. L. Williams, *Trans. Faraday Soc.*, **54**, 1120 (1958).

(9) J. Lascombe, Thèse, Bordeaux, 1960.

The $\nu(\text{C}=\text{O})$ monomer vibration is much less sensitive to solvent influence. Points corresponding to basic solvents are located over the straight line related to "inert solvents"; in this case indeed, the $>\text{C}=\text{O}$ vibrator is not directly involved in a hydrogen bond like methanol OH oscillator. When it can be observed, the autoassociated acid $\nu(\text{C}=\text{O})$ band is nearly insensible to solvent nature, corroborating the cyclic structure of dimer.

(10) P. Grange, J. Lascombe, and M. L. Josien, *Spectrochim. Acta*, **16**, 981 (1960).

(11) P. V. Huong, Thèse Bordeaux 1963. M. L. Josien, J. Lascombe, and P. V. Huong, *C. R. Gams*, **87** (1962).

LABORATOIRE DE SPECTROCHIMIE

MOLECULAIRE

FACULTE DES SCIENCES DE PARIS, 9, QUAI

SAINT-BERNARD, PARIS VE, FRANCE

LABORATOIRE DE CHIMIE PHYSIQUE DU C.N.R.S.

2, RUE HENRY-DUNANT, 94-THIAIS, FRANCE

M. KIRSZENBAUM

J. CORSET

M. L. JOSIEN*

RECEIVED SEPTEMBER 24, 1970

Perfluorinated Aliphatic Carboxylic Acids.

Nature of Association in Dilute Solutions

in Nonpolar Solvents

Publications costs assisted by Carothers Research Laboratory

Sir: Trifluoroacetic acid (TFA) is one of the strongest carboxylic acids known.¹ The available thermodynamic data for TFA indicates cyclic dimerization in the vapor phase;² but a dilution effect was observed within the band for hydrogen bonded carbonyl groups in carbon tetrachloride (CCl_4) solutions and this was interpreted as evidence for linear dimerization.³ This note reports that pentafluoropropionic (PFP) and heptafluorobutyric^{4b} (HFB) acids, which are as strong as TFA, show a similar dilution effect in CCl_4 solutions. Perfluorooctanoic acid⁵ also behaves similarly. Pentafluorobenzoic acid (PFB), which is a relatively weaker acid⁶ ($\text{p}K_a = 3.38$), behaves like acetic acid and does not show a dilution effect.

The relative hydrogen bonding acidities, as measured by ν_{OH} frequency shifts, of TFA, PFP, HFB, and PFB are compared in Table I. The ionization constant of TFA in aqueous solutions is under dispute at the present time.^{4a} Figures 1 and 2 show the dilution effect observed in the carbonyl stretching region for PFP and HFB, respectively, in CCl_4 solutions. Figure 3 shows the carbonyl stretching region of PFP in 1,2-dichloroethane (DCE) and *n*-hexane solutions. The results are very similar for PFP and HFB but not for PFB and these are summarized in Table II.

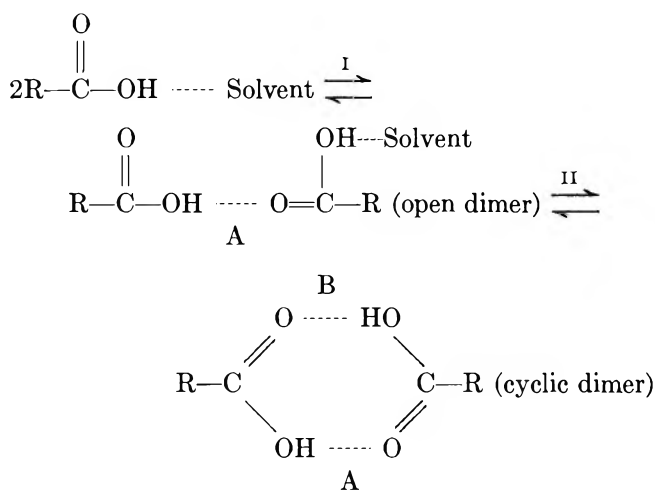
It is known that a given acid (for example, acetic acid^{7b}) is more dissociated in a basic solvent than hydrocarbon solvents. Similarly, in a given solvent

Table I: Hydroxyl Stretching Frequencies of TFA, PFP, HFB, and PFB in Various Solvents

Solvent	$\nu_{\text{OH}}, \text{cm}^{-1}$			
	TFA	PFP	HFB	PFB
Gas phase	3587 ^a	3581	3581	3559 ^b
<i>n</i> -Hexane	3524 (3524) ^a	3520	3520	
CCl_4	3500 (3504) ^a	3500	3500	3518 (3509) ^b
DCE	3385 (3391) ^a	3380	3375	3426

^a Reference 10. ^b J. M. Birchall, T. Clarke, and R. N. Haszeldine, *J. Chem. Soc.*, 4977 (1962).

the stronger acid self-associates to a lesser degree. Thus trichloroacetic acid (TCA) is less associated than di- and monochloroacetic acids in benzene.⁷ The equilibrium II represented below depends, besides other factors, on the enthalpy of hydrogen bond (B) formation which will be opposed by the entropy of cyclic dimer formation and the enthalpy of solvation of $-\text{OH}$ in the open dimer. In the vapor state an open



dimer may not survive because the enthalpy of hydrogen bond (B) formation (ΔH_f^B) can be taken to be approximately -7 kcal mol^{-1} ⁸ because all the car-

(1) (a) A. I. Popov, "The Chemistry of Nonaqueous Solvents," J. J. Lagowski, Ed., Vol. III, Academic Press, New York, N. Y.; (b) A. I. Popov summarized the data with references in Chapter 5.

(2) H. Dunken and G. Marx, *Abh. Deut. Akad. Wiss. Berlin, Kl. Math. Phys. Tech.*, **6**, 101 (1964).

(3) T. S. S. R. Murty and K. S. Pitzer, *J. Phys. Chem.*, **73**, 1426 (1969).

(4) (a) A. K. Covington, J. G. Freeman and T. H. Lilley, *ibid.*, **74**, 3773 (1970), and the references cited therein; (b) The ionization constants of TFA and HFB were reported as 0.59 and 0.68, respectively, A. L. Henne and C. J. Fox, *J. Amer. Chem. Soc.*, **73**, 2323 (1951).

(5) T. S. S. R. Murty, unpublished results.

(6) W. A. Sheppard, *J. Amer. Chem. Soc.*, **92**, 5419 (1970).

(7) J. Steigman and W. Cronkright, *Spectrochim. Acta, Part A*, **26**, 1805 (1970).

(8) T. C. Chaing and R. M. Hammaker, *J. Phys. Chem.*, **69**, 2715 (1965).

Table II: Carbonyl Stretching Frequencies of TFA, PFP, HFB, and PFB in Various Solvents

Solvent	TFA	PFP	$\nu_{C=O}$, cm^{-1}	HFB	PFB
Gas phase	1829, 1790 (1826, ^a 1781 ^a)	1824, 1782 (1825 ^b , 1779 ^b)		1823, 1782	
<i>n</i> -Hexane	1815, 1780 (1815, ^a 1780 ^a)	1812, 1775		1810, 1775	
CCl_4	1813, 1792, 1782	1807, 1785, 1773		1806, 1785, 1775	1764, 1724 (1764, ^b 1721 ^b)
DCE	1804, ^a 1782 ^a	1800, 1776		1800, 1777	1756, 1725

^a Reference 10. ^b J. K. Brown and K. J. Morgan, *Advan. Fluorine Chem.*, **4**, 253 (1965).

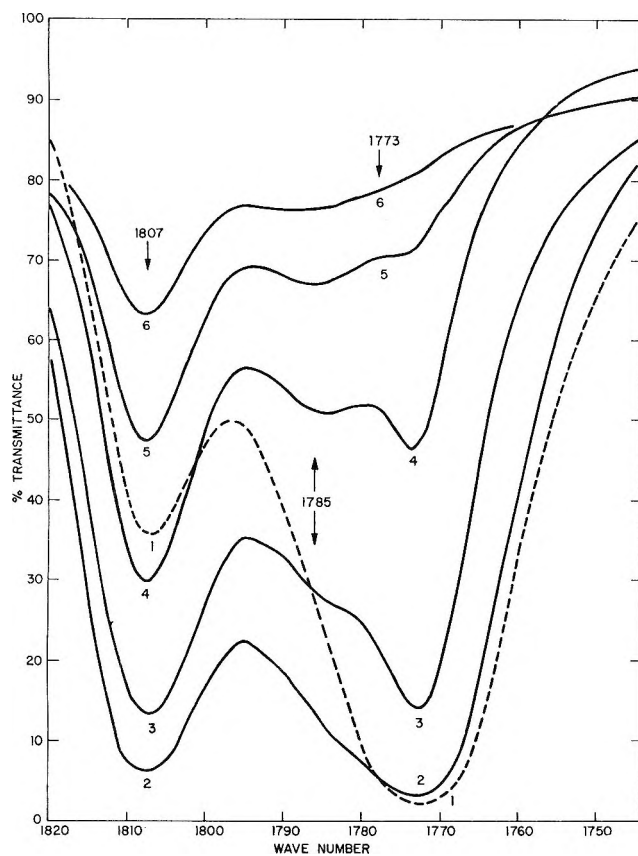


Figure 1. Carbonyl stretching region of PFP in CCl_4 solutions at room temperature: curve 1 (---) $2 \times 10^{-1} M$, 0.1 mm NaCl cells; curves 2, 3, 4, 5, and 6 (—) 1×10^{-2} , 5×10^{-3} , 2.5×10^{-3} , 1.25×10^{-3} and $6.3 \times 10^{-4} M$, respectively; 6-mm NaCl cells. The spectra were run using the scale of $10 \text{ cm}^{-1}/\text{in.}$ and at a speed of $20 \text{ cm}^{-1}/\text{min.}$

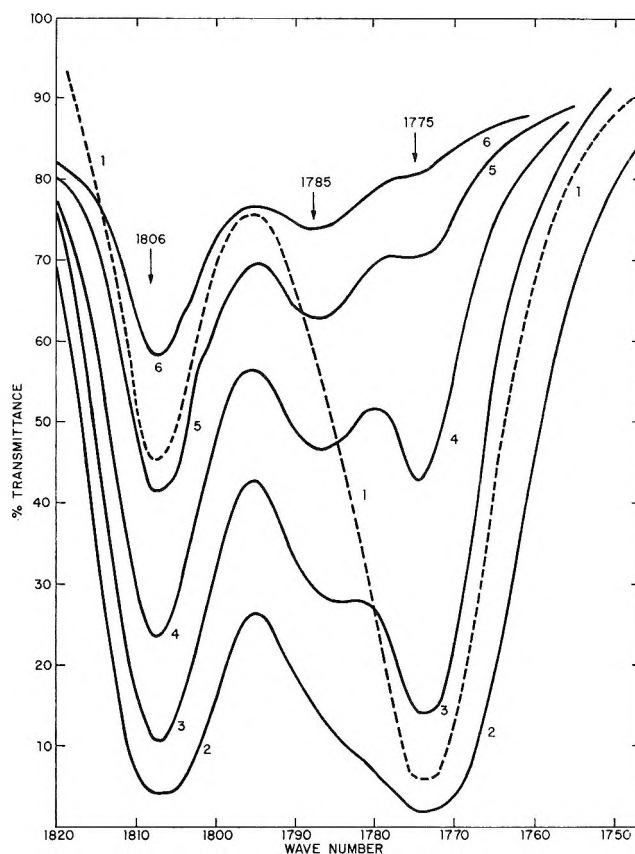


Figure 2. Carbonyl stretching region of HFB in CCl_4 at room temperature: curve 1 (---) $6.8 \times 10^{-2} M$, 0.1-mm NaCl cells; curves 2, 3, 4, 5 and 6 (—) 1×10^{-2} , 5×10^{-3} , 2.5×10^{-3} , 1.25×10^{-3} , and $6.3 \times 10^{-4} M$, respectively, 6-mm NaCl cells. The spectra were run using the scale of $10 \text{ cm}^{-1}/\text{in.}$ and at a speed of $20 \text{ cm}^{-1}/\text{min.}$

boxylic acids have a reported ΔH_f of nearly $-14 \text{ kcal mol}^{-1}$ ^{2,9}) more than compensates for the entropy of cyclic dimer formation. However, in a solvent the solvation of $-\text{OH}$ will become more and more important for a given acid as the solvent basicity increases or in a given solvent as the strength of the acid increases which could alter the equilibrium to favor open dimers.³ If the solvent becomes basic enough and/or the acid strong enough and/or the hydrogen bond (A) weak enough, only monomers hydrogen bonded to the solvent

exist. Thus, in freezing dioxane TCA appears, from cryoscopic measurements, to be entirely monomeric⁹ although it is dimerized in benzene.^{7,9} The spectral features associated with the nonbonded hydroxyl and carbonyl groups are much stronger for TFA,³ and in general for perfluorinated aliphatic carboxylic acids, than for other carboxylic acids.

The available data taken together seem to indicate

(9) G. Allen and E. F. Caldin, *Quart. Rev., Chem. Soc.*, **7**, 255 (1953).

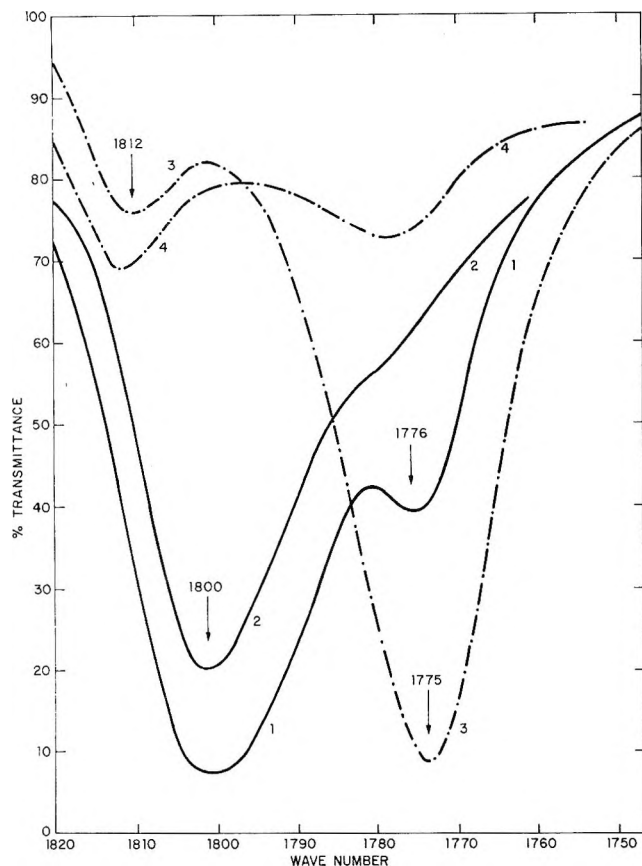


Figure 3. Carbonyl stretching region of PFP in DCE and *n*-hexane solutions at room temperature: curve 1, $1 \times 10^{-1} M$ in DCE, 0.1-mm NaCl cells; curve 2, $2 \times 10^{-3} M$ in DCE, 6-mm NaCl cells; curve 3, $9.4 \times 10^{-2} M$ in *n*-hexane, 0.1-mm NaCl cells; curve 4, $8 \times 10^{-4} M$ in *n*-hexane, 6-mm NaCl cells. The spectra were run using the scale of $10 \text{ cm}^{-1}/\text{in.}$ and at a speed of $20 \text{ cm}^{-1}/\text{min.}$

that the dilution effect observed, in CCl_4 in the band for hydrogen bonded carbonyl groups for the perfluorinated aliphatic carboxylic acids, is due to cyclic and open dimers and/or open polymers and dimers. In light of the data in CCl_4 it would be of interest to speculate on the nature of the dimer in *n*-hexane and DCE. In the latter two solvents no dilution effect of the bonded carbonyl groups is observed in the concentration range studied. For PFP in *n*-hexane the dimer band persists up to $8 \times 10^{-4} M$ and in DCE the dimer band is weak relative to the free carbonyl absorption

even at $1 \times 10^{-1} M$ and present only as a shoulder at $2 \times 10^{-3} M$. For TFA in DCE the dimer band is noticeable only at $4 \times 10^{-2} M$.¹⁰ The spectral data would be consistent with an argument that the dimer is cyclic in *n*-hexane (similar to vapor phase) but is open in DCE because of greater solvation of $-\text{OH}$. The nature of the dimers in these solvents can be understood better if accurate hydrogen bond enthalpy values are available. The question of cyclic and/or open dimers was raised and discussed in detail even for the relatively weak trimethylacetic acid⁸ ($\text{p}K_a = 5.02$) in CCl_4 .

It was originally reported³ that TFA in benzene revealed the presence of two absorption peaks (at 3400 and 3455 cm^{-1}) in the region assigned to free hydroxyl groups, and similar double peaks were obtained for TCA and tribromoacetic (TBA) acids though no dilution effect of the bonded carbonyl groups of TCA and TBA was observed. However, Kirszenbaum, *et al.*, point out that the 3455-cm^{-1} absorption^{10,11} is due to benzene solvent and this note confirms their observation. Also, the recent work on the dimerization constants of chlorinated acetic acids⁷ confirms that no double peaks are present in the free hydroxyl region for TCA (and therefore also for TBA) in benzene.

TFA (Columbia Organic Chemicals Co.), PFP (PCR Incorporated), HFB (Columbia Organic Chemicals Co.) were distilled. PFB (Aldrich Chemical Co.) was used without further purification. All the solvents were dried by standard methods.

The spectra were measured using a Beckman IR-12 spectrophotometer. The path length of the cells varied depending upon experimental convenience. Beckman NIR silica cells of 10 and 1 cm length, 0–6-mm Beckman variable path length, and 0.1-mm sodium chloride cells and 10-cm cells with sodium chloride windows were used.

(10) M. Kirszenbaum, J. Corset, and M. L. Josien, *J. Phys. Chem.*, **75**, 1327 (1971).

(11) R. D. Mair and D. F. Hornig, *J. Chem. Phys.*, **17**, 1236 (1949).

E. I. DUPONT DE NEMOURS AND CO., INC. T. S. S. R. MURTY
CAROTHERS RESEARCH LABORATORY
EXPERIMENTAL STATION
WILMINGTON, DELAWARE 19898

RECEIVED MARCH 15, 1971

Journal of Chemical and Engineering Data

APRIL 1971, Vol. 16, No. 2

TABLE OF CONTENTS

- 129** Enthalpies of Decalins and of *trans*-Decalin and *n*-Pentane Mixtures
J. M. Lenoir, K. E. Hayworth, and H. G. Hipkin
- 134** Compressibility Measurements of the Liquid Binary Systems $\text{KNO}_3\text{-Ca}(\text{NO}_3)_2$ and $\text{ZnCl}_2\text{-C}_5\text{H}_5\text{N}\cdot\text{HCl}$
L. J. Pollard, M. L. Crowe, and Werner Strauss
- 137** Vapor-Liquid Equilibrium Relationships of Binary Systems. Propane-*n*-Alkane Systems, *n*-Hexane and *n*-Heptane
W. B. Kay
- 141** Beckmann Rearrangement of Adamantanone Oxime
Peter Kovacic, K. W. Field, and T. A. Wnuk
- 143** Density, Viscosity, and Carbon Dioxide Solubility and Diffusivity in Aqueous Ethylene Glycol Solutions
Walter Hayduk and V. K. Malik
- 146** Vapor-Liquid Equilibria for Carbon Dioxide-Difluoromethane System.
R. A. Adams and F. P. Stein
- 149** Vapor-Liquid Equilibria in Binary Aromatic-Olefin Systems
J. H. Vera and J. M. Prausnitz
- 154** PVT Properties of Liquid *n*-Octane
M. S. Benson and Jack Winnick
- 158** Phase Equilibria Data for Helium-Methane System
W. E. DeVaney, H. L. Rhodes, and P. C. Tully
- 161** Methyl and Monoglycol Esters of Hydroxymethylabietaic Acid and Their Derivatives
K. K. Sugathan, W. A. Rohde, and G. W. Hedrick
- 164** Isobaric Vapor-Liquid Equilibria for Three Binary and Two Ternary Systems
Isamu Nagata and Tatsuhiko Ohta
- 167** Vapor Pressure of Dysprosium and Erbium
J. M. McCormack, P. R. Platt, and R. K. Saxer
- 170** Correlation Equation for Solubility of Carbon Dioxide in Water, Seawater, and Seawater Concentrates
Prem Munjal and P. B. Stewart
- 173** Some Heat Capacities of Argon in Ranges 5-1000 Atm and 180-450° K. Examination and Correction Using Sonic Velocity Data
G. E. Goring and J. N. Holyoak
- 178** Magnesium Complex and Ion-Pair in $\text{MgCO}_3\text{-CO}_2$ Solution System
F. S. Nakayama
- 181** Solution-Crystal Equilibrium for Pyridine-Water System
A. J. Glessner and A. L. Myres
- 185** Densities and Refraction in Some Binary Systems of Hexadecane and Normal Chloroalkanes at 25° C
E. L. Heric and B. M. Coursey
- 188** Vapor-Liquid Equilibrium at 29.3° C in System 2,6-Lutidine-Water
Z. M. Kurtyka
- 190** Interfacial Tensions Between Molten Magnesium and Salts of the $\text{MgCl}_2\text{-KCl-BaCl}_2$ System
J. N. Reding
- 195** Low-Temperature Heat Capacity and Entropy of Ammonium Tetrametaphosphate
Z. T. Wakefield, B. B. Luff, and R. C. Sheridan
- 197** Thermodynamic Study of Water and Propylene Oxide Solutions
K. W. Morcom and R. W. Smith
- 200** Salt Effects in Liquid-Liquid Equilibria
M. L. Desai and E. O. Eisen
- 203** Osmotic Coefficients of Aqueous Solutions of Calcium Chloride and Calcium Perchlorate at 25° C
R. A. Robinson and C. K. Lim
- 204** Densities of Some Nitrate and Sulfate Melts
L. G. Boxall and K. E. Johnson
- 206** Isomerization Equilibrium Constants of *n*-Butenes
John Happel, M. A. Hnatow, and Reiji Mezaki
- 210** Electrical Conductance and Density in the Fused Molybdate Systems, $\text{Li}_2\text{MoO}_4\text{-Na}_2\text{MoO}_4$ and $\text{Li}_2\text{MoO}_4\text{-K}_2\text{MoO}_4$
L. P. Brown K. B. Morris
- 212** Experimental Data and Procedures for Predicting Thermal Conductivity of Binary Mixtures of Nonpolar Gases
S. C. Saxena and P. K. Tondon
- 220** Dielectric Constants, Viscosities, Fusion Point Curves, and Other Properties of Three Nonaqueous Binary Systems
P. G. Sears, T. M. Stoeckinger, and L. R. Dawson

- 222** Density and Viscosity of Aqueous Solutions of Methanol and Acetone from the Freezing Point to 10° C
T. W. Yergovich, G. W. Swift, and Fred Kurata
- 226** Hittorf Transference Numbers in Aqueous Copper Sulfate at 25° C
M. J. Pikal and D. G. Miller
- 229** Apparent Molal Volumes of Aqueous Tetraphenyl Arsonium Chloride Solutions at 0°, 25°, and 50° C
F. J. Millero
- 232** Torsion-Effusion Study of Sublimation of Barium Nitride
R. C. Blair and Z. A. Munir
- 234** Heat of Combustion of Isophthalamide
W. S. Hamilton and L. C. Witt
- 235** Solubility of Helium and Neon in Water and Seawater
R. F. Weiss
- 241** Properties of Organic-Water Mixtures. Activity Coefficients of Sodium Chloride at Saturation in Aqueous Solutions of Some Oxy-Oxa Compounds at 25° C
R. J. Raridon and K. A. Kraus

ORGANIC SECTION

- 244** Studies in the Heterocyclic Series II. 3,6-Diazaphenothiazine Sulfoxides and Other Potential Antiparasitic and Pesticidal Agents
C. O. Okafor
- 246** Organodichlorosilanes and Cyclotrisiloxanes Containing Polar Groups
T. C. Wu
- 249** Synthesis and Nmr Data of Some Variously Substituted Diphenylmethanes and Dibenzylbenzenes
Giorgio Montaudo, Paolo Finocchiaro, Salvatore Caccamese, and Francesco Bottino
- 254** Synthesis of Biphenyl Portion of Decinine
Benjamin Blank and Praful D. Vaidya
- 258** Preparation and Properties of Some Hydroxy Oximes and Their Precursors
J. F. Engel and C. C. Chappelow, Jr.
- 260** Deshielding of Ortho Proton of *N*-Acylanilines
T. L. Lemke
- 263** New Data Compilations
- 136, 259** Corrections

BROADEN

Your Chemical Information Base

Enter your low-cost charter subscription now to the American Chemical Society's exciting new "SINGLE ARTICLE ANNOUNCEMENT SERVICE" and select relevant current material from fifteen major ACS primary journals.

Now, you can vastly increase your available range of chemical data . . . in a fraction of your current reading time . . . and at a minimum of cost.

The ACS "SINGLE ARTICLE ANNOUNCEMENT SERVICE" brings subscribers twice-monthly announcements containing reproductions of contents pages from fifteen major ACS primary journals . . . as well as I&EC's "Research Results Service."

By scanning the tables of contents, you can decide which articles are pertinent to your needs. Then, using an order form included with the announcement, you can check the desired articles and return it to us. Your reprints will be sent to you via first class mail . . . within twenty-four hours of receipt.

Publications included in this service are: ANALYTICAL CHEMISTRY . . . BIOCHEMISTRY . . . ENVIRONMENTAL SCIENCE & TECHNOLOGY . . . I&EC-FUNDAMENTALS . . . I&EC-PROCESS DESIGN & DEVELOPMENT . . . I&EC-PRODUCT RESEARCH & DEVELOPMENT . . . INORGANIC CHEMISTRY . . . JOURNAL OF AGRICULTURAL AND FOOD CHEMISTRY . . . JOURNAL OF THE AMERICAN CHEMICAL SOCIETY . . . JOURNAL OF CHEMICAL DOCUMENTATION . . . JOURNAL OF CHEMICAL AND ENGINEERING DATA . . . JOURNAL OF MEDICINAL CHEMISTRY . . . JOURNAL OF ORGANIC CHEMISTRY . . . JOURNAL OF PHYSICAL CHEMISTRY . . . MACROMOLECULES . . . plus the "Research Results Service" (which provides titles and short summaries of all manuscripts being considered for future publication in the three I&EC Quarterlies).

Cost for the reprints is quite low: \$1 for the first individual reprint and \$.60 for each additional reprint order entered in the same request. Papers from the "Research Results Service" are available in manuscript form, at a nominal cost per page.

Enter your charter subscription now to the exciting "SINGLE ARTICLE ANNOUNCEMENT SERVICE" . . . and save 20% as a charter subscriber.

Single Article Announcement Service

American Chemical Society, 1155 16th Street, N.W., Washington, D.C. 20036

Yes—I wish to receive the ACS SINGLE ARTICLE ANNOUNCEMENT SERVICE at the one-year charter rate checked below.

	U.S.	Canada, PUAS	Other Nations
ACS Member <i>Personal Use</i> Charter One-Year Rate	<input type="checkbox"/> \$8.00	<input type="checkbox"/> \$11.00	<input type="checkbox"/> \$11.50
Nonmember Charter One-Year Rate	<input type="checkbox"/> \$16.00	<input type="checkbox"/> \$19.00	<input type="checkbox"/> \$19.50

Payment enclosed Bill me Bill company I am an ACS member I am not an ACS member

Name _____ Position _____

Address Home _____ (Specific title please)
 Business _____

City _____ State/Country _____ Zip _____

Your employer _____

Nature of your employer's business: Manufacturing or Processing _____
(Please indicate)

If manufacturer, type of products produced _____

Keep pace with the new...

through these basic research journals of the American Chemical Society

The Journal of the American Chemical Society

The premier American chemistry journal publishing original research papers in every field. Biweekly.

*ACS members: U.S. \$22.00 Canada, PUAS \$26.50 Other nations \$27.50
Nonmembers: U.S. \$44.00 Canada, PUAS \$48.50 Other nations \$49.50

The Journal of Organic Chemistry

Embraces the field, from synthesis to structure to behavior. Biweekly publication.

*ACS members: U.S. \$20.00 Canada, PUAS \$24.50 Other nations \$25.50
Nonmembers: U.S. \$40.00 Canada, PUAS \$44.50 Other nations \$45.50

The Journal of Physical Chemistry

Maintains a balance between classical areas of chemistry and modern structural quantum oriented areas. Biweekly.

*ACS members: U.S. \$20.00 Canada, PUAS \$24.00 Other nations \$25.00
Nonmembers: U.S. \$40.00 Canada, PUAS \$44.00 Other nations \$45.00

Biochemistry

Covers enzymes, proteins, carbohydrates, lipids, nucleic acids and their metabolism, genetics, biosynthesis. Biweekly.

*ACS members: U.S. \$20.00 Canada, PUAS \$23.00 Other nations \$23.50
Nonmembers: U.S. \$40.00 Canada, PUAS \$43.00 Other nations \$43.50

The Journal of Agricultural and Food Chemistry

Places special emphasis on the chemical aspects of agricultural and food chemistry. Bimonthly.

*ACS members: U.S. \$10.00 Canada, PUAS \$13.00 Other nations \$13.50
Nonmembers: U.S. \$20.00 Canada, PUAS \$23.00 Other nations \$23.50

The Journal of Medicinal Chemistry

Emphasis is on synthesis, mode of action and pharmacology of medicinal agents. Monthly.

*ACS members: U.S. \$15.00 Canada, PUAS \$18.00 Other nations \$18.50
Nonmembers: U.S. \$30.00 Canada, PUAS \$33.00 Other nations \$33.50

The Journal of Chemical and Engineering Data

Quarterly journal presenting data on properties and behavior of both new and known chemical systems.

*ACS members: U.S. \$15.00 Canada, PUAS \$18.00 Other nations \$18.50
Nonmembers: U.S. \$30.00 Canada, PUAS \$33.00 Other nations \$33.50

Inorganic Chemistry

Publishes original research, both experimental and theoretical, in all phases of inorganic chemistry.

*ACS members: U.S. \$18.00 Canada, PUAS \$21.00 Other nations \$21.50
Nonmembers: U.S. \$36.00 Canada, PUAS \$39.00 Other nations \$39.50

Macromolecules

Presents original research on all fundamental aspects of polymer chemistry. Bimonthly publication.

*ACS members: U.S. \$12.00 Canada, PUAS \$15.00 Other nations \$15.50
Nonmembers: U.S. \$24.00 Canada, PUAS \$27.00 Other nations \$27.50

American Chemical Society / 1155 Sixteenth Street, N.W., Washington, D.C. 20036

Please enter a one year subscription for the following journals:

1 _____	2 _____	3 _____
4 _____	5 _____	6 _____
7 _____	8 _____	9 _____
name _____		position _____
address _____		
city _____	state/country _____	zip _____
your company _____		nature of company's business _____

I am an ACS member I am not an ACS member Bill me for \$ _____

Payment enclosed (*payable to American Chemical Society*) in the amount of \$ _____. Payment must be made in U.S. currency, by international money order, UNESCO coupons, or U.S. bank draft; or order through your book dealer.

* NOTE: Subscriptions at ACS member rates are for personal use only.